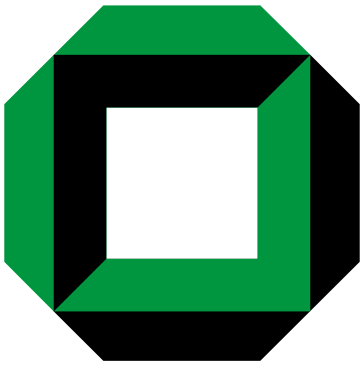

Karlsruher Institut für Technologie
Fakultät für Physik

Novel Applications of Nonreciprocal Quantum Amplifiers

Lindsay Orr

Dissertation

Karlsruhe 2025

Fakultät für Physik
Karlsruher Instituts für Technologie (KIT)
Wolfgang-Gaede-Str. 1
76131 Karlsruhe, Deutschland

Karlsruher Institut für Technologie

Fakultät für Physik
Institut für Theorie der Kondensierten Materie

Novel Applications of Nonreciprocal Quantum Amplifiers

Zur Erlangung des akademischen Grades eines

Doktors der Naturwissenschaften (Dr. rer. nat.)

von der KIT-Fakultät für Physik
des Karlsruher Instituts für Technologie (KIT)

genehmigte

Dissertation

von

Lindsay Orr, M.Sc.

aus Kanada

Tag der mündlichen Prüfung: 09/05/2025

Referentin: Prof. Dr. Anja Metelmann
Korreferent: Prof. Dr. Shlomi Kotler

I hereby declare that I have written the dissertation independently, that I have completely and accurately listed all resources used, that I have indicated everything that has been taken from the work of others whether unchanged or otherwise, and that I have observed the Statutes for Safeguarding Good Research Practice at the Karlsruhe Institute for Technology.

Berlin 2025

Lindsay Orr

Solvitur ambulando

Abstract

The implementation of quantum-limited amplifiers has been a necessity for the high-fidelity processing of signals involving few weak photons, commonly encountered in experiments involving superconducting microwave electronics. The need to protect sensitive quantum systems during these experiments demands the use of devices capable of directionally routing the noisy signals from these amplifiers away from the quantum system under observation, which is accomplished by breaking the symmetry of reciprocity. To reduce losses and improve fidelity, both characteristics may be realised in a single device: the nonreciprocal quantum amplifier. In this dissertation, we explore uses for nonreciprocal quantum amplifiers that go beyond these signal processing applications. These applications will depend on the quantum nature of the amplifier, and so cannot be realised using components operating in the classical regime. Two different utilisations are considered in this work. We first examine the ability of nonreciprocal amplifiers to entangle their output signals and find that not only does directional signal transmission not inhibit the formation of entangled states, but it simultaneously allows for the routing of unwanted noise away from these outputs. This allows for the generation of high-fidelity propagating entangled states in noisy channels. The second project is motivated by a desire to improve the efficiency of measuring the state of a superconducting transmon qubit. The measurement requires the use of a microwave resonator to convert information about the qubit state into a microwave photon signal, which must then be passed to a quantum-limited preamplifier. While it has been demonstrated that using a nonreciprocal preamplifier improves the measurement efficiency, it is still reduced due to the presence of extra wiring with the resonator. We therefore consider a case where the same device acts as both the measurement resonator and the nonreciprocal preamplifier. We demonstrate that the amplification allows for a robust and highly efficient qubit measurement, while the nonreciprocity concurrently prevents excess backaction on the qubit.

Acknowledgements

It's difficult for me to believe that five and a half years have already passed since I arrived at Flughafen Tegel. While not one iota of this time has gone exactly as I expected, I am happy to have had the chance to work alongside some terrific people, who have made my time as a doctoral student a rich and rewarding experience.

I must start by thanking Anja Metelmann for taking me on as the second doctoral student in the newly formed research group, providing the opportunity to work in such an invigorating field, and introducing me to my superb collaborators. Thank you for all of the illuminating discussions and for sharing your knowledge about engineered quantum systems.

I would also like to thank all of the members of the Arbeitsgruppe, past and present, with whom I have worked. I would particularly like to thank Victor Bittencourt for taking the time to give thoughtful comments and edits for this dissertation, and for hosting me during my visits to Strasbourg. Sina Böhling and Nicolás Díaz-Naufal, being the only other original doctoral students from the groups time at the Freie Universität Berlin, also deserve special thanks for their camaraderie and support during the years of homeoffice and the relocation to Karlsruhe. It's hard to imagine how many hours of delays from Deutsche Bahn we sat through during the commute, Sina! Thank you to Suocheng Zhao as well for sharing many delicious dinners, especially during the long months of writing.

I would also like to thank all of the collaborators I have had the opportunity to work with during the past years. Thank you to Shlomi Kotler for your keen insights, which helped push the project forward, for taking the time to travel to serve as the co-referee on my committee, and for your kind comments about my dissertation. To Saeed Khan, it was great working with you, and thank you for all of your assistance in improving the paper. Thank you to Florent Lecocq and Benton Miller; it was great to finally meet both of you in person at the March Meeting. Many thanks to Benton for patiently taking the time to answer my many, no doubt elementary, questions about the experiment.

Thank you to all of the members of the TKM and TFP who made working in Karlsruhe so enjoyable. After working at home in Berlin for the majority of my doctorate, I was grateful to find myself in such a friendly and welcoming department these past couple of years. I would particularly like to thank Iksu Jang for being a reliable companion for hikes in the Schwarzwald; Davide Valentinis, Sopheak Sorn, and Veronika Stangier, for also sharing in my deep love of food; Tamaghna Hazra for the groaning dad jokes; and Charlie Stewart for the tea and banter. I would also like to thank the members of staff from the two universities who helped me so much with navigating the labyrinthine administration for each university, Sonja König at KIT, and Marietta Wissmann at FUB.

I must also extend thanks to Jara Juana Bermejo-Vega, without whom I may never have heard about this position, and would certainly never have secured my apartment in Berlin. In my mind, I like to think the Sichuan dinner I made for you during your visit to the University of Waterloo lodged me in your mind.

There are many other people from UW who also deserve recognition. I would especially like to thank my master's supervisor, Pierre-Nicholas Roy, for teaching me how to be a research scientist and for your support during my years in your research group. Thank you as well to my collaborator during that time, Lisandro Hernández de la Peña, for urging me to take up doctoral studies and continue in academia. To the rest of the people I knew during my time at UW who supported me in my academic career, whether professionally or through friendship, and who are too many to list here, I also offer my deepest thanks.

Moving abroad shortly in advance of a global pandemic also meant that meeting and forming close bonds with new people was challenging. So I would like to thank Anastasia Mikheeva, whom I met on my first day in Berlin, for being such a solid base during those initial tough years. I also relied on the support of many of my friends from back in Canada during this time, many of whom, due to the effects of distance and time, I no longer see or talk to nearly as much as I would like. Many thanks to William Gertler for your support, for keeping in touch during these past years, and for taking the time to visit me in Berlin. That excerpt you shared with me about the fig tree when I was being indecisive about moving abroad from Sylvia Plath's The Bell Jar will probably always be etched into my memory. Gordon Hatt, thank you for hanging out for a couple of months and chatting about art and movies. Thanks also to my old friends from my time in Kitchener-Waterloo who encouraged me in academia: Al, Cary, Emma, John, Simon, and so many others. I hope to see you all in person again soon!

Lastly, I would like to thank my family who, although they don't understand what I research or why I would spend all of this time on these degrees, have given me their unconditional love and support from the beginning to today. Thank you to my Mom and Dad, Nathan and Sharon, and Nolan.

Contents

List of Symbols

Symbol	Description
$\mathbf{A}, \boldsymbol{A}, \mathbf{H}, \boldsymbol{H}, \ldots$	Bold upper-case Latin letters correspond to matrices.
$\mathrm{A}_{jk}, A_{jk}, \mathrm{H}_{jk}, H_{jk}, \ldots$	Matrix element of the above, located at j-th row and k-th column.
$\mathbf{a}, \boldsymbol{a}, \mathbf{h}, \boldsymbol{h}, \ldots$	Bold lower-case Latin letters correspond to vectors.
$\mathrm{a}_j, a_j, \mathrm{h}_j, h_j, \ldots$	Vector element of the above, corresponds to j-th position in the array.
$\mathbf{I}_m$	Identity matrix of dimension $m \times m$.
$\mathbf{0}_m$	Zero matrix, also called the null matrix, of dimension $m \times m$.
$\mathbf{0}, \mathbf{I}, \mathbf{X}, \mathbf{Z}, \mathbf{J}$	Matrices of dimension 2×2 used to write larger matrices in block-form. Defined as: $\mathbf{0} := \begin{pmatrix} 0 & 0 \\ 0 & 0 \end{pmatrix}$ $\mathbf{I} := \begin{pmatrix} 1 & 0 \\ 0 & 1 \end{pmatrix}$ $\mathbf{X} := \begin{pmatrix} 0 & 1 \\ 1 & 0 \end{pmatrix}$ $\mathbf{Z} := \begin{pmatrix} 1 & 0 \\ 0 & -1 \end{pmatrix}$ $\mathbf{J} := \begin{pmatrix} 0 & 1 \\ -1 & 0 \end{pmatrix}$.
$\hat{a}_j, \hat{a}_j^\dagger$	Creation and annihilation operators for a system with label j.
$\hat{\boldsymbol{a}}$	Vector of creation and annihilation operators; order is generally specified.
$\hat{q}_j, \hat{p}_j$	Position and momentum quadrature operators for a system with label j.
$\hat{\boldsymbol{r}}$	Vector of quadrature operators, whose elements are the Hermitian operators $\hat{r}_k = \hat{r}_k^\dagger$.
$\boldsymbol{\Omega}$	The anti-symmetric symplectic form, $\boldsymbol{\Omega}^T = -\boldsymbol{\Omega}$. Elements are $\Omega_{jk} = -\Omega_{kj}$. Written as $\boldsymbol{\Omega}_m$ when the dimension $2m \times 2m$ needs to be specified.
$\boldsymbol{\mu}$	Vector of means, with elements defined as $\mu_k := \langle \hat{r}_k \rangle$.
$\boldsymbol{\sigma}$	Covariance matrix, whose elements are $\sigma_{jk} := \frac{1}{2}\langle \hat{r}_j \hat{r}_k + \hat{r}_k \hat{r}_j \rangle - \langle \hat{r}_j \rangle \langle \hat{r}_k \rangle$.
$\mathbf{S}$	Scattering matrix.
$\boldsymbol{\nu}$	Diagonal matrix of symplectic eigenvalues, ν_k, of a covariance matrix.
$W_f(\boldsymbol{r})$	Corresponding Wigner function for an arbitrary operator $\hat{f}$.
$w_f(\boldsymbol{\xi})$	Characteristic function of the Wigner function $W_f(\boldsymbol{r})$.
$\boldsymbol{r}$	Vector of phase-space quadrature symbols, elements are the real-valued r_k.
$\boldsymbol{\xi}$	Coordinates of reciprocal Fourier space, elements are ξ_k.
$\mathcal{L}(\hat{\rho})$	Lindblad, or quantum Liouvillian, superoperator.
$\mathcal{D}[\hat{z}](\hat{\rho})$	Dissipation superoperator with jump-operator $\hat{z}$.
$E_{\mathcal{N}}^{(j,k)}$	Bipartite logarithmic negativity for systems labelled j and k.
$\mathcal{P}^{(j,k)}$	Joint purity for subsystems labelled j and k.
SNR	Signal-to-Noise Ratio.
Γ_{meas}	Measurement rate.
Γ_{d}	Dephasing rate of qubit due to coupled modes.
η	Measurement efficiency, $\eta := \Gamma_{\mathrm{meas}}/\Gamma_{\mathrm{d}}$.
$\boldsymbol{\kappa}$	Diagonal matrix of dissipation rates. κ_j is not the j-th entry.
κ_j	Dissipation rate, also called damping or decay rate, for a system with label j.
$\bar{n}_j$	Thermal occupancy of bath coupled to system j.
g_{jk}	Coherent coupling rate between two systems labelled j and k.
$\mathcal{C}_{jk}$	Cooperativity for coherent two-mode interaction, $\mathcal{C}_{jk} := 4g_{jk}^2/\kappa_j\kappa_k$.
$\mathcal{C}_\lambda$	Cooperativity for single-mode squeezing with amplitude λ, $\mathcal{C}_\lambda := 2\lambda/\kappa_j$.
$\mathcal{X}$	Dispserive coupling to qubit χ normalised by the mode damping rate, $\mathcal{X} := 2\chi/\kappa_j$.
δ_{jk}	The Kronecker delta.
$\delta(x)$	The Dirac delta-distribution.
$\chi_k(\omega)$	Susceptibility function, $\chi_k(\omega) := (\kappa_k/2 - i\omega)^{-1}$.

1 Introduction

Advances in the ability to fabricate and manipulate quantum systems with specifically engineered properties during the past several decades have led to the rapid emergence and expansion of the field of quantum technologies [1], roughly a century after the birth of quantum theory itself [2]. The field has led to developments in quantum sensing [3] and metrology [4], and most enticingly quantum information processing [5, 6], which promises advancements in communication [7], cryptography [8], and computation [9]. The unique properties of these devices rely on quantum phenomena, which are easily susceptible to degradation from sources of noise, requiring that they be well isolated from the external world. It is, nevertheless, impossible to protect against all sources of noise: vacuum fluctuations will always be present, and the need to perform measurements to determine the state of these engineered devices necessarily perturbs the system, forcing us to think about noise at the quantum level [10]. Additionally, the final detection of the measurement outcome may occur outside of the shielded environment, introducing the problem of environmental noise. Since the measurement outcome is generally of low power, and hence is susceptible to noise, if those of us who live in the realm of classical physics are to have any chance at observing it, amplifiers must be used to increase the strength of the signal [11].

A series of amplifiers in a measurement chain may be used to successively amplify the low-power measurement above the noise floor in the laboratory, thereby converting the information in the quantum device into a signal that can be measured by classical means. These amplifiers also unavoidably add noise at each step and are, in general, reciprocal devices, meaning that they will not only direct amplified signal up the measurement chain towards the laboratory, but will also send amplified noise back down the measurement chain. This is undesirable when performing a continuous measurement, since the noisy back-propagating signal can interfere with the measurement results, and even affect the state of the quantum device through unwanted backaction. In order to prevent this, *nonreciprocal* signal-processing devices are required, such as circulators and isolators, which allow for directional routing of signals and therefore have the ability to redirect or terminate any back-propagating signal. The inclusion of these extra devices within the measurement chain, along with the required additional connections, will add more noise, and some also come at the cost of further reducing the fidelity of the measurement.

Since noise during signal processing is unavoidable, and only acts to decrease the efficiency of the measurement, it is desirable to minimise the amount of added noise; this is critical for the first components in the measurement chain, where the measurement signal is the weakest and most sensitive to contamination. It is therefore best if these first components add the minimum possible amount of noise, which can be achieved if they are themselves quantum systems whose noise is said to be *quantum-limited* [10–12], which is possible for amplifiers and nonreciprocal devices based on superconducting circuits operating at and below the microwave frequency regime [5]. While research into realising amplifiers in superconducting circuits was first undertaken in the 1960s [13], these devices attracted minimal attention in the decades before the advent of superconducting qubits [14], where they are now an integral component for the preamplification of qubit measurement signals. The issue of qubit measurement has also been a primary driver of research in nonreciprocal quantum devices, and hence theoretical [15, 16] and experimental developments [17–22] have also only occurred within the past decade. The desire to improve losses and so decrease noise through a reduction in the number of connections between different components has also led to devices which can perform both amplification and directional signal routing: *nonreciprocal quantum amplifiers* [23–29].

The development of nonreciprocal quantum amplifiers is therefore well motivated from a signal processing perspective, where the aim is to improve the noise characteristics of delicate quantum signals. While their study necessitates the use of quantum theory, the signal processing properties under consideration are also features of classical systems and hence are not uniquely quantum. The goal of this dissertation is to consider two applications which cannot be realised using classical devices: entanglement of photons and the direct measurement of a transmon qubit.

To this end, in Chapter 2 we focus on the common theory required to understand the physical modelling of nonreciprocal linear quantum amplifiers. The fundamental building blocks of these amplifiers are parametrically coupled harmonic oscillators subjected to linear dynamics, where amplification is achieved through the proper modulation of the parametric couplings. The quantum states of these linear amplifiers belong to a larger class of

continuous variable quantum states termed Gaussian states, and given their central role in the work to follow, we open with a summary of their properties, specifically focusing on how they transform under the dynamics of open quantum systems. After this, we review the basics of parametrically coupled physics, before moving on to a detailed description of the symmetry of reciprocity and how one may break it to realise nonreciprocity. We start with an explanation of the phenomenon in classical electromagnetic systems, before proceeding to extend the concept to open quantum systems. Two approaches to nonreciprocity in open quantum systems are discussed, one based on engineered dissipative processes [15], and the other based on the interference of scattered signals [16], both of which are shown to be equivalent when applied to Gaussian quantum systems. The section is finished by assembling all the components in order to introduce the two nonreciprocal amplifier configurations that will be considered in this dissertation, both of which have been realised in experimental setups, called the delta [18, 19] and bowtie amplifiers [20, 30]. The following chapters present the results from two projects, both focused on purely quantum mechanical applications of these nonreciprocal amplifiers. These chapters build on the material in Chapter 2 but are otherwise independent, and begin with their own specific introductory material.

Chapter 3 presents an investigation of the ability of nonreciprocal amplifiers to generate entangled states. This chapter begins with a review of entanglement quantification with the purity and the logarithmic negativity entanglement, along with the deleterious effect that unwanted noise in the form of thermal fluctuations has on the fidelity of entangled states. We then motivate the application of these measures to investigate the fidelity of the entangled states formed between the propagating signals emanating from quantum amplifiers. This formalism is then used to investigate the effect of nonreciprocity on the entangled propagating states generated by quantum amplifiers. This chapter expands on existing published work in the following article [31]:

> L. Orr, S. A. Khan, N. Buchholz, S. Kotler, and A. Metelmann. "High-Purity Entanglement of Hot Propagating Modes Using Nonreciprocity," PRX Quantum 4, 020344 (2023).

Chapter 4 considers the use of a nonreciprocal amplifier for the readout of a superconducting transmon qubit, where the amplifier is not simply a standalone component in a measurement chain, but is coupled directly to the qubit, and so measures the qubit state and amplifies the result of said measurement simultaneously. The chapter begins with an overview of the fundamental aspects of qubit measurement, focusing on the specifics for superconducting systems. Of particular importance is the review of the intrinsic limits placed on the rate of qubit measurement, which cannot surpass the rate at which the measurement process destroys the coherence of the qubit state through dephasing. The closer these measurement and dephasing rates are in value, the more efficient the measurement, and so to determine the efficiency of the nonreciprocal amplifier acting as a measurement device, both of these quantities must be calculated exactly. While this is a simple process for the measurement rate, things are more complicated for the rate of dephasing, which has only been calculated for simple systems. To facilitate dephasing calculations for the nonreciprocal amplifier, along with other qubit measurement systems, an existing method based on Wigner phase-space distributions was expanded; this forms one of the main results for the chapter. The measurement efficiency of the nonreciprocal amplifier is then investigated using this method, and an optimal regime for qubit measurement is found. The results presented here comprise the theoretical work done for a collaborative project with members of the Advanced Microwave Photonics Group from the National Institute of Standards and Technology (NIST).

2 Theoretical Background

2.1 Gaussian States in Quantum Mechanics

The physical models considered in this work are all based on systems of coupled bosonic modes, and therefore correspond to *continuous variable* (CV) quantum systems. Crucially, it is assumed that the states of these CV quantum systems are always *Gaussian states*; in order for a CV state to be Gaussian, it must be possible to characterise the state entirely using the first and second moments of the physical variables, with the quantum state as the probability density function. As a result of this assumption, the dynamics, whether closed or open, should always preserve the *Gaussianity* of the state. Such transformations, which take a Gaussian state to another Gaussian state, are called *Gaussian transformations*. Gaussian states, along with Gaussian transformations, are the fundamental elements of linear quantum optics and photonics [32]. Here, the bosonic modes correspond to normal modes of the quantised electromagnetic field, modelled as individual harmonic oscillators, with the photon creation and annihilation operators acting as the continuous variables of the system. The set of Gaussian states for such systems includes the well-known vacuum and coherent states of a quantum harmonic oscillator, along with squeezed states and thermal states.

These assumptions allow for the quantum states and transformations to be represented in a manner which is not only elegant but also practical. CV quantum systems are, by their nature, infinite-dimensional, meaning that any representation of the quantum state in a Hilbert space must also be infinite-dimensional. Additionally, any finite-dimensional approximation of the state grows exponentially depending on the number of bosonic modes. Gaussian states, however, may be simply represented in terms of their finite number of moments, with Gaussian transformations acting as matrix transformations on these moments. Since the number of moments scales quadratically with the number of bosonic modes, the system remains tractable when considering the multimode amplifiers at the core of this work. This is closely related to the *phase-space* representation of the quantum state and provides an alternative to working in infinite-dimensional Hilbert space. In this section, we will introduce the necessary mathematical details to efficiently treat Gaussian states and transformations for both coherent and open quantum systems, along with the intimate connection with phase-space quantum mechanics.

2.1.1 Operator Structure

We consider a system of N canonical bosonic modes, with the state space given by the Hilbert space $\mathcal{H} = \bigotimes_{k=1}^{N} \mathcal{H}_k$, where $\mathcal{H}_k$ is the usual Hilbert space for the pure states of an individual harmonic oscillator. Associated with each mode is a pair of creation and annihilation operators, $\hat{a}_k^\dagger$ and $\hat{a}_k$ respectively, where $k = 1, \ldots, N$. These operators satisfy the bosonic canonical commutation relations,

$$[\hat{a}_k, \hat{a}_l^\dagger] = \delta_{kl} \quad \text{and} \quad [\hat{a}_k, \hat{a}_l] = [\hat{a}_k^\dagger, \hat{a}_l^\dagger] = 0, \tag{2.1}$$

where δ_{kl} is the Kronecker delta. We refer to these as the *mode* or *ladder operators*, and they will act on the basis of number states $|n_1, \ldots, n_N\rangle$ in the usual manner, by either creating or annihilating a boson from their respective mode:

$$\hat{a}_k |n_1, \ldots, n_N\rangle = \sqrt{n_k}\, |n_1, \ldots, n_k - 1, \ldots, n_N\rangle \quad \text{and} \quad \hat{a}_k^\dagger |n_1, \ldots, n_N\rangle = \sqrt{n_k + 1}\, |n_1, \ldots, n_k + 1, \ldots, n_N\rangle . \tag{2.2}$$

For this work, the set of Hermitian *quadrature operators* will prove to be more useful for describing the system. In this operator basis, each mode has a pair of quadrature operators, $\hat{q}_k$ and $\hat{p}_k$, referred to as the position and momentum operators, respectively; these names are historical artefacts from the association with the harmonic oscillator, and simply refer to orthogonal variables of the quantum system and not to actual position and momentum variables.

These may be defined in terms of the mode operators as follows:

$$\hat{q}_k = \frac{1}{\sqrt{2}}\left(\hat{a}_k^\dagger + \hat{a}_k\right) \quad \text{and} \quad \hat{p}_k = \frac{i}{\sqrt{2}}\left(\hat{a}_k^\dagger - \hat{a}_k\right), \tag{2.3}$$

and so satisfy the usual canonical commutation relations

$$[\hat{q}_k, \hat{p}_l] = i\delta_{kl} \quad \text{and} \quad [\hat{q}_k, \hat{q}_l] = [\hat{p}_k, \hat{p}_l] = 0. \tag{2.4}$$

The definitions from Eq. (2.3) represent just one possible definition of the quadrature operators, and in fact, any set of Hermitian operators built from the creation and annihilation operators could serve as a set of quadrature operators. In order to free ourselves of the constraints imposed by choosing one basis, we will replace the N pairs of position and momentum operators, $\hat{q}_k$ and $\hat{p}_k$, with a vector of length $2N$, $\hat{\boldsymbol{r}}$, which contains a complete basis of quadrature operators, and where an element of this vector, $\hat{r}_k$, represents an arbitrary quadrature operator. This notation is adopted for all matrices and vectors, where the bold symbol denotes the entire array, and where the non-bold symbol denotes an element of the array along with a subscript for the array indices. This definition allows for the canonical commutation relation to be rewritten as:

$$[\hat{r}_k, \hat{r}_l] = i\Omega_{kl} \quad \text{where} \quad \Omega_{kl} = -\Omega_{lk} \quad \text{and} \quad \Omega_{kl}\Omega_{lk} = \boldsymbol{\Omega}^2 = -\mathbf{I}_{2N}, \tag{2.5}$$

where $\mathbf{I}_{2N}$ is the $2N \times 2N$ identity matrix, and the antisymmetric matrix $\boldsymbol{\Omega}$ is called the symplectic form. The above properties of the symplectic form indicate that its inverse is given by $\boldsymbol{\Omega}^{-1} = \boldsymbol{\Omega}^T = -\boldsymbol{\Omega}$, and that it has unit determinant, $\det[\boldsymbol{\Omega}] = 1$. In this work, we adopt the Einstein summation convention, where repeated indices in expressions are summed over, however, we keep all indices as subscripts for clarity. The two most commonly used conventions for defining the vector $\hat{\boldsymbol{r}}$, and as a consequence the symplectic form, are:

$$\hat{\boldsymbol{r}} := \left(\hat{q}_1, \hat{p}_1, \ldots, \hat{q}_N, \hat{p}_N\right)^T \quad \text{and} \quad \boldsymbol{\Omega} = \mathbf{I}_N \otimes \begin{pmatrix} 0 & 1 \\ -1 & 0 \end{pmatrix} \equiv \begin{pmatrix} 0 & 1 & & & \\ -1 & 0 & & & \\ & & \ddots & & \\ & & & 0 & 1 \\ & & & -1 & 0 \end{pmatrix},$$

$$\text{or} \quad \hat{\boldsymbol{r}} := \left(\hat{q}_1, \ldots, \hat{q}_N, \hat{p}_1, \ldots, \hat{p}_N\right)^T \quad \text{and} \quad \boldsymbol{\Omega} = \begin{pmatrix} 0 & 1 \\ -1 & 0 \end{pmatrix} \otimes \mathbf{I}_N \equiv \begin{pmatrix} \mathbf{0}_N & \mathbf{I}_N \\ -\mathbf{I}_N & \mathbf{0}_N \end{pmatrix}. \tag{2.6}$$

where $\mathbf{I}_N$ and $\mathbf{0}_N$ are the $N \times N$-dimensional identity and zero, or null, matrices, respectively. The first convention will be used within this work when writing explicit expressions for matrices in the quadrature basis, since it keeps pairs of variables for the same mode together and allows for single and multimode interactions to be clearly distinguished. With the basic operator structure defined, we can now proceed to introduce and define Gaussian quantum states.

2.1.2 Moments of a Gaussian State

A continuous variable state $\hat{\rho}$ is Gaussian if it can be entirely described through the first and second moments of the quadrature or ladder operators. We can therefore define a vector of length $2N$ of the first moments, $\boldsymbol{\mu}$, which constitute the *mean* values of the state:

$$\mu_j := \langle \hat{r}_j \rangle. \tag{2.7}$$

The second central moments may be represented by the matrix $\boldsymbol{\varsigma}$, with elements defined as:

$$\varsigma_{kl} := \langle \hat{r}_k \hat{r}_l \rangle - \langle \hat{r}_k \rangle \langle \hat{r}_l \rangle. \tag{2.8}$$

Expectation values for an arbitrary operator $\hat{A}$ are defined as $\langle \hat{A} \rangle := \mathrm{Tr}[\hat{\rho}\hat{A}]$. In order for the density operator $\hat{\rho}$ to be a true quantum state, the matrix of second central moments must be a Hermitian and positive semi-definite matrix, $\boldsymbol{\varsigma} \geq 0$, a restriction which comes from the fact that the density operator itself must be positive semi-definite, $\hat{\rho} \geq 0$. The matrix of second central moments may be split into a sum of symmetric and antisymmetric matrices; the elements of the antisymmetric matrix correspond to the expectation values $\langle \hat{r}_k \hat{r}_l - \hat{r}_l \hat{r}_k \rangle / 2 = \Omega_{kl}/2$, where we have immediately used the known commutation relation in Eq. (2.5) to replace the expectation value with the symplectic form. The antisymmetric component of $\boldsymbol{\varsigma}$ is therefore the same regardless of the system and so contains no novel information, and as a result, all of the non-trivial information about the second central moments is contained in the *symmetrised*

second central moments. We term this symmetric matrix the *covariance* matrix $\boldsymbol{\sigma}$, and define the matrix elements as

$$\sigma_{kl} := \frac{1}{2}\langle \hat{r}_k \hat{r}_l + \hat{r}_l \hat{r}_k \rangle - \langle \hat{r}_k \rangle \langle \hat{r}_l \rangle, \tag{2.9}$$

where we can see from this definition that, for a valid density operator, $\boldsymbol{\sigma}$ must be a real symmetric matrix. The arrays $\boldsymbol{\mu}$ and $\boldsymbol{\sigma}$ contain all the necessary information for describing a Gaussian state, since the higher-order moments of a Gaussian may be expressed in terms of $\boldsymbol{\mu}$ and $\boldsymbol{\sigma}$ using Isserlis' theorem, commonly referred to as Wick's theorem when applied to creation and annihilation operators. We can now write the matrix of second central moments entirely in terms of the covariance matrix and symplectic form, $\boldsymbol{\varsigma} = \boldsymbol{\sigma} + i\boldsymbol{\Omega}/2$, and from the fact that $\hat{\rho} \geq 0$ deduce that the covariance matrix must obey the following relation [33]:

$$\boldsymbol{\sigma} + \frac{i}{2}\boldsymbol{\Omega} \geq 0. \tag{2.10}$$

The above inequality is a compact way of expressing the uncertainty relation for any CV state, not just Gaussian states, and is equivalent to the Robertson-Schrödinger uncertainty relation. The exact nature of the relation between Eq. (2.10) and the uncertainty principle will be discussed further in Section 2.1.5, where it will be shown that Eq. (2.10) is instrumental in determining whether a Gaussian state is entangled. The uncertainty relation also implies that, for $\hat{\rho}$ to represent a true density operator, the covariance matrix must be strictly positive definite, $\boldsymbol{\sigma} > 0$.

2.1.3 Wigner Phase-Space Representation

As stated in the introduction to this section, the study of Gaussian states is inextricable from the phase-space formulation of quantum mechanics. The phase-space formulation will allow us to replace any wave function, density operator, and observable with corresponding quasi-probability distributions (QPDs) in phase space, akin to the Hamiltonian formulation of classical mechanics in spirit, but with significant differences. For a review of some technical aspects of the phase-space formulation of quantum mechanics, refer to Appendix A. We will specifically focus on QPDs in the Wigner phase space, hereafter termed *Wigner functions*. The Wigner function associated with an arbitrary state $\hat{\rho}$ is defined as:

$$W_\rho(\boldsymbol{r}) := \frac{1}{(2\pi)^{2N}} \int_{\mathbb{R}^{2N}} \mathrm{Tr}\Big[\hat{\rho} \exp\big[i\boldsymbol{\xi}\cdot\hat{\boldsymbol{r}}\big]\Big] \exp\big[-i\boldsymbol{\xi}\cdot\boldsymbol{r}\big]\, d^{2N}\boldsymbol{\xi} = \frac{1}{(2\pi)^{2N}} \int_{\mathbb{R}^{2N}} w_\rho(\boldsymbol{\xi}) \exp\big[-i\boldsymbol{\xi}\cdot\boldsymbol{r}\big]\, d^{2N}\boldsymbol{\xi} \tag{2.11}$$

where $\boldsymbol{\xi}$ is a vector of length $2N$ containing the Fourier space coordinates, ξ_k, and $\boldsymbol{r}$ is the vector of phase-space quadratures. Phase-space QPDs can be associated not only with density operators $\hat{\rho}$, but also with observables, using an identical definition.

As is well known, the product of operators in Hilbert space is generally noncommutative, a feature which is not shared by the usual commutative multiplication of functions in phase space. As a result, the Wigner transform of an operator product does not, except in the most trivial cases, correspond to the multiplication of Wigner functions, $f(\hat{\boldsymbol{r}})g(\hat{\boldsymbol{r}}) \not\to W_f(\boldsymbol{r})W_g(\boldsymbol{r})$. It is possible to define a noncommutative product on the phase space which is equivalent to the operator product; for the Wigner representation, this is the celebrated nonlocal *Moyal star-product* of QPDs [34, 35]. From the above definition of the Wigner function, we can write an explicit form of the Moyal star-product as follows:

$$f(\hat{\boldsymbol{r}})g(\hat{\boldsymbol{r}}) \to W_f(\boldsymbol{r}) \star W_g(\boldsymbol{r}) := W_f(\boldsymbol{r}) \exp\left[\frac{i\hbar}{2} \overleftarrow{\boldsymbol{\partial r}}^T \boldsymbol{\Omega}\, \overrightarrow{\boldsymbol{\partial r}}\right] W_g(\boldsymbol{r}). \tag{2.12}$$

Here, $\boldsymbol{\partial r}$ is a vector of derivatives with respect to the phase-space quadratures, $\partial/\partial r_k$, with the arrows denoting the direction of the derivatives. It is crucial to note that $f(\hat{\boldsymbol{r}})$ and $g(\hat{\boldsymbol{r}})$ do not share the same functional form as their Wigner functions $W_f(\boldsymbol{r})$ and $W_g(\boldsymbol{r})$, however, using the logic that operator products are replaced with the Moyal star-product when casting such functions to phase space, the Wigner function can be calculated using $W_f(\boldsymbol{r}) = f(\star\boldsymbol{r})$. This noncommutative phase-space product ensures that the symplectic structure of the canonical commutation relation is preserved among the phase-space quadrature symbols:

$$[\hat{r}_k, \hat{r}_l] = i\Omega_{kl} \to (r_k \star r_l - r_l \star r_k) = i\Omega_{kl}. \tag{2.13}$$

The Hilbert space for a single bosonic mode is therefore replaced with a two-dimensional real space with a symplectic structure, denoted $\mathcal{M}_k(\mathbb{R}^2, \boldsymbol{\Omega}_1)$. For the total phase space, the tensor product structure is replaced by the direct sum of the individual local phase spaces for each bosonic mode, $\mathcal{M}(\mathbb{R}^{2N}, \boldsymbol{\Omega}_N) = \bigoplus_{k=1}^{N} \mathcal{M}_k(\mathbb{R}^2, \boldsymbol{\Omega}_1)$.

Returning to the Wigner function from Eq. (2.11), provided that the density operator is Hermitian, $\hat{\rho} = \hat{\rho}^\dagger$, the kernel of the Fourier transform satisfies $w_\rho(\boldsymbol{\xi})^\dagger = w_\rho(-\boldsymbol{\xi})$, meaning that the Wigner function must be a real-valued

function. Despite this, the Wigner function $W_\rho(\boldsymbol{r})$ is called a QPD since it does not obey all the axioms of a true probability distribution; one of the most significant differences is that $W_\rho(\boldsymbol{r})$ can contain areas of negative probability density. However, for the Gaussian states we are considering, this is not the case, and so the Wigner function is guaranteed to be positive valued over the entire phase space. Despite this, the structure of the Wigner phase space still means that even Gaussian Wigner functions do not correspond to true probability distributions. As might be expected, the name *Gaussian state* comes from the fact that the respective Wigner function is a real Gaussian distribution, which may be expressed generally as

$$W_\rho(\boldsymbol{r}) = \frac{1}{(2\pi)^N \sqrt{\det[\boldsymbol{\sigma}]}} \exp\left[-\frac{1}{2}(\boldsymbol{r}-\boldsymbol{\mu})^T \boldsymbol{\sigma}^{-1}(\boldsymbol{r}-\boldsymbol{\mu})\right] \tag{2.14}$$

where $\boldsymbol{\mu}$ and $\boldsymbol{\sigma}$ are the previously defined vector of means and covariance matrix, respectively. The Wigner function can also be completely defined through its characteristic function, which is simply the Fourier transform of Eq. (2.14), and so is equivalent to the kernel of the Fourier transform used to define the Wigner function in Eq. (2.11):

$$w_\rho(\boldsymbol{\xi}) := \mathrm{Tr}\Big[\hat{\rho}\exp\big[i\boldsymbol{\xi}\cdot\hat{\boldsymbol{r}}\big]\Big] = \exp\left[-\frac{1}{2}\boldsymbol{\xi}^T\boldsymbol{\sigma}\boldsymbol{\xi} + i\boldsymbol{\mu}^T\boldsymbol{\xi}\right]. \tag{2.15}$$

Much like the characteristic function of a true probability distribution, derivatives of $w_\rho(\boldsymbol{\xi})$ can be used to obtain the moments of the phase-space quadrature symbols r_k, which correspond to symmetrised expectation values of the original quadrature operators $\hat{r}_k$,

$$\mu_k = -i\frac{\partial}{\partial\xi_k} w_\rho(\boldsymbol{\xi})\Big|_{\boldsymbol{\xi}=0} \qquad \sigma_{kl} + \mu_k\mu_l = -\frac{\partial^2}{\partial\xi_k\partial\xi_l} w_\rho(\boldsymbol{\xi})\Big|_{\boldsymbol{\xi}=0}. \tag{2.16}$$

When calculating expectation values in phase space, inner products and traces are replaced by the act of integrating over phase-space quadratures. Tracing over the entirety of the Hilbert space is therefore equivalent to integrating over the entire phase space, or equivalently, taking the value of the characteristic function at the origin in the reciprocal Fourier space. This allows us to represent the normalisation condition for $\hat{\rho}$ as:

$$1 = \mathrm{Tr}[\hat{\rho}] = \int_{\mathbb{R}^{2N}} W_\rho(\boldsymbol{r})\, d^{2N}\boldsymbol{r} = w_\rho(\boldsymbol{\xi}=0). \tag{2.17}$$

Instead of integrating over the entire phase space, we can instead integrate over specific quadratures to obtain marginal distributions of the total Wigner function. Performing a partial trace over a specific mode is therefore equivalent to integrating over their quadratures in phase space; as an example, integrating over one bosonic mode, which is labelled k, is equivalent to

$$\mathrm{Tr}_k[\hat{\rho}] = \int_{\mathbb{R}^2} W_\rho(\boldsymbol{r})\, dq_k\, dp_k = w_\rho(\boldsymbol{\xi})\Big|_{\xi_{qk},\xi_{pk}=0}. \tag{2.18}$$

Since the Wigner function for Gaussian states is a multivariate Gaussian distribution, the resulting marginal distribution is necessarily the Wigner function of a Gaussian state; writing the moments of $W_\rho(\boldsymbol{r})$ in block form, dividing them between the mode k to be integrated over and the remaining modes, which are labelled m, the moments of the marginal distribution are:

$$\begin{pmatrix} \boldsymbol{\sigma}_{mm} & \boldsymbol{\sigma}_{mk} \\ \boldsymbol{\sigma}_{km} & \boldsymbol{\sigma}_{kk} \end{pmatrix} \xrightarrow{\mathrm{Tr}_k} \boldsymbol{\sigma}_{mm} \qquad \begin{pmatrix} \boldsymbol{\mu}_m \\ \boldsymbol{\mu}_k \end{pmatrix} \xrightarrow{\mathrm{Tr}_k} \boldsymbol{\mu}_m. \tag{2.19}$$

The marginal distributions of the Wigner function also have a unique property not shared by any other phase-space representation: the probability distribution corresponding to a measurement of a $\hat{\rho}$ in the quadrature $\hat{r}$ is obtained by integrating over all other quadratures, labelled $\boldsymbol{r}_{\mathrm{int}}$, in phase space,

$$\langle r|\hat{\rho}|r\rangle = \int_{\mathbb{R}^{2N-1}} W_\rho(\boldsymbol{r})\, d^{2N-1}\boldsymbol{r}_{\mathrm{int}}. \tag{2.20}$$

In this work, we are solely interested in processes which preserve the Gaussian nature of the state $\hat{\rho}$, ensuring that the Wigner function of the state may always be expressed as in Eq. (2.14). While it is possible to perform these transformations on the Wigner function itself, it is much easier to study how the moments evolve under such Gaussian transformations, since these are always sufficient to characterise the entire state. In the next section, we will start by examining a specific class of transformations which preserves the Gaussianity of the state, called the symplectic-affine transformations.

2.1.4 Symplectic Transformations

The set of symplectic-affine transformations is of specific interest among all possible Gaussian transformations, since they are the only Gaussian transformations which preserve the canonical commutation relation Eq. (2.4), and are therefore canonical transformations. Such transformations include both symplectic transformations and translations, $\hat{\boldsymbol{r}} \to \mathbf{S}\hat{\boldsymbol{r}} + \mathbf{d}$, where $\mathbf{d} \in \mathbb{R}^{2N}$ is a real vector of length $2N$ representing translations, and $\mathbf{S}$ is a $2N \times 2N$ real symplectic matrix. Being a symplectic matrix, $\mathbf{S} \in Sp(2N, \mathbb{R})$ must satisfy the following properties:

$$\mathbf{S}^T \boldsymbol{\Omega} \mathbf{S} = \boldsymbol{\Omega} \quad \text{and} \quad \det[\mathbf{S}] = 1. \tag{2.21}$$

Using the given relations, the inverse of the symplectic matrix $\mathbf{S}$ may be expressed as $\mathbf{S}^{-1} = -\boldsymbol{\Omega}\mathbf{S}^T\boldsymbol{\Omega}$. We can now confirm that transformations of this type preserve the canonical commutation relation:

$$[\hat{r}_k, \hat{r}_l] = i\Omega_{kl} \to [\mathrm{S}_{km}\hat{r}_m + \mathrm{d}_k, \mathrm{S}_{ln}\hat{r}_n + \mathrm{d}_l] = \mathrm{S}_{km}[\hat{r}_m, \hat{r}_n]\mathrm{S}^T_{nl} = i\mathrm{S}_{km}\Omega_{mn}\mathrm{S}^T_{nl} = i\Omega_{kl}. \tag{2.22}$$

Given that unitary transformations, $\hat{\boldsymbol{r}} \to \hat{U}^\dagger \hat{\boldsymbol{r}} \hat{U}$, also preserve commutation relations, it may be deduced that certain unitary transformations may be represented as symplectic-affine transformations:

$$\hat{\boldsymbol{r}} \to \hat{U}^\dagger \hat{\boldsymbol{r}} \hat{U} \equiv \mathbf{S}\hat{\boldsymbol{r}} + \mathbf{d}. \tag{2.23}$$

Invertible transformations of this form are termed *Gaussian unitary transformations*, which, as mentioned in the previous section, preserve the Gaussian structure of CV states. Such transformations can also be applied to the expectation values $\langle \hat{r}_k \rangle$ and $\langle \hat{r}_k \hat{r}_l \rangle$, and hence can also be cast as a transformation on the means $\boldsymbol{\mu}$ and covariance matrix $\boldsymbol{\sigma}$:

$$\boldsymbol{\mu} \to \mathbf{S}\boldsymbol{\mu} + \mathbf{d} \quad \text{and} \quad \boldsymbol{\sigma} \to \mathbf{S}\boldsymbol{\sigma}\mathbf{S}^T. \tag{2.24}$$

Therefore, a Gaussian unitary transformation on a Gaussian state in Hilbert space is equivalent to a symplectic transformation on the moments of the Gaussian Wigner function in phase space. Expressing this unitary transformation as the exponential of an anti-Hermitian operator, $\hat{U} = \exp[-i\hat{H}]$, $\hat{U}$ is a Gaussian unitary transformation so long as the Hermitian operator $\hat{H}$ is at most a quadratic polynomial of the quadrature operators [36]:

$$\hat{H} = \frac{1}{2}\hat{\boldsymbol{r}}^T \boldsymbol{H}^{(2)} \hat{\boldsymbol{r}} + \hat{\boldsymbol{r}}^T \boldsymbol{h}^{(1)}. \tag{2.25}$$

where $\boldsymbol{H}^{(2)}$ is a $2N \times 2N$ real symmetric matrix, and $\boldsymbol{h}^{(1)}$ is a real vector of length $2N$. We can write explicit expressions for the symplectic-affine transformation in Eq. (2.23) in terms of the elements of $\hat{H}$ by applying the following lemma of the Baker–Campbell–Hausdorff (BCH) formula [37]:

$$e^X Y e^{-X} = \sum_{k=0}^{\infty} \frac{1}{k!}[(X)^k, Y] \quad \text{where} \quad [(X)^k, Y] \equiv \underbrace{[X, \cdots [X, [X}_{k \text{ times}}, Y]] \cdots] \ , \ [(X)^0, Y] \equiv Y. \tag{2.26}$$

Using the canonical commutation relations, the following expressions can be retrieved for $\mathbf{S}$ and $\mathbf{d}$:

$$\mathbf{S} = \exp\left[\boldsymbol{\Omega}\boldsymbol{H}^{(2)}\right] \quad \text{and} \quad \mathbf{d} = \frac{\exp\left[\boldsymbol{\Omega}\boldsymbol{H}^{(2)}\right] - \mathbf{I}_{2N}}{\boldsymbol{\Omega}\boldsymbol{H}^{(2)}}\, \boldsymbol{\Omega}\boldsymbol{h}^{(1)}, \tag{2.27}$$

where $\mathbf{d}$ is to be interpreted as a formal power series of the matrix $\boldsymbol{\Omega}\boldsymbol{H}^{(2)}$. It may be confirmed that $\mathbf{S}$ does indeed satisfy the conditions for a symplectic matrix outlined in Eq. (2.21) using the above power series, demonstrating that the unitary transformation induced by a quadratic Hamiltonian corresponds to a symplectic-affine transformation. The reverse, as it turns out, is not true: starting with a symplectic transformation, it is not possible in general to find a corresponding unitary transformation generated by a single quadratic Hamiltonian. The solution, as discussed in Appendix C.1, is to use a product of multiple Gaussian unitary transformations. Having established that symplectic transformations correspond to unitary transformations in Hilbert space, we will now present one of the most important structural properties of the covariance matrix, the Williamson normal form, which will be of particular importance when discussing the entanglement of Gaussian CV states in Chapter 3.

2.1.5 The Williamson Normal Form

The Williamson normal form is a matrix decomposition which may be applied to covariance matrices and is equivalent to a normal mode decomposition for Gaussian states. The result is due to Williamson's theorem [38], which states that for any real symmetric matrix, there is a symplectic matrix which diagonalises it. Additionally, the elements of the

diagonal matrix come in pairs. For a system of N modes, the Williamson normal form of the covariance matrix $\boldsymbol{\sigma}$ is:

$$\boldsymbol{\sigma} = \mathbf{S}\boldsymbol{\nu}\mathbf{S}^T \quad \text{where} \quad \boldsymbol{\nu} := \bigoplus_{k=1}^{N} \nu_k \mathbf{I}_2. \tag{2.28}$$

The matrix $\mathbf{S}$ is a real symplectic matrix, and so corresponds to a Gaussian unitary transformation, as indicated in Eq. (2.27). The matrix $\boldsymbol{\nu}$ is called the Williamson form of $\boldsymbol{\sigma}$, and the elements ν_k are called the symplectic eigenvalues of $\boldsymbol{\sigma}$. The standard method of obtaining the set of symplectic eigenvalues is to compute the spectrum of the matrix $\boldsymbol{\Omega\sigma}$; the solution is $\{\pm i\nu_1, \ldots, \pm i\nu_N\}$, which contains the symplectic eigenvalues that we seek. While calculating the symplectic eigenvalues is simple, obtaining an expression for the symplectic matrix $\mathbf{S}$ in the Williamson normal form is considerably more difficult [39]. These symplectic eigenvalues are closely connected to the uncertainty relation in Eq. (2.10), which may be expressed equivalently as:

$$\text{The uncertainty relation, } \boldsymbol{\sigma} + \frac{i}{2}\boldsymbol{\Omega} \geq 0, \text{ is obeyed if } \nu_k \geq \frac{1}{2} \text{ for all symplectic eigenvalues.} \tag{2.29}$$

The above can be demonstrated by first using the normal form of $\boldsymbol{\sigma}$ and the definition of the symplectic matrix to rewrite the uncertainty relation as $\mathbf{S}(\boldsymbol{\nu} + i\boldsymbol{\Omega}/2)\mathbf{S}^T \geq 0$, which reduces to $\boldsymbol{\nu} + i\boldsymbol{\Omega}/2 \geq 0$. We can always pick the form of $\mathbf{S}$ such that $\boldsymbol{\nu} + i\boldsymbol{\Omega}/2$ may be expressed in block diagonal form, with the blocks written as $\left(\begin{smallmatrix} \nu_k & i/2 \\ -i/2 & \nu_k \end{smallmatrix}\right)$. The eigenvalues of each block are $\nu_k \pm 1/2$, and since the matrix $\boldsymbol{\nu} + i\boldsymbol{\Omega}/2$ is positive semi-definite only if the eigenvalues of each individual block are greater than zero, this yields the condition: $\nu_k \pm 1/2 \geq 0$. We can discard the weaker condition, and so conclude that $\nu_k \geq 1/2$ must be true for every symplectic eigenvalue if the uncertainty relation is to be obeyed.

The condition that $\nu_k \geq 1/2$ means that the variance for every normal mode of a Gaussian state must be equal to or larger than the variance of a vacuum state, which is $\nu_{\text{vac}} = 1/2$. This lower bound means that every symplectic eigenvalue can also be written as $\nu_k = \bar{n}_k + 1/2$, where $\bar{n}_k$ indicates fluctuations above that of the vacuum. The variance for each normal mode is therefore $\left(\begin{smallmatrix} \bar{n}_k+1/2 & 0 \\ 0 & \bar{n}_k+1/2 \end{smallmatrix}\right)$, which is the covariance matrix of *thermal state*; details are provided in Appendix C.4. The fluctuations above the vacuum $\bar{n}_k$ may therefore be interpreted as the number of thermal quanta in the normal mode. The covariance matrix of the N uncoupled normal modes, defined as the Williamson form $\boldsymbol{\nu}$ in Eq. (2.28), is therefore equivalent to the covariance of an N-mode thermal state. Since the symplectic transformation $\mathbf{S}$ is equivalent to a unitary transformation, the Williamson normal form also says that any Gaussian state is unitarily equivalent to a thermal state, a fact that will, once again, be of relevance in Chapter 3.

2.2 Open Quantum Systems and Gaussian Transformations

As has been shown, the unitary evolution of a Gaussian state can be understood through transformations applied to its moments. Thus, the time evolution of a Gaussian state under Gaussian dynamics can be completely described through dynamical equations for the moments. We are particularly interested in the form that these dynamical systems take for an open quantum system, which may be modelled as a large collection of environment modes, E, coupled to a finite number of modes which constitute the primary system, S. At this point, the total dynamics is captured by the following Hamiltonian

$$\hat{H}_T = \hat{H}_E + \hat{H}_S + \hat{H}_I, \tag{2.30}$$

where the $\hat{H}_I$ is the interaction Hamiltonian between the system and environment, $\hat{H}_S$ acts solely on the system, and $\hat{H}_E$ on the environment, also termed the bath or reservoir. The dynamics of the system and environment is wholly coherent, $\hat{\rho}_T(t) = \hat{U}^\dagger(t)\hat{\rho}_T(0)\hat{U}(t)$, where the unitary operator is the usual $\hat{U}(t) = \exp[-it\hat{H}_T]$, and where $\hat{\rho}_T(t)$ represents the combined system-environment density operator; both of these are linear operators on the combined Hilbert space, $\mathcal{H}_S \otimes \mathcal{H}_E$. The density operator for the system may be obtained by tracing over the environment degrees of freedom

$$\hat{\rho}_S(t) = \text{Tr}_E[\hat{\rho}_T(t)]. \tag{2.31}$$

In this chapter, we will introduce tractable models for the time evolution of $\hat{\rho}_S(T)$ which retain only the essential elements of the environment. Provided that the total Hamiltonian $\hat{H}_T$ is at most a quadratic polynomial of the system and environment quadrature operators, then upon tracing over the environment degrees of freedom, the system-environment interaction will be reduced to a *Gaussian quantum channel* acting on the remaining modes of the primary system. A quantum channel has the important property that it is a completely-positive trace-preserving (CPTP) map; as a result, a quantum channel applied to an initial density operator $\hat{\rho}_S(0)$ preserves the positive semi-definiteness of the density operator along with the unit trace. If $\hat{\rho}_S(0)$ is a Gaussian state, then a Gaussian

channel will transform its first and second central moments as follows,

$$\boldsymbol{\mu} \to \mathbf{T}\boldsymbol{\mu} + \mathbf{d} \quad \text{and} \quad \boldsymbol{\sigma} \to \mathbf{T}\boldsymbol{\sigma}\mathbf{T}^T + \boldsymbol{V} \tag{2.32}$$

where $\mathbf{d}$ is a real vector of length $2N$, $\mathbf{T}$ and $\mathbf{V}$ are both $2N \times 2N$ real matrices, and $\mathbf{V}$ is additionally a symmetric matrix. A Gaussian quantum channel is therefore a CPTP map that also preserves the Gaussian nature of the system state [40]. The restriction on the system-environment interaction is sufficient for the systems under consideration in this work, and we will make the further assumption that the environment modes are Markovian Gaussian white-noise processes. We will focus on two distinct, yet complementary, formalisms when modelling the dynamics of our open system: the Lindblad master equation and the Heisenberg-Langevin equations. We will further use the Heisenberg-Langevin equations and input-output theory to characterise the scattering behaviour of the system. But before tackling the open system dynamics, we will begin with a review of unitary dynamics for Gaussian states.

2.2.1 Coherent Dynamics of Gaussian Moments

The coherent dynamics of a state $\hat{\rho}$ can be described in the Shrödinger picture by the von Neumann equation,

$$\frac{d}{dt}\hat{\rho} = -i[\hat{H}, \hat{\rho}], \tag{2.33}$$

whose solution is the usual unitary time evolution. Equivalently, we can push the time dependence to observables $\hat{A}$ in the Heisenberg picture, and calculate the coherent dynamics using the Heisenberg equation:

$$\frac{d}{dt}\hat{A} = i[\hat{H}, \hat{A}] + \frac{\partial}{\partial t}\hat{A}. \tag{2.34}$$

In order to write the equations of motion for the moments of a Gaussian state, we will work in the Heisenberg picture and invoke the Ehrenfest theorem to write an equation of motion for the expectation value of an operator:

$$\frac{d}{dt}\langle\hat{A}\rangle = i\langle[\hat{H}, \hat{A}]\rangle + \left\langle \frac{\partial}{\partial t}\hat{A} \right\rangle. \tag{2.35}$$

We can express the quadratic Hamiltonian as a polynomial in the quadrature basis as follows,

$$\hat{H} = \frac{1}{2}\hat{\boldsymbol{r}}^T \boldsymbol{H}^{(2)} \hat{\boldsymbol{r}} + \hat{\boldsymbol{r}}^T \boldsymbol{h}^{(1)} = \frac{1}{2}\hat{r}_k H^{(2)}_{kl} \hat{r}_l + h^{(1)}_k \hat{r}_k \quad \text{where} \quad \left(H^{(2)}_{kl}\right)^T \equiv H^{(2)}_{lk} = H^{(2)}_{kl} \tag{2.36}$$

so that we can readily apply the canonical commutation relations from Eq. (2.5). We can now write the dynamical equation for the first and second order combinations of the quadrature operators:

$$\frac{d}{dt}\hat{r}_j = \Omega_{jk}\left(H^{(2)}_{kl}\hat{r}_l + h^{(1)}_k\right) \quad \text{and} \quad \frac{d}{dt}(\hat{r}_j\hat{r}_k) = \Omega_{jl}\left(H^{(2)}_{lm}\hat{r}_m + h^{(1)}_l\right)\hat{r}_k - \hat{r}_j\left(\hat{r}_m H^{(2)}_{ml} + h^{(1)}_l\right)\Omega_{lk}. \tag{2.37}$$

Using the definition of the first and second central moments along with the Ehrenfest theorem, we can write the following dynamical equations for the central moments,

$$\frac{d}{dt}\mu_j = \Omega_{jk}\left(H^{(2)}_{kl}\mu_l + h^{(1)}_k\right) \quad \text{and} \quad \frac{d}{dt}\sigma_{jk} = \Omega_{jl}H^{(2)}_{lm}\sigma_{mk} - \sigma_{jm}H^{(2)}_{ml}\Omega_{lj}, \tag{2.38}$$

or equivalently in terms of their arrays, using the fact that $\boldsymbol{H}^{(2)}$ is symmetric and $\boldsymbol{\Omega}$ is antisymmetric,

$$\frac{d}{dt}\boldsymbol{\mu} = \boldsymbol{\Omega}\big(\boldsymbol{H}^{(2)}\boldsymbol{\mu} + \boldsymbol{h}^{(1)}\big) \quad \text{and} \quad \frac{d}{dt}\boldsymbol{\sigma} = \big(\boldsymbol{\Omega}\boldsymbol{H}^{(2)}\big)\boldsymbol{\sigma} + \boldsymbol{\sigma}\big(\boldsymbol{\Omega}\boldsymbol{H}^{(2)}\big)^T. \tag{2.39}$$

We know from the solution to the von Neumann equation that the time evolution of $\hat{\rho}$ must be unitary, and therefore the solution to the dynamical equations of the Gaussian moments will be given by a symplectic transformation, as discussed in Section 2.1.4. If the Hamiltonian is time-independent, then we can immediately write the solution to the dynamical equations as,

$$\boldsymbol{\mu}(t) = \mathbf{S}(t)\boldsymbol{\mu}(0) + \mathbf{d}(t) \quad \text{and} \quad \boldsymbol{\sigma}(t) = \mathbf{S}(t)\boldsymbol{\sigma}(0)\mathbf{S}(t)^T, \tag{2.40}$$

where we can write explicit expressions for the time-dependent symplectic and translation transformations entirely in terms of the coefficients of $\hat{H}$ when written in the quadrature basis:

$$\mathbf{S}(t) = \exp\left[t\boldsymbol{\Omega}\boldsymbol{H}^{(2)}\right] \qquad \mathbf{d}(t) = \frac{\exp\left[t\boldsymbol{\Omega}\boldsymbol{H}^{(2)}\right] - \mathbf{I}_{2N}}{\boldsymbol{\Omega}\boldsymbol{H}^{(2)}}\,\boldsymbol{\Omega}\boldsymbol{h}^{(1)}. \tag{2.41}$$

With the coherent dynamics solved, we can now proceed to derive similar dynamical equations for the Gaussian moments for open quantum systems coupled to Markovian environments.

2.2.2 The Lindblad Master Equation

2.2.2.1 Open System Dynamics of Gaussian Moments

The first model of an open quantum system that we will examine is the celebrated Markovian *Lindblad master equation* [41, 42]. Working in the Schrödinger picture, the most general form of the Lindblad master equation, which satisfies the properties of a Gaussian channel, is

$$\frac{d}{dt}\hat{\rho} = \mathcal{L}(\hat{\rho}) \quad \text{where} \quad \mathcal{L}(\hat{\rho}) = -i[\hat{H},\hat{\rho}] + \sum_{j,k=1}^{2N}\Gamma_{jk}\left(\hat{r}_k\hat{\rho}\hat{r}_j - \frac{1}{2}[\hat{r}_j\hat{r}_k,\hat{\rho}]_+\right), \tag{2.42}$$

where the system Hamiltonian $\hat{H}$ must be at most a quadratic function of the quadrature operators, and hence may be written as in Eq. (2.36). The $2N\times 2N$ matrix of environment couplings $\boldsymbol{\Gamma}$ is assumed to be Hermitian and positive semi-definite. Provided that the Hamiltonian and the couplings to the environment are all time-independent, the solution to the Lindblad master equations is

$$\hat{\rho}(t) = e^{t\mathcal{L}}\hat{\rho}(0), \tag{2.43}$$

where the evolution is no longer unitary due to the dissipative environmental coupling, and so the CPTP dynamical map in Eq. (2.43) is not invertible. We can also express this in the Heisenberg picture, $\mathrm{Tr}[\hat{A}(e^{t\mathcal{L}}\hat{\rho})] \equiv \mathrm{Tr}[(e^{t\mathcal{L}^\dagger}\hat{A})\hat{\rho}]$, in order to write an adjoint version of the Lindblad master equation for observables, which is only well-defined under certain circumstances[1] [41]:

$$\frac{d}{dt}\hat{A} = \mathcal{L}^\dagger(\hat{A}) \quad \text{where} \quad \mathcal{L}^\dagger(\hat{A}) = i[\hat{H},\hat{A}] + \sum_{j,k=1}^{2N}\Gamma^*_{jk}\left(\hat{r}_j\hat{A}\hat{r}_k - \frac{1}{2}[\hat{r}_k\hat{r}_j,\hat{A}]_+\right). \tag{2.44}$$

If one is only interested in the time-evolution of operator expectation values, then it is possible to solve the following master equation in all cases,

$$\frac{d}{dt}\langle\hat{A}\rangle = \langle\mathcal{L}^\dagger(\hat{A})\rangle, \tag{2.45}$$

where $\mathcal{L}^\dagger(\hat{A})$ is defined as in Eq. (2.44). It is possible to calculate the dynamical equations for the Gaussian moments using this expression, as was done in the previous section for the coherent dynamics, however, the dissipative part of the Lindblad master equation makes this calculation tedious. A simpler method is to instead use the Wigner phase-space representation to write the Lindblad master equation as a partial differential equation of the Wigner function:

$$\frac{d}{dt}\hat{\rho} = \mathcal{L}(\hat{\rho}) \xleftrightarrow[\text{Wigner}]{\text{Weyl}} \frac{\partial}{\partial t}W_\rho(\boldsymbol{r}) = \left[-\boldsymbol{\partial r}^T\boldsymbol{\Omega}\boldsymbol{h}^{(1)} - \frac{1}{2}\boldsymbol{\partial r}^T\big(\boldsymbol{\Omega}\mathrm{Re}[\boldsymbol{\Gamma}]\boldsymbol{\Omega}\big)\boldsymbol{\partial r} - \boldsymbol{\partial r}^T\left(\boldsymbol{\Omega}\boldsymbol{H}^{(2)} + \boldsymbol{\Omega}\mathrm{Im}[\boldsymbol{\Gamma}]\right)\boldsymbol{r}\right]W_\rho(\boldsymbol{r}). \tag{2.46}$$

Transforming from the Wigner phase-space back to the Hilbert space is accomplished using the Weyl transformation; see Appendix A for further details. The vector $\boldsymbol{\partial r}$ has length $2N$ and contains the partial derivatives with respect to the phase-space variables $\boldsymbol{r}$, and can be written as $\boldsymbol{\partial r} := (\partial/\partial r_1,\ldots,\partial/\partial r_{2N})^T$. The above second-order differential

[1] This manner of writing an adjoint Lindblad master equation for observables, although used in some common sources [43], is not rigorous, and ignores technical complications regarding the continuity of the adjoint dynamical map. To summarise the problem, such a master equation can only be defined when the generator of the dynamical semi-group is strongly continuous. The flow $\hat{\rho}(t) = e^{t\mathcal{L}}\hat{\rho}(0)$ is guaranteed to be strongly-continuous since it is continuous for every density operator, allowing one to write the Lindblad master equation in Eq. (2.42) using $\mathcal{L}$. Strong continuity is not preserved when considering the generator of the dual semi-group, which acts on the adjoint space of observables, and so $\hat{A}(t) = e^{t\mathcal{L}^\dagger}\hat{A}(0)$ is not continuous for all observables. Instead, it is said to be weakly continuous, since only $\langle\hat{A}(t)\rangle = \mathrm{Tr}[(e^{t\mathcal{L}^\dagger}\hat{A}(0))\hat{\rho}]$ is guaranteed to always be continuous by virtue of the strong continuity of $e^{t\mathcal{L}}\hat{\rho}(0)$; as a result, only the dynamical equation in Eq. (2.45) is well defined for all observables. Observables do exist for which time evolution is continuous, and it is for these operators only that the adjoint Lindblad master equation in Eq. (2.44) may be defined. Such restrictions do not exist if $\mathcal{L}$ corresponds to unitary evolution.

equation is known as a Fokker-Planck equation, and will preserve the Gaussian nature of the Wigner function $W_\rho(\boldsymbol{r})$. It is easier to extract the moments of the Gaussian from the characteristic function $w_\rho(\boldsymbol{\xi})$, so a Fourier transform is performed over the phase-space coordinates, which yields another Fokker-Planck differential equation:

$$\xrightarrow{\text{Fourier}} \frac{\partial}{\partial t} w_\rho(\boldsymbol{\xi}) = \left[-i\boldsymbol{\xi}^T \boldsymbol{\Omega} \boldsymbol{h}^{(1)} + \frac{1}{2}\boldsymbol{\xi}^T \big(\boldsymbol{\Omega}\text{Re}[\boldsymbol{\Gamma}]\boldsymbol{\Omega}\big)\boldsymbol{\xi} + \boldsymbol{\xi}^T \Big(\boldsymbol{\Omega}\boldsymbol{H}^{(2)} + \boldsymbol{\Omega}\text{Im}[\boldsymbol{\Gamma}]\Big)\boldsymbol{\partial}\boldsymbol{\xi} \right] w_\rho(\boldsymbol{\xi}). \tag{2.47}$$

The vector $\boldsymbol{\partial}\boldsymbol{\xi}$ has length $2N$ and is defined analogously to $\boldsymbol{\partial}\boldsymbol{r}$, where $\boldsymbol{\partial}\boldsymbol{\xi} := (\partial/\partial\xi_1, \ldots, \partial/\partial\xi_{2N})^T$. By substituting the general form for the characteristic function of a Gaussian state from Eq. (2.15) into the above Fokker-Planck equation, we can work out the following dynamical equations for the first and second moments:

$$\frac{d}{dt}\boldsymbol{\mu}(t) = \mathbf{A}\boldsymbol{\mu}(t) + \mathbf{f} \quad \text{and} \quad \frac{d}{dt}\boldsymbol{\sigma}(t) = \mathbf{A}\boldsymbol{\sigma}(t) + \boldsymbol{\sigma}(t)\mathbf{A}^T + \mathbf{C}, \tag{2.48}$$

where the matrices and vectors may be written as

$$\mathbf{A} = \boldsymbol{\Omega}\boldsymbol{H}^{(2)} + \boldsymbol{\Omega}\text{Im}[\boldsymbol{\Gamma}] \qquad \mathbf{C} = -\boldsymbol{\Omega}\text{Re}[\boldsymbol{\Gamma}]\boldsymbol{\Omega} \qquad \mathbf{f} = \boldsymbol{\Omega}\boldsymbol{h}^{(1)}. \tag{2.49}$$

The matrix $\mathbf{A}$ is specifically referred to as the *dynamical matrix*. The dynamical equations are readily solved in the steady state, where the equation for $\boldsymbol{\sigma}$ becomes a Lyapunov equation, and the equation for $\boldsymbol{\mu}$ is a simple linear matrix equation. It is, in fact, possible to solve the dynamical equations of the Gaussian moments when both $\hat{H}$ and $\boldsymbol{\Gamma}$ are wholly independent of time [44]:

$$\boldsymbol{\mu}(t) = \mathbf{T}(t)\boldsymbol{\mu}(0) + \mathbf{d}(t) \quad \text{and} \quad \boldsymbol{\sigma}(t) = \mathbf{T}(t)\boldsymbol{\sigma}(0)\mathbf{T}(t)^T + \boldsymbol{V}(t) \tag{2.50}$$

where the transformations can be written as follows[2]:

$$\mathbf{T}(t) = \exp[t\mathbf{A}] \qquad \mathbf{d}(t) = \frac{\exp[t\mathbf{A}] - \mathbf{I}_{2N}}{\mathbf{A}}\mathbf{f} \qquad \mathbf{V}(t) = \text{vec}^{-1}\left(\frac{\exp[t(\mathbf{A}\otimes\mathbf{A})] - \mathbf{I}_{4N^2}}{(\mathbf{A}\otimes\mathbf{A})} \text{vec}(\mathbf{C}) \right). \tag{2.51}$$

An important difference between the above expression and those for unitary evolution is that the symplectic transformation $\mathbf{S}(t)$ has been replaced by $\mathbf{T}(t) = \exp[t\mathbf{A}]$, which is not a symplectic transformation; in order to determine under what condition $\mathbf{T}(t)$ is symplectic, and hence unitary and invertible, we can use the definition of a symplectic matrix from Eq. (2.21) to construct an equivalent condition for the dynamical matrix $\mathbf{A}$ in the exponential:

$$\boldsymbol{\Omega}\mathbf{A} + \mathbf{A}^T\boldsymbol{\Omega} = 0 \quad \text{or equivalently} \quad \boldsymbol{\Omega}\mathbf{A} - (\boldsymbol{\Omega}\mathbf{A})^T = 0. \tag{2.52}$$

Using the definition of the dynamical matrix $\mathbf{A}$ from Eq. (2.49), the coherent dynamics represented by $\boldsymbol{\Omega}\boldsymbol{H}^{(2)}$ will satisfy the above condition because $\boldsymbol{H}^{(2)}$ is a symmetric matrix, while the component arising from the coupling to the environment, $\boldsymbol{\Omega}\text{Im}[\boldsymbol{\Gamma}]$, will not since $\text{Im}[\boldsymbol{\Gamma}]$ is antisymmetric. Thus, symplectic transformations only correspond to invertible unitary transformations of the density operator, and so dissipative environmental couplings necessarily result in nonunitary, and therefore non-invertible, dynamics.

2.2.2.2 The Quantum Optical Master Equation

The Lindbladian $\mathcal{L}$ in Eq. (2.42) is the infinitesimal generator of a one-parameter dynamical semi-group [41], and is the most general form for a Markovian Gaussian quantum channel. The general form may be derived based on mathematical grounds, however, it is also possible to use the so-called microscopic derivation so as to obtain the Lindbladian based on purely physical arguments. For this work, we are specifically interested in the model known as the quantum optical master equation, detailed microscopic derivations of which may be found in Refs. [43, 45–47]; we will provide an overview of the derivation, drawing from a number of the listed sources, making sure to highlight the important assumptions, which will be relevant for our physical models.

The dynamics of the combined system is governed by a total time-independent Hamiltonian $\hat{H}_T$, with identical form to Eq. (2.30); we will specify the exact form of $\hat{H}_T$ later on, but for the first part of this derivation it is simpler to keep the expressions abstract. We assume that the system and environment are weakly coupled, so the coupling described by the interaction Hamiltonian $\hat{H}_I$ is a weak perturbation of the independent Hamiltonians, $\hat{H}_S + \hat{H}_E$; this is the *weak-coupling approximation*. The system Hamiltonian is initially written in its energy eigenbasis, while the

[2]The function vec($\mathbf{C}$) is the vectorisation operation; the definition used here transposes the rows of the matrix $\mathbf{C}$, and then stacks them to create a column vector of length $4N^2$, thereby vectorising the matrix. The function $\text{vec}^{-1}(\cdot)$ denotes the inverse of this operation.

interaction Hamiltonian is written as a sum,

$$\hat{H}_S = \sum_k \varepsilon_k \left|\varepsilon_k\right\rangle\!\left\langle\varepsilon_k\right| \qquad \hat{H}_I = \sum_k \hat{A}_k \otimes \hat{E}_k = \sum_k \hat{A}_k^\dagger \otimes \hat{E}_k^\dagger \tag{2.53}$$

where $\hat{A}_k$ and $\hat{E}_k$ are linear operators on the primary system and environment Hilbert spaces, respectively. It is convenient to also write the system operators $\hat{A}$ in the basis of $\hat{H}_S$ eigenstates, since this will allow us to determine the timescales of the different processes in $\hat{H}_I$ later on; we therefore rewrite the individual $\hat{A}_k$ as,

$$\hat{A}_k = \sum_{l,m} \left|\varepsilon_l\right\rangle\!\left\langle\varepsilon_l\right|\hat{A}_k\left|\varepsilon_m\right\rangle\!\left\langle\varepsilon_m\right| \equiv \sum_\omega \hat{A}_k(\omega) \quad \text{where} \quad \hat{A}_k(\omega) = \sum_{\omega=\varepsilon_l-\varepsilon_m} \left\langle\varepsilon_l\right|\hat{A}_k\left|\varepsilon_m\right\rangle \left|\varepsilon_l\right\rangle\!\left\langle\varepsilon_m\right|, \tag{2.54}$$

where the sum in $\hat{A}_k(\omega)$ is over eigenenergies with identical differences in energy, represented by the frequency ω. We can now move to an interaction picture by applying the unitary transformation $\hat{U}(t) = \exp[it(\hat{H}_S + \hat{H}_E)]$ to the Schrödinger picture operators; the Hamiltonian therefore transforms as

$$\begin{aligned} &\hat{H}_T \to \hat{U}(t)\hat{H}_T\hat{U}^\dagger(t) + i\left(\frac{d}{dt}\hat{U}(t)\right)\hat{U}^\dagger(t) = \hat{U}(t)\hat{H}_I\hat{U}^\dagger(t) =: \tilde{H}_I(t) \\ &\text{where} \quad \tilde{H}_I(t) = \sum_{k,\omega} e^{i\hat{H}_S t}\hat{A}_k(\omega)e^{-i\hat{H}_S t} \otimes e^{i\hat{H}_E t}\hat{E}_k e^{-i\hat{H}_E t} = \sum_{k,\omega} e^{-i\omega t}\hat{A}_k(\omega) \otimes \tilde{E}_k(t). \end{aligned} \tag{2.55}$$

In order to take the derivative of t$\hat{U}(t)$ with respect to time, we can use the fact that any unitary operator may written as the exponential of an anti-Hermitian operator $i\hat{H}(t)$, that is $\hat{U}(t) = e^{i\hat{H}(t)}$, and so use the following expressions for the derivative of the exponential map $e^{X(t)}$ [48],

$$\frac{d}{dt}e^X = e^X\left(\sum_{k=0}^\infty \frac{(-1)^k}{(k+1)!}[(X)^k, dX/dt]\right) = \left(\sum_{k=0}^\infty \frac{1}{(k+1)!}[(X)^k, dX/dt]\right)e^X, \tag{2.56}$$

where $[(X)^k, Y]$ is the iterated commutator, previously defined in Eq. (2.26). A dynamical equation can then be written for the total density operator in the interaction frame as follows:

$$\frac{d}{dt}\tilde{\rho}_T(t) = -i[\tilde{H}_I(t), \tilde{\rho}_T(t)] \quad \text{where} \quad \tilde{\rho}_T(t) := \hat{U}(t)\hat{\rho}_T(t)\hat{U}^\dagger(t). \tag{2.57}$$

This differential equation is integrated to yield a formal solution, which is then substituted back into the original differential equation to obtain an exact integro-differential equation for $\tilde{\rho}_T(t)$:

$$\frac{d}{dt}\tilde{\rho}_T(t) = -i[\tilde{H}_I(t), \tilde{\rho}_T(t_0)] - \int_{t_0}^t [\tilde{H}_I(t), [\tilde{H}_I(t'), \tilde{\rho}_T(t')]\,]\,dt'. \tag{2.58}$$

To progress from here we further assume that there is no coupling between the system and environment before the initial time t_0, so they are initially uncorrelated, $\tilde{\rho}_T(t_0) = \tilde{\rho}_S(t_0) \otimes \tilde{\rho}_E(t_0)$. Additionally, the number of modes in the environment is taken to be much larger than the system, which, when combined with the initial assumption of weak coupling, results in no backaction from the system on the environment, and hence there is no change in the spectrum of the environment due to the system; this is known as the *Born approximation*. As a result of this, the state of the bath is constant and uncorrelated with the system, which in the interaction frame means that the initial-state is the steady state, $\tilde{\rho}_T(t) \approx \tilde{\rho}_S(t) \otimes \tilde{\rho}_E(t_0)$.

We can now trace out the environment in Eq. (2.58) to obtain a dynamical equation for the system density operator, $\dot{\tilde{\rho}}_S(t) = \mathrm{Tr}_E[\dot{\tilde{\rho}}_T(t)]$. Tracing over the environment will yield first- and second-order expectation values of the operators $\tilde{E}_k(t)$, which must now be evaluated. By construction, the expectation value of the environmental operators must vanish entirely:

$$\mathrm{Tr}_E\left[[\tilde{H}_I(t), \tilde{\rho}_T(t_0)]\right] = 0 \quad \to \quad \mathrm{Tr}_E\left[\tilde{E}_k(t)\tilde{\rho}_E(t_0)\right] \equiv \langle\tilde{E}_k(t)\rangle = 0. \tag{2.59}$$

Only the second-order expectation values of the environmental operators will remain in the dynamical equation for $\tilde{\rho}_s(t)$, which are functions of two points in time, and may be written as

$$\langle\tilde{E}_k^\dagger(t)\tilde{E}_l(t')\rangle \equiv \mathrm{Tr}_E\left[\tilde{E}_k^\dagger(t)\tilde{E}_l(t')\hat{\rho}_E(t_0)\right] = \mathrm{Tr}_E\left[\tilde{E}_k^\dagger(t-t')\tilde{E}_l(0)\hat{\rho}_E(t_0)\right]. \tag{2.60}$$

Since the density operator $\hat{\rho}_E(t_0)$ does not evolve with time in the interaction picture, it commutes with the operator

$e^{i\hat{H}_E t}$, and as a result the second order expectation value can be characterised entirely by the difference in time, $t - t' = \tau$, commonly called the lag; the environment therefore corresponds to a wide-sense stationary process [49].

The next major assumption that we invoke is the *Markov approximation*, which sets vastly different time scales for the time evolution of the environment and the system. By taking the environment to be Markovian, the timescale of its dynamics is assumed to be far shorter than that the of the system; this ensures that the correlation time of the environment is so short that, when viewed on system-timescales, it can be assumed to have no dependence on earlier times and hence *no memory*. This has two effects on the dynamical equation in Eq. (2.58), which will finally allow us to cast this as a Markovian master equation. First, we can assume that due to the rapid decay of the environmental correlations that the integrand sufficiently decays to zero faster than $\tilde{\rho}_S(t')$ can change, allowing for the replacement $\tilde{\rho}_S(t') \to \tilde{\rho}_S(t)$. Secondly, the rapid decay of the integrand also allows for the upper limit of the integral to go to infinity; we additionally set the initial time to zero without any loss of generality. Combining these approximations yields, in the interaction picture, the Born-Markov master equation:

$$\begin{aligned}\frac{d}{dt}\tilde{\rho}_S(t) &= -\int_0^\infty \mathrm{Tr}_E\left[[\tilde{H}_I(t), [\tilde{H}_I(t-\tau), \tilde{\rho}_S(t)\otimes\tilde{\rho}_E]]\right] dt' \\ &= \sum_{\omega,\omega'}\sum_{k,l} e^{i(\omega'-\omega)t} C_{kl}(\omega)\left(\hat{A}_l(\omega)\tilde{\rho}_S(t)\hat{A}_k^\dagger(\omega') - \hat{A}_k^\dagger(\omega')\hat{A}_l(\omega)\tilde{\rho}_S(t)\right) + \text{h.c.}\end{aligned} \tag{2.61}$$

The decompositions of the interaction Hamiltonian from Eqs. (2.53) and (2.55) were used to obtain the second expression. The function $C_{kl}(\omega)$ corresponds to the one-sided Fourier transform of the environment correlation function from Eq. (2.60):

$$C_{kl}(\omega) := \int_0^\infty e^{i\omega\tau}\langle\tilde{E}_k^\dagger(\tau)\tilde{E}_l(0)\rangle\, d\tau \tag{2.62}$$

This function is generally complex-valued and may be written in terms of a real component, which corresponds to purely dissipative interactions between the system and environment, and an imaginary component, which gives rise to some additional coherent dynamics in the system. Writing $C_{kl}(\omega) = \frac{1}{2}\gamma_{kl}(\omega) + i\ell_{kl}(\omega)$, we then have:

$$\gamma_{kl}(\omega) = \frac{1}{2}\left(C_{kl}(\omega) + C_{kl}^*(\omega)\right) \qquad \ell_{kl}(\omega) = \frac{1}{2i}\left(C_{kl}(\omega) - C_{kl}^*(\omega)\right). \tag{2.63}$$

The coefficients $\gamma_{kl}(\omega)$ are now elements of a Hermitian matrix, as was assumed at the beginning of this section, and correspond to a full Fourier transform of the environmental correlators, or equivalently, the power-spectral density of the environment:

$$\gamma_{kl}(\omega) = \int_{-\infty}^\infty e^{i\omega\tau}\langle\tilde{E}_k^\dagger(\tau)\tilde{E}_l(0)\rangle\, d\tau. \tag{2.64}$$

The imaginary parts $\ell_{kl}(\omega)$ can be combined to form a Hermitian Hamiltonian operator, called the *Lamb shift* Hamiltonian:

$$\hat{H}_{\text{LS}} := \sum_\omega\sum_{k,l}\ell_{kl}(\omega)\hat{A}_k^\dagger(\omega)\hat{A}_l(\omega) \quad \text{where} \quad [\hat{H}_S, \hat{H}_{\text{LS}}] = 0. \tag{2.65}$$

As the name implies, the Lamb shift Hamiltonian corresponds to a shift of the bare energy levels of the system, which occurs due to coupling with the environment. Since it commutes with the system Hamiltonian, its form will be preserved when shifting back to the Shrödinger picture.

We can now invoke the final assumption in this derivation, the so-called *secular approximation*, which eliminates all the off-resonant, or non-secular, terms where the transition frequencies of the system operators are not identical, $\omega \neq \omega'$. This approximation relies on non-resonant transitions within the system oscillating too rapidly compared to the relaxation time of the system to have any appreciable effect on the dynamics, and they are therefore dropped from our final expression. Transforming the system back to the Shrödinger picture, we finally arrive at the optical Lindblad master equation:

$$\frac{d}{dt}\hat{\rho}_S(t) = -i[\hat{H}_S + \hat{H}_{\text{LS}}, \hat{\rho}_S(t)] + \sum_\omega\sum_{k,l}\gamma_{kl}(\omega)\left(\hat{A}_l(\omega)\hat{\rho}_S(t)\hat{A}_k^\dagger(\omega) - \frac{1}{2}[\hat{A}_k^\dagger(\omega)\hat{A}_l(\omega), \hat{\rho}_S(t)]_+\right). \tag{2.66}$$

For physical systems, the Lamb shift Hamiltonian is a small correction to the system Hamiltonian energies, and therefore it is normally ignored; for the purposes of this work, we will justifiably do the same.

2.2.2.3 Noise from a Thermal Reservoir

With the above expression in hand, the Lindblad master equations for specific models of the system and environment can be quickly obtained; we are particularly interested in modelling the environment as a thermal reservoir. We start by assuming that the system and environment are comprised of bosonic modes, modelled as quantum harmonic oscillators, each with its own resonant frequency. The environments are comprised of a large number of modes, each of which is assumed to be wholly independent, resulting in no cross-mode coupling through the environmental degrees of freedom. The components from the total Hamiltonian in Eq. (2.30) which act purely on the system and environment are then:

$$\hat{H}_E = \sum_{j=1}^{N} \sum_{\omega_b} \omega_b \hat{b}_j^\dagger(\omega_b)\hat{b}_j(\omega_b) \quad \text{and} \quad \hat{H}_S = \hat{H}_0 + \hat{H}_Q\,,\ \hat{H}_0 = \sum_{j=1}^{N} \omega_j \hat{a}_j^\dagger \hat{a}_j. \tag{2.67}$$

The $\hat{a}_j^{(\dagger)}$ operators act on the system modes and obey the same commutation relations as in Eq. (2.1). The operators $\hat{b}_k^{(\dagger)}(\omega_b)$ are the creation and annihilation operators for the bosonic bath modes coupled to the system mode j, with the commutation relations $[\hat{b}_k(\omega_b), \hat{b}_l^\dagger(\omega_b)] = \delta_{kl}$. The system Hamiltonian is written as the sum of an N-mode harmonic oscillator Hamiltonian, $\hat{H}_0$, leaving the quadratic Hamiltonian, $\hat{H}_Q$, unspecified.

Turning to the system-environment interaction Hamiltonian, we assume that the coupling between the system and environment is quadratic, and only involves the exchange of single excitations:

$$\hat{H}_I = \sum_{j=1}^{N} \sum_{\omega_b} i\left(f_j^*(\omega_b)\hat{b}^\dagger(\omega_b)\hat{a}_j - f_j(\omega_b)\hat{b}_j(\omega_b)\hat{a}_j^\dagger\right) = \sum_{j=1}^{N}\left(\hat{B}_j^\dagger \hat{a}_j + \hat{B}_j \hat{a}_j^\dagger\right) \quad \text{where} \quad \hat{B}_j = -i\sum_{\omega_b} f_j(\omega_b)\hat{b}_j(\omega_b). \tag{2.68}$$

With this, we can identify the environment operators $\hat{E}_k$ as the $\hat{B}_j^{(\dagger)}$ operators, whereas the system operators $\hat{A}_k$ are the ladder operators. Notice that while no restrictions were placed on the Hamiltonian in the previous section, these definitions mean that the dynamics generated by $\hat{H}_T$ corresponds to a unitary Gaussian transformation, as detailed in Section 2.2.1. Provided that the total state $\hat{\rho}_T$ is also Gaussian, then, upon tracing out the environment, the state of the primary system must also necessarily be Gaussian at all times, and so the resulting Lindblad master equation must be a Gaussian channel.

Writing $\hat{A}_k$ in terms of the level-spacing dependent operators $\hat{A}_k(\omega)$ requires the diagonalisation of $\hat{H}_S$, which has been left unspecified. In order to simplify this process, we assume that the Hamiltonian $\hat{H}_Q$ corresponds to a weak correction to the energy levels of $\hat{H}_0$. This is well motivated when working in the microwave regime, where the modes have a bare frequency on the order of $\sim 1 - 10\,\mathrm{GHz}$, while the interactions in $\hat{H}_Q$ have strengths up to $\sim 10\,\mathrm{MHz}$. In this case, the eigenbasis of $\hat{H}_S$ is approximately the basis of multimode number states from Eq. (2.2), with a constant spacing of $\pm\omega_j$ between the energy levels for the j-th mode. Since the mode operators act as ladder operators between regularly spaced number states, the system operators in Eq. (2.66) only depend on the frequency of their respective mode. The sum over ω collapses to a sum over the constant energy spacings, $\pm\omega_j$, with the system operators replaced by $\hat{A}_k(-\omega_j) \to \hat{a}_j$ and $\hat{A}_k(+\omega_j) \to \hat{a}_j^\dagger$.

We must now evaluate the correlation functions $\gamma_{kl}(\pm\omega_j)$ to obtain the desired master equation. As stated above, we assume that the environment forms a thermal reservoir coupled to the system. Based on the assumptions made in the derivation, the effects of $\hat{H}_I$ can be neglected by invoking the weak-coupling approximation. The constant environmental state is assumed to be in thermal equilibrium, with the density operator corresponding to the canonical ensemble:

$$\hat{\rho}_E = \frac{e^{-\beta\hat{H}_E}}{\mathrm{Tr}_E\left[e^{-\beta\hat{H}_E}\right]} = \bigotimes_{k,\omega_b} \hat{\rho}_k^{\mathrm{th}}(\omega_b) \quad \text{where} \quad \hat{\rho}_k^{\mathrm{th}}(\omega_b) = \frac{1}{1-e^{-\beta\omega_b}} e^{-\beta\omega_b \hat{b}_k^\dagger(\omega_b)\hat{b}_k(\omega_b)} \tag{2.69}$$

where $\beta = 1/k_B T$, and k_B is Boltzmann's constant. The above state corresponds to a collection of uncorrelated thermal states for each bath mode, each of which has some characteristic thermal occupancy determined by the frequency of the bath mode,

$$\bar{n}(\omega_b) = \frac{e^{-\beta\omega_b}}{1-e^{-\beta\omega_b}}. \tag{2.70}$$

With $\hat{\rho}_E$ defined, the expectation values of the environment ladder operators can now be defined; to facilitate the evaluation of $\gamma_{kl}(\omega_j)$, we replace the discrete sum over the bath frequencies with an integral, $\sum_{\omega_b} \to \int d\omega_b$. Under this replacement, only two correlation functions take non-zero values:

$$\langle \hat{b}_k^\dagger(\omega_b)\hat{b}_l(\omega_b')\rangle = \bar{n}(\omega_b)\delta_{kl}\delta(\omega_b - \omega_b') \qquad \langle \hat{b}_k(\omega_b)\hat{b}_l^\dagger(\omega_b')\rangle = (\bar{n}(\omega_b)+1)\delta_{kl}\delta(\omega_b - \omega_b'). \tag{2.71}$$

Each field is therefore only correlated with other ladder operators of identical frequency. These correlators also

indicate that the dissipative coupling $\gamma_{kl}(\omega_j)$ is only non-zero when $k = l$, due to the assumed independence of the environments for different modes of the system. We can now compute the only two non-zero values of $\gamma_{kl}(\omega_j)$:

$$\int_{-\infty}^{\infty} e^{-i\omega\tau}\langle\tilde{B}_k(\tau)\tilde{B}_k^\dagger(0)\rangle\, d\tau = \iint f_k^*(\omega_b) f_l(\omega_b') \int_{-\infty}^{\infty} e^{-i(\omega_j-\omega_b)\tau}\langle\hat{b}_k^\dagger(\omega_b)\hat{b}_k(\omega_b')\rangle\, d\tau\, d\omega_b\, d\omega_b' = 2\pi\left|f_k(\omega_j)\right|^2(\bar{n}(\omega_j)+1)$$
$$\int_{-\infty}^{\infty} e^{i\omega\tau}\langle\tilde{B}_k^\dagger(\tau)\tilde{B}_k(0)\rangle\, d\tau = \iint f_k^*(\omega_b) f_l(\omega_b') \int_{-\infty}^{\infty} e^{i(\omega_j-\omega_b)\tau}\langle\hat{b}_k^\dagger(\omega_b)\hat{b}_k(\omega_b')\rangle\, d\tau\, d\omega_b\, d\omega_b' = 2\pi\left|f_k(\omega_j)\right|^2\bar{n}(\omega_j). \tag{2.72}$$

As a result of our approximations, the modes of the principal system only couple to modes in the environment with similar frequencies, and hence the thermal occupancy of the reservoir corresponds to the frequency of the principal system modes; for identical temperatures, a higher frequency mode will in general see a bath with lower occupancy compared to a lower frequency mode. This should be understood to be an approximation, as there are other factors present in physical devices which contribute to the amount of thermal noise impinging on a mode from the environment that have not been taken into account here, such as pumps used to drive the system.

Since all non-trivial dependence on the frequencies of the bath modes has dropped out, we make the substitutions $\bar{n}(\omega_j) \to \bar{n}_j$ and $2\pi\left|f_k(\omega_j)\right|^2 \to \kappa_j$. We can now replace all unknown quantities in the Lindblad master equation in Eq. (2.66), making sure to use $\hat{a}_j^{(\dagger)}$ in place of the system operators, which leads us to our final result:

$$\frac{d}{dt}\hat{\rho}_S = -i[\hat{H}_S,\hat{\rho}_S] + \sum_{k=1}^{N}\Big(\kappa_k\big(\bar{n}_k+1\big)\mathcal{D}[\hat{a}_k](\hat{\rho}_S) + \kappa_k\bar{n}_k\mathcal{D}[\hat{a}_k^\dagger](\hat{\rho}_S)\Big) \quad \text{where} \quad \mathcal{D}[\hat{L}](\hat{\rho}) := \hat{L}\hat{\rho}\hat{L}^\dagger - \frac{1}{2}[\hat{L}^\dagger\hat{L},\hat{\rho}]_+. \tag{2.73}$$

The constant κ_k parameters represent decay rates from the system to the environment, and are set by the system-environment coupling. Looking at the dissipative component of Eq. (2.73), we see that upon tracing over the environment, the single particle exchange between the system and bath in the interaction Hamiltonian from Eq. (2.68) has given rise to two incoherent single-photon processes: single-particle dissipation into the environment which proceeds with the rate $\kappa_k(\bar{n}_k+1)$, and single-particle excitation with rate $\kappa_k\bar{n}_k$, which is absent when the environment is in the vacuum state.

The Lindblad master equation in Eq. (2.73) is naturally expressed in terms of the creation and annihilation operator basis, however, to use the dynamical equations in Eq. (2.48) we require that the dissipation terms be expressed in the quadrature basis:

$$\begin{aligned}&\kappa_k\big(\bar{n}_k+1\big)\mathcal{D}[\hat{a}_k](\hat{\rho}) + \kappa_k\bar{n}_k\mathcal{D}[\hat{a}_k^\dagger](\hat{\rho})\\ &= \kappa_k\left(\bar{n}_k+\frac{1}{2}\right)\left(\mathcal{D}[\hat{q}_k](\hat{\rho})+\mathcal{D}[\hat{p}_k](\hat{\rho})\right) - \kappa_k\frac{i}{2}\left(\hat{q}_k\hat{\rho}\hat{p}_k - \frac{1}{2}[\hat{p}_k\hat{q}_k,\hat{\rho}]_+\right) + \kappa_k\frac{i}{2}\left(\hat{p}_k\hat{\rho}\hat{q}_k - \frac{1}{2}[\hat{q}_k\hat{p}_k,\hat{\rho}]_+\right).\end{aligned} \tag{2.74}$$

We can now write the coefficient matrix for thermal dissipation, and from that the matrices $\mathbf{\Omega}\mathrm{Im}[\mathbf{\Gamma}]$ and $\mathbf{\Omega}\mathrm{Re}[\mathbf{\Gamma}]\mathbf{\Omega}$:

$$\mathbf{\Gamma} = \bigoplus_{k=1}^{N}\frac{\kappa_k}{2}\begin{pmatrix}2\bar{n}_k+1 & i\\ -i & 2\bar{n}_k+1\end{pmatrix} \to \mathbf{\Omega}\mathrm{Im}[\mathbf{\Gamma}] = -\bigoplus_{k=1}^{N}\frac{\kappa_k}{2}\mathbf{I}_2 \quad \text{and} \quad \mathbf{\Omega}\mathrm{Re}[\mathbf{\Gamma}]\mathbf{\Omega} = -\bigoplus_{k=1}^{N}\kappa_k\left(\bar{n}_k+\frac{1}{2}\right)\mathbf{I}_2. \tag{2.75}$$

With the addition of a quadratic system Hamiltonian, $\hat{H}_S$, these expressions allow for the moment differential equations from Eqs. (2.48) and (2.49) to be adapted for the Lindladian in Eq. (2.73):

$$\mathbf{A} = \mathbf{\Omega}\boldsymbol{H}^{(2)} - \bigoplus_{k=1}^{N}\frac{\kappa_k}{2}\mathbf{I}_2 \qquad \mathbf{C} = \bigoplus_{k=1}^{N}\kappa_k\left(\bar{n}_k+\frac{1}{2}\right)\mathbf{I}_2 \qquad \mathbf{f} = \mathbf{\Omega}\boldsymbol{h}^{(1)}. \tag{2.76}$$

In the next section, we will review the differential Heisenberg-Langevin equations. By again assuming that the environment is a Markovian thermal reservoir, we will demonstrate that the same moment equations can be obtained using the Heisenberg-Langevin equations, revealing the equivalence with the quantum optical master equation for the purpose of calculating the expectation values of the internal system modes.

2.2.3 Heisenberg-Langevin Equations and Input-Output Theory

2.2.3.1 Derivation of the Dynamical Equations

The Heisenberg-Langevin equations provide a complementary approach to open quantum systems, which, compared to the Lindblad master equation, can be consistently defined in the Heisenberg picture. For these equations, along with the related input-output theory, we will follow the seminal work by Gardiner and Collett [50], where the relation with

the Lindblad master equation is also established. This general equivalence will not be demonstrated here, however, it will be shown that, under the same approximations, the Heisenberg-Langevin equations generate the same equations of motion for the moments of a Gaussian state, as in Eq. (2.76).

The derivation starts with the same total Hamiltonian from the microscopic derivation of the Lindblad master equation, $\hat{H}_T$, which was defined in Eqs. (2.67) and (2.68). The system Hamiltonian, $\hat{H}_S$, is again at most dependent on quadratic and bilinear terms of the primary system ladder operators. For $\hat{H}_E$ and $\hat{H}_I$, the sum over bath frequencies is pre-emptively replaced with an integral, so the environment and system-environment interaction Hamiltonians are as follows:

$$\hat{H}_E = \sum_{k=1}^{N} \int_{-\infty}^{\infty} \omega_b \hat{b}_k^\dagger(\omega_b)\hat{b}_k(\omega_b)\, d\omega_b \qquad \hat{H}_I = \sum_{k=1}^{N} \int_{-\infty}^{\infty} i\left(f_k^*(\omega_b)\hat{b}^\dagger(\omega_b)\hat{a}_k - f_k(\omega_b)\hat{b}_k(\omega_b)\hat{a}_k^\dagger\right) d\omega_b. \tag{2.77}$$

Although there cannot be any modes with negative frequency, the range of integration is over the entire real line, rather than just the positive frequency values. As stated in Gardiner and Collett, this is only an idealisation, and can be accounted for by assuming that we are in a frame rotating with some angular frequency which gives the appearance of negative frequency modes; this frequency must also be larger than the bandwidth of the system modes, so the integral may be extended to negative infinity.

Heisenberg equations of motion can be written for the environment operators $\hat{b}_k(\omega_b; t)$, which now include some time dependence, along with arbitrary operators acting on the primary system $\hat{A}(t)$. The Heisenberg equation for $\hat{b}_k(\omega_b; t)$ can be formally solved and substituted into the Heisenberg equation for $\hat{A}(t)$ to yield the following:

$$\begin{aligned}\frac{d}{dt}\hat{A}(t) = i[\hat{H}_S(t), \hat{A}(t)] &- \sum_{k=1}^{N} \int_{-\infty}^{\infty} \Big(f_k(\omega_b)e^{-i\omega_b(t-t_0)}\hat{b}_k(\omega_b; t_0)[\hat{a}_k^\dagger(t), \hat{A}(t)] \\ &\qquad - f_k^*(\omega_b)e^{i\omega_b(t-t_0)}\hat{b}_k^\dagger(\omega_b; t_0)[\hat{a}_k(t), \hat{A}(t)]\Big) d\omega_b \\ &+ \sum_{k=1}^{N} \int_{-\infty}^{\infty} |f_k(\omega_b)|^2 \int_{t_0}^{t} \Big(e^{-i\omega_b(t-t')}[\hat{a}_k^\dagger(t), \hat{A}(t)]\hat{a}_k(t') \\ &\qquad - e^{i\omega_b(t-t')}\hat{a}_k^\dagger(t')[\hat{a}_k(t), \hat{A}(t)]\Big) dt'\, d\omega_b.\end{aligned} \tag{2.78}$$

The so-called *first Markov approximation* is now applied to the environment, which determines the time scale of the system and bath dynamics. As a result of the fleeting correlation time for the environment compared to the system, the response of the environment becomes almost flat as a function of frequency, ω_b. The coupling between the environment and the system is therefore assumed to be independent of frequency, which corresponds to the approximation $2\pi |f_k(\omega_b)|^2 \to \kappa_k$ in the above expression, where κ_k can be understood as a damping or decay rate; the coupling to the bath is therefore replaced by a frequency-independent damping term. From this point, the phase of the interaction between the system and bath resulting from the complex coefficient $f_k(\omega_b)$ will be ignored without loss of generality.

Now that the coupling has no frequency dependence, we will define an *input field* for a system mode in terms of the bath operators,

$$\hat{a}_{k,\mathrm{in}}(t) := \frac{1}{\sqrt{2\pi}} \int_{-\infty}^{\infty} e^{-i\omega_b(t-t_0)}\hat{b}_k(\omega_b; t_0)\, d\omega_b \quad \text{where} \quad [\hat{a}_{k,\mathrm{in}}(t), \hat{a}_{l,\mathrm{in}}^\dagger(t')] = \delta_{kl}\delta(t-t'). \tag{2.79}$$

With this definition, the differential equation for $\hat{A}(t)$ may be simplified to yield the *Heisenberg-Langevin equation*:

$$\begin{aligned}\frac{d}{dt}\hat{A}(t) = i[\hat{H}_S(t), \hat{A}(t)] + \sum_{k=1}^{N} \Bigg(&[\hat{a}_k^\dagger(t), \hat{A}(t)] \left(\sqrt{\kappa_k}\hat{a}_{k,\mathrm{in}}(t) + \frac{\kappa_k}{2}\hat{a}_k(t)\right) \\ &- \left(\sqrt{\kappa_k}\hat{a}_{k,\mathrm{in}}^\dagger(t) + \frac{\kappa_k}{2}\hat{a}_k^\dagger(t)\right)[\hat{a}_k(t), \hat{A}(t)]\Bigg).\end{aligned} \tag{2.80}$$

Further assuming that the form of the system Hamiltonian is identical to Eq. (2.36), the above equations can be used to construct equations of motion for the ladder operators of the system $\hat{a}_k^{(\dagger)}$,

$$\frac{d}{dt}\hat{a}_k^{(\dagger)}(t) = i[\hat{H}_S(t), \hat{a}_k^{(\dagger)}] - \frac{\kappa_k}{2}\hat{a}_k^{(\dagger)} - \sqrt{\kappa_k}\hat{a}_{k,\mathrm{in}}^{(\dagger)}(t), \tag{2.81}$$

along with the quadrature operators $\hat{r}_k$:

$$\begin{aligned}
&\frac{d}{dt}\hat{r}_k(t) = i[\hat{H}_S(t), \hat{r}_k(t)] - \frac{\kappa_k}{2}\hat{r}_k(t) - \sqrt{\kappa_k}\hat{r}_{k,\text{in}}(t) \\
\longrightarrow\ &\frac{d}{dt}\hat{\boldsymbol{r}}(t) = \mathbf{A}\hat{\boldsymbol{r}}(t) + \mathbf{f} - \sqrt{\boldsymbol{\kappa}}\hat{\boldsymbol{r}}_{\text{in}}(t) \quad \text{where} \quad \boldsymbol{\kappa} = \bigoplus_{k=1}^{N}\frac{\kappa_k}{2}\mathbf{I}_2\ ,\ \mathbf{A} = \boldsymbol{\Omega}\boldsymbol{H}^{(2)} - \frac{1}{2}\boldsymbol{\kappa}\ ,\ \mathbf{f} = \boldsymbol{\Omega}\boldsymbol{h}^{(1)}.
\end{aligned} \tag{2.82}$$

Here, $\hat{r}_{k,\text{in}}$ are the input-field operators in the quadrature basis, with the position and momentum input-field operators defined as $\hat{q}_{k,\text{in}} = (\hat{a}_{k,\text{in}} + \hat{a}^\dagger_{k,\text{in}})/\sqrt{2}$ and $\hat{p}_{k,\text{in}} = -i(\hat{a}_{k,\text{in}} - \hat{a}^\dagger_{k,\text{in}})/\sqrt{2}$. Compared to the derivation of the Lindblad master equation, no trace is performed over the bath, and hence no assumption has been made regarding the state of the bath. However, in order to turn the above Heisenberg-Langevin equation for the quadrature operators into dynamical equations for moments of a Gaussian state, the expectation value of the input-field operators will need to be considered, which will necessarily involve applying further approximations to the environment.

Input-Field Operators and Noise

The input-field operator represents a noise process impinging on the system due to its coupling with the environment. The form given in Eq. (2.79) corresponds to a wave packet of bath mode operators $\hat{b}(\omega_b; t_0)$, which is freely evolving under $\hat{H}_E$ starting at some earlier time t_0 until it interacts with the primary system at time t. The state of the primary system and environment are therefore assumed to be separable before any interaction occurs, at times $t \leq t_0$.

The input-field operators are assumed to correspond to *Gaussian white noise process*, meaning that they are determined entirely by their first two expectation values. Given that this is white noise, the mean must be zero, while the variance arises due to zero-point, or vacuum, fluctuations of the field, plus any additional increase in the variance due to thermal fluctuations. The expectation values of the input field are then:

$$\langle \hat{a}^{(\dagger)}_{k,\text{in}}(t)\rangle = 0 \qquad \langle \hat{a}_{j,\text{in}}(t)\hat{a}^\dagger_{k,\text{in}}(t')\rangle = (\bar{n}_k + 1)\delta_{jk}\delta(t-t') \qquad \langle \hat{a}^\dagger_{j,\text{in}}(t)\hat{a}_{k,\text{in}}(t')\rangle = \bar{n}_k\delta_{jk}\delta(t-t'). \tag{2.83}$$

Note that the thermal photon number $\bar{n}_k$ is not dependent on the frequency of the mode, and hence is flat as a function of the bath bandwidth. As a result, the state of the input field cannot be assumed to be a thermal state as in Eq. (2.69), since $\bar{n}_k$ would then have some frequency dependence [50]. We therefore impose the value of $\bar{n}_k$ to be the same as in Eq. (2.72) by hand. As a result of the above definitions, the input operators must have the following expectation value when written in the quadrature basis:

$$\langle \hat{r}_{k,\text{in}}(t)\rangle = 0 \qquad \langle \hat{r}_{j,\text{in}}(t)\hat{r}_{k,\text{in}}(t')\rangle = \left(\delta_{jk}\left(\bar{n}_k + \frac{1}{2}\right) + \frac{i}{2}\Omega_{jk}\right)\delta(t-t'). \tag{2.84}$$

With the above expression, along with Eq. (2.82), we can easily work out the dynamical equation for the moments:

$$\frac{d}{dt}\mu_k = \frac{d}{dt}\langle \hat{r}_k\rangle \qquad \frac{d}{dt}\sigma_{jk} = \frac{d}{dt}\left(\frac{1}{2}\langle \hat{r}_j\hat{r}_k + \hat{r}_k\hat{r}_j\rangle - \langle \hat{r}_j\rangle\langle \hat{r}_k\rangle\right). \tag{2.85}$$

It is easily confirmed that the dynamical equation for $\boldsymbol{\mu}$ is identical to the corresponding equation generated by the Lindblad master equation, while a bit more work is required for the covariance matrix. In order to evaluate the second order correlators, we can use the fact that the Heisenbeg-Langevin equations obey the usual rules of calculus, that is $\frac{d}{dt}(\hat{r}_j\hat{r}_k) = (\frac{d}{dt}\hat{r}_j)\hat{r}_k + \hat{r}_j(\frac{d}{dt}\hat{r}_k)$. To calculate the correlators of the form $\langle \hat{r}_j(\frac{d}{dt}\hat{r}_k)\rangle$ we must use both the differential equation in Eq. (2.82) along with its solution; the following formal solution may be written assuming that the system Hamiltonian has no explicit time dependence:

$$\hat{r}_j(t) = \mathrm{T}_{jl}(t, t_0)\hat{r}_l(t_0) - \int_{t_0}^{t}\mathrm{T}_{jl}(\tau, t_0)\left(\sqrt{\kappa_l}\hat{r}_{l,\text{in}}(\tau) - \mathrm{f}_l\right)d\tau \quad \text{where} \quad \mathbf{T}(t, t_0) = \exp\left[(t-t_0)\mathbf{A}\right]. \tag{2.86}$$

With this solution, the same-time correlation function between the system operator and the input field can also be worked out using the known correlation functions of the input fields, along with the assumption that both system and environment are uncorrelated at different times, $\langle \hat{r}_l(t_0), \hat{r}_{k,\text{in}}(t)\rangle = 0$, and so:

$$\frac{1}{2}\langle \hat{r}_j(t)\hat{r}_{k,\text{in}}(t) + \hat{r}_{k,\text{in}}(t)\hat{r}_j(t)\rangle = -\delta_{jk}\frac{\sqrt{\kappa_k}}{2}\left(\bar{n}_k + \frac{1}{2}\right). \tag{2.87}$$

By combining the various given expressions above into the definition from Eq. (2.85), we arrive at the desired result

for the moment differential equations:

$$\begin{aligned} &\frac{d}{dt}\langle \hat{r}_j\rangle = A_{jl}\langle \hat{r}_l\rangle + f_j \qquad &&\frac{d}{dt}\langle \hat{r}_j\hat{r}_k\rangle = A_{jl}\langle \hat{r}_l\hat{r}_k\rangle + \langle \hat{r}_j\hat{r}_l\rangle\big(A^T\big)_{lk} + \mathrm{f}_j\langle \hat{r}_k\rangle + \langle \hat{r}_j\rangle \mathrm{f}_k + \delta_{jk}\kappa_k\left(\bar{n}_k + \frac{1}{2}\right) \\ \longrightarrow \quad &\frac{d}{dt}\mu_j = A_{jl}\mu_l + f_j \qquad &&\frac{d}{dt}\sigma_{jk} = A_{jl}\sigma_{lk} + \sigma_{jl}\big(A^T\big)_{lk} + \delta_{jk}\kappa_k\left(\bar{n}_k + \frac{1}{2}\right). \end{aligned} \tag{2.88}$$

This confirms that the dynamics of the Gaussian moments obtained using the Heisenberg-Langevin equations, under the assumption that the environment is a Markovian thermal bath, are identical to those obtained using the Lindblad master equation, since the arrays in the above equations are the same as those in Eq. (2.76).

2.2.3.2 Time-Reversed Dynamics and Input-Output Theory

The Heisenberg-Langevin equation derived in the previous section relied on solving the Heisenberg equations for the environmental ladder operators using their initial conditions, $\hat{b}_k(\omega_b; t_0)$ where $t_0 < t$, however, it is also possible to construct a solution using the future state of the environmental modes after their interaction with the system, $\hat{b}_k(\omega_b; t_1)$ where $t_1 > t$. Using this solution, we can construct a time-reversed Heisenberg-Langevin equation for system operators:

$$\begin{aligned} \frac{d}{dt}\hat{A}(t) = i[\hat{H}_S(t), \hat{A}(t)] + \sum_{k=1}^{N}\Bigg(&[\hat{a}_k^\dagger(t), \hat{A}(t)]\left(\sqrt{\kappa_k}\hat{a}_{k,\mathrm{out}}(t) - \frac{\kappa_k}{2}\hat{a}_k(t)\right) \\ &- \left(\sqrt{\kappa_k}\hat{a}_{k,\mathrm{out}}^\dagger(t) - \frac{\kappa_k}{2}\hat{a}_k^\dagger(t)\right)[\hat{a}_k(t), \hat{A}(t)]\Bigg), \end{aligned} \tag{2.89}$$

where the damping on the system has been replaced with anti-damping in the reversed-time picture. The input-field operators have also been replaced by *output fields*, defined as:

$$\hat{a}_{k,\mathrm{out}}(t) := \frac{1}{\sqrt{2\pi}}\int_{-\infty}^{\infty} e^{-i\omega_b(t-t_1)}\hat{b}_k(\omega_b; t_1)\, d\omega_b \quad \text{where} \quad [\hat{a}_{k,\mathrm{out}}(t), \hat{a}_{l,\mathrm{out}}^\dagger(t')] = \delta_{kl}\delta(t-t'). \tag{2.90}$$

Whereas the input-field operators describe the environment before interaction with the primary system, the output-field operator describes the environment after this interaction, as the wave-packet propagates freely away from the system. In addition, since the initial state $\hat{\rho}_{\mathrm{in}}$ is Gaussian, by nature of the assumption that the input field is Gaussian white noise, then the state of the system at any time will remain Gaussian as a result of the linear dynamics of the Hamiltonian $\hat{H}_T$, including the state of the input field, $\hat{\rho}_{\mathrm{out}}$.

While the covariances of the input fields can be specified using the initial conditions of the environment, the covariances of the output fields rely on the knowledge of the system state since $\hat{\rho}_{\mathrm{out}}$ is dependent on the system-environment interaction. The relationship between these three quantities can be determined using the fact that the dynamics described by the time-forward and time-reversed Heisenberg-Langevin equations in Eqs. (2.80) and (2.89), respectively, must be identical. The interdependence between the input and output fields, along with the primary system, may then be expressed through the *input-output relation*:

$$\hat{a}_{k,\mathrm{out}}(t) - \hat{a}_{k,\mathrm{in}}(t) = \sqrt{\kappa_k}\hat{a}_k(t) \quad \text{or, equivalently,} \quad \hat{r}_{k,\mathrm{out}}(t) - \hat{r}_{k,\mathrm{in}}(t) = \sqrt{\kappa_k}\hat{r}_k(t). \tag{2.91}$$

As can be seen, in the absence of any interaction with the primary system, the input and output fields will be identical, $\hat{r}_{k,\mathrm{out}}(t) = \hat{r}_{k,\mathrm{in}}(t)$. The ability to model the bath before and after interaction is the key difference between the input-output formalism and the Lindblad master equation approach, where only the dynamics of the primary system may be calculated. This is incredibly useful when dealing with systems where the environment itself can be observed, such as when the primary system is composed of ported modes connected to some external wiring or transmission line. The input-output formalism also allows for each mode to be connected to multiple environments, representing monitored and unmonitored environments; examples of the latter include material defects, which result in losses to an environment which cannot be observed. In this work, we will consider such loss channels as insignificant and so only consider systems with observable propagating fields.

2.2.3.3 Scattering Relations and the Frequency Domain

The input-output relation in Eq. (2.91) can also be interpreted as a scattering process, where the primary system represents a scattering centre for the propagating environmental field operators. To develop this viewpoint, it is more convenient to work in frequency space, and to this end, we define the Fourier transform of a time-dependent operator,

along with the inverse transformation, using the unitary Fourier transform convention:

$$\mathcal{F}[\hat{A}(t)](\omega) = \frac{1}{\sqrt{2\pi}} \int_{-\infty}^{\infty} e^{i\omega t} \hat{A}(t)\, dt =: \hat{A}[\omega] \qquad \mathcal{F}^{-1}[\hat{A}[\omega]](t) = \frac{1}{\sqrt{2\pi}} \int_{-\infty}^{\infty} e^{-i\omega t} \hat{A}[\omega]\, d\omega = \hat{A}(t). \tag{2.92}$$

Applying this Fourier transform to the mode operators, we define $\mathcal{F}[\hat{a}_k(t)](\omega) \equiv \hat{a}_k[\omega]$ and $\mathcal{F}[\hat{a}_k^\dagger(t)](\omega) \equiv \hat{a}_k^\dagger[\omega]$. Note that, due to the complex exponential in the Fourier transform, $\hat{a}_k^\dagger[\omega]$ is no longer the conjugate-transpose of $\hat{a}_k[\omega]$, which is instead $(\hat{a}_k[\omega])^\dagger = \hat{a}_k^\dagger[-\omega]$. The Hermiticity of operators is also not preserved under the Fourier transform since the transpose operation will also change the sign of the frequency argument; hence for the quadrature operators $\mathcal{F}[\hat{r}_k(t)](\omega) \equiv \hat{r}_k[\omega]$ it must be noted that $(\hat{r}_k[\omega])^\dagger = \hat{r}_k[-\omega]$.

Focusing on the scattering of the quadrature operators undergoing linear dynamics, the Fourier transform is applied to the Heisenberg-Langevin equation in Eq. (2.82) to yield the following linear system of equations in the frequency domain:

$$-i\omega \hat{\boldsymbol{r}}[\omega] = \mathbf{A}\hat{\boldsymbol{r}}[\omega] + \mathbf{f} - \sqrt{\boldsymbol{\kappa}}\hat{\boldsymbol{r}}_{\mathrm{in}}[\omega]. \tag{2.93}$$

The input-output relation in Eq. (2.91) may also be transformed to generate an equivalent relation between frequency-dependent operators:

$$\hat{\boldsymbol{r}}_{\mathrm{out}}[\omega] - \hat{\boldsymbol{r}}_{\mathrm{in}}[\omega] = \sqrt{\boldsymbol{\kappa}}\hat{\boldsymbol{r}}[\omega]. \tag{2.94}$$

A scattering relation may be obtained using these two expressions, which is applicable only in the steady state, where any dependence of the internal mode on its initial state has decayed away. In this instance, the internal state of the primary system is solely a function of the noise from the input fields; this may be determined from Eq. (2.86), where the presence of decay within the system will ensure that in the infinite time limit $\lim_{t\to\infty} \mathrm{T}_{jl}(t, t_0) = 0$. The scattering relation is therefore only explicitly dependent on the input and output fields:

$$\hat{\boldsymbol{r}}_{\mathrm{out}}[\omega] = \mathbf{S}[\omega]\hat{\boldsymbol{r}}_{\mathrm{in}}[\omega] + \mathbf{V}[\omega]\mathbf{f} \quad \text{where} \quad \begin{aligned} \mathbf{S}[\omega] &:= \sqrt{\boldsymbol{\kappa}}(\mathbf{A} + i\omega\mathbf{I}_{2N})^{-1}\sqrt{\boldsymbol{\kappa}} + \mathbf{I}_{2N}, \\ \mathbf{V}[\omega] &:= \sqrt{\boldsymbol{\kappa}}(\mathbf{A} + i\omega\mathbf{I}_{2N})^{-1}. \end{aligned} \tag{2.95}$$

The matrix $\mathbf{S}[\omega]$ is called the scattering matrix, and contributes two terms to the output field: the scattering of the input fields off the primary system, along with an added term for the input field which is always present in the environment. The other matrix $\mathbf{V}[\omega]$ corresponds to the displacement of the input field scattering off the primary system, which only occurs when the primary system is itself displaced by some other field $\mathbf{f}$. This can occur when there are linear drive terms in the Hamiltonian, represented in the quadrature basis by the vector $\mathbf{f} = \boldsymbol{\Omega}\boldsymbol{h}^{(1)}$. Since these drive terms may be applied through the port, they may be included in a redefined input field $\tilde{\boldsymbol{r}}_{\mathrm{in}}[\omega] = \hat{\boldsymbol{r}}_{\mathrm{in}}[\omega] - \boldsymbol{\kappa}^{-1/2}\mathbf{f}$, allowing for the entire scattering relation in Eq. (2.95) to be described by $\mathbf{S}[\omega]$ only. In this case, the input fields have identical second moments but non-zero means. While only the relations for the quadrature operators are provided here, similar expressions may be obtained for the ladder operators using the Heisenberg-Langevin equation in Eq. (2.81), along with the input-output relation Eq. (2.91).

Further insight into the scattering process may be gleaned by Fourier transforming the input and output-field operators from Eqs. (2.79) and (2.90):

$$\hat{a}_{k,\mathrm{in}}[\omega] = \mathcal{F}[\hat{a}_{k,\mathrm{in}}(t)](\omega) = e^{i\omega t_0}\hat{b}_k(\omega; t_0) \qquad \hat{a}_{k,\mathrm{out}}[\omega] = \mathcal{F}[\hat{a}_{k,\mathrm{out}}(t)](\omega) = e^{i\omega t_1}\hat{b}_k(\omega; t_1). \tag{2.96}$$

The Fourier-transformed operators are the bath mode operators in the interaction picture at the initial and final times, t_0 and t_1, respectively. The entirety of the system evolution is therefore subsumed within the scattering relation, which takes the bath operator from its initial to final-time configurations.

Given that the state of the bath and the system in the time domain are Gaussian states, this property also carries over to the corresponding objects in the frequency domain. We can therefore characterise the input and output fields entirely by their first and second moments. The correlation functions for the input fields can be obtained by expressing the frequency-domain operators as the Fourier transform of their respective time-domain operators, and then using the known time-domain correlators; when the correlators of the input fields correspond to thermal noise, as in Eq. (2.83), the equivalent expressions in the frequency domain are:

$$\langle \hat{a}_{j,\mathrm{in}}^{(\dagger)}[\omega] \rangle = 0 \qquad \langle \hat{a}_{j,\mathrm{in}}[\omega]\hat{a}_{k,\mathrm{in}}^\dagger[\omega'] \rangle = (\bar{n}_j + 1)\delta_{jk}\delta(\omega + \omega') \qquad \langle \hat{a}_{j,\mathrm{in}}^\dagger[\omega]\hat{a}_{k,\mathrm{in}}[\omega'] \rangle = \bar{n}_j\delta_{jk}\delta(\omega + \omega'). \tag{2.97}$$

The input noise is therefore still Gaussian white noise in the frequency domain. The correlators for the output fields can then be constructed entirely using the above expressions, as indicated by the scattering relation in Eq. (2.95).

Compact expressions for the moments can be obtained for the steady-state input and output fields, which oscillate resonantly with the fundamental frequencies of the primary system modes; provided we are in an interaction picture where we rotate with the bare frequencies of the system modes, the resonance frequency will be given by $\omega = 0$.

The steady-state correlators of the input and output fields on resonance therefore correspond to the correlators of $\hat{a}_{k,\mathrm{in}}[0] = \lim_{t_0\to-\infty}\hat{b}_k(0;t_0)$ and $\hat{a}_{k,\mathrm{out}}[0] = \lim_{t_1\to\infty}\hat{b}_k(0;t_1)$, respectively. The mean of the input fields is still zero, $\mu_{\mathrm{in},k} = 0$, while the mean of the output fields depends on the presence or absence of any displacement in the primary system, $\mu_{out,k} = \mathrm{V}_{kj}[0]\mathrm{f}_j$. Finally, the steady-state covariance matrices on resonance may be expressed as follows:

$$\boldsymbol{\sigma}_{\mathrm{in}} = \bigoplus_{k=1}^{N}\left(\bar{n}_k + \frac{1}{2}\right)\mathbf{I}_2 \quad \text{and} \quad \boldsymbol{\sigma}_{\mathrm{out}} = \mathbf{S}[0]\boldsymbol{\sigma}_{\mathrm{in}}\mathbf{S}^T[0], \tag{2.98}$$

where $\boldsymbol{\sigma}_{\mathrm{in}}$ is the covariance matrix of an uncorrelated N-mode thermal state, and $\boldsymbol{\sigma}_{\mathrm{out}}$ is obtained using the scattering relation. Interestingly, the scattering matrix on resonance, when written in the quadrature basis, corresponds to a real symplectic matrix; as noted in Section 2.1.4, this means that $\mathbf{S}[0]$ corresponds to a unitary transformation of the propagating input fields.

2.2.4 Applicability of the Lindblad and Heisenberg-Langevin Equations

In this section, we have reviewed two approaches for modelling open quantum systems with Markovian environments: the Lindblad master equation and the Heisenberg-Langevin equations. While both approaches yield identical equations of motion for the moments of a Gaussian state in the primary system, their treatment of the environment results in different scopes of application. Additionally, since the Lindblad master equation traces over the environment, it provides a practical means for solving the density operator of the primary system. The Heisenberg-Langevin equations, on the other hand, do not constitute a practical approach to solving the dynamics of the primary system operators outside of expectation values, since the input and output fields are still treated as a continuum of bath modes. The upside is that these propagating fields allow one to actually model the state of the bath, which is not possible in the Lindblad master equation; this allows for the construction of the invaluable input-output theory, along with scattering relations for the bath fields.

It may then be surprising that both methods yield the same dynamics for the internal modes, especially given that the microscopic derivation of the Lindblad master equation invokes the Born approximation, where the state of the bath is assumed to be unaffected by the system dynamics. The input-output relations obviously rely on the fact that the interaction between the environment and system does, in fact, change the state of the former. This contradiction then prompts the question: why do both approaches result in the same dynamics for the primary system?

For the master equation, the Born approximation results in a bath which only evolves under its own Hamiltonian, and hence is always in the same initial state when working in the interaction picture. In the Heisenberg-Langevin equations, the input field also only evolves under its own Hamiltonian while the wave propagates towards the system, and hence it is treated as if it is unaffected by the system until the time of interaction. The result of this interaction is the output field, but since this is assumed to propagate away from the system and never interact with the incoming input fields, the fact that the "state" of the bath has been changed is irrelevant. We can then conclude that the reason for this apparent equivalence when modelling the internal system is that both approaches, when combined with the Markov approximation, result in an environment which is an unchanging Gaussian white noise process from the point of view of the primary system; since we have set the correlation functions for both approaches to be identical, the expectation values for the internal states must also be the same.

When considering the state of the primary system, both approaches can therefore be used interchangeably. However, the systems in this work are to be treated as *ported* devices, where the internal modes are connected to some transmission lines which can send and receive signals, with the primary system as the intermediary. Since these signals are to be modelled as propagating input and output fields, the behaviour of the environment is to be understood from the perspective of the Heisenberg-Langevin equations and input-output theory. This formalism is incredibly useful for modelling the signals emanating from amplifiers, where the amplification of incoming signals is described entirely by the scattering matrix, without the need to concern oneself with the internal state of the system, which only acts as a scattering centre. In the next section, this formalism will be put to work, as we introduce how these amplifiers may be engineered through the appropriate driving of parametrically coupled systems.

2.3 Parametric Coupling in Quantum Systems

In this section, we will introduce the concept of *parametric couplings*, whereby different interactions between coupled harmonic modes may be specifically engineered through the modulation of system parameters. The control afforded by this modulation will allow for interactions to be made resonant between systems which are otherwise weakly coupled or otherwise off-resonant due to differences in fundamental frequencies. Portions of this section are inspired by the reviews of parametrically coupled physics in Refs. [51, 52]. This section will use parametric couplings in

superconducting circuits as a motivating physical example, though the formalism presented is not specific to this platform.

2.3.1 Engineering Parametrically Modulated Interactions

Parametric couplings may be written generically as $\mathrm{M}(t)\,\hat{r}_j\hat{r}_k$, where two quadrature operators are coupled via a time-dependent modulation term $\mathrm{M}(t)$. Such an interaction is intrinsically nonlinear since it involves the coupling of two quadrature operators with the modulation term, which is controlled through some other system, which we will call a *pump*. Although the preceding sections were concerned with Gaussian states and linear dynamics, provided that the pumps are treated as classical-like systems with large amplitudes, and the interaction between the harmonic modes is at most quadratic, these systems may be modelled using the formalism for Gaussian states and transformations.

In the superconducting circuit platform, these harmonic modes correspond to the resonances of the electromagnetic field in some superconducting material. The quantised resonant modes are modelled as LC-circuits using a lumped-element model [53], which oscillate at their own resonance frequency given by $\omega_r = 1/\sqrt{LC}$, where C and L are the capacitance and inductance. The quantum LC-circuits behave as independent harmonic oscillators, with quantised magnetic flux $\hat{\Phi}$ and charge $\hat{Q}$ serving as canonical variables, $[\hat{\Phi}, \hat{Q}] = \pm i$, where the choice of sign depends on convention; for further details on the quantisation of circuits, refer to Chapter 4.

The nonlinear coupling between the quantised modes is engineered through the use of *Josephson junctions* [54, 55], where an insulating barrier is placed between two superconductors. The nonlinearity is a result of the Josephson effect, where a supercurrent, comprised of tunnelling electron Cooper pairs, flows across the barrier in the absence of an applied voltage; this effect may be described using the Josephson equations [56]:

$$I(t) = I_c \sin(2\pi\Phi(t)/\Phi_0) \qquad \frac{d}{dt}\Phi(t) = V(t). \tag{2.99}$$

Here, $\Phi(t) = \Phi_0\varphi/2\pi$ is the magnetic flux, $\Phi_0 = h/2e$ is the unit of quantisation called the magnetic flux quantum, and φ is the difference in phase of the supercurrent across the junction. The final parameter I_c is called the critical current and represents the maximum value of the supercurrent. These expressions demonstrate the dependence of the current I and voltage V across the junction on the magnetic flux in the circuit, and can be used to calculate the inductance of the Josephson junction:

$$V(t) = L(\Phi)\frac{d}{dt}I(t) \quad \longrightarrow \quad L(\Phi) = \frac{\Phi_0}{2\pi\cos(2\pi\Phi/\Phi_0)}. \tag{2.100}$$

The Josephson junction is therefore a nonlinear inductor, and it is this property which will allow for the nonlinear mixing required for parametric coupling. The energy stored in this inductor corresponds to a potential when constructing a Hamiltonian for the system, which is termed the Josephson potential, $\hat{H}_{JJ} = -(I_c\Phi_0/2\pi)\cos(2\pi\hat{\Phi}/\Phi_0)$.

Keeping with the lumped element model, connecting the LC-circuits and Josephson junction in a single circuit allows for nonlinear mixing of the resonant mode fluxes due to the fact that $\hat{H}_{JJ}$ is a nonlinear function of the magnetic flux across the junction. While a single Josephson junction can be used for nonlinear mixing, the simple cosine potential, $\hat{H}_{JJ} \propto \cos(\varphi)$, means that the dominant nonlinear term has a fourth-order dependence on the phase across the junction. The nonlinearity φ^4 term not only provides the necessary mixing for parametric modulation, but also results in so-called *Kerr terms* of a similar magnitude which cause large undesired nonlinear shifts in the fundamental frequencies ω_r of the resonant harmonic modes as the pumps are modulated [57]. In order to avoid this, it is preferable to have a leading nonlinear term of order φ^3 in the potential. This is achieved by using loops with multiple Josephson junctions instead of a singular junction; numerous circuit designs combining both Josephson junctions and LC-circuits are present in the literature. Some specific Josephson junction configurations which have been used to create parametric amplifiers [14] are: the DC-SQUID [14, 58–60], SLUG [61–64], SNAIL [65–67][3], and Josephson Ring Modulator (JRM) [18, 68–72].

Operation of these Josephson loops is dependent on the threading of an external direct current (DC) magnetic flux through the loop; this induces a DC bias current within the Josephson loop to oppose the change in magnetic flux. The nonlinear nature of the Josephson loop potential results in nonlinear mixing of the harmonic modes' fluxes and the DC bias flux Φ_b. The DC bias flux acts as a quasi-static operating point, and it is by varying the external magnetic flux about this flux-bias point that parametric modulation is achieved in these systems. The choice of DC flux-bias will also shift the frequencies of the resonant modes, $\omega_{r,\mathrm{eff}} = 1/\sqrt{L_\mathrm{eff}C}$, since connecting to the Josephson loop means the effective inductance L_eff for each resonant mode is now dependent on Φ_b.

A general Hamiltonian may be written as $\hat{H} = \hat{H}_0 + \hat{H}_V$, where $\hat{H}_0$ is the free Hamiltonian for the independent

[3]The mollusc-themed device acronyms are the superconducting quantum interference device (SQUID), Superconducting Low-Inductance Undulatory Galvanometer (SLUG), and Superconducting Nonlinear Asymmetric Inductive Element (SNAIL).

resonant harmonic modes, where ω_j are the mode frequencies for a fixed DC flux-bias. The potential term $\hat{H}_V$ contains the nonlinear mixing terms of the harmonic mode quadratures due to the Josephson junction loop:

$$\hat{H}_0 = \sum_j \omega_j \hat{a}_j^\dagger \hat{a}_j \qquad \hat{H}_V = \sum_{j,k} c_{jk}^{(2)} \hat{r}_j \hat{r}_k + \sum_{j,k,l} c_{jkl}^{(3)} \hat{r}_j \hat{r}_k \hat{r}_l + \dots \,, \; \hat{r}_j = \frac{1}{\sqrt{2}} \left(\hat{a}_j^\dagger e^{-i\phi_j} + \hat{a}_j e^{i\varphi_j} \right). \tag{2.101}$$

It is to be understood that the potential $\hat{H}_V$ is a Taylor expansion about the quasi-static DC flux-bias Φ_b; note that the sums in $\hat{H}_V$ may include coupling between quadratures of the same mode. It is the modulation of the coefficients in the series expansion of $\hat{H}_V$ which gives rise to the desired parametric coupled system.

This may be achieved by modulating the second-order quadrature coupling parameters in time, as was done in Ref. [19]. In that work, the DC flux is varied by applying additional alternating current (AC) charge drives on top of the DC current. This generates AC magnetic flux threading the loop on top of the DC magnetic flux, causing oscillations in the Josephson loop about the DC flux-bias point. This results in the modulation of $c_{jk}^{(2)}(t)$ necessary for parametric couplings, where the amplitude and frequency are controlled using the current and frequency of the AC charge drive, respectively. In addition, multiple pump tones can be realised through a superposition of multiple AC currents.

Alternatively, the third-order quadrature coupling (or three-wave mixing) terms may be used to generate the necessary pumping, as in the case of the JRM in Refs. [57, 67]. In these setups, the pumping is achieved by driving one of the resonant harmonic modes through its port, resulting in an effective displacement of the mode quadratures by the time-dependent pump field, $\hat{a}_j \to \hat{a}_j + \alpha_j^\mathrm{p}(t)$. Because the three-wave mixing of the quantised magnetic fluxes dominates, the field used to pump one of the modes generates parametric modulation of the interaction between the *other* two resonant modes in the third-order interaction.

In both of these cases, incorporating the effects of the pumping into $\hat{H}_V$ results in an explicitly time-dependent parametrically modulated Hamiltonian; the simplest pumping scheme will yield the following

$$\hat{H}_V^\mathrm{p}(t) = \sum_{j,k,l} 2g_{jk}^{(l)} \cos(\omega_l^\mathrm{p} t + \phi_l^\mathrm{p}) \left(\hat{a}_j^\dagger e^{i\phi_j} + \hat{a}_j e^{-i\phi_j} \right) \left(\hat{a}_k^\dagger e^{i\phi_k} + \hat{a}_k e^{-i\phi_k} \right) + \text{nonlinear terms}. \tag{2.102}$$

Here, ω_l^p is the frequency of the pump tone, and ϕ_l^p is the phase of the complex pump amplitude, $\alpha_l^\mathrm{p} = |\alpha_l^\mathrm{p}|\, e^{i\phi_l^\mathrm{p}}$; the pump amplitude has been absorbed into the constant coupling rate, $g_{jk}^{(l)} \propto |\alpha_l^\mathrm{p}|$. The *stiff-pump approximation* has therefore been invoked, resulting in a pump amplitude which is identical at the input and output, and so is assumed to be constant in time, $\alpha_l^\mathrm{p}(0) = \alpha_l^\mathrm{p}(t)$. The pump field is therefore assumed to be constant in the face of added sources of noise, say due to quantum fluctuations, and is not diminished by its pumping of the parametric interaction. Since the energy from pump photons are consumed in the process of linear parametric amplification, this approximation can break down in cases, leading to pump depletion [73] and an amplifier with a nonlinear relation between its input and output power. To ensure that the approximation is always valid, we assume that the amplitudes of all pumps are large in comparison to the amplitude of all output fields.

As will be shown in the next section, parametric modulation of these interactions will require precise tuning of the pump frequencies ω^p based on the fundamental frequencies of the modes. This requirement means that, while the pumps cannot be too weak if the stiff-pump approximation is to be invoked, they can also not be too strong, since the frequencies of the resonant modes are dependent on the applied flux-bias. Sufficiently large variations about the DC flux-bias therefore result in nonlinear oscillations of the mode frequencies, which creates difficulty in matching the pump frequencies with the mode frequencies. The origin of this effect comes from the nonlinear terms in Eq. (2.102), specifically the self-Kerr terms, which create shifts in the frequencies of the system modes dependent on the pump power. While their effect is taken to be negligible in this work, the need to suppress these Kerr terms still motivates recent work directed at realising Kerr-free potentials [57, 74].

2.3.2 Resonant and Off-Resonant Interactions

As evidenced in Eq. (2.102), pumping nonlinearly coupled systems gives rise to a system which may be approximately modelled as Gaussian, provided that any Kerr-terms are sufficiently small. Depending on the choice of pump frequency, ω^p, certain parametric interactions will be resonant, and so dominate the interaction between the coupled harmonic modes, while others will be rendered off-resonant, allowing us to ignore their impact on the dynamics of the system. In this section, we will see how modulation of the pump provides the ability to select which interactions we wish to make resonant, and which assumptions must be invoked in order to do so. We start with a toy system comprised of two harmonic modes with an interaction which is parametrically modulated by a single pump tone:

$$\hat{H}^\mathrm{p} = \omega_j \hat{a}_j^\dagger \hat{a}_j + \omega_k \hat{a}_k^\dagger \hat{a}_k + 2g \cos\left(\omega^\mathrm{p} t + \phi^\mathrm{p}\right) \left(\hat{a}_j^\dagger e^{i\phi_j} + \hat{a}_j e^{-i\phi_j} \right) \left(\hat{a}_k^\dagger e^{i\phi_k} + \hat{a}_k e^{-i\phi_k} \right). \tag{2.103}$$

The single pump tone will only allow us to drive one interaction between the two modes; more pump tones are therefore required to realise additional resonant interactions. To determine which interactions are rendered resonant for different choices of the pump frequency ω^{p}, we move into an interaction picture rotating with the frequencies ω_j and ω_k via the unitary transformation $\hat{U}(t) = \exp[it(\omega_j \hat{a}_j^\dagger \hat{a}_j + \omega_k \hat{a}_k^\dagger \hat{a}_k)]$:

$$\begin{aligned}\hat{H}_I^{\mathrm{p}} &= g\left(e^{i(\omega^{\mathrm{p}}t+\phi^{\mathrm{p}})} + e^{-i(\omega^{\mathrm{p}}t+\phi^{\mathrm{p}})}\right)\left(\hat{a}_j^\dagger e^{i(\omega_j t+\phi_j)} + \hat{a}_j e^{-i(\omega_j t+\phi_j)}\right)\left(\hat{a}_k^\dagger e^{i(\omega_k t+\phi_k)} + \hat{a}_k e^{-i(\omega_k t+\phi_k)}\right)\\ &= g\Big(\hat{a}_j^\dagger \hat{a}_k^\dagger e^{i(\omega_j+\omega_k-\omega^{\mathrm{p}})t} e^{i(\phi_j+\phi_k-\phi^{\mathrm{p}})} + \hat{a}_j^\dagger \hat{a}_k e^{i(\omega_j-\omega_k-\omega^{\mathrm{p}})t} e^{i(\phi_j-\phi_k-\phi^{\mathrm{p}})}\\ &\qquad + \hat{a}_j^\dagger \hat{a}_k^\dagger e^{i(\omega_j+\omega_k+\omega^{\mathrm{p}})t} e^{i(\phi_j+\phi_k+\phi^{\mathrm{p}})} + \hat{a}_j^\dagger \hat{a}_k e^{i(\omega_j-\omega_k+\omega^{\mathrm{p}})t} e^{i(\phi_j-\phi_k+\phi^{\mathrm{p}})} + \mathrm{h.c.}\Big).\end{aligned} \tag{2.104}$$

Depending on the choice of pump frequency, certain terms can be rendered time-independent, and therefore resonant, in the interaction picture; terms which are still time-dependent after the pump frequencies have been selected are called *counter-rotating* (CR) terms. The goal is to ensure that these CR terms are off-resonant, and so are oscillating with sufficiently high frequencies that their effect on the system dynamics may be neglected; provided that they are, we may invoke the *rotating-wave approximation* (RWA), and discard the CR terms. The frequencies ω_j and decay rates κ_j of the harmonic modes must satisfy certain properties for the CR to be ignored, and hence for the RWA to be valid. In order to explain the assumptions that must be made, we must examine the response functions of the harmonic modes.

Response in the Frequency Domain

In this discussion on parametrically coupled physics, we have so far omitted the fact that these modes are to be treated as ported open systems if they are to be used for signal processing. Since the modes now have some finite decay rate, κ_j, their response is no longer discretely peaked at their fundamental frequency, ω_j, but has some finite width. In order to determine the bare response of a ported harmonic mode in the absence of coupling to any other mode, we start with the free Hamiltonian for a harmonic oscillator $\hat{H}_0 = \omega_j \hat{a}_j^\dagger \hat{a}_j$, which is coupled to an environment with damping rate κ_j. The dynamics of the open system can be represented using the Heisenberg-Langevin equation from Eq. (2.81), which yields the following equations:

$$\frac{d}{dt}\hat{a}_j(t) = -\left(\frac{\kappa_j}{2} + i\omega_j\right)\hat{a}_j(t) - \sqrt{\kappa_j}\hat{a}_{j,\mathrm{in}}(t) \xrightarrow{\text{Fourier}} \hat{a}_j[\omega] = -\sqrt{\kappa_j}\chi_j(\omega-\omega_j)\hat{a}_{j,\mathrm{in}}[\omega]. \tag{2.105}$$

The function $\chi_j(\omega) := (\kappa_j/2 - i\omega)^{-1}$, where $\chi_j(\omega) = \chi_j^*(-\omega)$, is the susceptibility, and its magnitude corresponds to the fundamental response of the mode $\hat{a}^{(\dagger)}[\omega]$ in the frequency domain. The magnitude-squared gives an idea about the shape of this function in the frequency domain,

$$|\chi_j(\omega-\omega_j)|^2 = \frac{1}{(\kappa_j/2)^2 + (\omega-\omega_j)^2}, \tag{2.106}$$

which corresponds to a Lorentzian line shape centred at the resonant frequency for the mode, ω_j, with the characteristic linewidth[4] given by the decay rate κ_j. We can therefore interpret Eq. (2.105) as saying that a driving term applied to $\hat{a}_j$ through its port will result in a response with the line shape $\kappa_j |\chi_j(\omega-\omega_p)|^2$ in frequency space. For the conjugate operator, $\hat{a}_j^\dagger(t)$, the susceptibility is $\chi_j(\omega+\omega_j)$, and therefore the response is centred at the negative frequency, $-\omega_j$. To ensure that $\hat{a}_j$ constitutes a distinct mode in frequency space, we require that the response functions be sharply peaked around the resonant frequency, and so the linewidth must be small compared to the fundamental frequency, that is, $\kappa_j \ll \omega_j$.

If we now include modulated coupling to another mode $\hat{a}_k$, as in the pumped Hamiltonian Eq. (2.103), then the dynamical equation for $\hat{a}_j(t)$ and corresponding frequency domain equation for $\hat{a}_k[\omega]$ are:

$$\begin{aligned}&\frac{d}{dt}\hat{a}_j(t) = -\left(\frac{\kappa_j}{2} + i\omega_j\right)\hat{a}_j(t) - \sqrt{\kappa_k}\hat{a}_{j,\mathrm{in}}(t) - 2ige^{i\phi_j}\cos(\omega^{\mathrm{p}}t+\phi^{\mathrm{p}})\left(\hat{a}_k^\dagger(t)e^{i\phi_k} + \hat{a}_k(t)e^{-i\phi_k}\right)\\ \longrightarrow\ &\hat{a}_j[\omega] = \chi_j(\omega-\omega_j)\Big(-\sqrt{\kappa_j}\hat{a}_{j,\mathrm{in}}[\omega] - ige^{i(\phi_j+\phi^{\mathrm{p}})}\left(\hat{a}_k^\dagger[\omega+\omega^{\mathrm{p}}]e^{i\phi_k} + \hat{a}_k[\omega+\omega^{\mathrm{p}}]e^{-i\phi_k}\right)\\ &\qquad - ige^{i(\phi_j-\phi^{\mathrm{p}})}\left(\hat{a}_k^\dagger[\omega-\omega^{\mathrm{p}}]e^{i\phi_k} + \hat{a}_k[\omega-\omega^{\mathrm{p}}]e^{-i\phi_k}\right)\Big).\end{aligned} \tag{2.107}$$

The other mode will naturally have its own response function defined by the susceptibility $\chi_k(\omega-\omega_k)$, with linewidth κ_k, and peaks at ω_k and $-\omega_k$ for $\hat{a}_k[\omega]$ and $\hat{a}_k^\dagger[\omega]$, respectively. It is again required that $\kappa_k \ll \omega_k$ for a_k to be a

[4]The linewidth is technically defined as the "full width at half maximum" (FWHM) of the Lorentzian function.

distinct mode, but since there is now some non-zero overlap between the response functions for both modes, if we wish for the modes to be nondegenerate then both response functions must also be well separated in frequency space, meaning that ω_j and ω_k must far apart compared to the decay of the two Lorentzian response functions.

Examining Eq. (2.107), it may be seen that the single pump tone results in couplings between $\hat{a}_j[\omega]$ and the mode $\hat{a}_k[\omega']$ at four different frequencies. An appropriate choice of pump frequency will render some of these terms off-resonant, so that their interaction with $\hat{a}_j[\omega]$ may be neglected; this assumption is just the RWA, but from the point of view of the frequency, rather than the time, domain. The expression for $\hat{a}_j[\omega]$ in Eq. (2.107) also demonstrates that in order for the RWA to be applied, the pump amplitude g must also be sufficiently small. Since the response of $\hat{a}_j[\omega]$ to these other frequency domain "modes" is governed by $g^2\left|\chi_j(\omega-\omega_j)\right|^2$, if g is large enough then the response function will not decay fast enough at frequencies away from ω_j to justify the use of the RWA. To ensure the response functions remain distinct and well separated, it is generally required that the coherent coupling rate must be much smaller than the mode frequencies, $g_{jk} \ll \omega_j, \omega_k$. This demonstrates the utility of working in the frequency domain, since this assumption would not be immediately evident by examining the time-dependent Hamiltonian in Eq. (2.104) alone.

2.3.3 Frequency Conversion and Amplification

Parametrically coupled systems are composed of two basic two-mode interactions, which are often termed frequency conversion (FC) and parametric amplification (PA) in the language of parametrically coupled systems; we will alternatively use the more optically motivated terms of beam splitter (BS) and single- and two-mode squeezing (SMS and TMS) when discussing these interactions. With the necessary assumptions laid out, we are now ready to provide a practical demonstration of how these interactions can be made resonant using parametric modulation. Since these interactions induce linear dynamics for the system modes, the formalism introduced in the previous sections for handling linear Gaussian systems, particularly the input-output theory from Section 2.2.3, will be crucial here.

Frequency Conversion

The first interaction we will consider is frequency conversion, so named because it exchanges photons between two harmonic modes with unequal frequencies. This interaction is made resonant by pumping at the difference of the mode frequencies, $\omega^{\mathrm{p}} = |\omega_j - \omega_k|$, where we assume that this is satisfied exactly, so there is no pump detuning. The interaction Hamiltonian may then be written as

$$\hat{H}_I^{\mathrm{p}}(t) = \hat{H}_{\mathrm{FC}} + \hat{H}_{\mathrm{CR}}(t) \quad \text{where} \quad \hat{H}_{\mathrm{FC}} = g_{jk}\left(\hat{a}_j^\dagger \hat{a}_k e^{i\phi} + \hat{a}_j \hat{a}_k^\dagger e^{-i\phi}\right)\ ,\ \phi := \phi_j - \phi_k \pm \phi^{\mathrm{p}}, \tag{2.108}$$

where $\hat{H}_{\mathrm{CR}}(t)$ contains the CR terms, comprised of parametric amplification and frequency conversion processes which have some explicit time-dependence at this pump frequency. Applying the RWA, we take these counter-rotating terms to be off-resonant, and eliminate them from the dynamics, leaving only $\hat{H}_{\mathrm{FC}}$. Continuing to work in this rotating frame, we can write the Heisenberg-Langevin equations for the mode operators using Eq. (2.81):

$$\frac{d}{dt}\hat{\boldsymbol{a}}_{\mathrm{FC}}(t) = \tilde{\mathbf{A}}_{\mathrm{FC}}\hat{\boldsymbol{a}}_{\mathrm{FC}}(t) - \sqrt{\boldsymbol{\kappa}_{\mathrm{FC}}}\hat{\boldsymbol{a}}_{\mathrm{FC,in}}(t)\ ,\ \tilde{\mathbf{A}}_{\mathrm{FC}} = \begin{pmatrix}\mathbf{A}_{\mathrm{FC}} & \mathbf{0}_2\\ \mathbf{0}_2 & \overline{\mathbf{A}}_{\mathrm{FC}}\end{pmatrix}\ ,\ \mathbf{A}_{\mathrm{FC}} = \begin{pmatrix}-\kappa_j/2 & -ie^{i\phi}g_{jk}\\ -ie^{-i\phi}g_{jk} & -\kappa_k/2\end{pmatrix}, \tag{2.109}$$

where $\hat{\boldsymbol{a}}_{\mathrm{FC}} = (\hat{a}_j, \hat{a}_k, \hat{a}_j^\dagger, \hat{a}_k^\dagger)$ is the vector of modes operators, and $\tilde{\boldsymbol{\kappa}}_{\mathrm{FC}} = \mathrm{diag}(\kappa_j, \kappa_k, \kappa_j, \kappa_k)$ is the matrix of dissipation rates. This ordering is chosen in order to write the dynamical matrix $\tilde{\mathbf{A}}_{\mathrm{FC}}$ in block form. In addition, $\overline{\mathbf{A}}_{\mathrm{FC}}$ denotes the element-wise conjugation of $\mathbf{A}_{\mathrm{FC}}$. Fourier transforming the above equation and applying the input-output relation, we can write $\hat{\boldsymbol{a}}_{\mathrm{FC,out}}[\omega] = \tilde{\mathbf{S}}_{\mathrm{FC}}[\omega]\hat{\boldsymbol{a}}_{\mathrm{FC,in}}[\omega]$, where the scattering matrix is:

$$\tilde{\mathbf{S}}_{\mathrm{FC}}[\omega] = \begin{pmatrix}\mathbf{S}_{\mathrm{FC}}[\omega] & \mathbf{0}_2\\ \mathbf{0}_2 & \overline{\mathbf{S}}_{\mathrm{FC}}[-\omega]\end{pmatrix}\ ,\ \mathbf{S}_{\mathrm{FC}}[\omega] = \chi_{\mathrm{FC}}(\omega)\begin{pmatrix}g_{jk}^2 - \chi_j^{-1}(-\omega)\chi_k^{-1}(\omega) & ie^{i\phi}g_{jk}\sqrt{\kappa_j\kappa_k}\\ ie^{-i\phi}g_{jk}\sqrt{\kappa_j\kappa_k} & g_{jk}^2 - \chi_j^{-1}(\omega)\chi_k^{-1}(-\omega)\end{pmatrix}. \tag{2.110}$$

The function $\chi_{\mathrm{FC}}^{-1}(\omega) = (g_{jk}^2 + \chi_j^{-1}(\omega)\chi_k^{-1}(\omega))^{-1}$ is the susceptibility of the joint two-mode system. The poles of $\chi_{\mathrm{FC}}^{-1}(\omega)$, denoted $\omega_\pm$, correspond to the resonances within the parametrically coupled system, which are termed the normal, or hybrid, modes. The real and imaginary components of the poles are related to the resonant frequencies and decay rates of these normal modes. The normal modes of the system can also be calculated from the eigenvalues of the dynamical matrix $\mathbf{A}_{\mathrm{FC}}$, which we denote $\lambda_\pm$. Since the system dynamics may be determined by solving $e^{\mathbf{A}t} = \mathbf{Q}^{-1}\mathrm{diag}(e^{\lambda_+ t}, e^{\lambda_- t})\mathbf{Q}$, we can see that real part of $-\lambda_\pm$ corresponds to the decay rate of the normal modes, while the imaginary component gives the normal mode frequency with respect to the frame.

When calculating the scattering matrix, it can be seen that the poles of $\chi_{\mathrm{FC}}^{-1}(\omega)$ are related to the eigenvalues of the dynamical matrix through $\chi_{\mathrm{FC}}^{-1}(\omega) = \det[\mathbf{A}_{\mathrm{FC}} + i\omega\mathbf{I}_2]$, and hence the poles of the scattering matrix correspond to

the complex-conjugates of the system eigenvalues. These eigenvalues may be solved analytically to yield the pair:

$$\lambda_{\pm} = -\left(\frac{\kappa_j + \kappa_k}{4}\right) \pm \sqrt{\left(\frac{\kappa_j - \kappa_k}{4}\right)^2 - g_{jk}^2}. \tag{2.111}$$

Using these definitions, the susceptibility of the system can then be expressed as the product of the normal mode susceptibilities, $\chi_{\mathrm{FC}}(\omega) = \chi_+(\omega)\chi_-(\omega)$, where $\chi_{\pm}(\omega) = (-\lambda_{\pm}^* - i\omega)^{-1}$. The eigenvalues are completely real for sufficiently small coherent coupling rates, $g_{jk} < |\kappa_j - \kappa_k|/4$, where both normal modes will have distinct decay rates and have no apparent rotation. In the regime $g_{jk} \geq |\kappa_j - \kappa_k|/4$, the rate of coherent exchange of photons exceeds their dissipation through the normal modes, leading to an effect known as normal-mode splitting. Here, the decay rates become degenerate, and the modes rotate with opposite frequency with respect to the frame. When normal-mode splitting occurs, the separation in frequency space between the normal modes increases with g. Importantly, the decay rate for either normal mode can never be pushed to non-positive values, and hence the system is always stable.

On resonance, $\omega = 0$, the scattering matrix may be expressed in terms of the phases and the cooperativity, $\mathcal{C}_{jk} := 4g_{jk}^2/\kappa_j\kappa_k$, which is defined as the ratio between the coherent and dissipative rates:

$$\mathbf{S}_{\mathrm{FC}}[0] = \frac{1}{\mathcal{C}_{jk}+1}\begin{pmatrix} \mathcal{C}_{jk}-1 & 2ie^{i\phi}\sqrt{\mathcal{C}_{jk}} \\ 2ie^{-i\phi}\sqrt{\mathcal{C}_{jk}} & \mathcal{C}_{jk}-1 \end{pmatrix}. \tag{2.112}$$

In the above matrix, the diagonal elements correspond to the reflection of the input signal, whereas the off-diagonal elements represent the amount of transmitted or "frequency-converted" signal from the other mode. The covariance of the output fields may also be calculated,

$$\langle \hat{a}_{j,\mathrm{out}}^2 \rangle = |\mathrm{S}_{jj}|^2 \langle \hat{a}_{j,\mathrm{in}}^2 \rangle + |\mathrm{S}_{jk}|^2 \langle \hat{a}_{k,\mathrm{in}}^2 \rangle = \left(\frac{\mathcal{C}_{jk}-1}{\mathcal{C}_{jk}+1}\right)^2 \langle \hat{a}_{j,\mathrm{in}}^2 \rangle + \frac{4\mathcal{C}_{jk}}{(\mathcal{C}_{jk}+1)^2}\langle \hat{a}_{k,\mathrm{in}}^2 \rangle, \tag{2.113}$$

where an identical expression for $\langle \hat{a}_{k,\mathrm{out}}^2 \rangle$ can be obtained by exchanging labels. This demonstrates that, provided the input noise is vacuum, the output noise is also vacuum noise since the scattering matrix elements obey the relation $|\mathrm{S}_{jj}|^2 + |\mathrm{S}_{jk}|^2 = 1$. Therefore, no extra energy has been added to the system by the pump.

This relation between the scattering matrix elements also allows for the definition of a dimensionless transmission ratio, $\mathrm{t} = 2\sqrt{\mathcal{C}_{jk}}/(\mathcal{C}_{jk}+1)$, which captures the portion of the input which is frequency converted to the other mode; the portion of the signal which is reflected is therefore $\sqrt{1-\mathrm{t}^2} = |\mathcal{C}_{jk}-1|/(\mathcal{C}_{jk}+1)$, where both quantities dependent purely on the cooperativity. In the case where there is perfect conversion, $\mathrm{t} = 1$, the cooperativity is $\mathcal{C}_{jk} = 1$, indicating that this requires that the rate of dissipation be perfectly matched with the coherent coupling between the two modes. When $\mathrm{t} = 0$, there is only reflection, which occurs in two limits: when $\mathcal{C}_{jk} = 0$, where there is no coherent coupling and hence no conversion, and $\mathcal{C}_{jk} \to \infty$, where there is no conversion due to the large separation in frequency space between the split normal modes.

The full scattering matrix $\tilde{\mathbf{S}}_{\mathrm{FC}}[\omega]$ can also be written in the quadrature basis, $\hat{\boldsymbol{r}} = (\hat{q}_j, \hat{p}_j, \hat{q}_k, \hat{p}_k)$ as follows:

$$\begin{aligned}\tilde{\mathbf{S}}_{\mathrm{FC}}[0] &= \frac{1}{\mathcal{C}_{jk}+1}\begin{pmatrix} (\mathcal{C}_{jk}-1)\mathbf{I} & -2\sqrt{\mathcal{C}_{jk}}\,(\cos(\phi)\mathbf{J} + \sin(\phi)\mathbf{I}) \\ -2\sqrt{\mathcal{C}_{jk}}\,(\cos(\phi)\mathbf{J} - \sin(\phi)\mathbf{I}) & (\mathcal{C}_{jk}-1)\mathbf{I} \end{pmatrix} \\ &= \begin{pmatrix} \cos(\theta)\mathbf{I} & \sin(\theta)\,(\cos(\phi)\mathbf{J} + \sin(\phi)\mathbf{I}) \\ \sin(\theta)\,(\cos(\phi)\mathbf{J} - \sin(\phi)\mathbf{I}) & \cos(\theta)\mathbf{I} \end{pmatrix}.\end{aligned} \tag{2.114}$$

The scattering behaviour is therefore equivalent to the symplectic transformation associated with a unitary beam splitter transformation, defined in Appendix C.3, where the angle is $\theta = 2\arctan\left(1/\sqrt{\mathcal{C}_{jk}}\right)$. For the remainder of this work, we will therefore refer to interactions of the form $\hat{H}_{\mathrm{FC}}$ as *beam splitters*.

Parametric Amplification

While the frequency-converter only exchanges excitations between the parametrically coupled modes, parametric amplification actively creates excitations in the system modes, a necessity when amplifying signals. Parametric amplification is generated by pumping at the sum of the frequencies, $\omega^{\mathrm{p}} = \omega_j + \omega_k$, leading to the following interaction Hamiltonian:

$$\hat{H}_I^{\mathrm{p}}(t) = \hat{H}_{\mathrm{PA}} + \hat{H}_{\mathrm{CR}}(t) \quad \text{where} \quad \hat{H}_{\mathrm{PA}} = g_{jk}\left(\hat{a}_j^\dagger \hat{a}_k^\dagger e^{i\phi} + \hat{a}_j \hat{a}_k e^{-i\phi}\right)\ ,\ \phi := \phi_j + \phi_k - \phi^{\mathrm{p}}. \tag{2.115}$$

The off-resonant parametric processes $\hat{H}_{\mathrm{CR}}(t)$ are again neglected under the RWA. Defining the vector of mode operators as $\hat{\boldsymbol{a}}_{\mathrm{PA}} = (\hat{a}_j, \hat{a}_k^\dagger, \hat{a}_j^\dagger, \hat{a}_k)$, along with $\boldsymbol{\kappa}_{\mathrm{PA}} = \boldsymbol{\kappa}_{\mathrm{FC}}$, the Heisenberg-Langevin equations for the mode operators

may be written as:

$$\frac{d}{dt}\hat{\boldsymbol{a}}_{\mathrm{PA}}(t) = \tilde{\mathbf{A}}_{\mathrm{PA}}\hat{\boldsymbol{a}}_{\mathrm{PA}}(t) - \sqrt{\boldsymbol{\kappa}_{\mathrm{PA}}}\hat{\boldsymbol{a}}_{\mathrm{PA,in}}(t)\ ,\ \tilde{\mathbf{A}}_{\mathrm{PA}} = \begin{pmatrix} \mathbf{A}_{\mathrm{PA}} & \mathbf{0}_2 \\ \mathbf{0}_2 & \overline{\mathbf{A}}_{\mathrm{PA}} \end{pmatrix}\ ,\ \mathbf{A}_{\mathrm{PA}} = \begin{pmatrix} -\kappa_j/2 & -ie^{i\phi}g_{jk} \\ ie^{-i\phi}g_{jk} & -\kappa_k/2 \end{pmatrix}. \tag{2.116}$$

Using the input-output relation, the scattering matrix, $\hat{\boldsymbol{a}}_{\mathrm{PA,out}}[\omega] = \tilde{\mathbf{S}}_{\mathrm{PA}}[\omega]\hat{\boldsymbol{a}}_{\mathrm{PA,in}}[\omega]$, is then:

$$\tilde{\mathbf{S}}_{\mathrm{PA}}[\omega] = \begin{pmatrix} \mathbf{S}_{\mathrm{PA}}[\omega] & \mathbf{0}_2 \\ \mathbf{0}_2 & \overline{\mathbf{S}}_{\mathrm{PA}}[-\omega] \end{pmatrix}\ ,\ \mathbf{S}_{\mathrm{PA}}[\omega] = \chi_{\mathrm{PA}}(\omega)\begin{pmatrix} g_{jk}^2 - \chi_j^{-1}(-\omega)\chi_k^{-1}(\omega) & -ie^{i\phi}g_{jk}\sqrt{\kappa_j\kappa_k} \\ ie^{-i\phi}g_{jk}\sqrt{\kappa_j\kappa_k} & g_{jk}^2 - \chi_j^{-1}(\omega)\chi_k^{-1}(-\omega) \end{pmatrix} \tag{2.117}$$

The susceptibility for the parametric amplifier is $\chi_{\mathrm{PA}}(\omega) = (g_{jk}^2 - \chi_j^{-1}(\omega)\chi_k^{-1}(\omega))^{-1}$, where, as with the frequency converter, the poles of this function correspond to the frequency and decay rates of the normal modes. Since these properties can also be obtained from the eigenvalues of the dynamical matrix $\mathbf{A}_{\mathrm{PA}}$, these two objects are related via $\chi_{\mathrm{PA}}^{-1}(\omega) = \det[\mathbf{A}_{\mathrm{PA}} + i\omega\mathbf{I}_2]$. As a result, $\chi_{\mathrm{PA}}(\omega)$ may also be expressed as the product of the normal mode susceptibilities. To examine the behaviour of the parametric amplifier, we must again calculate the eigenvalues of the system:

$$\lambda_{\pm} = -\left(\frac{\kappa_j + \kappa_k}{4}\right) \pm \sqrt{\left(\frac{\kappa_j - \kappa_k}{4}\right)^2 + g_{jk}^2}. \tag{2.118}$$

The PA eigenvalues are always entirely real, and so no normal-mode splitting will occur for this system. However, it can be seen that for certain parameter values is possible that $\lambda_+ \geq 0$, indicating that one of the normal modes has negative effective damping, or anti-damping, resulting in an unstable system where the steady-state scattering matrix description no longer applies; this occurs when the rate of coherent photon creation in the system exceeds the innate decay rates, $g_{jk} \geq \sqrt{\kappa_j\kappa_k}/2$. For the system to be stable, we therefore require that $\mathcal{C}_{jk} < 1$, where we have again used the cooperativity, $\mathcal{C}_{jk} := 4g_{jk}^2/\kappa_j\kappa_k$.

To analyse the behaviour of a parametric amplifier, we return to the scattering matrix, focusing on the scattering on resonance, $\omega = 0$, where it is again dependent only on the phase and the cooperativity:

$$\mathbf{S}_{\mathrm{PA}}[0] = -\frac{1}{1-\mathcal{C}_{jk}}\begin{pmatrix} \mathcal{C}_{jk}+1 & -2ie^{i\phi}\sqrt{\mathcal{C}_{jk}} \\ 2ie^{-i\phi}\sqrt{\mathcal{C}_{jk}} & \mathcal{C}_{jk}+1 \end{pmatrix}. \tag{2.119}$$

Amplification occurs when the amplitude of the output field $\hat{a}_{j,\mathrm{out}}$ is larger than that of the input field, $\hat{a}_{j,\mathrm{in}}$, which can be determined by examining the amplitude of the diagonal entries in the matrix above. In the language of amplifiers, the input field $\hat{a}_{j,\mathrm{in}}$ is referred to as the *signal*; the other input field that mixes with the signal during amplification, in this case $\hat{a}_{k,\mathrm{in}}$, is called the *idler*. In the process of parametric amplification, photons from the pump are down-converted into signal and idler photons, thereby increasing the amplitude of the output fields.

The amplification of the signal photons can be characterised by the *gain*, which is defined in the above scattering matrix using the magnitude of the diagonal matrix elements, $\sqrt{G} = (1+\mathcal{C}_{jk})/(1-\mathcal{C}_{jk})$. In the case where there is no coherent coupling, $\mathcal{C}_{jk} = 0$, then $G = 1$, meaning the input field is simply reflected to the output field, resulting in no gain and no amplification. As the cooperativity approaches the point of instability, $\mathcal{C}_{jk} \to 1$, the magnitude of the scattering element can be increased without bound, $G \to \infty$, resulting in infinite gain. The opposite case, where the magnitude of the scattering matrix element is less than one, is termed *isolation*, and while this is not possible for this scattering matrix, it can occur in more complicated amplifier configurations. A feature of linear parametric amplification is that amplified photons from the idler are also present in the signal output, with the magnitude of this scattering element given by $\sqrt{G-1} = 2\sqrt{\mathcal{C}_{jk}}/(1-\mathcal{C}_{jk})$. This added noise is fundamentally unavoidable in linear quantum amplifiers [11, 12].

In order to better understand the limits on the added noise from the idler, we will consider two cases of parametric amplification. In the first case, the signal and idler have distinct frequencies, and so correspond to distinct modes; this is termed *nondegenerate parametric amplification*. To examine the behaviour of the output noise due to parametric amplification, it is simpler to express the scattering matrix in the quadrature basis, defined as $\hat{\boldsymbol{r}} = (\hat{q}_j, \hat{p}_j, \hat{q}_k, \hat{p}_k)$:

$$\mathbf{S}_{\mathrm{TMS}}[0] = -\frac{1}{1-\mathcal{C}_{jk}}\begin{pmatrix} (\mathcal{C}_{jk}+1)\mathbf{I} & 2\sqrt{\mathcal{C}_{jk}}(-\cos(\phi)\mathbf{X} + \sin(\phi)\mathbf{Z}) \\ 2\sqrt{\mathcal{C}_{jk}}(-\cos(\phi)\mathbf{X} + \sin(\phi)\mathbf{Z}) & (\mathcal{C}_{jk}+1)\mathbf{I} \end{pmatrix} \tag{2.120}$$

The above scattering matrix is, up to a global change of phase, identical to the corresponding symplectic transformation of a coherent two-mode squeezer (TMS) unitary transformation, defined in Appendix C.3. Amplification not only increases the number of photons in the output, but it also increases the noise above that of the vacuum state, thereby making it more robust against added sources of noise from the environment or other external devices. Picking one

mode to be the signal and the other the idler, the variance of both quadratures of the signal output may be written as:

$$\langle \hat{q}^2_{s,\text{out}} \rangle = G\left(\langle \hat{q}^2_{s,\text{in}} \rangle + \frac{G-1}{G}\left(\cos^2(\phi)\langle \hat{p}^2_{i,\text{in}} \rangle + \sin^2(\phi)\langle \hat{q}^2_{i,\text{in}} \rangle \right) \right)$$
$$\langle \hat{p}^2_{s,\text{out}} \rangle = G\left(\langle \hat{p}^2_{s,\text{in}} \rangle + \frac{G-1}{G}\left(\cos^2(\phi)\langle \hat{q}^2_{i,\text{in}} \rangle + \sin^2(\phi)\langle \hat{p}^2_{i,\text{in}} \rangle \right) \right). \tag{2.121}$$

These expressions are valid regardless of which mode, a_j or a_k, is the signal or idler. Assuming that the input noise is thermal noise, Eq. (2.85) demonstrates that the input noise is independent of the choice of quadrature, $\langle \hat{q}^2_{i,\text{in}} \rangle = \langle \hat{p}^2_{i,\text{in}} \rangle$, and therefore the added noise from the idler is independent of the choice of phase ϕ. Both quadratures of the signal therefore see the same amount of noise from the idler, and are amplified identically regardless of the choice of phase since $\langle \hat{q}^2_{s,\text{in}} \rangle = \langle \hat{p}^2_{s,\text{in}} \rangle$ as well. Since the choice of phase is irrelevant, this is referred to as *phase-insensitive* or *phase-preserving* amplification. Provided the amount of noise from the idler is just vacuum, $\langle \hat{r}_{i,\text{in}} \rangle = 1/2$, then the amount of noise added to the signal is bounded above by $1/2$ quanta, with this limit only being reached in the limit of infinite gain.

In the second case, the frequencies of the signal and idler fields are identical, resulting in *degenerate parametric amplification*. In this instance both modes are the same, $\hat{a}_j = \hat{a}_k$, and the parametric coupling is rewritten as $(\lambda_k/2)\left(e^{i\phi}\hat{a}_k^{2\,\dagger} + e^{-i\phi}\hat{a}_k^2\right)$ in order to simplify the results. Working in the quadrature basis, $\hat{\boldsymbol{r}} = (\hat{q}_k, \hat{p}_k)$, and additionally redefining the cooperativity as $\mathcal{C}_\lambda = 2\lambda_k/\kappa_k$, the scattering matrix for this degenerate parametric amplifier (DPA) is

$$\mathbf{S}_{\text{SMS}}[0] = -\frac{1}{1-\mathcal{C}_\lambda^2}\begin{pmatrix} 1+\mathcal{C}_\lambda^2+2\mathcal{C}_\lambda\sin(\phi) & -2\mathcal{C}_\lambda\cos(\phi) \\ -2\mathcal{C}_\lambda\cos(\phi) & 1+\mathcal{C}_\lambda^2-2\mathcal{C}_\lambda\sin(\phi) \end{pmatrix}. \tag{2.122}$$

In contrast to the case of nondegenerate parametric amplification, the above is identical to the symplectic transformation of a single-mode squeezer (SMS) unitary operation, again given in Appendix C.3. Defining the gain as $\sqrt{G} = (1+\mathcal{C}_\lambda)/(1-\mathcal{C}_\lambda)$, the variances of the output quadratures may be expressed as:

$$\langle \hat{q}^2_{k,\text{out}} \rangle = \frac{1}{4G}\left(\left[(1-\sin(\phi)) + G(1+\sin(\phi)\right]^2 \langle \hat{q}^2_{k,\text{in}} \rangle + (G-1)^2\cos^2(\phi)\langle \hat{p}^2_{k,\text{in}} \rangle \right)$$
$$\langle \hat{p}^2_{k,\text{out}} \rangle = \frac{1}{4G}\left(\left[(1+\sin(\phi)) + G(1-\sin(\phi)\right]^2 \langle \hat{p}^2_{k,\text{in}} \rangle + (G-1)^2\cos^2(\phi)\langle \hat{q}^2_{k,\text{in}} \rangle \right). \tag{2.123}$$

In the above, the phase $\phi = +\pi/2$ results in the amplification of the position quadrature, $\langle \hat{q}^2_{k,\text{out}} \rangle = G\langle \hat{q}^2_{k,\text{out}} \rangle$, where there is no longer any added noise mixed with the output due to the degeneracy of the signal and idler. For this choice of phase, the orthogonal momentum quadrature is de-amplified or squeezed, $\langle \hat{p}^2_{k,\text{out}} \rangle = G^{-1}\langle \hat{p}^2_{k,\text{out}} \rangle$; this behaviour is reversed for the opposite phase $\phi = -\pi/2$. Since the amplified quadrature is explicitly dependent on the choice of phase, this is termed *phase-sensitive* or *phase-dependent* amplification.

An important characteristic in both of the above examples is that amplification is present in the outputs of all ports. This is undesirable if we wish to protect certain systems connected to a parametric amplifier from excess backaction due to amplified noise. Therefore, to prevent the emission of this amplified noise from certain ports, it is required that the amplifier also be directional; this requires that the system break the symmetry of *reciprocity*, a concept that will be introduced in the next section.

2.4 What is Nonreciprocity?

2.4.1 Nonreciprocity in Classical Electromagnetism

Given that quantum amplifiers are based on photonic systems, which involve the manipulation of light in the form of photons, we will concern ourselves with the symmetry of reciprocity as it relates to the field of electromagnetism. The specific symmetry we will consider is termed *Lorentz reciprocity*, which, given its namesake, is certainly no longer new physics [75–77]. Despite this, the principle of reciprocity, or rather the breaking of it, underpins a great deal of contemporary technology operating in the radio-frequency, microwave, and optical regimes. Systems which do not obey reciprocity are termed *nonreciprocal*, however, despite the fundamental nature of nonreciprocity in signal processing applications, the concept is still misunderstood often enough to warrant recent scientific publications dedicated to answering the question: what exactly constitutes nonreciprocal behaviour in electromagnetic systems [78, 79]?

The term *reciprocity* originates from Latin and means something akin to "back and forth," which could lead one to believe at first glance that the symmetry is related to some time-reversal invariance in the system, though as will be explained herein, the exact nature of reciprocity is a little more subtle than it may initially seem. An intuitive

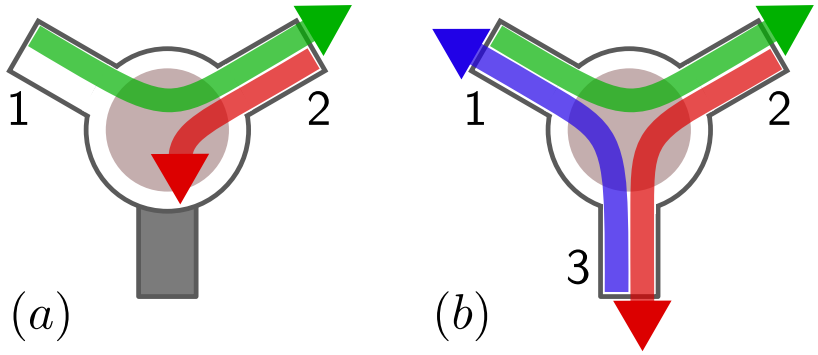

Figure 2.1: Representation of a three-port device acting as an (a) isolator and (b) circulator. The circulator routes incoming signals to only one of the neighbouring ports, while preventing the reflection of the signal. The signal transmission in the isolator is similar, except that the third port is now terminated. The signal from port 2 does not leave through either of the monitored ports in the isolator, and the transmission of the signal from port 1 is unaffected. The scattering behaviour of the isolator can be represented by the scattering matrix in Eq. (2.124).

definition starts by considering a system with some number of ports, which provide a connection to transmit signals to and from some external system. The ports can be collected into two groups, one labelled the "sources" and the other the "detectors": the system is called reciprocal if the behaviour of the transmitted fields is invariant when the ports acting as sources and detectors are exchanged. Systems which break this symmetry are therefore termed nonreciprocal.

This definition is particularly useful when characterising the reciprocity of linear-time invariant (LTI) systems, that is, linear systems with no explicit time-dependence which receive input signals at the system ports, and through some internal physical processes, produce output signals which leave the system through these same ports. The internal processes in the system can be collectively described through a scattering matrix, where the LTI system is only reciprocal in instances where the scattering matrix is symmetric, up to a shift in phase. Nonreciprocal LTI systems must therefore have an asymmetric scattering matrix [78]. For example, we can consider an isolator with two ports, whose field can be described by the modes of the electromagnetic field, a_1 and a_2, respectively. In order for this two-port system to act as an isolator, only signals entering through one of the ports are transmitted through the other port, with no reflection; all other signals are necessarily blocked through some combination of interference or dissipation within the medium. The scattering relation for an isolator is therefore given by

$$\begin{pmatrix} a_{1,\text{out}} \\ a_{2,\text{out}} \end{pmatrix} = \begin{pmatrix} 0 & 0 \\ 1 & 0 \end{pmatrix} \begin{pmatrix} a_{1,\text{in}} \\ a_{2,\text{in}} \end{pmatrix}. \tag{2.124}$$

Labelling port a_1 as source and port a_2 as detector, it is obvious that the scattering behaviour is not identical if these labels were to be exchanged, so this system is necessarily nonreciprocal. An important point is that, while nonreciprocity leads to asymmetric transmission of the signal in the system, the inverse is not true, and it is possible for there to be asymmetric propagation in systems which obey Lorentz reciprocity [79]. This is not an uncommon misconception, even within recent works claiming to realise nonreciprocity in quantum mechanical systems, and highlights the subtle nature of the definition.

As previously stated, the concept of nonreciprocity is also related to time-reversal symmetry breaking in certain cases. To make this connection more mathematically solid, we can use the Lorentz reciprocity theorem. To derive this theorem, we start with two current densities, $\mathbf{J}_k$ with arbitrary labels $k = 1, 2$, which independently produce an electric field, $\mathbf{E}_k$, and magnetic field, $\mathbf{H}_k$. Faraday's law for $\mathbf{E}_k$ and the Ampère–Maxwell law for $\mathbf{H}_k$ may be constructed and then Fourier transformed from the time to the frequency domain to turn the differential equations into linear functions of frequency,

$$\nabla \times \mathbf{E}_k = -\frac{\partial}{\partial t}\mathbf{B}_k\,,\ \nabla \times \mathbf{H}_k = \mathbf{J}_k + \frac{\partial}{\partial t}\mathbf{D}_k \quad \longrightarrow \quad \nabla \times \check{\mathbf{E}}_k = i\omega\check{\mathbf{B}}_k\,,\ \nabla \times \check{\mathbf{H}}_k = \check{\mathbf{J}}_k - i\omega\check{\mathbf{D}}_k, \tag{2.125}$$

where $\mathbf{B}_k$ is the magnetic flux density, $\mathbf{D}_k$ is the electric flux density; the Fourier transformed fields are defined as $\check{\mathbf{A}}(\omega) := \mathcal{F}[\mathbf{A}(t)](\omega) = \frac{1}{\sqrt{2\pi}}\int_{-\infty}^{\infty} f(t)e^{i\omega t}\,dt$. The electric and magnetic fields and flux densities are related the components of the electromagnetic field by $\epsilon_{lm}\mathrm{E}_m = \mathrm{D}_l$ and $\mu_{lm}\mathrm{H}_m = \mathrm{B}_l$, where ϵ_{lm} and μ_{lm} are the permittivity and permeability tensors of the medium, respectively. The tensor expressions are used to accommodate situations where the material is anisotropic, which results in nonidentical permittivity or permeability along different axes in the material. Since ϵ_{lm} and μ_{lm} may vary in time, it is easier to work with the flux density vectors in the frequency

domain. The theorem is obtained from the Fourier-transformed Maxwell's equations through the use of some basic arithmetic and vector identities [80], after which, we arrive at the Lorentz reciprocity theorem, which states that if the following equality holds, then the system is reciprocal [79]:

$$\left(\check{\mathbf{J}}_1 \cdot \check{\mathbf{E}}_2 - \check{\mathbf{J}}_2 \cdot \check{\mathbf{E}}_1\right) = \nabla \cdot \left(\check{\mathbf{H}}_1 \times \check{\mathbf{E}}_2 - \check{\mathbf{H}}_2 \times \check{\mathbf{E}}_1\right) + i\omega \left(\check{\mathbf{D}}_1 \cdot \check{\mathbf{E}}_2 - \check{\mathbf{D}}_2 \cdot \check{\mathbf{E}}_1 - \check{\mathbf{B}}_1 \cdot \check{\mathbf{H}}_2 + \check{\mathbf{B}}_2 \cdot \check{\mathbf{H}}_1\right). \tag{2.126}$$

This may also be formulated in integral form over a volume V with smooth surface S, and normal vector $\mathbf{n}$:

$$\begin{aligned}\int_V &\left(\check{\mathbf{J}}_1 \cdot \check{\mathbf{E}}_2 - \check{\mathbf{J}}_2 \cdot \check{\mathbf{E}}_1\right) dV \\ &= \oint_S \left(\check{\mathbf{H}}_1 \times \check{\mathbf{E}}_2 - \check{\mathbf{H}}_2 \times \check{\mathbf{E}}_1\right) \cdot \mathbf{n}\, dS + i\omega \int_V \left(\check{\mathbf{D}}_1 \cdot \check{\mathbf{E}}_2 - \check{\mathbf{D}}_2 \cdot \check{\mathbf{E}}_1 - \check{\mathbf{B}}_1 \cdot \check{\mathbf{H}}_2 + \check{\mathbf{B}}_2 \cdot \check{\mathbf{H}}_1\right) dV.\end{aligned} \tag{2.127}$$

The above expressions are always invariant under the exchange of labels, and their violation results in the system being termed nonreciprocal. These expressions provide a bridge between the notion reciprocity as a result of the time-reversal symmetric propagation of fields, and reciprocity as a result of the invariance of transmitted fields under exchange of ports, where the transmitted fields correspond to the current densities $\mathbf{J}_1$ and $\mathbf{J}_2$.

With the Lorentz reciprocity theorem defined, we can now demonstrate that nonreciprocity, under certain circumstances, is also equivalent to time-reversal symmetry breaking. We define the time-reversed systems using a time-reversal map T, which takes the time-forward system to the time-reversed system,

$$T : (\mathbf{J}(t), \mathbf{E}(t), \mathbf{H}(t)) \to (\mathbf{J}'(t), \mathbf{E}'(t), \mathbf{H}'(t)). \tag{2.128}$$

Since Maxwell's equations are necessarily invariant under time-reversal, $(\mathbf{J}'(t), \mathbf{E}'(t), \mathbf{H}'(t))$ must also obey both the time and frequency-domain equations in Eq. (2.125); the systems $(\mathbf{J}_k(t), \mathbf{E}_k(t), \mathbf{H}_k(t))$ used to derive the condition for Lorentz reciprocity in Eq. (2.126) can therefore be replaced by the time-forward and time-reversed systems. Systems which follow $(\mathbf{J}'(t), \mathbf{E}'(t), \mathbf{H}'(t)) = (-\mathbf{J}(-t), \mathbf{E}(-t), -\mathbf{H}(-t))$ will satisfy Eq. (2.125) and hence are reciprocal. In order to break reciprocity, the evolution of the time-reversed Maxwell's equations must yield different fields from the time-forward equations; this may be achieved by altering the permittivity or the permeability so that propagation of the electromagnetic field through the media is asymmetric under time-reversal, leading to different dynamics for different directions of current flow.

An example is the Faraday effect, where the polarisation of the electromagnetic field undergoes a rotation when moving through a material; this is a nonreciprocal effect since, upon reflection, the rotation is not undone, but instead the polarisation rotates again by the same angle. Such a material is modelled using a non-diagonal tensor for the permeability [81], which causes signals propagating in different directions in the medium to experience different magnetic permeabilities. This permeability tensor can be realised through the application of an external magnetic field to a susceptible material. Since the magnetic field is external to the system, and hence unaffected by the time reversal of the internal fields, Maxwell's equations of motion will be distinct for both directions of time, breaking time-reversal symmetry and Lorentz reciprocity in Eq. (2.125), thereby giving rise to nonreciprocity. The Faraday effect may therefore be used to engineer reciprocal transmission through the constructive and destructive interference of signals in the material, which is possible due to the rotation of the field amplitude. This interference may be used to control which ports a signal exists and is used to realise optical and microwave isolators and circulators.

This notion of nonreciprocity as time-reversal symmetry breaking does not account for potential sources of loss or gain within the system. The issue is that loss and gain are the reverse processes of one another; however, in a system with loss attenuation of the signal amplitude occurs regardless of which way time flows. Since reversing time in a lossy system cannot produce gain, time-reversal symmetry is always broken, and so by this definition, a lossy system would never appear to be reciprocal. The same reasoning holds true for systems with gain. Therefore, the Lorentz reciprocity theorem in Eq. (2.126) does not apply to such systems. In order to provide a definition of nonreciprocity for mediums with loss and gain, we do not focus on the bare amplitude of the signals, but instead on their ratio [79]. Systems with loss and gain are therefore nonreciprocal when the ratio of the signal amplitudes is not identical under time-reversal. This point is particularly important to keep in mind for the quantum systems to be examined in this work, since the gain in quantum amplifiers will increase signal amplitude, and the open nature of the quantum systems will introduce sources of loss; neither, however, will serve as sources of nonreciprocity in quantum systems.

2.4.2 Nonreciprocity in Dissipative Quantum Systems

2.4.2.1 Nonreciprocity Through Engineered Dissipation

In the previous section, we showed how altering the apparent permittivity or permeability of a medium can break time-reversal symmetry, allowing for nonreciprocal signal routing. For systems made of ferrimagnetic material, this is achieved by applying a magnetic bias field, however, the large size and strong magnetic fields inhibit integration with sensitive quantum systems, which necessarily live in well-shielded and very cold environments. Integrated nonreciprocal devices must therefore also be quantum and must realise nonreciprocity by an entirely different mechanism. We focus on one approach to nonreciprocity using engineered dissipation from Metelmann and Clerk [15, 82, 83], a concept closely connected to the theory of cascaded quantum systems [84, 85]. We start with two independent systems, labelled A and B, which are coupled via the following coherent, and reciprocal, interaction,

$$\hat{H} = g\left(\hat{A}^\dagger \hat{B}^\dagger + \hat{A}\hat{B}\right). \tag{2.129}$$

where $\hat{A}$ and $\hat{B}$ act on systems A and B, respectively. No assumptions need be made on the form of the operators, with the exception that the operators acting on different systems commute, $[\hat{A}^{(\dagger)}, \hat{B}^{(\dagger)}] = 0$. To make this coherent interaction nonreciprocal, systems A and B are additionally coupled to a common environment, which mediates a so-called "dissipative interaction" between the two systems, resulting in non-unitary dynamics. For the interaction between the two systems to become nonreciprocal, the form of the dissipative coupling must be properly engineered to match that of the coherent process, and the system parameters must be balanced correctly. Assuming the common environment is Markovian, the necessary system can be described using the following Lindblad master equation,

$$\frac{d}{dt}\hat{\rho} = -i[\hat{H}, \hat{\rho}] + \gamma\mathcal{D}[\hat{z}](\hat{\rho}) \quad \text{where} \quad \hat{z} = \hat{A} + \zeta e^{i\phi}\hat{B}^\dagger \quad \text{or} \quad \hat{A}^\dagger - \zeta e^{-i\phi}\hat{B}, \tag{2.130}$$

where $\mathcal{D}[\hat{L}](\hat{\rho}) = \hat{L}\hat{\rho}\hat{L}^\dagger - \frac{1}{2}[\hat{L}^\dagger\hat{L}, \hat{\rho}]_+$. The form of the jump operator in the dissipator is not unique, and in this case, two different choices can give rise to nonreciprocity for an identical set of parameters. To determine these necessary parameter values, we will examine the dynamics of two arbitrary observables of systems A and B, $\hat{O}_A$ and $\hat{O}_B$, where both observables commute with all operators of the other system. Using the above Lindblad master equation, along with the first jump-operator, $\hat{z} = \hat{A} + \zeta e^{i\phi}\hat{B}^\dagger$, the equations of motion for the observables expectation values are:

$$\begin{aligned}
\frac{d}{dt}\langle\hat{O}_A\rangle &= \frac{1}{2}\left(2g + i\gamma\zeta e^{-i\phi}\right)\langle i[\hat{A}, \hat{O}_A]\hat{B}\rangle + \frac{1}{2}\left(2g - i\gamma\zeta e^{+i\phi}\right)\langle i[\hat{A}^\dagger, \hat{O}_A]\hat{B}^\dagger\rangle + \gamma\langle\mathcal{D}^\dagger[\hat{A}](\hat{O}_A)\rangle \\
\frac{d}{dt}\langle\hat{O}_B\rangle &= \frac{1}{2}\left(2g - i\gamma\zeta e^{-i\phi}\right)\langle i[\hat{B}, \hat{O}_B]\hat{A}\rangle + \frac{1}{2}\left(2g + i\gamma\zeta e^{+i\phi}\right)\langle i[\hat{B}^\dagger, \hat{O}_B]\hat{A}^\dagger\rangle + \gamma\zeta^2\langle\mathcal{D}^\dagger[\hat{B}^\dagger](\hat{O}_B)\rangle
\end{aligned} \tag{2.131}$$

where $\langle\hat{O}\rangle \equiv \mathrm{Tr}[\hat{\rho}\hat{O}]$, and $\mathcal{D}^\dagger[\hat{L}](\hat{O}) = \hat{L}^\dagger\hat{O}\hat{L} - \frac{1}{2}[\hat{L}^\dagger\hat{L}, \hat{O}]_+$. In both expressions, the engineered dissipation gives rise to an additional coupling between the two systems, along with two additional independent dissipation channels. In order to render the coupling nonreciprocal, the strength of the coherent and dissipative interactions must be properly balanced, and the phase of the jump operator set to the correct value, so that the desired couplings may be cancelled exactly in Eq. (2.131):

$$2g = \gamma\zeta \quad \text{and} \quad \phi = \pm\frac{\pi}{2}. \tag{2.132}$$

The direction of the nonreciprocal interaction is controlled through the sign of the phase ϕ, with $\phi = -\pi/2$ corresponding to the case where the dynamics of system A are completely independent of system B, and vice versa for $\phi = +\pi/2$. Applying the nonreciprocity conditions from Eq. (2.132) to the equations of motion in Eq. (2.131), the dynamical equations for the observables simplify to:

$$\begin{aligned}
A \to B: \frac{d}{dt}\langle\hat{O}_A\rangle &= \gamma\langle\mathcal{D}^\dagger[\hat{A}](\hat{O}_A)\rangle & \frac{d}{dt}\langle\hat{O}_B\rangle &= 2g\langle i[\hat{B}, \hat{O}_B]\hat{A}\rangle + 2g\langle i[\hat{B}^\dagger, \hat{O}_B]\hat{A}^\dagger\rangle + \gamma\zeta^2\langle\mathcal{D}^\dagger[\hat{B}^\dagger](\hat{O}_B)\rangle \\
A \leftarrow B: \frac{d}{dt}\langle\hat{O}_B\rangle &= \gamma\zeta^2\langle\mathcal{D}^\dagger[\hat{B}^\dagger](\hat{O}_B)\rangle & \frac{d}{dt}\langle\hat{O}_A\rangle &= 2g\langle i[\hat{A}, \hat{O}_A]\hat{B}\rangle + 2g\langle i[\hat{A}^\dagger, \hat{O}_A]\hat{B}^\dagger\rangle + \gamma\langle\mathcal{D}^\dagger[\hat{A}](\hat{O}_A)\rangle.
\end{aligned} \tag{2.133}$$

In both cases, the dynamics of one system will decouple from the other and will only see added dissipation due to the engineered environment. The other system, meanwhile, is still coherently coupled to this system, but through an effective Hamiltonian with twice the coupling strength. Due to the presence of dissipation, nonreciprocity in this instance does not arise from the breaking of time-reversal symmetry, but due to the fact that the dynamics is unidirectional, and hence there is no invariance of the system under exchange of source and detector.

Engineered dissipation of this form arises as a result of properly coupling to an auxiliary system which has the properties of a reservoir; for our purposes, the most relevant physical implementation is a bosonic mode, $\hat{a}_l$, with

a large damping rate κ_l. By increasing the damping of this auxiliary mode so that it becomes the fastest rate in the system, the dynamics of the mode can be removed through adiabatic elimination [46], resulting in a Markovian dissipation channel coupled to systems A and B. Starting with a Hamiltonian comprised of Eq. (2.129) plus some additional coupling to the auxiliary mode, $\hat{H}_{\text{aux}}$, and then adiabatically eliminating the open bosonic mode leads to engineered dissipation,

$$\hat{H}_{\text{aux}} = \frac{\sqrt{\gamma\kappa_l}}{2}\left(\hat{a}_l^\dagger \hat{z} + \hat{z}^\dagger \hat{a}_l\right) \to \gamma\mathcal{D}[\hat{z}] \tag{2.134}$$

thus retrieving the Lindblad master equation in Eq. (2.130); we will revisit this example shortly in Section 2.4.2.3.

2.4.2.2 Nonreciprocity Through Scattering Interference

Since no assumptions were made about the form of the primary systems in the previous section, the engineered dissipation approach to nonreciprocity may be applied to nonlinear quantum systems and interactions. There exists another approach from Ranzani and Aumentado [16, 86], which applies specifically to linear systems which can be modelled using the scattering matrix description in Section 2.2.3.2; since this work is focused on open quantum systems comprised of linearly coupled harmonic oscillators, with defined input and output fields, this viewpoint is also relevant. This approach views the scattering matrix as a collection of graphs representing different coupling paths within the system, where properly balancing the system parameters can result in path interference, leading to nonreciprocal scattering. Nonreciprocity in this instance manifests as asymmetry in the scattering matrix; for a scattering matrix in an arbitrary basis, the system is said to be reciprocal if the scattering matrix obeys [16]

$$\mathbf{S}^\dagger = \mathbf{U}_\varphi \mathbf{S} \mathbf{U}_\varphi^\dagger. \tag{2.135}$$

The matrix $\mathbf{U}_\varphi$ is comprised of phase shifts applied to the individual modes, and hence arises from a unitary transformation of the form $\hat{U}_\varphi = \exp\left[i\sum_{k=1}^N \varphi_k \hat{a}_k^\dagger \hat{a}_k\right]$. For the quadrature basis, the matrix $\mathbf{U}_\varphi$ is therefore a direct sum of orthogonal rotation matrices. This statement of nonreciprocity is equivalent to the demand that $\mathbf{S}^T$ and $\mathbf{S}$ be equivalent under some set of single-mode unitary transformations. This definition highlights that any asymmetry in scattering due to a difference in the phase is irrelevant, and so the focus is instead on asymmetry in the amplitude of the scattering. This allows for a way to measure the degree of asymmetry, and hence nonreciprocity, in the system. For this, we start by writing the scattering and unitary phase-shift matrices in 2×2 block form,

$$\mathbf{S} = \begin{pmatrix} \mathbf{S}_{11} & \mathbf{S}_{12} & \cdots & \mathbf{S}_{1N} \\ \mathbf{S}_{21} & \mathbf{S}_{22} & \cdots & \mathbf{S}_{2N} \\ \vdots & \vdots & \ddots & \vdots \\ \mathbf{S}_{N1} & \mathbf{S}_{N2} & \cdots & \mathbf{S}_{NN} \end{pmatrix} \quad \text{and} \quad \mathbf{U}_\varphi = \bigoplus_{k=1}^N \mathbf{U}_k \ , \ \det[\mathbf{U}_k] = 1, \tag{2.136}$$

where $\mathbf{S}_{jk}$ is the two-mode block corresponding to scattering from the input of mode a_k to the output of mode a_j, and $\mathbf{U}_k$ corresponds to an arbitrary phase-shift applied to mode a_k. For linear systems, we are interested in the asymmetry of scattering between pairs of modes, a_j and a_k, where, according to Eq. (2.135), reciprocity between this mode pair only occurs when $\mathbf{S}_{jk}$ and $\mathbf{S}_{kj}$ satisfy the following condition:

$$\mathbf{S}_{kj}^\dagger = \mathbf{U}_j \mathbf{S}_{jk} \mathbf{U}_k^\dagger. \tag{2.137}$$

In order for the scattering to be reciprocal, $\mathbf{S}_{jk}$ and $\mathbf{S}_{kj}^\dagger$ must therefore be equivalent matrix; a necessary condition for equivalence is $\text{Tr}[\mathbf{S}_{jk}\mathbf{S}_{jk}^\dagger] = \text{Tr}[\mathbf{S}_{kj}\mathbf{S}_{kj}^\dagger]$. In order quantify any asymmetry, we therefore use this identity to construct the following function, termed the normalised degree of nonreciprocity[5]:

$$N^{(j,k)} := \frac{||\mathbf{S}_{kj}||_F^2 - ||\mathbf{S}_{jk}||_F^2}{||\mathbf{S}_{kj}||_F^2 + ||\mathbf{S}_{jk}||_F^2}, \tag{2.138}$$

where $||\mathbf{A}||_F := \sqrt{\text{Tr}[\mathbf{A}\mathbf{A}^\dagger]}$ is the Frobenius norm. This measure is defined such that it will lie in a bounded interval, $N^{(j,k)} \in [-1, 1]$, and will capture the difference in the amplitude, as well as the preferred direction, of the scattering between pairs of modes; obviously, the sign of the function changes when permuting the modes, $N^{(j,k)} = -N^{(k,j)}$. By construction, $N^{(j,k)} = 0$ when the scattering between a pair of modes is reciprocal. For all other non-zero values,

[5] This function is constructed so as to be independent of the choice of basis for the scattering matrix, however, while $||\mathbf{A}||_F^2 = ||\mathbf{B}||_F^2$ is a necessary condition for unitary matrix equivalence, $\mathbf{A} = \mathbf{U}_1\mathbf{B}\mathbf{U}_2$ where $\mathbf{U}_k$ is unitary, it has not been checked whether it is a sufficient condition for 2×2 matrices. Contrast this to unitarily similar 2×2 matrices, $\mathbf{A} = \mathbf{U}_1\mathbf{B}\mathbf{U}_1$, which must have identical Frobenius norms, along with $\text{Tr}[\mathbf{A}] = \text{Tr}[\mathbf{B}]$ and $\text{Tr}[\mathbf{A}^2] = \text{Tr}[\mathbf{B}^2]$, by Specht's theorem.

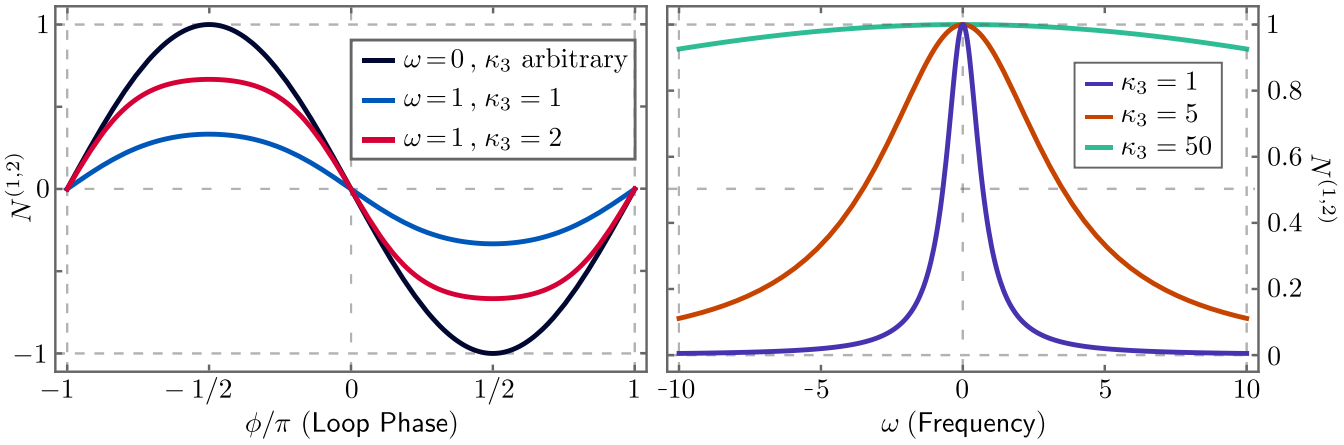

Figure 2.2: Plots of the generalised degree of nonreciprocity $N^{(1,2)}$, [Left] as function of the phase of the three-mode loop Hamiltonian in Eq. (2.139), and [Right] as a function of the frequency of the associated scattering matrix $\mathbf{S}[\omega]$ at the phase $\phi = -\pi/2$. All couplings obey the relation $g_{jk} = 4/\kappa_j\kappa_k$, where the decay rates for the two primary modes are fixed at $\kappa_1 = 1$ and $\kappa_2 = 1$, and the decay rate κ_3 is varied. Fixing the decay rates ensures that the condition $g_{12} = 2g_{13}g_{23}/\kappa_3$ is always obeyed. When $N^{(1,2)} = 1$ the direction of the nonreciprocal interaction is $a_1 \to a_2$, and when $N^{(1,2)} = -1$ the direction is $a_1 \leftarrow a_2$.

$N^{(j,k)} \neq 0$, the scattering matrix is asymmetric and hence the scattering process must be nonreciprocal, with the function taking positive values when the amplitude of the scattering means that the direction $a_j \to a_k$ is dominant, and negative values when the direction $a_j \leftarrow a_k$ is preferred. When the function reaches $N^{(j,k)} = \pm 1$ the scattering is perfectly asymmetric, in which case $||\mathbf{S}_{jk}||_F$ or $||\mathbf{S}_{kj}||_F$ vanishes exactly, depending on the direction.

2.4.2.3 Equivalence for Gaussian Systems

For Gaussian systems, the engineered dissipation approach of Metelmann and Clerk and the graph-based interference approach of Ranzani and Aumentado are complementary approaches to realising nonreciprocity. Going back and forth between the two approaches is possible for systems comprised entirely of linearly coupled open bosonic modes by adiabatically eliminating certain modes to realise engineered dissipation channels, or conversely, converting engineered dissipation channels into additional bosonic modes as in Eq. (2.134). Through this, we can see that, at a minimum, we require three bosonic modes to realise nonreciprocity in a quantum system. As a motivating example, consider a system of passively coupled bosonic modes with the Hamiltonian

$$\hat{H} = g_{12}\left(\hat{a}_1^\dagger\hat{a}_2 + \hat{a}_1\hat{a}_2^\dagger\right) + g_{13}\left(\hat{a}_1^\dagger\hat{a}_3 + \hat{a}_1\hat{a}_3^\dagger\right) + g_{23}\left(e^{-i\phi}\hat{a}_2^\dagger\hat{a}_3 + e^{i\phi}\hat{a}_2\hat{a}_3^\dagger\right) \tag{2.139}$$

whose open system dynamics can be modelled using the following Lindblad master equation

$$\frac{d}{dt}\hat{\rho} = \mathcal{L}(\hat{\rho}) \quad \text{where} \quad \mathcal{L}(\hat{\rho}) = -i[\hat{H},\hat{\rho}] + \sum_{k=1,2,3}\kappa_k\mathcal{D}[\hat{a}_k](\hat{\rho}). \tag{2.140}$$

If we wish to determine the conditions for nonreciprocity between modes a_1 and a_2, this can be easily accomplished in the regime where a_3 is highly damped, allowing for the adiabatic elimination of this auxiliary mode. Using Eq. (2.134), the resulting master equation is simply:

$$\begin{aligned}\frac{d}{dt}\hat{\rho}_{12} &= -i[\hat{H}_{12},\hat{\rho}_{12}] + \gamma\mathcal{D}[\hat{z}](\hat{\rho}_{12}) + \sum_{k=1,2}\kappa_k\mathcal{D}[\hat{a}_k](\hat{\rho}_{12}) \\ \text{where} \quad \hat{H}_{12} &= g_{12}\left(\hat{a}_1^\dagger\hat{a}_2 + \hat{a}_1\hat{a}_2^\dagger\right) \ , \ \hat{z} = \hat{a}_1 + \zeta e^{i\phi}\hat{a}_2 \quad \text{and} \quad \hat{\rho}_{12} = \mathrm{Tr}_3[\hat{\rho}].\end{aligned} \tag{2.141}$$

The damping rate and asymmetry are entirely arbitrary, but for simplicity we choose $\gamma = 4g_{13}^2/\kappa_3$ and $\zeta = g_{23}/g_{13}$; the results shown in Section 2.4.2.1 demonstrate that nonreciprocity occurs when the conditions in Eq. (2.132) are met, which correspond to the following expressions for this system:

$$2g = \zeta\gamma \to g_{12} = 2g_{13}g_{23}/\kappa_3 \quad \text{and} \quad \phi = \pm\frac{\pi}{2}. \tag{2.142}$$

Alternatively, we can demonstrate the equivalence between the master equation and scattering approaches to nonreciprocity by calculating the scattering matrix, $\mathbf{S}[\omega]$, for the open three-mode system described by the Lindblad master equation in Eq. (2.140). The conditions in Eq. (2.142) may be applied to this scattering matrix, and the results for $N^{(1,2)}$ are shown in Figure 2.2. Here, we can see in the left-most plot that not only is $\phi = \pm\frac{\pi}{2}$ necessary to reach $N^{(1,2)} = \pm 1$, but that this only occurs when scattering is at the resonance frequency, which is $\omega = 0$ in this example since we are in a rotating frame; this is confirmed in the right-most plot. This occurs because the engineered Markovian environment has been replaced by a mode with a finite damping rate, which means that the response of this mode now has a finite bandwidth and is therefore no longer flat over the entire frequency domain. As a result, perfectly asymmetrical scattering can now only be realised for a single frequency. So, while it is not required that the auxiliary mode be highly damped, the width of $N^{(1,2)}$ as a function of frequency increases for larger values of κ_3.

It is important to point out that nonreciprocity, as defined in Section 2.4.2.1, is concerned with the dynamics of the internal modes of the system, while the definition in Section 2.4.2.2 concerns the scattering properties, and hence the behaviour of the input and output fields. This example has therefore demonstrated that the occurrence of nonreciprocal behaviour in the internal and propagating modes is related and appears under the same parameter conditions.

2.5 Introducing the Nonreciprocal Quantum Amplifiers

A variety of topics have been introduced in this chapter to provide the required theoretical background for this work, which warrants a summary. The chapter began with an introduction to Gaussian states and their structural properties, demonstrating that such states can be represented entirely using their means and covariances. Such a representation, which is intimately connected with the Wigner phase space, frees us from representing such states in the infinite-dimensional Hilbert space. It was then demonstrated that dynamical processes which preserve Gaussian states can also be easily represented as transformations on these moments. This included the dynamics for open quantum systems, where both the Lindblad master equation and Heisenberg-Langevin equations yield the same dynamical equations for the moments of the internal system modes. This Gaussian description of states was also extended to propagating bath modes, which also satisfied the necessary requirements. Subsequently, input-output theory allowed for the transformation of input fields to output fields to be expressed entirely in terms of a scattering matrix.

The realities of physically engineering such systems through the modulation of parametric couplings were then introduced in the following section. Using superconducting circuits as a motivating example, it was demonstrated that the coupling between a pair of harmonic modes and a classical-like pump could be used to engineer specific coherent interactions between the quantum modes of the system. These interactions allowed for the conversion of photons between modes of different frequencies, along with the enhancement of input fields through linear parametric amplification. We finally introduced the concept of nonreciprocity, where it was shown that two approaches based on engineered dissipation and the interference of scattering processes yielded the same conditions for nonreciprocity when applied to Gaussian systems. An important result is that nonreciprocity, and hence directional signal routing, requires a minimum of three harmonic modes, all coupled via Gaussian coherent processes.

With this information, we can conclude that any nonreciprocal linear quantum amplifier must necessarily be composed of at least three harmonic modes. In fact, there are two three-mode configurations which have been realised in superconducting circuit systems: we refer to these as the *delta amplifier* [18, 19] and the *bowtie amplifier* [20, 30]. The name of these amplifiers derives from a graphical representation of the dynamical couplings between the ladder operators, as shown in Figure 2.3. To finish this section, we will demonstrate how parametrically coupled systems can be used to obtain the desired Hamiltonians; details regarding the scattering behaviour will be omitted, but may be found in the aforementioned references.

The first configuration we will consider is the delta amplifier, which may be operated as a directional phase-preserving amplifier. We can start with a pumped Hamiltonian for a three-mode loop

$$\hat{H}^{\mathrm{p}}_{\mathrm{loop}} = \sum_{k=1,2,3} \omega_k \hat{a}_k^\dagger \hat{a}_k + \sum_{(j,k)\in V_\Delta} 2g_{jk} \cos\left(\omega^{\mathrm{p}}_{jk} t + \phi^{\mathrm{p}}_{jk}\right)\left(\hat{a}_j^\dagger e^{i\phi_j} + \hat{a}_j e^{-i\phi_j}\right)\left(\hat{a}_k^\dagger e^{i\phi_k} + \hat{a}_k e^{-i\phi_k}\right), \tag{2.143}$$

where $V_\Delta = \{(1,2),(1,3),(2,3)\}$ is the set of mode pairs. This amplifier requires that two of the interactions be nondegenerate parametric amplifiers, while the third is a frequency converter, or equivalently two two-mode squeezers and a beam splitter. This imposes the following constraints on the pump frequencies: $\omega^{\mathrm{p}}_{12} = \omega_1 + \omega_2$, $\omega^{\mathrm{p}}_{23} = \omega_2 + \omega_3$, and $\omega^{\mathrm{p}}_{13} = |\omega_1 - \omega_3|$. In order for the RWA to be applied, all mode frequencies must be well-separated and the linewidths small, $\kappa_k \ll \omega_k$. Under this assumption, the Hamiltonian may be written in the rotating frame as

$$\hat{H}_\Delta = g_{12}\left(\hat{a}_1^\dagger \hat{a}_2^\dagger + \hat{a}_1 \hat{a}_2\right) + g_{13}\left(\hat{a}_1^\dagger \hat{a}_3 + \hat{a}_1 \hat{a}_3^\dagger\right) + g_{23}\left(e^{i\phi}\hat{a}_2^\dagger \hat{a}_3^\dagger + e^{-i\phi}\hat{a}_2 \hat{a}_3\right), \tag{2.144}$$

where ϕ is referred to as the loop-phase. To obtain the above expression, two of the arbitrary pump phases were set to $\phi_{12}^{\mathrm{p}} = \phi_1 + \phi_2$ and $\phi_{13}^{\mathrm{p}} = |\phi_1 - \phi_3|$; the loop phase may then be written entirely in terms of the pump phases, $\phi \equiv \phi_{12}^{\mathrm{p}} \pm \phi_{13}^{\mathrm{p}} - \phi_{23}^{\mathrm{p}}$. Since this phase has no dependence on the phases of the modes, it cannot be eliminated via a gauge transformation, and hence is always present. As discussed in the previous section, correctly tuning this phase will be necessary for controlling the direction of signal propagation between the ports of a nonreciprocal three-mode system.

The other configuration is the bowtie amplifier, which behaves as a directional phase-sensitive amplifier under proper operation. In this case, we start with the pumped loop Hamiltonian $\hat{H}_{\mathrm{loop}}^{\mathrm{p}}$ again, and apply a fourth pump tone to one of the modes to realise a single-mode squeezing interaction,

$$\hat{H}_{\mathrm{loop}}^{\mathrm{p}} + \lambda \cos\left(\omega_2^{\mathrm{p}} t + \phi_2^{\mathrm{p}}\right)\left(\hat{a}_2^\dagger e^{i\phi_2} + \hat{a}_2 e^{-i\phi_2}\right)^2 . \tag{2.145}$$

The pump frequencies between the mode pairs are chosen to realise three beam splitter interactions, $\omega_{12}^{\mathrm{p}} = |\omega_1 - \omega_2|$, $\omega_{23}^{\mathrm{p}} = |\omega_2 - \omega_3|$, and $\omega_{13}^{\mathrm{p}} = |\omega_1 - \omega_3|$, which on their own can be used to create a circulator device as described in Figure 2.1. The fourth pump frequency must be twice the mode frequency $\omega_2^{\mathrm{p}} = 2\omega_2$ in order to realise degenerate parametric amplification. Assuming the system parameters allow for the invocation of the RWA, the Hamiltonian for the bowtie amplifier is

$$\hat{H}_{\bowtie} = g_{12}\left(\hat{a}_1^\dagger \hat{a}_2 + \hat{a}_1 \hat{a}_2^\dagger\right) + g_{13}\left(\hat{a}_1^\dagger \hat{a}_3 + \hat{a}_1 \hat{a}_3^\dagger\right) + g_{23}\left(e^{i\phi}\hat{a}_2^\dagger \hat{a}_3 + e^{-i\phi}\hat{a}_2 \hat{a}_3^\dagger\right) + \frac{\lambda}{2}\left(e^{i\theta}\hat{a}_2^{\dagger\,2} + e^{-i\theta}\hat{a}_2^2\right). \tag{2.146}$$

The irremovable loop phase ϕ is once again present in the Hamiltonian, ensuring that we can control the direction of propagation of the amplified output signals. The phase $\theta = 2\phi_2 - \phi_2^{\mathrm{p}}$ is also always present, and determines which quadratures are amplified by the DPA.

As demonstrated in Section 2.4.2.3, nonreciprocity between a pair of interacting harmonic modes is dependent not only on the choice of phases but also on the proper balancing of the coherent and dissipative rates in the system. Both the delta and bowtie amplifiers are comprised of three pair-wise interactions between the modes, and any one of these three interactions can be made nonreciprocal with the proper choice of system parameters. Choosing which interactions to make nonreciprocal will depend on what behaviour is desired of the amplifier: in Chapter 3, the demand to realise bipartite entanglement of the output fields for different modes means that the amplifiers are required to act as directional multiport devices, where amplified signals are emitted in multiple directions. In Chapter 4, on the other hand, the constraints imposed by the motivating physical device mean that the signal should enter and leave through the same port, and so this amplifier is operated as a single-port device. Additionally, it must direct amplified noise away from the sensitive qubit. Given the disparity in operation, the conditions for, and consequences of, nonreciprocity in these three-mode amplifiers will therefore be deferred until required in each chapter.

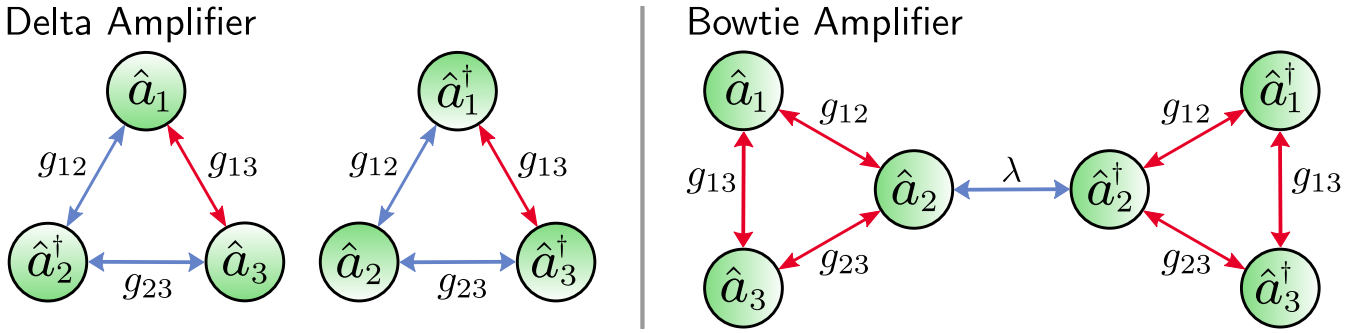

Figure 2.3: Graphical representation of the two three-mode amplifiers considered in this work, which inspire their names: [Left] the delta amplifier, and [Right] the bowtie amplifier. The graphs represent the coupling between the ladder operators in the dynamical equations for the delta and bowtie amplifier, which are a result of the Hamiltonians in Eqs. (2.144) and (2.146), respectively. Blue arrows denote parametric amplification, or squeezing, interactions, while red arrows denote frequency conversion, or beam splitters. These colours are chosen because pumping the PA interaction for any pair of modes requires a higher pump frequency than the FC interaction. The coupling between the ladder operators is simple for the delta amplifier, which decomposes into two graphs, each comprised of two PAs with rate g_{12} and g_{23}, and one FC with rate g_{13}. The graph for the bowtie amplifier is comprised of two connected loops, each consisting of three FC interactions with rates g_{12}, g_{13}, and g_{23}, which are coupled via a DPA with rate λ.

3 Entanglement Generation in Nonreciprocal Quantum Amplifiers

The generation of high-fidelity entangled states is fundamental for the realisation of quantum information processing (QIP) and communication protocols. While qubits are well-suited for local QIP operations, photons present the best option [87] for realising distributed quantum information processing and communication protocols over long distances between modes in a quantum network [88–93]. The branch of QIP that focuses on the manipulation of photons is called *continuous variable quantum information* [94–99], the basis components of which are the Gaussian states and transformations introduced in Chapter 2. The distribution of maximally entangled states is, however, hampered by the presence of decoherence channels and other sources of environmental noise, which induce errors and reduce the fidelity of the entangled state. While the error correction of CV states can be achieved through the use of linear optical elements, corresponding to Gaussian transformations [100, 101], improving the fidelity through distillation and purification cannot be achieved through the use of Gaussian transformations alone [102]. As a result, nonlinear transformations are required [103–109] which are currently difficult to implement in the microwave and radio-frequency (RF) regimes.

Thermal fluctuations in the environment provide one source of decoherence, which may be mitigated by operating at cryogenic temperatures provided that $k_b T \ll \hbar\omega$. Thus, the impact of thermal noise may be reduced for mode frequencies in the microwave domain. In lower frequency bands, such as the RF domain that is ubiquitous in modern communication, thermal fluctuations are still a significant barrier, appreciable even at the coldest operating temperatures [110–112], presenting challenges for RF quantum communication and sensing. Given the limitations with exist at cryogenic temperatures, alternative approaches must be considered to generate high-fidelity entanglement in systems with hot modes. In this chapter, we present an approach utilising engineered nonreciprocity to directionally route these thermal fluctuations, allowing for the generation of high-purity entangled states with an increased robustness to thermal excitations. For this purpose, we will use the previously introduced delta and bowtie linear nonreciprocal quantum amplifiers.

Linear quantum amplifiers create entanglement between photons using the same mechanism that enables them to amplify weak signals: through squeezing. For these ported systems, two forms of entanglement are possible, termed the *intracavity* and *output* entanglement, shown pictorially in Figure 3.1. Intracavity entanglement is formed between the coherently coupled internal modes of the amplifier, while output entanglement is generated between the propagating output fields emitted through the amplifier ports. These propagating output fields correspond to resonant modes of the electromagnetic field within the transmission line or resonators coupled to the amplifier ports, and so will alternatively be referred to as *cavities*. While the amount of intracavity entanglement correlations is inherently limited, there is no bound on the strength of these correlations between the propagating modes, allowing the latter to form highly entangled states. We are interested in operating these amplifiers as multiport devices, so that these highly entangled propagating states can be directed towards different nodes in a quantum network.

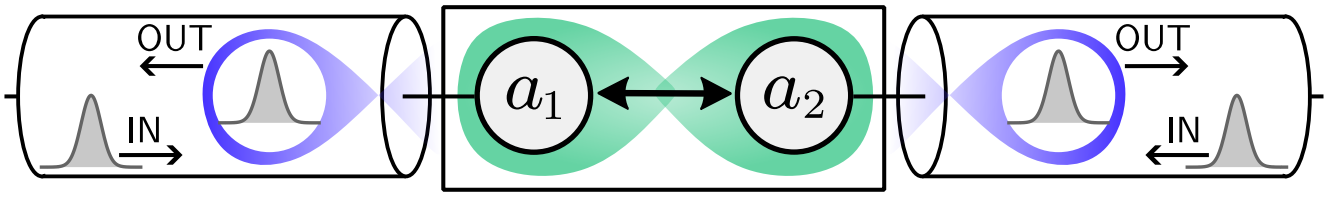

Figure 3.1: A diagram of two coherently interacting harmonic modes, a_1 and a_2, each coupled to a transmission line resonator. The resonant modes of the transmission lines support propagating fields, in the form of incoming input fields and outgoing output fields. Two types of entanglement are present in the system: entanglement between the internal harmonic modes, termed intracavity entanglement, and entanglement between the output fields, termed output entanglement. The input fields are uncorrelated Gaussian white noise processes, and hence are never entangled.

While several proposals and recent experiments consider the entanglement of the output fields of cold modes coupled via an intermediate hot mode [113–119], we consider situations where the output fields to be entangled themselves are effectively coupled to high-temperature baths. The presence of this noise, which is particularly evident in RF modes, can severely limit the entanglement fidelity of the emitted output from such hot modes at a given pump power through the degradation of the joint-state purity. We will demonstrate that the use of nonreciprocity is crucial to alleviate the effects through its ability to continuously reroute thermal excitations towards a cold output. This enables the entanglement of propagating photons with much higher purity than is possible using a completely reciprocal two-mode entangling interaction between the hot modes of interest. To determine the optimum regime of the delta and bowtie amplifier for this thermal routing, we will also investigate the effects of nonreciprocity on the generation of output entanglement, as this goes beyond the traditional signal processing applications. We will begin with an introduction to the ingredients which will be used in this section to characterise the quantum state: the separability criterion for a CV state, the entanglement monotone known as the logarithmic negativity, and the purity.

3.1 Entanglement in Continuous Variable Systems

3.1.1 Introduction

Entanglement is a type of correlation unique to composite quantum systems, which is present when the states of the subsystems cannot be described independently of each other. To investigate the ability of these nonreciprocal quantum amplifiers to generate entangled states, specific methods must be introduced which can be used to characterise this phenomenon. We must therefore make clear the distinction between a separable and an entangled state. We first bipartition the Hilbert space of the composite system, $\mathcal{H} = \mathcal{H}_A \otimes \mathcal{H}_B$, therefore dividing it between two parties A and B. A state of the composite system, $\hat{\rho}$, is defined as *separable* on this bipartition if it can be written as a convex combination of product states,

$$\hat{\rho} = \sum_k p_k \, |\psi_k^A\rangle\langle\psi_k^A| \otimes |\psi_k^B\rangle\langle\psi_k^B| \quad \text{where} \quad p_k \geq 0 \, , \sum_k p_k = 1. \tag{3.1}$$

A state is defined as *entangled* if it cannot be written in the above form. Separable states can always be created using local quantum operations performed independently by parties A and B, as well as classical communication, by which the two parties can coordinate and optimise their local operations [120]. As a result, such operations, termed *local operations and classical communication* (LOCC), are unable to generate entanglement correlations.

Now that we have some basic notion of what entanglement is, we must define a measure of entanglement so that when given an arbitrary state, we have some way of quantifying how entangled it is. One measure is the entropy of entanglement [121], however, this measure is only defined for pure states. The situation becomes complicated when considering mixed states, as there is no single measure of entanglement [120, 122], and many of the measures which have been introduced are difficult to compute. The easiest to calculate is the *logarithmic negativity* [123], and it is the one that will be used in this work. The logarithmic negativity has been proven to satisfy the properties of an *entanglement monotone* [124], which means it satisfies the following three properties: it should quantify entanglement using a non-negative real number, it should return zero if the state is separable, and it should not increase on average through the use of LOCCs. The last property is particularly important: since LOCCs alone can only generate separable states, they should never increase the amount of entanglement in a system, and so any method of calculating the amount of entanglement should not return a larger number after the application of LOCCs on a state. An *entanglement measure* has the added property that, when applied to a pure state, it is identical to the entropy of entanglement [120].

Entanglement is an important resource for quantum information processing applications [122], however, these applications generally require states which are maximally entangled [94, 97, 98], which means that they must be pure and highly entangled. However, quantum states are fragile, and performing operations or transmitting the state can decrease the purity and entanglement. By performing state purification and distillation, the local parties can turn several copies of states with low purity or entanglement into a smaller number of maximally entangled states using LOCC [121, 125, 126]. For continuous variable Gaussian states, it has been proven that this is not possible using LOCC with only Gaussian transformations, and that nonlinear processes are therefore required [102, 104, 106, 107]. The entanglement correlations that can be extracted in this process are known as the *distillable entanglement*; importantly, the logarithmic negativity provides an upper bound on the amount of distillable entanglement in a bipartite system [123]. There may be entanglement correlations which cannot be accessed by LOCC alone, known as *bound entanglement* [127, 128], and which are therefore unusable in distillation protocols. Having given a descriptive overview of quantum entanglement, we can now proceed to the specific technical definitions we will use to characterise the entanglement and purity of Gaussian continuous variable states.

3.1.2 Separability of Bipartite States

3.1.2.1 Positive Partial Transpose Criterion

The condition we will use to determine if a state is separable is the Peres–Horodecki criterion [129–131], also called the *positive partial transpose criterion* (PPT criterion). In order to explain this criterion, we must first define the partial transpose operation. We begin with a bipartite system, with the two parties labelled A and B; for a density operator $\hat{\rho}$, written in some arbitrary basis as

$$\hat{\rho} = \sum_{j,k|l,m} p_{j,k|l,m} \left|\psi_j^A\right\rangle\!\left\langle\psi_k^A\right| \otimes \left|\psi_l^B\right\rangle\!\left\langle\psi_m^B\right|, \tag{3.2}$$

the partial transpose with respect to B, denoted $\hat{\rho}^{T_B}$, is defined as

$$\hat{\rho}^{T_B} := \sum_{j,k|l,m} p_{j,k|l,m} \left|\psi_j^A\right\rangle\!\left\langle\psi_k^A\right| \otimes \left|\psi_m^B\right\rangle\!\left\langle\psi_l^B\right|. \tag{3.3}$$

The partial transpose obviously has the property $(\hat{\rho}^{T_A})^T = \hat{\rho}^{T_B}$. The PPT criterion says that a bipartitioned state is separable if its partial transpose is also positive semi-definite, $\hat{\rho}^{T_B} \geq 0$ or, equivalently, $\hat{\rho}^{T_A} \geq 0$, and is therefore also a density operator. Since the partial transpose of $\hat{\rho}$ is also Hermitian and has trace one, this is the only property of a density operator that the partial transpose can possibly violate. A physical interpretation of this criterion comes from the fact that the transpose operation corresponds to *time reversal* at the level of the density operator [127], so a state is separable if the partially time-reversed state is also a bona fide quantum state.

For finite level systems, this criterion has been shown to be necessary and sufficient for determining whether a state is separable for two cases of bipartite systems: a pair of two-level systems, and a pair of one two-level and one three-level system [130]. For Gaussian states, the criterion is necessary and sufficient for a bipartite system consisting of a pair of bosonic modes [132], for a bipartition consisting of one bosonic mode in one partition and N bosonic modes in the other partition [128], and for a class of Gaussian states which is termed bisymmetric [133]. For all other states, it fails to be a sufficient condition, since there exist states which satisfy the PPT criterion but are entangled, which are called bound entangled states [128]; in such cases, other criteria must be considered [134–136]. Despite this, violating the PPT criterion is still a sufficient test to determine whether an entangled state can be distilled [105, 137], and so bound states contain no distillable entanglement correlations.

The nonreciprocal amplifiers we are considering consist of three bosonic modes, so no matter which bipartition we choose, the use of the PPT criterion will be necessary and sufficient to determine whether the resulting state is separable. Since computing the logarithmic negativity for the three $(2,1)$-mode bipartitions does not generate any additional information that is not already provided by the three $(1,1)$-mode partitions, we will focus on computing the latter. Focusing on the entanglement between only pairs of bosonic modes also means that, provided the states are entangled, it is guaranteed that all entanglement correlations are distillable. To provide some insight into what the logarithmic negativity is computing when applied to Gaussian states, we will go into greater depth about what the PPT criterion means for Gaussian states.

3.1.2.2 Separability Criterion for Continuous Variable States

We consider a continuous variable system bipartitioned into two sets of bosonic modes, A and B. Partitions A and B have N_A and N_B bosonic modes, respectively, along with their own sets of quadrature operators, $(\hat{\boldsymbol{q}}_A, \hat{\boldsymbol{p}}_A)$ and $(\hat{\boldsymbol{q}}_B, \hat{\boldsymbol{p}}_B)$. We proceed to map the Gaussian state $\hat{\rho}$ to its Wigner function:

$$\hat{\rho} \longleftrightarrow W_\rho(\boldsymbol{q}_A, \boldsymbol{p}_A, \boldsymbol{q}_B, \boldsymbol{p}_B). \tag{3.4}$$

Applying the transpose to the state $\hat{\rho}$ corresponds to time reversal for the associated Wigner function, which on the level of phase space corresponds to a sign reversal on the momentum coordinates [98, 132]. The partial transpose therefore corresponds to a time reversal applied to one of the two sets of momenta, which we choose to apply to partition B:

$$\hat{\rho}^{T_B} \longleftrightarrow W_\rho(\boldsymbol{q}_A, \boldsymbol{p}_A, \boldsymbol{q}_B, -\boldsymbol{p}_B). \tag{3.5}$$

If we define this specific ordering of the coordinates as the following column vector $\boldsymbol{r}_{AB} := \mathrm{col}(\boldsymbol{q}_A, \boldsymbol{p}_A, \boldsymbol{q}_B, \boldsymbol{p}_B)$, then the partial transpose of B can be implemented as a matrix transformation, $\boldsymbol{\Lambda} := \mathrm{diag}(\mathbf{I}_{N_A}, \mathbf{I}_{N_A}, \mathbf{I}_{N_B}, -\mathbf{I}_{N_B})$. The means of this state can be set to any value by a purely local displacement transformation on the state, and so they are not important for determining whether a state is separable or entangled, since they can be altered by LOCC.

The important quantity to look at is the covariance matrix, which for the partially transposed state we define as

$$\tilde{\boldsymbol{\sigma}} := \boldsymbol{\Lambda}\boldsymbol{\sigma}\boldsymbol{\Lambda}. \tag{3.6}$$

The PPT criterion can then be expressed in the following manner: If $W_\rho(\boldsymbol{r})$ is a Wigner function of a true quantum state then it is separable if $W_\rho(\boldsymbol{\Lambda r})$ is also the Wigner function of a true quantum state [98, 132]. We recall from Eq. (2.10) that the covariance matrix of a true Wigner function must obey the uncertainty relation; this fact allows us to express the PPT criterion for Gaussian states in terms of the following requirement on the covariance matrices:

$$\text{If} \quad \boldsymbol{\sigma} + \frac{i}{2}\boldsymbol{\Omega} \geq 0 \quad \text{and} \quad \tilde{\boldsymbol{\sigma}} + \frac{i}{2}\boldsymbol{\Omega} \geq 0 \quad \text{then } \hat{\rho} \text{ is separable.} \tag{3.7}$$

Since the relation for $\boldsymbol{\sigma}$ is always satisfied for a true quantum state, the PPT criterion then states that if $\tilde{\boldsymbol{\sigma}}$ violates uncertainty, the state may be entangled. We emphasise that regardless of the above, even if the Wigner function no longer represents a true quantum state, it must still be a Gaussian distribution, and as such the trace of $\hat{\rho}^{T_B}$ must still converge, indicating that the Wigner function must be integrable, and hence $\tilde{\boldsymbol{\sigma}} \geq 0$.

3.1.2.3 Simon's Criterion

As previously stated, since satisfying the PPT criterion is generally only a necessary but not sufficient condition for the state to be separable, there are states which satisfy the criteria which turn out to be entangled. It is, however, necessary and sufficient when each party has one bosonic mode, where the PPT criterion is equivalent to the well-known Simon's criterion [132]. Another necessary and sufficient criterion for systems of two bosonic modes has also been introduced, known as Duan's criterion [138], which is based on the variance of Einstein–Podolsky–Rosen (EPR) type operators constructed using the covariance matrix of a two-mode Gaussian state. Simon's criterion, on the other hand, is based on certain symplectic invariants of the partial transposed covariance matrix, and since the partial transpose is used when calculating the chosen measure of entanglement [123], it is the one we use when checking whether a state is entangled.

In order to demonstrate the idea behind Simon's criterion, we start with the uncertainty relations Eq. (3.7) for a Gaussian state. The uncertainty relations for a true quantum state always hold, and so for a Gaussian state, they are necessarily invariant under all Gaussian unitary transformations acting on the Hilbert space. We recall from Section 2.1.4 that Gaussian unitary transformations on Gaussian states correspond to symplectic transformations on the covariance matrix, meaning that the uncertainty, $\boldsymbol{\sigma} + i\boldsymbol{\Omega}_2/2 \geq 0$, for a two-mode state is always invariant under $Sp(4,\mathbb{R})$. For a separable state, the uncertainty relation for the partially time-reversed state must also be preserved, $\tilde{\boldsymbol{\sigma}} + i\boldsymbol{\Omega}_2/2 \geq 0$. Both conditions are only satisfied under the set of independent local Gaussian unitary transformations, which corresponds to the set of operations from $Sp(2,\mathbb{R})$ applied to the individual modes; the entire set of local Gaussian unitary operations is then the subset $Sp(2,\mathbb{R}) \oplus Sp(2,\mathbb{R}) \subset Sp(4,\mathbb{R})$. It is required that the criterion be invariant under transformations from $Sp(2,\mathbb{R}) \oplus Sp(2,\mathbb{R})$, since this is equivalent to stating that LOCC cannot generate entanglement correlations,

The uncertainty relation for covariance matrices, $\boldsymbol{\sigma} + i\boldsymbol{\Omega}_2/2 \geq 0$, can be expressed in terms of quantities of the covariance matrix which do not change under the set of local transformations, $Sp(2,\mathbb{R}) \oplus Sp(2,\mathbb{R})$:

$$\det[\mathbf{A}]\det[\mathbf{B}] + \left(\frac{1}{4} - \det[\mathbf{C}]\right)^2 - \mathrm{Tr}\left[\mathbf{A}\boldsymbol{\Omega}_1\mathbf{C}\boldsymbol{\Omega}_1\mathbf{B}\boldsymbol{\Omega}_1\mathbf{C}^T\boldsymbol{\Omega}_1\right] \geq \frac{1}{4}\big(\det[\mathbf{A}] + \det[\mathbf{B}]\big). \tag{3.8}$$

Here, $\boldsymbol{\Omega}_1 := \left(\begin{smallmatrix} 0 & 1 \\ -1 & 0 \end{smallmatrix}\right)$ is the symplectic form for a single mode system, and the covariance matrix is written in terms of 2×2 blocks, $\boldsymbol{\sigma} = \left(\begin{smallmatrix} \mathbf{A} & \mathbf{C} \\ \mathbf{C}^T & \mathbf{B} \end{smallmatrix}\right)$. The only $Sp(2,\mathbb{R}) \oplus Sp(2,\mathbb{R})$ invariant quantity which changes for the covariance matrix of the partially time-reversed state, $\tilde{\boldsymbol{\sigma}}$, is the sign of $\det[\mathbf{C}]$. The uncertainty relation for $\tilde{\boldsymbol{\sigma}}$ is therefore identical to Eq. (3.8), but with a sign change on the $\det[\mathbf{C}]$ term, $(1/4 - \det[\mathbf{C}])^2 \to (1/4 + \det[\mathbf{C}])^2$. If $\det[\mathbf{C}] \geq 0$, then the fact that $\boldsymbol{\sigma}$ obeys Eq. (3.8) means that $\tilde{\boldsymbol{\sigma}}$ will also obey the uncertainty relation, and is therefore also a true quantum state. Hence, two-mode Gaussian states with $\det[\mathbf{C}] \geq 0$ are always separable. If $\det[\mathbf{C}] < 0$, then the uncertainty relation for $\boldsymbol{\sigma}$ is stronger than the one for $\tilde{\boldsymbol{\sigma}}$; since it is not possible to determine in general whether or not $\tilde{\boldsymbol{\sigma}}$ satisfies the uncertainty relation here, the state defined by $\boldsymbol{\sigma}$ may be separable or entangled in this instance. Bringing both cases together, the PPT criterion Eq. (3.7) may then be expressed in the following form for a two-mode Gaussian state,

$$\det[\mathbf{A}]\det[\mathbf{B}] + \left(\frac{1}{4} - |\det[\mathbf{C}]|\right)^2 - \mathrm{Tr}\left[\mathbf{A}\boldsymbol{\Omega}_1\mathbf{C}\boldsymbol{\Omega}_1\mathbf{B}\boldsymbol{\Omega}_1\mathbf{C}^T\boldsymbol{\Omega}_1\right] \geq \frac{1}{4}\big(\det[\mathbf{A}] + \det[\mathbf{B}]\big). \tag{3.9}$$

which is known as Simon's criterion.

3.1.3 The Logarithmic Negativity

With the PPT criterion established as a necessary criterion for entangled states, we can now proceed to use the partially transposed state to quantify how entangled a state is. Two easily computable entanglement monotones can be constructed using the partially transposed state: the negativity and the logarithmic negativity [123]. The positive semi-definite criterion for a density operator, $\hat{\rho}$, means that all eigenvalues must satisfy $\lambda_k \geq 0$. The negativity uses the fact that some eigenvalues, $\tilde{\lambda}_k$, of the partially transposed state can take negative values if the state is entangled to quantify the entanglement:

$$\mathcal{N}(\hat{\rho}) := \frac{1}{2}\Big(||\hat{\rho}^{T_B}||_1 - 1\Big) \equiv \frac{1}{2}\sum_n \big|\tilde{\lambda}_k\big| - \tilde{\lambda}_k. \tag{3.10}$$

Here, $||\mathbf{A}||_1 := \mathrm{Tr}\big[\sqrt{\mathbf{A}^\dagger \mathbf{A}}\,\big]$ is the trace norm. The more commonly used logarithmic negativity may be defined in terms of the negativity as,

$$E_{\mathcal{N}}(\hat{\rho}) := \ln\big(||\hat{\rho}^{T_B}||_1\big) = \ln(2\mathcal{N}(\hat{\rho}) + 1), \tag{3.11}$$

and will be the entanglement monotone used in this work, since it has more useful properties compared to the negativity. The two most important properties are that it is additive for tensor products of states, $E_{\mathcal{N}}(\hat{\rho}^A \otimes \hat{\rho}^B) = E_{\mathcal{N}}(\hat{\rho}^A) + E_{\mathcal{N}}(\hat{\rho}^B)$, and that it provides an upper bound on the amount of distillable entanglement [124].

For Gaussian states, the logarithmic negativity may be expressed in terms of the symplectic eigenvalues of the partially transposed state [123]. This is done by applying the Williamson normal mode decomposition from Section 2.1.5 to unitarily diagonalise the partially transposed state as a product state of thermal states. Using the fact that the logarithmic negativity is additive for tensor products, we can instead express $E_{\mathcal{N}}(\hat{\rho})$ as a sum over the thermal normal modes as,

$$E_{\mathcal{N}}(\hat{\rho}) \equiv \sum_{k=1}^{N} \ln\big(||\hat{\rho}_k^{\mathrm{th}}||_1\big) \quad \text{where} \quad \hat{\rho}^{T_B} = \hat{U}\left(\bigotimes_{k=1}^{N} \hat{\rho}_k^{\mathrm{th}}\right)\hat{U}^\dagger. \tag{3.12}$$

The thermal density operators may be written in the number eigenstate basis as $\hat{\rho}_k^{\mathrm{th}} = (1 - z_k)\sum_n z_k^n \,|n\rangle_k\langle n|_k$ where $z_k = \bar{n}_k/(\bar{n}_k + 1)$ is a function of the mean number of photons in the thermal state. We recall that the symplectic eigenvalues of $\hat{\rho}^{T_B}$ can also be expressed as $\tilde{\nu}_k = \bar{n}_k + 1/2$, meaning that we can write $\tilde{\nu}_k = (1 - z_k)^{-1} - 1/2$. Now, quantum states which obey the uncertainty principle have symplectic eigenvalues which are bounded below by the uncertainty of a vacuum state, $\tilde{\nu}_k \geq 1/2$, which implies that $\bar{n}_k \geq 0$.

However, the partially transposed $\hat{\rho}^{T_B}$ may not be a true quantum state if $\hat{\rho}$ is entangled by the PPT criterion, and so its symplectic eigenvalues can have variance below the vacuum, $\tilde{\nu}_k < 1/2$, violating the uncertainty relation. The Wigner function of $\hat{\rho}^{T_B}$ should still correspond to an integrable Gaussian function so $\tilde{\boldsymbol{\sigma}} > 0$, meaning that even if the uncertainty relation is violated, the symplectic eigenvalues are still bounded from below, $0 < \tilde{\nu}_k$. If a symplectic eigenvalue is in the range $0 < \tilde{\nu}_k < 1/2$, then the effective thermal occupation would be negative for that normal mode. The implication is that z_k is negative if $\tilde{\nu}_k < 1/2$, and therefore the trace norm must be $||\hat{\rho}||_1 = (1 - z_k)/(1 - |z_k|)$, which is equal to one if $\tilde{\nu}_k \geq 1/2$. Using the preceding expressions, we can finally write the logarithmic negativity in terms of the symplectic eigenvalues of the partially transposed state:

$$E_{\mathcal{N}}(\hat{\rho}) = \sum_{k=1}^{N} \begin{cases} 0 & \text{for } \tilde{\nu}_k \geq 1/2 \\ -\ln(2\tilde{\nu}_k) & \text{for } 0 < \tilde{\nu}_k < 1/2 \end{cases}. \tag{3.13}$$

If the PPT criterion from Eq. (3.7) is satisfied then the above is necessarily zero, however, if $\tilde{\boldsymbol{\sigma}} + i\boldsymbol{\Omega}/2 < 0$ then we are guaranteed that are least some of the symplectic eigenvalues for the partially transposed state violated uncertainty, $\tilde{\nu}_K < 1/2$, and the degree to which they violated this condition is captured by the logarithmic negativity. The entangled for Gaussian states as measured by the logarithmic negativity therefore increases without bound, $E_{\mathcal{N}}(\hat{\rho}) \to \infty$, as $\tilde{\nu}_k$ approaches the minimum allowed value, $\tilde{\nu}_k \to 0$. The logarithmic negativity will also increase as more normal modes of the partially transposed state violate uncertainty.

In the simplest case, where there are only two modes in the composite system, analytic expressions are guaranteed for the symplectic eigenvalues of the partially transposed state. The characteristic equation for $\boldsymbol{\Omega}_2\tilde{\boldsymbol{\sigma}}$ can be written as,

$$\tilde{\nu}^4 + \eta\tilde{\nu}^2 + \det[\boldsymbol{\sigma}] = 0 \quad \text{where} \quad \eta = \det[\mathbf{A}] + \det[\mathbf{B}] - 2\det[\mathbf{C}] \quad \text{and} \quad \boldsymbol{\sigma} = \begin{pmatrix} \mathbf{A} & \mathbf{C} \\ \mathbf{C}^T & \mathbf{B} \end{pmatrix}. \tag{3.14}$$

The characteristic equation has the solutions $\pm\tilde{\nu}_+$ and $\pm\tilde{\nu}_-$, which can be expressed as follows,

$$\tilde{\nu}_\pm = \frac{1}{\sqrt{2}}\sqrt{\eta \pm \sqrt{\eta - 4\det[\boldsymbol{\sigma}]}}. \tag{3.15}$$

It can be shown that $\tilde{\nu}_+$, the maximum symplectic eigenvalue, obeys $\tilde{\nu}_+ \geq 1/2$ and so always satisfies the uncertainty relation. The minimum symplectic eigenvalue, $\tilde{\nu}_-$, can violate uncertainty, and does so for covariance matrices which violate Simon's criterion. The logarithmic negativity for a two-mode system may then be expressed succinctly as:

$$E_{\mathcal{N}}(\hat{\rho}) = \begin{cases} 0 & \text{for } \tilde{\nu}_- \geq 1/2 \\ -\ln(2\tilde{\nu}_-) & \text{for } 0 < \tilde{\nu}_- < 1/2 \end{cases}. \tag{3.16}$$

3.1.4 Purity of Gaussian States

The final measure we will consider is the purity, which naturally quantifies how mixed the state is. In this work, we define the purity, $\mathcal{P}$, as follows,

$$\mathcal{P} := \mathrm{Tr}\big[\hat{\rho}^2\big] \quad \text{where the purity is bounded by} \quad 0 < \mathcal{P} \leq 1. \tag{3.17}$$

A state is considered pure if the measure is $\mathcal{P} = 1$, in which case the density operator is idempotent, $\hat{\rho}^2 = \hat{\rho}$, and hence may be expressed as a projector onto some state vector $|\psi\rangle$, by $\hat{\rho} = |\psi\rangle\langle\psi|$. If the purity is, however, strictly less than unity, $\mathcal{P} < 1$, then the state is considered mixed. For quantum systems with finite dimension, d, the purity is easily calculated using a matrix representation of the density operator. The purity can also be shown to be bounded from below, $\mathcal{P} \geq 1/d$, and states which saturate this lower bound are called maximally mixed states.

For continuous variable systems, the Hilbert space is infinite dimensional, and so for ease we use the Wigner function associated with $\hat{\rho}$, which will allow us to perform the trace by integrating over the Wigner phase space. The purity may then be written as,

$$\mathcal{P} = \int_{\mathbb{R}^{2N}} W_\rho(\boldsymbol{r}) \star W_\rho(\boldsymbol{r})\, d^{2N}\boldsymbol{r} = \int_{\mathbb{R}^{2N}} W_\rho(\boldsymbol{r})^2\, d^{2N}\boldsymbol{r}, \tag{3.18}$$

where the simplification comes from the fact that exactly one Moyal star-product may be replaced by a scalar product when integrating over the entire phase space of the Wigner representation; refer to Eq. (A.18) in Appendix A. If $W_\rho(\boldsymbol{r})$ corresponds to a Gaussian state, we are then performing a phase space integral of the function,

$$W_\rho(\boldsymbol{r})^2 = \frac{1}{(2\pi)^{2N}\det[\boldsymbol{\sigma}]} \exp\Big[-(\boldsymbol{r}-\boldsymbol{\mu})^T\boldsymbol{\sigma}^{-1}(\boldsymbol{r}-\boldsymbol{\mu})\Big], \tag{3.19}$$

which yields the following definition for the purity of a Gaussian state, which is only dependent on the covariance matrix:

$$\mathcal{P} = \frac{1}{2^N\sqrt{\det[\boldsymbol{\sigma}]}}. \tag{3.20}$$

Defining the purity in terms of the covariance matrix also allows for marginal purities to be quickly calculated since the partial trace of a Gaussian state is guaranteed to produce another Gaussian state. In the case of a two-mode system, inequalities can be established between the marginal purities and the global purity, which determine whether the state is separable or entangled [139], however, this test is not always conclusive.

We can further express the purity for any Gaussian state in terms of the symplectic eigenvalues of its covariance matrix by using the Williamson normal mode decomposition from Section 2.1.5, $\boldsymbol{\sigma} = \mathbf{S}\boldsymbol{\nu}\mathbf{S}^T$, and the fact that a symplectic matrix has unit determinant, $\det[\mathbf{S}] = 1$. The determinant of the covariance matrix is therefore equal to the determinant of the diagonal matrix of symplectic eigenvalues, $\det[\boldsymbol{\sigma}] = \det[\boldsymbol{\nu}]$. Since the symplectic eigenvalues come in pairs, the purity is then

$$\mathcal{P} = \left(\prod_{k=1}^{N} 2\nu_k\right)^{-1}. \tag{3.21}$$

Since the uncertainty relation for a true quantum state constrains the symplectic eigenvalues to $\nu_k \geq 1/2$, the purity calculated using the above expression is in the range $0 < \mathcal{P} \leq 1$. Importantly, we can see that a Gaussian state is pure if and only if its normal mode form is equivalent to a multimode vacuum state, where all symplectic eigenvalues are $\nu_k = 1/2$. The above expression shows that purity can also be pushed arbitrarily close to zero even if only one of the ν_k grows arbitrarily large. Since a symplectic eigenvalue which is larger than the minimum allowed by uncertainty can be interpreted as having some amount of effective thermal noise, $\nu_k = \bar{n}_k + 1/2$, the purity of a Gaussian state can be significantly diminished due to the presence of some effective thermal noise in at least one of its normal modes.

On the other hand, Eq. (3.21) tells us that the purity cannot be altered by application of a symplectic transformation, or indeed any transformation that has a determinant of one. As a result, the purity of a Gaussian state cannot be changed through the application of Gaussian unitary transformations. Thermal noise present in the normal modes of the system acts to reduce the purity of the state, necessitating the use of purification schemes.

3.2 Squeezing and Entanglement

3.2.1 The Two-Mode Squeezed State

In Gaussian systems, entanglement correlations are generated through the use of squeezing, where the two-mode squeezed vacuum (TMSV) state is often treated as the gold standard for entangled two-mode Gaussian states, since the state is pure and the amount of entanglement scales linearly with the magnitude of the squeezing. Since the focus in this chapter is on mitigating the effects of thermal noise on entangled states, we will start by explicitly demonstrating how thermal noise affects the two-mode squeezed state. Two-mode squeezing is performed by the unitary transformation,

$$\hat{U}_{S2} := \exp\left[-ir\left(e^{i\theta}\hat{a}_A^\dagger\hat{a}_B^\dagger + e^{-i\theta}\hat{a}_A\hat{a}_B\right)\right] \equiv \exp\Big[-ir\Big(\cos(\theta)\big(\hat{q}_A\hat{q}_B - \hat{p}_A\hat{p}_B\big) + \sin(\theta)\big(\hat{q}_A\hat{p}_B + \hat{p}_A\hat{q}_B\big)\Big)\Big], \tag{3.22}$$

which corresponds to the following symplectic transformation in phase space

$$\boldsymbol{S}_2(r,\theta) = \begin{pmatrix} \cosh(r)\mathbf{I} & \sinh(r)\left(\sin(\theta)\mathbf{Z} - \cos(\theta)\mathbf{X}\right) \\ \sinh(r)\left(\sin(\theta)\mathbf{Z} - \cos(\theta)\mathbf{X}\right) & \cosh(r)\mathbf{I} \end{pmatrix}. \tag{3.23}$$

In order to incorporate thermal effects in the system, we assume that the two modes are both in thermal states before the squeezing is applied, and so the initial covariance matrix is

$$\boldsymbol{\sigma}_{\text{th}} = \begin{pmatrix} \left(\bar{n}_A + \frac{1}{2}\right)\mathbf{I} & \mathbf{0} \\ \mathbf{0} & \left(\bar{n}_B + \frac{1}{2}\right)\mathbf{I} \end{pmatrix}. \tag{3.24}$$

Applying the symplectic transformation to the thermal state covariance matrix, $\boldsymbol{S}_2(r,\theta)\boldsymbol{\sigma}_{\text{th}}(\boldsymbol{S}_2(r,\theta))^T =: \boldsymbol{\sigma}_{\text{TMS}}$, yields the covariance matrix for a two-mode squeezed thermal state:

$$\boldsymbol{\sigma}_{\text{TMS}} = \begin{pmatrix} \left[\left(\bar{n}_A + \frac{1}{2}\right)\cosh^2(r) + \left(\bar{n}_B + \frac{1}{2}\right)\sinh^2(r)\right]\mathbf{I} & \begin{matrix}(\bar{n}_A + \bar{n}_B + 1)\cosh(r)\sinh(r) \\ \times(\sin(\theta)\mathbf{Z} - \cos(\theta)\mathbf{X})\end{matrix} \\ \begin{matrix}(\bar{n}_A + \bar{n}_B + 1)\cosh(r)\sinh(r) \\ \times(\sin(\theta)\mathbf{Z} - \cos(\theta)\mathbf{X})\end{matrix} & \left[\left(\bar{n}_B + \frac{1}{2}\right)\cosh^2(r) + \left(\bar{n}_A + \frac{1}{2}\right)\sinh^2(r)\right]\mathbf{I} \end{pmatrix}. \tag{3.25}$$

To get an idea of the impact of thermal quanta and squeezing on the entanglement of the system, we work out Simon's criterion for this covariance matrix, which states that the state is separable if the following inequality is satisfied:

$$\bar{n}_A\bar{n}_B(\bar{n}_A + 1)(\bar{n}_B + 1) - \sinh^2(r)\cosh^2(r)(\bar{n}_A + \bar{n}_B + 1)^2 \geq 0. \tag{3.26}$$

We can immediately notice that in the case where one of the thermal occupations is zero that the above inequality reduces to

$$-\sinh^2(r)\cosh^2(r)(\bar{n}_A + 1)^2 \geq 0 \quad \text{when} \quad n_B = 0, \tag{3.27}$$

which is trivially satisfied when there is no squeezing in the system $r = 0$. As a consequence, the two modes are entangled for any non-zero amount of squeezing, provided that only one is initially in a thermal state. If both modes are initially in a thermal state, then the squeezing is insufficient to generate entanglement if it satisfies the following inequality,

$$\frac{1}{2}\ln\left(\frac{2\bar{n}_A\bar{n}_B + \bar{n}_A + \bar{n}_B + 1 + 2\sqrt{\bar{n}_A\bar{n}_B\left(\bar{n}_A + 1\right)\left(\bar{n}_B + 1\right)}}{\bar{n}_A + \bar{n}_B + 1}\right) \geq r, \tag{3.28}$$

and so there are non-zero values of the squeezing which are insufficient for the generation of entanglement. However, since the left-hand side grows at the rate of a logarithmic function, increases in the number of thermal quanta do not rapidly increase the threshold that the squeezing must surpass in order to violate Simon's criterion. To see the effect on the entanglement more explicitly, we calculate the symplectic eigenvalues of the partially transposed covariance matrix,

$$\tilde{\nu}_\pm = \sqrt{(\delta\bar{n})^2 + (2\bar{n} + 1)^2\cosh(4r) \pm \sqrt{(2\bar{n} + 1)^2\left(1 + \cosh(4r)\right)\Big(2(\delta\bar{n})^2 + (2\bar{n} + 1)^2(-1 + \cosh(4r))\Big)}}, \tag{3.29}$$

where we have used the following definitions to simplify the above expression,

$$\bar{n} = \frac{1}{2}\big(\bar{n}_A + \bar{n}_B\big) \quad \text{and} \quad \delta\bar{n} = \left|\bar{n}_A - \bar{n}_B\right|. \tag{3.30}$$

In the case where both modes are initially in vacuum, the symplectic eigenvalues and logarithmic negativity take on the ideal forms:

$$\tilde{\nu}_{\pm} = \frac{1}{2}e^{\pm 2r} \quad \text{and} \quad E_{\mathcal{N}} = \ln(2\tilde{\nu}_{-}) = 2r. \tag{3.31}$$

The entanglement therefore grows linearly with the amount of squeezing for a TMSV. When one of the modes is initially in a thermal state, the expressions for the symplectic eigenvalues lose this simple form. To determine if the photons in the thermal state are inhibiting the formation of entanglement in any way, we work out the series expansion in the limit of large $\bar{n}_A$, taking $\bar{n}_B = 0$:

$$\tilde{\nu}_{-} = \frac{1}{2}\text{sech}(2r) + \mathcal{O}\big[(\bar{n}_A)^{-1}\big] \qquad \tilde{\nu}_{+} = \bar{n}_A \cosh(2r) + \frac{1}{2}\cosh(4r)\text{sech}(2r) + \mathcal{O}\big[(\bar{n}_A)^{-1}\big]. \tag{3.32}$$

The minimum symplectic eigenvalues is therefore independent of the average number of thermal quanta in the limit $\bar{n}_A \to \infty$, whereas the leading order term in the maximum symplectic eigenvalue is linearly dependent on the average number of thermal quanta, and therefore increases without bound. With this, we know that the logarithmic negativity is bounded by,

$$\ln(\cosh(2r)) \leq E_{\mathcal{N}} \leq 2r \;\text{ for } \bar{n}_A \geq 0 \text{ and } \bar{n}_B = 0. \tag{3.33}$$

So, although increasing the occupation of the thermal state will reduce the amount of entanglement, the lower bound is still non-zero. In fact, with increased squeezing, the relative difference between the upper and lower bounds of $E_{\mathcal{N}}$ can be made arbitrarily small, indicating that, although entanglement is diminished if one mode is in a thermal state, this effect can be mitigated by squeezing harder.

We now turn our attention to the case where both modes have non-zero thermal occupation. In order to simplify the expression for the logarithmic negativity, the thermal occupation of both modes is set to the same value, $\bar{n}_A, \bar{n}_B = \bar{n}$. The symplectic eigenvalues and logarithmic negativity are then,

$$\tilde{\nu}_{\pm} = e^{\pm 2r}\left(\bar{n} + \frac{1}{2}\right) \quad \text{and} \quad E_{\mathcal{N}} = 2r - \ln\big(2\bar{n} + 1\big). \tag{3.34}$$

This expression for the logarithmic negativity assumes that $\tilde{\nu}_{-} < 1/2$, or equivalently $2r > \ln(2\bar{n} + 1)$, which only occurs when Simon's criterion, expressed in Eq. (3.28), is violated. The presence of thermal quanta linearly increases both symplectic eigenvalues, representing an increase in the variance of the normal modes of the partially transposed state; if the variance is sufficiently large, then the partially transposed state will no longer violate the uncertainty relation, resulting in no entanglement.

The last quantity we wish to examine is the purity, which is unaffected for the global state by the presence two-mode squeezing, since the purity is unchanged under symplectic transformations. The global purity for the covariance matrices $\boldsymbol{\sigma}$ is therefore,

$$\mathcal{P} = \frac{1}{(2\bar{n}_A + 1)(2\bar{n}_B + 1)}. \tag{3.35}$$

This is expected since the two-mode squeezing unitary transformation cannot change the purity of the Gaussian state as it has a determinant of one, $\det[\boldsymbol{S}_2(r,\theta)] = 1$. As a result, $\det[\boldsymbol{\sigma}_{\text{th}}] = \det[\boldsymbol{\sigma}_{\text{TMS}}]$, and so the purity of the initial two-mode thermal state and squeezed thermal state have identical values.

3.2.2 Two-Mode Squeezing in an Open System

Before considering the two nonreciprocal amplifiers, we will analyse the behaviour of entangled states in an open system. This reference system consists of a nondegenerate coherent two-mode squeezing (TMS) interaction between two harmonic modes,

$$\hat{H}_{\text{TMS}} = g_{12}\left(e^{i\vartheta}\hat{a}_1^{\dagger}\hat{a}_2^{\dagger} + e^{-i\vartheta}\hat{a}_1\hat{a}_2\right). \tag{3.36}$$

The behaviour of this coherent system was analysed in the previous section, Section 3.2.1, but now we will treat this as an open quantum system. Each mode is therefore coupled to the environment, which we assume to be independent baths, each of which is in a thermal state. This two-mode squeezed open system can therefore be described by the following Lindblad master equation,

$$\frac{d}{dt}\hat{\rho} = \mathcal{L}_{\text{TMS}}(\hat{\rho}) \quad \text{where} \quad \mathcal{L}_{\text{TMS}}(\hat{\rho}) = -i[\hat{H}_{\text{TMS}}, \hat{\rho}] + \sum_{k=1,2}\kappa_k\left((\bar{n}_k + 1)\mathcal{D}[\hat{a}_k](\hat{\rho}) + \bar{n}_k\mathcal{D}[\hat{a}_k^{\dagger}](\hat{\rho})\right). \tag{3.37}$$

The dynamics induced by this master equation are entirely linear, so provided that the state is initially a Gaussian, it will remain Gaussian for all time. In addition, we consider the environment to be akin to a transmission line, so that

there are also output fields propagating away from the system. We can therefore examine the entanglement behaviour for two sets of modes: the coherently coupled open modes which make up the physical system described by the above Lindblad master equation, which we will refer to as the intracavity modes, and the output modes representing the propagating fields leaving the system ports, which can be handled using input-output theory from Section 2.2.3.2.

In both instances, we are solely concerned with the steady-state entanglement, so we must determine whether the system is stable. To do this, we first write the Heisenberg-Langevin equation for this system in the quadrature basis given by the vector $\hat{\boldsymbol{r}} = (\hat{q}_1, \hat{p}_1, \hat{q}_2, \hat{p}_2)$ as

$$\frac{d}{dt}\hat{\boldsymbol{r}}(t) = \mathbf{A}_{\mathrm{TMS}}\hat{\boldsymbol{r}}(t) - \sqrt{\boldsymbol{\kappa}}\hat{\boldsymbol{r}}_{\mathrm{in}}(t) \tag{3.38}$$

where $\boldsymbol{\kappa} = \mathrm{diag}(\kappa_1, \kappa_1, \kappa_2, \kappa_2)$ is the matrix of dissipation rates. The system stability is determined by the dynamical matrix $\mathbf{A}_{\mathrm{TMS}}$, which may be written as follows in this basis, using the methods in Sections 2.2.2 and 2.2.3:

$$\mathbf{A}_{\mathrm{TMS}} = \begin{pmatrix} (-\kappa_1/2)\,\mathbf{I} & g_{12}(\sin(\vartheta)\mathbf{Z} - \cos(\vartheta)\mathbf{X}) \\ g_{12}(\sin(\vartheta)\mathbf{Z} - \cos(\vartheta)\mathbf{X}) & (-\kappa_2/2)\,\mathbf{I} \end{pmatrix}, \tag{3.39}$$

In order to ensure the system has a steady state, we need to ensure that the eigenvalues of the dynamical matrix all have a negative real part. The conditions for this can be determined using the necessary and sufficient Routh-Hurwitz stability criterion [140, 141], and so the system is stable if both of the following inequalities are satisfied:

$$0 < \frac{\kappa_1}{2} + \frac{\kappa_2}{2} \quad \text{and} \quad 0 < 1 - \mathcal{C}_{12}\,, \text{ where } \mathcal{C}_{12} := \frac{4g_{12}^2}{\kappa_1\kappa_2}. \tag{3.40}$$

The parameter $\mathcal{C}_{12}$ is the cooperativity, defined as a ratio of the strengths of the coherent and dissipative processes in the system. The second inequality puts a limit on the strength of the squeezing interaction, above which the system becomes unstable, which limits the cooperativity to the range $0 \leq \mathcal{C}_{12} < 1$. The first criterion means that there is no net antidamping from the bath couplings, and coupled with the second inequality, means that neither of the decay rates can take non-negative values.

3.2.2.1 Entanglement of the Intracavity Modes

We first consider the behaviour of the intracavity modes; we can apply the results from Section 2.2.2 to the Lindblad master equation given by Eq. (3.37) to write a differential equation for the covariance matrix of the intracavity modes:

$$\frac{d}{dt}\boldsymbol{\sigma}_{\mathrm{int}}(t) = \mathbf{A}_{\mathrm{TMS}}\boldsymbol{\sigma}_{\mathrm{int}}(t) + \boldsymbol{\sigma}_{\mathrm{int}}(t)\mathbf{A}_{\mathrm{TMS}}^T + \mathbf{C} \quad \text{where} \quad \mathbf{C} = \begin{pmatrix} \kappa_1\left(\bar{n}_1 + \frac{1}{2}\right)\mathbf{I} & \mathbf{0} \\ \mathbf{0} & \kappa_2\left(\bar{n}_2 + \frac{1}{2}\right)\mathbf{I} \end{pmatrix}. \tag{3.41}$$

We are interested in the intracavity covariance matrix when the internal Gaussian state is in the steady state, $\boldsymbol{\sigma}_{\mathrm{int}} := \lim_{t\to\infty}\boldsymbol{\sigma}_{\mathrm{int}}(t)$, which corresponds to the solution of a Lyapunov equation:

$$\mathbf{A}_{\mathrm{TMS}}\boldsymbol{\sigma}_{\mathrm{int}} + \boldsymbol{\sigma}_{\mathrm{int}}\mathbf{A}_{\mathrm{TMS}}^T + \mathbf{C} = 0 \quad \rightarrow \quad \boldsymbol{\sigma}_{\mathrm{int}} = \int_0^\infty e^{\tau\mathbf{A}_{\mathrm{TMS}}}\,\mathbf{C}\,e^{\tau\mathbf{A}_{\mathrm{TMS}}^T}\,d\tau \tag{3.42}$$

Provided that the system obeys the stability criteria in Eq. (3.40), this integral converges, so the steady-state intracavity covariance matrix can be retrieved:

$$\boldsymbol{\sigma}_{\mathrm{int}} = \frac{1}{(1-\mathcal{C}_{12})(\kappa_1+\kappa_2)}\begin{pmatrix} \boldsymbol{\varsigma}_{11} & \boldsymbol{\varsigma}_{12} \\ \boldsymbol{\varsigma}_{12} & \boldsymbol{\varsigma}_{22} \end{pmatrix} \text{ where } \begin{aligned} \boldsymbol{\varsigma}_{11} &= \Big(\big(\kappa_1(1-\mathcal{C}_{12})+\kappa_2\big)\left(\bar{n}_1+\tfrac{1}{2}\right) + \kappa_2\mathcal{C}_{12}\left(\bar{n}_2+\tfrac{1}{2}\right)\Big)\mathbf{I} \\ \boldsymbol{\varsigma}_{22} &= \Big(\big(\kappa_2(1-\mathcal{C}_{12})+\kappa_1\big)\left(\bar{n}_2+\tfrac{1}{2}\right) + \kappa_1\mathcal{C}_{12}\left(\bar{n}_1+\tfrac{1}{2}\right)\Big)\mathbf{I} \\ \boldsymbol{\varsigma}_{12} &= \sqrt{\mathcal{C}_{12}\kappa_1\kappa_2}\,(\bar{n}_1+\bar{n}_2+1)\,(\sin(\vartheta)\mathbf{Z} - \cos(\vartheta)\mathbf{X})\,. \end{aligned} \tag{3.43}$$

Checking Simon's criterion tells us that the modes are separable if the following inequality is satisfied,

$$0 \leq \Big(\bar{n}_1\bar{n}_2(\kappa_1+\kappa_2)^2(1-\mathcal{C}_{12}) + \mathcal{C}_{12}\,(\bar{n}_1+\bar{n}_2+1)\left(\kappa_1^2\bar{n}_1 + \kappa_2^2\bar{n}_2 - \kappa_1\kappa_2\right)\Big). \tag{3.44}$$

If both environments are in the vacuum state, then this inequality is always violated, and hence the intracavity modes are always entangled. If only one of the environments is in the vacuum, say $\bar{n}_2 = 0$, then the state is entangled for all non-zero values of the cooperativity, provided that the remaining free parameters violate the inequality $\bar{n}_1 \geq \kappa_2/\kappa_1$. Since a large dissipation rate generally indicates a colder bath temperature and hence fewer thermal fluctuations in

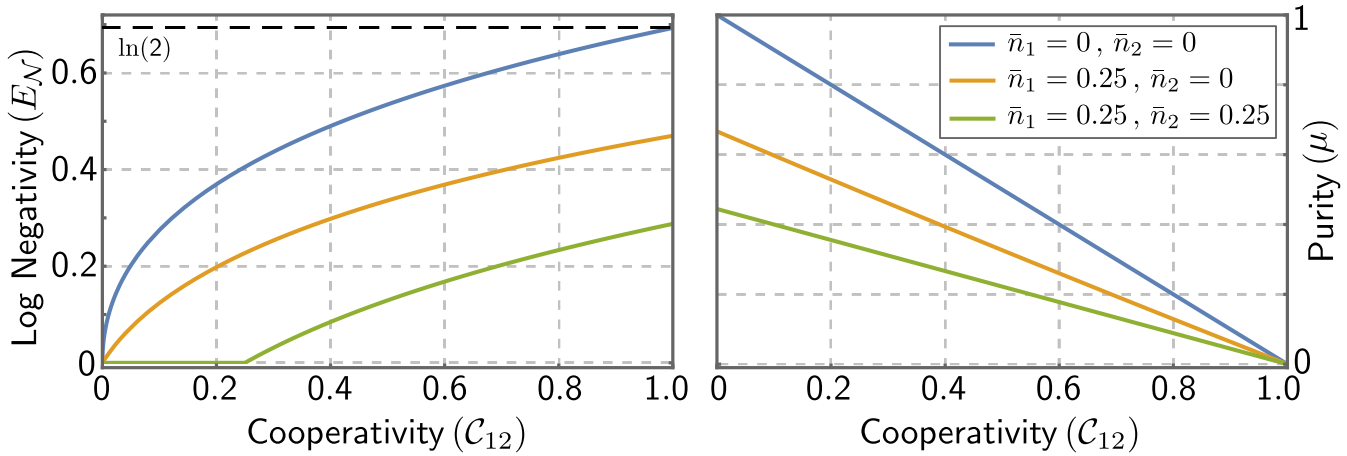

Figure 3.2: [Left] Logarithmic negativity $E_{\mathcal{N}}^{(j,k)}$ and [Right] purity $\mathcal{P}^{(j,k)}$ of the steady-state intracavity states of the open two-mode squeezer, plotted as a function of the squeezing cooperativity. The dissipation rates for both modes are set to the same value in both plots, $\kappa_1/\kappa_2 = 1$, resulting in no asymmetry. Results for the bipartitie state are shown for three sets of values of the thermal noise coming from the baths: $\bar{n}_1 = 0$ and $\bar{n}_2 = 0$ (blue), $\bar{n}_1 = 0.25$ and $\bar{n}_2 = 0$ (orange), $\bar{n}_1 = 0.25$ and $\bar{n}_2 = 0.25$ (green). Notice in the left plot that the logarithmic negativity only reaches the maximum allowable value of ln(2) when both baths contribute vacuum noise. When both baths have some small amount of thermal fluctuations, the entanglement is zero until the amount of squeezing, represented by $\mathcal{C}_{12}$, is sufficiently large. In the left plot, all values of the purity go to zero as the squeezing is increased, regardless of thermal noise. Increases in the logarithmic negativity therefore come at the cost of a reduction in purity.

the bath, we should expect that κ_2 will indeed be larger than κ_1. Things become more complicated when both baths are in a thermal state. Analysis here shows that for a non-zero number of thermal quanta in both environments, the minimum value of the cooperativity required to entangle the two modes occurs when the two dissipation rates are equal, $\kappa_1/\kappa_2 = 1$. As the asymmetry between the two dissipation rates increases, $\kappa_1/\kappa_2 \neq 1$, it will eventually become impossible to entangle the two modes for stable systems. Naturally, increasing the number of thermal quanta is also detrimental to the entanglement.

So as to better understand how the entanglement behaves in this system, we will perform the Williamson normal mode decomposition on the intracavity covariance matrix to compare this covariance matrix with that of a two-mode squeezed state from Eq. (3.25). This will allow us to use the previous analysis from Section 3.2.1 to determine the optimal values of logarithmic negativity and the purity. The decomposition should yield the following form,

$$\boldsymbol{\sigma}_{\text{int}} = \boldsymbol{S}_2(r,\vartheta) \begin{pmatrix} \left(\bar{n}_A + \frac{1}{2}\right)\mathbf{I} & \mathbf{0} \\ \mathbf{0} & \left(\bar{n}_B + \frac{1}{2}\right)\mathbf{I} \end{pmatrix} \boldsymbol{S}_2(r,\vartheta)^T, \tag{3.45}$$

where $\boldsymbol{S}_2(r,\vartheta)$ is defined in Eq. (3.23). The total squeezing in the system is

$$r = \ln\left(\sqrt{\frac{\kappa_1+\kappa_2}{2\sqrt{\varkappa}} + \frac{1}{2}} + \sqrt{\frac{\kappa_1+\kappa_2}{2\sqrt{\varkappa}} - \frac{1}{2}}\right) \text{ where } \varkappa = (\kappa_1+\kappa_2)^2 - 4\mathcal{C}_{12}\kappa_1\kappa_2. \tag{3.46}$$

Since $\mathcal{C}_{12} \in [0,1)$, we have $\varkappa \in \left((\kappa_1-\kappa_2)^2, (\kappa_1+\kappa_2)^2\right]$.

The squeezing is not only dependent on the cooperativity, but is again dependent on the dissipation rates, and specifically the ratio of these rates. The behaviour of the squeezing as the cooperativity approaches the point of instability is of most interest, since it is at this point that the strength of the coherent two-mode squeezing interaction is maximised, meaning that the squeezing should be maximised as well:

$$\lim_{\mathcal{C}_{12}\to 1} r = \ln\left(\frac{\sqrt{\kappa_1}+\sqrt{\kappa_2}}{\sqrt{|\kappa_1-\kappa_2|}}\right). \tag{3.47}$$

This demonstrates that the squeezing can only reach arbitrarily large values when the dissipation rates are identical for both modes, $\kappa_1 = \kappa_2$, otherwise, the amount of squeezing obtainable for stable systems is finite and set by the ratio of the dissipation rate and not their absolute values.

It is therefore impossible for the coherent squeezing interaction to create an ideal two-mode squeezed state if there

is some asymmetry in the dissipation rates. The reason is that, in the steady state, there is a balance between the coherent and dissipative processes in the system. While the coherent process works to create a two-mode squeezed state, dissipation causes this state to decay and works to thermalise the two modes with their respective environments. Provided that there is no asymmetry between the dissipation rates, then the squeezed correlations created in both modes decay at the same rate. However, if there is some asymmetry in these rates, then the squeezed correlations are dissipated away faster from one mode compared to the other. As a result of this imbalance, it is not possible to create an idealised two-mode squeezed state, and so the amount of squeezing that can be generated is limited.

Next, we examine the average thermal occupation of the normal mode thermal states, which are given by the following expressions:

$$\begin{aligned}\bar{n}_A &= \frac{1}{2(1-\mathcal{C}_{12})(\kappa_1+\kappa_2)}\Big(\bar{n}_1\left[\kappa_1(1-2\mathcal{C}_{12})+\kappa_2+\sqrt{\varkappa}\right]+(\bar{n}_2+1)\left[-\kappa_1-\kappa_2(1-2\mathcal{C}_{12})+\sqrt{\varkappa}\right]\Big)\\ \bar{n}_B &= \frac{1}{2(1-\mathcal{C}_{12})(\kappa_1+\kappa_2)}\Big(\bar{n}_2\left[\kappa_2(1-2\mathcal{C}_{12})+\kappa_1+\sqrt{\varkappa}\right]+(\bar{n}_1+1)\left[-\kappa_2-\kappa_1(1-2\mathcal{C}_{12})+\sqrt{\varkappa}\right]\Big).\end{aligned} \tag{3.48}$$

The number of thermal quanta in the normal modes is not only dependent on the thermal fluctuations in the bath, but is also dependent on the cooperativity and relative values of the dissipation rates. When there is no coherent interaction between the modes, $\mathcal{C}_{12}=0$, the normal modes are independent, and thermalise with their baths in the steady state as expected, $\bar{n}_A=\bar{n}_1$ and $\bar{n}_B=\bar{n}_2$. To understand how the thermal noise behaves as we attempt to maximise the squeezing, we will examine the behaviour of the normal mode populations near the point of instability, $\mathcal{C}_{12}\to 1$. If there is some asymmetry between the dissipation rates, say $\kappa_1>\kappa_2$, then the normal mode populations may be expressed as:

$$\begin{aligned}\bar{n}_A &= \frac{\kappa_1^2\bar{n}_1+\kappa_2^2\left(\bar{n}_2+1\right)}{\kappa_1^2-\kappa_2^2}+\mathcal{O}\left([1-\mathcal{C}_{12}]^1\right)\\ \bar{n}_B &= \frac{\left(\bar{n}_1+\bar{n}_2+1\right)(\kappa_1-\kappa_2)}{(\kappa_1+\kappa_2)(1-\mathcal{C}_{12})}+\frac{2\kappa_1\kappa_2\left(\bar{n}_1+\bar{n}_2+1\right)-\kappa_2^2\bar{n}_2-\kappa_1^2\left(\bar{n}_1+1\right)}{\kappa_1^2-\kappa_2^2}+\mathcal{O}\left([1-\mathcal{C}_{12}]^1\right).\end{aligned} \tag{3.49}$$

As the cooperativity increases, the thermal occupation $\bar{n}_A$ approaches a finite value, while $\bar{n}_B$ will diverge. This is a problem for the entanglement; recall that thermal quanta in both normal modes will decrease the amount of entanglement in the system, and while increased squeezing can overcome this, the amount of squeezing that can be generated in this instance is limited as the dissipation rates are not equal. In some cases, the squeezing will be insufficient to overcome the growth in the number of thermal quanta, in which case the entanglement collapses to zero. Since having unequal dissipation rates is not optimal if we want unbounded squeezing, we now focus on the thermal occupations when both dissipation rates are identical:

$$\begin{aligned}\bar{n}_A &= \frac{\bar{n}_1+\bar{n}_2+1}{2\sqrt{1-\mathcal{C}_{12}}}+\frac{1}{2}\left(\bar{n}_1-\bar{n}_2-1\right)+\mathcal{O}\left([1-\mathcal{C}_{12}]^1\right)\\ \bar{n}_B &= \frac{\bar{n}_1+\bar{n}_2+1}{2\sqrt{1-\mathcal{C}_{12}}}+\frac{1}{2}\left(-\bar{n}_1+\bar{n}_2-1\right)+\mathcal{O}\left([1-\mathcal{C}_{12}]^1\right).\end{aligned} \tag{3.50}$$

The number of thermal quanta in the normal modes will still grow without bound as the cooperativity approaches the point of instability, so if we want to push the squeezing to arbitrarily large values, the trade-off is that both $\bar{n}_A$ and $\bar{n}_B$ will increase as well. Despite this, setting $\kappa_1=\kappa_2$ is still the optimal choice. The above expressions also demonstrate that the thermal occupation in the normal modes is non-zero, but is minimised if both baths are in the vacuum state. So, in the regime where $\kappa_1=\kappa_2$ and $\bar{n}_1,\bar{n}_2=0$, the squeezing and normal mode thermal occupations are:

$$r=\ln\left(\sqrt{\frac{1}{2\sqrt{1-\mathcal{C}_{12}}}+\frac{1}{2}}+\sqrt{\frac{1}{2\sqrt{1-\mathcal{C}_{12}}}-\frac{1}{2}}\right)\quad\text{and}\quad\bar{n}_A,\bar{n}_B=\frac{1}{2\sqrt{1-\mathcal{C}_{12}}}-\frac{1}{2}. \tag{3.51}$$

Using Eq. (3.34), the logarithmic negativity can then be written as

$$E_{\mathcal{N}}=2\ln\left(\frac{1}{\sqrt{2}}\left[\sqrt{1+\sqrt{1-\mathcal{C}_{12}}}+\sqrt{1-\sqrt{1-\mathcal{C}_{12}}}\right]\right), \tag{3.52}$$

which approaches the following value as the system approaches the point of instability,

$$\lim_{\mathcal{C}_{12}\to 1}E_{\mathcal{N}}=\ln(2). \tag{3.53}$$

We can see that, even in the optimal parameter regime, the intracavity entanglement that may be generated is fundamentally limited in the steady state. The reason for this is that increasing the strength of the coherent two-mode squeezing interaction not only increases r, but also increases $\bar{n}_A$ and $\bar{n}_B$. The net effect is that the logarithmic negativity is restricted to values below $\ln(2)$. Turning our attention now to the purity, for this two-mode system, it may be simply expressed using the normal mode thermal occupation numbers:

$$\mathcal{P} = \frac{1}{(2\bar{n}_A + 1)(2\bar{n}_B + 1)}. \tag{3.54}$$

Eqs. (3.49) and (3.50) indicate that the purity of the entangled state will always go to zero if the squeezing within the system is increased, since one or both of the normal mode occupations will grow without bound:

$$\lim_{\mathcal{C}_{12} \to 1} \mathcal{P} = 0. \tag{3.55}$$

This holds regardless of the ratio between the two decay rates, and will occur even if both baths are in the vacuum state. The intracavity entanglement is therefore fundamentally limited in the amount of entanglement it can create, and even this comes at the cost of a highly impure state. Having analysed the behaviour of the intracavity states, we will now turn our attention to the output modes, which do not suffer from these limitations.

3.2.2.2 Entanglement of the Output Modes

In order to characterise the behaviour of the steady-state output fields, we use the standard approach outlined in Section 2.2.3. We begin with the Heisenberg-Langevin equation from Eq. (3.38), which is then Fourier transformed from the time to the frequency domain. From here, we use input-output theory to calculate the scattering matrix in the frequency domain, $\hat{\boldsymbol{r}}_{\text{out}}[\omega] = \mathbf{S}_{\text{TMS}}[\omega]\hat{\boldsymbol{r}}_{\text{in}}[\omega]$. We will specifically focus on scattering at the resonance frequency of the system, $\omega = 0$; for simplicity, we will drop the frequency dependence when writing the scattering matrix at the resonance frequency, $\mathbf{S}_{\text{TMS}}[0] \equiv \mathbf{S}_{\text{TMS}}$. The scattering matrix is written in the quadrature basis as follows:

$$\mathbf{S}_{\text{TMS}} = -\frac{1}{1 - \mathcal{C}_{12}} \begin{pmatrix} (1 + \mathcal{C}_{12})\,\mathbf{I} & 2\sqrt{\mathcal{C}_{12}}\,(\sin(\vartheta)\mathbf{Z} - \cos(\vartheta)\mathbf{X}) \\ 2\sqrt{\mathcal{C}_{12}}\,(\sin(\vartheta)\mathbf{Z} - \cos(\vartheta)\mathbf{X}) & (1 + \mathcal{C}_{12})\,\mathbf{I} \end{pmatrix}. \tag{3.56}$$

The scattering matrix on resonance acts as a symplectic transformation on the input covariance matrix, yielding the covariance matrix for the output modes on resonance:

$$\boldsymbol{\sigma}_{\text{out}} = \mathbf{S}_{\text{TMS}}\,\boldsymbol{\sigma}_{\text{in}}\,\mathbf{S}_{\text{TMS}}^{T} \quad \text{where} \quad \boldsymbol{\sigma}_{\text{in}} = \begin{pmatrix} \left(\bar{n}_1 + \frac{1}{2}\right)\mathbf{I} & \mathbf{0} \\ \mathbf{0} & \left(\bar{n}_2 + \frac{1}{2}\right)\mathbf{I} \end{pmatrix}. \tag{3.57}$$

Combining the above expressions, the output mode covariance matrix is then,

$$\boldsymbol{\sigma}_{\text{out}} = \frac{1}{(1 - \mathcal{C}_{12})^2} \begin{pmatrix} \varsigma_{11} & \varsigma_{12} \\ \varsigma_{12} & \varsigma_{22} \end{pmatrix} \text{ where } \begin{aligned} \varsigma_{11} &= \left((1 + \mathcal{C}_{12})^2 \left(\bar{n}_1 + \tfrac{1}{2}\right) + 4\mathcal{C}_{12}\left(\bar{n}_2 + \tfrac{1}{2}\right)\right)\mathbf{I} \\ \varsigma_{22} &= \left((1 + \mathcal{C}_{12})^2 \left(\bar{n}_2 + \tfrac{1}{2}\right) + 4\mathcal{C}_{12}\left(\bar{n}_1 + \tfrac{1}{2}\right)\right)\mathbf{I} \\ \varsigma_{12} &= 2\sqrt{\mathcal{C}_{12}}(1 + \mathcal{C}_{12})\,(\bar{n}_1 + \bar{n}_2 + 1)\,(\sin(\vartheta)\mathbf{Z} - \cos(\vartheta)\mathbf{X})\,. \end{aligned} \tag{3.58}$$

We can compare now this covariance matrix to the covariance matrix for a two-mode squeezed state, Eq. (3.25). Since the output mode covariance matrix is just a symplectic transformation of the input covariance matrix, it is already in the Williamson normal mode form. The number of thermal quanta in each of the two normal modes is therefore equal to the number of thermal quanta created by the baths. The squeezing and cooperativity are related to each other through the following expressions:

$$\mathcal{C}_{12} = \left(\frac{e^r - 1}{e^r + 1}\right)^2 \qquad r = \ln\left(\frac{1 + \sqrt{\mathcal{C}_{12}}}{1 - \sqrt{\mathcal{C}_{12}}}\right). \tag{3.59}$$

From the above, we can see that as the cooperativity approaches the point of instability, the squeezing grows without bound, and therefore, the output modes can contain an arbitrarily large amount of squeezing. Since the number of thermal quanta in the normal modes does not change, the entangling behaviour is identical to the ideal form of a two-mode squeezed state from Section 3.2.1. In the worst case, where both baths have the same thermal occupation, $\bar{n}_1, \bar{n}_2 = \bar{n}$, the logarithmic negativity can be written as,

$$E_{\mathcal{N}} = 2\ln\left(\frac{1 + \sqrt{\mathcal{C}_{12}}}{1 - \sqrt{\mathcal{C}_{12}}}\right) - \ln\left(2\bar{n} + 1\right). \tag{3.60}$$

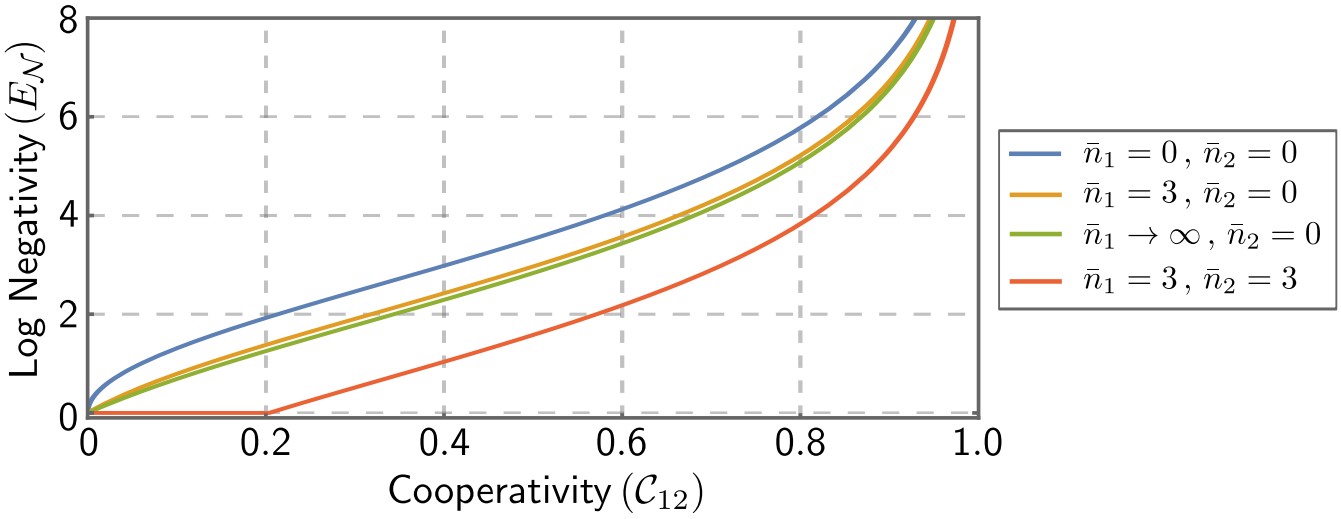

Figure 3.3: Logarithmic negativity of the steady-state output states of the open two-mode squeezer, plotted as a function of the squeezing cooperativity, $\mathcal{C}_{12}$. Results for bipartite state are shown for three sets of values for the thermal noise coming from the baths: $\bar{n}_1 = 0$ and $\bar{n}_2 = 0$ (blue), $\bar{n}_1 = 3$ and $\bar{n}_2 = 0$ (orange), $\bar{n}_1 \to \infty$ and $\bar{n}_2 = 3$ (green), $\bar{n}_1 = 3$ and $\bar{n}_2 = 3$ (red). Notice how the entanglement is only ever zero for non-zero values of $\mathcal{C}_{12}$ when the baths for both modes contain some thermal noise. In all cases, increasing $\mathcal{C}_{12}$ leads to unbounded values of the logarithmic negativity when the cooperativity approaches the point of instability, $\mathcal{C}_{12} \to 1$.

The amount of entanglement that can be generated between the output modes is therefore, in principle, unbounded, no matter the thermal occupation,

$$\lim_{\mathcal{C}_{12}\to 1} E_{\mathcal{N}} = \infty. \tag{3.61}$$

This behaviour contrasts with the intracavity entanglement, which has a strict upper bound due to the increase in the thermal occupancy of the normal modes with increasing cooperativity. The purity of the joint output mode state is simple to calculate since it is identical to that of the input state:

$$\mathcal{P} = \frac{1}{(2\bar{n}_1 + 1)(2\bar{n}_2 + 1)}. \tag{3.62}$$

Provided the thermal noise in the baths is just vacuum noise, the entangled state of the output modes can be highly pure, $\mathcal{P} = 1$. Any thermal noise will degrade the purity, an effect which cannot be altered by adjusting the other system parameters. Regardless, the output modes have the benefit that a highly entangled state can be generated without the increase in the squeezing also degrading the purity, as opposed to the case of the intracavity state. Due to this limitation and the fact that the intracavity mode entanglement is fundamentally bounded, we will therefore focus purely on the output modes. Now that we have fully characterised the ideal behaviour of the entanglement between two modes in a continuous variable system and shown how thermal noise degrades the fidelity of this entangled state, we will turn our attention to the two nonreciprocal quantum amplifiers, and demonstrate how they can be used to protect against the effects of thermal noise when entangling propagating output modes.

3.3 Delta Amplifier

3.3.1 System Setup

3.3.1.1 Dynamical Equations

We begin by examining the entangling behaviour of the delta amplifier; this section follows and builds on previous work published by the author in Ref. [31]. The coherent processes in this system can be modelled using the following Hamiltonian for a three-mode loop; this involves two two-mode squeezing (TMS) interactions and one beam splitter (BS) interaction, along with a loop phase, $\phi \in [-\pi, \pi]$. We work in the interaction picture, where we are rotating with the mode frequencies, and assume no pump detunings for the three parametric processes. The Hamiltonian can then

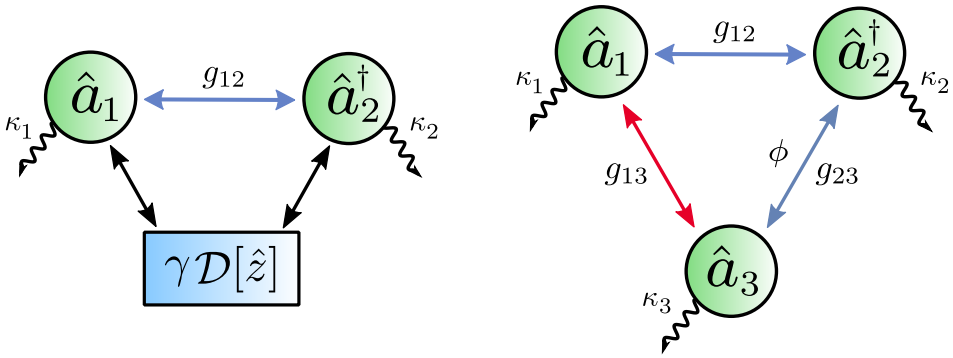

Figure 3.4: [Left] Diagram of an open two-mode squeezer where both modes are coupled to the nonlocal dissipator $\gamma\mathcal{D}[\hat{z}]$. The two harmonic modes are coupled via a TMS interaction with rate g_{12}. [Right] Diagram of the delta amplifier system, consisting of three open modes. Modes a_1 and a_2 are coupled via a TMS with rate g_{12}, as are modes a_2 and a_3, where the TMS has rate g_{23}. Modes a_1 and a_3 are coupled via a BS interaction with rate g_{13}. The tunable loop phase is placed on the TMS interaction between modes a_2 and a_3. If mode a_3 is adiabatically eliminated in the delta amplifier, then the loop is equivalent to the system to the left, with nonlocal jump operator $\hat{z} = \hat{a}_1 + \zeta e^{i\phi}\hat{a}_2^\dagger$.

be expressed as:

$$\hat{H}_\Delta = g_{12}\left(\hat{a}_1^\dagger\hat{a}_2^\dagger + \hat{a}_1\hat{a}_2\right) + g_{13}\left(\hat{a}_1^\dagger\hat{a}_3 + \hat{a}_1\hat{a}_3^\dagger\right) + g_{23}\left(e^{i\phi}\hat{a}_2^\dagger\hat{a}_3^\dagger + e^{-i\phi}\hat{a}_2\hat{a}_3\right). \tag{3.63}$$

This is also an open quantum system with each mode coupled to an independent environment, allowing thermal noise to enter the amplifier through the system ports. The open quantum system, comprised of the three-mode loop and the environment with which it interacts through its ports, constitutes the delta amplifier, which is described by the following quantum-optical master equation:

$$\frac{d}{dt}\hat{\rho} = \mathcal{L}_\Delta(\hat{\rho}) \quad \text{where} \quad \mathcal{L}_\Delta(\hat{\rho}) = -i[\hat{H}_\Delta, \hat{\rho}] + \sum_{k=1,2,3}\kappa_k\left((\bar{n}_k+1)\mathcal{D}[\hat{a}_k](\hat{\rho}) + \bar{n}_k\mathcal{D}[\hat{a}_k^\dagger](\hat{\rho})\right). \tag{3.64}$$

Recalling the reciprocal open TMS system, described by Eqs. (3.36) and (3.37) and discussed in Section 3.2.2, the delta amplifier can be viewed as the system which naturally arises when attempting to render the TMS interaction nonreciprocal. This can be understood using the graph-based approach for parametrically coupled systems [16], or using the engineered dissipation approach involving the addition of a nonlocal dissipator to the original TMS [83], both of which were introduced in Section 2.4.2. Applying the latter approach to the TMS, the master equation will take the following form:

$$\frac{d}{dt}\hat{\rho} = \mathcal{L}_{\text{TMS}}(\hat{\rho}) + \gamma\mathcal{D}[\hat{z}](\hat{\rho}). \tag{3.65}$$

The use of either nonlocal collapse operator, $\hat{z} = \hat{a}_1 + \zeta e^{i\phi}\hat{a}_2^\dagger$ or $\hat{z} = \hat{a}_1^\dagger + \zeta e^{-i\phi}\hat{a}_2$, will cause the TMS to be nonreciprocal provided that the interaction strength γ, asymmetry ζ, and, most crucially, phase ϕ, are appropriately chosen [83]. The delta amplifier described by Eq. (3.64) can be reduced to Eq. (3.65) when the mode a_3 can be adiabatically eliminated, that is, when its damping rate κ_3 is the largest system parameter. Assuming that the damping rate of mode a_3 is large also implies that the input noise from the environment on mode a_3 should be vacuum noise. Upon adiabatically eliminating mode a_3, the jump operator $\hat{z} = \hat{a}_1 + \zeta e^{i\phi}\hat{a}_2^\dagger$ is realised, where the asymmetric coupling is equal to $\zeta = g_{23}/g_{13}$, as depicted in Figure 3.4. Since we need to explicitly include the dynamics of mode a_3 in order to properly explore the routing of both scattered fields and their correlations, the full system described by Eq. (3.64) will be used.

It is important to note that the required jump operators $\hat{z}$ are non-Hermitian, nonlocal collapse operators. It has been demonstrated that nonreciprocal interactions involving dissipators with Hermitian collapse operators are equivalent to measurement-based feed-forward schemes [83]. Such a scheme is equivalent to measuring one part of the total system and then using the result to evolve another part of the system, breaking the reciprocity of the interaction between the subsystems. Such a scheme amounts to performing LOCC on the entire system, and hence it cannot generate any entanglement between the two subsystems. In contrast, the non-Hermitian collapse operators required here have no such mapping and can, in principle, generate entanglement.

3.3.1.2 Stability Conditions

Given that we are only investigating the behaviour of the system in the steady state, we must work out the conditions on the system parameters to ensure that the system reaches the steady state. To do this, we again have to investigate the eigenvalues of the dynamical matrix. If the vector of quadrature operators is given by $\hat{\boldsymbol{r}} = (\hat{q}_1, \hat{p}_1, \hat{q}_2, \hat{p}_2, \hat{q}_3, \hat{p}_3)$, then the dynamical matrix takes the form:

$$\mathbf{A}_\Delta = \begin{pmatrix} (-\kappa_1/2)\mathbf{I} & -g_{12}\mathbf{X} & g_{13}\mathbf{J} \\ -g_{12}\mathbf{X} & (-\kappa_2/2)\mathbf{I} & g_{23}(\sin(\phi)\mathbf{Z} - \cos(\phi)\mathbf{X}) \\ g_{13}\mathbf{J} & g_{23}(\sin(\phi)\mathbf{Z} - \cos(\phi)\mathbf{X}) & (-\kappa_3/2)\mathbf{I} \end{pmatrix}. \tag{3.66}$$

The eigenvalues can then be calculated from the characteristic polynomial for the dynamical matrix,

$$\det[\mathbf{A}_\Delta - s\mathbf{I}_6] = P(s)^2 + 4g_{12}^2 g_{13}^2 g_{23}^2 \cos^2(\phi) \quad \text{where} \quad P(s) = s^3 + u_2 s^2 + u_1 s + u_0. \tag{3.67}$$

The coefficients of the third-order polynomial $P(s)$ have the following form:

$$\begin{aligned} u_2 &= \frac{\kappa_1}{2} + \frac{\kappa_2}{2} + \frac{\kappa_3}{2} \\ u_1 &= -g_{12}^2 + g_{13}^2 - g_{23}^2 + \frac{\kappa_1}{2}\frac{\kappa_2}{2} + \frac{\kappa_1}{2}\frac{\kappa_3}{2} + \frac{\kappa_2}{2}\frac{\kappa_3}{2} \\ u_0 &= -g_{12}^2\frac{\kappa_3}{2} + g_{13}^2\frac{\kappa_2}{2} - g_{23}^2\frac{\kappa_1}{2} + \frac{\kappa_1}{2}\frac{\kappa_2}{2}\frac{\kappa_3}{2}. \end{aligned} \tag{3.68}$$

In general, analytic expressions in terms of radicals are not possible for roots of sixth-order polynomials. Selecting the loop phases $\phi = \pm\pi/2$ reduces the characteristic polynomial to a product of two third-order polynomials, $P(s)^2$, thereby simplifying the conditions for stability by reducing the complexity of the roots. We recall from the introduction to nonreciprocity in Section 2.4.2 that the optimum values for realising nonreciprocity in a three-mode loop are $\phi = \pm\pi/2$, so focusing solely on the stability at this point is well motivated.

In order to determine when the roots of $P(s)$ have negative real parts, indicating that the system is stable, we use the necessary and sufficient Routh-Hurwitz stability criterion. For a third-order characteristic polynomial, the Routh-Hurwitz criterion for stability requires that all coefficients of $P(s)$ must be strictly positive, $u_k > 0$. Additionally, it is required that $u_1 u_2 - u_0$ be positive; this last quantity can be written as:

$$u_1 u_2 - u_0 = -g_{12}^2\left(\frac{\kappa_1}{2} + \frac{\kappa_2}{2}\right) + g_{13}^2\left(\frac{\kappa_1}{2} + \frac{\kappa_3}{2}\right) - g_{23}^2\left(\frac{\kappa_2}{2} + \frac{\kappa_3}{2}\right) + \left(\frac{\kappa_1}{2} + \frac{\kappa_2}{2}\right)\left(\frac{\kappa_1}{2} + \frac{\kappa_3}{2}\right)\left(\frac{\kappa_2}{2} + \frac{\kappa_3}{2}\right). \tag{3.69}$$

Replacing the coherent couplings g_{jk} with the cooperativity $\mathcal{C}_{jk}$, the criteria for stability are then:

$$\begin{aligned} &0 < \kappa_1 + \kappa_2 + \kappa_3 \\ &0 < \kappa_1\kappa_2(1 - \mathcal{C}_{12}) + \kappa_1\kappa_3(1 + \mathcal{C}_{13}) + \kappa_2\kappa_3(1 - \mathcal{C}_{23}) \\ &0 < \kappa_1\kappa_2\kappa_3\left(1 - \mathcal{C}_{12} + \mathcal{C}_{13} - \mathcal{C}_{23}\right) \\ &0 < (\kappa_1 + \kappa_2)(\kappa_1 + \kappa_3)(\kappa_2 + \kappa_3) - \kappa_1\kappa_2\mathcal{C}_{12}(\kappa_1 + \kappa_2) + \kappa_1\kappa_3\mathcal{C}_{13}(\kappa_1 + \kappa_3) - \kappa_2\kappa_3\mathcal{C}_{23}(\kappa_2 + \kappa_3). \end{aligned} \tag{3.70}$$

As was the case for the TMS, the scattering matrix for this system can be expressed entirely in terms of the cooperativities when on resonance. As a result, the most important criterion for stability for our future analysis is the expression

$$0 < 1 - \mathcal{C}_{12} + \mathcal{C}_{13} - \mathcal{C}_{23} \tag{3.71}$$

which constrains the strength of the TMS interactions in the delta amplifier. The presence of a strong BS interaction, corresponding to $\mathcal{C}_{13}$, on the other hand, improves the stability of the system. Since the decay rates do not explicitly appear in the scattering matrix, it is assumed that the values they take are such that the other stability criteria hold. The above criteria at a minimum constrain the individual decay rates to be greater than zero to ensure that the steady state can be reached, $\kappa_k > 0$ for $k = 1, 2, 3$.

3.3.2 Scattering Properties

3.3.2.1 A Change of Basis

We again follow the standard approach outlined in Section 2.2.3 for calculating the scattering matrix in the frequency domain. The scattering matrix is dense and unwieldy in the quadrature basis, even at the resonance frequency. To more easily analyse the scattering behaviour, we move to the complex basis of creation and annihilation operators.

Here the dynamical matrix can be split into two 3×3 blocks, which is more apparent if we adopt the following convention for the vector of operators, $\hat{\boldsymbol{a}}_\Delta = (\hat{a}_1, \hat{a}_2^\dagger, \hat{a}_3, \hat{a}_1^\dagger, \hat{a}_2, \hat{a}_3^\dagger)$. The Heisenberg-Langevin equation for $\hat{\boldsymbol{a}}_\Delta$ can be obtained by performing a basis transformation on the equations for the quadrature operators $\hat{\boldsymbol{r}}$, which yields the following

$$\frac{d}{dt}\hat{\boldsymbol{a}}_\Delta(t) = \tilde{\mathbf{A}}_\Delta \hat{\boldsymbol{a}}_\Delta(t) - \sqrt{\tilde{\boldsymbol{\kappa}}_\Delta}\hat{\boldsymbol{a}}_{\Delta,\text{in}}(t) \tag{3.72}$$

where $\tilde{\mathbf{A}}_\Delta$ is the dynamical matrix, $\tilde{\boldsymbol{\kappa}}_\Delta = \text{diag}(\kappa_1, \kappa_2, \kappa_3, \kappa_1, \kappa_2, \kappa_3)$ is a diagonal matrix of the mode damping rates, and $\hat{\boldsymbol{a}}_{\Delta,\text{in}}(t)$ is the vector of input noise operators in the basis of creation and annihilation operators, with correlators given by Eq. (2.83). In this basis, the dynamical matrix can be expressed as

$$\tilde{\mathbf{A}}_\Delta = \begin{pmatrix} -\kappa_1/2 & -ig_{12} & -ig_{13} & 0 & 0 & 0 \\ ig_{12} & -\kappa_2/2 & ie^{-i\phi}g_{23} & 0 & 0 & 0 \\ -ig_{13} & -ie^{i\phi}g_{23} & -\kappa_3/2 & 0 & 0 & 0 \\ 0 & 0 & 0 & -\kappa_1/2 & ig_{12} & ig_{13} \\ 0 & 0 & 0 & -ig_{12} & -\kappa_2/2 & -ie^{i\phi}g_{23} \\ 0 & 0 & 0 & ig_{13} & ie^{-i\phi}g_{23} & -\kappa_3/2 \end{pmatrix}. \tag{3.73}$$

The scattering matrix $\tilde{\mathbf{S}}_\Delta[\omega]$ can be obtained as usual, by Fourier transforming the Heisenberg-Langevin equations to the frequency domain, then solving the set of linear equations and using input-output theory. The input and output fields are therefore related by the expression: $\hat{\boldsymbol{a}}_{\Delta,\text{out}}[\omega] = \tilde{\mathbf{S}}_\Delta[\omega]\hat{\boldsymbol{a}}_{\Delta,\text{in}}[\omega]$. The scattering matrix on resonance, $\tilde{\mathbf{S}}_\Delta[0] \equiv \tilde{\mathbf{S}}_\Delta$, can be written in block form:

$$\tilde{\mathbf{S}}_\Delta = \begin{pmatrix} \mathbf{S}_\Delta^{aa} & \mathbf{0}_3 \\ \mathbf{0}_3 & \mathbf{S}_\Delta^{a^\dagger a^\dagger} \end{pmatrix} \tag{3.74}$$

where $\mathbf{0}_3$ is the 3×3 null matrix, and the non-trivial sub-blocks are element-wise complex conjugates of one another on resonance $\overline{\mathbf{S}_\Delta^{aa}} = \mathbf{S}_\Delta^{a^\dagger a^\dagger}$. We therefore only need to define the elements of one sub-block,

$$\mathbf{S}_\Delta^{aa} = \frac{1}{D}\begin{pmatrix} D + 2(1 - \mathcal{C}_{23}) & -2\left(i\sqrt{\mathcal{C}_{12}} + e^{i\phi}\sqrt{\mathcal{C}_{13}\mathcal{C}_{23}}\right) & -2\left(i\sqrt{\mathcal{C}_{13}} - e^{-i\phi}\sqrt{\mathcal{C}_{12}\mathcal{C}_{23}}\right) \\ 2\left(i\sqrt{\mathcal{C}_{12}} + e^{-i\phi}\sqrt{\mathcal{C}_{13}\mathcal{C}_{23}}\right) & D + 2(1 + \mathcal{C}_{13}) & 2\left(ie^{-i\phi}\sqrt{\mathcal{C}_{23}} + \sqrt{\mathcal{C}_{12}\mathcal{C}_{13}}\right) \\ 2\left(i\sqrt{\mathcal{C}_{13}} - e^{i\phi}\sqrt{\mathcal{C}_{12}\mathcal{C}_{23}}\right) & -2\left(ie^{i\phi}\sqrt{\mathcal{C}_{23}} + \sqrt{\mathcal{C}_{12}\mathcal{C}_{13}}\right) & D + 2(1 - \mathcal{C}_{12}) \end{pmatrix} \tag{3.75}$$

where $D = -(1 - \mathcal{C}_{12} + \mathcal{C}_{13} - \mathcal{C}_{23}) - 2i\sqrt{\mathcal{C}_{12}\mathcal{C}_{13}\mathcal{C}_{23}}\cos(\phi)$.

Again, on resonance, the scattering matrix may be expressed purely in terms of the cooperativities, $\mathcal{C}_{jk} := 4g_{jk}^2/\kappa_j\kappa_k$. The off-diagonal elements reflect how the input field of one mode is scattered into the output field of another mode, and as can be seen in the above matrix, these elements do not have the same expression. The matrix is, therefore, in general not symmetric, and hence the scattering between each pair of modes can be made nonreciprocal. This is achieved by balancing the cooperativities and adjusting the loop phase ϕ. The diagonal elements represent the reflection of a mode's input field into its output, which can similarly be blocked through careful choice of the system parameters. Since we are interested in how input noise is scattered by the system, we must consider how all of the scattering parameters can be controlled, and so delve into the details below.

3.3.2.2 Nonreciprocal Scattering

For nonreciprocal systems, we are primarily interested in the asymmetry of scattering between modes a_j and a_k, which we will measure using the normalised degree of nonreciprocity, $N^{(j,k)}$, defined in Eq. (2.138) from Chapter 2. We recall that when scattering between a pair of modes is reciprocal that $N^{(j,k)} = 0$, and that for all other values, $N^{(j,k)} \neq 0$, the amplitudes are asymmetric, and hence the scattering between the mode pair must be nonreciprocal. When $N^{(j,k)} = \pm 1$, the scattering is totally asymmetric, and one of the submatrices controlling scattering between modes a_j and a_k is the zero matrix. We refer to these as points of *perfect* nonreciprocity, and they have the special property that signal transmission is only allowed in one direction. The main focus of this chapter is the behaviour of the system at these points, and the impact that unidirectional scattering has on entanglement.

To properly characterise when the scattering is nonreciprocal, we apply an element-wise absolute value operation, $\text{abs}(\mathbf{O})$ to the scattering matrix $\tilde{\mathbf{S}}_\Delta$ to eliminate any phase information and render the matrix symmetric; since the elements of the two sub-blocks are complex conjugates, we must have $\text{abs}(\mathbf{S}_\Delta^{aa}) = \text{abs}(\mathbf{S}_\Delta^{a^\dagger a^\dagger})$. The absolute value

squared is calculated for simplicity:

$$\mathrm{abs}\left(\mathbf{S}_{\Delta}^{aa}\right)^2 = \frac{1}{|D|^2}\begin{pmatrix} \left(1+\mathcal{C}_{12}-\mathcal{C}_{13}-\mathcal{C}_{23}\right)^2 & 4\left(\mathcal{C}_{12}+\mathcal{C}_{13}\mathcal{C}_{23}\right) & 4\left(\mathcal{C}_{13}+\mathcal{C}_{12}\mathcal{C}_{23}\right) \\ +4\mathcal{C}_{12}\mathcal{C}_{13}\mathcal{C}_{23}\cos^2(\phi) & +8\sqrt{\mathcal{C}_{12}\mathcal{C}_{13}\mathcal{C}_{23}}\sin(\phi) & +8\sqrt{\mathcal{C}_{12}\mathcal{C}_{13}\mathcal{C}_{23}}\sin(\phi) \\ 4\left(\mathcal{C}_{12}+\mathcal{C}_{13}\mathcal{C}_{23}\right) & \left(1+\mathcal{C}_{12}+\mathcal{C}_{13}+\mathcal{C}_{23}\right)^2 & 4\left(\mathcal{C}_{23}+\mathcal{C}_{12}\mathcal{C}_{13}\right) \\ -8\sqrt{\mathcal{C}_{12}\mathcal{C}_{13}\mathcal{C}_{23}}\sin(\phi) & +4\mathcal{C}_{12}\mathcal{C}_{13}\mathcal{C}_{23}\cos^2(\phi) & +8\sqrt{\mathcal{C}_{12}\mathcal{C}_{13}\mathcal{C}_{23}}\sin(\phi) \\ 4\left(\mathcal{C}_{13}+\mathcal{C}_{12}\mathcal{C}_{23}\right) & 4\left(\mathcal{C}_{23}+\mathcal{C}_{12}\mathcal{C}_{23}\right) & \left(1-\mathcal{C}_{12}-\mathcal{C}_{13}+\mathcal{C}_{23}\right)^2 \\ -8\sqrt{\mathcal{C}_{12}\mathcal{C}_{13}\mathcal{C}_{23}}\sin(\phi) & -8\sqrt{\mathcal{C}_{12}\mathcal{C}_{13}\mathcal{C}_{23}}\sin(\phi) & +4\mathcal{C}_{12}\mathcal{C}_{13}\mathcal{C}_{23}\cos^2(\phi) \end{pmatrix} \tag{3.76}$$

$$\text{where} \quad |D|^2 = \left(1-\mathcal{C}_{12}+\mathcal{C}_{13}-\mathcal{C}_{23}\right)^2 + 4\mathcal{C}_{12}\mathcal{C}_{13}\mathcal{C}_{23}\cos^2(\phi).$$

We can see that the above matrix is symmetric, and hence the scattering reciprocal, only when the loop phase takes the values $\phi = 0, \pm\pi$ and nowhere else. This reciprocity is satisfied independently of the value of any other parameters in the system. As a result, the system exhibits nonreciprocal scattering to varying degrees for all other values of the loop phase ϕ.

Using Eq. (3.76) in conjunction with Eq. (3.75), we can determine that the points of perfect nonreciprocal scattering can only occur when the loop phase takes the values $\phi = \pm\pi/2$, as expected from Section 2.4.2. The choice of loop phase will also determine the direction of the nonreciprocal scattering. But proper choice of the loop phase is insufficient, we must also balance the strength of the coherent and dissipative processes, which here takes the form of balancing the three cooperativities. An important consequence is that the cooperativities are no longer independent quantities, and the range of values they can take becomes limited since we need to satisfy the inequality in Eq. (3.71) to keep the system stable. The required conditions on the loop phase and cooperativities are summarised below, as well as the limits this places on the cooperativities to ensure stability. The arrows denote the direction in which signal transmission is allowed, with scattering matrix elements in the reverse direction vanishing exactly:

Coop. Condition	$\phi = -\pi/2$	$\phi = +\pi/2$	Stability Criteria
$\mathcal{C}_{12} = \mathcal{C}_{13}\mathcal{C}_{23}$	$a_1 \to a_2$	$a_1 \leftarrow a_2$	$0 \le \mathcal{C}_{13}$ & $0 \le \mathcal{C}_{23} < 1$
$\mathcal{C}_{23} = \mathcal{C}_{12}\mathcal{C}_{13}$	$a_2 \to a_3$	$a_2 \leftarrow a_3$	$0 \le \mathcal{C}_{13}$ & $0 \le \mathcal{C}_{12} < 1$
$\mathcal{C}_{13} = \mathcal{C}_{12}\mathcal{C}_{23}$	$a_1 \to a_3$	$a_1 \leftarrow a_3$	$0 \le \mathcal{C}_{12} < 1$ & $0 \le \mathcal{C}_{23} < 1$

(3.77)

3.3.2.3 Reflection of the Input Fields

We are interested in controlling more than asymmetrical scattering between pairs of modes; it is also important to control how a mode's input field is reflected into the output field. This is critical if we wish to prevent amplified thermal noise from the input field from appearing in the output of the same mode. We can therefore modulate the amount of reflection by balancing the system parameters in the diagonal elements of Eq. (3.75). We extract the diagonal elements and write them below:

$$\begin{aligned}
(\mathrm{S}_{\Delta}^{aa})_{11} &= 1 + \frac{2}{D}(1-\mathcal{C}_{23}) = \frac{1}{D}\left(1+\mathcal{C}_{12}-\mathcal{C}_{13}-\mathcal{C}_{23}-2i\sqrt{\mathcal{C}_{12}\mathcal{C}_{13}\mathcal{C}_{23}}\cos(\phi)\right) \\
(\mathrm{S}_{\Delta}^{aa})_{22} &= 1 + \frac{2}{D}(1+\mathcal{C}_{13}) = \frac{1}{D}\left(1+\mathcal{C}_{12}+\mathcal{C}_{13}+\mathcal{C}_{23}-2i\sqrt{\mathcal{C}_{12}\mathcal{C}_{13}\mathcal{C}_{23}}\cos(\phi)\right) \\
(\mathrm{S}_{\Delta}^{aa})_{33} &= 1 + \frac{2}{D}(1-\mathcal{C}_{12}) = \frac{1}{D}\left(1-\mathcal{C}_{12}-\mathcal{C}_{13}+\mathcal{C}_{23}-2i\sqrt{\mathcal{C}_{12}\mathcal{C}_{13}\mathcal{C}_{23}}\cos(\phi)\right).
\end{aligned} \tag{3.78}$$

Blocking the reflected signal in the output of a specific mode a_k then corresponds to the scattering matrix element $(\mathrm{S}_{\Delta}^{aa})_{kk}$ going to zero. From the above expressions, we can see that this is again only possible when the loop phase takes the values $\phi = \pm\pi/2$. The cooperativities must be appropriately balanced as well, and we summarise the conditions in the table below:

	Phase	Coop. Conditions
$a_{1,\mathrm{in}} \not\to a_{1,\mathrm{out}}$	$\phi = \pm\pi/2$	$0 = 1+\mathcal{C}_{12}-\mathcal{C}_{23}-\mathcal{C}_{13}$ & $\mathcal{C}_{13} \le 1+\mathcal{C}_{12}$
$a_{2,\mathrm{in}} \not\to a_{2,\mathrm{out}}$	–	Not possible
$a_{3,\mathrm{in}} \not\to a_{3,\mathrm{out}}$	$\phi = \pm\pi/2$	$0 = 1-\mathcal{C}_{12}+\mathcal{C}_{23}-\mathcal{C}_{13}$ & $\mathcal{C}_{13} \le 1+\mathcal{C}_{23}$

(3.79)

Blocking the reflected input field is not possible for mode a_2 in this setup due to the fact that the cooperativities cannot take negative values. We can also see from Eq. (3.76) that the magnitude of the reflected signal is always greater than unity, $|(\mathrm{S}_{\Delta}^{aa})_{22}| \ge 1$, indicating that not only is it impossible to block reflection for mode a_2, but that the

input noise reflected in the output field is potentially amplified. This behaviour should be anticipated since the mode is coherently coupled to the two other modes in the system via TMS interactions.

3.3.2.4 Scattering in the Quadrature Basis

Having identified the loop phases $\phi = \pm\pi/2$ as points of interest, we now move back to the quadrature basis. We pick the order for the vector of quadrature operators $\hat{\boldsymbol{r}}$ that was originally used when defining the dynamical matrix, Eq. (3.66). We start with the Heisenberg-Langevin equation for the quadrature operators,

$$\frac{d}{dt}\hat{\boldsymbol{r}}(t) = \mathbf{A}_\Delta \hat{\boldsymbol{r}}(t) - \sqrt{\boldsymbol{\kappa}_\Delta}\hat{\boldsymbol{r}}_{\text{in}}(t) \tag{3.80}$$

where $\boldsymbol{\kappa}_\Delta = \text{diag}(\kappa_1, \kappa_1, \kappa_2, \kappa_2, \kappa_3, \kappa_3)$, and perform the usual procedure to obtain the scattering matrix as a function of frequency, $\hat{\boldsymbol{r}}_{\text{out}}[\omega] = \mathbf{S}_\Delta[\omega]\hat{\boldsymbol{r}}_{\text{in}}[\omega]$. The scattering matrix on resonance takes a particularly simple form for the loop phases $\phi = \pm\pi/2$:

$$\mathbf{S}_\Delta^{(\pm\pi/2)} = \frac{-1}{1-\mathcal{C}_{12}+\mathcal{C}_{13}-\mathcal{C}_{23}} \begin{pmatrix} (1+\mathcal{C}_{12}-\mathcal{C}_{13}-\mathcal{C}_{23})\mathbf{I} & -2(\sqrt{\mathcal{C}_{12}} \pm \sqrt{\mathcal{C}_{13}\mathcal{C}_{23}})\mathbf{X} & 2(\sqrt{\mathcal{C}_{13}} \pm \sqrt{\mathcal{C}_{12}\mathcal{C}_{23}})\mathbf{J} \\ -2(\sqrt{\mathcal{C}_{12}} \mp \sqrt{\mathcal{C}_{13}\mathcal{C}_{23}})\mathbf{X} & (1+\mathcal{C}_{12}+\mathcal{C}_{13}+\mathcal{C}_{23})\mathbf{I} & 2(\pm\sqrt{\mathcal{C}_{23}} + \sqrt{\mathcal{C}_{12}\mathcal{C}_{13}})\mathbf{Z} \\ 2(\sqrt{\mathcal{C}_{13}} \mp \sqrt{\mathcal{C}_{12}\mathcal{C}_{23}})\mathbf{J} & 2(\pm\sqrt{\mathcal{C}_{23}} - \sqrt{\mathcal{C}_{12}\mathcal{C}_{13}})\mathbf{Z} & (1-\mathcal{C}_{12}-\mathcal{C}_{13}+\mathcal{C}_{23})\mathbf{I} \end{pmatrix}. \tag{3.81}$$

Crucially, Eq. (3.81) is a real symplectic matrix, and hence corresponds to a unitary transformation on the Gaussian state of the input modes, as discussed in Section 2.1.4. So, even though the above matrix represents the steady-state scattering of an *open* quantum system, it is effectively equivalent to a *coherent* unitary transformation applied to the input fields. This is true for all other values of the loop phase, however, this pseudo-coherent process is simpler to describe for $\phi = \pm\pi/2$; for more detail, refer to Appendix D.3.

However, even in this simplified form, this scattering matrix still represents a complicated set of linear operations acting on the input fields. It can be brought to a simpler form by applying one of the conditions from the above tables in order to realise nonreciprocal scattering or to block reflected input noise. The next section will specifically focus on the case where scattering between modes a_1 and a_2, and alternatively a_2 and a_3, is made nonreciprocal. In these cases, the behaviour of the nonreciprocal scattering matrix easily predicted by modelling the steady-state scattering as a series of optical transformations, which will prove invaluable for describing the behaviour of the entangled output states.

3.3.3 Circuit Decomposition at Points of Perfect Nonreciprocal Scattering

Since the steady-state scattering matrix belongs to the group of real symplectic matrices, $\mathbf{S}_\Delta \in Sp(6, \mathbb{R})$, a variety of decomposition schemes [142, 143] are available to represent the scattering matrix more efficiently. An important property is that the decomposed forms are solely in terms of symplectic matrices, and hence represent successive applications of Gaussian unitary processes. Taking inspiration from Ref. [144], we interpret these decompositions as sequential operations in a linear circuit that acts unitarily on the state of the input modes; the state at the end of the circuit therefore corresponds to the state of the output modes.

Perhaps the most prominent example used in quantum optics is the Bloch-Messiah decomposition, however, we find that the less commonly used polar decomposition provides simpler results for the perfectly nonreciprocal delta amplifier. Both are discussed in detail in Appendix C.2. The polar decomposition allows us to write a matrix in the form $\mathbf{R}_L\mathbf{U}_L$, referred to as its left polar decomposition, or in the form $\mathbf{U}_R\mathbf{R}_R$, which is termed the right polar decomposition. Since the matrix to be decomposed is symplectic, the matrices in the decompositions are also symplectic. Physically, the $\mathbf{U}_L$ and $\mathbf{U}_R$ matrices represent passive optical transformations, specifically beam splitters and phase shifters. The $\mathbf{R}_L$ and $\mathbf{R}_R$ matrices represent active transformations, which correspond to single and two-mode squeezing interactions. Additionally, the left and right polar decompositions are, in general, distinct from each other.

The polar decomposition typically leads to dense and complicated forms for the $\mathbf{R}_{L/R}$ and $\mathbf{U}_{L/R}$ matrices. As previously stated, the scattering matrix describing the system has a remarkably simple form for the left and/or right polar decomposition at points of nonreciprocal scattering for two of the modes pairs, $N^{(1,2)} = \pm 1$ and $N^{(2,3)} = \pm 1$. This simple form is valid up to a global change in the phase of the scattering matrix, $-\mathbf{S}_\Delta$. This phase flip is applied since the phase convention that was chosen for the Heisenberg-Langevin equations in this text means the output fields scattered by $\mathbf{S}_\Delta$ propagate in the opposite direction of the input fields. If we wish to decompose $\mathbf{S}_\Delta$ as a circuit, where both the input and the output propagate in the same direction, we must change the global phase, an operation which is equivalent to applying a series of phase shifters to $\mathbf{S}_\Delta$. It is important to emphasise that due to the structure of the output covariance matrix that this change of phase will not affect the resulting covariances. For these simple

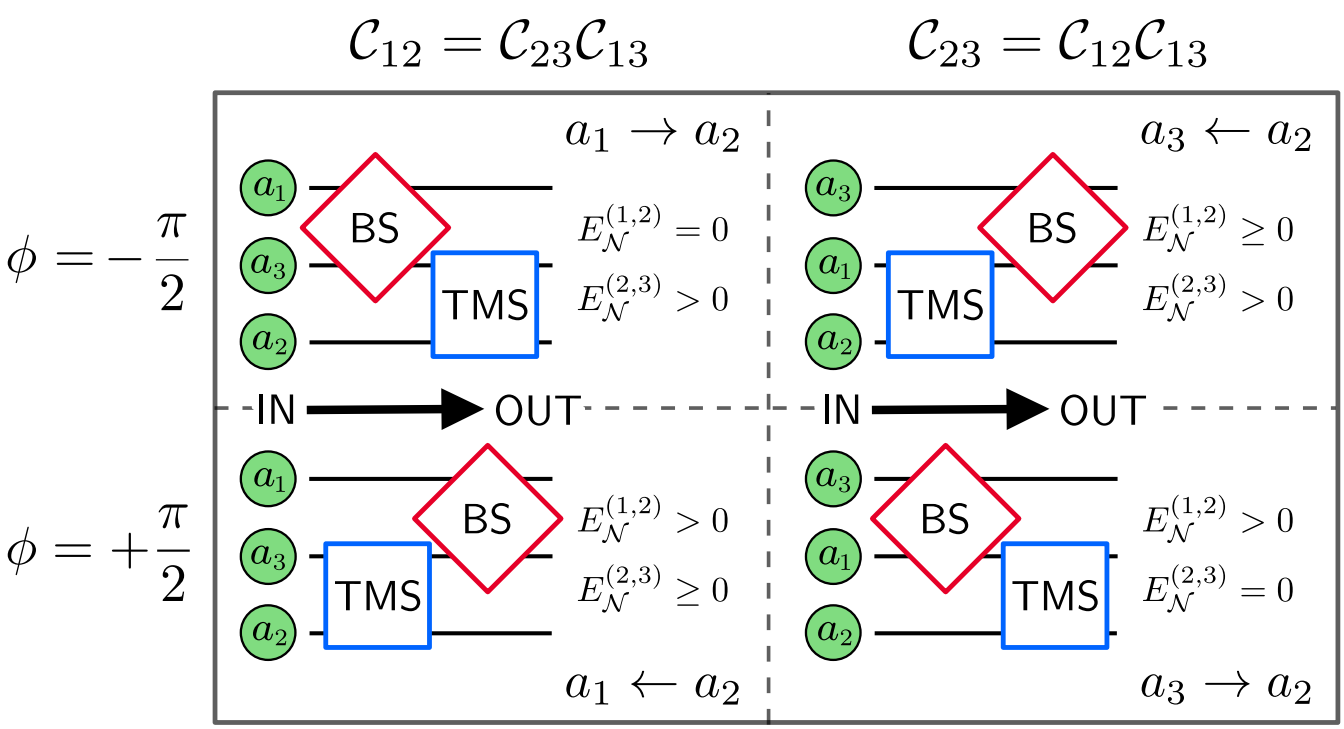

Figure 3.5: Circuit descriptions of the delta amplifier at the points of perfect nonreciprocal scattering, where the normalised degree of nonreciprocity takes the values [Left] $N^{(1,2)} = \pm 1$, and [Right] $N^{(2,3)} = \pm 1$. Two values of the loop phase are shown: [Top] $\phi = +\pi/2$, and [Bottom] $\phi = -\pi/2$, which correspond to the two directions for the nonreciprocal scattering between the mode pairs. The position of modes a_1 and a_3 within the circuit diagrams are swapped between the left and right columns, since the two-mode-squeezer couples the mode pair (a_2, a_3) when $N^{(1,2)} = \pm 1$, and (a_1, a_2) when $N^{(2,3)} = \pm 1$. The beam splitter element always couples the mode pair (a_1, a_3). Input is initially uncorrelated and moves from left to right. The specific forms of the two-mode squeezing and beam splitter interactions can be found in Eq. (3.83).

cases, the symplectic matrices in the polar decomposition involve only a single interaction between one mode pair. At this point, we recall Eqs. (2.23) and (2.27), which provide a way to relate symplectic transformations on Gaussian states to unitary transformations:

$$\mathbf{S}\hat{\boldsymbol{r}} \equiv \hat{U}^\dagger \hat{\boldsymbol{r}} \hat{U} \quad \text{where} \quad \hat{U} = \exp\left[-\frac{i}{2}\hat{\boldsymbol{r}}^T \boldsymbol{H}^{(2)} \hat{\boldsymbol{r}}\right] \quad \text{implies that} \quad \mathbf{S} = \exp\left[\boldsymbol{\Omega}\boldsymbol{H}^{(2)}\right]. \tag{3.82}$$

The three symplectic matrices required to characterise the scattering behaviour will then correspond to the following unitary transformations, written in the basis of creation and annihilation operators:

$$\begin{aligned}
\mathbf{R}^{(1,2)} &\longleftrightarrow \hat{U}_{\text{TMS}}^{(1,2)} := \exp\left[-2i \operatorname{artanh}\left(\sqrt{\mathcal{C}_{12}}\right)\left(\hat{a}_1^\dagger \hat{a}_2^\dagger + \hat{a}_1 \hat{a}_2\right)\right] \\
\mathbf{U}^{(1,3)} &\longleftrightarrow \hat{U}_{\text{BS}}^{(1,3)} := \exp\left[-2i \arctan\left(\sqrt{\mathcal{C}_{13}}\right)\left(\hat{a}_1^\dagger \hat{a}_3 + \hat{a}_1 \hat{a}_3^\dagger\right)\right] \\
\mathbf{R}_{\text{sgn}(\phi)}^{(2,3)} &\longleftrightarrow \hat{U}_{\text{TMS}}^{(2,3)} := \exp\left[-2i\,\text{sgn}(\phi) \operatorname{artanh}\left(\sqrt{\mathcal{C}_{23}}\right)\left(i\hat{a}_2^\dagger \hat{a}_3^\dagger - i\hat{a}_2 \hat{a}_3\right)\right].
\end{aligned} \tag{3.83}$$

These three interactions correspond to the three coherent interactions which appear in the Hamiltonian for the delta amplifier, Eq. (3.63), when the loop phase is $\phi = \pm\pi/2$. We start with the case where the scattering between modes a_1 and a_2 is perfectly nonreciprocal, $N^{(1,2)} = \pm 1$. Here, the polar decomposition consists of two of the above symplectic transformations, $\mathbf{U}^{(1,3)}$ and $\mathbf{R}_{\pm}^{(2,3)}$. We find that both the left and right polar decompositions can provide useful, complementary insight into the scattering behaviour at these points of perfect nonreciprocity. For the loop phase $\phi = -\pi/2$, it is the left polar decomposition which takes on a simple form:

$$-\mathbf{S}_\Delta = \mathbf{R}_{-}^{(2,3)}\,\mathbf{U}^{(1,3)} \quad \text{when} \quad \phi = -\frac{\pi}{2} \quad \text{and} \quad \mathcal{C}_{12} = \mathcal{C}_{13}\mathcal{C}_{23}. \tag{3.84}$$

As illustrated in Figure 3.5, modes a_1 and a_3 interact first via a beam splitter $\mathbf{U}^{(1,3)}$ which acts to exchange input

from a_1 to a_3, and vice versa. This operation is followed by a two-mode squeezer $\mathbf{R}_{-}^{(2,3)}$ between modes a_2 and a_3, where the output of mode a_2 then becomes dependent on the input of mode a_1, thus realising directional transmission from $a_1 \to a_2$. The output of mode a_1 cannot have any dependence on the input of a_2 because it can only arrive at the output of mode a_3 via the same two-mode squeezer. For the opposite sign of the loop phase, $\phi = +\pi/2$, the right polar decomposition is simpler, and yields:

$$-\mathbf{S}_\Delta = \mathbf{U}^{(1,3)}\,\mathbf{R}_{+}^{(2,3)} \;\text{ when }\; \phi = +\frac{\pi}{2} \;\text{ and }\; \mathcal{C}_{12} = \mathcal{C}_{13}\mathcal{C}_{23}, \tag{3.85}$$

which describes the same component operations as Eq. (3.84) but applied in *reverse* order, along with a global sign change on $\mathbf{R}_{+}^{(2,3)}$ to account for the reversal in sign of the loop phase. As a result, the scattering behaviour is reversed and still nonreciprocal, allowing transmission from $a_1 \leftarrow a_2$.

Similar decompositions are obtained when the scattering between modes a_2 and a_3 is nonreciprocal, $N^{(2,3)} = \pm 1$, but which instead involve $\mathbf{U}^{(1,3)}$ and $\mathbf{R}^{(1.2)}$. In this case, for the loop phase $\phi = -\pi/2$, it is the right polar decomposition which takes on a simple form:

$$-\mathbf{S}_\Delta = \mathbf{U}^{(1,3)}\,\mathbf{R}^{(1,2)} \;\text{ when }\; \phi = -\frac{\pi}{2} \;\text{ and }\; \mathcal{C}_{23} = \mathcal{C}_{12}\mathcal{C}_{23}. \tag{3.86}$$

And for the other possible value of the loop phase, $\phi = +\pi/2$, the left polar decomposition is now the simpler decomposition of the two:

$$-\mathbf{S}_\Delta = \mathbf{R}^{(1,2)}\,\mathbf{U}^{(1,3)} \;\text{ when }\; \phi = +\frac{\pi}{2} \;\text{ and }\; \mathcal{C}_{23} = \mathcal{C}_{12}\mathcal{C}_{23}. \tag{3.87}$$

The same physical interpretation can be applied to this circuit as was done for the mode pair a_1 and a_2. Again, we see that depending on the order of the optical elements, directional transmission can be realised between the mode pair a_2 and a_3.

The relatively simple form of these circuits provides a heuristic picture of nonreciprocal scattering in this system, where changing the direction of the nonreciprocal scattering is equivalent to changing the order of operations in the circuit. However, note that the nonreciprocal behaviour in both instances is not explained just by sequential beam splitters, but also involves two-mode squeezing interactions. This already hints at the possibility of generating nontrivial quantum correlations in scattered output fields, and thus connects to entangling properties of the three-mode system, as we will see in the following section.

3.3.4 Entanglement of Propagating Modes

The output state of the delta amplifier, and all of its entangling capabilities, is completely characterised by the covariance matrix of the output field quadrature operators, as previously defined in Section 2.2.3.2. The steady-state output covariance matrix on resonance takes the form:

$$\boldsymbol{\sigma}_{\Delta,\text{out}} = \mathbf{S}_\Delta \boldsymbol{\sigma}_{\text{in}} \mathbf{S}_\Delta^T. \tag{3.88}$$

where $\boldsymbol{\sigma}_{\text{in}}$ is the matrix of correlations of the input fields. Assuming the input noise for different modes is uncorrelated Gaussian white noise, $\boldsymbol{\sigma}_{\text{in}}$ contains variances determined by the thermal occupation number $\bar{n}_k$ and vacuum fluctuations:

$$\boldsymbol{\sigma}_{\text{in}} = \begin{pmatrix} \left(\bar{n}_1 + \frac{1}{2}\right)\mathbf{I}_2 & \mathbf{0} & \mathbf{0} \\ \mathbf{0} & \left(\bar{n}_2 + \frac{1}{2}\right)\mathbf{I}_2 & \mathbf{0} \\ \mathbf{0} & \mathbf{0} & \left(\bar{n}_3 + \frac{1}{2}\right)\mathbf{I}_2 \end{pmatrix}. \tag{3.89}$$

From this covariance matrix, we aim to calculate useful entanglement metrics for different bipartitions of the output fields in order to investigate the effects of nonreciprocal scattering. These include Simon's criterion for the separability of Gaussian states defined in Eq. (3.9), as well as the logarithmic negativity for pairs of modes defined in Eq. (3.16), and written here as $E_{\mathcal{N}}^{(j,k)}$ to indicate that this is applied to the shared output state of modes a_j and a_k. Similarly, we define the marginal purity $\mathcal{P}^{(j,k)}$ of a given bipartition of the output field of modes using Eq. (3.20). We will only consider the mode pairs (a_1, a_2) and (a_2, a_3), because the output of modes a_1 and a_3 are *never* entangled on resonance, $E_{\mathcal{N}}^{(1,3)} = 0$. This can be confirmed by examining Simon's criterion for the (a_1, a_3) mode pair.

3.3.4.1 Output Entanglement in the Presence of Vacuum Noise

We begin by examining the entanglement properties and purity of the output fields under vacuum input, $\bar{n}_k = 0$, for all modes. In this instance the initial matrix of correlations consists of vacuum noise and is therefore proportional to the identity matrix, $\boldsymbol{\sigma}_{\text{in}} = \frac{1}{2}\mathbf{I}_6$, so the output covariance matrix is $\boldsymbol{\sigma}_{\Delta,\text{out}} = \frac{1}{2}\mathbf{S}_\Delta \mathbf{S}_\Delta^T$. We will first consider the case

where scattering between modes a_1 and a_2 could be nonreciprocal by balancing the cooperativities $\mathcal{C}_{12} = \mathcal{C}_{13}\mathcal{C}_{23}$. The logarithmic negativity between the output modes is plotted in the top panel of Figure 3.6, where we notice the strong dependence on the value of the loop phase.

The covariance matrix for the $a_1 \to a_2$ direction of perfect nonreciprocal scattering may be written using the polar form of the scattering matrix from Eq. (3.84):

$$\boldsymbol{\sigma}_{\Delta,\text{out}} = \frac{1}{2}\mathbf{R}_{-}^{(2,3)}\left(\mathbf{R}_{-}^{(2,3)}\right)^{T} \text{ when } \phi = -\frac{\pi}{2} \text{ and } \mathcal{C}_{12} = \mathcal{C}_{13}\mathcal{C}_{23}. \tag{3.90}$$

where the beam splitter component does not appear because it is an orthogonal transformation. The entangling behaviour for this direction of the nonreciprocal scattering is therefore equivalent to a two-mode squeezer between modes a_2 and a_3; hence we must have $E_{\mathcal{N}}^{(2,3)} > 0$. Since modes a_1 and a_2 do not share any squeezing in this representation, there will be no entanglement generated between these two modes, as seen in Figure 3.6.

We can then ask whether there are other operating points where the entanglement between the output of modes a_1 and a_2 vanishes. It is possible to determine this for all system parameters, and not just at the points of perfect nonreciprocity, by examining Simon's criterion for the output of modes a_1 and a_2:

$$\sqrt{\mathcal{C}_{12}\mathcal{C}_{23}\mathcal{C}_{13}}\left(\sqrt{\frac{\mathcal{C}_{12}}{\mathcal{C}_{23}\mathcal{C}_{13}}} + \sqrt{\frac{\mathcal{C}_{23}\mathcal{C}_{13}}{\mathcal{C}_{12}}} + 2\sin(\phi)\right) \leq 0. \tag{3.91}$$

The output fields of modes a_1 and a_2 are separable so long as the above inequality is satisfied, which, assuming non-zero values for the cooperativities, only occurs for one set of parameters: $\mathcal{C}_{12} = \mathcal{C}_{13}\mathcal{C}_{23}$ and $\phi = -\pi/2$, which is the point of perfect nonreciprocal scattering with direction $a_1 \to a_2$. This is then the only point of operation where the entanglement of the output of modes a_1 and a_2 vanishes, $E_{\mathcal{N}}^{(1,2)} = 0$, and away from this point the output for these two modes will therefore always be entangled.

For the reverse direction, $a_1 \leftarrow a_2$, we can use Eq. (3.85) to write the covariance matrix as

$$\boldsymbol{\sigma}_{\Delta,\text{out}} = \frac{1}{2}\mathbf{U}^{(1,3)}\,\mathbf{R}_{+}^{(2,3)}\left(\mathbf{R}_{+}^{(2,3)}\right)^{T}\left(\mathbf{U}^{(1,3)}\right)^{T} \text{ when } \phi = +\frac{\pi}{2} \text{ and } \mathcal{C}_{12} = \mathcal{C}_{13}\mathcal{C}_{23}. \tag{3.92}$$

Importantly, the beam splitter between modes a_1 and a_3 appears and therefore plays an important role in the entanglement generation here. The two-mode squeezer acts first to entangle modes a_2 and a_3, while the later action of the beam splitter swaps some of these squeezed correlations from mode a_3 to a_1, generating entanglement between the output of modes a_1 and a_2.

Moreover, at $\phi = \pi/2$ there exists only one specific mode of operation where the entanglement between mode a_2 and a_3 vanishes: when $\mathcal{C}_{13} = 1$ the beam splitter in Eq. (3.83) acts to *perfectly* swap all squeezing from mode a_3 to a_1, and swap all the uncorrelated vacuum noise from mode a_1 to a_3. This results in the formation of a TMSV state between the output modes a_1 and a_2, and so $E_{\mathcal{N}}^{(1,2)}$ will be equivalent to the value achieved by the output of the open TMS from Section 3.2.2.2, as seen in Figure 3.6. Since the output modes a_2 and a_3 no longer share any squeezed correlations, the measured entanglement between them must vanish, $E_{\mathcal{N}}^{(2,3)} = 0$.

This point of perfect swapping, where $\mathcal{C}_{12} = \mathcal{C}_{23}$ and $\mathcal{C}_{13} = 1$ is unique in that the scattering between a_2 and a_3 is also nonreciprocal, and not just the scattering between modes a_1 and a_2. This occurs because the appropriate condition for balancing the cooperativities, $\mathcal{C}_{23} = \mathcal{C}_{12}\mathcal{C}_{13}$, along with the phase condition, are also satisfied at this point. In order to discuss the behaviour at this point, we examine the form of output covariance matrix for the two direction of nonreciprocal scattering between modes a_2 and a_3, which is also shown at the points where the loop phase takes the values $\phi = \pm\pi/2$ in Figure 3.6. For the case where the direction of perfect nonreciprocal scattering is $a_2 \to a_3$, the covariance matrix may be written using the scattering matrix from Eq. (3.87):

$$\boldsymbol{\sigma}_{\Delta,\text{out}} = \frac{1}{2}\mathbf{U}^{(1,3)}\,\mathbf{R}^{(1,2)}\left(\mathbf{R}^{(1,2)}\right)^{T}\left(\mathbf{U}^{(1,3)}\right)^{T} \text{ when } \phi = -\frac{\pi}{2} \text{ and } \mathcal{C}_{23} = \mathcal{C}_{12}\mathcal{C}_{13}. \tag{3.93}$$

The entangling behaviour for this direction is similar to the $a_1 \leftarrow a_2$ direction of nonreciprocal scattering, but with mode a_1 and a_3 swapped. Here, the beam splitter once again acts to swap squeezed correlations, but the squeezed state is originally created between a_1 and a_2, with the beam splitter acting later to swap from mode a_1 to a_3. When the cooperativities are again balanced to allow for perfect swapping, it is now uncorrelated vacuum noise which is being swapped from a_3 to a_1, leaving the output of modes a_2 and a_3 in a TMSV. This perfectly mirrors the behaviour of the perfect swap, which occurs at the opposite phase.

For the other direction of nonreciprocal scattering, $a_2 \leftarrow a_3$, we can write the covariance matrix in terms of

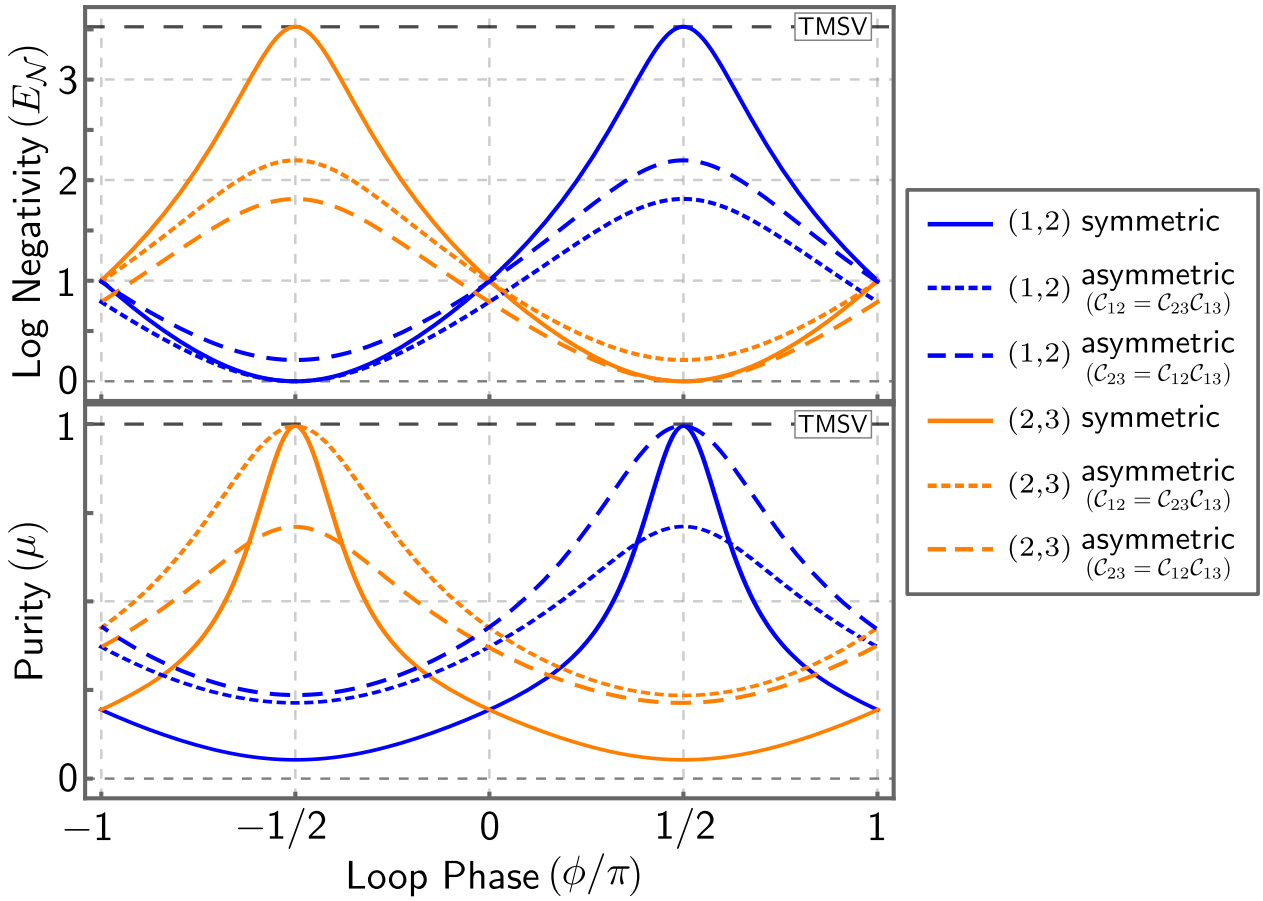

Figure 3.6: [Top] Logarithmic negativity $E_{\mathcal{N}}^{(j,k)}$ and [Bottom] purity $\mathcal{P}^{(j,k)}$ of the stationary output states of the delta amplifier. Results are shown for the bipartite output states of modes a_1 and a_2 (blue), along with a_2 and a_3 (orange). For the symmetric case (solid) the scattering between both mode pairs, (a_1, a_2) and (a_2, a_3), are perfectly nonreciprocal at the loop phases $\phi = \pm\pi/2$: the cooperativities are $\mathcal{C}_{23} = \mathcal{C}_{12} = 0.5$ and $\mathcal{C}_{13} = 1$, and so both cooperativity balancing conditions, $\mathcal{C}_{12} = \mathcal{C}_{23}\mathcal{C}_{13}$ and $\mathcal{C}_{23} = \mathcal{C}_{12}\mathcal{C}_{13}$ are met. In the first asymmetric case, only the scattering between the mode pair (a_1, a_2) is perfectly nonreciprocal (dotted): here $\mathcal{C}_{12} = 0.5$, $\mathcal{C}_{23} = 0.25$, and $\mathcal{C}_{13} = 2$. For the other asymmetric case, it is the scattering between the mode pair (a_2, a_3) which is perfectly nonreciprocal (dashed): here $\mathcal{C}_{12} = 0.25$, $\mathcal{C}_{23} = 0.5$, and $\mathcal{C}_{13} = 2$. All baths are in the vacuum state. The dashed black lines at the top of both plots correspond to the logarithmic negativity and purity for the output state of a *reciprocal* two-mode squeezed system with vacuum input (TMSV), $\mathcal{C}_{12} = \mathcal{C}_{13} = 0$.

Eq. (3.87), using the fact that the orthogonal transformations will commute with the identity matrix,

$$\boldsymbol{\sigma}_{\Delta,\text{out}} = \frac{1}{2}\mathbf{R}^{(1,2)}\left(\mathbf{R}^{(1,2)}\right)^T \text{ when } \phi = +\frac{\pi}{2} \text{ and } \mathcal{C}_{23} = \mathcal{C}_{12}\mathcal{C}_{13}. \tag{3.94}$$

Here we see that the output modes a_2 and a_3 share no squeezed correlations, so their joint state is separable, $E_{\mathcal{N}}^{(2,3)} = 0$, and it is now the output modes a_1 and a_2 which will always be entangled, $E_{\mathcal{N}}^{(1,2)} > 0$. Again using Simon's criterion, the output of a_2 and a_3 will be separable so long as the following inequality is satisfied:

$$\sqrt{\mathcal{C}_{12}\mathcal{C}_{23}\mathcal{C}_{13}}\left(\sqrt{\frac{\mathcal{C}_{23}}{\mathcal{C}_{12}\mathcal{C}_{13}}} + \sqrt{\frac{\mathcal{C}_{12}\mathcal{C}_{13}}{\mathcal{C}_{23}}} - 2\sin(\phi)\right) \leq 0. \tag{3.95}$$

This criterion is only violated when $\mathcal{C}_{23} = \mathcal{C}_{12}\mathcal{C}_{13}$ and $\phi = -\pi/2$, which is the point of perfect nonreciprocal scattering with direction $a_2 \leftarrow a_3$. The required phase here is now the opposite phase requirement from Eq. (3.95).

It is evident that the direction of the nonreciprocal scattering, and therefore the value of the phase ϕ, plays a crucial role in the behaviour of the output field entanglement, as depicted in Figure 3.6. $E_{\mathcal{N}}^{(1,2)}$ and $E_{\mathcal{N}}^{(2,3)}$ reach maximum values for this parameter regime, where they both achieve the same entanglement of a reciprocal two-mode squeezer, however, the maxima are achieved at different values of the phase. In addition, this is also the only operating regime

where both $E_{\mathcal{N}}^{(1,2)}$ and $E_{\mathcal{N}}^{(2,3)}$ reach the absolute minimum value of zero.

The point of perfect swapping discussed earlier deserves additional attention. We recall that at this point, the loop phase is $\phi = \pm\pi/2$ and the cooperativities obey the relations $\mathcal{C}_{12} = \mathcal{C}_{23}$ and $\mathcal{C}_{13} = 1$, resulting in perfect nonreciprocal scattering for both of the mode pairs (a_1, a_2) and (a_2, a_3). This point is notable because it also corresponds to points where the input signal is not reflected in the output signals for modes a_1 and a_3. Referring to the conditions for blocking reflection listed in Eq. (3.79), it may be seen that it is only possible to satisfy the conditions for both modes when performing a perfect swap. From here on, we will refer to the regime where $\mathcal{C}_{13} = 1$ as the "symmetric" case since $\mathcal{C}_{12} = \mathcal{C}_{23}$. We therefore label the regime where $\mathcal{C}_{13} \neq 1$ the "asymmetric" case.

The circuit decomposition also allows for a heuristic explanation of the behaviour of the marginal purities, seen in the bottom plot of Figure 3.6. Since the initial covariance matrix is $\boldsymbol{\sigma}_{\text{in}} = \mathbf{I}_6/2$ for vacuum inputs, the marginal purities for the input states will be $\mathcal{P}^{(1,2)} = 1$ and $\mathcal{P}^{(2,3)} = 1$. These purities will remain unchanged in the output state provided the 2-mode block can be reached by a symplectic transformation. This follows since the determinant of a symplectic transformation is $\det[\mathbf{S}] = 1$, and therefore $\det[\mathbf{SOS}^T] = \det[\mathbf{O}]$ for any matrix $\mathbf{O}$.

We start again bu balancing the cooperativities such that $\mathcal{C}_{12} = \mathcal{C}_{13}\mathcal{C}_{23}$. Since the covariance matrix for $\phi = -\pi/2$, Eq. (3.90), simply describes a two-mode squeezing interaction between modes a_2 and a_3, the marginal purity will always be maximised for these parameter values, $\mathcal{P}^{(2,3)} = 1$. On the other hand, the marginal purity of the output state between modes a_1 and a_2 is below one, $\mathcal{P}^{(1,2)} < 1$, in this case since the 2-mode block $\boldsymbol{\sigma}_{\Delta,\text{out}}^{(1,2)}$ cannot be reached by any combination of symplectic transformations. This same reasoning applies to the opposite phase $\phi = +\pi/2$, where $\mathcal{P}^{(2,3)} < 1$ always holds and $\mathcal{P}^{(1,2)} < 1$ only in the asymmetric case. The exception is the symmetric case, where the purity $\mathcal{P}^{(1,2)} = 1$ is realised because $\boldsymbol{\sigma}_{\Delta,\text{out}}^{(1,2)}$ is equivalent to the covariance matrix for a two-mode squeezed vacuum state. In fact, the condition that saturates the marginal purity $\mathcal{P}^{(1,2)} = 1$ is equivalent to the condition for which $E_{\mathcal{N}}^{(2,3)} = 0$, see Eq. (3.95), meaning only the output of modes a_1 and a_2 are entangled. An identical analysis can be performed when the cooperativities are balanced such that $\mathcal{C}_{23} = \mathcal{C}_{12}\mathcal{C}_{13}$, but where the behaviour of the mode pairs, (a_1, a_2) and (a_2, a_3), is swapped for opposite values of the loop phase $\phi \to -\phi$.

In this section, we have observed and explained how entanglement arises in a nonreciprocal system. Crucially, we find that the points of perfect nonreciprocity play a special role in maximising the achievable output entanglement. We also note how the special symmetric case allows for the purity of the output states to be maximised, and also prevents the reflection of noise from the input fields. We are now in a position to analyse the role of nonreciprocity in entanglement generation in the presence of thermal fluctuations.

3.3.4.2 Rerouting Thermal Fluctuations Using Nonreciprocity

Thermal noise is an unwanted feature when attempting to generate entanglement. In the case of a reciprocal two-mode squeezer, thermal noise incident on one or both modes will only serve to degrade the logarithmic negativity. While this can be overcome by increasing the strength of the two-mode squeezing interaction, the same is not true for the purity of the generated output state. More precisely, the purity for a two-mode squeezed system with thermal noise at the inputs for both modes is independent of the degree of squeezing, which is shown in Eq. (3.35).

One might expect that reciprocally coupling an auxiliary cold mode to the hot modes of interest would help in mitigating this impact. However, while such a coupling can reduce the internal occupation of the hot modes, it is unable to continuously route thermal inputs in a specified direction: away from the propagating output fields. Combining this cold auxiliary mode with nonreciprocity enables unidirectional scattering of coherent input signals, which extends to the routing of thermal fluctuations, while also allowing for the output of the target modes to be entangled. While it is also possible for a three-mode reciprocal system to route thermal fluctuations, no entanglement can be generated between the outputs of the target modes, which is demonstrated in Appendix D.2.

The delta amplifier provides a way for us to avoid these effects on the state shared between the output of modes a_1 and a_2, or a_2 and a_3, by setting the parameters to the symmetric case. At this point, there is no reflection of the inputs from modes a_1 and a_3, which are instead perfectly swapped between the two modes; in this instance, the two modes are said to be impedance matched. We focus, without loss of generality, on improving the purity of the shared state of the output of modes a_1 and a_2. Provided that the input of mode a_3 is in vacuum, if we set $\phi = +\pi/2$, thermal noise incident on the input of mode a_1 can be rerouted to the output of mode a_3. Using the left polar decomposition for the scattering matrix, Eq. (3.85), the output covariance matrix has the following form:

$$\boldsymbol{\sigma}_{\Delta,\text{out}} = \mathbf{U}_{\text{swap}}^{(1,3)} \mathbf{R}_{+}^{(2,3)} \boldsymbol{\sigma}_{\text{in}} \left(\mathbf{R}_{+}^{(2,3)}\right)^T \left(\mathbf{U}_{\text{swap}}^{(1,3)}\right)^T. \tag{3.96}$$

where

$$\mathbf{U}_{\text{swap}}^{(1,3)} \longleftrightarrow \hat{U}_{\text{swap}}^{(1,3)} := \exp\left[-i\frac{\pi}{2}\left(\hat{a}_1^\dagger \hat{a}_3 + \hat{a}_1 \hat{a}_3^\dagger\right)\right]. \tag{3.97}$$

The circuit description shown in Figure 3.5 provides a succinct explanation of the scattering: modes a_2 and a_3 are

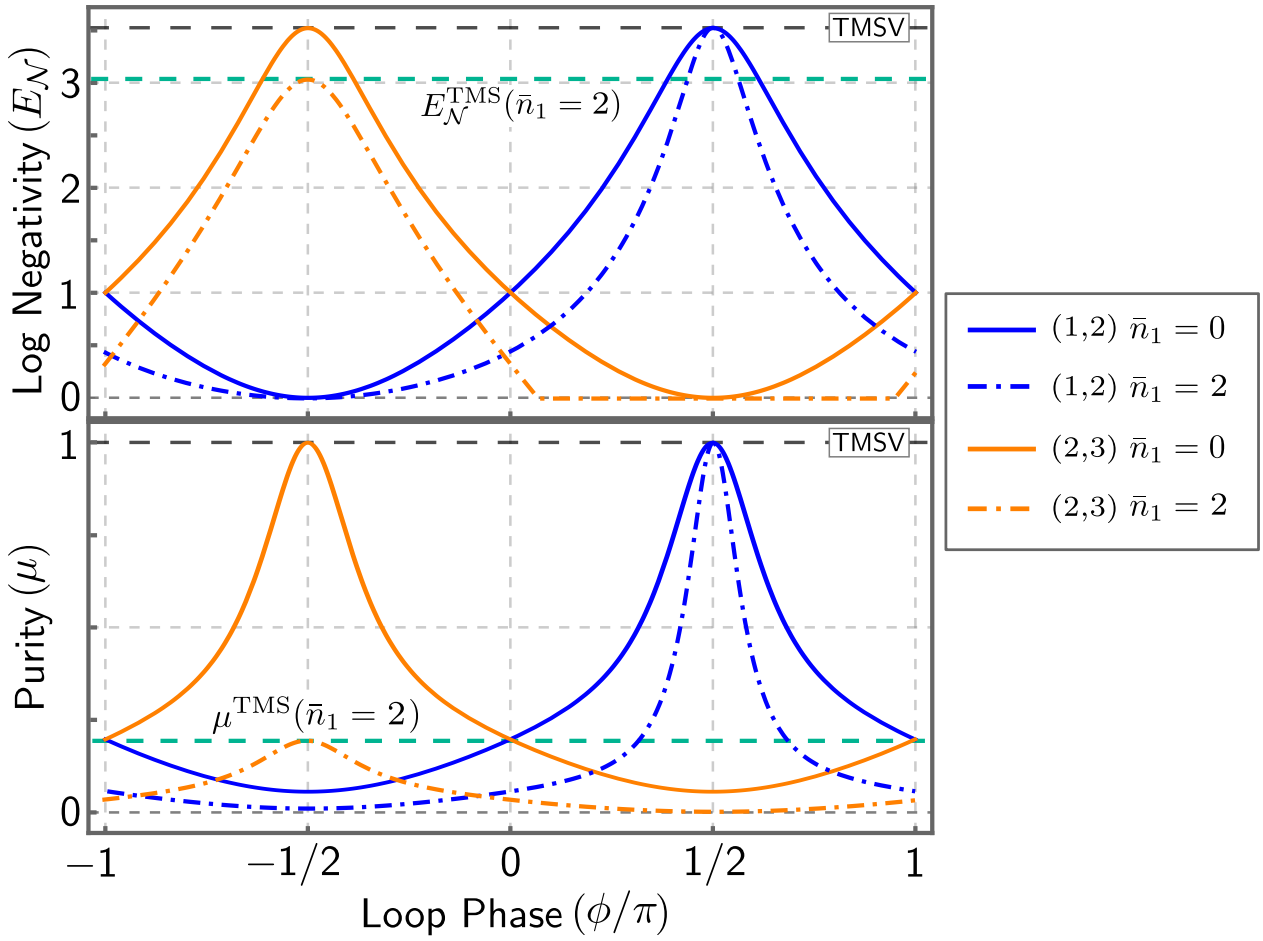

Figure 3.7: [Top] Logarithmic negativity and [Bottom] purity of the delta amplifier output states as a function of the loop phase in the presence of thermal noise. Two values for the noise from the bath for mode a_1 are shown: vacuum noise $\bar{n}_1 = 0$ (solid), and thermal noise $\bar{n}_1 = 2$ (dashed-dotted line). The modes a_2 and a_3 only experience vacuum noise from the bath, $\bar{n}_2 = \bar{n}_3 = 0$. The results shown are for the symmetric case where $\mathcal{C}_{12} = \mathcal{C}_{23} = 0.5$ and $\mathcal{C}_{13} = 1$, describing the joint output states of modes a_1 and a_2 (blue), and modes a_2 and a_3 (orange). We also show the results for a two-mode squeezed state where $\bar{n}_1 = 2$ and $\bar{n}_2 = 0$ (green). The dashed black line indicates both the logarithmic negativity and purity for a two-mode squeezed vacuum state (TMSV).

entangled, and the subsequent beam splitter acts as a perfect swap of the states of modes a_1 and a_3. Since $\bar{n}_1 \neq 0$, the output of mode a_3 will receive the unwanted thermal noise, while the output of mode a_1 forms a two-mode squeezed state with mode a_2. Provided that the input for mode a_2 is also vacuum noise, the shared state for the output of modes a_1 and a_2 will be a TMSV state with maximum purity and entanglement, unaffected by the value of $\bar{n}_1$, as seen in Figure 3.7.

In this symmetric regime, a right polar decomposition given by Eq. (3.87) can also be used, and therefore the covariance matrix described by Eq. (3.96) can be written in an alternate, but equivalent form. Due to the presence of thermal noise, the initial covariance matrix is no longer proportional to the identity matrix, and hence the beam splitter no longer has a trivial effect on the covariances of the input states. The output covariance matrix then also has the form:

$$\boldsymbol{\sigma}_{\Delta,\mathrm{out}} = \mathbf{R}^{(1,2)}\,\mathbf{U}_{\mathrm{swap}}^{(1,3)}\boldsymbol{\sigma}_{\mathrm{in}}\left(\mathbf{U}_{\mathrm{swap}}^{(1,3)}\right)^{T}\left(\mathbf{R}^{(1,2)}\right)^{T}. \tag{3.98}$$

Here, the action of the beam splitter on $\boldsymbol{\sigma}_{\mathrm{in}}$ swaps the thermal noise from mode a_1 with the input from mode a_3, which is vacuum noise. This is followed by a two-mode squeezer acting directly to entangle modes a_1 and a_2, creating a state with maximum purity and entanglement. It is important to note that mode a_1 is not cooled using this scheme, and that the nonreciprocal scattering only allows for the thermal noise to be rerouted so that it does not appear in the output field.

If we tune ϕ away from the points of perfect nonreciprocity and impedance matching, the entanglement and purity of modes a_1 and a_2 degrade as before. However, comparing Figure 3.7 and the previous results when only considering vacuum inputs, Figure 3.6, we note that the degradation is more pronounced when the input field of mode a_1 has

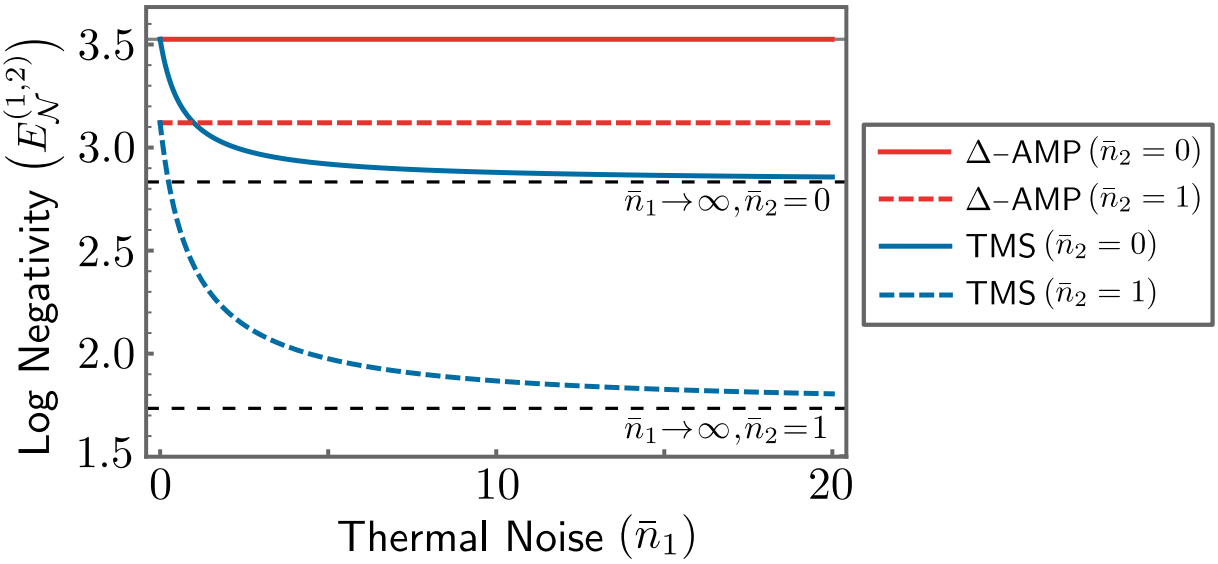

Figure 3.8: The entanglement between the stationary output of the modes a_1 and a_2 as measured by the logarithmic negativity, as a function of the strength of thermal noise input $\bar{n}_1$ on mode a_1. We compare the results from an open two-mode squeezed system (TMS, blue) with the delta amplifier (Δ-AMP, red). In both cases, the squeezing interaction between modes a_1 and a_2 has cooperativity $\mathcal{C}_{12} = 0.5$. The symmetric case is shown for the delta amplifier, so $\mathcal{C}_{23} = 0.5$, $\mathcal{C}_{13} = 1$, and $\phi = +\pi/2$. The thermal occupation of mode a_2 is set to $\bar{n}_2 = 0$ (solid) and $\bar{n}_2 = 1$ (dashed). Mode a_3 is always taken to have vacuum input noise. The dashed black lines correspond to the logarithmic negativity for a TMS where $\bar{n}_1 \to \infty, \bar{n}_2 = 0$ and $\bar{n}_1 \to \infty, \bar{n}_2 = 1$.

non-zero thermal occupancy. This observation further highlights the importance of nonreciprocity in implementing perfect swaps of thermal inputs.

Finally, while thermal noise in one mode is detrimental to both entanglement and purity, the effects are compounded when both modes contain some thermal noise input. Figure 3.8 demonstrates the effects of incident thermal noise on both modes of an entangled pair. The delta amplifier has the benefit that, regardless of the amount of thermal noise incident on mode a_2, the thermal noise incident on mode a_1 is always swapped away in the output. The usual two-mode squeezed state, on the other hand, will experience extra degradation of the entanglement and purity as $\bar{n}_1$ increases for even relatively small values of $\bar{n}_2$, as discussed in Section 3.2.1. The conditions for blocking reflection listed in Eq. (3.79) make it clear that it is not possible to prevent $\bar{n}_2$ from appearing in the output of mode a_2. However, provided that the noise incident on mode a_1 is at a higher temperature than the noise incident on mode a_3, $\bar{n}_1 > \bar{n}_3$, then the delta amplifier will always improve the fidelity of the entangled output state for modes a_1 and a_2 when compared to the usual TMS at the same interaction strength.

3.4 Bowtie Amplifier

3.4.1 System Setup

3.4.1.1 Dynamical Equations

With the entangling behaviour of the delta amplifier fully characterised, we can now proceed to investigate the other three-mode nonreciprocal amplifier: that of the bowtie amplifier. Motivated by the fact that the delta amplifier is capable of routing thermal noise under certain conditions, the primary goal of this section will be to determine the conditions under which this is possible with the bowtie amplifier configuration. The Hamiltonian for this system involves four coherent processes, three beam splitter (BS) interactions coupling the three modes with one of the BS interactions carrying the loop phase, $\phi \in [-\pi, \pi]$; the squeezing for entanglement is provided by a single-mode squeezing (SMS) interaction applied to one of the modes. Assuming no detuning of the pump frequencies, the Hamiltonian for this configuration may be written in the rotated frame as,

$$\hat{H}_{\bowtie} = g_{12}\left(\hat{a}_1^\dagger \hat{a}_2 + \hat{a}_1 \hat{a}_2^\dagger\right) + g_{23}\left(\hat{a}_2^\dagger \hat{a}_3 + \hat{a}_2 \hat{a}_3^\dagger\right) + g_{13}\left(e^{i\phi}\hat{a}_1^\dagger \hat{a}_3 + e^{-i\phi}\hat{a}_1 \hat{a}_3^\dagger\right) + \frac{\lambda}{2}\left(e^{i\theta}\hat{a}_2^{\dagger 2} + e^{-i\theta}\hat{a}_2^2\right). \tag{3.99}$$

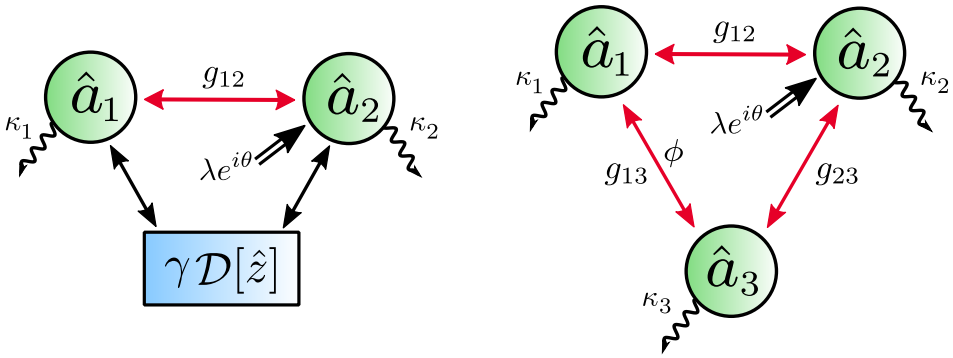

Figure 3.9: [Left] Diagram of an open system comprised of a beam splitter interaction plus single-mode squeezing applied to one mode, coupled to the nonlocal dissipator $\gamma\mathcal{D}[\hat{z}]$. The rates of the BS and SMS interactions are g_{12} and λ, respectively. The SMS interaction has an additional phase to control which quadrature is amplified, θ. [Right] Diagram of the bowtie amplifier, consisting of three open modes. All mode pairs (a_j, a_k) are coupled via beam splitter interactions with rates g_{jk}, with single-mode squeezing applied to mode a_2 with rate λ and phase θ. The tunable loop phase is placed on the interaction between modes a_1 and a_3. If mode a_3 is adiabatically eliminated, this three-mode loop is equivalent to the system depicted to the left with the jump operator given by $\hat{z} = \hat{a}_1 + \zeta e^{i\phi}\hat{a}_2$.

Assuming that each mode is coupled to an independent Markovian bath, the open-system dynamics of the bowtie amplifier may be modelled using the following Lindblad master equation:

$$\frac{d}{dt}\hat{\rho} = \mathcal{L}_{\bowtie}(\hat{\rho}) \quad \text{where} \quad \mathcal{L}_{\bowtie}(\hat{\rho}) = -i[\hat{H}_{\bowtie}, \hat{\rho}] + \sum_{k=1,2,3} \kappa_k \left((\bar{n}_k + 1)\mathcal{D}[\hat{a}_k](\hat{\rho}) + \bar{n}_k \mathcal{D}[\hat{a}_k^\dagger](\hat{\rho}) \right). \tag{3.100}$$

Since the bowtie amplifier contains no two-mode squeezing interactions, it is not the nonreciprocal extension of the open TMS system from Section 3.2.2, but instead an open system with the following two-mode Hamiltonian,

$$\hat{H}_{\text{BS-SMS}} = g_{12}\left(\hat{a}_1^\dagger \hat{a}_2 + \hat{a}_1 \hat{a}_2^\dagger\right) + \frac{\lambda}{2}\left(e^{i\theta}\hat{a}_2^{\dagger\,2} + e^{-i\theta}\hat{a}_2^2\right), \tag{3.101}$$

where the two modes are coherently coupled by a beam splitter interaction, and where squeezing is applied to the mode a_2. As with the bowtie amplifier, the modes are coupled to independent Markovian baths with some thermal fluctuations. The Lindblad master equation for the total system is then,

$$\frac{d}{dt}\hat{\rho} = \mathcal{L}_{\text{BS-SMS}}(\hat{\rho}) \quad \text{where} \quad \mathcal{L}_{\text{BS-SMS}}(\hat{\rho}) = -i[\hat{H}_{\text{BS-SMS}}, \hat{\rho}] + \sum_{k=1,2} \kappa_k \left((\bar{n}_k + 1)\mathcal{D}[\hat{a}_k](\hat{\rho}) + \bar{n}_k \mathcal{D}[\hat{a}_k^\dagger](\hat{\rho}) \right). \tag{3.102}$$

We will refer to the two-mode open system described by the Lindbladian $\mathcal{L}_{\text{BS}-\text{SMS}}$ as the beam splitter plus single-mode squeezer (BS-SMS) setup. Using the engineered dissipation approach to nonreciprocity from Section 2.4.2, the BS-SMS interaction can be made nonreciprocal through the addition of an appropriate nonlocal dissipator to the Lindblad master equation [83],

$$\frac{d}{dt}\hat{\rho} = \mathcal{L}_{\text{BS-SMS}}(\hat{\rho}) + \gamma\mathcal{D}[\hat{z}](\hat{\rho}), \tag{3.103}$$

along with appropriate tuning of system parameters. There are two correct choices for nonlocal jump operators, $\hat{z} = \hat{a}_1 + \zeta e^{i\phi}\hat{a}_2$ or $\hat{z} = \hat{a}_1^\dagger + \zeta e^{i\phi}\hat{a}_2^\dagger$, which are determined solely by the coupling between modes a_1 and a_2, and are independent of any single mode processes. Unlike with the delta amplifier, replacing the nonlocal dissipator with a highly damped mode does not result in equivalent three-mode systems for either choice of these two jump operators. Starting with the master equation for the bowtie amplifier in Eq. (3.100), adiabatically eliminating mode a_3 will yield the first jump operator, $\hat{z} = \hat{a}_1 + \zeta e^{i\phi}\hat{a}_2$, as shown in Figure 3.9. In this instance, the nonlocal dissipator coupling is $\gamma = 4g_{13}^2/\kappa_3$, and the asymmetric coupling is $\zeta = g_{23}/g_{13}$.

Whereas squeezing in the delta amplifier arose due to the two TMS interactions between the system modes, the squeezing in the bowtie amplifier, necessary for amplification as well as entanglement generation, is generated at only one mode. The three passive beam splitters are required to distribute the squeezed correlations among the three modes in the loop, a task which cannot be accomplished by TMS interactions, which cannot transfer correlations. As will be demonstrated, despite these differences, the entangling behaviours of the two systems are remarkably similar. This connection will be established using a circuit decomposition of the bowtie amplifier, which will demonstrate that it is also capable of generating high-fidelity flying entangled states through the routing of thermal fluctuations.

3.4.1.2 Stability Conditions

We will apply the Routh-Hurwitz criterion to the dynamical matrix of the bowtie amplifier to determine the necessary conditions to ensure the parameters are within the stable regime. Writing the quadrature basis vector as $\hat{\boldsymbol{r}} = (\hat{q}_1, \hat{p}_1, \hat{q}_2, \hat{p}_2, \hat{q}_3, \hat{p}_3)$, the dynamical matrix for the bowtie amplifier is

$$\mathbf{A}_{\bowtie} = \begin{pmatrix} (-\kappa_1/2)\mathbf{I} & g_{12}\mathbf{J} & g_{13}(\sin(\phi)\mathbf{I} + \cos(\phi)\mathbf{J}) \\ g_{12}\mathbf{J} & (-\kappa_2/2)\mathbf{I} + \lambda(\sin(\theta)\mathbf{Z} - \cos(\theta)\mathbf{X}) & g_{23}\mathbf{J} \\ g_{13}(-\sin(\phi)\mathbf{I} + \cos(\phi)\mathbf{J}) & g_{23}\mathbf{J} & (-\kappa_3/2)\mathbf{I} \end{pmatrix}. \tag{3.104}$$

The characteristic polynomial for this dynamical matrix is,

$$\det[\mathbf{A}_{\bowtie} - s\mathbf{I}_6] = P(s,+\lambda)P(s,-\lambda) + 4g_{12}^2 g_{13}^2 g_{23}^2 \cos^2(\phi) \text{ where } P(s,\pm\lambda) = s^3 + u_2(\pm\lambda)s^2 + u_1(\pm\lambda)s + u_0(\pm\lambda), \tag{3.105}$$

where the coefficients of the third-order polynomial $P(s,\pm\lambda)$ are:

$$\begin{aligned} u_2(\pm\lambda) &= \frac{\kappa_1}{2} + \frac{\kappa_2 \mp 2\lambda}{2} + \frac{\kappa_3}{2} \\ u_1(\pm\lambda) &= g_{12}^2 + g_{13}^2 + g_{23}^2 + \frac{\kappa_1}{2}\frac{\kappa_2 \mp 2\lambda}{2} + \frac{\kappa_2 \mp 2\lambda}{2}\frac{\kappa_3}{2} + \frac{\kappa_1}{2}\frac{\kappa_3}{2} \\ u_0(\pm\lambda) &= g_{12}^2\frac{\kappa_3}{2} + g_{13}^2\frac{\kappa_2 \mp 2\lambda}{2} + g_{13}^2\frac{\kappa_1}{2} + \frac{\kappa_1}{2}\frac{\kappa_2 \mp 2\lambda}{2}\frac{\kappa_3}{2}. \end{aligned} \tag{3.106}$$

Focusing on the points of perfect nonreciprocity, the optimal values for loop phase are $\phi = \pm\pi/2$, which reduces the above characteristic polynomial to the product of two third-order polynomials, $P(s,+\lambda)P(s,-\lambda)$. The Routh-Hurwitz criterion can be generated for the two individual polynomials, which mandates that all coefficients must be greater than zero, $u_k(\pm\lambda) > 0$. Additionally, the coefficients must also satisfy the condition $u_2(\pm\lambda)u_1(\pm\lambda) - u_0(\pm\lambda) > 0$ in order for the system to be stable; this term may be written as

$$\begin{aligned} u_2(\pm\lambda)u_1(\pm\lambda) - u_0(\pm\lambda) = {} & g_{12}^2\left(\frac{\kappa_1}{2} + \frac{\kappa_2 \mp 2\lambda}{2}\right) + g_{13}^2\left(\frac{\kappa_1}{2} + \frac{\kappa_3}{2}\right) + g_{23}^2\left(\frac{\kappa_2 \mp 2\lambda}{2} + \frac{\kappa_3}{2}\right) \\ & + \left(\frac{\kappa_1}{2} + \frac{\kappa_2 \mp 2\lambda}{2}\right)\left(\frac{\kappa_1}{2} + \frac{\kappa_3}{2}\right)\left(\frac{\kappa_2 \mp 2\lambda}{2} + \frac{\kappa_3}{2}\right). \end{aligned} \tag{3.107}$$

In both cases, the magnitude of the single-mode squeezing interaction, λ, modifies the effective damping on the a_2 mode, resulting in additional damping, or antidamping. The stability criteria are always met by the polynomial where mode a_2 receives extra damping, $P(s,+\lambda)$, and so we only need to consider the conditions for the $P(s,-\lambda)$ polynomial, where mode a_2 is antidamped. Rewriting the conditions in terms of the cooperativities yields the following stability criteria:

$$\begin{aligned} 0 &< \kappa_1 + \kappa_2\,(1 - \mathcal{C}_\lambda) + \kappa_3 \\ 0 &< \kappa_1\kappa_2(1 + \mathcal{C}_{12} - \mathcal{C}_\lambda) + \kappa_1\kappa_3(1 + \mathcal{C}_{13}) + \kappa_2\kappa_3(1 + \mathcal{C}_{23} - \mathcal{C}_\lambda) \\ 0 &< \kappa_1\kappa_2\kappa_3\big(1 + \mathcal{C}_{12} + \mathcal{C}_{13} + \mathcal{C}_{23} - \mathcal{C}_\lambda(1 + \mathcal{C}_{13})\big) \\ 0 &< \kappa_1\kappa_2\mathcal{C}_{12}\big(\kappa_1 + \kappa_2(1 - \mathcal{C}_\lambda)\big) + \kappa_1\kappa_3\mathcal{C}_{13}\big(\kappa_1 + \kappa_3\big) + \kappa_2\kappa_3\mathcal{C}_{23}\big(\kappa_2(1 - \mathcal{C}_\lambda) + \kappa_3\big) \\ &\quad + \big(\kappa_1 + \kappa_2(1 - \mathcal{C}_\lambda)\big)\big(\kappa_1 + \kappa_3\big)\big(\kappa_2(1 - \mathcal{C}_\lambda) + \kappa_3\big). \end{aligned} \tag{3.108}$$

Here, $\mathcal{C}_{jk} := 4g_{jk}^2/\kappa_j\kappa_k$ are the beam splitter cooperativities, and $\mathcal{C}_\lambda := 2\lambda/\kappa_2$ is the cooperativity for the single-mode squeezer. Since the scattering matrix depends solely on the cooperativity, the most relevant of these conditions is the following:

$$0 < 1 + \mathcal{C}_{12} + \mathcal{C}_{13} + \mathcal{C}_{23} - \mathcal{C}_\lambda(1 + \mathcal{C}_{13}). \tag{3.109}$$

This condition sets the upper limit on the amount of squeezing that can be generated in the system, which is the source of instability. The remaining conditions are explicitly dependent on the decay rates of the individual modes, which we assume to always be tuned appropriately to ensure stability, regardless of the values of the cooperativities.

3.4.1.3 Scattering Properties

Routing of thermal noise between the modes of the amplifier requires proper tuning of the system parameters, so to determine the appropriate conditions, we must examine the scattering matrix for the nonreciprocal amplifier. For

simplicity, we will do this in the basis of creation and annihilation operators for the system, $\hat{\boldsymbol{a}}_{\bowtie} = (\hat{a}_1, \hat{a}_2, \hat{a}_3, \hat{a}_1^\dagger, \hat{a}_2^\dagger, \hat{a}_3^\dagger)$, which has a different ordering from the basis used for the delta amplifier. The Heisenberg-Langevin in this basis may be written as

$$\frac{d}{dt}\hat{\boldsymbol{a}}_{\bowtie}(t) = \tilde{\mathbf{A}}_{\bowtie}\hat{\boldsymbol{a}}_{\bowtie}(t) - \sqrt{\tilde{\boldsymbol{\kappa}}_{\bowtie}}\hat{\boldsymbol{a}}_{\bowtie,\text{in}}(t) \tag{3.110}$$

where $\tilde{\mathbf{A}}_{\bowtie}$ is the dynamical matrix, $\tilde{\boldsymbol{\kappa}}_{\bowtie} = \text{diag}(\kappa_1, \kappa_2, \kappa_3, \kappa_1, \kappa_2, \kappa_3)$ is a diagonal matrix of damping rates, and $\hat{\boldsymbol{a}}_{\bowtie,\text{in}}(t)$ is the vector of time-dependent input-noise operators. The dynamical matrix in this basis is:

$$\tilde{\mathbf{A}}_{\bowtie} = \begin{pmatrix} -\kappa_1/2 & -ig_{12} & -ie^{i\phi}g_{13} & 0 & 0 & 0 \\ -ig_{12} & -\kappa_2/2 & -ig_{23} & 0 & -ie^{i\theta}\lambda & 0 \\ -ie^{-i\phi}g_{13} & -ig_{23} & -\kappa_3/2 & 0 & 0 & 0 \\ 0 & 0 & 0 & -\kappa_1/2 & ig_{12} & ie^{-i\phi}g_{13} \\ 0 & ie^{-i\theta}\lambda & 0 & ig_{12} & -i\kappa_2/2 & ig_{23} \\ 0 & 0 & 0 & ie^{i\phi}g_{13} & ig_{23} & -\kappa_3/2 \end{pmatrix}. \tag{3.111}$$

We solve for the steady-state scattering matrix by first Fourier transforming the system of Heisenberg-Langevin equations to the frequency domain, and then proceed to use input-output theory to write $\hat{\mathbf{a}}_{\bowtie,\text{out}}[\omega] = \tilde{\mathbf{S}}_{\bowtie}[\omega]\hat{\mathbf{a}}_{\bowtie,\text{in}}[\omega]$. The full scattering matrix on resonance $\tilde{\mathbf{S}}_{\bowtie}[0] \equiv \tilde{\mathbf{S}}_{\bowtie}$ may then be decomposed into 3×3 blocks:

$$\tilde{\mathbf{S}}_{\bowtie} = \begin{pmatrix} \mathbf{S}_{\bowtie}^{aa} & \mathbf{S}_{\bowtie}^{aa^\dagger} \\ \mathbf{S}_{\bowtie}^{a^\dagger a} & \mathbf{S}_{\bowtie}^{a^\dagger a^\dagger} \end{pmatrix}. \tag{3.112}$$

The scattering matrix is considerably denser than that of the delta amplifier, thanks to the presence of the single-mode squeezing in the off-diagonal blocks of the dynamical matrix. To simplify the analysis, we use the fact that when the scattering is on resonance, the sub-blocks of the scattering matrix obey $\overline{\mathbf{S}_{\bowtie}^{aa}} = \mathbf{S}_{\bowtie}^{a^\dagger a^\dagger}$ and $\overline{\mathbf{S}_{\bowtie}^{a^\dagger a}} = \mathbf{S}_{\bowtie}^{aa^\dagger}$, and so we only need to explicitly examine two of the sub-blocks:

$$\mathbf{S}_{\bowtie}^{aa} = \frac{1}{D}\begin{pmatrix} D + 2C(1+\mathcal{C}_{23}) + 2\mathcal{C}_\lambda^2(1+\mathcal{C}_{13}) & -2C\big(i\sqrt{\mathcal{C}_{12}} + e^{i\phi}\sqrt{\mathcal{C}_{13}\mathcal{C}_{23}}\big) & -2C\big(ie^{i\phi}\sqrt{\mathcal{C}_{13}} + \sqrt{\mathcal{C}_{12}\mathcal{C}_{23}}\big) \\ & & -2ie^{i\phi}\sqrt{\mathcal{C}_{13}}\mathcal{C}_\lambda^2(1+\mathcal{C}_{13}) \\ -2C\big(i\sqrt{\mathcal{C}_{12}} + e^{-i\phi}\sqrt{\mathcal{C}_{13}\mathcal{C}_{23}}\big) & D + 2C(1+\mathcal{C}_{13}) & -2C\big(i\sqrt{\mathcal{C}_{23}} + e^{i\phi}\sqrt{\mathcal{C}_{12}\mathcal{C}_{23}}\big) \\ -2C\left(ie^{-i\phi}\sqrt{\mathcal{C}_{13}} + \sqrt{\mathcal{C}_{12}\mathcal{C}_{23}}\right) & -2C\big(i\sqrt{\mathcal{C}_{23}} + e^{-i\phi}\sqrt{\mathcal{C}_{12}\mathcal{C}_{23}}\big) & D + 2C(1+\mathcal{C}_{12}) + 2\mathcal{C}_\lambda^2(1+\mathcal{C}_{13}) \\ -2ie^{-i\phi}\sqrt{\mathcal{C}_{13}}\mathcal{C}_\lambda^2(1+\mathcal{C}_{13}) & & \end{pmatrix}$$

$$\mathbf{S}_{\bowtie}^{a^\dagger a} = \frac{\mathcal{C}_\lambda e^{-i\theta}}{D}\begin{pmatrix} 2i\big(i\sqrt{\mathcal{C}_{12}} - e^{-i\phi}\sqrt{\mathcal{C}_{13}\mathcal{C}_{23}}\big) & -2i(1+\mathcal{C}_{13}) & -2i\big(i\sqrt{\mathcal{C}_{12}} - e^{-i\phi}\sqrt{\mathcal{C}_{13}\mathcal{C}_{23}}\big) \\ \times\big(i\sqrt{\mathcal{C}_{12}} + e^{-i\phi}\sqrt{\mathcal{C}_{13}\mathcal{C}_{23}}\big) & \times\big(i\sqrt{\mathcal{C}_{12}} - e^{-i\phi}\sqrt{\mathcal{C}_{13}\mathcal{C}_{23}}\big) & \times\big(i\sqrt{\mathcal{C}_{23}} + e^{i\phi}\sqrt{\mathcal{C}_{12}\mathcal{C}_{13}}\big) \\ 2i(1+\mathcal{C}_{13}) & & 2i(1+\mathcal{C}_{13}) \\ \times\big(i\sqrt{\mathcal{C}_{12}} + e^{-i\phi}\sqrt{\mathcal{C}_{13}\mathcal{C}_{23}}\big) & -2i(1+\mathcal{C}_{13})^2 & \times\big(i\sqrt{\mathcal{C}_{23}} + e^{i\phi}\sqrt{\mathcal{C}_{12}\mathcal{C}_{13}}\big) \\ 2i\big(i\sqrt{\mathcal{C}_{12}} + e^{-i\phi}\sqrt{\mathcal{C}_{13}\mathcal{C}_{23}}\big) & -2i(1+\mathcal{C}_{13}) & 2i\big(i\sqrt{\mathcal{C}_{23}} + e^{i\phi}\sqrt{\mathcal{C}_{12}\mathcal{C}_{13}}\big) \\ \times\big(i\sqrt{\mathcal{C}_{23}} - e^{i\phi}\sqrt{\mathcal{C}_{12}\mathcal{C}_{13}}\big) & \times\big(i\sqrt{\mathcal{C}_{23}} - e^{i\phi}\sqrt{\mathcal{C}_{12}\mathcal{C}_{13}}\big) & \times\big(i\sqrt{\mathcal{C}_{23}} - e^{i\phi}\sqrt{\mathcal{C}_{12}\mathcal{C}_{13}}\big) \end{pmatrix}$$

$$\text{where} \quad D = |C|^2 - \mathcal{C}_\lambda^2(1+\mathcal{C}_{13})^2 \quad \text{and} \quad C = -(1+\mathcal{C}_{12}+\mathcal{C}_{13}+\mathcal{C}_{23}) - 2i\sqrt{\mathcal{C}_{12}\mathcal{C}_{13}\mathcal{C}_{23}}\cos(\phi). \tag{3.113}$$

Here, $\mathbf{S}_{\bowtie}^{aa}$ takes the annihilation operators of the input modes to the output modes, while $\mathbf{S}_{\bowtie}^{a^\dagger a}$ represents the scattering of the annihilation operators for the input to the creation operators of the output modes.

3.4.1.4 Controlling Scattering: Nonreciprocity and Reflection

With the scattering matrix defined, we can now provide the conditions required to realise perfect nonreciprocal scattering between the different mode pairs, as well as the separate conditions required to block unwanted noise from being reflected in a mode's output field. Starting with the former: the degree of nonreciprocity between two modes a_j and a_k is given by the $N^{(j,k)} \in [-1, 1]$ function defined in Eq. (2.138), which measures the difference in scattering amplitude between the scattering process $a_{j,\text{in}} \to a_{k,\text{out}}$ and $a_{k,\text{in}} \to a_{j,\text{out}}$. This function only reaches its extremum when the scattering between the modes a_j and a_k is perfectly nonreciprocal, which requires all elements representing scattering in one direction between these modes to vanish in both the $\mathbf{S}_{\bowtie}^{aa}$ and $\mathbf{S}_{\bowtie}^{a^\dagger a}$ matrices. For the bowtie amplifier,

we can only realise perfect nonreciprocal scattering between the mode pairs (a_1, a_2) and (a_2, a_3) when there is some non-zero squeezing in the system. The necessary conditions are detailed in the following table:

Coop. Condition	$\phi = -\pi/2$	$\phi = +\pi/2$	Stability Criteria
$\mathcal{C}_{12} = \mathcal{C}_{13}\mathcal{C}_{23}$	$a_1 \to a_2$	$a_1 \leftarrow a_2$	$\mathcal{C}_\lambda < 1 + \mathcal{C}_{23}$ & $0 \leq \mathcal{C}_{13}$
$\mathcal{C}_{23} = \mathcal{C}_{12}\mathcal{C}_{13}$	$a_2 \to a_3$	$a_2 \leftarrow a_3$	$\mathcal{C}_\lambda < 1 + \mathcal{C}_{12}$ & $0 \leq \mathcal{C}_{13}$
$\mathcal{C}_{13} = \mathcal{C}_{12}\mathcal{C}_{23}$ & $\mathcal{C}_\lambda = 0$	$a_3 \to a_1$	$a_3 \leftarrow a_1$	$0 \leq \mathcal{C}_{12}$ & $0 \leq \mathcal{C}_{23}$

(3.114)

In order to make the effects of the nonreciprocity conditions clear, the highlighted terms in $\mathbf{S}_{\bowtie}^{aa}$ and $\mathbf{S}_{\bowtie}^{a^\dagger a}$ go to zero exactly when the corresponding cooperativity and phase matching conditions are applied from the above table.

For modes a_1 and a_3, perfect nonreciprocal scattering is only possible when the amplitude of the squeezing interaction is zero, $\mathcal{C}_\lambda = 0$, meaning there is no amplification. This is a result of the squeezing altering the damping rate of mode a_2, which results in additional damping on one of the a_2 normal modes, while the other normal mode was antidamped, $\kappa_2/2 \pm \lambda$. This effects the required balancing condition for nonreciprocity between modes a_1 and a_3, which is no longer given by $\mathcal{C}_{13} = \mathcal{C}_{12}\mathcal{C}_{23}$, or equivalently, $g_{13} = g_{12}g_{23}/(\kappa_2/2)$, but is instead $g_{13} = g_{12}g_{23}/(\kappa_2/2 \pm \lambda)$. Nonreciprocity between the (a_1, a_3) mode pair therefore requires satisfying the condition where the damped and antidamped decay rates, and not the innate decay rate of a_2, are used, which is only possible when $\lambda = 0$.

The split in the damping rate also prevents thermal noise from the input of mode a_2 from being blocked from the reflected output field. As a result, we can conclude that thermal noise cannot be rerouted away from mode a_2 by the bowtie amplifier if the output modes are to be entangled. The bath for this mode must therefore be cold if an entangled state with the output of either of the other two modes is to have maximum purity. The scattering parameters controlling reflection for both modes a_1 and a_3 can both vanish, meaning that the routing of thermal noise is possible. Examining the scattering matrix allows us to determine the necessary conditions, which are summarised for all modes in the following table:

	Phase	Coop. Conditions
$a_{1,\text{in}} \not\to a_{1,\text{out}}$	$\phi = \pm\pi/2$	$0 = 1 - \mathcal{C}_{12} + \mathcal{C}_{23} - \mathcal{C}_{13}$, $\mathcal{C}_{13} = 1$ & $0 \leq \mathcal{C}_\lambda < 1 + \mathcal{C}_{23}$
$a_{2,\text{in}} \not\to a_{2,\text{out}}$	$\phi = \pm\pi/2$	$0 = 1 + \mathcal{C}_{12} + \mathcal{C}_{23} - \mathcal{C}_{13}$ & $\mathcal{C}_\lambda = 0$
$a_{3,\text{in}} \not\to a_{3,\text{out}}$	$\phi = \pm\pi/2$	$0 = 1 + \mathcal{C}_{12} - \mathcal{C}_{23} - \mathcal{C}_{13}$, $\mathcal{C}_{13} = 1$ & $0 \leq \mathcal{C}_\lambda < 1 + \mathcal{C}_{12}$

(3.115)

In order to block the reflection of the input noise, elements from $\mathbf{S}_{\bowtie}^{aa}$ and $\mathbf{S}_{\bowtie}^{a^\dagger a}$ must vanish; examining $\mathbf{S}_{\bowtie}^{a^\dagger a}$ in particular, we can see that $(\mathbf{S}_{\bowtie}^{a^\dagger a})_{11} = 0$ and $(\mathbf{S}_{\bowtie}^{a^\dagger a})_{33} = 0$ when certain nonreciprocity conditions, highlighted in Eq. (3.114) are fulfilled. As a result, the conditions for blocking input noise reflection, detailed in Eq. (3.115), also correspond to points of perfect nonreciprocity, with one added condition: the cooperativity between modes a_1 and a_3 must satisfy $\mathcal{C}_{13} = 1$, meaning the rates of the coherent and dissipative processes are perfectly matched. These are identical to the conditions that were necessary for thermal noise rerouting in the delta amplifier, detailed in Section 3.3.4.2, indicating that similar behaviour will be possible to realise with the bowtie amplifier. Despite this similarity, there are some subtle differences in the entangling behaviour which will be expounded upon in the next section.

3.4.2 Entanglement of Propagating Modes

3.4.2.1 A New Reference System

Given that the bowtie amplifier is the nonreciprocal loop formed from the open BS-SMS system described by Eq. (3.103), and not an open TMS system as was the case with the delta amplifier, it is expected that the entangling behaviour of the bowtie amplifier hews to that of the BS-SMS. As a result, before diving into an analysis of the bowtie amplifier, we must first investigate the entanglement of the propagating modes for the BS-SMS, and will do so by comparing the entanglement generation to the open TMS from Section 3.2. First, we determine the stability criteria of the open BS-SMS system using the dynamical matrix written in the quadrature basis defined by $\hat{\boldsymbol{r}} = (\hat{q}_1, \hat{p}_1, \hat{q}_2, \hat{p}_2)$:

$$\mathbf{A}_{\text{BS-SMS}} = \begin{pmatrix} -(\kappa_1/2)\mathbf{I} & g_{12}\mathbf{J} \\ g_{12}\mathbf{J} & -(\kappa_2/2)\mathbf{I} + \lambda(-\cos(\theta)\mathbf{X} + \sin(\theta)\mathbf{Z}) \end{pmatrix}. \tag{3.116}$$

We can determine the Routh-Hurwitz stability criteria for this dynamical matrix:

$$0 < \left(\frac{\kappa_1}{2} \pm \lambda\right) + \frac{\kappa_2}{2} \quad \text{and} \quad 0 < 1 + \mathcal{C}_{12} \pm \mathcal{C}_\lambda\,, \quad \text{where} \quad \mathcal{C}_{12} := \frac{4g_{12}^2}{\kappa_1\kappa_2}\,, \mathcal{C}_\lambda := \frac{2\lambda}{\kappa_2}. \tag{3.117}$$

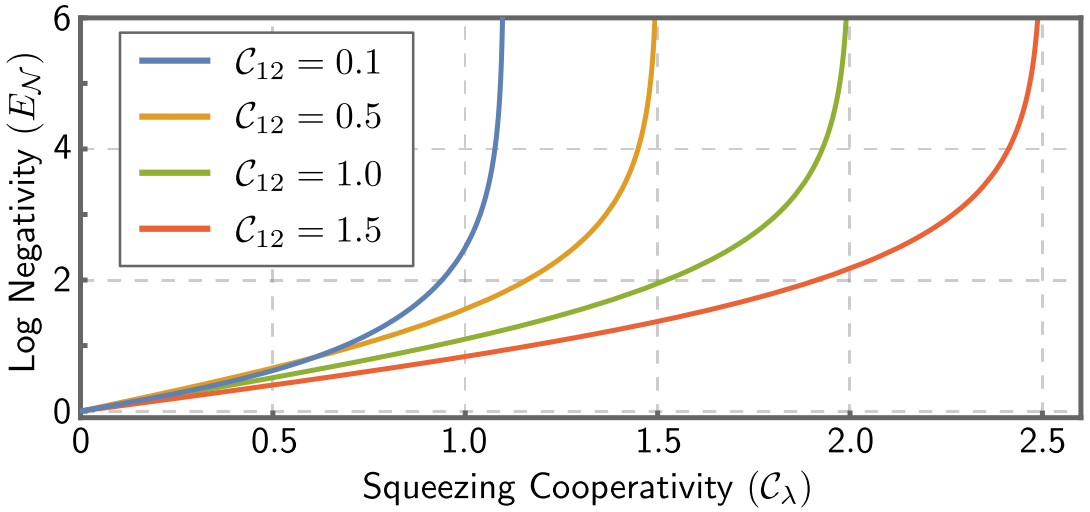

Figure 3.10: The logarithmic negativity for the output modes of the beam splitter plus single-mode squeezer system, plotted against the strength of the single-mode squeezer, represented by the cooperativity $\mathcal{C}_\lambda = 2\lambda/\kappa_2$. The beam splitter cooperativity, $\mathcal{C}_{12} = 4g_{12}^2/\kappa_1\kappa_2$, is fixed along each curve. All baths are assumed to be in the vacuum, $\bar{n}_1, \bar{n}_2 = 0$. The range of stable values of $\mathcal{C}_\lambda$ increases for larger $\mathcal{C}_{12}$, however, the entangling behaviour is the same along all curves since they all diverge as the squeezing approaches the point of instability, $\mathcal{C}_\lambda \to 1 + \mathcal{C}_{12}$.

As with the bowtie amplifier, the single-mode squeezing results in added damping and antidamping on mode a_2, and it is the antidamping which can make the system unstable. Using the dynamical matrix and input-output theory, the steady-state scattering matrix on resonance for the BS-SMS system is then:

$$\mathbf{S}_{\text{BS-SMS}} = -\frac{1}{(1+\mathcal{C}_{12})^2 - \mathcal{C}_\lambda^2} \begin{pmatrix} (1-\mathcal{C}_{12}^2-\mathcal{C}_\lambda^2)\mathbf{I} & 2\sqrt{\mathcal{C}_{12}}(1+\mathcal{C}_{12})\mathbf{J} \\ +2\mathcal{C}_\lambda\mathcal{C}_{12}(-\cos(\theta)\mathbf{X}+\sin(\theta)\mathbf{Z}) & -2\mathcal{C}_\lambda\sqrt{\mathcal{C}_{12}}(\cos(\theta)\mathbf{Z}+\sin(\theta)\mathbf{X}) \\ 2\sqrt{\mathcal{C}_{12}}(1+\mathcal{C}_{12})\mathbf{J} & (1-\mathcal{C}_{12}^2+\mathcal{C}_\lambda^2)\mathbf{I} \\ +2\mathcal{C}_\lambda\sqrt{\mathcal{C}_{12}}(\cos(\theta)\mathbf{Z}+\sin(\theta)\mathbf{X}) & +2\mathcal{C}_\lambda(-\cos(\theta)\mathbf{X}+\sin(\theta)\mathbf{Z}) \end{pmatrix}. \tag{3.118}$$

This matrix is not symmetric, and hence neither it nor the corresponding covariance matrix for the output modes corresponds to that of a two-mode squeezer. Thus, the entanglement is not cleanly related to the amount of squeezing generated by the SMS interaction, but is instead given by a rather ungainly expression. Assuming vacuum noise at the inputs, the steady-state output covariance matrix on resonance for the BS-SMS system is $\boldsymbol{\sigma}_{\text{out}} = \frac{1}{2}\mathbf{S}_{\text{BS-SMS}}\mathbf{S}_{\text{BS-SMS}}^T$, from which the logarithmic negativity for the output mode pair (a_1, a_2) can be calculated for an arbitrary phase, θ, of the SMS:

$$\begin{aligned} E_{\mathcal{N}}^{(1,2)} = &\ln\Big((1+\mathcal{C}_{12}+\mathcal{C}_\lambda)(1+\mathcal{C}_{12}-\mathcal{C}_\lambda)\Big) \\ &-\frac{1}{2}\ln\left((1+\mathcal{C}_{12}+\mathcal{C}_\lambda)^2(1+\mathcal{C}_{12}-\mathcal{C}_\lambda)^2+32\mathcal{C}_\lambda^2\mathcal{C}_{12}-8\mathcal{C}_\lambda\sqrt{\mathcal{C}_{12}}\sqrt{(1+\mathcal{C}_{12}+\mathcal{C}_\lambda)^2(1+\mathcal{C}_{12}-\mathcal{C}_\lambda)^2+16\mathcal{C}_\lambda^2\mathcal{C}_{12}}\right). \end{aligned} \tag{3.119}$$

The above expression guarantees that the amount of entanglement that may be generated between the output modes is still unbounded, as it was for the open TMS, as demonstrated in Figure 3.10. The joint state for the output modes is also perfectly pure in the absence of thermal noise, $\mathcal{P}^{(1,2)} = 1$.

Understanding the interplay between the beam splitter and the single-mode squeezing in generating entanglement will be important when the bowtie amplifier is finally considered. Since the analysis of the bowtie amplifier will rest on a circuit decomposition, we will simplify that analysis by first performing a circuit decomposition on the BS-SMS system in the form of a Bloch-Messiah decomposition. In this case, the resulting equivalent circuit involves a series of single-mode squeezers sandwiched between two groups of passive elements. For the BS-SMS system, the necessary elements for the circuit decomposition are the following transformations:

$$\begin{aligned} \mathbf{U}^{(1,2)} &\longleftrightarrow \hat{U}_{\text{BS}}^{(1,2)} := \exp\left[-i\arctan\left(\sqrt{\mathcal{C}_{12}}\right)\left(\hat{a}_1^\dagger\hat{a}_2+\hat{a}_1\hat{a}_2^\dagger\right)\right] \\ \mathbf{R}^{(2)} &\longleftrightarrow \hat{U}_{\text{SMS}}^{(2)} := \exp\left[-i\frac{1}{2}\ln\left(\frac{1+\mathcal{C}_{12}+\mathcal{C}_\lambda}{1+\mathcal{C}_{12}-\mathcal{C}_\lambda}\right)\left(e^{i\theta}\hat{a}_2^{\dagger 2}+e^{-i\theta}\hat{a}_2^2\right)\right]. \end{aligned} \tag{3.120}$$

Although this is not a polar decomposition, to keep the notation consistent with that used for the delta amplifier, we denote passive elements using $\mathbf{U}$ and active elements using $\mathbf{R}$. The first transformation, $\mathbf{U}^{(1,2)}$, denotes a beam splitter between the outputs of modes a_1 and a_2, with the angle set by the beam splitter cooperativity, $\mathcal{C}_{12}$. The active element, $\mathbf{R}^{(2)}$, corresponds to a single-mode squeezer with phase θ applied to mode a_2, where the amount of squeezing is given by,

$$r = \ln\left(\frac{1+\mathcal{C}_{12}+\mathcal{C}_{\lambda}}{1+\mathcal{C}_{12}-\mathcal{C}_{\lambda}}\right), \tag{3.121}$$

which will diverge as $\mathcal{C}_{\lambda} \to 1+\mathcal{C}_{12}$. Grouping all elements, the BS-SMS system admits the following non-unique circuit decomposition:

$$-\mathbf{S}_{\text{BS-SMS}} = \mathbf{U}^{(1,2)}\,\mathbf{R}^{(2)}\,\mathbf{U}^{(1,2)}. \tag{3.122}$$

The covariance matrix for the output modes in the presence of vacuum noise from the baths may then be represented as

$$\boldsymbol{\sigma}_{\text{out}} = \frac{1}{2}\mathbf{U}^{(1,2)}\,\mathbf{R}^{(2)}\left(\mathbf{R}^{(2)}\right)^{T}\left(\mathbf{U}^{(1,2)}\right)^{T}. \tag{3.123}$$

Taking this one step at a time, the first non-trivial element is the squeezing interaction, which first creates the covariance matrix of a single-mode squeezed vacuum state (SMSV); the succeeding beam splitters then act to swap some of these squeezed correlations to the output of mode a_1, with the output of mode a_2 receiving vacuum correlations in return. The dependence of Eq. (3.119) on the beam splitter cooperativity $\mathcal{C}_{12}$ is a result of the unequal distribution of the squeezed correlations between the two modes. The swapping of these correlations will only be perfectly balanced when the angle of the beam splitter is $\pi/4$, which only occurs when $\mathcal{C}_{12}=1$. This point is special since the coherent and dissipative processes in the system are perfectly matched. In this case, the rate at which the squeezing which is generated at mode a_2 leaves through its port is balanced by the rate at which the squeezing is swapped to mode a_1 by the beam splitter, where it leaves through this port; the squeezing is then evenly distributed between the two modes. The logarithmic negativity of the BS-SMS from Eq. (3.119) then simplifies to,

$$E_{\mathcal{N}}^{(1,2)} = \ln\left(\frac{2+\mathcal{C}_{\lambda}}{2-\mathcal{C}_{\lambda}}\right) \quad \text{when} \quad \mathcal{C}_{12}=1. \tag{3.124}$$

In this case, and this case only, the logarithmic negativity is given by $E_{\mathcal{N}}^{(1,2)} = 2r_{\text{eff}}$, where the effective squeezing of each mode is half the total squeezing introduced into the system by the single-mode squeezer from Eq. (3.121), $r_{\text{eff}} = r/2$. Even at this point, the system does not behave in the same manner as the TMS since the scattering matrix is still not symmetric.

Including thermal noise from the input fields therefore complicates the behaviour of the BS-SMS system, since the circuit decomposition demonstrates that only some of the thermal noise correlations in the output fields are squeezed. The situation is therefore not entirely analogous to the two-mode squeezed state from Section 3.2.1, where all thermal noise from the input fields is squeezed. Given that the logarithmic negativity in Eq. (3.119) is complicated enough without the addition of thermal noise, we forgo an exact analysis of the effects of the thermal noise on entanglement, although we can surmise based on all previously examined systems that it will be deleterious. Since the system still acts on the input correlations as a symplectic transformation, the purity of the output state must be identical to the input, and so the thermal noise in this case will still degrade the purity of the composite output state. If the input noise is $\bar{n}_1$ and $\bar{n}_2$, then the purity for this reciprocal system must be $\mathcal{P}^{(1,2)} = 1/(2\bar{n}_1+1)(2\bar{n}_2+1)$, which is the same as the input and is therefore unchanged by the system. If the initial state has vacuum correlations, the maximum value of the purity is therefore $\mathcal{P}^{(1,2)}=1$. With the analysis of this reference system complete, we can now proceed to characterise the entangling behaviour of the three-mode bowtie amplifier.

3.4.2.2 Circuit Decomposition of the Bowtie Amplifier

In order to model the scattering behaviour of the bowtie amplifier, we perform a matrix decomposition of the symplectic scattering matrix, $\mathbf{S}_{\bowtie} \in Sp(6,\mathbb{R})$. The polar decomposition does not provide compact expressions for this system, so we instead turn to the Bloch-Messiah decomposition [144]. This decomposition allows us to write a symplectic matrix as $\mathbf{O}_1\mathbf{D}\mathbf{O}_2$, where, physically, the orthogonal matrices $\mathbf{O}_1$ and $\mathbf{O}_2$ correspond to some collection of passive optical transformations. Sandwiched between these passive elements is the matrix $\mathbf{D}$, which represents a series of single-mode squeezers. When the scattering between modes a_1 and a_2 is nonreciprocal, $N^{(1,2)} = \pm 1$, the

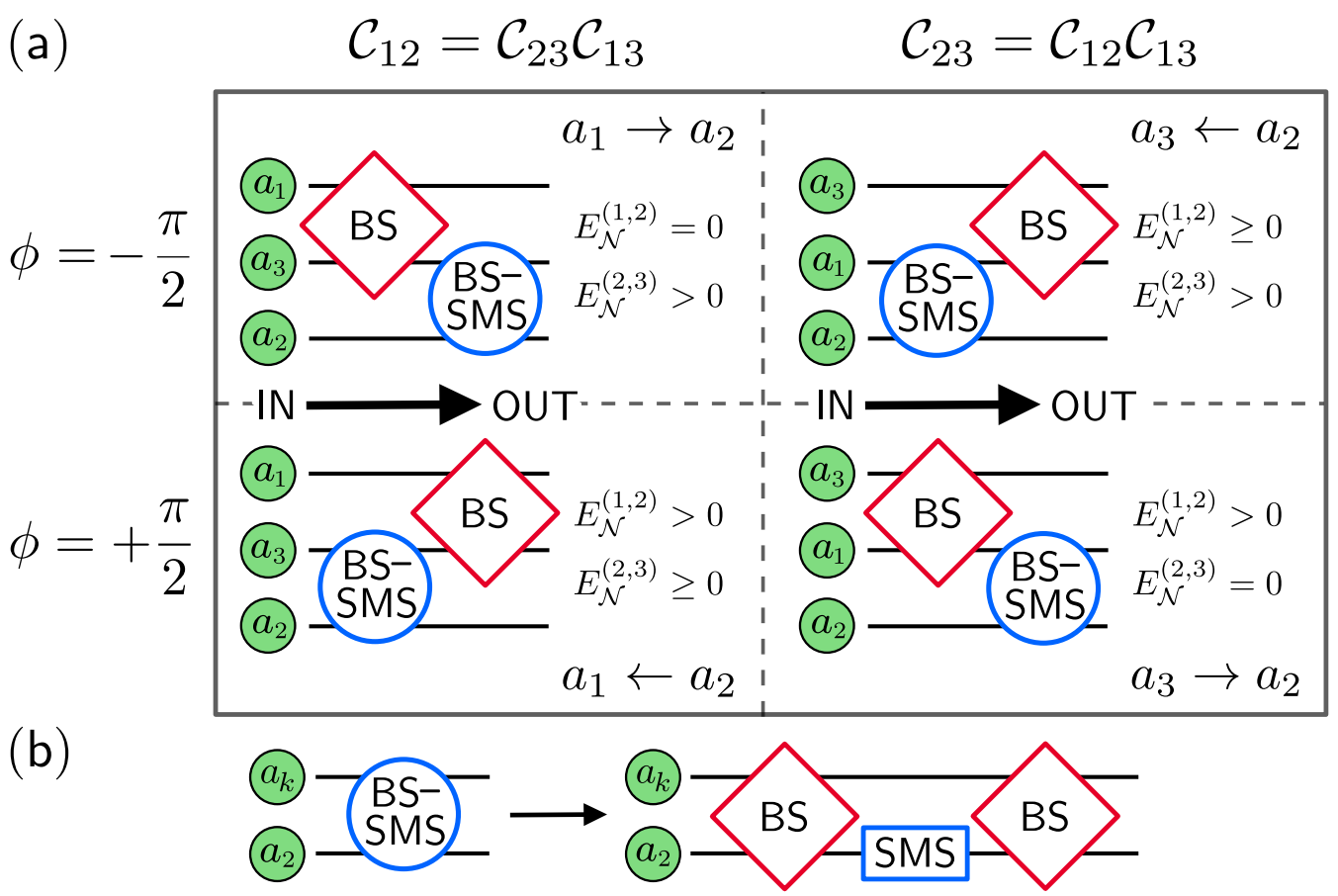

Figure 3.11: (a) Circuit descriptions of the bowtie amplifier at the points of perfect nonreciprocal scattering, where [Left] $N^{(1,2)} = \pm 1$, and [Right] $N^{(2,3)} = \pm 1$. Two values of loop phase are shown: [Top] $\phi = +\pi/2$, and [Bottom] $\phi = -\pi/2$, which correspond to the two directions of nonreciprocal scattering. The position of modes a_1 and a_3 within the circuit diagrams are swapped between the left and right columns, since the combined beam splitter plus single-mode squeezing (BS-SMS) interaction couples the mode pair (a_2, a_3) when $N^{(1,2)} = \pm 1$, and (a_1, a_2) when $N^{(2,3)} = \pm 1$. The beam splitter element always couples the mode pair (a_1, a_3). The input is initially uncorrelated and moves from left to right. The specific forms of the single-mode squeezing and beam splitter interactions can be found in Eqs. (3.125) and (3.128). (b) Breakdown of the combined BS-SMS interaction into a single-mode squeezer applied to mode a_2, sandwiched between two identical beam splitter interactions, which are not identical in form to the beam splitter between the mode pair $(a, 1, a_3)$ from (a).

matrix decomposition can be written in terms of the following interactions:

$$\begin{aligned}
\mathbf{U}_{\mathrm{sgn}(\phi)}^{(1,3)} &\longleftrightarrow \hat{U}_{\mathrm{BS}}^{(1,3)} := \exp\left[-2i\,\mathrm{sgn}(\phi)\,\arctan\left(\sqrt{\mathcal{C}_{13}}\right)\left(i\hat{a}_1^\dagger\hat{a}_3 - i\hat{a}_1\hat{a}_3^\dagger\right)\right] \\
\mathbf{U}^{(2,3)} &\longleftrightarrow \hat{U}_{\mathrm{BS}}^{(2,3)} := \exp\left[-i\arctan\left(\sqrt{\mathcal{C}_{23}}\right)\left(\hat{a}_2^\dagger\hat{a}_3 + \hat{a}_2\hat{a}_3^\dagger\right)\right] \\
\mathbf{R}_{23}^{(2)} &\longleftrightarrow \hat{U}_{\mathrm{SMS}}^{(2,3)} := \exp\left[-\frac{i}{2}\ln\left(\frac{1+\mathcal{C}_{23}+\mathcal{C}_\lambda}{1+\mathcal{C}_{23}-\mathcal{C}_\lambda}\right)\left(e^{i\theta}\hat{a}_2^{\dagger 2} + e^{-i\theta}\hat{a}_2^2\right)\right].
\end{aligned} \tag{3.125}$$

These two beam splitters and one single-mode squeezer are the three separate interactions present in the Hamiltonian for the bowtie amplifier, Eq. (3.63), when the loop phase is $\phi = \pm\pi/2$ and $\mathcal{C}_{12} = \mathcal{C}_{13}\mathcal{C}_{23}$, and are all that is required to model $\mathbf{S}_{\bowtie}$ for these system parameters. For the loop phase $\phi = -\pi/2$ the circuit decomposition takes the form,

$$-\mathbf{S}_{\bowtie} = \mathbf{U}^{(2,3)}\,\mathbf{R}_{23}^{(2)}\,\mathbf{U}^{(2,3)}\,\mathbf{U}_{-}^{(1,3)} \;\text{ when }\; \phi = -\frac{\pi}{2} \;\text{ and }\; \mathcal{C}_{12} = \mathcal{C}_{13}\mathcal{C}_{23}, \tag{3.126}$$

where we have made sure to perform a global phase rotation on the scattering matrix. The first element in this circuit is a beam splitter, which acts to mix the input signal from modes a_1 and a_3. The remainder of the elements in the circuit are *identical* to the circuit decomposition of the BS-SMS system from Eq. (3.122), and so comprise an entangling operation between modes a_2 and a_3. Since the beam splitter between modes a_1 and a_3 comes first in the

circuit, followed by the entangling between modes a_2 and a_3, the input of mode a_1 can reach the output of mode a_2, but not the reverse. This perfectly agrees with the direction of the nonreciprocal scattering for this set of parameters, $a_1 \to a_2$. Turning now to the opposite loop phase, $\phi - +\pi/2$, the Bloch-Messiah decomposition yields

$$-\mathbf{S}_{\bowtie} = \mathbf{U}_{+}^{(1,3)}\,\mathbf{U}^{(2,3)}\,\mathbf{R}_{23}^{(2)}\,\mathbf{U}^{(2,3)} \;\text{ when }\; \phi = +\frac{\pi}{2} \;\text{ and }\; \mathcal{C}_{12} = \mathcal{C}_{13}\mathcal{C}_{23}. \tag{3.127}$$

With the exception of a global change of phase on the beam splitter between a_2 and a_3, the interactions are the same as in Eq. (3.126) but applied in the reverse order, as was the case with the delta amplifier. It follows that the unidirectional transmission represented by this circuit decomposition is the reverse of Eq. (3.126), and so has direction $a_2 \leftarrow a_1$.

When the scattering between modes a_2 and a_3 is nonreciprocal, $N^{(2,3)} = \pm 1$, the Bloch-Messiah decomposition still consists of the beam splitter between modes a_2 and a_3, but the components forming the BS-SMS entangling interaction now act on modes a_1 and a_2:

$$\begin{aligned}\mathbf{U}^{(1,2)} &\longleftrightarrow \hat{U}_{\mathrm{BS}}^{(1,2)} := \exp\left[-i\arctan\left(\sqrt{\mathcal{C}_{12}}\right)\left(\hat{a}_1^\dagger\hat{a}_2 + \hat{a}_1\hat{a}_2^\dagger\right)\right]\\ \mathbf{R}_{12}^{(2)} &\longleftrightarrow \hat{U}_{\mathrm{SMS}}^{(1,2)} := \exp\left[-\frac{i}{2}\ln\left(\frac{1+\mathcal{C}_{12}+\mathcal{C}_\lambda}{1+\mathcal{C}_{12}-\mathcal{C}_\lambda}\right)\left(e^{i\theta}\hat{a}_2^{\dagger 2} + e^{-i\theta}\hat{a}_2^2\right)\right].\end{aligned} \tag{3.128}$$

Starting with the loop phase $\phi = -\pi/2$, the corresponding linear circuit is,

$$-\mathbf{S}_{\bowtie} = \mathbf{U}_{-}^{(1,3)}\,\mathbf{U}^{(1,2)}\,\mathbf{R}_{12}^{(2)}\,\mathbf{U}^{(1,2)} \;\text{ when }\; \phi = -\frac{\pi}{2} \;\text{ and }\; \mathcal{C}_{23} = \mathcal{C}_{12}\mathcal{C}_{13}, \tag{3.129}$$

where the entangling interaction between modes a_1 and a_2 comes first in the circuit, followed by the beam splitter between modes a_2 and a_3, meaning that the output of mode a_1 must be independent of the input of mode a_3, and hence $a_3 \to a_1$. For the opposite loop phase, $\phi = +\pi/2$, the interactions are naturally reversed,

$$-\mathbf{S}_{\bowtie} = \mathbf{U}^{(1,2)}\,\mathbf{R}_{12}^{(2)}\,\mathbf{U}^{(1,2)}\,\mathbf{U}_{+}^{(1,3)} \;\text{ when }\; \phi = +\frac{\pi}{2} \;\text{ and }\; \mathcal{C}_{23} = \mathcal{C}_{12}\mathcal{C}_{13}. \tag{3.130}$$

and so the nonreciprocal scattering now has the direction $a_3 \leftarrow a_1$. The scattering exhibited by the bowtie amplifier at the points of perfect nonreciprocity behaves in a similar manner to that of the delta amplifier, discussed in Section 3.3.3, where the elements in the decomposition are switched when reversing the direction of nonreciprocal scattering, as shown in Figure 3.11.

3.4.2.3 Output Entanglement in the Presence of Vacuum Noise

With the scattering behaviour of the bowtie amplifier at the points of perfect nonreciprocity now understood, the behaviour of the logarithmic negativity and purity of the output modes can be analysed. The steady-state output covariance matrix on resonance for the bowtie amplifier is,

$$\boldsymbol{\sigma}_{\bowtie,\mathrm{out}} = \mathbf{S}_{\bowtie}\boldsymbol{\sigma}_{\mathrm{in}}\mathbf{S}_{\bowtie}^T. \tag{3.131}$$

The input noise from the three baths is assumed to be uncorrelated, with each having the covariance of a Gaussian thermal state, resulting in the same input covariance matrix as in Eq. (3.89). We will start with the assumption that the thermal occupancy for each bath is zero, and so the input covariance matrix is that of a three mode vacuum state, $\boldsymbol{\sigma}_{\mathrm{in}} = \frac{1}{2}\mathbf{I}_6$, and hence $\boldsymbol{\sigma}_{\bowtie,\mathrm{out}} = \frac{1}{2}\mathbf{S}_{\bowtie}\mathbf{S}_{\bowtie}^T$. To simplify the expressions for the output covariance matrix, it is useful to define circuit elements which combine the three interactions comprising the entangling BS-SMS interaction into a single element:

$$\mathbf{Q}^{(1,2)} := \mathbf{U}^{(1,2)}\,\mathbf{R}_{12}^{(2)}\,\mathbf{U}^{(1,2)} \qquad \mathbf{Q}^{(2,3)} := \mathbf{U}^{(2,3)}\,\mathbf{R}_{23}^{(2)}\,\mathbf{U}^{(2,3)}. \tag{3.132}$$

This element is the entangling operation for the bowtie amplifier in the circuit decomposition, and takes the place of the two-mode squeezer present in the decomposition of the delta amplifier, thereby allowing us to draw clear connections between the behaviour of the entanglement and purity for these two amplifiers. One notable difference, discussed in Section 3.4.2.1, is that open quantum systems described by Eq. (3.132) do not entangle in the same way as a two-mode squeezer. Regardless, since it is a symplectic operation, the entangled output state is still pure provided that the input is vacuum noise.

Starting with the case where the scattering between modes a_1 and a_2 is perfectly nonreciprocal, the output

covariance matrices for both directions can be constructed using the scattering matrices from Eqs. (3.126) and (3.127):

$$a_1 \to a_2 \,:\, \boldsymbol{\sigma}_{\bowtie,\text{out}} = \frac{1}{2}\mathbf{Q}^{(2,3)}\left(\mathbf{Q}^{(2,3)}\right)^T \text{ when } \phi = -\frac{\pi}{2} \text{ and } \mathcal{C}_{12} = \mathcal{C}_{13}\mathcal{C}_{23} \tag{3.133}$$

$$a_1 \leftarrow a_2 \,:\, \boldsymbol{\sigma}_{\bowtie,\text{out}} = \frac{1}{2}\mathbf{U}_+^{(1,3)}\mathbf{Q}^{(2,3)}\left(\mathbf{Q}^{(2,3)}\right)^T\left(\mathbf{U}_+^{(1,3)}\right)^T \text{ when } \phi = +\frac{\pi}{2} \text{ and } \mathcal{C}_{12} = \mathcal{C}_{13}\mathcal{C}_{23}. \tag{3.134}$$

For both directions, entanglement is generated between the propagating modes a_2 and a_3, and it is the placement of the passive beam splitter element between a_1 and a_3 in the circuit decomposition which dictates whether the output of modes a_1 and a_2 will be entangled. In Eq. (3.134), the entangled state between the propagating modes a_2 and a_3 is generated first, with the successive beam splitter acting to distribute these entanglement correlations to the other modes of the system. In Eq. (3.133), the beam splitter precedes the generation of entanglement, and hence it cannot generate entanglement since there are no entanglement correlations to swap; this is demonstrated in Figure 3.12, where only $E_{\mathcal{N}}^{(2,3)} > 0$ at $\phi = -\pi/2$. We can determine when the output modes a_1 and a_2 are entangled using Simon's criterion:

$$\mathcal{C}_\lambda^2\sqrt{\mathcal{C}_{12}\mathcal{C}_{23}\mathcal{C}_{13}}\left(\sqrt{\frac{\mathcal{C}_{12}}{\mathcal{C}_{13}\mathcal{C}_{23}}} + \sqrt{\frac{\mathcal{C}_{13}\mathcal{C}_{23}}{\mathcal{C}_{12}}} + 2\sin(\phi)\right) \leq 0. \tag{3.135}$$

Thus, the state is separable when the conditions for nonreciprocal scattering with direction $a_1 \to a_2$ are met, corresponding to the output covariance matrix Eq. (3.133). When $a_1 \leftarrow a_2$, the beam splitter guarantees that $E_{\mathcal{N}}^{(1,2)} > 0$, and will in certain circumstances dependent on the value of $\mathcal{C}_{13}$, swap all entanglement correlations from a_3 to a_1, resulting in $E_{\mathcal{N}}^{(2,3)} = 0$.

Moving on to the case where scattering between modes a_3 and a_2 is nonreciprocal, the covariance matrices are generated using Eqs. (3.129) and (3.130):

$$a_2 \to a_3 \,:\, \boldsymbol{\sigma}_{\bowtie,\text{out}} = \frac{1}{2}\mathbf{U}_-^{(1,3)}\mathbf{Q}^{(1,2)}\left(\mathbf{Q}^{(1,2)}\right)^T\left(\mathbf{U}_-^{(1,3)}\right)^T \text{ when } \phi = -\frac{\pi}{2} \text{ and } \mathcal{C}_{12} = \mathcal{C}_{13}\mathcal{C}_{23} \tag{3.136}$$

$$a_2 \leftarrow a_3 \,:\, \boldsymbol{\sigma}_{\bowtie,\text{out}} = \frac{1}{2}\mathbf{Q}^{(1,2)}\left(\mathbf{Q}^{(1,2)}\right)^T \text{ when } \phi = +\frac{\pi}{2} \text{ and } \mathcal{C}_{12} = \mathcal{C}_{13}\mathcal{C}_{23}. \tag{3.137}$$

We can see that by exchanging the labels of a_1 and a_3, and changing the sign of the loop-phase $\phi \to -\phi$, that the behaviour of the entanglement is identical to the case where scattering between modes a_1 and a_2 is nonreciprocal. The entanglement $E_{\mathcal{N}}^{(2,3)}$ is therefore expected to be zero only when the nonreciprocal scattering has direction $a_3 \to a_1$, which is evident in Figure 3.12. The separability of the joint output state for modes a_2 and a_3 at this point may be confirmed by checking Simon's criterion:

$$\mathcal{C}_\lambda^2\sqrt{\mathcal{C}_{12}\mathcal{C}_{23}\mathcal{C}_{13}}\left(\sqrt{\frac{\mathcal{C}_{23}}{\mathcal{C}_{12}\mathcal{C}_{13}}} + \sqrt{\frac{\mathcal{C}_{12}\mathcal{C}_{13}}{\mathcal{C}_{23}}} - 2\sin(\phi)\right) \leq 0. \tag{3.138}$$

It is apparent from Eqs. (3.135) and (3.138), that the entanglement measures $E_{\mathcal{N}}^{(1,2)}$ and $E_{\mathcal{N}}^{(2,3)}$ are only zero when the nonreciprocal scattering is directed towards mode a_2, $a_1 \to a_2$ and $a_3 \to a_2$, respectively. In the bowtie amplifier, all squeezing and therefore all entanglement correlations originate from mode a_2, hence, we can determine that the absence of entanglement in these cases is due to nonreciprocity blocking squeezed correlations from reaching the outputs of modes a_1 or a_3, resulting in no entanglement correlations.

This behaviour has important consequences for the entanglement between the output of modes a_1 and a_3, which may be entangled by the bowtie amplifier, as shown in Figure 3.12. This behaviour contrasts with the delta amplifier, where the output of modes a_1 and a_3 is always separable. We note that $E_{\mathcal{N}}^{(1,3)}$ can also vanish here when certain nonreciprocity conditions are met. In order to determine when this occurs for the output state of the (a_1, a_3) mode pair, we can once again use Simon's criterion:

$$\mathcal{C}_\lambda^2\mathcal{C}_{12}\mathcal{C}_{23}\mathcal{C}_{13}\left(\sqrt{\frac{\mathcal{C}_{12}}{\mathcal{C}_{13}\mathcal{C}_{23}}} + \sqrt{\frac{\mathcal{C}_{13}\mathcal{C}_{23}}{\mathcal{C}_{12}}} + 2\sin(\phi)\right)\left(\sqrt{\frac{\mathcal{C}_{23}}{\mathcal{C}_{12}\mathcal{C}_{13}}} + \sqrt{\frac{\mathcal{C}_{12}\mathcal{C}_{13}}{\mathcal{C}_{23}}} - 2\sin(\phi)\right) \leq 0. \tag{3.139}$$

In this instance, the criterion for separability is a product of the Simon's criteria for the other two output mode pairs, (a_1, a_2) and (a_2, a_3), given in Eqs. (3.135) and (3.138). As a result, $E_{\mathcal{N}}^{(1,3)} = 0$ when either $E_{\mathcal{N}}^{(1,2)} = 0$ or $E_{\mathcal{N}}^{(2,3)} = 0$, corresponding to the $a_1 \to a_2$ and $a_3 \to a_2$ directions of perfect nonreciprocal scattering, respectively. This is expected, since by preventing the exchange of entanglement correlations from a_2 to either a_1 or a_3, the joint output state for (a_1, a_3) will therefore share no squeezing correlations, and hence it must be separable.

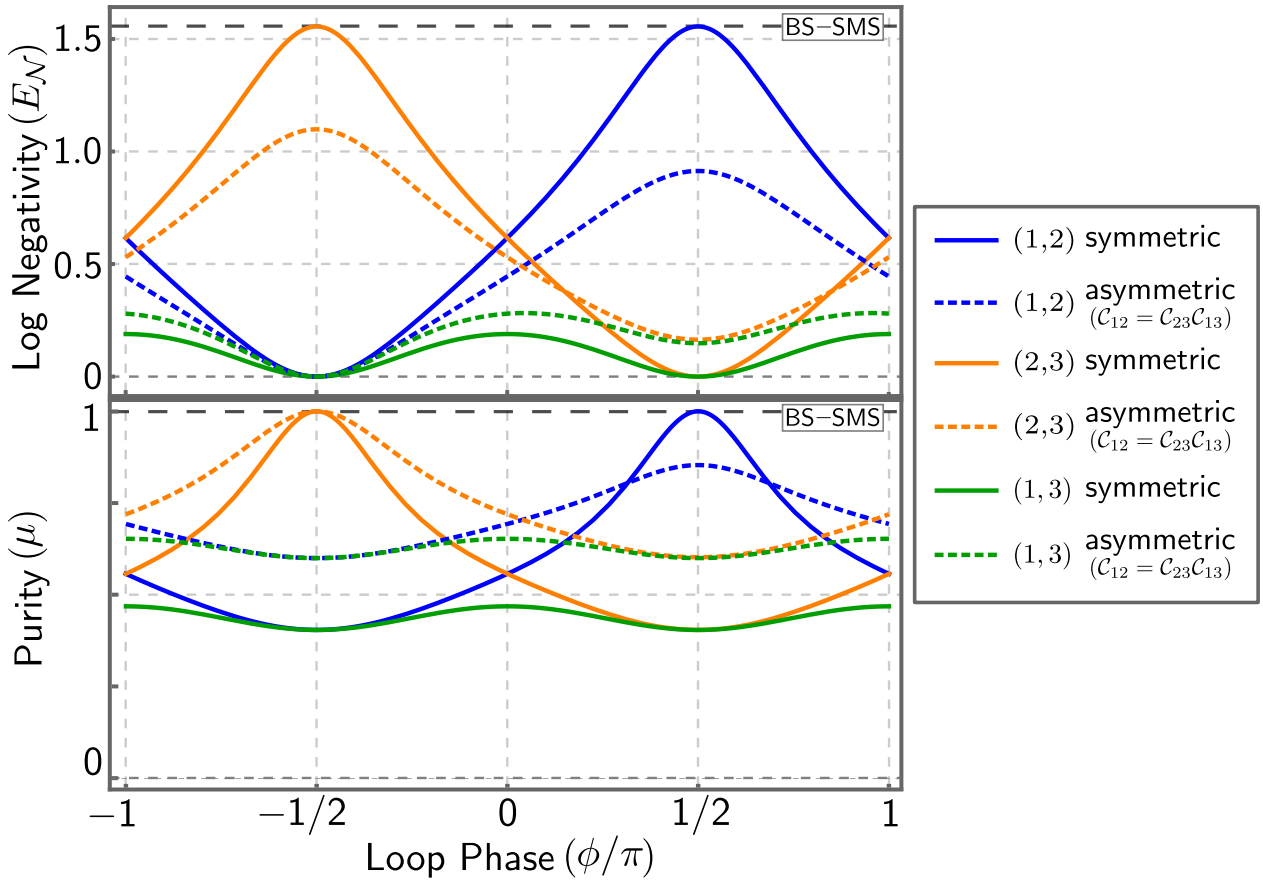

Figure 3.12: [Top] Logarithmic negativity $E_{\mathcal{N}}^{(j,k)}$ and [Bottom] purity $\mathcal{P}^{(j,k)}$ of the stationary output states of the bowtie amplifier. Results are shown for the bipartite output states of modes a_1 and a_2 (blue), a_2 and a_3 (orange), and a_1 and a_3 (green). For the symmetric case (solid) the scattering between both mode pairs, (a_1, a_2) and (a_2, a_3), are perfectly nonreciprocal at the loop phases $\phi = \pm\pi/2$: the beam splitter cooperativities are $\mathcal{C}_{12} = \mathcal{C}_{23} = 0.5$ and $\mathcal{C}_{13} = 1$, and so both cooperativity balancing conditions, $\mathcal{C}_{12} = \mathcal{C}_{23}\mathcal{C}_{13}$ and $\mathcal{C}_{23} = \mathcal{C}_{12}\mathcal{C}_{13}$, are met. In the asymmetric case, only the scattering between the mode pair (a_1, a_2) is perfectly nonreciprocal (dotted): here $\mathcal{C}_{12} = 0.5$, $\mathcal{C}_{23} = 1$, and $\mathcal{C}_{13} = 0.5$, so only the condition $\mathcal{C}_{12} = \mathcal{C}_{23}\mathcal{C}_{13}$ is met. In both cases, the cooperativity for the squeezing interaction is $\mathcal{C}_{\lambda} = 1$. All baths are in the vacuum state. The dashed black lines at the top of both plots correspond to the logarithmic negativity and purity for the output state of a *reciprocal* two-mode system comprised of a beam splitter plus single-mode squeezer (BS-SMS), $\mathcal{C}_{13} = \mathcal{C}_{23} = 0$.

3.4.2.4 Rerouting Thermal Fluctuations Using Nonreciprocity

Given the similarities in the circuit decomposition between the bowtie and delta amplifiers at the points of perfect nonreciprocal scattering, and the consequent likeness in their entangling behaviour when the input fields have vacuum correlations, we can therefore expect that the bowtie amplifier is also capable of routing thermal fluctuations from the input fields to obtain high-purity entangled output states. We will focus on the case where the input of mode a_1 is hot, and hence $\bar{n}_1$ has some non-zero value, and attempt to realise a highly pure entangled state between the outputs of modes a_1 and a_2 by rerouting this thermal noise.

From Figure 3.12 we can see that the marginal purity of joint output states subject to vacuum input noise can reach the maximum value of one. In the case of the mode pair (a_1, a_2), the purity is saturated when Simon's criterion for the separability of the (a_2, a_3) output state from Eq. (3.138) is satisfied. In the case of thermal input noise on mode a_1, we can therefore expect that this condition must also be met for $\mathcal{P}^{(1,2)} = 1$, which will require that nonreciprocal scattering between a_2 and a_3 have direction $a_3 \to a_2$. In order to prevent thermal noise from the input of mode a_1 from contaminating the output of mode a_2, and thereby reducing the purity, we should also like for scattering to be directed towards mode a_1 and away from mode a_2, and therefore also require that the conditions for the $a_2 \to a_1$ direction of perfect nonreciprocal scattering be met.

Matching both nonreciprocity conditions simultaneously results in a balance of cooperativities we previously referred to as the *symmetric* regime, where modes a_1 and a_3 were said to be impedance matched. In this case, the entanglement and purity of the output states for the (a_1, a_2) and (a_2, a_3) mode pairs are mirrored with respect to the loop phase,

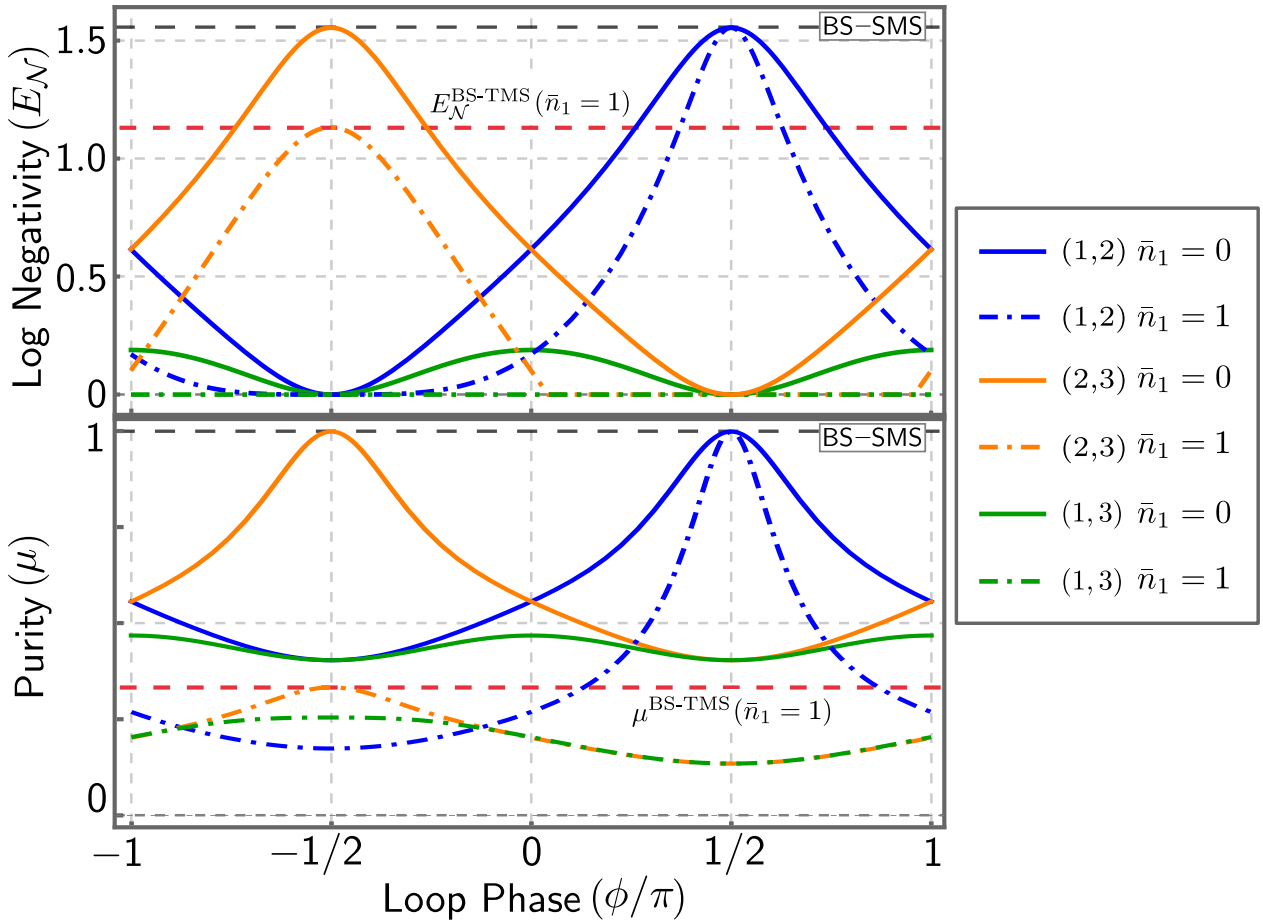

Figure 3.13: [Top] Logarithmic negativity and [Bottom] purity of the bowtie amplifier output states as a function of the loop phase in the presence of thermal noise. Two values for the noise from the bath for mode a_1 are shown: vacuum noise $\bar{n}_1 = 0$ (solid), and thermal noise $\bar{n}_1 = 1$ (dashed-dotted line). Modes a_2 and a_3 only experience vacuum noise from the bath, $\bar{n}_2 = \bar{n}_3 = 0$. The results shown are for the symmetric case where $\mathcal{C}_{12} = \mathcal{C}_{23} = 0.5$ and $\mathcal{C}_{13} = 1$, describing the joint output states of modes a_1 and a_2 (blue), modes a_2 and a_3 (orange), and modes a_1 and a_3 (green). We also show the results for a BS-SMS system where $\bar{n}_1 = 1$ and $\bar{n}_2 = 0$ (dashed, red). The dashed black line indicates both the logarithmic negativity and purity for a BS-SMS system in vacuum, $\mathcal{C}_{12} = 0.5$, and $\mathcal{C}_{13} = \mathcal{C}_{23} = 0$. The strength the squeezing in all cases is $\mathcal{C}_\lambda = 1$.

as shown in Figure 3.12. Here, the cooperativities obey the balancing conditions, $\mathcal{C}_{12} = \mathcal{C}_{23}$ and $\mathcal{C}_{13} = 1$, and so the beam splitter between modes a_1 and a_3 in the circuit decomposition acts to perfectly swap correlations between the two modes:

$$\mathbf{U}^{(1,3)}_{\text{sgn}(\phi),\text{swap}} \longleftrightarrow \hat{U}^{(1,3)}_{\text{BS}} := \exp\left[\text{sgn}(\phi)\frac{\pi}{2}\left(\hat{a}_1^\dagger \hat{a}_3 - \hat{a}_1 \hat{a}_3^\dagger\right)\right]. \tag{3.140}$$

The covariance matrix in the symmetric case can now be constructed using two equivalent circuit decompositions, and since we wish to entangle the outputs of mode a_1 and a_2, the decompositions at the loop-phase $\phi = +\pi/2$ are chosen:

$$\boldsymbol{\sigma}_{\bowtie,\text{out}} = \mathbf{U}^{(1,3)}_{+,\text{swap}}\, \mathbf{Q}^{(2,3)}\, \boldsymbol{\sigma}_{\text{in}} \left(\mathbf{Q}^{(2,3)}\right)^T \left(\mathbf{U}^{(2,3)}_{+,\text{swap}}\right)^T \tag{3.141}$$

$$\boldsymbol{\sigma}_{\bowtie,\text{out}} = \mathbf{Q}^{(1,2)}\, \mathbf{U}^{(1,3)}_{+,\text{swap}}\, \boldsymbol{\sigma}_{\text{in}} \left(\mathbf{U}^{(1,3)}_{+,\text{swap}}\right)^T \left(\mathbf{Q}^{(1,2)}\right)^T. \tag{3.142}$$

Since $\bar{n}_1 \neq 0$, the input covariance matrix $\boldsymbol{\sigma}_{\text{in}}$ is no longer proportional to the identity matrix and so does not trivially commute with the passive circuit elements. The result is similar to the delta amplifier, in that a high-purity entangled state is generated between the output of modes a_1 and a_2, where $\mathcal{P}^{(1,2)} = 1$ can be realised provided that the input for modes a_2 and a_3 corresponds to vacuum noise. While this is not technically a TMSV state, the amount of entanglement that may be generated is still unbounded, as demonstrated in Figure 3.10.

In the symmetric parameter regime, the output of mode a_3 receives all the thermal noise from the input of mode a_1, and is additionally not entangled with the other two modes. This is expected, since perfect nonreciprocity not

only ensures that noise entering mode a_1 is never scattered to mode a_2, but also prevents this thermal noise from being reflected in the output of mode a_1 since the condition for blocking reflection from Eq. (3.115) is also met. With nowhere else to go, the thermal noise must necessarily appear in the output of mode a_3. Importantly, as indicated in Figure 3.13, this noise-swapping behaviour is only observed for the appropriate loop phase $\phi = +\pi/2$. Both $E_{\mathcal{N}}^{(1,2)}$ and $\mathcal{P}^{(1,2)}$ decrease away from the ideal value of ϕ, with the rate of decline increasing for larger thermal fluctuations $\bar{n}_1$.

An important caveat is that this noise swapping scheme is only robust against thermal noise in one mode. Thermal noise entering mode a_2 cannot be rerouted for any parameter regime, as Eq. (3.115) indicates that it is not possible to block the reflection of input noise from a_2 while also generating entanglement in the system, due to the requirement that $\mathcal{C}_\lambda = 0$. This same limitation exists for the delta amplifier, indicating that high-purity entangled states cannot be generated between two hot modes through the use of a single three-mode nonreciprocal amplifier. Despite this, the ability to reroute some thermal noise will still result in an entangled state with greater fidelity than can be achieved by the analogous reciprocal two-mode BS-SMS system in Section 3.4.2.1.

3.5 Summary and Outlook

In this chapter, we reviewed how entanglement may be defined for continuous variable Gaussian states, along with two different ways to characterise the fidelity of entangled states: the logarithmic negativity and the more familiar notion of purity. The former was shown to provide a measure of entanglement based on Simon's criterion, where a state is considered entangled if the partially time-reversed state violates the uncertainty principle, and therefore fails to be a bona fide quantum state itself. The stronger the uncertainty condition is violated, the larger the value of the logarithmic negativity. These quantities were used to demonstrate that, in the ideal scenario, the propagating modes emanating from an open quantum system are pure and can realise unlimited entanglement. Dissipation of the modes through additional loss channels, in the form of internal losses or unmonitored ports, would result in deviations from the ideal behaviour, but for the purpose of this work, it is considered to be insignificant compared to dissipation through the main ports, and hence has been omitted. The presence of thermal noise, however, was detrimental to both measures, and while the entanglement could be improved by squeezing the system harder, it was not possible to improve the purity in a two-mode system using Gaussian unitary transformations.

It was proposed that nonreciprocity could be used to handle this noise, and given that the amplifiers realise gain through the anti-squeezing of their output fields, the two three-mode nonreciprocal amplifier configurations were selected as test systems. This required analysing the effect of nonreciprocity beyond that of asymmetric scattering for signal routing, which can also be realised in classical systems, and, in particular, exploring its influence on quantum correlations and the steady-state entanglement of output fields. While it is not a priori obvious that it should be possible to entangle outputs from two modes when signal scattering is unidirectional, we show that this is indeed possible, provided the system is configured correctly. It was demonstrated that for both three-mode amplifier configurations, the entanglement of the output fields depended strongly on the direction of nonreciprocal scattering. To explain the entanglement behaviour, a heuristic picture for both systems was developed based on matrix decompositions of the symplectic scattering matrix. This description allows for the nonreciprocal scattering to be mapped to sequential Gaussian circuit operations, including passive beam splitters and, more importantly, single and two-mode squeezers, which generate the necessary entanglement correlations.

The analysis revealed slight differences in the scattering behaviour between the bowtie and delta amplifiers, which gave rise to differences in the optimum achievable entangled output states. While the delta amplifier could realise a two-mode squeezed vacuum state, this is not possible with the bowtie amplifier. This difference can be seen as a result of the fact that the delta amplifier is a phase-preserving amplifier, as is the open two-mode squeezer, as shown in Section 2.3.3. The generation of a TMSV therefore stems from the ability to amplify all quadratures of the output fields. The bowtie configuration, on the other hand, is a phase-sensitive amplifier and so is incapable of generating a TMSV since amplification of one quadrature implies de-amplification of the orthogonal quadrature. Despite this disparity, both amplifier configurations shared the same qualitative entangling and thermal routing behaviour.

Two interchangeable modes, labelled a_1 and a_3 in this chapter, were found to always form a separable pair in the delta amplifier, whereas in the bowtie amplifier, separability only occurred at the points of perfect nonreciprocity. The circuit picture helps us to see that, while nonreciprocity may not allow for the sharing of entangled correlations between these two modes, they can still exchange correlations between each other. Provided that the system is properly tuned, this exchange can be done perfectly, allowing for output correlations to be exactly swapped between the two modes. The third mode, labelled a_2, is the odd one out in these nonreciprocal amplifiers, since it can never be engineered to exactly swap correlations with the other two modes within the loop. It was found that this is necessary, since it is the output of this mode which can form an entangled state with the outputs of the other two indistinguishable modes. It is the direction of nonreciprocal scattering between mode a_2 and the others which determines whether the mode pair is entangled or not: when the unidirectional transmission is directed *away* from this mode, then the outputs are entangled, and when it is directed *towards* the output of this mode the outputs form

a separable state. For both amplifiers, the circuit decomposition was necessary to understand this behaviour, as well as the exact nature of the entangled state.

Finally, combining these two behaviours allows us to arrive at the key result: thermal fluctuations from a hot mode can be directed towards the output of a cold reservoir mode, allowing for the formation of an entangled vacuum state with the other cold mode in the amplifier loop. The hot mode and cold reservoir mode are the passively coupled a_1 and a_3 modes, and entanglement is generated between the hot mode and the cold a_2 mode. Here, the swap of hot thermal noise with cold vacuum noise is achieved by matching the coherent and dissipative coupling rates between modes a_1 and a_3. At the same time, nonreciprocal scattering is engineered between the hot mode and the a_2 mode, so that the thermal noise from the hot mode is also blocked from the output of the a_2 mode, while still allowing for the output of these two modes to form an entangled state. Provided that the input noise for mode a_2 is also vacuum noise, then the joint output state is optimally entangled and has maximum purity. In this way, the output entanglement can be made much more robust against thermal fluctuations when compared to a reciprocal two-mode system.

While the three-mode nonreciprocal amplifiers allow for the generation of a highly pure entangled state between one hot and one cold mode, the same is not possible between hot modes within one loop. A possible way to entangle the outputs of two hot modes is to use two copies of the nonreciprocal amplifiers and employ a measurement-based entanglement-swapping protocol [31, 145, 146]. Such a scheme still relies on only one mode in the amplifier being hot, where the other two must necessarily be cold. In order to entangle two hot modes within the same nonreciprocal amplifier, more cold modes are required for the routing of thermal fluctuations from multiple sources. Four-mode nonreciprocal amplifier configurations have been proposed [147], which are capable of realising the necessary routing behaviour, allowing for the generation of a TMSV between two coupled hot modes, conditioned on the other two modes in the amplifier being cold. However, unlike the three-mode amplifiers discussed here, there is currently no experimental realisation of these amplifiers.

This work is relevant to the generation of stationary entanglement of itinerant low-frequency modes, where thermal occupations can be appreciable even at cryogenic temperatures. The analysis also brings to light the possible uses of nonreciprocity in entanglement generation. With recent interest in multipartite entanglement in quantum systems of increasing scale, our work invites the exploration of whether engineered nonreciprocity can be a useful resource in improving the robustness of multipartite entanglement in low-frequency modes. Beyond entanglement, there is also interest in the applications of other uniquely quantum correlations which, while not present in classical systems, can exist in *separable*, and hence unentangled, mixed quantum states. These nonclassical correlations are known as *quantum discord*, and have been shown to be more robust against dissipation. It has been demonstrated that quantum discord is a resource for certain quantum information applications [148–150], and given that a computable measure exists for Gaussian states exists [151, 152] an analysis of the effects of nonreciprocity on quantum discord may therefore also be of interest.

4 Fast and Efficient Qubit Readout with an Integrated Nonreciprocal Amplifier

For an experimental platform to be used for quantum computation, it must fulfill several criteria [153], the most relevant of these criteria for this work is the ability to measure a qubit's state rapidly and with a high degree of fidelity. One of the most promising candidates for quantum computation realises qubits in superconducting systems [154–156], where measurement of the qubit state is performed by scattering a microwave signal off a coupled readout-cavity [10, 157]. The photons from this microwave signal become entangled with the qubit state during this interaction, and through their detection, the information about the qubit that they carry allows for the determination of its state.

Acquiring knowledge of the qubit state is therefore accomplished by detecting this microwave signal, which is typically comprised of a small number of photons. Given the relatively low frequency of photons in the microwave regime, the energy of each photon is correspondingly small, and hence the signal from the measurement system is weak. Single photon measurement in the microwave regime is currently not feasible due to the low power of the individual photons, necessitating the use of amplifiers to increase the amplitude of the signal. Since measurement of the amplified field is not performed in the shielded cryogenic environment, where the superconducting device is housed, but with devices operating at room temperature, the amount of environmental noise increases dramatically as the signal moves up the measurement chain. This feeble signal must therefore go through successive stages of amplification to ensure that it is not swamped by environmental noise as it propagates through the receiver circuit. The amplifiers themselves add their own noise to the measurement chain and are generally reciprocal devices, and so will reflect an amplified signal back down the measurement chain towards the qubit, resulting in unwanted qubit backaction. To avoid this, nonreciprocal signal processing devices in the form of circulators and isolators are placed between the amplifiers and the measurement system to prevent unwanted backwards propagation.

All of these added components come at the cost of reducing the overall measurement efficiency, which can be defined as the ratio of qubit-state information observed to the amount of qubit-state information extracted during the measurement. While a high-fidelity measurement can be obtained by repeating many low-efficiency measurements, this results in a longer measurement time for superconducting quantum computing. Fast measurements are necessary in order to implement measurement-based control protocols of the qubit, such as error-correcting codes, and measurement-based entanglement teleportation. It is therefore paramount that the amount of added noise be kept to a minimum to improve the efficiency of superconducting qubit measurements.

Given the delicate nature of the signal that initially comes from the cryogenic environment, the first amplifier in this chain is chosen to be a superconducting parametric amplifier, which is ideally as close to the quantum-noise-limit as possible [11]. Passive nonreciprocal devices must be placed between the measurement device and the first reciprocal amplifier. These devices are, by their very nature, large and lossy, being on the order of centimeters, and are made of ferrimagnetic materials that require the use of magnetic fields to operate. Both of these aspects inhibit their integration with superconducting circuits, necessitating the use of additional wiring. As a result, the signal, and hence the measurement efficiency, are significantly degraded even before the first stage of amplification.

Current state-of-the-art measurement chains replace these lossy components with highly efficient microwave superconducting devices. Replacing these individual components with a directional nonreciprocal amplifier allows for the signal isolation and amplification to be performed using a single device. Recent advances have seen nonreciprocal devices connected directly to the qubit measurement cavity with corresponding increases in efficiency [30, 158]; however, the added wiring and connectors mean some additional noise is added to the measurement signal, resulting in a corresponding reduction in the measurement efficiency.

In an attempt to overcome the intrinsic limitations on efficiency which arise due to losses which occur before the measurement signal even reaches the first quantum amplifier, we propose a different architecture where the nonreciprocal amplifier is co-located with the qubit, thereby improving the overall measurement efficiency by integrating the nonreciprocal amplifier and measurement system. This project is motivated by an existing device operated by the Advanced Microwave Photonics group from the National Institute of Standards and Technology (NIST); system parameters are based on those that may be achieved by this device. This work comprises the theory component of this collaboration. Our goal is to determine how to properly operate an integrated nonreciprocal amplifier in order to

realise qubit measurement that is sufficiently amplified to protect the measurement signal from sources of noise further up the measurement chain, and which also reduces the amount of backaction on the qubit due to the amplified noise. Accurate calculation of the measurement backaction on the qubit, which takes the form of loss of qubit-state coherence called *dephasing*, is important for any measurement system. Since the measurement backaction results in the loss of qubit-state information, it can present a serious limitation if it significantly exceeds the rate at which we can acquire the qubit-state information. We therefore generalise an existing method for calculating this dephasing, one which is applicable when the state of the measurement system is guaranteed to be Gaussian. This method uses the fact that the dynamics of such states can be characterised using their first two moments, as was shown in Section 2.2. As will be demonstrated here, although the addition of a coupled qubit introduces a highly nonlinear element to the system, a modified version of this moment method can still be used to calculate the state of the measurement system under certain circumstances. Before we proceed to this new work, we will introduce the necessary theoretical background to understand how qubit measurement is performed in superconducting systems. We will start by quantifying the two elements required for the calculation of the measurement efficiency: the measurement rate and the dephasing rate.

4.1 Fundamentals of Qubit Measurement

4.1.1 Qubit-State Readout with Pointer States

The measurement of a microscopic quantum system requires the use of a sufficiently macroscopic system whose state is accessible to us [10]. In order to extract information from the quantum system, the coupling to the macroscopic system must be engineered so that, as the system evolves, the state of the macroscopic system becomes dependent on the state of the quantum system. The macroscopic system therefore acts as a *pointer*, and the measurement of the *pointer state* thereby allows us to acquire information about the quantum system [159]. For our purposes, the quantum system is the qubit, and the pointer system is the coupled measurement apparatus, comprised of some number of harmonic oscillator modes; for the physical systems under consideration, these harmonic modes are resonant modes of a microwave field confined to a cavity. Our goal is to determine whether the qubit is in the ground or excited state, $|g\rangle$ or $|e\rangle$, so the qubit-harmonic mode interaction must allow for the oscillator component of the state to become dependent on the qubit state as the system evolves. If the qubit is initially prepared in a coherent superposition and is initially uncoupled to the oscillator state $|\psi\rangle$, as the measurement proceeds, the state will evolve into an entangled qubit-harmonic mode state:

$$\left(c_e\,|e\rangle + c_g\,|g\rangle\right)|\psi\rangle \rightarrow e^{i\delta}c_e\,|e\rangle\,|\psi_e\rangle + e^{-i\delta}c_g\,|g\rangle\,|\psi_g\rangle\,. \tag{4.1}$$

The qubit-state conditioned oscillator states, $|\psi_e\rangle$ and $|\psi_g\rangle$, are therefore the pointer states of our system. It is important to note that, unlike the qubit states $|e\rangle$ and $|g\rangle$, the oscillator system states $|\psi_e\rangle$ and $|\psi_g\rangle$ are not necessarily orthogonal, and as a result, there may be some overlap between the pointer states. The larger the overlap between the pointer states, the less certain we are about *which* pointer state was measured, which leads to a larger uncertainty in our ability to infer the state of the qubit. To improve our chance of correctly discerning the qubit state, it is therefore crucial that the overlap between the pointer states be minimised, which is achieved by ensuring that the qubit and harmonic modes have sufficient time to interact.

This interaction, and indeed the process of measurement itself, does come at the cost of disturbing the system, referred to as backaction. Some of this is unavoidable, like the loss of coherence that occurs in the qubit due to the extraction of information via the entangled harmonic modes. Backaction can also arise when the observable is not a constant of motion, that is to say, it does not commute with the Hamiltonian, which results in an increase in the uncertainty of the observable as the system evolves. This form of backaction is avoidable, however, and measurements which manage to evade it are termed *quantum nondemolition* (QND) measurements [160, 161]. A QND measurement ensures that the pointer states are exactly correlated to their respective qubit state, as in Eq. (4.1). It is important to note that a QND measurement only preserves the state of the qubit when it is an eigenstate of the QND-observable, and that in all other instances, the state is collapsed randomly onto one of these eigenstates. Subsequent measurements of a QND-observable are guaranteed to produce the same result, and the expectation value of the observable is preserved.

Since we wish to realise a measurement of either $|g\rangle$ or $|e\rangle$, the QND-observable must be $\hat{\sigma}_z = |e\rangle\langle e| - |g\rangle\langle g|$. As a result, the Hamiltonian can only be proportional to the $\hat{\sigma}_z$ operator or the identity operator in the qubit Hilbert space, which necessarily preserves the probabilities of the superposition in Eq. (4.1). The system Hamiltonian must therefore be of the form $\hat{H}_r + \hat{H}_{qr}\hat{\sigma}_z$, where $\hat{H}_r$ and $\hat{H}_{qr}$ act solely on the harmonic mode Hilbert space. Under such an interaction, the harmonic modes evolve under a Hamiltonian which is dependent on the state of the qubit, either $\hat{H}_r - \hat{H}_{qr}$ or $\hat{H}_r + \hat{H}_{qr}$, which will result in evolution from an initial state $|\psi\rangle$ to one of the pointer states, $|\psi_g\rangle$ or $|\psi_e\rangle$. A pictorial view of this evolution is shown in Figure 4.1.

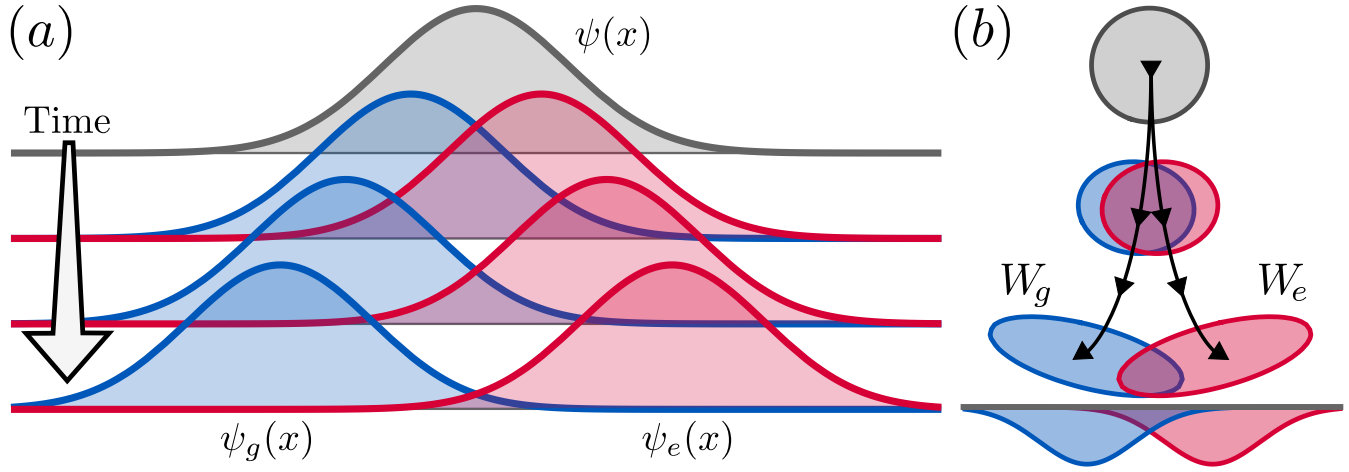

Figure 4.1: Time evolution of the cavity oscillator pointer states. In this picture, the oscillator is initially in the vacuum state, where the wave-function $\psi(x)$ is initially a Gaussian. The qubit and oscillator are coupled so that, as time progresses, the initial vacuum state (grey) evolves into either a ground (blue) or excited (red) qubit-state conditioned pointer state. (a) Here, we see slices of the time evolution of the wave function. The qubit-oscillator coupling is chosen so that the oscillator state remains a canonical coherent state, and as such, still has vacuum statistics. In this example, the qubit-state information is encoded in the position of the coherent state, $\psi_{e/g}(x) = \pi^{-1/4}\exp[-(x-\sqrt{2}\mathrm{Re}[\alpha_{e/g}(t)])^2/2]$. (b) Depicted here is the trajectory of the Gaussian Wigner functions for the cavity pointer state, represented as error ellipses in phase space. As time progresses, both the displacement and variance of the Gaussian Wigner functions change depending on the state of the qubit. Shown at the bottom are the marginal distributions for the final states along the optimum measurement quadrature, showing the overlap between the two Wigner functions; the choice of the measured quadrature is therefore important, since the marginal distributions for both pointer states would be indistinguishable along the orthogonal axis. In both diagrams, as time progresses, the displacement increases, resulting in a decreased overlap and hence increased distinction between the pointer states. For physical systems, this is not always the case; for example, refer to the top right of Figure 4.2, where this overlap does not increase monotonically with time.

During this evolution, the output from the system of harmonic modes is monitored, resulting in a time-integrated measurement signal called the *measurement operator*, $\hat{m}(t)$. The *signal-to-noise ratio* (SNR) is then the separation of the qubit-state conditioned expectation values of $\hat{m}(t)$, divided by the standard deviation of the signal; for ease, we write the square of the SNR:

$$\mathrm{SNR}^2(t) := \frac{1}{4}\frac{|\mu_e(t)-\mu_g(t)|^2}{s_e^2(t)+s_g^2(t)} \quad \text{where} \quad \mu_{\sigma_z}(t) = \langle \hat{m}(t)\rangle_{\sigma_z}\,,\; s^2_{\sigma_z}(t) = \langle \hat{m}^2(t)\rangle_{\sigma_z} - \langle \hat{m}(t)\rangle^2_{\sigma_z}\,,\; \sigma_z = e,g. \tag{4.2}$$

The variance corresponds to noise in the system, and is a combination of the variance of the Wigner functions along with other sources of noise which may alter the variance of the output distributions. In this phase-space picture, the pointer states of the harmonic mode system may be associated with the Wigner functions W_g and W_e, which evolve along trajectories determined by the state of the qubit. The qubit state can be distinguished provided that the overlap between the two Wigner functions is minimal, where the overlap is dependent on which axis in phase space we choose to integrate over. As shown in Figure 4.1, the overlap is minimised with respect to one quadrature in phase space, however, the Wigner functions are indistinguishable in the orthogonal quadrature. It is therefore necessary to pick the appropriate measurement operator such that the SNR is maximised.

As previously stated, this measurement will necessarily result in a loss of the phase coherence for the qubit state. This can be seen by analysing the off-diagonal element of the reduced qubit density matrix, obtained after tracing over the harmonic oscillator degrees of freedom:

$$\rho_{eg}(t) = \mathrm{Tr}_r\big[\,|\psi_e\rangle\langle\psi_g|\,\big]e^{2i\delta}c_e c_g^* \equiv e^{2i\delta}\,\langle\psi_g|\psi_e\rangle\,\rho_{eg}(0). \tag{4.3}$$

The inner product between the two pointer states, $0 \le |\langle\psi_g|\psi_e\rangle| \le 1$, is generally complex but is bounded to be less than one for normalised states. The argument of this inner product corresponds to a shift in the qubit frequency, whereas the magnitude of the inner product alters the magnitude of the off-diagonal element $\rho_{eg}(t)$. As the overlap between the two pointer states decreases, the magnitude of this inner product decreases. While this results in a more distinct measurement, the magnitude of the off-diagonal element necessarily decreases as well, indicating that phase

coherence of the qubit has been lost: this process is termed *measurement-induced dephasing*. If the pointer states become orthogonal, then all phase coherence is lost, and the qubit ends up in a mixed state. The definition of the SNR in Eq. (4.2) shows that as the overlap between the pointer state decreases, there is an increase in the signal of the measurement. These expressions provide a heuristic connection between the measurement and the dephasing: the more distinct the measurement signal, the larger the backaction from the measurement in the form of dephasing. In the next section, we will establish the connection between these two quantities in a more rigorous manner.

4.1.2 Intrinsic Limits on Measurement

In the same way that the SNR can be used to characterise the information gained during measurement, we can also define a rate of dephasing, $\Gamma_{\mathrm{d}}(t)$, to quantify the loss of phase coherence in the qubit state as a result of this measurement. As above, this is defined in terms of the off-diagonal element of the reduced qubit density matrix:

$$|\rho_{eg}(t)| = \exp\left[-\int_0^t \Gamma_{\mathrm{d}}(\tau)\, d\tau\right] |\rho_{eg}(0)|\,. \tag{4.4}$$

There is an intimate relationship between these two quantities which places a fundamental upper limit on what we can expect a measurement scheme to achieve. Specifically, the rate at which we acquire information about the qubit state cannot exceed the rate at which information is destroyed in the qubit due to the measurement:

$$\mathrm{SNR}^2(t) \leq \int_0^t \Gamma_{\mathrm{d}}(\tau)\, d\tau. \tag{4.5}$$

The ratio of these two quantities can be used to define a measurement efficiency, which has an upper bound of one when the measurement is perfectly efficient. In the case where a steady state exists for the harmonic mode system, these quantities reach their respective steady-state rates,

$$\Gamma_{\mathrm{meas}} := \lim_{t\to\infty} \frac{\mathrm{SNR}^2(t)}{t} \quad \text{and} \quad \Gamma_{\mathrm{d}} := \lim_{t\to\infty} \frac{1}{t}\int_0^t \Gamma_{\mathrm{d}}(\tau)\, d\tau \tag{4.6}$$

where Γ_{meas} is termed the *measurement rate* and Γ_{d} is the *dephasing rate*. In the steady state, the measurement efficiency can then be defined as

$$\eta := \frac{\Gamma_{\mathrm{meas}}}{\Gamma_{\mathrm{d}}}\ ,\ 0 \leq \eta \leq 1. \tag{4.7}$$

Proof of the bounds in Eq. (4.7) can be found in Ref. [10] using a quantum noise approach. We will take a slightly different approach motivated by a Bayesian interpretation of the measurement from Ref. [162], and provide a demonstration of Eq. (4.5), which will by extension imply Eq. (4.7). This relies on the fact that the reduced qubit density matrix must be a positive semi-definite Hermitian matrix, which means that the matrix elements must obey the inequality

$$|\rho_{eg}(t)| \leq \sqrt{\rho_{ee}(t)\rho_{gg}(t)}. \tag{4.8}$$

The left-hand side can be replaced by the time-integrated dephasing from Eq. (4.4), whereas the right-hand side is simply the probabilities that the qubit is in the ground or excited state, which are constant for a QND measurement. Importantly, the above inequality is also valid regardless of the realisation of the measurement. For a single realisation of the quadrature $\langle\hat{m}\rangle$, we can rewrite the above inequality as $P(|\rho_{eg}(t)|\,|\,\langle\hat{m}\rangle) \leq P(\sqrt{\rho_{ee}(t)\rho_{gg}(t)}\,|\,\langle\hat{m}\rangle)$, where the inequality is now conditional on the realisation of $\langle\hat{m}\rangle$. The expressions are dependent on time, but this is omitted to simplify the notation. By integrating over all possible realisations of $\langle\hat{m}\rangle$, we retrieve the new inequality:

$$\begin{aligned}\int P(|\rho_{eg}(t)|\,|\,\langle\hat{m}\rangle)\, P(\langle\hat{m}\rangle)\, d\langle\hat{m}\rangle \;&\leq \int P(\sqrt{\rho_{ee}(t)\rho_{gg}(t)}\,|\,\langle\hat{m}\rangle)\, P(\langle\hat{m}\rangle)\, d\langle\hat{m}\rangle \\ &\leq \int \sqrt{P(e\,|\langle\hat{m}\rangle) P(g\,|\langle\hat{m}\rangle)}\, P(\langle\hat{m}\rangle)\, d\langle\hat{m}\rangle.\end{aligned} \tag{4.9}$$

A lot of new terms are introduced, so we will go through them slowly. First, in order to integrate over all realisations $\langle\hat{m}\rangle$, we must integrate over the distribution $P(\langle\hat{m}\rangle)$, which corresponds to the probability of realising a particular value of $\langle\hat{m}\rangle$ at a specific time:

$$P(\langle\hat{m}\rangle) := P(e)P(\langle\hat{m}\rangle|\, e) + P(g)P(\langle\hat{m}\rangle|\, g). \tag{4.10}$$

Here we have introduced more variables: $P(e)$ and $P(g)$ are the probabilities that the qubit is in the excited or the ground state, respectively. Since the measurement is QND, these are constant and equal to their initial values, $P(e) = \rho_{ee}(0)$ and $P(g) = \rho_{gg}(0)$. The distributions, $P(\langle\hat{m}\rangle|\,\sigma_z)$ where $\sigma_z = e, g$, give the probability that $\langle\hat{m}\rangle$ is

realised given the qubit was in the state $|\sigma_z = e, g\rangle$. Provided that the qubit is in state $|\sigma_z\rangle$, then the harmonic mode system is in one of the pointer states, and the probability distribution is just a marginal distribution of the associated Wigner function for the pointer state. Assuming that the Wigner functions are Gaussian, we can write,

$$P(\langle\hat{m}\rangle|\,\sigma_z) := \frac{1}{\sqrt{2\pi s^2_{\sigma_z}(t)}} \exp\left[-\frac{\big(\langle\hat{m}\rangle - \mu_{\sigma_z}(t)\big)^2}{2s^2_{\sigma_z}(t)}\right] \tag{4.11}$$

where the mean $\mu_{\sigma_z}(t)$ and variance $s^2_{\sigma_z}(t)$ are the same quantities used to define the SNR in Eq. (4.2). The definition of the distribution $P(\langle\hat{m}\rangle)$ given in Eq. (4.11) is therefore a weighted sum of two pointer state Wigner distributions. On the left-hand side of Eq. (4.9), we made the replacement $P(\sqrt{\rho_{ee}(t)\rho_{gg}(t)}\,|\,\langle\hat{m}\rangle) = \sqrt{P(e\,|\langle\hat{m}\rangle)P(g\,|\langle\hat{m}\rangle)}$, where the distributions $P(\sigma_z\,|\langle\hat{m}\rangle)$ correspond to the probability that the qubit was in the state $|\sigma_z = e, g\rangle$ given that $\langle\hat{m}\rangle$ was measured. We can invert these posterior probabilities by invoking Bayes' theorem,

$$P(\sigma_z\,|\langle\hat{m}\rangle) = \frac{P(\langle\hat{m}\rangle|\,\sigma_z)P(\sigma_z)}{P(\langle\hat{m}\rangle)}. \tag{4.12}$$

With all necessary components defined, we can simplify the right-hand side of Eq. (4.9):

$$\begin{aligned}\int \sqrt{P(e\,|\langle\hat{m}\rangle)P(g\,|\langle\hat{m}\rangle)}\,P(\langle\hat{m}\rangle)\,d\langle\hat{m}\rangle \;&= \sqrt{\rho_{ee}(0)\rho_{gg}(0)}\int \sqrt{P(\langle\hat{m}\rangle|\,e)P(\langle\hat{m}\rangle|\,g)}\,d\langle\hat{m}\rangle \\ &= \sqrt{\rho_{ee}(0)\rho_{gg}(0)}\left(\frac{1}{2}\left(\frac{s_e(t)}{s_g(t)} + \frac{s_g(t)}{s_e(t)}\right)\right)^{-1/2} \exp\left[-\frac{\big(\mu_e(t) - \mu_g(t)\big)^2}{4(s_e^2(t) + s_g^2(t))}\right] \\ &\leq \sqrt{\rho_{ee}(0)\rho_{gg}(0)}\exp\Big[-\mathrm{SNR}^2(t)\Big].\end{aligned} \tag{4.13}$$

Moving on to the left-hand side, this may be simplified under the assumption that the qubit dephasing resulting from measurement is independent of the realisation of the measurement:

$$\int P(|\rho_{eg}(t)|\;|\,\langle\hat{m}\rangle)\,P(\langle\hat{m}\rangle)\,d\langle\hat{m}\rangle = |\rho_{eg}(t)|\int P(\langle\hat{m}\rangle)\,d\langle\hat{m}\rangle = |\rho_{eg}(t)|\,. \tag{4.14}$$

The right-hand side can therefore be replaced by Eq. (4.4). Assuming that the qubit is initially in a coherent state, $|\rho_{eg}(0)|^2 = \rho_{ee}(0)\rho_{gg}(0)$, we retrieve the expression

$$\exp\left[-\int_0^t \Gamma_{\mathrm{d}}(\tau)\,d\tau\right] \leq \exp\Big[-\mathrm{SNR}^2(t)\Big] \tag{4.15}$$

thereby confirming that the qubit dephases as a result of the measurement at least as fast as we can measure the state of the qubit, as expressed in Eq. (4.5). While it should be intuitive that this relation is true, given that this chapter is concerned with the efficiency of a novel measurement apparatus, it was important to give concrete justification for Eq. (4.5). This section relied on an information-theoretic argument to establish this connection; in the next section, we will demonstrate how these two quantities are related physically when performing a dispersive measurement of the qubit.

4.1.3 Qubit Measurement in Circuit QED

4.1.3.1 Engineering Light-Matter Interactions in Circuit QED

Although the methods applied in this chapter are not restricted to a specific paradigm, as stated in the introduction, the motivation comes from the field of superconducting circuits. Superconducting qubits and microwave photons in superconducting circuits can be engineered to allow for a strong interaction, allowing for the realisation of qubit control, the application of one and two-qubit gates, and, critically, fast qubit measurement [157]. These systems can be understood through the field of *circuit quantum electrodynamics* (circuit QED) [163], an outgrowth of the older field of cavity quantum electrodynamics [164]. In this section, we will provide as brief an introduction as possible to the quantum mechanical model for the measurement setup, along with all necessary approximations involved to go from the Hamiltonian describing the circuit model to the final light-matter Hamiltonian. We will then proceed to show how a QND measurement of the qubit state can be performed, before finishing the introduction with a review of the qubit measurement procedure in circuit QED.

Circuit Quantisation

To obtain a quantum mechanical model of the superconducting circuit, we start with a well-understood classical physical model of the system, and then, through some procedure, turn this classical system into a quantum model through a process known as *quantisation*. In the standard approach to circuit quantisation [165], Kirchhoff's laws are used to construct a Lagrangian for the lumped-element circuit model in terms of the charge and flux variables. Canonical momenta are then defined, and a Legendre transformation is performed to move to a Hamiltonian formalism with canonically conjugate charge and flux variables. The canonical quantisation procedure of Dirac [166] is then performed, and the system finally moves to the Hilbert space, yielding a pair of non-commuting charge and flux operators. While circuit quantisation has proved to be an incredibly successful approach in describing the quantum behaviour of superconducting circuits, the "process" of quantising a classical system is rife with technical details that must be considered for anything beyond the simplest models. As a result, there is no single unifying procedure by which one may quantise a system, and the procedure for quantising circuits is still a matter of debate.

Nonlinear systems have to deal with the fact that no quantisation procedure will yield a set of commutation relations which preserves all classical Poisson bracket relations between nonlinear polynomials of conjugate variables [34]. For nonlinear elements which give rise to periodic variables, canonical quantisation will fail since it is not possible to define a conjugate pair of operators on such spaces [167], though the system may still be quantised using different operators [168]. An example of this is the phase variable of the Josephson junctions, where the nonlinear dependence of the inductance on the magnetic flux [54, 55, 169] gives rise to a potentially[1] 2π-periodic phase variable. Kirchhoff's laws may also result in systems where the conservation of charge and energy results in constraints on the variables in the Lagrangian. In such constrained systems, the canonical variables are not independent, and so the Lagrangian is said to be singular, meaning no Legendre transformation can be defined. Since there is no Hamiltonian description, the system cannot be canonically quantised for a singular system using the standard method [171]. To handle this, Dirac and Bergmann proposed their own solutions to the quantisation of constrained systems [172–174]. Recent works in the field have taken a variety of approaches based on the geometry of the system configuration space, such as using the related quantisation method of Faddeev–Jackiw for constrained systems [175], or starting with a Hamiltonian description of the system to avoid dealing with the Lagrangian formalism altogether [176]. Other works have even argued that Kirchhoff's laws cannot be used as variable constraints when quantising superconducting circuits [177, 178]. For this work, we will ignore any such technicalities and individually quantise the linear measurement resonator and nonlinear transmon qubit.

Linear Resonator

The first circuit component that we will consider is the linear resonator, which contains the "light" component of the circuit QED model in the form of microwave photons. The linear resonator is effectively just a lump of superconducting material through which electrical current flows. In principle, quantisation of the electromagnetic field depends on the type of resonator in use [157, 165, 179, 180], however, the general approach uses the fact that the finite boundary conditions of the resonator results in an electromagnetic field within the resonator with a discrete spectrum of normal modes. The normal modes of this resonator may be modelled as LC-circuits, with some capacitance C and inductance L, whose values come from the physical parameters of the superconducting material, along with the frequency of the normal mode, $\omega_r = 1/\sqrt{LC}$. Oscillations in the electromagnetic field are a result of the current generated by the flow of the electron condensate within the superconducting circuit. The current in the superconducting circuit can be treated as a single macroscopic degree of freedom, which, using the LC-circuit model, generates a magnetic field in the inductor by transferring the energy stored in the electric field of the capacitor, and vice versa. These oscillations are harmonic in nature, leading to a simple quantisation procedure since the system is entirely linear. The resulting Hamiltonian for the quantised LC-circuit is then simply equivalent to a quantum harmonic oscillator,

$$\hat{H}_{\mathrm{LC}} = \frac{\hat{\Phi}^2}{2L} + \frac{\hat{Q}^2}{2C} \quad \text{where} \quad [\hat{\Phi}, \hat{Q}] = i. \tag{4.16}$$

The canonical variables for the oscillator are the electric charge, $\hat{Q}$, and the magnetic flux, $\hat{\Phi}$. The quantised charge and flux operators can be expressed in terms of the creation and annihilation operators for the cavity electromagnetic field as

$$\hat{\Phi} = \Phi_{\mathrm{zpf}}(\hat{a} + \hat{a}^\dagger) \qquad \hat{Q} = -iQ_{\mathrm{zpf}}(\hat{a} - \hat{a}^\dagger). \tag{4.17}$$

where $\Phi_{\mathrm{zpf}} = \sqrt{Z_r/2}$ and $Q_{\mathrm{zpf}} = \sqrt{1/2Z_r}$ are the zero-point fluctuations in the magnetic and electric fields, and $Z_r = \sqrt{L/C}$ is the characteristic impedance. The superconductivity of the circuit is essential to ensure long-lived oscillations in the absence of any external couplings, as the resistance within the circuit would otherwise dampen these oscillations over time.

[1] There is still some contention about whether the phase of the Josephson junction is a compact or extended variable [170].

Since measurement requires that the resonator be populated with microwave photons, which must then be collected, the ends of the resonator are capacitively coupled to external transmission lines, which will act as the input and output ports of the resonator. Since the resonator is now an open system, the individual normal modes now have some characteristic linewidths, which are assumed to be identical. The model of the normal modes as individual LC-resonators only holds for frequencies which are very close to the individual resonances, and hence it must be assumed that the system is always at these points. To this end, in order to make sure that the normal modes are distinct and well separated, the quality factor of the resonator, $\mathrm{Q} = \omega_0/\kappa$, must be large to avoid significant overlap in the mode response functions in frequency space. Here, ω_0 is the frequency between the different normal modes, and $\kappa = \kappa_{\mathrm{ext}} + \kappa_{\mathrm{int}}$ is the mode linewidth, which is a combination of the loss rate through the monitored ports, κ_{ext}, along with additional internal losses within the circuit itself, κ_{int}. In addition, for the purpose of this section, we assume that only one of these normal modes is close enough in frequency to couple to the superconducting qubit, with the remainder being too far off-resonant to be physically relevant.

Transmon Qubit

While linear components are important for quantum information processing applications, true quantum computation requires some nonlinearity in the system, even in the case of Gaussian quantum computation [98]. This is the "matter" component of the light-matter interaction, which takes the form of an atom placed in the cavity in cavity QED, whereas in circuit QED this is realised using a so-called artificial atom in the form of a nonlinear circuit termed a *superconducting qubit*. While there are numerous ways to realise superconducting qubits [156, 181–184], motivated by the device at hand, we will focus on the transmon qubit [185], a relative of the earlier Cooper pair box [186].

A basic requirement of all superconducting qubits is that the energy levels of the system have non-uniform spacing, an effect achieved by the use of a nonlinear circuit, allowing for the system to be approximated by a spectrally separated two-level system since transitions to other energy levels are highly disfavoured. This nonlinear effect is introduced by the use of a Josephson junction, where two superconductors are separated by a thin insulating barrier. A supercurrent can flow between these across the barrier in the form of tunnelling Cooper pairs of electrons, a phenomenon known as the Josephson effect [54, 169]. Replacing the inductor of the LC-circuit with the Josephson junction results in a nonlinear circuit whose quantum state can be characterised by the net-number of electron Cooper pairs which have tunnelled across the junction, $|m\rangle$ where $m \in \mathbb{Z}$, referred to as *charge states*[2] which can take positive or negative values depending on the direction of the current flow. The Hamiltonian for this nonlinear circuit is a combination of the charging energy for the Cooper pairs, along with a potential term from their tunnelling across the junction,

$$\hat{H}_{\mathrm{TMN}} = \sum_{m=-\infty}^{\infty} \left(4E_C(m - n_g)^2 \, |m\rangle\langle m| - \frac{E_J}{2}\big(\, |m\rangle\langle m+1| + |m+1\rangle\langle m| \, \big) \right) \tag{4.18}$$

where E_C is the charging energy of one electron, E_J is the Josephson energy, and n_g is an offset in the total charge energy due to an external electric field. The behaviour of Eq. (4.18) is well known to be analogous to a planar quantum rotor under a cosine potential, with the charge states taking the place of the angular momentum eigenstates. We can therefore express the Hamiltonian in an equivalent form

$$\hat{H}_{\mathrm{TMN}} = 4E_C \left(\hat{n} - n_g\right)^2 - E_J \cos\hat{\varphi} \tag{4.19}$$

where we can define the cosine potential in terms of the phase operator $\cos\hat{\varphi} := (e^{i\hat{\varphi}} + e^{-i\hat{\varphi}})/2$. These operators have the following definitions in the charge basis

$$\hat{n} = \sum_{m=-\infty}^{\infty} m \, |m\rangle\langle m| \qquad e^{i\hat{\varphi}} = \sum_{m=-\infty}^{\infty} |m\rangle\langle m+1| \qquad e^{-i\hat{\varphi}} = \sum_{m=-\infty}^{\infty} |m+1\rangle\langle m|$$

with the associated commutation relations[3]

$$[e^{i\hat{\varphi}}, e^{-i\hat{\varphi}}] = 0 \qquad [\hat{n}, e^{i\hat{\varphi}}] = e^{i\hat{\varphi}} \qquad [\hat{n}, e^{-i\hat{\varphi}}] = -e^{-i\hat{\varphi}}. \tag{4.20}$$

[2] Depending on the configuration, one side of the Josephson junction may form an island of superconducting current while the other side is connected to ground, or both sides of the junction may form superconducting islands. In the latter case, each island has some number of Cooper pairs N_1 and N_2, where the quantum number m counts the difference in the number of Cooper pairs between the two islands, $|m\rangle \equiv |N_1 + m, N_2 - m\rangle$.

[3] It is commonly claimed in works on the transmon qubit that the bare phase operator and the charge operator are conjugate variables, $[\hat{\varphi}, \hat{n}] = i$. It has been known for a long time that this relation is fallacious, and that these two operators do not in fact form a conjugate operator pair [167]. The defectiveness of this commutation relation is evident here when taking a matrix element in the charge basis, where the assumption that $\hat{n}$ is Hermitian leads to a contradictory result: $\langle m|[\hat{\varphi}, \hat{n}]|m'\rangle = i\,\langle m|m'\rangle \to (m' - m)\,\langle m|\hat{\varphi}|m'\rangle = i\delta_{mm'}$. Along with this, the bare phase variable is also ill-posed and leads to an unphysical uncertainty relation. The solution is to only work with the periodic phase operators, such as the unitary operator pair defined in Eq. (4.20) [168].

To find the eigenstates of this nonlinear circuit, it is simplest to express Eq. (4.19) in the basis of phase states, $|\varphi\rangle$, where $\varphi \in [0, 2\pi)$. The resulting Schrödinger equation is then equivalent to Mathieu's differential equation, whose solutions are the 2π-periodic Mathieu functions [182]. They are termed the *transmon states*, but for convenience, we write these eigenstates as $|j\rangle$ where $j \in \mathbb{N}$, and define ω_j as the associated eigenenergies. The energy spectrum of this Hamiltonian is controlled by the ratio of the charge and Josephson energies, E_J/E_C. A charge qubit is realised when $E_J/E_C \ll 1$ [186–188]; in this regime, the eigenstates $|j\rangle$ become highly localised functions in the charge basis $|m\rangle$, and so fluctuations in charge noise coming from the external field, represented as n_g, result in a loss of coherence in the charge qubit. This effect is so severe that research into charge qubits has largely been abandoned. A transmon qubit is realised in the opposite regime, where $E_J/E_C \gg 1$ [185, 189], where the lowest lying eigenstates become highly localised in phase and are centred at the minimum of the cosine potential. Due to the high degree of phase localisation, the eigenstates do not see the entire nonlinear potential, and can be approximated by the eigenstates of a weakly anharmonic oscillator. In this limit, the eigenenergies of the anharmonic oscillator are independent of the external field n_g, and so the low-lying states are no longer susceptible to charge noise[4]. This protection comes at the cost of a reduction in the nonlinear spacing between the lowest energy levels in the transmon, an effect which comes into play when considering qubit measurement.

Light-Matter Interaction

Now that the models of the two main elements have been described, we can proceed to couple them. By capacitively coupling the microwave resonator and transmon qubit, the offset charge in Eq. (4.19) is now dependent on the charging energy of the LC-circuit, and so is replaced by an operator, $n_g \to -\hat{n}_r$, which is necessarily dependent on $\hat{Q}$. Making sure to include the free Hamiltonian of the LC-circuit, the coupled circuit Hamiltonian is

$$\hat{H}_{\mathrm{TMN-LC}} = 4E_c\left(\hat{n} + \hat{n}_r\right)^2 - E_J \cos\hat{\varphi} + \left(\frac{\hat{\Phi}^2}{2L} + \frac{\hat{Q}^2}{2C}\right) \quad \text{where} \quad \hat{n}_r \propto \hat{Q}. \tag{4.21}$$

Expanding the $(\hat{n} + \hat{n}_r)^2$ term would reveal that the capacitive coupling has also shifted the charging energy, and hence the fundamental frequency, of the LC-circuit. To retrieve the desired light-matter interaction between these two elements, we first replace the LC-circuit operators with the photon-field operators, and express the transmon component in terms of its basis states:

$$\hat{H}_{\mathrm{TMN-LC}} = \omega_r \hat{a}^\dagger \hat{a} + \sum_{j=0}^{\infty} \omega_j \left|j\right\rangle\!\left\langle j\right| + \sum_{j,j'} g_{j,j'} \left|j\right\rangle\!\left\langle j'\right| \left(\hat{a}^\dagger + \hat{a}\right). \tag{4.22}$$

The interaction term at the end comes from the coupling $\hat{n}\hat{Q}$ which arises when expanding $(\hat{n} + \hat{n}_r)^2$ from Eq. (4.21), where the coupling energy $g_{j,j'} = g^*_{j',j}$ is a function of numerous system parameters. The charge operator $\hat{n}$ is dense in the basis of the transmon states of $\hat{H}_{\mathrm{TMN}}$, and so can generate any state transition. Thankfully, most of the state transitions in Eq. (4.22) can be safely ignored based on several criteria. As the anharmonicity of the potential decreases by increasing E_J/E_C, the charge operator only strongly couples nearest neighbours, and so we can restrict transitions to $j \leftrightarrow j+1$. To explain this, we recall that the transmon behaves as a weakly anharmonic oscillator, and so the lower transmon states can be approximated as perturbed Fock states in a region around the potential minimum. In this regime, the charge operator can also be roughly approximated as conjugate to phase, and in analogy with the harmonic oscillator system, begins to obey the same properties as a momentum-type operator. As with a true weak anharmonic oscillator, the transition is strongest for nearest neighbours, $\langle j|\hat{n}|j+1\rangle$, and we expect that the other transitions vanish entirely as E_J/E_C increases, $\lim_{E_J/E_C\to\infty}\langle j|\hat{n}|j+k\rangle \to 0$ [185]. Applying the rotating-wave approximation, we eliminate interactions which do not preserve total quanta as off-resonant, resulting in the following Hamiltonian

$$\hat{H}_{\mathrm{TMN-LC}} \approx \omega_r \hat{a}^\dagger \hat{a} + \sum_{j=0}^{\infty} \omega_j \left|j\right\rangle\!\left\langle j\right| + \sum_{j} g_{j,j+1}\Big(\left|j\right\rangle\!\left\langle j+1\right| \hat{a}^\dagger + \left|j+1\right\rangle\!\left\langle j\right| \hat{a}\Big). \tag{4.23}$$

As a final step, we assume that there is still enough nonlinearity in the system to permit us to operate this system as a qubit by restricting ourselves to two transmon states with the lowest energy. Defining the computational basis as $|j=0\rangle := |g\rangle$ and $|j=1\rangle := |e\rangle$, we at last arrive at the Jaynes-Cummings Hamiltonian

$$\hat{H}_{\mathrm{JC}} = \omega_r \hat{a}^\dagger \hat{a} + \frac{\omega_q}{2}\hat{\sigma}_z + g(\hat{a}^\dagger \hat{\sigma}_- + \hat{a}\hat{\sigma}_+) \tag{4.24}$$

[4] Beyond charge noise, noise from magnetic flux is also present in such systems. Although flux noise is typically about two orders of magnitude weaker than charge noise, it still significantly contributes to the relaxation and dephasing of transmon qubits [190, 191]. Since transmon qubits are innately susceptible to flux noise its suppression is correspondingly difficult; this has lead to the development of new qubit architectures which are better protected against errors from both types of noise [184, 192, 193].

where $\hat{\sigma}_z = |e\rangle\langle e| - |g\rangle\langle g|$, $\hat{\sigma}_+ = |e\rangle\langle g|$, and $\hat{\sigma}_- = |g\rangle\langle e|$. While this approximation will form the basis for the measurement theory, in reality it is known that resonator photons will create excitations during the measurement process, resulting in unwanted transitions within the transmon to states outside the computational subspace [185, 194, 195], a topic that will come up again when we move to the dispersive regime.

4.1.3.2 The Dispersive Regime

In order to perform efficient qubit-state measurement, it is a requirement that $\hat{\sigma}_z$ be a QND-observable of the system Hamiltonian, a property which is not, on the face of it, obeyed by the Jaynes-Cummings Hamiltonian in Eq (4.24). It is, however, possible to bring the Jaynes-Cummings into a regime where $\hat{\sigma}_z$ becomes a QND-observable of the effective Hamiltonian; this is known as the *dispersive regime*. In the dispersive regime, the detuning between the qubit and resonator, $\Delta = \omega_q - \omega_r$, is much larger than the coupling strength, $|\Delta| \gg g$ [47]. As a result of this large detuning, the exchange of excitations between the qubit and resonator is highly disfavoured, and the two only interact via virtual photon processes; in the absence of particle exchange, the qubit effectively no longer experiences transitions between its excited and ground state. Since the qubit state is now conserved, $\hat{\sigma}_z$ is a conserved quantity of the effective dispersive regime Hamiltonian, and so measurement of the qubit state is QND.

To bring $\hat{H}_{JC}$ into the dispersive regime, we must first diagonalise the Jaynes-Cummings Hamiltonian. This is possible because a Jaynes-Cummings interaction preserves the total number of quanta in the system, and so the diagonalisation can be performed on the individual subspaces. Writing the qubit-resonator state as $|\text{qubit}, \text{resonator}\rangle$, each of these subspaces consists of two states with total quanta n, $|e, n-1\rangle$ and $|g, n\rangle$, with the exception of the ground state $|g, 0\rangle$. Restricting Eq. (4.24) to the two-state subspace, the occupation of the resonator becomes a fixed parameter, so the Hamiltonian now takes the form of a two-level system, $\hat{H}_n = (\omega_r + 1/2)n + \Delta\bar{\sigma}_z/2 + g\sqrt{n}\bar{\sigma}_x$ [196]. In this subspace, $|e, n-1\rangle$ and $|g, n\rangle$ correspond to the excited and ground states, respectively, with corresponding spin-operators $\bar{\sigma}_z$ and $\bar{\sigma}_x$. This Hamiltonian is diagonalised through a rotation of the $\bar{\sigma}_z$ eigenstates using the unitary operator $\hat{U}_n = \exp[-i\theta_n\bar{\sigma}_y/2]$ where the angle of rotation is $\theta_n = \arctan(2\varepsilon\sqrt{n})$, and $\varepsilon = g/\Delta$. To write this unitary operator in terms of the original qubit-resonator operators, we have to replace n with an operator $\hat{N}$ which counts the total quanta, and the spin-operator $\bar{\sigma}_y$ with a suitable operator which acts on the full state space using $\sqrt{n}\bar{\sigma}_y \to i(\hat{a}^\dagger\hat{\sigma}_- - \hat{a}\hat{\sigma}_+)$. The set of unitary operators $\hat{U}_n$ can now be collected into a single unitary operator acting on the full system [197]:

$$\hat{U}_\text{D} = \exp\left[\Lambda(\hat{N})\left(\hat{a}^\dagger\hat{\sigma}_- - \hat{a}\hat{a}^\dagger\right)\right] \quad \text{where} \quad \Lambda(\hat{N}) = \frac{\arctan\left(2\varepsilon\sqrt{\hat{N}}\right)}{2\sqrt{\hat{N}}} \quad \text{and} \quad \hat{N} = \hat{a}^\dagger\hat{a} + |e\rangle\langle e|\,. \tag{4.25}$$

The operator $\hat{N}$ corresponds to the total number of quanta in the system, and so commutes with the original Jaynes-Cummings Hamiltonian since this is a conserved quantity. This unitary operator brings the Jaynes-Cummings Hamiltonian to the following dressed form:

$$\hat{H}_\text{D} = \hat{U}_\text{D}^\dagger\hat{H}_\text{JC}\hat{U}_\text{D} = \omega_r\hat{a}^\dagger\hat{a} + \frac{\omega_q}{2}\hat{\sigma}_z - \frac{\Delta}{2}\left(1 - \sqrt{1 + 4\varepsilon^2\hat{N}}\right)\hat{\sigma}_z. \tag{4.26}$$

The ground state of the dressed Hamiltonian is unchanged, while the remainder of the dressed eigenstates can be written as follows [164]:

$$|\overline{g, n}\rangle = \cos(\theta_n/2)\,|g, n\rangle - \sin(\theta_n/2)\,|e, n-1\rangle \qquad |\overline{e, n-1}\rangle = \sin(\theta_n/2)\,|g, n\rangle + \cos(\theta_n/2)\,|e, n-1\rangle\,. \tag{4.27}$$

When the qubit and resonator have similar frequencies, $\Delta \sim 0$, the dressed states are highly entangled combinations of the bare qubit and resonator states. Since the qubit states are not well-defined, the measurement of the qubit state is naturally not QND. As previously stated, for the purposes of measurement and general quantum information processing, we want to work in the dispersive regime, where the qubit-resonator detuning is much larger than the coupling strength, $|\Delta| \gg g$. Expanding the square root in Eq. (4.26), and truncating higher order terms in $\varepsilon = g/\Delta \ll 1$, we retrieve the dispersive Hamiltonian:

$$\hat{H}_\text{disp} = \omega_r\hat{a}^\dagger\hat{a} + \frac{\tilde{\omega}_q}{2}\hat{\sigma}_z + \chi\hat{a}^\dagger\hat{a}\hat{\sigma}_z \quad \text{where} \quad \chi = \frac{g^2}{\Delta},\ \tilde{\omega}_q = \omega_q + \frac{g^2}{\Delta}. \tag{4.28}$$

Before we consider using this Hamiltonian as a model for our qubit measurement, we have one final constraint to consider: the dispersive regime ensures that the original angle $\theta_n = \arctan(2g\sqrt{n}/\Delta)$ is now approximated by $\theta_n \approx 2g\sqrt{n}/\Delta$. In order to ensure that the qubit state is well-defined, we require that $\theta_n \ll 1$, an assumption that can be broken even in the dispersive regime if the resonator occupancy is too large. The maximum allowable value of the photon occupancy must therefore be well below a certain critical photon number so that the entanglement between

the qubit and resonator is guaranteed not to be too strong, $n \ll n_{\text{crit}} = \Delta^2/4g^2$. This criterion is also necessary to ensure that any virtual interactions between the resonator and higher energy levels of the transmon qubit are negligible; the necessity of this requirement is apparent if we had instead first applied the dispersive approximation to the generalised Jaynes-Cummings Hamiltonian in Eq. (4.23), which contains couplings between the different energy levels of the transmon [185, 198].

Up to this point, we have conspicuously ignored the fact that these elements are all open-quantum systems, so to more accurately model the open system, the coupling between the system and collective environment should be included in the form of a system-bath Hamiltonian. For the microwave resonator, as mentioned previously, this consists of external losses through the monitored transmission lines, which are desirable for measurement, as well as internal losses, which can arise due to unmonitored ports or defects in the material. These internal losses will result in inefficiencies in the measurement, but for the purpose of this work, they are assumed to be negligible compared to the external losses necessary for measurement. For the transmon qubit, there are numerous sources of loss, which can originate from the wiring, imperfections in materials, and extrinsic sources of noise, among others. The collective effect is energy relaxation and loss of state coherence, which results in an overall decrease in the lifetime of the qubit state, however, advances in engineering and fabrication are leading to steady improvements over time [156]. The system-bath Hamiltonians used to model all of these processes are not unchanged when moving to the dispersive regime, where the formerly independent system-bath couplings of the resonator and qubit become intertwined [197]. Deriving an effective qubit master equation in this regime allows one to see that the qubit relaxation time becomes dependent on the photon loss rate, $\kappa\varepsilon^2$, which is a result of qubit decay through the resonator loss channel, known as the Purcell effect [199]. These corrections are at least quadratic in ε, and so their inclusion leads to a breakdown in the QND nature of the physical model. In this work, these correction terms are taken to be weak, and so they are safely ignored.

4.1.3.3 Backaction from the Dispersive Shift

Now that we are operating in the dispersive regime, $\hat{\sigma}_z$ finally commutes with the dispersive Hamiltonian $\hat{H}_{\text{disp}}$, and so measurement of the qubit will be QND. In a *dispersive measurement*, the dispersive coupling in $\hat{H}_{\text{disp}}$ results in a shift of the resonant frequency of the harmonic mode conditioned on the state of the qubit, $(\omega_r + \sigma_z\chi)\hat{a}^\dagger\hat{a}$, where $\sigma_z = \pm 1$. To acquire this information, the resonator is populated with photons, resulting in a displaced state within the resonator. Using the measurement description from Eq. (4.1), as the system evolves and the resonator extracts the qubit information, this state will evolve depending on the state of the qubit, either under $\hat{H}_{\text{disp},e} = (\omega_r + \chi)\hat{a}^\dagger\hat{a}$ or $\hat{H}_{\text{disp},g} = (\omega_r - \chi)\hat{a}^\dagger\hat{a}$, into one of two coherent pointer states, $|\alpha_e\rangle$ or $|\alpha_g\rangle$, respectively. In phase space, the dispersive Hamiltonian corresponds to a rotation of the state about the origin, and therefore if we rotate at the resonant frequency of the oscillator ω_r, the action of $\hat{H}_{\text{disp},e}$ and $\hat{H}_{\text{disp},g}$ will correspond to rotations in opposite directions. The dispersive shift therefore only results in a difference of phase between the two pointer states, and so their displacement vectors must necessarily have the same magnitude in phase space. As a result, for arbitrary time, the coherent pointer states can be expressed as $|\alpha_e\rangle = |e^{i\theta}\alpha\rangle$ and $|\alpha_g\rangle = |e^{-i\theta}\alpha\rangle$.

The QND nature of the measurement also results in a minimisation of the qubit dephasing during measurement. Since the virtual interaction results in no energy exchange between the resonator and qubit in our idealised model, there is no backaction resulting from the qubit absorbing photon energy. There is still backaction on the qubit from the dispersive measurement in the form of a frequency shift, often called an ac-Stark shift, and qubit dephasing. The qubit frequency shift is a result of the non-zero photon occupation in the resonator, and can be inferred from the dispersive coupling, $(\tilde{\omega}_q/2 + \chi\langle\hat{a}^\dagger\hat{a}\rangle)\hat{\sigma}_z$. The dephasing results from the same interaction, and can be understood as a broadening of the qubit-linewidth resulting from resonator photon number fluctuations in the form of shot noise [200–203], which translates to an increase in qubit-state fluctuations and a corresponding loss of coherence.

We know that the qubit dephasing is related to the overlap of the pointer states through Eq. (4.3); assuming that these pointer states are the two coherent states above, we can express this overlap as $|\langle\alpha_e|\alpha_g\rangle| = e^{-|\alpha|^2(1-2\cos(2\theta))}$. In the steady-state, the rate of dephasing of the qubit is then $\Gamma_{\text{d}} \propto |\alpha|^2 \sin^2(\theta)$. This confirms the expectation that the dephasing increases as the pointer states become more distinguishable through a larger photon occupation $|\alpha|^2$, and phase separation θ. Calculating the measurement rate is another matter, since it is acquired not from the intracavity resonator state, but from the measured output field.

4.1.3.4 Measurement of the Output Signal

The output signal from the transmission line must pass through the entire chain of off-chip devices before being measured. The effects of this measurement chain on the output signal differ depending on the setup and conventions used when defining certain quantities, such as the measurement rate. These details are not pertinent for this theoretical work, and so the description will be in broad brushstrokes. We start with the output resonator field, which can be

obtained using standard input-output theory, $\hat{a}_{\text{out}}(t) = \sqrt{\kappa_{\text{ext}}}\hat{a}(t) + \hat{a}_{\text{in}}(t) + \sqrt{\kappa_{\text{int}}}\hat{b}(t)$, where the $\hat{b}(t)$ operator is included to account for any additional noise introduced due to internal loss channels, which we assume to be Gaussian white-noise processes. Each element of the measurement chain has a characteristic bandwidth, which is assumed to be larger than the bandwidth of the initial output field. The effect of the measurement chain on the signal bandwidth can be gathered into a single filter function, which is convolved with the signal of the output mode:

$$\hat{a}_f(t) = \int_{-\infty}^{\infty} f(t-\tau)\,\hat{a}_{\text{out}}(t)\,dt. \tag{4.29}$$

The filter is assumed to be a normalised function over the entire time domain, a requirement which must be met in order to preserve the canonical commutation relation for the filtered output fields, $[\hat{a}_f(t), \hat{a}_f^\dagger(t)] = 1$. This allows for the definition of position and momentum-like quadratures for the filtered output field,

$$\hat{q}_f = \frac{1}{\sqrt{2}}\left(\hat{a}_f^\dagger + \hat{a}_f\right) \qquad \hat{p}_f = \frac{i}{\sqrt{2}}\left(\hat{a}_f^\dagger - \hat{a}_f\right). \tag{4.30}$$

At the end of the measurement chain, the output signal is transformed into a voltage signal with a characteristic amplitude and phase, which can be parametrised in terms of the in-phase and quadrature component operators, $\hat{I}$ and $\hat{Q}$, respectively. These signals can be expressed in terms of the filtered output fields, along with additional noise arising from the measurement chain. Definitions of the component operators vary, and in some cases are treated as oscillating functions of $\hat{q}_f$ and $\hat{p}_f$. For simplicity, we assume that we are in a rotating frame where the component operators are treated as fixed combinations of the time-dependent output fields, and define the operators as follows:

$$\hat{I}(t) = V\left[\cos(\phi)\hat{q}_f(t) + \sin(\phi)\hat{p}_f(t)\right] + \hat{V}_{\text{noise},I}(t) \qquad \hat{Q}(t) = V\left[\cos(\phi)\hat{p}_f(t) - \sin(\phi)\hat{q}_f(t)\right] + \hat{V}_{\text{noise},Q}(t). \tag{4.31}$$

The voltage amplitude V of the signal is dependent on all prior components in the measurement chain, both passive and active, and so is a function of the gain of the amplifiers, transmittance of the circulators, losses from these components, and other parameters from the numerous signal-processing devices. The operators $\hat{V}_{\text{noise},I/Q}(t)$ represent the collective added noise from these off-chip components. The commutator of this noise can be inferred from the fact that the in-phase and quadrature component operators represent orthogonal components of an electromagnetic field, and so must form a pair of canonically conjugate variables, $[\hat{I}(t), \hat{Q}(t)] = i$. The measured signal is a weighted combination of these two operators, integrated over the course of the measurement, and can be represented by the measurement operator:

$$\hat{m}(t) := \int_0^t \left(\mathrm{w}_I(\tau)\hat{I}(\tau) + \mathrm{w}_Q(\tau)\hat{Q}(\tau)\right) d\tau. \tag{4.32}$$

The weight functions, $\mathrm{w}_I = \langle\hat{I}\rangle_e - \langle\hat{I}\rangle_g$ and $\mathrm{w}_Q = \langle\hat{Q}\rangle_e - \langle\hat{Q}\rangle_g$, correspond to an additional final filter applied to the measurement signal to ensure that the qubit-state information acquired is maximised [204, 205]. For example, if the qubit information acquired by the pointer states is found entirely in $\hat{I}$, then no part of $\hat{Q}$ will be measured since the mean is independent of the qubit state, and so no unnecessary signal is recorded in the measurement. Looking at this from the $I-Q$ phase space, the axis defined by the integrand, $\mathrm{w}_I(\tau)\hat{I}(\tau) + \mathrm{w}_Q(\tau)\hat{Q}(\tau)$, is always the one which contains the largest displacement between the two pointer states, thereby maximising the distinction during the measurement. This definition also ensures that the weights are larger when the pointer states are more easily distinguished, and so these contribute more to the entire integral. Finally, this definition ensures that the signal at long times is given minimal weight, which is necessary since the qubit relaxes during the measurement, resulting in a gradual loss in the distinguishability of the pointer states [163]. With the measurement operator defined, we can finally rewrite the SNR in Eq. (4.2) in terms of a physically meaningful variable,

$$\mathrm{SNR}^2(t) := \frac{\left|\langle\hat{m}(t)\rangle_e - \langle\hat{m}(t)\rangle_g\right|^2}{\langle\hat{m}_N^2(t)\rangle_e + \langle\hat{m}_N^2(t)\rangle_g} \quad \text{where} \quad \hat{m}_N(t) = \hat{m}(t) - \langle\hat{m}(t)\rangle_{\sigma_z}\ ,\ \sigma_z = e, g. \tag{4.33}$$

In this work, we will apply several approximations to the measurement operator in Eq. (4.32); these assumptions will serve to maximise the above SNR, and so by invoking them we will obtain the maximum amount of qubit information allowed by theory. The first assumption is that internal losses in the resonator are minimal, and so the only contribution to the cavity linewidth comes from coupling to the transmission line; this ensures that all qubit information extracted by the resonator is collected through the output port, and none is lost due to internal losses. In addition, we assume for simplicity that the measurement chain has infinite bandwidth, meaning that the filter function in Eq. (4.29) is a Delta distribution, and so the filtered output can be replaced by the usual output operators in all subsequent definitions. Additionally, we assume that the added noise corresponds to Gaussian white-noise processes, which are uncorrelated with the output quadrature operators. As a result of this final assumption, the

expectation values of the off-chip noise operators are zero, $\langle \hat{V}_{\text{noise},I/Q}(t)\rangle = 0$, and so their presence does not reduce the measurement efficiency by degrading the signal component of the SNR in Eq. (4.33). By assuming that this off-chip noise is uncorrelated with the output quadratures, the noise component of the SNR is therefore the sum of two components: the noise from the output signal and the noise of the off-chip components.

Assuming that the qubit relaxation time is far longer than the duration of the measurement, and that a steady state exists for the system, in the long-time limit of the measurement, the component operators will also reach a steady state. In this regime, the integrand in Eq. (4.32) converges to a constant value, and the square of the SNR scales linearly in time as a result. This motivates the definition of a steady-state measurement rate, as was done in Eq. (4.6). A new time-independent representation of the measurement operator $\hat{M}(t)$ is now required. This can be defined using the steady-state value of the output fields, which correspond to the Fourier-transformed output operators, $\hat{q}_{\text{out}}[\omega]$ and $\hat{p}_{\text{out}}[\omega]$, at the resonance frequency of the system. Combining the various phases from Eqs. (4.31) and (4.32), and moving to the frequency domain, the steady-state measurement operator can be expressed entirely in terms of the output field quadratures:

$$\hat{M}[\omega] = \cos(\vartheta)\,\hat{q}_{\text{out}}[\omega] + \sin(\vartheta)\,\hat{p}_{\text{out}}[\omega]. \tag{4.34}$$

The trigonometric functions of the angle ϑ are the normalised weight functions for this time-independent measurement operator[5], which may be constructed analogously to those used in the definition of the time-dependent measurement operator from Eq. (4.32):

$$\cos(\vartheta) = \frac{\mathrm{w}_q[\omega]}{\sqrt{\mathrm{w}_q[\omega]^2 + \mathrm{w}_p[\omega]^2}} \qquad \sin(\vartheta) = \frac{\mathrm{w}_p[\omega]}{\sqrt{\mathrm{w}_q[\omega]^2 + \mathrm{w}_p[\omega]^2}}, \tag{4.35}$$

where,

$$\mathrm{w}_q[\omega] = \langle \hat{q}_{\text{out}}[\omega]\rangle_e - \langle \hat{q}_{\text{out}}[\omega]\rangle_g \qquad \mathrm{w}_p[\omega] = \langle \hat{p}_{\text{out}}[\omega]\rangle_e - \langle \hat{p}_{\text{out}}[\omega]\rangle_g. \tag{4.36}$$

The off-chip noise operators, $\hat{V}_{\text{noise},I/Q}$, have been ignored in this definition of the measurement operator, but their effect on the measurement will not be omitted. The collective noise from these off-chip sources can be collected into a constant number of *added photons*, $\bar{n}_{\text{add}}$, which is independent of the qubit state. With this definition, and assuming that the cavity resonance is ω_r, the steady-state measurement rate is:

$$\Gamma_{\text{meas}} = \lim_{t\to\infty} \frac{\mathrm{SNR}^2(t)}{t} = \frac{\left|\langle \hat{M}[\omega_r]\rangle_e - \langle \hat{M}[\omega_r]\rangle_g\right|^2/4}{\bar{S}_{MM,e}[\omega_r] + \bar{S}_{MM,g}[\omega_r] + 2\bar{n}_{\text{add}}}. \tag{4.37}$$

Where $\left|\langle \hat{M}[\omega_r]\rangle_e - \langle \hat{M}[\omega_r]\rangle_g\right|^2$ now corresponds to the measurement signal, and the standard deviation in the SNR has been replaced with the symmetrised output noise-power of the resonator:

$$\begin{aligned}\bar{S}_{MM,\sigma_z}[\omega] &= \frac{1}{2}\int_{-\infty}^{\infty} \Big\langle \left(\hat{M}(t) - \langle \hat{M}(t)\rangle_{\sigma_z}\right)\left(\hat{M}(0) - \langle \hat{M}(0)\rangle_{\sigma_z}\right) + \left(\hat{M}(0) - \langle \hat{M}(0)\rangle_{\sigma_z}\right)\left(\hat{M}(t) - \langle \hat{M}(t)\rangle_{\sigma_z}\right) \Big\rangle_{\sigma_z} e^{i\omega t}\, dt \\ &= \frac{1}{2}\int_{-\infty}^{\infty} \Big\langle \left(\hat{M}[\omega] - \langle \hat{M}[\omega]\rangle_{\sigma_z}\right)\left(\hat{M}[\omega'] - \langle \hat{M}[\omega']\rangle_{\sigma_z}\right) + \left(\hat{M}[\omega'] - \langle \hat{M}[\omega']\rangle_{\sigma_z}\right)\left(\hat{M}[\omega] - \langle \hat{M}[\omega]\rangle_{\sigma_z}\right) \Big\rangle_{\sigma_z} d\omega',\end{aligned} \tag{4.38}$$

where the Fourier transform of an operator is defined in Eq. (2.92).

4.1.3.5 Qubit Readout in the Dispersive Regime

We are now in a place where we can examine how well the standard dispersive measurement setup, comprising a single qubit and resonator cavity, measures the state of the qubit by characterising the time-dependent SNR as well as the steady-state measurement rate. In order for the cavity state of the resonator to acquire qubit information, its state must be displaced, which is achieved by the addition of a drive term to the dispersive measurement setup. The effects of the transmission line are included through the addition of a dissipation channel to the cavity. Applying the Born-Markov approximation when modelling the transmission line, and working in the frame-rotating with the applied drive, the system can be modelled by the following Lindblad master equation [206]:

$$\frac{d}{dt}\hat{\rho} = -i[\hat{H}_s, \hat{\rho}] + \kappa\mathcal{D}[\hat{a}](\hat{\rho}) \quad \text{where} \quad \hat{H}_s = \Delta_r \hat{a}^\dagger\hat{a} + \frac{\tilde{\omega}_q}{2}\hat{\sigma}_z + \chi\hat{a}^\dagger\hat{a}\hat{\sigma}_z + \left(\epsilon(t)\hat{a}^\dagger + \epsilon^*(t)\hat{a}\right), \tag{4.39}$$

[5] A caveat: while these weights will maximise the *signal* component of the measurement rate, it is not guaranteed that they will necessarily maximise the measurement rate *overall* for every set of parameters. If the noise along the quadrature with maximum signal is sufficiently amplified, then it may decrease the measurement rate enough that the measurement of another quadrature will yield a higher value for the measurement rate. For the systems under consideration here, this edge case is not relevant, and so these weights are always used. This will not be an issue if the noise is identical along every possible measurement quadrature.

where $\Delta_r = \omega_r - \omega_d$ is the cavity-drive detuning. The loss channels for the qubit are omitted for the moment since they do not impact the dephasing induced by the measurement, but will be included when a more general method for dephasing calculations is introduced in Section 4.2.1. In the absence of any squeezing or thermal noise, the pointer states start as the vacuum state $|0\rangle$, and gradually evolve into their corresponding canonical coherent states, $|\alpha_e(t)\rangle$ and $|\alpha_g(t)\rangle$. The time evolution of the field amplitudes can be determined by calculating the time evolution of the expectation values $\alpha_{\sigma_z} = \langle \hat{a} \rangle_{\sigma_z}$, where $\sigma_z = e, g$, using Eq. (2.45). The Hamiltonian can be split into a resonator-only and qubit-resonator component, $\hat{H}_s = \hat{H}_r + \hat{H}_{qr}\hat{\sigma}_z$, where $\hat{H}_{qr} = \chi \hat{a}^\dagger \hat{a}$. The effective Hamiltonian governing the evolution of each pointer state is then dependent on the state of the qubit, $\langle \hat{\sigma}_z \rangle = \pm 1$, so $\hat{H}_s = \hat{H}_r + \hat{H}_{qr}$ when the qubit is in the excited state, and $\hat{H}_s = \hat{H}_r - \hat{H}_{qr}$ when it is in the ground state. The dynamical equations can now be obtained for the field amplitude of the pointer states, which evolve independently of one another,

$$\frac{d}{dt}\alpha_e(t) = \left(-\frac{\kappa}{2} - i(\Delta_r + \chi)\right)\alpha_e(t) - i\epsilon(t) \qquad \frac{d}{dt}\alpha_g(t) = \left(-\frac{\kappa}{2} - i(\Delta_r - \chi)\right)\alpha_g(t) - i\epsilon(t). \tag{4.40}$$

As we have established, the SNR as well as the accumulated dephasing are related to the intracavity field of the pointer states directly through the relations [205]:

$$\mathrm{SNR}^2(t) = \frac{\kappa}{2}\int_0^t |\alpha_e(\tau) - \alpha_g(\tau)|^2 \, d\tau \qquad \int_0^t \Gamma_\mathrm{d}(\tau)\, d\tau = 2\chi \int_0^t \mathrm{Im}[\alpha_g(\tau)\alpha_e^*(\tau)]\, d\tau. \tag{4.41}$$

This expression demonstrates that the SNR increases as the distance between the coherent pointer states increases; in the absence of added photons, the noise contribution of the SNR will always be that of a vacuum state. Using the differential equations in Eq. (4.40), the expressions for the SNR and dephasing can be shown to be equivalent when using the optimal weights for the SNR [205]. Before the introduction of off-chip noise, the maximum efficiency of the measurement is therefore one, $\eta = 1$, and so the rate at which qubit information is destroyed by the measurement is equal to the rate of an optimal measurement.

This does not mean that any choice of parameters will lead to the best measurement. The innate relaxation and dephasing of the qubit as also present and will destroy the qubit state over time, meaning that the measurement should proceed as quickly as possible. To see how the parameters of the system affect the timescale of the measurement, we will solve the cavity amplitudes in the steady-state, and so assume that the drive takes a constant value, $\epsilon(t) \to \epsilon$. The steady-state response is simply:

$$\alpha_{e/g} = \frac{-\epsilon}{(\Delta_r \pm \chi) - i\kappa/2} \quad \text{or} \quad \left|\alpha_{e/g}\right| = \frac{\epsilon}{\sqrt{(\kappa/2)^2 + (\Delta_r \pm \chi)^2}}\,, \arg(\alpha_{e/g}) = \arctan\left(\frac{\Delta_r \pm \chi}{\kappa/2}\right). \tag{4.42}$$

The detuning between the drive and cavity strongly affects the amplitude and phase of the intracavity fields. If this detuning is large, the result is a very small field amplitude, resulting in very weak entanglement between the resonator and qubit; the measurement rate, and hence dephasing, are very small in this regime and so it is optimal for situations where the minimal decoherence of the qubit state is desired, such as the application of qubit gates [207]. For the purposes of measurement, the opposite regime is chosen, where there is no detuning $\Delta_r = 0$. In this case, the pointer states are rotated by the dispersive shift in opposite directions, with identical field amplitude. The steady-state measurement and dephasing rates are then,

$$\Gamma_\mathrm{meas}\,, \Gamma_\mathrm{d} = \frac{2\,|\epsilon|^2\,\chi^2\kappa}{(\kappa^2/4 + \chi^2)^2} = \frac{16\,|\alpha|^2\,\chi(2\chi/\kappa)}{(1 + (2\chi/\kappa)^2)^2}. \tag{4.43}$$

As we can again see, in the ideal case where there is no off-chip noise, the measurement is perfectly efficient since both rates are identical, $\Gamma_\mathrm{meas}/\Gamma_\mathrm{d} = 1$. The measurement rate is controlled by the amplitude of the drive field, $|\epsilon|^2$, and the ratio of the dispersive coupling with the cavity loss rate, $\chi/(\kappa/2)$. Populating the cavity with more photons by increasing $|\epsilon|^2$ will increase the coupling between the qubit and cavity, as well as the strength of the output signal, naturally resulting in a faster measurement. This improvement is not without limits, as this increases the intracavity photon population of the resonator, eventually resulting in a breakdown of the model when approaching the critical photon number n_crit. In this regime, there is stronger entanglement between the resonator and qubit, resulting in a breakdown of the dispersive approximation and an increase in energy exchange between the qubit and resonator. The stronger interaction will also result in a non-negligible increase in the transition rate to higher transmon states, so we can no longer approximate the transmon as a two-level system. Both processes cause the measurement to be non-QND and hence reduce the efficiency of the measurement scheme.

The ratio $\chi/(\kappa/2)$ can be seen as balancing two rates: χ, which represents the rate at which a photon can acquire qubit information, and $\kappa/2$, which corresponds to the lifetime of a photon created in the cavity before it decays through the output port. The measurement rate is maximised when these two rates are perfectly balanced, and so

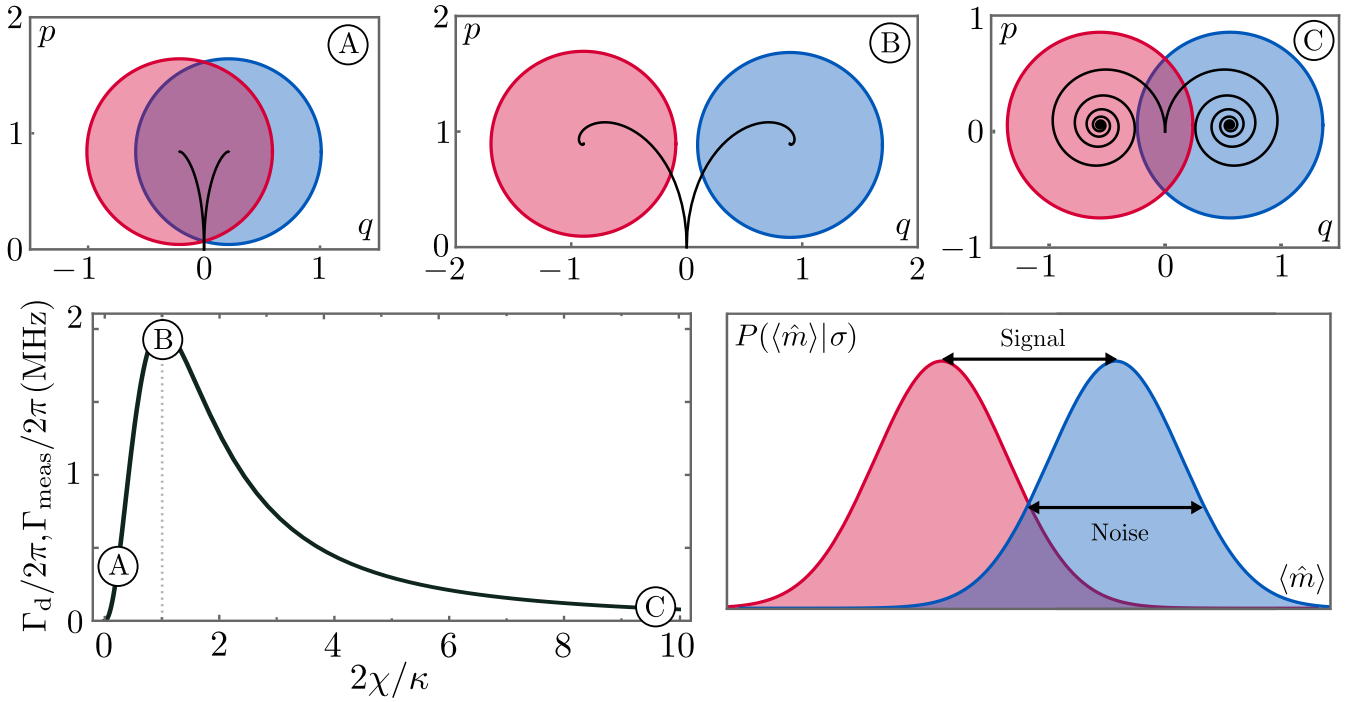

Figure 4.2: [Top] Steady-state intracavity fields for the excited (red) and ground (blue) pointer states, with accompanying paths traced by the Wigner functions in phase space. The error ellipses correspond to vacuum noise. The drive amplitude is fixed at $\epsilon = \sqrt{\kappa}$ and the dispersive coupling is set to $\chi/2\pi = 2.5\,\text{MHz}$. Three regimes are displayed, (A) $2\chi/\kappa = 1/4$, (B) $2\chi/\kappa = 1$, and (C) $2\chi/\kappa = 10$, with corresponding points marked in the bottom left plot. [Bottom left] Steady-state dephasing and measurement rate, Γ_d and Γ_meas, plotted as a function of $2\chi/\kappa$, where the drive amplitude is set to $\epsilon = -\sqrt{\kappa}$. [Bottom right] Marginal probability distributions of the excited (red) and ground (blue) qubit-state conditioned pointer states with respect to the measurement operator $\hat{m}$. The signal component of the SNR corresponds to the distance between the means of the marginal distributions, while the noise corresponds to the standard deviation of the Gaussian. Marginal distributions can be obtained by integrating the full Gaussian Wigner functions. This diagram is inspired by a figure in Ref. [157].

$\chi/(\kappa/2) = 1$ [206, 208]. As shown in Figure 4.2, the measurement rate will decrease as one rate starts to dominate the other. In the regime where $\chi \ll \kappa/2$, the lifetime of the photon in the cavity is too short to acquire enough qubit information before it exits through the output, evidenced by the minimal difference in the relative phase of the pointer states. The reason for the decrease in the $\chi \gg \kappa/2$ regime is more subtle. Here, the increase in the decay rate results in a large variance in the average photon lifetime within the cavity compared to the time it takes to acquire a discernible phase shift due to the dispersive coupling; this increase in the photon variance results in an increase in the uncertainty of the measurement, decreasing our ability to determine the state of the qubit. The measurement rate can also be increased by keeping $\chi/(\kappa/2)$ fixed, and increasing the value of the dispersive shift χ. An increase in χ also has limits, since higher-order interactions will need to be included when expanding the Jaynes-Cummings Hamiltonian in the dressed frame. Given that the critical photon number decreases with increasing χ, $n_\text{crit} = \Delta/4\chi$, the dispersive model will at some point no longer hold as the allowable upper limit on the intracavity photon population decreases.

While this measurement is perfectly efficient in the ideal case, the amount of added off-chip photons significantly increases the noise in the SNR and measurement rate beyond vacuum noise. Since the increase in the signal strength is limited by the model, the efficiency necessarily suffers, but the inclusion of a directional amplifier as the first component of the measurement chain can help to improve this efficiency [17, 30]. Integrating the amplifier with the qubit in an attempt to improve the efficiency even further is the next step, however, this integration comes at the cost of additional dephasing beyond the measurement rate [209]. In this case, the pointer states are no longer pure coherent states, and so do not satisfy the assumptions used to characterise the dephasing in this section. To calculate the dephasing for the significantly more complicated setup involving a nonreciprocal amplifier, we will use a method based on the properties of Gaussian distributions in the Wigner phase space, which will be introduced in the next section.

4.2 Gaussian Moment Method For Calculating Measurement Backaction

In order to accurately characterise the efficiency of the qubit-state measurement, it is critical to be able to calculate the qubit dephasing that results from the backaction of the coupled harmonic modes which form the on-chip measurement apparatus. While calculating the SNR or measurement rate is straightforward, the dephasing is another matter. In practice, this calculation involves solving the dynamics of the coupled harmonic modes and then tracing over their Hilbert space; this process will also allow us to calculate the qubit frequency shift. One popular method involves applying a polaron-type transformation to move to a dressed displaced frame where the oscillator pointer states appear as vacuum states [197, 206]. Tracing over the harmonic mode Hilbert space is simple in this displaced frame, and after finally transforming back to the lab frame, the added dephasing from the harmonic modes will then appear in the reduced master equation for the qubit. While this method is exact, it is limited for two reasons: the polaron transformation becomes significantly more complicated upon the inclusion of squeezing, and it is unable to handle thermal states.

A more tractable approach uses the characteristic function of the Wigner phase-space representation for Gaussian states. Here, the dynamics of the harmonic mode state can be entirely described using the equations of motion for the moments, and the trace over the Hilbert space becomes a phase-space integral of a Gaussian distribution. This method has been used to solve for the dephasing and frequency shift for dispersively coupled single-mode systems in the presence of driven vacuum noise [202], thermal noise [210], and single-mode squeezing [209], in addition to measurement setups with a different dispersive qubit-harmonic mode coupling [211, 212], and measurements which are approximately QND only at short times [213]. This section aims to demonstrate how this phase-space moment method can be extended to multimode systems coupled to a single qubit. This method can also be applied to multimode dispersive measurement [214], longitudinal measurement [207, 215, 216], and any other measurement schemes [217] which obey the properties to be discussed in the next section.

4.2.1 Gaussian Master Equations

4.2.1.1 Scope of the Method

The use of the moment method places certain constraints on the allowable form of the master equation that may be used to model the system. In order to detail what interactions are allowed, we start by expressing the master equation for the joint qubit-harmonic mode density operator $\hat{\rho}$ as a sum of three Lindblad super-operators,

$$\frac{d}{dt}\hat{\rho} = \big(\mathcal{L}_r + \mathcal{L}_q + \mathcal{L}_{qr}\big)(\hat{\rho}) \tag{4.44}$$

where $\mathcal{L}_r$ represents the open system dynamics for the harmonic modes, $\mathcal{L}_q$ is the open system dynamics for the qubit only, and $\mathcal{L}_{qr}$ comprises the interacting terms between the qubit and the harmonic modes. The joint qubit-harmonic mode density operator can be written as follows in the basis of the excited and ground states of the qubit, $|e\rangle$ and $|g\rangle$, respectively:

$$\hat{\rho} = \hat{\rho}_{ee}\,|e\rangle\langle e| + \hat{\rho}_{gg}\,|g\rangle\langle g| + \hat{\rho}_{eg}\,|e\rangle\langle g| + \hat{\rho}_{ge}\,|g\rangle\langle e| \equiv \begin{pmatrix} \hat{\rho}_{ee} & \hat{\rho}_{eg} \\ \hat{\rho}_{ge} & \hat{\rho}_{gg} \end{pmatrix} \tag{4.45}$$

where $\hat{\rho}_{ge} = (\hat{\rho}_{eg})^\dagger$. Tracing over the qubit Hilbert state will return a harmonic mode state which corresponds to the sum of the two pointer states, $\hat{\rho}_{ee} + \hat{\rho}_{gg}$, which is guaranteed to be a true density operator. As a result, the Wigner function associated with $\hat{\rho}_{ee} + \hat{\rho}_{gg}$ is guaranteed to always be a real-valued function, where integrating over the entire phase space returns a value of one. By definition, the same is not true for the off-diagonal elements, $\hat{\rho}_{eg}$ and $\hat{\rho}_{ge}$, which in general are not properly normalised Hermitian operators. As a result, their respective Wigner quasiprobability distributions (QPDs) correspond to complex functions which are not properly normalised, and so integrating these functions over the entire phase space will yield complex numbers. As will be seen later in this section, this is required if we are to calculate the backaction of the measurement on the qubit, where the magnitude of this complex number will yield the induced dephasing, and the phase will correspond to a measurement-induced shift of the qubit frequency.

Although it may seem counter-intuitive to talk of a complex-valued Wigner QPD, this to be expected when dealing with non-Hermitian operators; the Wigner distribution for the annihilation operator $\hat{a} = (\hat{q} + i\hat{p})/\sqrt{2}$ is of course a complex-valued function in the phase space with real-valued q-p quadrature coordinates. Additionally, the Wigner QPDs for $\hat{\rho}_{eg}$ and $\hat{\rho}_{ge}$ will always be integrable over the entire phase space. This is a result of the fact that Eq. (4.45) must still be a positive semi-definite matrix even after integrating over the resonator degrees of freedom, $\mathrm{Tr}_r[\hat{\rho}] \geq 0$. This demand therefore results in the following inequality, $|\mathrm{Tr}_r[\hat{\rho}_{eg}]|^2 \leq \mathrm{Tr}_r[\hat{\rho}_{gg}]\mathrm{Tr}_r[\hat{\rho}_{ee}]$. Since both $\hat{\rho}_{ee}$ and $\hat{\rho}_{gg}$ correspond to true density operators upon proper rescaling, their phase-space integrals always converge to some positive finite value which is equal to their trace, $0 \leq \mathrm{Tr}_r[\hat{\rho}_{gg}], \mathrm{Tr}_r[\hat{\rho}_{ee}] \leq 1$. As a result, the integral of the Wigner QPD for $\hat{\rho}_{eg}$ over the entire phase space must converge since $|\mathrm{Tr}_r[\hat{\rho}_{eg}]|^2$ will always take some positive finite value.

We can rest assured that mapping $\hat{\rho}_{eg}$ to the Wigner phase space is a sensible operation and that we can define equations of motion for the resulting Wigner QPD. To use the moment method to calculate the dynamics of the harmonic mode components of Eq. (4.45), it is necessary that the elements have the following property:

- The operator $\hat{\rho}_{jk}$, $j,k \in \{e,g\}$, can be described entirely by its first and second moments, along with its norm.

For $\hat{\rho}_{ee}$ and $\hat{\rho}_{gg}$ this condition means that their Wigner QPDs will be non-normalised real-valued Gaussian distributions, whereas $\hat{\rho}_{eg}$ and $\hat{\rho}_{ge}$ map to non-normalised complex Gaussian distributions. In order for these components to remain Gaussian for all time, the initial state must naturally obey this condition, and the system dynamics must preserve it. This will constrain the different terms that can be included in the Lindbladian, which must also conform to the following conditions:

- The component of the dynamics acting on the harmonic modes, present in the super-operators $\mathcal{L}_r$ and $\mathcal{L}_{qr}$, must be Gaussian channels, as discussed in Section 2.2.2.
- The only qubit operator that may be present in the super-operators $\mathcal{L}_q$ and $\mathcal{L}_{qr}$ is the spin-z operator, $\hat{\sigma}_z$. If this is not the case, then the elements $\hat{\rho}_{jk}$ will couple to one another, and the resulting operator cannot, in general, be characterised by its first two moments.

The second property is necessary not just for the mathematical machinery to work, but as discussed in Section 4.1, was also a requirement for the measurement of the qubit state to be QND. We can see that if the measurement fails to be QND that the dynamics of the pointer state density operators, $\hat{\rho}_{ee}$ and $\hat{\rho}_{gg}$, will be coupled, whereupon the pointer states become superpositions of two Gaussians and are no longer uniquely dependent on the ground or excited state of the qubit. Since the sum of two nonidentical Gaussian distributions does not result in a Gaussian distribution, the resulting states cannot be characterised by only the means and covariances, and so the moment method is incapable of handling them. These two properties are therefore inextricably linked.

4.2.1.2 General Form of the Master Equation

Using these two conditions, we can provide general expressions for the Lindblad master equation. Since the component of the dynamics acting purely on the harmonic modes must correspond to a Gaussian channel, the form of the Lindbladian $\mathcal{L}_r$ comes directly from Section 2.2.2:

$$\mathcal{L}_r(\hat{\rho}) = -i[\hat{H}_r, \hat{\rho}] + \sum_{j,k=1}^{2N} \Gamma_{jk}\left(\hat{r}_k\hat{\rho}\hat{r}_j - \frac{1}{2}[\hat{r}_j\hat{r}_k, \hat{\rho}]_+\right) \tag{4.46}$$

where the Hamiltonian $\hat{H}_r$ is at most a quadratic polynomial of the quadrature operators. Since the Lindbladian containing the purely qubit dynamics, $\mathcal{L}_q$, can only depend on $\hat{\sigma}_z$, it only comprises one coherent and one dissipative process:

$$\mathcal{L}_q(\hat{\rho}) = -i\frac{\tilde{\omega}_q}{2}[\hat{\sigma}_z, \hat{\rho}] + \frac{\Gamma_\varphi}{2}\mathcal{D}[\hat{\sigma}_z](\hat{\rho}). \tag{4.47}$$

By describing the qubit state as a vector on or within the Bloch sphere, this coherent interaction simply results in a rotation of the vector around the z-axis. The dephasing term, $\mathcal{D}[\hat{\sigma}_z]$, results in a gradual collapse of the vector onto the z-axis, representing a loss of coherence. Importantly, $\hat{\sigma}_z$ is a QND-observable of this Lindbladian, $\mathcal{L}_q^\dagger(\hat{\sigma}_z) = 0$, and so this open-system dynamics can be handled by our method. As a result, the probability of observing the qubit in the ground or excited state is preserved.

Things are slightly more complicated for the qubit-harmonic mode component of the dynamics due to the fact that dissipation terms coupling the modes and qubit are technically allowed. In general, $\mathcal{L}_{qr}$ can take the following form

$$\mathcal{L}_{qr}(\hat{\rho}) = -i[\hat{H}_{qr}\hat{\sigma}_z, \hat{\rho}] + \sum_{j,k=1}^{2N}\Big(\Gamma_{jk,z0}\,\mathcal{J}[\hat{r}_k\hat{\sigma}_z, \hat{r}_j](\hat{\rho}) + \Gamma_{jk,0z}\,\mathcal{J}[\hat{r}_k, \hat{r}_j\hat{\sigma}_z](\hat{\rho}) + \Gamma_{jk,zz}\,\mathcal{J}[\hat{r}_k\hat{\sigma}_z, \hat{r}_j\hat{\sigma}_z](\hat{\rho})\Big), \tag{4.48}$$

where, for convenience, we have defined a new super-operator to handle the complicated form of the dissipation terms:

$$\mathcal{J}[\hat{L}_1, \hat{L}_2](\hat{\rho}) := \hat{L}_1\hat{\rho}\hat{L}_2^\dagger - \frac{1}{2}[\hat{L}_2^\dagger\hat{L}_1, \hat{\rho}]_+ \quad \text{where} \quad \mathcal{J}[\hat{L}, \hat{L}](\hat{\rho}) \equiv \mathcal{D}[\hat{L}](\hat{\rho}) := \hat{L}\hat{\rho}\hat{L}^\dagger - \frac{1}{2}[\hat{L}^\dagger\hat{L}, \hat{\rho}]_+. \tag{4.49}$$

The Hamiltonian $\hat{H}_{qr}$ is again at most a quadratic polynomial of the quadrature operators, and does not contain any qubit operators. Since coupled qubit-harmonic mode dissipation terms are generally not included in physical models, no physical interpretation will be considered. The coherent coupling between the modes and the qubit, on the other hand, is the source of the added backaction on the qubit that we wish to calculate.

Qubit Dissipation

An important consequence of our constraints is that the qubit dissipation terms, so-called *T1-processes*, have been omitted. These T1-processes couple the diagonal elements of the density operator, $\hat{\rho}_{ee}$ and $\hat{\rho}_{gg}$, meaning that the pointer states no longer perfectly correlate to the state of the qubit, resulting in a non-QND measurement. This loss of correlation between the pointer states and their respective qubit state increases over the course of the measurement, resulting in a decrease of measurement efficiency [218]. In order for the master equation in Eq. (4.44) to be a valid model for our measurement scheme, we therefore require that the rate of these T1-processes be very slow in comparison to every other process in the system, so that by the time they are relevant, the measurement will be finished. In practice, it is assumed that the timescale on which these T1-processes occur is infinite compared to the rest of the system, a safe assumption as transmon qubit lifetimes increase year-on-year [156].

However, when calculating the dephasing, it is only required that $\hat{\rho}_{eg}$ and $\hat{\rho}_{ge}$ do not couple to other elements of the density operator, and so retain their Gaussian-like properties. For dephasing calculations, we can therefore reintroduce certain qubit dissipation terms to our calculations, as discussed in Appendix E. The moment method is then able to handle qubit Lindbladians of the form

$$\mathcal{L}_q(\hat{\rho}) = -i\frac{\tilde{\omega}_q}{2}[\hat{\sigma}_z, \hat{\rho}] + \Gamma_- \mathcal{D}[\hat{\sigma}_-](\hat{\rho}) + \Gamma_+ \mathcal{D}[\hat{\sigma}_+](\hat{\rho}) + \frac{\Gamma_\varphi}{2}\mathcal{D}[\hat{\sigma}_z](\hat{\rho}), \tag{4.50}$$

and qubit-harmonic mode Lindbladians of the form

$$\begin{aligned}\mathcal{L}_{qr}(\hat{\rho}) = -i[\hat{H}_{qr}\hat{\sigma}_z, \hat{\rho}] + \sum_{j,k=1}^{2N} \Big(&\Gamma_{jk,-}\, \mathcal{J}[\hat{r}_k\hat{\sigma}_-, \hat{r}_j\hat{\sigma}_-](\hat{\rho}) + \Gamma_{jk,+}\, \mathcal{J}[\hat{r}_k\hat{\sigma}_+, \hat{r}_j\hat{\sigma}_+](\hat{\rho}) \\ &+ \Gamma_{jk,z0}\, \mathcal{J}[\hat{r}_k\hat{\sigma}_z, \hat{r}_j](\hat{\rho}) + \Gamma_{jk,0z}\, \mathcal{J}[\hat{r}_k, \hat{r}_j\hat{\sigma}_z](\hat{\rho}) + \Gamma_{jk,zz}\, \mathcal{J}[\hat{r}_k\hat{\sigma}_z, \hat{r}_j\hat{\sigma}_z](\hat{\rho}) \Big).\end{aligned} \tag{4.51}$$

In both cases, the only difference from the previous expressions is the inclusion of additional dissipation terms. Coherent interactions which result in transitions between the ground and excited state cannot be handled since they couple the off-diagonal elements $\hat{\rho}_{eg}$ and $\hat{\rho}_{ge}$ with the diagonal elements $\hat{\rho}_{ee}$ and $\hat{\rho}_{gg}$; this includes the Jaynes-Cummings Hamiltonian. We note that $\mathcal{L}_{qr}$ includes combined qubit-harmonic mode dissipation and dephasing terms; these can arise when applying the dispersive transformation to the Jaynes-Cummings master equation [197], though in general they are weak corrections. As a result, we will ignore any joint qubit-harmonic mode decay terms for the remainder of this section, however, qubit dissipation will be included in the following sections in the form of thermal noise coming from a bosonic bath.

4.2.1.3 Reduced Master Equations

In order to establish the connection between the dynamics of the harmonic mode system and the added backaction on the qubit, we will now examine the master equations that one obtains for the qubit after tracing over the harmonic mode degrees of freedom, as well as the effective master equations one obtains for the harmonic modes. We start with the Lindbladian for the full density operator defined by Eq. (4.44), where the mode dynamics are described by Eq. (4.46). Assuming that the modes and the qubit are coherently coupled, and that the qubit is additionally coupled to a bath which results in fluctuations of the qubit energy, $\mathcal{L}_q$ and $\mathcal{L}_{qr}$ can be expressed as

$$\mathcal{L}_q(\hat{\rho}) = -i\frac{\tilde{\omega}_q}{2}[\hat{\sigma}_z, \hat{\rho}] + \Gamma_- \mathcal{D}[\hat{\sigma}_-](\hat{\rho}) + \Gamma_+ \mathcal{D}[\hat{\sigma}_+](\hat{\rho}) + \frac{\Gamma_\phi}{2}\mathcal{D}[\hat{\sigma}_z](\hat{\rho}) \quad \text{and} \quad \mathcal{L}_{qr}(\hat{\rho}) = -i[\hat{H}_{qr}\hat{\sigma}_z, \hat{\rho}]. \tag{4.52}$$

The qubit dissipation has been reintroduced to demonstrate how it impacts the total dephasing. Tracing over the harmonic mode degrees of freedom in the total master equation will yield a reduced qubit master equation. Since we have ensured that $\hat{\sigma}_z$ is a QND-observable for both $\mathcal{L}_r$ and $\mathcal{L}_{qr}$, the extra interactions that these will contribute to the reduced qubit master equation must also have $\hat{\sigma}_z$ as a QND-observable, and the only two interactions which satisfy this requirement are a coherent frequency shift and some added qubit dephasing. The reduced qubit master equations must therefore take the following form

$$\frac{d}{dt}\hat{\rho}^q = -\frac{i}{2}(\tilde{\omega}_q + B(t))[\hat{\sigma}_z, \hat{\rho}^q] + \Gamma_- \mathcal{D}[\hat{\sigma}_-](\hat{\rho}^q) + \Gamma_+ \mathcal{D}[\hat{\sigma}_+](\hat{\rho}^q) + \frac{\Gamma_\varphi + \Gamma_\mathrm{d}(t)}{2}\mathcal{D}[\hat{\sigma}_z](\hat{\rho}^q), \tag{4.53}$$

where $B(t)$ and $\Gamma_\mathrm{d}(t)$ are the induced frequency shift and dephasing, respectively. $\tilde{\omega}_q$ is the frequency of the qubit in this frame, and $\Gamma_\pm$ are the coupling rates of the qubit with a bosonic bath, where $\bar{n}_q$ is the thermal occupation of said bath. Γ_φ is the dephasing rate of the qubit due to coupling to the environment. The operator $\hat{\rho}^q$ is the density

operator obtained after tracing over the harmonic mode degrees of freedom, defined as

$$\hat{\rho}^q := \mathrm{Tr}_r[\hat{\rho}]. \tag{4.54}$$

If we expand the reduced qubit density operator in the basis of ground and excited states,

$$\hat{\rho}^q = \rho^q_{gg}\,|g\rangle\langle g| + \rho^q_{ee}\,|e\rangle\langle e| + \rho^q_{eg}\,|e\rangle\langle g| + \rho^q_{ge}\,|g\rangle\langle e| \equiv \begin{pmatrix} \rho^q_{ee} & \rho^q_{eg} \\ \rho^q_{ge} & \rho^q_{gg} \end{pmatrix}, \tag{4.55}$$

then, using the reduced qubit master equation, we obtain the following set of equations:

$$\frac{d}{dt}\rho^q_{ee} = -\Gamma_-\rho^q_{ee} + \Gamma_+\rho^q_{gg} \qquad \frac{d}{dt}\rho^q_{eg} = \left[-i\left(\tilde{\omega}_q + B(t)\right) - \left(\frac{\Gamma_+ + \Gamma_-}{2} + \Gamma_\varphi + \Gamma_\mathrm{d}(t)\right)\right]\rho^q_{eg}. \tag{4.56}$$

The equations for the other two elements can be obtained using $\rho^q_{gg} = 1 - \rho^q_{ee}$ and $\rho^q_{ge}(t) = (\rho^q_{eg}(t))^*$. It is the dynamics of the off-diagonal elements that are of most interest since they contain the added backaction from the readout modes. The dynamical equation for the $\rho^q_{eg}(t)$ component has the following solution,

$$\rho^q_{eg}(t) = \exp\left[-t\left(i\tilde{\omega}_q + \frac{\Gamma_+ + \Gamma_-}{2} + \Gamma_\varphi\right) - \int_0^t \left[iB(\tau) + \Gamma_\mathrm{d}(\tau)\right]\,d\tau\right]\rho^q_{eg}(0). \tag{4.57}$$

Both dissipation terms in the reduced qubit master equation therefore contribute to the dephasing. The exchange of excitations with the bosonic bath will naturally result in dephasing as the coherence of the qubit state is lost due to thermalisation; this process proceeds at the rate $(\Gamma_+ + \Gamma_-)/2$. The other dephasing process, occurring with rate Γ_φ, is a result of the bath coupling causing fluctuations in the transition frequency of the qubit [197]. Both of these processes define relaxation and pure dephasing times for the qubit, $T_1 := 2/(\Gamma_+ + \Gamma_-)$ and $T_2 := 1/\Gamma_\varphi$, respectively.

Calculating $B(t)$ and $\Gamma_\mathrm{d}(t)$ requires that the dynamics of the modes be solved and then traced over. To model the dynamics of the harmonic modes, the decomposition Eq. (4.45) of the total density operator is used; the elements of this decomposition, $\hat{\rho}_{jk}(t)$, contain a mix of harmonic mode and qubit dynamics. Using the Lindbladians from Eq. (4.46) and Eq. (4.52), we can construct effective equations of motion for the off-diagonal element $\hat{\rho}_{eg}(t)$:

$$\frac{d}{dt}\hat{\rho}_{eg} = \mathcal{L}_r(\hat{\rho}_{eg}) - \left(i\tilde{\omega}_q + \frac{\Gamma_+ + \Gamma_-}{2} + \Gamma_\varphi\right)\hat{\rho}_{eg} - i[\hat{H}_{qr}, \hat{\rho}_{eg}]_+. \tag{4.58}$$

The rotation and dissipation terms coming from the qubit can be eliminated by defining

$$\hat{\rho}_{eg}(t) = e^{-t(i\tilde{\omega}_q + \tilde{\Gamma}_\phi)}\rho^q_{eg}(0)\hat{\rho}^r_{eg}(t) \tag{4.59}$$

where $\tilde{\Gamma}_\varphi = \Gamma_\varphi + (\Gamma_+ + \Gamma_-)/2$ is the total innate dephasing rate of the qubit. This quantity can be used to define a dephasing time in the absence of any measurement, which we define as $T_2^* := 1/\tilde{\Gamma}_\varphi = 2T_1T_2/(2T_1 + T_2)$. We recall from the definition Eq. (4.54) that the qubit density matrix is obtained by partially tracing over the mode Hilbert space, so the elements of the qubit density matrix in Eq. (4.55) can be related to the above expressions by applying the partial trace:

$$\rho^q_{eg}(t) \equiv \mathrm{Tr}_r[\hat{\rho}_{eg}(t)] = e^{-t(i\tilde{\omega}_q + \tilde{\Gamma}_\varphi)}\rho^q_{eg}(0)\mathrm{Tr}_r[\hat{\rho}^r_{eg}(t)]. \tag{4.60}$$

Finally, provided that our ansatz for the reduced qubit master equation Eq. (4.53) is correct, comparing the above expressions to the solutions in Eq. (4.57) allows us to relate the trace of $\hat{\rho}^r_{eg}(t)$ and $\hat{\rho}^r_{ge}(t)$ to the induced dephasing and frequency shift,

$$\mathrm{Tr}_r[\hat{\rho}^r_{eg}(t)] = \exp\left[-\int_0^t \left[iB(\tau) + \Gamma_\mathrm{d}(\tau)\right]\,d\tau\right]. \tag{4.61}$$

We can rewrite these to obtain expressions for the frequency shift and dephasing,

$$\Gamma_\mathrm{d}(t) = \frac{d}{dt}\mathrm{Re}\Big[-\ln\left(\mathrm{Tr}_r[\hat{\rho}^r_{eg}(t)]\right)\Big] \quad \text{and} \quad B(t) = \frac{d}{dt}\mathrm{Im}\Big[-\ln\left(\mathrm{Tr}_r[\hat{\rho}^r_{eg}(t)]\right)\Big]. \tag{4.62}$$

The expressions in terms of $\hat{\rho}^r_{ge}$ are similar. The final step in this process is to substitute the expressions for the combined qubit-harmonic mode operators from Eq. (4.59) into the dynamical equations in Eq. (4.58) to obtain dynamical equations for $\hat{\rho}^r_{eg}$ and $\hat{\rho}^r_{ge}$ only,

$$\frac{d}{dt}\hat{\rho}^r_{eg} = \mathcal{L}_r(\hat{\rho}^r_{eg}) - i[\hat{H}_{qr}, \hat{\rho}^r_{eg}]_+ \quad \text{and} \quad \frac{d}{dt}\hat{\rho}^r_{ge} = \mathcal{L}_r(\hat{\rho}^r_{ge}) + i[\hat{H}_{qr}, \hat{\rho}^r_{ge}]_+. \tag{4.63}$$

The coherent qubit-harmonic mode interaction $\hat{H}_{qr}\hat{\sigma}_z$ results in an anti-commutator term in Eq. (4.63), and so these equations of motion are *not* of Lindblad type. As a result, $\hat{\rho}^r_{eg}(t)$ and $\hat{\rho}^r_{ge}(t)$ are not true density operators. This has two consequences for these operators: the norm in no longer preserved under the evolution defined by Eq. (4.63), and $\hat{\rho}^r_{eg}(t)$ and $\hat{\rho}^r_{ge}(t)$ are in general not Hermitian. However, so long as we assume that the harmonic mode system is initially in a Gaussian state, the elements $\hat{\rho}^r_{jk}(t)$ will retain one crucial feature: they can be described entirely by their first and second moments along with their norm, since the dynamics in Eq. (4.63) is entirely linear.

It is evident from Eq. (4.62) that a complex and non-normalised trace means that there is backaction on the qubit. We recall from Eq. (4.3) that this is related to the overlap of the pointer states, and here we apply the same interpretation: as the pointer states become mode distinct the trace of the off-diagonal element will become smaller, leading to larger backaction from the multimode system in accordance with Eq. (4.62). This heuristic explanation works well when considering only pure states, however, the connection is less clear in this case since the joint qubit-harmonic mode state could be mixed. Even though we can no longer directly relate the dephasing with the dynamics of the pointer states, as we will see, the moment method will still allow us to discern how interactions in $\mathcal{L}_r$ and $\mathcal{L}_{qr}$ impact the dephasing. In particular, we gain the ability to see how the inclusion of squeezing, thermal noise, and non-dispersive coupling affects the qubit dephasing. Having worked out the necessary expressions in Hilbert space, we will now pass over to Wigner space to obtain an explicit expression for the moments of the multimode operators.

4.2.2 The Moment Method

4.2.2.1 Working in the Wigner Phase Space

When passing over to Wigner phase space, we must take into account the fact that the operator $\hat{\rho}^r_{eg}$ is not a true density operator because it neither Hermitian nor has a trace of one, and hence does not correspond to a probability distribution in phase space. To reiterate a point from Section 4.2.1.1, it follows that the corresponding Wigner function, $W_{eg}(\boldsymbol{r})$, will be complex valued and will not have a properly normalised phase-space integral, these being the equivalent properties in phase space as discussed in Section 2.1.3. As per usual, it is not the Wigner function itself but the associated characteristic function that we are interested in when defining equations of motion for the moments. In this instance, the characteristic function takes the form:

$$w_{eg}(\boldsymbol{\xi}) = \exp\left[-\frac{1}{2}\boldsymbol{\xi}^T\boldsymbol{\sigma}\boldsymbol{\xi} + i\boldsymbol{\mu}^T\boldsymbol{\xi} - \upsilon\right]. \tag{4.64}$$

Since $W_{eg}(\boldsymbol{r})$ is a complex function, the covariance matrix $\boldsymbol{\sigma}$ and the means $\boldsymbol{\mu}$ will be complex. The definition of the covariance matrix is still the same with $\sigma_{jk} = \sigma_{kj}$, so although the covariances are complex-valued, the matrix itself is still symmetric, $\boldsymbol{\sigma} = \boldsymbol{\sigma}^T$; although complex-symmetric matrices of central second moments are often referred to as pseudo-covariance matrices, we will still refer to $\boldsymbol{\sigma}$ as the covariance matrix. In addition, we have included a new term in the characteristic function, υ, equivalent to account for the fact that the total mass of the Wigner QPD, obtained from the phase-space integral of $W_{eg}(\boldsymbol{r})$, is in general not equal to one. The trace of $\hat{\rho}^r_{eg}$, and hence the induced dephasing and frequency shift, can be related to the υ parameter, using the fact that the trace of this operator must be

$$\mathrm{Tr}_r[\hat{\rho}^r_{eg}] = \int_{\mathbb{R}^{2N}} W_{eg}(\boldsymbol{r})\, d\boldsymbol{r} = w_{eg}(0), \tag{4.65}$$

and so the trace of the time-dependent operator is

$$\mathrm{Tr}_r[\hat{\rho}^r_{eg}(t)] = \exp\left[-\upsilon(t)\right]. \tag{4.66}$$

As discussed in Section 4.2.1.1, $W_{eg}(\boldsymbol{r})$ must always be integrable over the entire phase space, and hence $w_{eg}(0)$ is always some finite complex number. The trace of $\hat{\rho}^r_{eg}$ was also calculated in the previous section, so combining the above with Eq. (4.61), we can relate $\upsilon(t)$ to the induced backaction from the multimode system,

$$\upsilon(t) = \int_0^t \left[iB(\tau) + \Gamma_{\mathrm{d}}(\tau)\right] d\tau, \tag{4.67}$$

or equivalently,

$$\Gamma_{\mathrm{d}}(t) = \mathrm{Re}[\dot{\upsilon}(t)] \quad \text{and} \quad B(t) = \mathrm{Im}[\dot{\upsilon}(t)]. \tag{4.68}$$

In order to calculate $\dot{\upsilon}(t)$, the equations of motion for the covariances and means must be solved. The approach here is the same as in Section 2.2.2; we therefore convert the dynamical equation for the operator $\hat{\rho}^r_{eg}$ to an equivalent PDE

for $W_{eg}(\boldsymbol{r})$, and then perform a Fourier transform over the phase-space coordinates to obtain another PDE for $w_{eg}(\boldsymbol{\xi})$:

$$\frac{d}{dt}\hat{\rho}^r_{eg} \xrightarrow{\text{Wigner}} \frac{\partial}{\partial t}W_{eg}(\boldsymbol{r}) \xrightarrow{\text{Fourier}} \frac{\partial}{\partial t}w_{eg}(\boldsymbol{\xi}). \tag{4.69}$$

The system of ODEs for the moments can then be generated from this final PDE. The full details for performing these calculations can be found in Appendix B. We start with the dynamical equation for $\hat{\rho}^r_{eg}$ from the previous section,

$$\frac{d}{dt}\hat{\rho}^r_{eg} = -i[\hat{H}_r, \hat{\rho}^r_{eg}] - i[\hat{H}_{qr}, \hat{\rho}^r_{eg}]_+ + \sum_{j,k=1}^{N} \Gamma_{jk}\left(\hat{r}_j\hat{\rho}^r_{eg}\hat{r}_k - \frac{1}{2}[\hat{r}_k\hat{r}_j, \hat{\rho}^r_{eg}]_+\right). \tag{4.70}$$

For what follows the Hamiltonians $\hat{H}_r$ and $\hat{H}_{qr}$ will be expressed as

$$\hat{H}_r = \frac{1}{2}\hat{\boldsymbol{r}}^T\boldsymbol{H}^{(2)}_r\hat{\boldsymbol{r}} + \hat{\boldsymbol{r}}^T\boldsymbol{h}^{(1)}_r + h^{(0)}_r \quad \text{and} \quad \hat{H}_{qr} = \frac{1}{2}\hat{\boldsymbol{r}}^T\boldsymbol{H}^{(2)}_{qr}\hat{\boldsymbol{r}} + \hat{\boldsymbol{r}}^T\boldsymbol{h}^{(1)}_{qr} + h^{(0)}_{qr} \tag{4.71}$$

where $\boldsymbol{H}^{(2)}_r$ and $\boldsymbol{H}^{(2)}_{qr}$ are real symmetric matrices, $\boldsymbol{h}^{(1)}_r$ and $\boldsymbol{h}^{(1)}_{qr}$ are real-valued vectors, and $h^{(0)}_r$ and $h^{(0)}_{qr}$ are real-valued constants. In addition, the dissipation rates Γ_{jk} form a Hermitian matrix, $\boldsymbol{\Gamma} = \boldsymbol{\Gamma}^\dagger$. The phase-space PDE for the Wigner function can then be written as

$$\begin{aligned}\frac{\partial}{\partial t}W_{eg}(\boldsymbol{r}) = \Bigg[&- \boldsymbol{\partial r}^T\boldsymbol{\Omega h}^{(1)}_r - \frac{1}{2}\boldsymbol{\partial r}^T\left(\boldsymbol{\Omega}\text{Re}[\boldsymbol{\Gamma}]\boldsymbol{\Omega}\right)\boldsymbol{\partial r} - \boldsymbol{\partial r}^T\left(\boldsymbol{\Omega H}^{(2)}_r + \boldsymbol{\Omega}\text{Im}[\boldsymbol{\Gamma}]\right)\boldsymbol{r} \\ &- 2ih^{(0)}_{qr} - 2i\boldsymbol{r}^T\boldsymbol{h}^{(1)}_{qr} - \frac{i}{4}\boldsymbol{\partial r}^T\left(\boldsymbol{\Omega H}^{(2)}_{qr}\boldsymbol{\Omega}\right)\boldsymbol{\partial r} - i\boldsymbol{r}^T\boldsymbol{H}^{(2)}_{qr}\boldsymbol{r}\Bigg]W_{eg}(\boldsymbol{r}).\end{aligned} \tag{4.72}$$

In the above, taking $\boldsymbol{\Gamma}$ to be Hermitian allowed for the replacements $\text{Im}[\boldsymbol{\Gamma}] = -i(\boldsymbol{\Gamma} - \boldsymbol{\Gamma}^T)/2$ and $\text{Re}[\boldsymbol{\Gamma}] = (\boldsymbol{\Gamma} + \boldsymbol{\Gamma}^T)/2$, since the transpose is equal to element-wise conjugation of the matrix, $\boldsymbol{\Gamma}^T = \boldsymbol{\Gamma}^*$. The above PDE can be seen as a generalised Fokker-Planck equation, and so provided that the function is initially Gaussian, the solution will always be a Gaussian, albeit a complex unnormalised Gaussian function. As can be seen, the complex nature comes about due to qubit-coupling, which introduces imaginary terms into the PDE, and so the real part of the PDE comes entirely from the open-system dynamics within the harmonic mode system. Finally, transforming to Fourier space yields the following PDE for the characteristic function,

$$\begin{aligned}\frac{\partial}{\partial t}w_{eg}(\boldsymbol{\xi}) = \Bigg[&- i\boldsymbol{\xi}^T\boldsymbol{\Omega h}^{(1)}_r + \frac{1}{2}\boldsymbol{\xi}^T\left(\boldsymbol{\Omega}\text{Re}[\boldsymbol{\Gamma}]\boldsymbol{\Omega}\right)\boldsymbol{\xi} + \boldsymbol{\xi}^T\left(\boldsymbol{\Omega H}^{(2)}_r + \boldsymbol{\Omega}\text{Im}[\boldsymbol{\Gamma}]\right)\boldsymbol{\partial\xi} \\ &- 2ih^{(0)}_{qr} + 2\boldsymbol{\partial\xi}^T\boldsymbol{h}^{(1)}_{qr} + \frac{i}{4}\boldsymbol{\xi}^T\left(\boldsymbol{\Omega H}^{(2)}_{qr}\boldsymbol{\Omega}\right)\boldsymbol{\xi} + i\boldsymbol{\partial\xi}^T\boldsymbol{H}^{(2)}_{qr}\boldsymbol{\partial\xi}\Bigg]w_{eg}(\boldsymbol{\xi}).\end{aligned} \tag{4.73}$$

Substituting the expression for the characteristic function from Eq. (4.64) into the above expression, we can finally obtain time-dependent expressions for the moments.

4.2.2.2 Moment Differential Equations and Dephasing

For a system of N harmonic modes, the total set of differential equations involves $N(2N+1)$ ODEs for the complex covariances, $2N$ for the complex means, and a single ODE for υ. Prior works using the moment method considered specific single-mode systems and did not consider extending and generalising the method. The results here present a generalised system of equations that can be used to quickly generate systems of ODEs to calculate the induced backaction without having to churn through a phase space derivation for every unique system configuration. Since the number of ODEs grows quickly with the number of modes, we have expressed the system of ODEs as differential equations for $\boldsymbol{\sigma}$, $\boldsymbol{\mu}$, and υ. The result is a so-called Riccati matrix differential equation (RMDE) for the covariance matrix, and a simple linear matrix differential equation for $\boldsymbol{\mu}$. Details of this calculation can again be found in Appendix B, and the resulting equations of motion are:

$$\begin{aligned}\dot{\boldsymbol{\sigma}} &= \mathbf{A}\boldsymbol{\sigma} + \boldsymbol{\sigma}\mathbf{A}^T - \boldsymbol{\sigma}\mathbf{B}\boldsymbol{\sigma} + \mathbf{C} \\ \dot{\boldsymbol{\mu}} &= (\mathbf{A} - \boldsymbol{\sigma}\mathbf{B})\boldsymbol{\mu} + \mathbf{f} - \boldsymbol{\sigma}\mathbf{g} \\ \dot{\upsilon} &= -\varpi + \mathbf{g}^T\boldsymbol{\mu} + \frac{1}{2}\boldsymbol{\mu}^T\mathbf{B}\boldsymbol{\mu} + \frac{1}{2}\text{Tr}\left[\mathbf{B}\boldsymbol{\sigma}\right].\end{aligned} \tag{4.74}$$

The arrays in the above expressions can be written in terms of the elements of $\hat{H}_r$, $\hat{H}_{qr}$, and $\mathbf{\Gamma}$:

$$\begin{aligned} \mathbf{A} &= \mathbf{\Omega}\boldsymbol{H}_r^{(2)} + \mathbf{\Omega}\mathrm{Im}[\mathbf{\Gamma}] & \mathbf{B} &= 2i\boldsymbol{H}_{qr}^{(2)} & \mathbf{C} &= -\frac{i}{2}\mathbf{\Omega}\boldsymbol{H}_{qr}^{(2)}\mathbf{\Omega} - \mathbf{\Omega}\mathrm{Re}[\mathbf{\Gamma}]\mathbf{\Omega} \\ \mathbf{f} &= \mathbf{\Omega}\boldsymbol{h}_r^{(1)} & \mathbf{g} &= 2i\boldsymbol{h}_{qr}^{(1)} & \varpi &= -2ih_{qr}^{(0)}. \end{aligned} \tag{4.75}$$

Substituting in the expressions for the arrays in the above equations, we can write an equation for $\dot{\upsilon}(t)$ entirely in terms of the elements of $\hat{H}_{qr}$:

$$\frac{d}{dt}\upsilon(t) = i\left(2h_{qr}^{(0)} + 2\boldsymbol{\mu}^T\boldsymbol{h}_{qr}^{(1)} + \boldsymbol{\mu}^T\boldsymbol{H}_{qr}^{(2)}\boldsymbol{\mu} + \mathrm{Tr}\left[\boldsymbol{H}_{qr}^{(2)}\boldsymbol{\sigma}\right]\right). \tag{4.76}$$

Using Eq. (4.68), we can write explicit expressions for backaction terms, starting with the frequency shift

$$B(t) = 2h_{qr}^{(0)} + 2\mathrm{Re}[\boldsymbol{\mu}]^T\boldsymbol{h}_{qr}^{(1)} + \mathrm{Re}[\boldsymbol{\mu}]^T\boldsymbol{H}_{qr}^{(2)}\mathrm{Re}[\boldsymbol{\mu}] - \mathrm{Im}[\boldsymbol{\mu}]^T\boldsymbol{H}_{qr}^{(2)}\mathrm{Im}[\boldsymbol{\mu}] + \mathrm{Tr}\left[\boldsymbol{H}_{qr}^{(2)}\mathrm{Re}[\boldsymbol{\sigma}]\right]. \tag{4.77}$$

Analysis of the dephasing is more important for this work, and it can be understood to be comprised of two unique contributions, which we will term the *parasitic* and *measurement* dephasing:

$$\Gamma_{\mathrm{d}}(t) = \underbrace{-\left(2\mathrm{Im}[\boldsymbol{\mu}]^T\boldsymbol{h}_{qr}^{(1)} + \mathrm{Re}[\boldsymbol{\mu}]^T\boldsymbol{H}_{qr}^{(2)}\mathrm{Im}[\boldsymbol{\mu}] + \mathrm{Im}[\boldsymbol{\mu}]^T\boldsymbol{H}_{qr}^{(2)}\mathrm{Re}[\boldsymbol{\mu}]\right)}_{\Gamma_{\mathrm{d,m}}\text{ : measurement dephasing}} \underbrace{-\ \mathrm{Tr}\left[\boldsymbol{H}_{qr}^{(2)}\mathrm{Im}[\boldsymbol{\sigma}]\right]}_{\Gamma_{\mathrm{d,p}}\text{ : parasitic dephasing}}. \tag{4.78}$$

The parasitic dephasing only arises when the imaginary component of the covariance matrix is non-zero, and therefore is not always present. From the differential equation for $\boldsymbol{\sigma}$ in Eq. (4.74), it can be seen that the covariance matrix is entirely real only when $-\boldsymbol{\sigma}\mathbf{B}\boldsymbol{\sigma} + i\mathrm{Im}[\mathbf{C}] = 0$, which corresponds to the expression $4\boldsymbol{\sigma}\boldsymbol{H}_{qr}^{(2)}\boldsymbol{\sigma} = -\mathbf{\Omega}\boldsymbol{H}_{qr}^{(2)}\mathbf{\Omega}$. This is satisfied when the covariance matrix is that of the vacuum state, $\boldsymbol{\sigma} = \mathbf{I}_{2N}/2$. For this to occur, the coherent part of the dynamical matrix $\mathbf{A}$ can only contain passive phase shifters and beam splitters, so that $\mathbf{\Omega}\boldsymbol{H}_r^{(2)}$ is unitary. The modes must also be coupled to uncorrelated baths, which can only be sources of vacuum noise. Provided this is satisfied then $4\boldsymbol{\sigma}\boldsymbol{H}_{qr}^{(2)}\boldsymbol{\sigma} = \boldsymbol{H}_{qr}^{(2)}$, and so in addition, it is required that $\boldsymbol{H}_{qr}^{(2)} = -\mathbf{\Omega}\boldsymbol{H}_{qr}^{(2)}\mathbf{\Omega}$. The covariance matrix is then constant, $\dot{\boldsymbol{\sigma}} = 0$, resulting in no parasitic dephasing, so long as $\boldsymbol{H}_r^{(2)}$ and $\boldsymbol{H}_{qr}^{(2)}$ contain only passive processes.

Parasitic dephasing is thus absent when no squeezing or thermal noise is present, or else when there is no quadratic coupling between the qubit and the cavity system. This contribution to the dephasing is termed parasitic because it corresponds to additional measurements which are not observable in the displaced output field. This parasitic measurement can arise due to qubit state information being acquired by the phase and magnitude of the squeezed cavity state. For the measurement signal, this results in changes to the noise of the signal and not the displacement. The presence of thermal noise increases the variance in the intra-mode photon fluctuations, which can enhance the dephasing. This can, in turn, be used to measure the thermal occupation of the multimode system by observing the qubit dephasing [210]; since the qubit state measurement is not enhanced by the presence of thermal noise, we also consider this to be a parasitic measurement.

The measurement-induced dephasing comes from $\boldsymbol{\mu}$, and so is a result of the displacement of the internal fields of the harmonic modes. This is a combination of measurements from the quadratic, $\boldsymbol{H}_{qr}^{(2)}$, and linear, $\boldsymbol{h}_{qr}^{(1)}$, couplings. It is this component of the dephasing which provides an upper bound for the measurement rate, though in general it will always be larger, $\Gamma_{\mathrm{d,m}} \geq \Gamma_{\mathrm{meas}}$. The exact conditions that must be met for both rates to be identical have not yet been determined. Since the differential equation for $\boldsymbol{\mu}$ is dependent on $\boldsymbol{\sigma}$, the measurement-induced dephasing is dependent on the variance of the intra-mode fields, and by extension, the parasitic dephasing rate.

The system of ODEs in Eq. (4.74) is easily solved using numerical integration; however, obtaining analytic results is more difficult. If we assume that the dynamics rapidly approach a steady state during measurement, then it is possible in certain circumstances to obtain analytic results for the dephasing and frequency shift. The most difficult part is solving the steady state of the RMDE, commonly called the *continuous algebraic Riccati equation* (CARE). Specific details on solving the CARE are given in Appendix F, along with worked examples for relevant systems.

4.2.2.3 Pointer States

Calculating the dynamics of $\hat{\rho}_{eg}^r$ and $\hat{\rho}_{ge}^r$ is considerably more involved compared to the dynamics of the pointer states. The same moment method can be used to calculate the state of these intra-modal fields. Since T1-processes couple the two pointer states, as seen in Eq. (4.56), they alter the probabilities of the two pointer states over time, rendering the measurement non-QND. While T1-processes could be included when we calculated the dephasing, they must therefore be excluded in order for the mode system to be Gaussian. The ansatz for the reduced qubit master equation

takes on a slightly different form from Eq. (4.53):

$$\frac{d}{dt}\hat{\rho}^q = -\frac{i}{2}(\tilde{\omega}_q + B(t))[\hat{\sigma}_z, \hat{\rho}^q] + \frac{\Gamma_\varphi + \Gamma_\mathrm{d}(t)}{2}\mathcal{D}[\hat{\sigma}_z](\hat{\rho}^q). \tag{4.79}$$

The relevant coefficients in the expansion of the full density operator from Eq (4.45) can then be written as $\hat{\rho}_{ee}(t) = \hat{\rho}^r_{ee}(t)\rho^q_{ee}(0)$ and $\hat{\rho}_{gg}(t) = \hat{\rho}^r_{gg}(t)\rho^q_{gg}(0)$, where the coefficients $\rho^q_{ee}(0)$ and $\rho^q_{gg}(0)$ are constant, indicating that there are no transitions between the ground and excited states. The pointer states, $\hat{\rho}^r_{ee}$ and $\hat{\rho}^r_{gg}$, will correspond to true density operators by construction. Effective equations of motion can be written for these two elements in a similar manner to Eq. (4.63):

$$\frac{d}{dt}\hat{\rho}^r_{ee} = \mathcal{L}_r(\hat{\rho}^r_{ee}) - i[\hat{H}_{qr}, \hat{\rho}^r_{ee}] \quad \text{and} \quad \frac{d}{dt}\hat{\rho}^r_{gg} = \mathcal{L}_r(\hat{\rho}^r_{gg}) + i[\hat{H}_{qr}, \hat{\rho}^r_{gg}]. \tag{4.80}$$

These equations of motion are of Lindblad type, so we can use the moment expressions from Section 2.2.2:

$$\begin{aligned}\dot{\boldsymbol{\sigma}} &= \mathbf{A}\boldsymbol{\sigma} + \boldsymbol{\sigma}\mathbf{A}^T + \mathbf{C} \\ \dot{\boldsymbol{\mu}} &= \mathbf{A}\boldsymbol{\mu} + \mathbf{f}.\end{aligned} \tag{4.81}$$

The form of the arrays depends on the state of the qubit, which determines the sign of the qubit-harmonic mode Hamiltonian $\hat{H}_{qr}$:

$$\hat{\rho}^r_{kk}\,,\, k = e, g\,:\;\; \mathbf{A} = \boldsymbol{\Omega}\left(\boldsymbol{H}^{(2)}_r + \sigma_z \boldsymbol{H}^{(2)}_{qr}\right) + \boldsymbol{\Omega}\mathrm{Im}[\boldsymbol{\Gamma}] \qquad \mathbf{C} = -\boldsymbol{\Omega}\mathrm{Re}[\boldsymbol{\Gamma}]\boldsymbol{\Omega} \qquad \mathbf{f} = \boldsymbol{\Omega}\left(\boldsymbol{h}^{(1)}_r + \sigma_z \boldsymbol{h}^{(1)}_{qr}\right), \tag{4.82}$$

where $|e\rangle \to \sigma_z = +1$ and $|g\rangle \to \sigma_z = -1$. It is desirable to relate the moments of the two pointer states to those used to calculate the dephasing from Eq. (4.74). This relation is clear when using the previously discussed dressed frame approach to calculate the dephasing for dispersive measurement [197, 206], in which case the two pointer states are just coherent states. This relation can also be established using the moment method, where the dephasing can be extracted entirely from the displacement of the vacuum states. Since the pointer states have vacuum statistics, this comparison is simple, as there is no parasitic dephasing present. The inclusion of squeezing and thermal noise complicates the analysis, and so a direct connection in the case of non-vacuum statistics has not yet been established.

4.3 Dispersive Qubit Measurement with an Integrated Nonreciprocal Amplifier

Having introduced the measurement rate along with a general method to calculate the induced dephasing on a qubit from an integrated measurement device, we will now investigate how one can use a three-mode nonreciprocal amplifier to perform a dispersive qubit measurement. To begin, the three harmonic modes are passively coupled by three beam splitter interactions to form a loop which may be operated as a circulator. Amplification is realised by squeezing on mode a, hereafter called the *amplifier* mode. The displacement needed to determine the qubit state will come from a drive applied to mode b, which will therefore act as the interface between the on-chip components and the rest of the measurement chain. Mode b will therefore be termed the *buffer* mode. Finally, the qubit is located inside a resonator, and following the circuit QED model, is dispersively coupled to a single resonant mode, labelled mode c. The other two modes are engineered so as not to couple to the qubit, and therefore acquire qubit state information via the beam splitter coupling to the cavity mode. A clear choice of name for the dispersively coupled mode c is simply the *cavity* mode. The Hamiltonian for this setup is then

$$\begin{aligned}\hat{H}_{\triangledown} = {} & g_{ab}\left(\hat{a}^\dagger\hat{b} + \hat{a}\hat{b}^\dagger\right) + g_{bc}\left(\hat{b}^\dagger\hat{c} + \hat{b}\hat{c}^\dagger\right) + g_{ac}\left(e^{i\phi}\hat{a}^\dagger\hat{c} + e^{-i\phi}\hat{a}\hat{c}^\dagger\right) \\ & + \frac{\lambda}{2}\left(e^{i\theta}\hat{a}^{\dagger 2} + e^{-i\theta}\hat{a}^2\right) + \sqrt{\kappa_b}\,|\alpha|\left(e^{i\varphi}\hat{b}^\dagger + e^{-i\varphi}\hat{b}\right) + \chi\hat{c}^\dagger\hat{c}\hat{\sigma}_z + \frac{\tilde{\omega}_q}{2}\hat{\sigma}_z\end{aligned} \tag{4.83}$$

where $\hat{a}$, $\hat{b}$, and $\hat{c}$ are the bosonic mode operators. Additionally, the three bosonic modes are coupled to individual baths and so experience photon creation and annihilation due to thermal noise. The qubit is also modelled as an open system, and experiences dissipation and decay due to its bath couplings; however, we invoke the assumption that the decay rate is slow compared to the measurement rate and so remove it from the system dynamics. The Lindblad master equation for this open system is in the rotating frame, then

$$\frac{d}{dt}\hat{\rho} = -i[\hat{H}_{\triangledown}, \hat{\rho}] + \frac{\Gamma_\varphi}{2}\mathcal{D}[\hat{\sigma}_z](\hat{\rho}) + \sum_{z=a,b,c}\kappa_z\left((\bar{n}_z + 1)\mathcal{D}[\hat{z}](\hat{\rho}) + \bar{n}_z\mathcal{D}[\hat{z}^\dagger](\hat{\rho})\right). \tag{4.84}$$

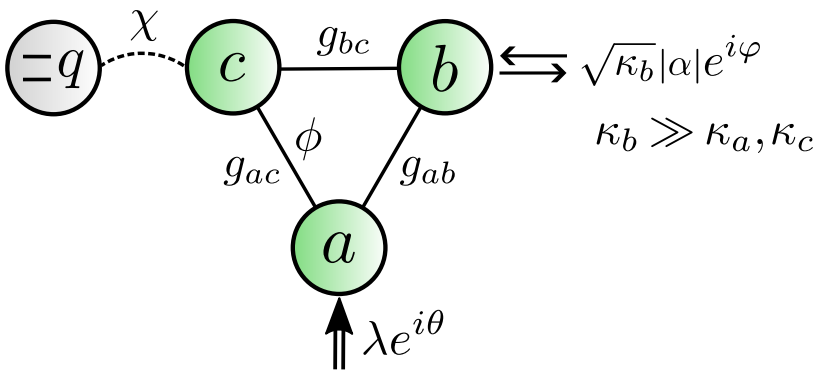

Figure 4.3: Mode diagram of the nonreciprocal amplifier which acts as our "measurement loop." The amplifier mode a, buffer mode b, and cavity mode c are all coupled parametrically via beam splitter interactions, g_{jk}. The tunable loop phase ϕ is placed on the interaction between the cavity and amplifier modes. Amplification is realised by the single-mode squeezer at the amplifier mode, which has its own amplitude λ and phase θ. A drive is applied to the buffer mode to create a displaced coherent state, with magnitude $\sqrt{\kappa_b}\,|\alpha|$ and phase φ. Since readout is performed through the buffer mode, its linewidth is much larger than the cavity and amplifier modes, $\kappa_b \gg \kappa_a, \kappa_c$. Lastly, the cavity mode is the only mode directly coupled to the qubit via a dispersive interaction, χ.

In order to properly operate this system, we must understand the effects of circulation and squeezing on the qubit measurement, which we will analyse separately. There are three physical properties which must be considered:

- Buffer Mode Output: Since this is a single-port measurement, the displaced coherent state created by the drive on the buffer mode must pass the cavity mode to acquire information about the qubit state, and then pass the amplifier mode to become a squeezed state, before returning to the buffer mode and leaving through its port to be measured. To ensure that the output of the buffer contains as much information as possible about the qubit state, the amount of the signal lost through the ports of the other two modes must be minimised.
- Minimising Measurement Backaction: The added noise from the amplifier mode will necessarily increase the total dephasing of the qubit, and therefore it is preferable that any signal leaving the amplifier mode be circulated away from the cavity mode.
- Optimising the Squeezing: To enhance the separation between the two pointer states, the phases of the drive and the amplifier must be appropriately chosen to enhance the difference between the two pointer states. The trade-off here is that the noise will be necessarily larger than that of a vacuum state if the measured quadrature is amplified, and so increasing the signal will also necessarily increase the noise component of the measurement rate.

The final point was answered in Eddins et al [209], where the effect of single-mode squeezing on a single cavity readout apparatus was investigated. The relevant results, and their application to our nonreciprocal amplifier, will be presented in Section 4.3.2. The first two points concern how the signals are circulated within the passive three-mode loop, and therefore can be answered by analysing the effect of a multimode circulator on dispersive qubit measurement. Such a measurement scheme has not yet been investigated, and as a result, we will first undertake a detailed analysis of the composite circulator-qubit system. Having completed that, will then bring the circulator and amplifier together.

4.3.1 Optimising The Mismatched Circulator

4.3.1.1 Balancing beam splitters and Dissipation

Operating the passive three-mode loop as a circulator requires that the coherent and dissipative processes be perfectly balanced to ensure that the input of one mode exits through the port of a neighbouring mode, thereby appearing in its output signal. This behaviour is useful when we wish to use the passive three-mode loop as a multiport device, but is not ideal when using the passive loop for a single-port measurement, since we wish for the signal to enter and exit through the same mode: the buffer mode. The input signal must therefore be reflected to the output of the buffer mode after traversing the loop. We will demonstrate here how the system parameters can be tuned to achieve this, beginning by showing how the usual choice of parameters fails through an analysis of the usual circulator scattering behaviour. This is more easily done in the basis of creation and annihilation operators, where for ease the operator

basis will be ordered as follows as $\hat{\boldsymbol{a}}_\circ = (\hat{a}, \hat{b}, \hat{c}, \hat{a}^\dagger, \hat{b}^\dagger, \hat{c}^\dagger)$. The Heisenberg-Langevin equations are then

$$\frac{d}{dt}\hat{\boldsymbol{a}}_\circ(t) = \tilde{\mathbf{A}}_\circ \hat{\boldsymbol{a}}_\circ(t) - \sqrt{\boldsymbol{\kappa}_\circ}\hat{\boldsymbol{a}}_{\circ,\mathrm{in}}(t) \tag{4.85}$$

where $\boldsymbol{\kappa}_\circ = \mathrm{diag}(\kappa_a, \kappa_b, \kappa_c, \kappa_a, \kappa_b, \kappa_c)$, and $\tilde{\mathbf{A}}_\circ$ is the following dynamical matrix:

$$\tilde{\mathbf{A}}_\circ = \begin{pmatrix} -\kappa_a/2 & -ig_{ab} & -ie^{i\phi}g_{ac} & 0 & 0 & 0 \\ -ig_{ab} & -\kappa_b/2 & -ig_{bc} & 0 & 0 & 0 \\ -ie^{-i\phi}g_{ac} & -ig_{bc} & -\kappa_c/2 - i\sigma_z\chi & 0 & 0 & 0 \\ 0 & 0 & 0 & -\kappa_a/2 & ig_{ab} & ie^{-i\phi}g_{ac} \\ 0 & 0 & 0 & ig_{ab} & -i\kappa_b/2 & ie^{-i\phi}g_{bc} \\ 0 & 0 & 0 & ie^{i\phi}g_{ac} & ig_{bc} & -\kappa_c/2 + i\sigma_z\chi \end{pmatrix}. \tag{4.86}$$

The dispersive coupling between the qubit and the cavity mode results in a shift of the resonant frequency of the cavity mode by $\pm\chi$, depending on whether the qubit is in the ground or excited state, $\sigma_z = \pm 1$. As a result, when calculating the scattering matrix, the resonance frequency is no longer $\omega = 0$ in the rotating frame. However, since the state of the qubit is unknown before the measurement, when calculating the scattering properties, we will split the difference between the resonance frequencies $\omega = \pm\chi$ of mode c, and so will continue to examine the behaviour of the scattering at zero frequency, $\omega = 0$. We then write the full scattering matrix in block form

$$\tilde{\mathbf{S}}_\circ = \begin{pmatrix} \mathbf{S}_\circ & \mathbf{0}_3 \\ \mathbf{0}_3 & \overline{\mathbf{S}}_\circ \end{pmatrix} \tag{4.87}$$

where $\mathbf{S}_\circ$ is the scattering matrix for the annihilation operator fields, and $\overline{\mathbf{S}}_\circ$is the scattering matrix for the creation operator fields, where these two matrices are by definition the element-wise complex conjugate of each other. We only need to consider one of the submatrices, and so pick the scattering matrix for the annihilation operator fields:

$$\mathbf{S}_\circ = \frac{1}{D}\begin{pmatrix} D + 2(1 + \mathcal{C}_{bc} + i\sigma_z\mathcal{X}) & \begin{matrix} -2\left(i\sqrt{\mathcal{C}_{ab}} + e^{i\phi}\sqrt{\mathcal{C}_{ac}\mathcal{C}_{bc}}\right) \\ +2\sigma_z\sqrt{\mathcal{C}_{ab}}\mathcal{X} \end{matrix} & -2\left(ie^{i\phi}\sqrt{\mathcal{C}_{ac}} + \sqrt{\mathcal{C}_{ab}\mathcal{C}_{bc}}\right) \\ \begin{matrix} -2\left(i\sqrt{\mathcal{C}_{ab}} + e^{-i\phi}\sqrt{\mathcal{C}_{ac}\mathcal{C}_{bc}}\right) \\ +2\sigma_z\sqrt{\mathcal{C}_{ab}}\mathcal{X} \end{matrix} & D + 2(1 + \mathcal{C}_{ac} + i\sigma_z\mathcal{X}) & -2\left(i\sqrt{\mathcal{C}_{bc}} + e^{i\phi}\sqrt{\mathcal{C}_{ab}\mathcal{C}_{ac}}\right) \\ -2\left(ie^{-i\phi}\sqrt{\mathcal{C}_{ac}} + \sqrt{\mathcal{C}_{ab}\mathcal{C}_{bc}}\right) & -2\left(i\sqrt{\mathcal{C}_{bc}} + e^{-i\phi}\sqrt{\mathcal{C}_{ab}\mathcal{C}_{ac}}\right) & D + 2(1 + \mathcal{C}_{ab}) \end{pmatrix} \tag{4.88}$$

where $D = -(1 + \mathcal{C}_{ab} + \mathcal{C}_{ac} + \mathcal{C}_{bc}) - i\sigma_z\mathcal{X}(1 + \mathcal{C}_{ab}) + 2i\sqrt{\mathcal{C}_{ab}\mathcal{C}_{ac}\mathcal{C}_{bc}}\cos(\phi)$.

Here, the cooperativities are $\mathcal{C}_{jk} := 4g_{jk}^2/\kappa_j\kappa_k$, and we have also defined a dimensionless parameter for the dispersive coupling strength by balancing it with the decay rate on the cavity mode, $\mathcal{X} := 2\chi/\kappa_c$. The loop phase controls the direction of the circulation within the passive three-mode loop. This can be realised in the above by setting the dispersive coupling to zero, $\mathcal{X} = 0$, and rendering every scattering process nonreciprocal by balancing the cooperativities using the relation $\mathcal{C}_{jk} = \mathcal{C}_{jl}\mathcal{C}_{lk}$, where (j, k, l) is some permutation of (a, b, c). When the three balancing conditions are met then every cooperativity must be equal to one, $\mathcal{C}_{jk} = 1$, meaning the rate of the beam splitter interaction is exactly balanced by the decay rates of the two coupled modes, $g_{jk}^2 = (\kappa_j/2)(\kappa_k/2)$. We can write the scattering matrices corresponding to the two optimal loop phases, $\phi = \pm\pi/2$, when no dispersive coupling is present, $\chi = 0$, as:

$$\phi = -\frac{\pi}{2} : \mathbf{S}_\circ = \begin{pmatrix} 0 & 0 & 1 \\ i & 0 & 0 \\ 0 & i & 0 \end{pmatrix} \qquad \phi = +\frac{\pi}{2} : \mathbf{S}_\circ = \begin{pmatrix} 0 & i & 0 \\ 0 & 0 & i \\ 1 & 0 & 0 \end{pmatrix}. \tag{4.89}$$

The two values of the loop phase therefore correspond to the following circulation directions within the loop:

$$\phi = -\frac{\pi}{2} : b \to c \to a \to b \qquad \phi = +\frac{\pi}{2} : b \to a \to c \to b. \tag{4.90}$$

Given the graphical configuration we have selected for the system, the circulation is *counter-clockwise* (CCW) when the loop phase is $\phi = -\pi/2$, and *clockwise* (CW) when $\phi = +\pi/2$.

The two circulator scattering matrices in Eq. (4.89) make it clear that for the purposes of qubit readout, we cannot operate the passive three-mode loop as a traditional circulator. By perfectly matching the beam splitter and decay rates, the input signal of one mode can be transmitted to the neighbouring mode, but because the decay rate is matched, this signal is immediately lost in the output channel of this neighbouring mode, and hence signal reflection

is not possible. In order to recover reflection in the output of buffer mode, there must therefore be some asymmetry between the strength of the beam splitters and the decay rates, $\mathcal{C}_{jk} \neq 1$; we will refer to this new mode of operation as the *mismatched circulator*.

If the decay rates are larger than the beam splitter couplings, indicating that $\mathcal{C}_{jk} < 1$, then the beam splitters are not strong enough to overcome the decay. There is increased reflection, but since this is just a result of the signal preferentially leaving through the same port immediately, there is no circulation around the loop, and any reflected signal will not contain much qubit information. To ensure that the beam splitters circulate the signal around the loop before it can be decayed away through the intermediate modes, it is required that $\mathcal{C}_{jk} > 1$. However, since the signal ideally only exits through the buffer mode, excess dissipation in the cavity and amplifier modes must be avoided. The decay rates for these two modes should therefore be small compared to the decay rate of the buffer mode. The amount of the reflected signal that we could hope to collect in the output can be determined by examining the magnitude of the scattering matrix element $(\mathrm{S}_\circ)_{bb}$; if this scattering element is less than one, then some loss has occurred within the loop. The magnitude squared is given since the expression is simpler:

$$\left|(\mathrm{S}_\circ)_{bb}\right|^2 = \frac{(-1+\mathcal{C}_{ab}+\mathcal{C}_{bc}-\mathcal{C}_{ac})^2+\mathcal{X}^2(1-\mathcal{C}_{ab})^2}{(1+\mathcal{C}_{ab}+\mathcal{C}_{bc}+\mathcal{C}_{ac})^2+\mathcal{X}^2(1+\mathcal{C}_{ab})^2}. \tag{4.91}$$

For finite parameter values we can see that the above scattering amplitude is always less than one, $\left|(\mathrm{S}_\circ)_{bb}\right|^2 < 1$, and additionally, that it vanishes exactly for the circulator cooperativity values of $\mathcal{C}_{jk} = 1$. This confirms that no qubit information can be collected by this port when no signal is reflected. It can also be seen from this expression that the amplitude of the reflected signal approaches one as the cooperativities are increased, as expected. This behaviour indicates that, even in the ideal case, some qubit information will always be lost on the way to the buffer mode, resulting in a measurement which can never be perfectly efficient. This will be confirmed when the measurement efficiency is calculated in a subsequent section.

4.3.1.2 Nonreciprocity and Measurement Backaction

Circulation in the passive loop is a result of nonreciprocal scattering between all mode pairs, and although perfect circulation inhibits qubit readout for a one-port device, we would still like to keep some nonreciprocity between the modes. The hope is that by diverting excess noise away from the dispersively coupled cavity mode, and by extension, away from the qubit, measurement backaction on the qubit can be minimised. To this end, we will examine the measurement-induced dephasing on the qubit at the necessary loop phases, $\phi = \pm\pi/2$. We assume that there is thermal noise at the input of every harmonic mode in the loop. As a result, parasitic dephasing will also be present; however, the analytic expression for $\Gamma_{\mathrm{d,p}}$ is far too complicated and so it may only be analysed through numerical computation. The measurement-induced dephasing for the ideal loop phase, on the other hand, may be expressed as follows,

$$\Gamma_{\mathrm{d,m}} = \frac{8\left|\alpha\right|^2\mathcal{X}^2 Z_{\mathrm{th}}\left(\mathrm{sgn}(\phi)\sqrt{\mathcal{C}_{ab}\mathcal{C}_{ac}}-\sqrt{\mathcal{C}_{bc}}\right)^2}{\left(\left(1+\mathcal{C}_{ab}+\mathcal{C}_{bc}+\mathcal{C}_{ac}\right)^2-\mathcal{X}^2\left(1+\mathcal{C}_{ab}\right)^2\right)^2+4\mathcal{X}^2Z_{\mathrm{th}}^2} \tag{4.92}$$

$$Z_{\mathrm{th}} = (2\bar{n}_a+1)\left(\sqrt{\mathcal{C}_{ab}\mathcal{C}_{bc}}+\mathrm{sgn}(\phi)\sqrt{\mathcal{C}_{ac}}\right)^2+(2\bar{n}_b+1)\left(\mathrm{sgn}(\phi)\sqrt{\mathcal{C}_{ab}\mathcal{C}_{ac}}-\sqrt{\mathcal{C}_{bc}}\right)^2+(2\bar{n}_c+1)\left(1+\mathcal{C}_{ab}\right)^2.$$

The function $\mathrm{sgn}(\phi)$ is a convenient shorthand to represent the global change in phase for the two optimal loop phases. The conditions for nonreciprocal scattering can be obtained from the matrix Eq. (4.88) when the qubit coupling is turned off, so there is no dispersive detuning, and are summarised in the following table:

Balance Condition	Cooperativity Condition	$\phi = -\pi/2$	$\phi = +\pi/2$
$g_{ab}\kappa_c/2 = g_{ac}g_{bc}$	$\mathcal{C}_{ab} = \mathcal{C}_{ac}\mathcal{C}_{bc}$	$a \to b$	$a \leftarrow b$
$g_{bc}\kappa_a/2 = g_{ab}g_{bc}$	$\mathcal{C}_{bc} = \mathcal{C}_{ab}\mathcal{C}_{ac}$	$b \to c$	$b \leftarrow c$
$g_{ac}\kappa_b/2 = g_{ab}g_{ac}$	$\mathcal{C}_{ac} = \mathcal{C}_{ab}\mathcal{C}_{bc}$	$c \to a$	$c \leftarrow a$

. (4.93)

As previously stated, the conditions which control the scattering to and from the cavity mode are of most interest to us, so we will start by applying the conditions individually. The effect of nonreciprocal scattering between the buffer and amplifier modes, b and a, will therefore be ignored.

We start by realising nonreciprocal scattering between modes a and c. The expressions reveal that when the scattering has direction $c \to a$, the thermal and vacuum noise terms from mode a drop out of the measurement

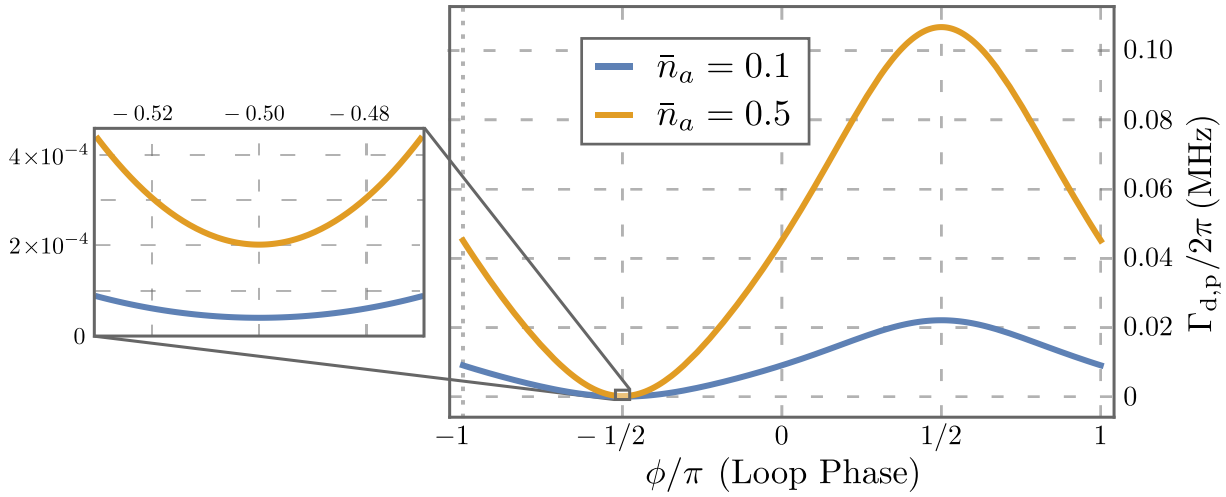

Figure 4.4: Parasitic dephasing $\Gamma_{\mathrm{d,p}}$ of the mismatched circulator due to thermal noise in mode a, $\bar{n}_a = 0.1$ (blue) and $\bar{n}_a = 0.5$ (orange), plotted as a function of the loop phase ϕ. All other thermal noise sources are in the vacuum state, $\bar{n}_b = 0$ and $\bar{n}_c = 0$. Decay rates for the three modes are $\kappa_a/2\pi = 0.2\,\mathrm{MHz}$, $\kappa_b/2\pi = 40.0\,\mathrm{MHz}$, and $\kappa_c/2\pi = 0.2\,\mathrm{MHz}$. The beam splitter rates are $g_{ab}/2\pi = 5.0\,\mathrm{MHz}$, $g_{bc}/2\pi = 5.0\,\mathrm{MHz}$, and $g_{ac}/2\pi = 1.25\,\mathrm{MHz}$. Qubit and mode c are coupled dispersively, $\chi/2\pi = 2.5\,\mathrm{MHz}$. Cooperativities are given by $\mathcal{C}_{ab} = 12.5$, $\mathcal{C}_{bc} = 12.5$, and $\mathcal{C}_{ac} = 156.25 = 12.5^2$. The cooperativities are balanced to ensure nonreciprocal scattering, $c \to a$ when $\phi = -\pi/2$, and $a \to c$ when $\phi = +\pi/2$.

dephasing, which may be written in this instance as

$$\mathcal{C}_{ac} = \mathcal{C}_{ab}\mathcal{C}_{bc}\,,\ \phi = -\frac{\pi}{2}\ :\ \Gamma_{\mathrm{d,m}} = \frac{8\,|\alpha|^2\,\mathcal{X}\,(\mathcal{C}_{bc}(\bar{n}_b+1)+(\bar{n}_c+1))}{\left((1+\mathcal{C}_{bc})^2-\mathcal{X}^2\right)^2+4\mathcal{X}^2\,(\mathcal{C}_{bc}(\bar{n}_b+1)+(\bar{n}_c+1))^2}. \tag{4.94}$$

This is in fact the measurement-induced dephasing that is obtained when all couplings to mode a are turned off, that is $\mathcal{C}_{ab}$ and $\mathcal{C}_{ac} = 0$. As a result, as far as the measurement-induced dephasing is concerned, there is no mode a in the measurement system. It is surprising that it is possible to cancel the contribution from mode a exactly here due to the detuning of mode c shifting the resonance frequency. If we examine the parasitic dephasing, shown in Figure 4.4 as a function of the loop phase, the effect of thermal noise from mode a is still present. This indicates that it is not possible to exactly cancel the backaction from this source of noise, which we can interpret to be a result of the finite bandwidth of the nonreciprocal behaviour along with the dispersive shift detuning the system from resonance. Here we can see that the parasitic dephasing due to $\bar{n}_a$ is minimised but still non-zero when the scattering has direction $c \to a$, and is maximised for the opposite direction of the nonreciprocal scattering, $a \to c$.

Although similar behaviour is observed when realising nonreciprocal scattering between the buffer and cavity modes, b and c, there is one major difference in this case: not only is the contribution due to thermal noise from b on the measurement dephasing cancelled, the measurement dephasing itself is exactly zero when the scattering has direction $c \to b$. Since photons from the drive enter the loop through the buffer mode, this behaviour is expected; if the displaced photons can never reach mode c then they can never dephase the qubit. For the opposite direction, $b \to c$, the displaced drive photons are directed to mode c, and hence the measurement-induced dephasing is always non-zero. The ability to set the measurement dephasing to zero by cancelling noise coming from the buffer mode is not useful, since this implies that the measurement rate must also be zero. In fact, it will be seen in the next section that the measurement rate will go to zero for both directions of nonreciprocal scattering between the cavity and buffer modes.

Finally, the above expressions indicate that it is not possible to cancel the thermal noise from c, since this mode is coupled directly to the qubit. We can therefore conclude that the best we can do is to redirect noise from mode a. Since this will act as the amplifier mode, it is critical that we are able to redirect noise from this mode so as to minimise backaction on the qubit. Having covered the backaction, we can now examine the effect of nonreciprocity on the measurement efficiency of the circulator.

4.3.1.3 Measurement Efficiency of the Mismatched Circulator

While in the previous section we were focused on decreasing the excess dephasing on the qubit due to thermal noise, the goal here is to see what sort of asymmetry can be expected between the measurement rate and the measurement dephasing. Since only the signal from the buffer mode contributes to the measurement, the steady-state measurement

operator evaluated on resonance, $\omega = 0$, may be written as a combination of the respective output quadratures

$$\hat{M}[0] = \cos(\vartheta)\hat{q}_{b,\mathrm{out}}[0] + \sin(\vartheta)\hat{p}_{b,\mathrm{out}}[0]. \tag{4.95}$$

To maximise the signal, the phase of the measurement operator is chosen using the ideal weights from Eq. (4.35), where it may be determined that for the ideal values of the loop phase, the optimal phase for the measurement operator happens to coincide with the phase of the drive applied to the buffer mode, $\vartheta = \varphi$. The trade-off in reducing the measurement backaction using nonreciprocal scattering is that the extra noise, which is directed away from the cavity mode, must go somewhere, and so instead ends up in the measurement signal leaving through the buffer mode port, thereby reducing the measurement rate. We must therefore find a way to enhance the strength of the measurement signal to make the measurement rate robust against the extra noise.

In order to determine the optimum behaviour of the measurement, from this point we set the thermal noise in every mode to zero, so all sources of input noise are only vacuum noise. In this case, the measurement rate is identical for both values of the loop phase, $\phi = \pm\pi/2$. Using Eq. (4.37), and assuming that no noise is added by off-chip processes, the measurement rate can be expressed as:

$$\Gamma_{\mathrm{meas}} = \frac{8\left|\alpha\right|^2 \mathcal{X}^2(\mathcal{C}_{ab}\mathcal{C}_{ac} - \mathcal{C}_{bc})^2}{\left((1 + \mathcal{C}_{ab} + \mathcal{C}_{bc} + \mathcal{C}_{ac})^2 + \mathcal{X}^2\left(1 + \mathcal{C}_{ab}\right)^2\right)^2}. \tag{4.96}$$

We can see that the measurement rate is zero when the cooperativities are balanced to ensure that the scattering between the buffer mode b and the cavity mode c is nonreciprocal, $\mathcal{C}_{bc} = \mathcal{C}_{ab}\mathcal{C}_{ac}$. This can be easily explained for both scattering directions. When $c \to b$, no displacement ever reaches the cavity mode, and so the output cannot contain any qubit information, whereas if $b \to c$, the displaced signal does acquire qubit state information; however, the signal never makes it back to the output of the buffer mode. In both cases, no information about the qubit state is present in the output signal of the buffer mode.

We also work out the measurement dephasing, which is the only contribution to the total dephasing from the measurement loop in the absence of thermal noise:

$$\Gamma_{\mathrm{d}} = \frac{8\left|\alpha\right|^2 \mathcal{X}^2\left(\mathrm{sgn}(\phi)\sqrt{\mathcal{C}_{ab}\mathcal{C}_{ac}} - \sqrt{\mathcal{C}_{bc}}\right)^2(1 + \mathcal{C}_{ab})(1 + \mathcal{C}_{ab} + \mathcal{C}_{bc} + \mathcal{C}_{ac})}{\left((1 + \mathcal{C}_{ab} + \mathcal{C}_{bc} + \mathcal{C}_{ac})^2 + \mathcal{X}^2\left(1 + \mathcal{C}_{ab}\right)^2\right)^2}. \tag{4.97}$$

The measurement rate and dephasing are shown in Figure 4.5 as functions of the loop phase. The behaviour of the measurement dephasing shows that, even though the conditions for circulation are not met here, there is still a preferred direction for circulating the photons around the passive loop. This is evidenced by the fact that the dephasing is higher for $\phi = -\pi/2$, where photons are preferentially circulated in the CCW direction, and so are directly swapped to the cavity mode after entering the buffer mode. When $\phi = +\pi/2$, where the photons preferentially move CW in the loop, the photons pass by mode a first, and hence some are decayed away. Therefore, fewer photons reach the dispersively coupled c mode when circulation is preferentially in the CW direction as compared to the CCW direction. This results in different values for the displacement of the c mode state, and as a consequence, there is less measurement-induced dephasing when the displaced measurement signal from mode b passes by mode a first.

The measurement rate, on the other hand, is identical for both directions because the average photon loss experienced by the measurement signal is independent of the direction of the signal through the loop, so that the same number of photons exit the buffer mode. Since the noise is always vacuum, this means that the total displacement of the measurement signal is identical for both directions of circulation, and in fact, the displacement will always be independent of the sign on the loop phase, even when thermal noise and squeezing are introduced. Things are different for the noise, since the rotation of the cavity state by the dispersively coupled qubit means that, in principle, it is different for the two directions of circulation. This will not be the case for measurements performed on passive systems with thermal noise from the inputs, such as this one, since the variance of the cavity states is the same along every quadrature axis. Asymmetry in the noise of the measurement signal is therefore only expected to become relevant when amplification is introduced, since the variances will be squeezed along different axes in phase space.

To determine how we can best maximise the measurement rate in comparison to the dephasing, we turn to the measurement efficiency:

$$\eta = \frac{\Gamma_{\mathrm{meas}}}{\Gamma_{\mathrm{d}}} = \frac{\left(\mathrm{sgn}(\phi)\sqrt{\mathcal{C}_{ab}\mathcal{C}_{ac}} + \sqrt{\mathcal{C}_{bc}}\right)^2}{\left(1 + \mathcal{C}_{ab} + \mathcal{C}_{bc} + \mathcal{C}_{ac}\right)\left(1 + \mathcal{C}_{ab}\right)}. \tag{4.98}$$

This expression only applies when $\mathcal{C}_{bc} \neq \mathcal{C}_{ab}\mathcal{C}_{ac}$ since otherwise the measurement rate, and hence the measurement efficiency, would be zero. For physical values of the cooperativity, $\mathcal{C}_{jk} > 0$, it is not possible for the measurement to be perfectly efficient, and so $\eta < 1$. This is to be expected since some photons carrying information about the qubit

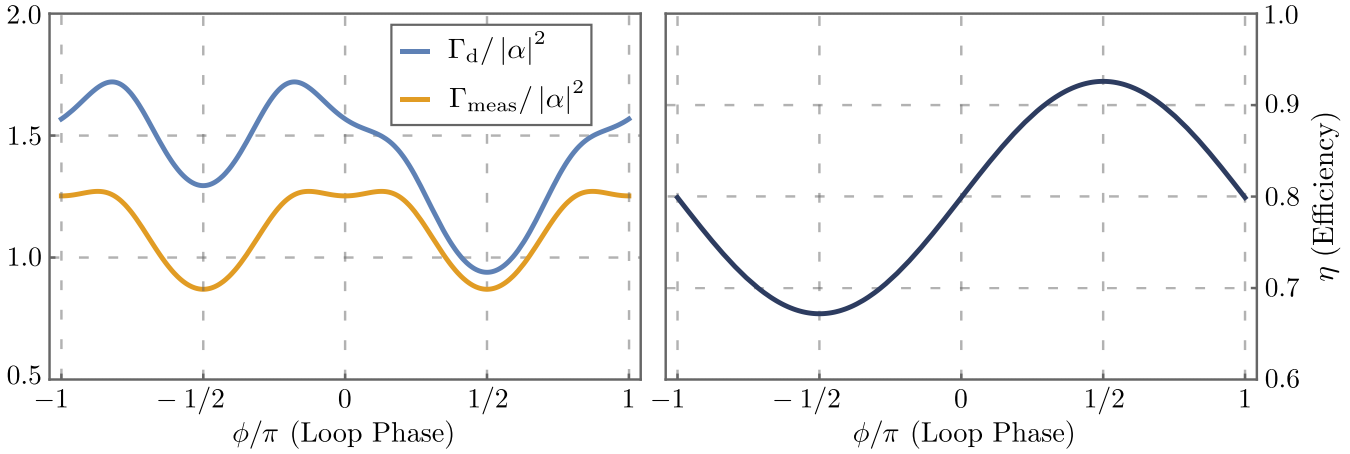

Figure 4.5: [Left] Measurement-induced dephasing $\Gamma_{d,m}/|\alpha|^2$ (orange) and measurement rate $\Gamma_{meas}/|\alpha|^2$ (blue) of the mismatched circulator normalised by the strength of the drive, and hence unitless, plotted as a function of the loop phase ϕ. [Right] The corresponding measurement efficiency, $\eta = \Gamma_{meas}/\Gamma_{d,m}$, is also plotted against the loop phase. Thermal noise contributions are zero for all modes: $\bar{n}_a$, $\bar{n}_b$, $\bar{n}_c = 0$, and no additional off-chip noise has been included. All other physical parameters are identical to those in Figure 4.4.

state will be lost when travelling from the cavity mode to the buffer mode, and so the measurement rate must always be lower than the rate of dephasing.

Since we wish to make the scattering between modes a and c nonreciprocal, we now apply the condition $\mathcal{C}_{ac} = \mathcal{C}_{ab}\mathcal{C}_{bc}$ to the measurement efficiency:

$$\phi = -\frac{\pi}{2} : \eta = \frac{(1-\mathcal{C}_{ab})^2\mathcal{C}_{bc}}{(1+\mathcal{C}_{ab})^2(1+\mathcal{C}_{bc})} \qquad \phi = +\frac{\pi}{2} : \eta = \frac{\mathcal{C}_{bc}}{1+\mathcal{C}_{bc}}. \tag{4.99}$$

In both cases, we can see that the measurement efficiency will approach unity $\eta \to 1$ as $\mathcal{C}_{ab}, \mathcal{C}_{bc} \to \infty$; since the value of $\mathcal{C}_{ac}$ is tied to the other two cooperativities, improved measurement efficiency requires that it grow faster than $\mathcal{C}_{ab}$ and $\mathcal{C}_{bc}$. In this parameter regime, the strength of the beam splitters is much larger than the decay rates, and so the displaced photons will make it back to the buffer mode to be measured faster than they can be decayed away in the other two modes. Since more photons are measured, the measurement rate can approach the dephasing rate, thereby improving the efficiency of the measurement. The efficiency for CCW circulation is dependent on $\mathcal{C}_{ab}$, unlike CW circulation, since the photons containing qubit information must first pass mode a, and so the measurement efficiency is attenuated.

Finally, it is not only the cooperativities which must be balanced to maximise the measurement rate. We recall from Section 4.1.3.5, that the ratio of the dispersive coupling and the linewidth of the dispersively coupled c mode, $2\chi/\kappa_c =: \mathcal{X}$, should also be considered when examining the measurement rate. There exists a critical ratio marking the transition from the weak to strong dispersive measurement regimes where the measurement rate is maximised. In the case of the measurement loop, the other two modes act to modify the effective linewidth and detuning on mode c. As a result, the optimum ratio between the innate cavity linewidth and detuning, $\kappa_c/2$ and χ, is $\mathcal{X} = (1+\mathcal{C}_{ab}+\mathcal{C}_{bc}+\mathcal{C}_{ac})/(1+\mathcal{C}_{ab})$. If the beam splitters between the modes are set to zero, the standard ratio $\mathcal{X} = 1$ is obtained.

4.3.2 Adding Amplification

With the behaviour of the mismatched circulator fully characterised, we can now add single-mode squeezing to the system to turn the three-mode measurement loop into a nonreciprocal amplifier. There are two new parameters which must be optimised here for the purposes of improving qubit measurement. The first is the phase of the single-mode squeezing, which controls which quadrature is squeezed and which is amplified, or anti-squeezed. The second property is the magnitude of the single-mode squeezing, which is tied to the amount of gain of the output signal, but is also constrained to ensure that the system is stable.

As previously mentioned, the presence of parametric amplification at the measurement mode was first discussed in Eddins et al [209]. In the paper, it was found that increasing the amount of single-mode squeezing, and hence the gain of the amplifier, led to a higher measurement rate along with an increase in the parasitic and measurement-induced dephasing rates. The increase in the parasitic dephasing could be compensated for by applying a stronger measurement

drive, where the larger drive amplitude naturally increased both the measurement rate and the measurement-induced dephasing, and resulted in the parasitic dephasing becoming a comparatively smaller part of the total induced dephasing. Higher efficiency could therefore be achieved through a combination of driving and single-mode squeezing. This is limited in practice, however, since a strong drive resulted in nonlinear effects, and stimulated transitions to higher energy levels of the transmon, thereby leading to a breakdown of the system model. It was also found that the increased amount of noise in the measurement signal due to the amplification was, in fact, not detrimental to the overall measurement efficiency. The reason was that the amplified noise in the measured quadrature overwhelmed the off-chip noise, and so it was important to improve the overall measurement efficiency.

4.3.2.1 Drive and Amplifier Phase

With this in mind, we start by examining the interplay between the phases of the drive, the amplifier, and the passive loop. The goal is to establish how the different components of the nonreciprocal amplifier shift and rotate the signal as it moves through the loop. For the two loop phases, $\phi = \pm\pi/2$, we provide a heuristic picture to explain the interplay between the drive and amplification by tracking the behaviour of the displaced signal as it circulates in its preferred direction around the loop. It must be emphasised that this is only a rough explanation; although there is a preferred direction of circulation, in reality, there are counter-propagating signals in the circuit, and it is their interference which gives rise to the steady-state behaviour.

Phase Space Description of the Interactions

Starting with the simplest component, the drive $e^{i\varphi}\hat{b}^\dagger + e^{-i\varphi}\hat{b}$, this term displaces the buffer mode Wigner function along the vector defined by $(q_b, p_b) = (\cos(\varphi - \pi/2), \sin(\varphi - \pi/2))$ in phase space. For example, if the drive phase is $\varphi = 0$ then the displacement in phase space will be along the negative p_b-axis. The effect of the beam splitter interaction $e^{i\phi}\hat{a}_j^\dagger\hat{a}_k + e^{-\phi}\hat{a}_j\hat{a}_k^\dagger$ is to swap the distribution between the two modes a_j and a_k. The exact behaviour is not important, and for the purpose of this explanation, it is only relevant that when the phase is $\phi = 0$ the Wigner distribution is rotated into an orthogonal axis as it is swapped to the other mode, whereas the distribution will be swapped to a parallel axis when the phase is $\phi = \pm\pi/2$.

The final interaction we have to consider is the single-mode squeezer, $e^{i\theta}\hat{a}^{\dagger 2} + e^{-i\theta}\hat{a}^2$. Here, amplification is along the axis $(q_a, p_a) = (\cos[\frac{1}{2}(\theta+\pi/2)], \sin[\frac{1}{2}(\theta+\pi/2)])$, and so the Wigner function will be squeezed along the orthogonal axis, $(q_a, p_a) = (\cos[\frac{1}{2}(\theta-\pi/2)], \sin[\frac{1}{2}(\theta-\pi/2)])$. If the amplifier phase is $\theta = \pi/2$, the amplification will be along the q_a-axis, and so the squeezing is along the p_a-axis. As a result, any displacement parallel to the q_a-axis will be enhanced, whereas any displacement in the p_a-axis is shrunk due to the squeezing. Correspondingly, the variance of the Wigner function will increase along the q_a-axis, and will become narrower along the p_a-axis. When the amplifier phase is set to $\theta = -\pi/2$, the behaviour is reversed, so that the amplification is along the p_a-axis, and the squeezing is along the q_a-axis.

Evolution of the Circulating Signal

We can now explain the ideal behaviour for each direction of circulation. We will start with the counter-clockwise circulation around the loop, corresponding to the loop phase $\phi = -\pi/2$. We recall that this results in preferred circulation of the signal from the buffer mode, to the cavity mode, to the amplifier mode, and then back to the buffer mode. A graphical representation is provided in Figure 4.6. To start, a drive with phase φ is applied to the buffer mode, creating a coherent state displaced in the $(q_b, p_b) = (\cos(\varphi - \pi/2), \sin(\varphi - \pi/2))$ direction. As this displaced state is swapped to the cavity mode, it is rotated and so lies along $(q_c, p_c) = (\cos(\varphi - \pi), \sin(\varphi - \pi))$. The dispersive coupling to the qubit proceeds to rotate the coherent state as it sits in the cavity mode, so that the acquired displacement that allows us to discriminate between the two qubit states is along the orthogonal axis, $(q_c, p_c) = (\cos(\varphi-\pi/2), \sin(\varphi-\pi/2))$. The Wigner function is then swapped by the beam splitter to the amplifier mode, where the difference between the pointer-state Wigner functions now lies along the $(q_a, p_a) = (\cos(\varphi-\pi/2), \sin(\varphi-\pi/2))$ axis. To enhance the displacement between these two states, the amplification must be applied along this axis, and therefore the phase of the single-mode squeezing must be $\theta = 2\varphi - \pi/2$. Finally, the third beam splitter swaps the state back to the buffer mode, where the separation between the pointer states is now along the $(q_b, p_b) = (\cos(\varphi), \sin(\varphi))$ axis. In order to maximise the measurement efficiency, the measurement quadrature should therefore have the same phase as the original drive.

Things are slightly different when the signal propagates clockwise through the loop, corresponding to a loop phase of $\phi = +\pi/2$. Here, the coherent state in the buffer mode is first swapped to the amplifier mode. The coherent state therefore lies along the $(q_a, p_a) = (\cos(\varphi - \pi), \sin(\varphi - \pi))$ axis when it is swapped to the amplifier mode. Since it has not acquired any qubit information, the optimal behaviour of the amplifier is to maximise the displacement, so the amplification should be applied along the same axis as the displacement, and hence the single-mode squeezing should have the phase $\theta = 2\varphi + \pi/2$. The amplified signal is then swapped to the dispersively coupled cavity mode,

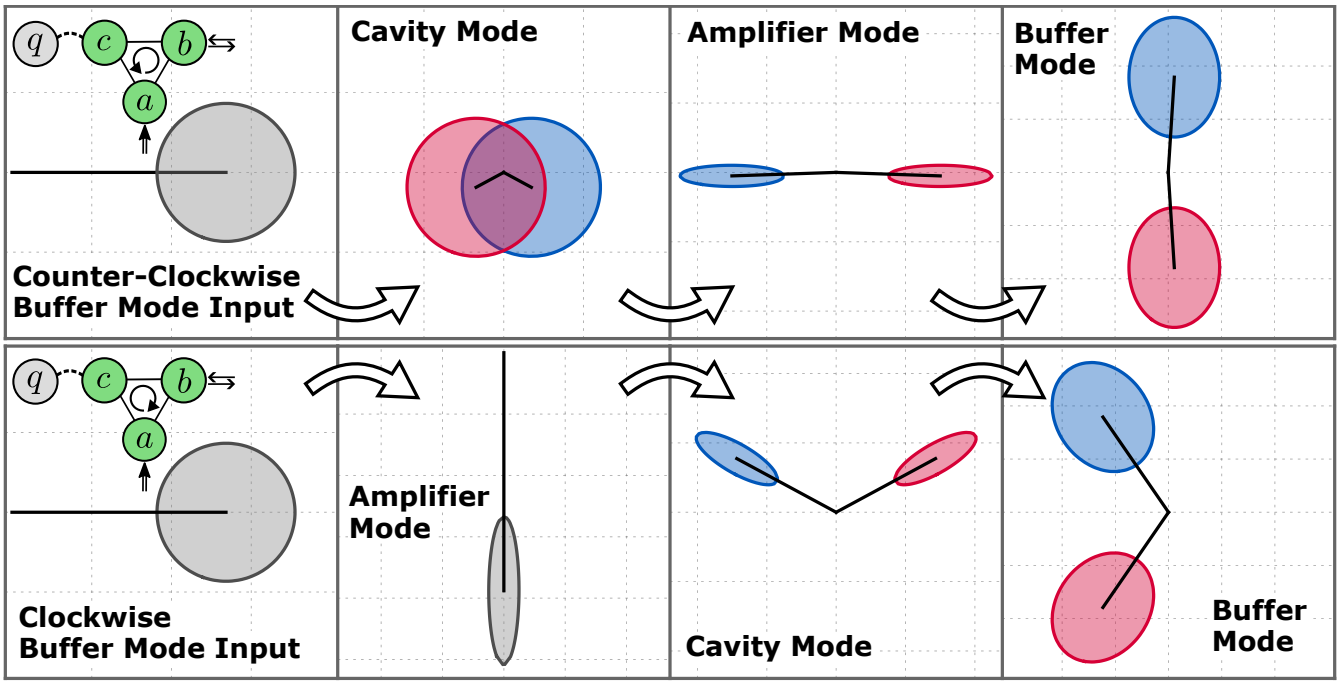

Figure 4.6: Wigner distribution confidence ellipses of the modes for the two circulation directions.
[Top] Counter-clockwise circulation: the initial coherent state entering the buffer mode is swapped to the cavity mode, where it rotates as a result of the dispersively coupled qubit. The signal is then amplified in the amplifier mode, and then this amplified signal is swapped to the buffer mode. There is an attenuation of the displacement and squeezing of the pointer state when swapping from the amplifier to the buffer mode. [Bottom] Clockwise circulation: the initial coherent state entering the buffer mode is swapped to the amplifier mode, where it is amplified. The signal then moves to the cavity mode, where the dispersive measurement of the qubit occurs, and then is swapped to the buffer mode. The displacement and squeezing of the final pointer state in the buffer mode are again attenuated.

acquires some qubit information, and then is swapped back to the buffer mode, where the signal now lies along the $(q_b, p_b) = (\cos(\varphi - \pi), \sin(\varphi - \pi))$ axis.

Although this explanation is not exact, the steady-state Wigner distributions of the various modes do closely correspond to those in Figure 4.6. In particular, the distribution of the amplifier mode shows almost no dependence on the qubit state for CW circulation, and the distribution for the cavity mode is nearly that of a vacuum state for CCW circulation. Since the true behaviour is very close to the ideal, we can make some predictions regarding the induced dephasing and measurement rate. We expect that the total induced dephasing is much larger for CW circulation compared to CCW circulation since the cavity mode state is highly squeezed in the former, and is nearly the vacuum state for the latter. Comparatively, the amount of noise in the measurement is expected to be larger for CCW circulation than for CW circulation since the qubit information is acquired after passing the single-mode squeezer when circulating CW, and so the noise seen in the measured quadrature is somewhere between perfectly amplified and squeezed noise. Since the single-mode squeezer is passed after the qubit measurement for CCW circulation, the noise in the measured quadrature is ideally amplified and squeezed for the orthogonal quadrature. The signal for both directions is the same, as will be shown in Section 4.3.3, meaning that more noise will be present in the measurement for CCW circulation, which will result in a lower measurement rate.

4.3.2.2 Stability and Amplifier Gain

Having thoroughly described the phase behaviour of the nonreciprocal amplifier, we will now provide limits on the amplitude of the squeezing. These limits come from the requirement that our system be stable, which is guaranteed if the normal modes have positive decay rates. To determine whether this is the case, we start with the dynamical matrix of the nonreciprocal amplifier, written in the quadrature basis given by $\hat{\boldsymbol{r}} = (\hat{q}_a, \hat{p}_a, \hat{q}_b, \hat{p}_b, \hat{q}_c, \hat{p}_c)$:

$$\mathbf{A}_{\triangledown} = \begin{pmatrix} -(\kappa_a/2)\mathbf{I} + \lambda(-\cos(\theta)\mathbf{X} + \sin(\theta)\mathbf{Z}) & g_{ab}\mathbf{J} & g_{ac}(\cos(\phi)\mathbf{J} + \sin(\phi)\mathbf{I}) \\ g_{ab}\mathbf{J} & -(\kappa_b/2)\mathbf{I} & g_{bc}\mathbf{J} \\ g_{ac}(\cos(\phi)\mathbf{J} - \sin(\phi)\mathbf{I}) & g_{bc}\mathbf{J} & -(\kappa_c/2)\mathbf{I} + \sigma_z\chi\mathbf{J} \end{pmatrix}. \tag{4.100}$$

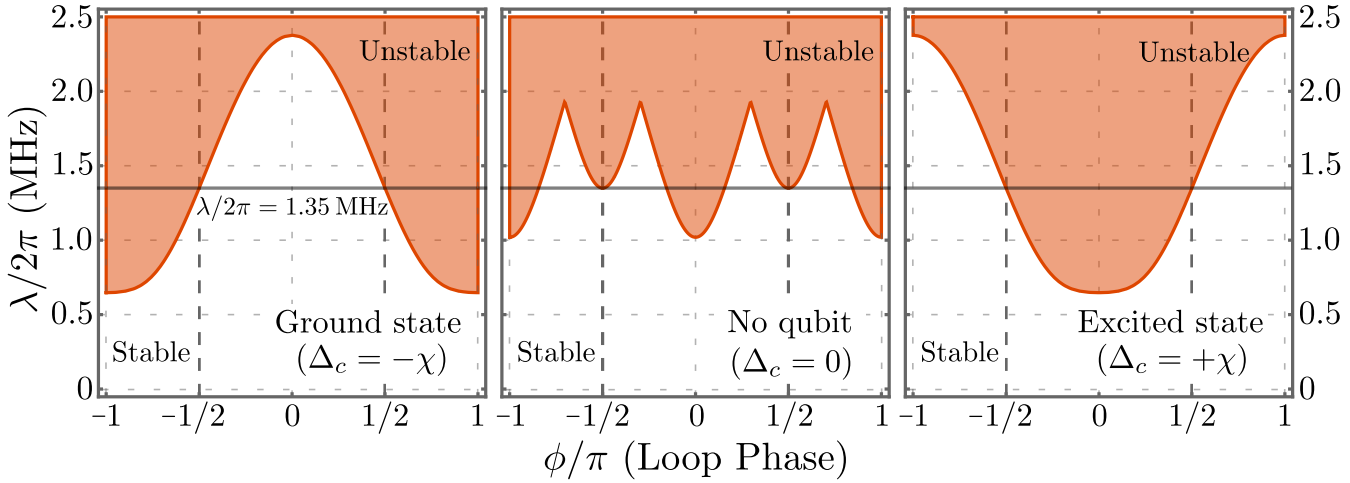

Figure 4.7: Stability plots for the nonreciprocal amplifier, as a function of the loop phase, ϕ, and strength of the squeezing on the amplifier mode, $\lambda/2\pi$. Stable regions are indicated in white, and unstable regions are coloured in red. The dispersive coupling to the qubit results in an effective detuning of the cavity mode, Δ_c, which is dependent on the state of the qubit, $\sigma_z = \pm 1$. Three cases are displayed, [Left] the qubit is in the ground state resulting in $\Delta_c = -\chi$, [Right] the qubit is in the excited state where the detuning is $\Delta_c = +\chi$, and [Middle] the dispersive coupling to the qubit is omitted so there is no detuning, $\Delta_c = 0$. The dispersive coupling between the qubit and cavity mode is $\chi/2\pi = 2.5\,\mathrm{MHz}$. The decay rates for the three modes are $\kappa_a/2\pi = 0.2\,\mathrm{MHz}$, $\kappa_b/2\pi = 40.0\,\mathrm{MHz}$, and $\kappa_c/2\pi = 0.2\,\mathrm{MHz}$. The beam splitter couplings are $g_{ab}/2\pi = 5.0\,\mathrm{MHz}$, $g_{bc}/2\pi = 5.0\,\mathrm{MHz}$, and $g_{ac}/2\pi = 1.25\,\mathrm{MHz}$. For these parameters, the necessary balancing condition required for nonreciprocal scattering between the amplifier and cavity mode is met, $g_{ac} = g_{ab}g_{bc}(2/\kappa_a)$. At this point, and this point only, the maximum strength of the squeezing λ allowed for the system to be stable is independent of the detuning of the cavity mode, provided the loop phase is set to the necessary values of $\phi = \pm\pi/2$. The condition which sets the maximum value of the squeezing, $\mathcal{C}_\lambda < 1 + \mathcal{C}_{ab}$, can be rewritten as $\lambda < (\kappa_a/2) + g_{ab}^2(2/\kappa_b)$. For these parameters, this indicates that the system becomes unstable for squeezing magnitudes at and beyond $\lambda/2\pi = 1.35\,\mathrm{MHz}$; this value is marked by a horizontal black line in all three plots.

As a reminder, σ_z is the realisation of the qubit measurement and so only takes the values $\sigma_z = \pm 1$. The stability criterion is equivalent to the requirement that the real part of the eigenvalues of this dynamical matrix be strictly negative. In order to check this, we must calculate the roots of the characteristic polynomial,

$$\begin{aligned}
&\det[\mathbf{A}_{\triangledown} - s\mathbf{I}_6] = P_0(s,+\lambda)P_0(s,-\lambda) + 4g_{ab}^2 g_{bc}^2 g_{ac}^2 \cos^2(\phi) + \chi^2 P_\chi(s,+\lambda)P_\chi(s,-\lambda) - 4\sigma_z \chi\, g_{ab}g_{bc}g_{ac}P_\chi(s,0)\cos(\phi) \\
&\text{where } P_0(s,\pm\lambda) = g_{ab}^2\left(\frac{\kappa_c}{2}+s\right) + g_{bc}^2\left(\frac{\kappa_a}{2}\mp\lambda+s\right) + g_{ac}^2\left(\frac{\kappa_b}{2}+s\right) + \left(\frac{\kappa_a}{2}\mp\lambda+s\right)\left(\frac{\kappa_b}{2}+s\right)\left(\frac{\kappa_c}{2}+s\right), \\
&\text{and } P_\chi(s,\pm\lambda) = g_{ab}^2 + \left(\frac{\kappa_a}{2}\mp\lambda+s\right)\left(\frac{\kappa_b}{2}+s\right).
\end{aligned} \tag{4.101}$$

The stability criteria are therefore independent of the phase of the squeezing, and are identical for the ideal values of the loop phase, $\phi = \pm\pi/2$. The Routh-Hurwitz criterion provides the necessary and sufficient conditions to render this system stable, equivalent to the requirement that all eigenvalues have a negative real part. However, the Routh-Hurwitz criteria for the general system are too complicated to analyse, and so provide little insight into the parameters required for stability. Consequently, the system must be simplified so that the criteria are manageable, which can be accomplished using nonreciprocity to reduce to number of independent parameters in the amplifier.

We recall from Section 4.3.1 that the mismatched circulator can block thermal noise originating at the amplifier mode from reaching the cavity mode by rendering the scattering between these two modes nonreciprocal. Realising nonreciprocity between the cavity and amplifier modes is also of interest for our nonreciprocal amplifier, since it allows us to reduce the backaction of the measurement on the qubit, provided that the signal is circulated CCW. By applying the necessary balancing condition for the cooperativities, $\mathcal{C}_{ac} = \mathcal{C}_{ab}\mathcal{C}_{bc}$, the stability requirements become independent of the dispersive coupling χ at the ideal values of the loop phase, $\phi = \pm\pi/2$, as shown in Figure 4.7. The detuning of the cavity mode due to the qubit can then be removed when analysing the system stability in this regime, greatly reducing the complexity of the stability criteria.

Applying these simplifications to the characteristic polynomial of $\mathbf{A}_{\triangledown}$, the stability of the system is then wholly dependent on the behaviour of the roots of $P_0(s,+\lambda)P_0(s,-\lambda)$. It can be shown that the Routh-Hurwitz criteria are

always fulfilled for the polynomial $P(s,-\lambda)$ but not for $P(s,+\lambda)$, so we only need to consider the latter. The stability criteria for the system at the points of nonreciprocity are then:

$$\begin{aligned}
0 &< \kappa_a(1-\mathcal{C}_\lambda)+\kappa_b+\kappa_c \\
0 &< \kappa_a\kappa_b\left(1-\mathcal{C}_\lambda+\mathcal{C}_{ab}\right)\left(\kappa_a(1-\mathcal{C}_\lambda)+\kappa_b\right)+\kappa_a\kappa_c\left(1-\mathcal{C}_\lambda+\mathcal{C}_{ab}\mathcal{C}_{bc}\right)\left(\kappa_a(1-\mathcal{C}_\lambda)+\kappa_c\right) \\
&\quad +\kappa_b\kappa_c\Big(2\kappa_a(1-\mathcal{C}_\lambda)+\left(1+\mathcal{C}_{bc}\right)\left(\kappa_b+\kappa_c\right)\Big) \\
0 &< \kappa_a\kappa_b\kappa_c\left(1+\mathcal{C}_{bc}\right)\left(1-\mathcal{C}_\lambda+\mathcal{C}_{ab}\right).
\end{aligned} \tag{4.102}$$

where we define the cooperativity for the squeezing as $\mathcal{C}_\lambda := 2\lambda/\kappa_a$. The first condition indicates that the squeezing results in anti-damping on the amplifier mode; however, the system is guaranteed to be stable so long as the net dissipation rate of the system is still positive. This condition is easily satisfied for the nonreciprocal measurement loop, since the decay rate of the buffer mode is engineered to be large, $\kappa_b \gg \kappa_a, \kappa_c$, to prevent dissipation of the signal within the loop. The second condition is the most complicated and difficult to interpret; however, the calculations shown in Figure 4.7 show that for physically motivated parameters, the stability of the system rests solely on the third condition. Since the decay rates and cooperativities must all be positive quantities, the third stability condition can be recast as,

$$\mathcal{C}_\lambda < 1+\mathcal{C}_{ab}. \tag{4.103}$$

This criterion sets the maximum allowable value of $\mathcal{C}_\lambda$, and therefore dictates the absolute upper limit for the magnitude of the single-mode squeezer, λ, the value of which is directly related to the gain of the amplifier. Since we are only monitoring the input and output of the amplifier through the buffer mode, the gain can be characterised by the scattering element $\hat{b}_{\text{out}} = \mathrm{S}_{bb}[0]\hat{b}_{\text{in}}$, which we evaluate at $\omega = 0$. Unlike the stability calculation, here we include the dispersive shift when calculating the scattering matrix. This reflection term is identical for both loop phases $\phi = \pm\pi/2$, and is given by:

$$\begin{aligned}
\mathrm{S}_{bb}[0] \;=\; & \frac{1}{(1+\mathcal{C}_{ab}+\mathcal{C}_{bc}+\mathcal{C}_{ac})^2-\mathcal{C}_\lambda^2(1+\mathcal{C}_{bc})^2+\mathcal{X}^2((1+\mathcal{C}_{ab})^2-\mathcal{C}_\lambda^2)} \\
& \times\Bigg[\mathcal{X}^2\left(-1+\mathcal{C}_{ab}^2+\mathcal{C}_\lambda^2\right)+2i\sigma_z\mathcal{X}\left(\mathcal{C}_{ab}\mathcal{C}_{ac}-\mathcal{C}_{bc}\left(1-\mathcal{C}_\lambda^2\right)\right) \\
& \quad +(1+\mathcal{C}_{ab}+\mathcal{C}_{bc}+\mathcal{C}_{ac})(-1+\mathcal{C}_{ab}+\mathcal{C}_{bc}-\mathcal{C}_{ac})-\mathcal{C}_\lambda^2\left(-1+\mathcal{C}_{bc}^2\right)\Bigg].
\end{aligned} \tag{4.104}$$

We note that this scattering element is independent of the choice of phase for the single-mode squeezer. Applying the nonreciprocity condition reduces this scattering matrix element to a particularly simple form:

$$\mathrm{S}_{bb}[0] = -\frac{\left((1-\mathcal{C}_{ab})(1+\mathcal{C}_{ab})-\mathcal{C}_\lambda^2\right)\left(1-\mathcal{C}_{bc}+i\sigma_z\mathcal{X}\right)}{\left((1+\mathcal{C}_{ab})^2-\mathcal{C}_\lambda^2\right)\left(1+\mathcal{C}_{bc}+i\sigma_z\mathcal{X}\right)}. \tag{4.105}$$

Using this quantity we can define two measures of gain; the amplitude gain, which is calculated using the magnitude of the scattering element, $|\mathrm{S}_{bb}[0]|$, and the power gain, which is calculated from the power of the output signal, that is the magnitude squared, $|\mathrm{S}_{bb}[0]|^2$. For this work, we will use the power gain, and so $\sqrt{\mathcal{G}_{bb}} := |\mathrm{S}_{bb}[0]|$. The gain can also be expressed in units of decibels as follows:

$$\mathcal{G}_{bb}(\mathrm{dB}) = 10\log_{10}|\mathrm{S}_{bb}[0]|^2 \quad \text{where} \quad |\mathrm{S}_{bb}[0]|^2 = \frac{\left((1-\mathcal{C}_{ab})(1+\mathcal{C}_{ab})-\mathcal{C}_\lambda^2\right)^2\left((1-\mathcal{C}_{bc})^2+\mathcal{X}^2\right)}{\left((1+\mathcal{C}_{ab})^2-\mathcal{C}_\lambda^2\right)^2\left((1+\mathcal{C}_{bc})^2+\mathcal{X}^2\right)}. \tag{4.106}$$

We can convert back from decibels using the definition $\mathcal{G}_{bb} := 10^{\mathcal{G}_{bb}(\mathrm{dB})/10}$. In the above expression, we notice that as the squeezing approaches the point of instability, $\mathcal{C}_\lambda \to 1+\mathcal{C}_{ab}$, the gain $\mathcal{G}_{bb}$ will diverge, so in theory there is no limit to how strongly the signal can be amplified; in practice this is of course not the case. When the single-mode squeezer is off, $\mathcal{C}_\lambda = 0$, Eq. 4.106 returns a negative value for the gain, indicating that the amplitude of the scattering element is less than one, $|\mathrm{S}_{bb}[0]| < 1$. This is to be expected, since there is inevitably some loss through the other two modes as the displaced signal circulates around the loop. As a result of this loss, in order for the signal to have a gain of zero, $\mathcal{G}_{bb} = 0\,\mathrm{dB}$ or $|\mathrm{S}_{bb}[0]|^2 = 1$, the amplitude of the single-mode squeezer must be non-zero. After turning on the single-mode squeezer, the amplifier mode must therefore initially do some work to overcome the attenuation in the reflected signal in order to realise positive gain, and hence amplification. For completeness, we can relate the amount

of squeezing to the power gain as follows,

$$\begin{aligned}\mathcal{C}_\lambda^2 = &\frac{1+\mathcal{C}_{ab}}{\mathcal{G}_{bb}\left((1+\mathcal{C}_{bc})^2+\mathcal{X}^2\right)-\left((1-\mathcal{C}_{bc})^2+\mathcal{X}^2\right)} \\ &\times\Bigg[-2\mathcal{C}_{ab}\sqrt{\mathcal{G}_{bb}\left((1+\mathcal{C}_{bc})^2+\mathcal{X}^2\right)\left((1-\mathcal{C}_{bc})^2+\mathcal{X}^2\right)} \\ &\quad+\mathcal{G}_{bb}(1+\mathcal{C}_{ab})\left((1+\mathcal{C}_{bc})^2+\mathcal{X}^2\right)-(1-\mathcal{C}_{ab})\left((1-\mathcal{C}_{bc})^2+\mathcal{X}^2\right)\Bigg].\end{aligned} \tag{4.107}$$

4.3.3 The Dispersive Measurement

With the analysis of each sub-component completed, we can compile everything that we have learned to examine the optimum behaviour when performing a dispersive qubit measurement with our single-port nonreciprocal amplifier. A lot has been covered, so the important points will be summarised first for clarity:

- For the single-port measurement to succeed, we require that as little signal as possible be lost through the other two modes. To accomplish this, the beam splitter rates should be larger than the decay rates, and ideally be as large as possible. This requirement can be written in terms of the cooperativity as $\mathcal{C}_{jk} \gg 1$.
- To minimise the backaction on the qubit due to noise coming from the amplifier mode, nonreciprocal scattering can be used to direct the signal away from the dispersively coupled cavity mode. This condition, $c \to a$, requires that the loop phase be set to $\phi = -\pi/2$, which naturally circulates the signal in the counter-clockwise direction. Realising nonreciprocal scattering requires that the beam splitter cooperativities be set to $\mathcal{C}_{ac} = \mathcal{C}_{ab}\mathcal{C}_{bc}$, or equivalently, $g_{ac} = g_{ab}g_{bc}(2/\kappa_b)$.
- To amplify the output and thereby maximise the measurement rate, the single-mode squeezing should be as strong as allowed by the stability conditions and the critical photon numbers. This is also necessary to compensate for added off-chip noise. In addition, the drive and squeezing should have a relative phase of $\theta - 2\varphi = -\pi/2$ for CCW circulation to enhance the displacement between the pointer states.

Although some of these properties have only been heuristically explained, or else only shown to work in the absence of single-mode squeezing, all will be confirmed to apply to the nonreciprocal amplifier as well in this section. To demonstrate this, we will examine the behaviour of the qubit dephasing as well as the measurement rate, before finishing with an analysis of measurement efficiency. For contrast, the results for CW circulation will also be analysed.

4.3.3.1 Measurement Backaction

We will start by characterising the induced backaction using the moment method in Section 4.2.2.2. The expressions which are necessary for calculating the dephasing will be given here, with full details provided in Appendix F.4. The total induced dephasing can be expressed as a combination of the parasitic and measurement-induced dephasing rates:

$$\begin{aligned}\Gamma_\mathrm{d} = \Gamma_\mathrm{d,p} + \Gamma_\mathrm{d,m} \quad \text{where} \quad \Gamma_\mathrm{d,p} &= \frac{1}{2}\mathrm{Re}\big[\mathrm{Tr}\left[\mathbf{B}\boldsymbol{\sigma}\right]\big] = -\chi\mathrm{Im}[\sigma_{q_cq_c}+\sigma_{p_cp_c}], \\ \text{and} \quad \Gamma_\mathrm{d,m} &= \frac{1}{2}\mathrm{Re}\big[\boldsymbol{\mu}^T\mathbf{B}\boldsymbol{\mu}\big] = -\chi\mathrm{Im}[\mu_{q_c}^2+\mu_{p_c}^2].\end{aligned} \tag{4.108}$$

Since the focus is on the rate of dephasing when the system is in the steady state, the arrays $\boldsymbol{\sigma}$ and $\boldsymbol{\mu}$ are the solutions to the following algebraic matrix equations

$$0 = \mathbf{A}\boldsymbol{\sigma} + \boldsymbol{\sigma}\mathbf{A}^T - \boldsymbol{\sigma}\mathbf{B}\boldsymbol{\sigma} + \mathbf{C} \qquad 0 = (\mathbf{A} - \boldsymbol{\sigma}\mathbf{B})\,\boldsymbol{\mu} + \mathbf{f}. \tag{4.109}$$

When defining the arrays in these expressions we work in the quadrature basis, $\hat{\boldsymbol{r}} = (\hat{q}_a, \hat{p}_a, \hat{q}_b, \hat{p}_b, \hat{q}_c, \hat{p}_c)$. The matrix $\mathbf{A}$ is the dynamical matrix of the nonreciprocal amplifier in the absence of any coupling to the qubit:

$$\mathbf{A} = \begin{pmatrix} -(\kappa_a/2)\mathbf{I} + \lambda(-\cos(\theta)\mathbf{X} + \sin(\theta)\mathbf{Z}) & g_{ab}\mathbf{J} & g_{ac}(\cos(\phi)\mathbf{J} + \sin(\phi)\mathbf{I}) \\ g_{ab}\mathbf{J} & -(\kappa_b/2)\mathbf{I} & g_{bc}\mathbf{J} \\ g_{ac}(\cos(\phi)\mathbf{J} - \sin(\phi)\mathbf{I}) & g_{bc}\mathbf{J} & -(\kappa_c/2)\mathbf{I} \end{pmatrix}. \tag{4.110}$$

The matrix $\mathbf{C}$ contains the usual vacuum and thermal noise terms from the baths, along with an added term which is present due to the coupling between the cavity mode and the qubit. This coupling also gives rise to the $\mathbf{B}$ matrix,

which generates a quadratic term in the matrix equation for $\boldsymbol{\sigma}$. These matrices take the form:

$$\mathbf{B} = \begin{pmatrix} \mathbf{0} & \mathbf{0} & \mathbf{0} \\ \mathbf{0} & \mathbf{0} & \mathbf{0} \\ \mathbf{0} & \mathbf{0} & 2i\chi\mathbf{I} \end{pmatrix} \qquad \mathbf{C} = \frac{1}{2}\begin{pmatrix} \kappa_a(2\bar{n}_a+1)\mathbf{I} & \mathbf{0} & \mathbf{0} \\ \mathbf{0} & \kappa_b(2\bar{n}_b+1)\mathbf{I} & \mathbf{0} \\ \mathbf{0} & \mathbf{0} & (i\chi+\kappa_c(2\bar{n}_c+1))\mathbf{I} \end{pmatrix}. \tag{4.111}$$

Lastly, the vector $\mathbf{f}$ in the equation for $\boldsymbol{\mu}$ comes from the drive term in the Hamiltonian:

$$\mathbf{f} = \sqrt{2\kappa_b}\,|\alpha|\begin{pmatrix} 0 & 0 & \sin(\varphi) & -\cos(\varphi) & 0 & 0 \end{pmatrix}^T. \tag{4.112}$$

These matrix equations are not solvable analytically over most of the parameter space, and so, with the exception of some specific system parameter values, they must be solved numerically.

Parasitic Dephasing

The parasitic component of the dephasing, as previously discussed in Section 4.2.2.2, arises when the variance of the system state is not identical to the vacuum state. Variances in the photon fluctuations above or below the vacuum enhance the dephasing by performing a parasitic measurement which does not impact the displacement of the pointer states, and is therefore unwanted. In Gaussian systems, the two processes which can cause this are single and two-mode squeezing, and thermal noise fluctuations from the environment. Squeezing must be present in the system to amplify the measurement, whereas thermal noise does nothing to enhance the measurement.

Since the coupling to the qubit rotates the state of the cavity mode, if this state is squeezed, then the parasitic measurement is a result of qubit information being lost due to the rotation of the squeezed and amplified quadratures of the cavity mode. This rotation is independent of the initial phase of the squeezed state that enters the cavity mode, and hence $\Gamma_{\mathrm{d,p}}$ must be independent of the single-mode squeezing phase. This fact is shown explicitly in Appendix F.4. The rotation of the quadrature due to the dispersive coupling will occur even if the squeezed state is not displaced, demonstrating that the parasitic dephasing is present even if the drive is off.

By circulating in the CCW direction, $\mathcal{C}_{ac} = \mathcal{C}_{ab}\mathcal{C}_{bc}$ and $\phi = -\pi/2$, thereby ensuring that noise from the amplifier mode is directed away from the cavity mode, we ideally expect that the state in the cavity mode is a displaced vacuum state coming from the drive on the buffer mode. For CW circulation, where $\phi = +\pi/2$, we therefore expect that the squeezed state is swapped directly from the amplifier mode to the cavity mode. The parasitic dephasing should then be at its lowest when circulating CCW, and highest when circulating CW, which can be seen in Figure 4.8, where $\Gamma_{\mathrm{d,p}}$ is plotted against the loop phase. The parasitic dephasing is directly dependent on the amplitude of the single-mode squeezing, λ, or equivalently amplifier gain, $\mathcal{G}_{bb}$, since this corresponds to an increase in the variance of photon fluctuations in the dispersively coupled cavity mode; this is also shown in Figure 4.8. Additionally, we note that the parasitic dephasing does not vanish exactly when $\phi = -\pi/2$, indicating that the state in the cavity mode is squeezed, if only slightly. This is expected, since we cannot perfectly apply the nonreciprocity condition across all frequencies.

To better demonstrate the differences in behaviour for the two circulation directions, the parasitic dephasing can be solved analytically for arbitrary values of the amplifier phase θ at specific values of the loop phase, that is, when $\phi = \pm\pi/2$:

$$\Gamma_{\mathrm{d,p}} = -\frac{1}{2}(\kappa_a+\kappa_b+\kappa_c) + \frac{1}{2}\mathrm{Re}\Big[\sqrt{\mathfrak{r}_1(+\lambda)} + \sqrt{\mathfrak{r}_2(+\lambda)} + \sqrt{\mathfrak{r}_3(+\lambda)} + \sqrt{\mathfrak{r}_1(-\lambda)} + \sqrt{\mathfrak{r}_2(-\lambda)} + \sqrt{\mathfrak{r}_3(-\lambda)}\Big], \tag{4.113}$$

where $\mathfrak{r}_k(\pm\lambda)$ are the roots of the following cubic polynomial,

$$0 = s^3 + v_2(\pm\lambda)s^2 + v_1(\pm\lambda)s + v_0(\pm\lambda, \mathrm{sgn}(\phi)) = (s-\mathfrak{r}_1(\pm\lambda))(s-\mathfrak{r}_2(\pm\lambda))(s-\mathfrak{r}_3(\pm\lambda)). \tag{4.114}$$

The coefficients have long expressions, and so are defined in Eq. (F.87) in Appendix F. The sign of the loop phase is only present in the $v_0(\pm\lambda, \mathrm{sgn}(\phi))$ term, and hence this is the only place where the direction of circulation appears when calculating the parasitic dephasing. Part of the effects of nonreciprocity on the parasitic dephasing can be gleaned from examining the $v_0(\pm\lambda, \mathrm{sgn}(\phi))$ term on its own, where applying the nonreciprocity condition between the amplifier and cavity modes removes the thermal noise contribution from the amplifier mode. The contributions from the squeezing are, however, untouched when applying the nonreciprocity condition to this term, along with the other two coefficients from the polynomial. The complicated form of the cubic roots, $\mathfrak{r}_k(\pm\lambda)$, means that it is not possible to explain the strong dependence of the parasitic dephasing on the circulation direction using the known analytic expressions. The effect of nonreciprocity on the squeezing is therefore currently only evidenced in numerical calculations, as seen in Figure 4.8, which serves to confirm the theoretical prediction that circulating in the CCW direction will minimise $\Gamma_{\mathrm{d,p}}$. Despite the difficulty in interpreting the analytic results, obtaining these expressions was necessary for calculating the measurement-induced dephasing.

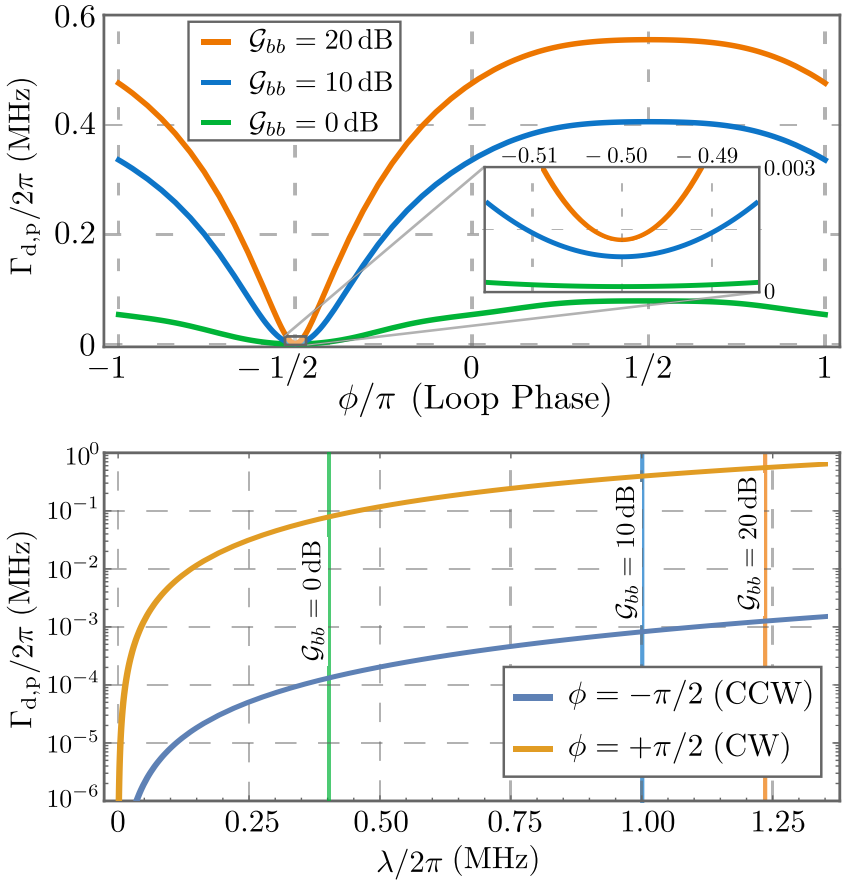

Figure 4.8: Parasitic dephasing $\Gamma_{\mathrm{d,p}}$ of the nonreciprocal amplifier due to noise from the single-mode squeezer at mode a. [Top] $\Gamma_{\mathrm{d,p}}$ as a function of the loop phase ϕ for three values of the squeezing λ, labelled in the plot using the related values of amplifier gain as measured at $\phi = \pm\pi/2$ in the absence of a dispersively coupled qubit: $\mathcal{G}_{bb} = 0\,\mathrm{dB}$ or $\lambda/2\pi \approx 0.4025\,\mathrm{MHz}$ (green), $\mathcal{G}_{bb} = 10\,\mathrm{dB}$ or $\lambda/2\pi \approx 1.0155\,\mathrm{MHz}$ (blue), and $\mathcal{G}_{bb} = 20\,\mathrm{dB}$ or $\lambda/2\pi \approx 1.2347\,\mathrm{MHz}$ (orange). Note that although the function is smooth and continuous over the entire range of loop phases, due to the instability of the pointer states, certain values of the loop phase are not accessible for $\lambda/2\pi \approx 1.0155\,\mathrm{MHz}$ and $1.2347\,\mathrm{MHz}$ as indicated in Figure 4.7. [Bottom] $\Gamma_{\mathrm{d,p}}$ as a function of the amplitude of the single-mode squeezer λ for two values of the loop phase: $\phi = -\pi/2$ corresponding to CCW circulation (blue), and $\phi = +\pi/2$ corresponding to CW circulation (blue). No thermal noise is present in the system $\bar{n}_a$, $\bar{n}_b =$, and $\bar{n}_c = 0$. All other system parameters are as in Figure 4.7.

Measurement Dephasing

In contrast to the parasitic dephasing, the measurement dephasing yields a comparatively simple form:

$$\begin{aligned}
\Gamma_{\mathrm{d,m}} = |\alpha|^2 \chi^2 \kappa_b \Bigg(& \frac{z_1(+\lambda)\big(\mathrm{sgn}(\phi) g_{ab} g_{ac} - g_{bc}(\kappa_a/2 - \lambda)\big)^2}{\big(z_0(+\lambda) - \chi^2 z_2(+\lambda)\big)^2 + \big(\chi z_1(+\lambda)\big)^2} \big(1 + \sin(\theta - 2\varphi)\big) \\
& + \frac{z_1(-\lambda)\big(\mathrm{sgn}(\phi) g_{ab} g_{ac} - g_{bc}(\kappa_a/2 + \lambda)\big)^2}{\big(z_0(-\lambda) - \chi^2 z_2(-\lambda)\big)^2 + \big(\chi z_1(-\lambda)\big)^2} \big(1 - \sin(\theta - 2\varphi)\big) \Bigg) \\
\text{where} \quad z_0(\pm\lambda) = & \big(g_{ab}^2 \kappa_c/2 + g_{bc}^2(\kappa_a/2 \mp \lambda) + g_{ac}^2 \kappa_b/2 + (\kappa_a/2 \mp \lambda)(\kappa_b/2)(\kappa_c/2)\big)^2 \\
z_1(\pm\lambda) = & \Big[\kappa_a(2\bar{n}_a + 1)\left(g_{ab} g_{bc} + \mathrm{sgn}(\phi) g_{ac} \kappa_b/2\right)^2 \\
& + \kappa_b(2\bar{n}_b + 1)\left(\mathrm{sgn}(\phi) g_{ab} g_{ac} - g_{bc}(\kappa_a/2 \mp \lambda)\right)^2 \\
& + \kappa_c(2\bar{n}_c + 1)\left(g_{ab}^2 + (\kappa_a/2 \mp \lambda)(\kappa_b/2)\right)^2\Big] \\
z_2(\pm\lambda) = & \big(g_{ab}^2 + (\kappa_a/2 \mp \lambda)(\kappa_b/2)\big)^2 .
\end{aligned} \tag{4.115}$$

The $z_k(\pm\lambda)$ coefficients are derived from the roots $\mathfrak{r}_k(\pm\lambda)$ of the polynomial in Eq. (4.114), which appeared when calculating the parasitic dephasing:

$$-v_0(\pm\lambda, \mathrm{sgn}(\phi)) = -\chi^2 z_2(\pm\lambda) + i\chi z_1(\pm\lambda) + z_0(\pm\lambda) = \mathfrak{r}_1(\pm\lambda)\,\mathfrak{r}_2(\pm\lambda)\,\mathfrak{r}_3(\pm\lambda). \tag{4.116}$$

The measurement dephasing can also be expressed in terms of the cooperativities for easier analysis:

$$\begin{aligned}
\Gamma_{\mathrm{d,m}} = 4\left|\alpha\right|^2 \mathcal{X}\Bigg(& \frac{Z_{1,+}\big(\mathrm{sgn}(\phi)\sqrt{\mathcal{C}_{ab}\mathcal{C}_{ac}} - \sqrt{\mathcal{C}_{bc}}(1-\mathcal{C}_\lambda)\big)^2}{\big(Z_{0,+} - \mathcal{X}^2 Z_{2,+}\big)^2 + \big(\mathcal{X} Z_{1,+}\big)^2}\big(1+\sin(\theta-2\varphi)\big) \\
& + \frac{Z_{1,-}\big(\mathrm{sgn}(\phi)\sqrt{\mathcal{C}_{ab}\mathcal{C}_{ac}} - \sqrt{\mathcal{C}_{bc}}(1+\mathcal{C}_\lambda)\big)^2}{\big(Z_{0,-} - \mathcal{X}^2 Z_{2,-}\big)^2 + \big(\mathcal{X} Z_{1,-}\big)^2}\big(1-\sin(\theta-2\varphi)\big)\Bigg) \\
\text{where}\quad Z_{0,\pm} &= \left((1+\mathcal{C}_{ab}+\mathcal{C}_{bc}+\mathcal{C}_{ac}) \mp \mathcal{C}_\lambda(1+\mathcal{C}_{bc})\right)^2 \\
Z_{1,\pm} &= \Big[(2\bar{n}_a+1)\big(\sqrt{\mathcal{C}_{ab}\mathcal{C}_{bc}} + \mathrm{sgn}(\phi)\sqrt{\mathcal{C}_{ac}}\big)^2 \\
&\qquad + (2\bar{n}_b+1)\big(\mathrm{sgn}(\phi)\sqrt{\mathcal{C}_{ab}\mathcal{C}_{ac}} - \sqrt{\mathcal{C}_{bc}}(1\mp\mathcal{C}_\lambda)\big)^2 \\
&\qquad + (2\bar{n}_c+1)\left(\mathcal{C}_{ab} + (1\mp\mathcal{C}_\lambda)\right)^2\Big] \\
Z_{2,\pm} &= \left(\mathcal{C}_{ab} + (1\mp\mathcal{C}_\lambda)\right)^2.
\end{aligned} \tag{4.117}$$

The measurement dephasing for the nonreciprocal amplifier Eq. (4.117) naturally reduces to the previously defined measurement dephasing for the passive mismatched circulator in Eq. (4.92) when the single-mode squeezer is turned off, $\lambda = 0$. Despite the addition of squeezing, the measurement-induced dephasing for the nonreciprocal amplifier and the mismatched circulator behaves similarly. In the above expression, it is still not possible to cancel thermal noise coming from the buffer mode or the cavity mode. Though it may seem possible with certain combinations of the cooperativities, loop phase, and relative amplifier-drive phase, the result is invariably either not physically possible since it violates one of the stability criteria, or else is uninteresting because the measurement dephasing goes to zero.

Cancelling thermal noise from the amplifier mode is still possible as before by applying the conditions for nonreciprocal scattering in the $c \to a$ direction, $\phi = -\pi/2$ and $\mathcal{C}_{ac} = \mathcal{C}_{ab}\mathcal{C}_{bc}$. Although it is not immediately obvious, the nonreciprocal scattering not only cancels the noise from $\bar{n}_a$ it also cancels the contributions from the squeezing *exactly*. The measurement dephasing becomes,

$$\mathcal{C}_{ac} = \mathcal{C}_{ab}\mathcal{C}_{bc}\,,\ \phi = -\frac{\pi}{2}\ :\ \Gamma_{\mathrm{d,m}} = \frac{8\left|\alpha\right|^2 \mathcal{X}\left(\mathcal{C}_{bc}(\bar{n}_b+1) + (\bar{n}_c+1)\right)}{\big(\left(1+\mathcal{C}_{bc}\right)^2 - \mathcal{X}^2\big)^2 + 4\mathcal{X}^2\left(\mathcal{C}_{bc}(\bar{n}_b+1) + (\bar{n}_c+1)\right)^2}, \tag{4.118}$$

which is identical to the previous result for the mismatched circulator in Eq. (4.94). The contribution from noise sources originating from the amplifier mode has disappeared, and the measurement dephasing is identical to the result we would have obtained by decoupling the amplifier mode entirely, $\mathcal{C}_{ab}$ and $\mathcal{C}_{ac} = 0$. This result is independent of the value of the relative phase between the single-mode squeezer and the drive, $\theta - 2\varphi$, as demonstrated in Figure 4.9. Although these noise terms have disappeared here, they are still present in the parasitic dephasing. This can be explained by remembering that the measurement dephasing comes purely from the drive on the buffer mode, and will vanish if the amplitude of that drive is zero, $|\alpha|^2$, indicating that the measurement dephasing is then entirely due to the net displacement of the cavity mode. As evidenced by the parasitic dephasing, nonreciprocity does not perfectly shield the cavity mode state from amplifier mode noise since we are not circulating perfectly, indicating that there are counter-propagating signals reaching the cavity state. The combination of these signals does not result in a state with the same variance as the vacuum state, resulting in the observed non-zero parasitic dephasing. What nonreciprocity does is combine the displacements of these different signals, destructively cancelling the contribution from the amplifier mode. As evidence, we can calculate the displacement of the cavity mode's internal field by solving:

$$\begin{aligned}
(q_{c,\mathrm{int}}^{\mathrm{ccw}}, p_{c,\mathrm{int}}^{\mathrm{ccw}}) &= \frac{2\sqrt{2}\left|\alpha\right|\sqrt{\mathcal{C}_{bc}/\kappa_c}}{(1+\mathcal{C}_{bc})^2 + \mathcal{X}^2}\Big((1+\mathcal{C}_{bc})\cos(\varphi) + \mathcal{X}\sin(\varphi), (1+\mathcal{C}_{bc})\sin(\varphi) - \mathcal{X}\cos(\varphi)\Big) \\
\longrightarrow \left|\alpha_{c,\mathrm{int}}^{\mathrm{ccw}}\right|^2 &= \frac{4\left|\alpha\right|^2 \mathcal{C}_{bc}/\kappa_c}{(1+\mathcal{C}_{bc})^2 + \mathcal{X}^2}.
\end{aligned} \tag{4.119}$$

These expressions are entirely independent of the squeezing λ, and so explain why the measurement dephasing is also independent of λ. Note that the effect of thermal noise on the measurement dephasing is still not well understood, since this only affects the variance and not the displacement of the internal state. Also, even in the absence of thermal

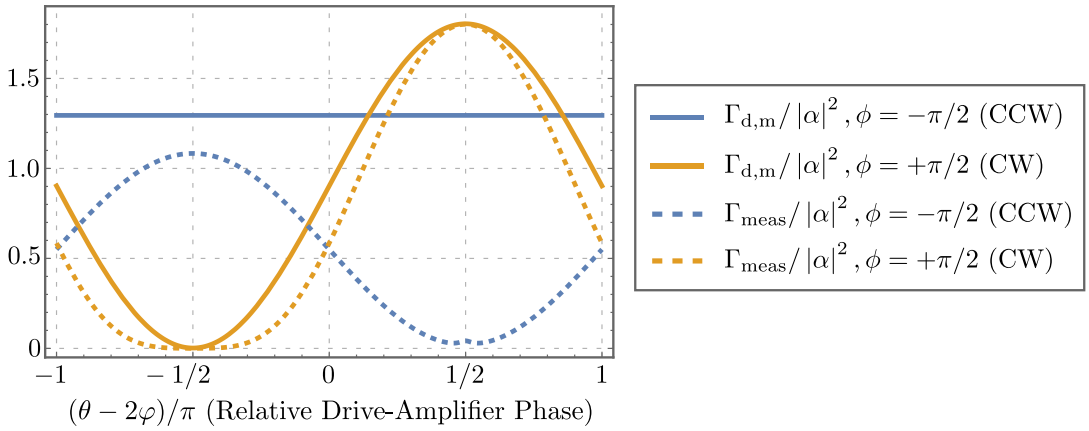

Figure 4.9: Measurement dephasing $\Gamma_{\mathrm{d,m}}$ (solid) and measurement rate Γ_{meas} (dotted) of the nonreciprocal amplifier, normalised by the amplitude of the buffer mode drive $|\alpha|^2$. Quantities are plotted against the relative phase between the single-mode squeezer and the drive, $\theta - 2\varphi$. The plotted rates correspond to two values of the loop phase: $\phi = -\pi/2$ (blue) and $\phi = +\pi/2$ (orange). The amplitude of the squeezer corresponds to a gain of $\mathcal{G}_{bb} = 10\,\mathrm{dB}$ or equivalently $\lambda/2\pi \approx 1.0155\,\mathrm{MHz}$. All other system parameters are identical to those in Figure 4.8.

noise, the above expression does not imply that the measurement dephasing can be trivially calculated from the internal state of the cavity mode in all cases.

When the scattering direction is reversed, $a \to c$, the displacement of the cavity mode state and the measurement dephasing are dependent on the phase and amplitude of the single-mode squeezer. This dependence is depicted in Figure 4.9, where it can be seen that the measurement dephasing for CW circulation reaches a maximum value when $\theta - 2\varphi = +\pi/2$, where the measurement dephasing increases along with the amplifier gain. Conversely, it reaches a minimum value at $\theta - 2\varphi = -\pi/2$, where the dephasing decreases as a function of the gain; see Figure 4.10. Since the first choice of phase corresponds to amplification along the displaced quadrature, the measurement dephasing will increase due to the enhancement of the cavity mode displacement. This can be demonstrated explicitly by calculating the magnitude of cavity mode displacement in phase space:

$$\left|\alpha_{c,\mathrm{int}}^{\mathrm{cw}}\right|^2 = \frac{4\,|\alpha|^2\,\mathcal{C}_{bc}/\kappa_c}{(1+\mathcal{C}_{bc})^2+\mathcal{X}^2} \times \frac{(1-\mathcal{C}_{ab}-\mathcal{C}_{\lambda})^2}{(1+\mathcal{C}_{ab}-\mathcal{C}_{\lambda})^2} \quad \text{when} \quad \theta - 2\varphi = \pi/2. \tag{4.120}$$

We notice there is a similarity to the CCW value, however, the presence of the amplifier increases the expected displacement. If the squeezing is along the displaced quadrature, then the amplifier is working to decrease the amount of displacement, leading to a decrease in the dephasing with increases in gain.

We also note that, depending on the phases, the measurement dephasing for CW circulation exceeds the rate for CCW circulation. We know that the measurement rate is ultimately tied to this rate of dephasing, and so we analyse this rate in the next section to determine whether the extra dephasing that comes with CCW circulation can also result in faster measurement of the qubit.

4.3.3.2 Measurement Rate

The analysis of the measurement rate will rest on the intuition developed in Section 4.3.2.1, where we determined that the phase of the measurement quadrature should match that of the drive when the loop phase is $\phi = \pm\pi/2$ to optimise the signal component. The steady-state measurement operators for the nonreciprocal amplifier and mismatched circulator are therefore identical for both of the optimum values of the loop phase,

$$\hat{M}[0] = \cos(\varphi)\hat{q}_{b,\mathrm{out}}[0] + \sin(\varphi)\hat{p}_{b,\mathrm{out}}[0]. \tag{4.121}$$

The behaviour of the measurement rate at these ideal loop phases also matches the expected behaviour from the heuristic explanation given in Section 4.3.2.1 exactly; this is demonstrated in Figure 4.9 where the measurement rate is at a maximum when the relative amplifier-drive phase is $\theta - 2\varphi = \pm\pi/2$. At this value of the relative phase, the amplification enhances the separation between the pointer states for CCW circulation, while for CW circulation, the amplification serves to increase the magnitude of the displacement before qubit measurement, thereby resulting in a larger signal as the pointer states rotate apart. These effects are enhanced with an increase in the amplifier gain. At the opposite relative phase, $\theta - 2\varphi = \mp\pi/2$, these quantities are squeezed, thereby decreasing the signal and lowering the overall measurement rate.

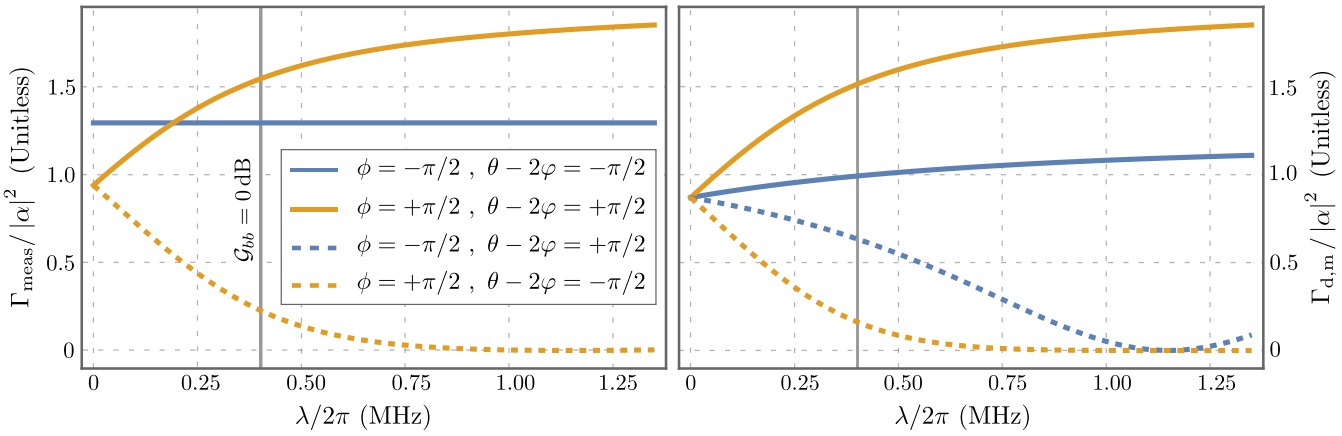

Figure 4.10: [Left] Measurement dephasing $\Gamma_{\mathrm{d,m}}$ and [Right] measurement rate Γ_{meas} of the nonreciprocal amplifier, normalised by the amplitude of the buffer mode drive $|\alpha|^2$. Quantities are plotted against the amplitude of the single-mode squeezer λ. The plotted rates correspond to two values of the loop phase: $\phi = -\pi/2$ (blue) and $\phi = +\pi/2$ (orange). The relative phase between the squeezer and the drive is tuned to realise amplification (solid) or squeezing (dotted) of the measurement signal. When the loop phase is $\phi = -\pi/2$, the dephasing is independent of the amplifier phase, and so these lines are identical. All other system parameters are identical to those in Figure 4.8.

Figure 4.9 also demonstrates that, for the same set of coupling strengths and decay rates, CW circulation can realise a faster measurement rate compared to CCW circulation. We can understand this by examining the individual parts of the total measurement rate. Starting with the signal component,

$$\frac{1}{4}\left|\langle\hat{M}[0]\rangle_e - \langle\hat{M}[0]\rangle_g\right|^2 = \frac{2\left|\alpha\right|^2\chi^2\kappa_b^2}{\det[\mathbf{A}_{\triangledown}]^2}\left(g_{ab}^2 g_{ac}^2 - g_{bc}^2\left(\frac{\kappa_a^2}{4} - \lambda^2\right) + 2\,\mathrm{sgn}(\phi)\lambda g_{ab}g_{ac}g_{bc}\sin(\theta - 2\varphi)\right)^2, \tag{4.122}$$

where $\det[\mathbf{A}_{\triangledown}]$ is the determinant of the dynamical matrix for our nonreciprocal amplifier, $\mathbf{A}_{\triangledown}$, defined in Eq. (4.100). Only one term in the above expression is dependent on the various phases of our system, and it is through this term that we can see that the signal is identical for CW and CCW circulation when $\theta - 2\varphi$ has the opposite phase:

$$\sin(\theta^{\mathrm{ccw}} - 2\varphi^{\mathrm{ccw}}) = -\sin(\theta^{\mathrm{cw}} - 2\varphi^{\mathrm{cw}}) \quad \longrightarrow \quad \theta^{\mathrm{ccw}} - 2\varphi^{\mathrm{ccw}} = \theta^{\mathrm{cw}} - 2\varphi^{\mathrm{cw}} \pm \pi. \tag{4.123}$$

The maximum obtainable signal is therefore identical for both directions of circulation, and so the number of photons reaching the output of the buffer mode must be identical. This was also seen in the mismatched circulator, where the overall measurement rate was identical since the noise of the output state was always in vacuum. The reason for the difference here is that the output noise power is not identical for both directions of circulation; exact expressions may be found in Appendix F.4. Since amplification occurs before the qubit measurement during CW circulation, the dispersive coupling to the qubit will rotate some of the amplified noise out of the measurement quadrature, so the output noise power is somewhere between squeezed and amplified noise. For CCW circulation amplification occurs after measurement, so the output noise-power of the measurement quadrature corresponds almost entirely to amplified noise, resulting in an inherently noisier measurement in comparison.

4.3.3.3 Measurement Efficiency

With the backaction and measurement rate now fully characterised, we can now proceed to calculate the efficiency of the measurement. In the ideal case, there is either no added noise coming from other sources acting to decrease the measurement rate, $\bar{n}_{\mathrm{add}} = 0$. We also assume that the phases are all tuned to their optimum values, and the backaction coming from parasitic measurements is sufficiently minimised. The last point can be achieved by increasing the amplitude of the drive so that it is much smaller in magnitude compared to the dephasing from the measurement drive, $\Gamma_{\mathrm{d,p}} \ll \Gamma_{\mathrm{d,m}}$. Provided these assumptions are met, the measurement efficiency can be approximated as,

$$\eta = \frac{\Gamma_{\mathrm{meas}}(\bar{n}_{\mathrm{add}})}{\Gamma_{\mathrm{d,p}} + \Gamma_{\mathrm{d,m}}} \approx \frac{\Gamma_{\mathrm{meas}}(0)}{\Gamma_{\mathrm{d,m}}} \quad \text{where} \quad \Gamma_{\mathrm{meas}}(\bar{n}_{\mathrm{add}}) = \frac{\left|\langle\hat{M}[0]\rangle_e - \langle\hat{M}[0]\rangle_g\right|^2/4}{\bar{S}_{MM,e}[0] + \bar{S}_{MM,g}[0] + 2\bar{n}_{\mathrm{add}}}. \tag{4.124}$$

The threshold for drive amplitude at which the measurement dephasing overpowers the parasitic dephasing is considerably different for CCW vs CW circulation. In Figure 4.11, the parasitic component is overwhelmed when the

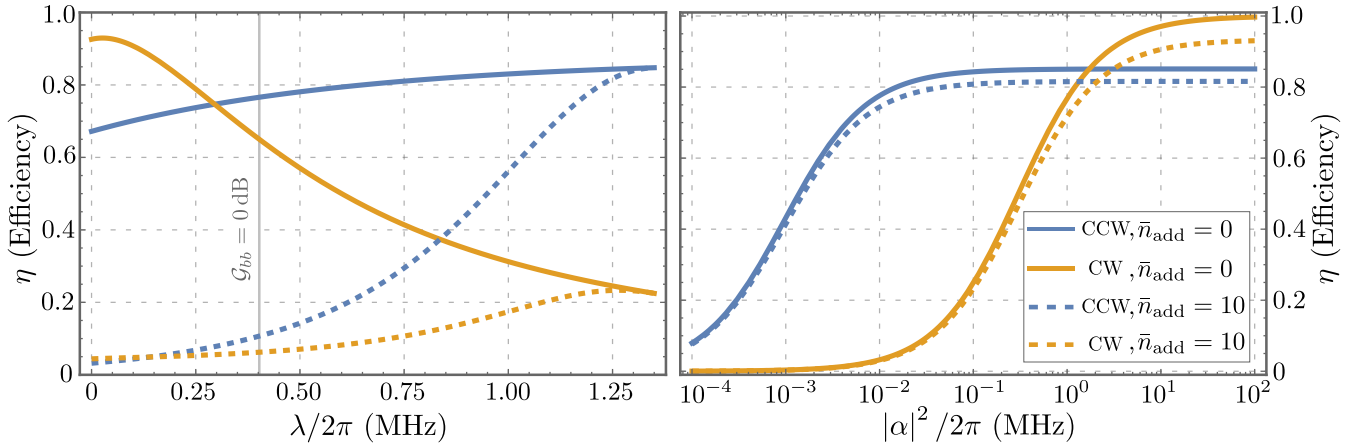

Figure 4.11: [Left] The measurement efficiency $\eta = \Gamma_{\text{meas}}/\Gamma_{\text{d}}$ of the nonreciprocal amplifier plotted against squeezing strength, $\lambda/2\pi$, with the drive amplitude set to $|\alpha|^2/2\pi = 0.1\,\text{MHz}$. [Right] Here, the measurement efficiency is plotted against the drive amplitude $|\alpha|^2/2\pi$, with the amplifier gain fixed to $\mathcal{G}_{bb} = 20\,\text{dB}$, equivalent to $\lambda/2\pi \approx 1.2347\,\text{MHz}$. Results for the two optimum values of the loop phase are shown, and for both values, the relative phase of the single-mode squeezer and drive are tuned so as to amplify the measurement signal. The plotted phase values are then: $\phi = -\pi/2$ and $\theta - 2\varphi = -\pi/2$ (blue), and, $\phi = +\pi/2$ and $\theta - 2\varphi = +\pi/2$ (orange). For these two sets of phases, we consider the case where there is no added off-chip noise, $\bar{n}_{\text{add}} = 0$ (solid), and where there is ten photons of added noise, $\bar{n}_{\text{add}} = 10$ (dashed). All other system parameters are identical to those in Figure 4.8. Although the right plot includes large values of $|\alpha|^2$, the entire range is not accessible since the cavity mode occupation must be well below the critical photon number, defined in Section 4.1.3 for the single mode case. Applying that result here, and assuming a cavity-qubit mode detuning of roughly $\Delta/2\pi \sim 1\,\text{GHz}$, the critical photon number is on the order of $n_{\text{crit}} = \Delta/4\chi \sim 100$. Using the classical cavity occupations from Eqs. (4.119) and (4.120), we arrive at rough photon occupations of $\left|\alpha_{c,\text{int}}^{\text{ccw}}\right|^2 \approx 0.31\,|\alpha|^2\,(\text{MHz}/2\pi)^{-1}$ and $\left|\alpha_{c,\text{int}}^{\text{ccw}}\right|^2 \approx 132.5\,|\alpha|^2\,(\text{MHz}/2\pi)^{-1}$. When circulating CCW the measurement dephasing safely overwhelms the parasitic dephasing before the cavity occupation becomes a problem, while for CW circulation the parasitic dephasing is not sufficiently minimised in comparison to the measurement dephasing until $|\alpha|^2 \sim 100$, by which point the internal occupation of the cavity mode has far surpassed the critical photon number, rendering the model unphysical.

efficiency becomes independent of increases in $|\alpha|^2$. Using the provided parameter values, for CCW circulation this behaviour does not occur until roughly $|\alpha^{\text{ccw}}|^2 \gtrsim 0.1$, while for CW circulation the required drive amplitude is two orders of magnitude larger, $|\alpha^{\text{cw}}|^2 \gtrsim 10$. The reason is that the parasitic dephasing is orders of magnitude smaller due to the circulation of amplifier noise away from the cavity mode. This is evident in Figure 4.8, where, for example, the difference is roughly $\Gamma_{\text{d,p}}^{\text{cw}} \sim 500\,\Gamma_{\text{d,p}}^{\text{ccw}}$ for all values of the single-mode squeezer amplitude λ.

Since it is easy to render the parasitic dephasing irrelevant with CCW circulation, we will continue our focus on this direction. Omitting any sources of thermal noise, the measurement dephasing can be written directly from Eq. (4.118):

$$\Gamma_{\text{d,m}}^{\text{ccw}} = \frac{8\,|\alpha|^2\,\mathcal{X}^2\mathcal{C}_{bc}(1+\mathcal{C}_{bc})}{\left((1+\mathcal{C}_{bc})^2+\mathcal{X}^2\right)^2}. \tag{4.125}$$

The measurement rate for CCW circulation, assuming no added off-chip noise, and an optimum relative phase of $\theta - 2\varphi = -\pi/2$ between the squeezer and drive, can be expressed as

$$\Gamma_{\text{meas}}^{\text{ccw}} = \frac{(-1+\mathcal{C}_{ab}+\mathcal{C}_{\lambda})^2}{(-1+\mathcal{C}_{ab}+\mathcal{C}_{\lambda})^2+4\mathcal{C}_{ab}} \times \frac{8\,|\alpha|^2\,\mathcal{X}^2\mathcal{C}_{bc}^2}{\left((1+\mathcal{C}_{bc})^2+\mathcal{X}^2\right)^2}. \tag{4.126}$$

As mentioned previously, $\Gamma_{\text{d,m}}^{\text{ccw}}$ is equivalent to the drive-induced dephasing for a measurement apparatus comprised of two modes coupled via a beam splitter where both modes only experience vacuum noise from their baths. Things are slightly different for the measurement rate $\Gamma_{\text{meas}}^{\text{ccw}}$, which, as seen above, can be expressed as the product of two parts. The term dependent on $\mathcal{C}_{bc}$ is the measurement rate for the passively coupled two-mode system with dephasing given by Eq. (4.125). The other term is dependent on the beam splitter between the amplifier and buffer mode, $\mathcal{C}_{ab}$, along with the amplifier strength, $\mathcal{C}_{\lambda}$. This term arises because, unlike the passively coupled two-mode system, the measurement signal is circulated past the amplifier mode before reaching the buffer. Despite the presence of amplification, the loss incurred by passing the amplifier mode attenuates the measurement rate so that it is below

that of the passively coupled two-mode system. This is the result of amplification of the measured quadrature, and is the price we pay to minimise the backaction on the qubit.

Assuming that the drive amplitude is sufficiently large, the efficiency can be approximated as follows:

$$\eta^{\mathrm{ccw}} \approx \frac{(-1+\mathcal{C}_{ab}+\mathcal{C}_{\lambda})^2}{(-1+\mathcal{C}_{ab}+\mathcal{C}_{\lambda})^2+4\mathcal{C}_{ab}} \times \frac{\mathcal{C}_{bc}}{\mathcal{C}_{bc}+1} \equiv \frac{1}{1+4\mathcal{C}_{ab}/(-1+\mathcal{C}_{ab}+\mathcal{C}_{\lambda})^2} \times \frac{1}{1+1/\mathcal{C}_{bc}}. \tag{4.127}$$

In order to maximise this measurement efficiency, we can take a lesson from the mismatched circulator and make the beam splitter couplings as large as possible to swap the measurement signal to the buffer before it can be decayed away. In the regime where $\mathcal{C}_{ab}, \mathcal{C}_{bc} \to \infty$ it can be confirmed that $\eta^{\mathrm{ccw}} \to 1$, and that this upper limit is independent of the strength of the amplifier $\mathcal{C}_{\lambda}$.

It is also important to analyse the dependence of the efficiency on the gain of the amplifier, which can be done by varying $\mathcal{C}_{\lambda}$ while fixing $\mathcal{C}_{ab}$. If the beam splitter rate is faster than the decay rates, $\mathcal{C}_{ab} > 1$, then this function increases over the range of single-mode squeezing amplitudes permitted by the stability criterion, $\mathcal{C}_{\lambda} \in [0, 1+\mathcal{C}_{ab})$. The measurement efficiency is therefore maximised when the system approaches instability, and so increasing the distinguishability of the signal outweighs the increase in output noise power. We can write a series expansion for the efficiency about the point of instability:

$$\lim_{\mathcal{C}_{\lambda}\to 1+\mathcal{C}_{ab}} \eta^{\mathrm{ccw}} \approx \frac{1}{1+1/\mathcal{C}_{bc}} \left(\frac{1}{1+1/\mathcal{C}_{ab}} - \frac{1+\mathcal{C}_{ab}-\mathcal{C}_{\lambda}}{(1+\mathcal{C}_{ab})^2} + \mathcal{O}\big[(1+\mathcal{C}_{ab}-\mathcal{C}_{\lambda})^2\big] \right). \tag{4.128}$$

To approach $\eta^{\mathrm{ccw}} \to 1$, we therefore still require that the beam splitter rates be as large as possible to overcome any attenuation in the system.

The efficiency exhibits strange behaviour when the decay rates match or overwhelm the beam splitter rate, $\mathcal{C}_{ab} \leq 1$. In this regime the efficiency goes exactly to zero, $\eta^{\mathrm{ccw}} = 0$, when $\mathcal{C}_{\lambda} = 1 - \mathcal{C}_{ab}$. The signal is therefore gone, and there is no way to distinguish between the pointer states. At this point the gain of the amplifier is actually negative, and is smaller than the gain that would be realised if the squeezer was turned off, $\mathcal{G}_{bb}(\mathcal{C}_{\lambda} = 1-\mathcal{C}_{ab}) \leq \mathcal{G}_{bb}(\mathcal{C}_{\lambda}=0)$ for $\mathcal{C}_{ab} \leq 1$. This implies that the measurement signal is, in fact, squeezed and not amplified. This behaviour is not explained by the intuition that we have built to this point because this was based on the assumption that the signal propagates perfectly in one direction through the circuit with a negligible amount of loss. Although the efficiency does increase as $\mathcal{C}_{\lambda}$ is increased over the range $\mathcal{C}_{\lambda} \in [1-\mathcal{C}_{ab}, 1+\mathcal{C}_{ab})$, we have no explanation for the behaviour of η^{ccw} in this regime.

For comparison, we examine the optimal measurement efficiency for CW circulation by assuming that $|\alpha|$ is sufficiently large, the phase condition $\theta - 2\varphi = +\pi/2$ is met, and that there is no added noise. Unlike before, the expressions for both rates are not compact. Motivated by the fact that numerical simulations show that the efficiency increases as the amplitude of the squeezer approaches the point of instability, we again examine the efficiency for CW circulation in this limit:

$$\lim_{\mathcal{C}_{\lambda}\to 1+\mathcal{C}_{ab}} \eta^{\mathrm{cw}} \approx 1-(1+\mathcal{C}_{ab}-\mathcal{C}_{\lambda})^2 \frac{(1+\mathcal{C}_{bc})^2\big((1+\mathcal{C}_{bc})^2+4\mathcal{C}_{ab}\mathcal{C}_{bc}\big)+2\mathcal{X}^2(1-\mathcal{C}_{bc}^2)+\mathcal{X}^4}{16\mathcal{X}^2\mathcal{C}_{ab}\mathcal{C}_{bc}^2(1+\mathcal{C}_{ab})^2} + \mathcal{O}\big[(1+\mathcal{C}_{ab}-\mathcal{C}_{\lambda})^3\big]. \tag{4.129}$$

This behaviour contrasts heavily with what was observed for CCW circulation, where the efficiency still relied on making $\mathcal{C}_{ab}$ and $\mathcal{C}_{bc}$ as large as possible to optimise efficiency. No such limitation exists for the CW circulation efficiency. Here we can see that the measurement efficiency is limited mainly by the gain of the amplifier, and can theoretically approach perfect efficiency, regardless of the beam splitter rates. This indicates that the presence of amplified noise improves the measurement efficiency, an effect seen in other works [215, 217, 219], and can help overcome any losses in the cavity mode before the signal moves to the buffer mode. Compared to CW circulation, CCW circulation has to contend with the problem of loss, since the signal is still nearly a vacuum state when it is in the cavity mode, and will experience added loss as it passes to the amplifier mode. This occurs when the cooperativity between modes a and c is small, $\mathcal{C}_{ac} \ll 1$, although and is not seen directly due to the absence of $\mathcal{C}_{ac}$ in Eq. (4.127) as a result application of the nonreciprocity condition having been applied.

Although Eq. (4.129) may appear to be optimal behaviour, in reality, the increase in the intracavity occupation due to a large $|\alpha|$ will cause a breakdown in the model before then, as was observed in Eddins et al [209]. As demonstrated in Figure 4.11, a naïve calculation shows that the critical drive strength for CW circulation will be reached at much smaller drive magnitudes compared to CCW circulation, $|\alpha_{\mathrm{crit}}^{\mathrm{cw}}|^2 \sim 430\,|\alpha_{\mathrm{crit}}^{\mathrm{ccw}}|^2$, demonstrating that circulating noise away from the cavity mode is also important to prevent the breakdown of our model.

The final point of concern is: how well does the nonreciprocal amplifier compensate for added off-chip noise? Using the definition for added noise from Eq. (4.124) we can see that to compensate for any decrease in efficiency due to $\bar{n}_{\mathrm{add}}$, that the output noise-power should be much larger to swamp this extra noise $\bar{S}_{MM,e/g}[0] \gg \bar{n}_{\mathrm{add}}$. The signal component of the measurement rate must also increase as well so that the measurement efficiency does not decrease;

as shown in Figure 4.11, we can realise this behaviour for both CW and CCW circulation. We can re-examine the ideal behaviour for CCW circulation when additional off-chip noise is taken into account:

$$\eta^{\mathrm{ccw}} \approx \frac{(-1+\mathcal{C}_{ab}+\mathcal{C}_{\lambda})^2}{4\mathcal{C}_{ab}\mathcal{C}_{\lambda}+(2\bar{n}_{\mathrm{add}}+1)(1+\mathcal{C}_{ab}-\mathcal{C}_{\lambda})^2} \times \frac{\mathcal{C}_{bc}}{\mathcal{C}_{bc}+1}. \tag{4.130}$$

This expression makes it clear that the added noise term is diminished as the strength of the single-mode squeezing approaches the point of instability, $\mathcal{C}_{\lambda} \to 1+\mathcal{C}_{ab}$, corresponding to increased amplifier gain and hence larger output noise-power. This behaviour is observed in Figure 4.11, where the curves with and without added noise converge to the same value for larger values of the squeezer amplitude λ. This figure also demonstrates that the same logic holds true for CW circulation, and that this is to be expected even when the parasitic dephasing is non-negligible.

4.4 Summary and Outlook

In this chapter, we provided a review of the fundamental limits for the QND measurement of the state of a qubit. We showed that the rate at which information about the qubit state is acquired by the measurement apparatus cannot exceed the rate at which the measurement dephases the qubit. Both quantities are necessary to determine the efficiency of the measurement, but while calculating the former quantity is easy, the latter is difficult. To accurately characterise the dephasing, we expanded a previously used method using the moments of a complex-valued non-normalised Wigner function, allowing for rapid solution of the dephasing for multimode systems involving active processes and environmental noise beyond vacuum fluctuations.

We then proceeded to investigate the use of a three-mode nonreciprocal amplifier dispersively coupled to the qubit to realise fast and efficient measurement. This device was taken to be a single-port amplifier due to the constraints of the motivating physical system, where the measurement signal was injected and collected through the same port; an investigation of different measurement schemes using this amplifier was not undertaken, but would also be of interest for comparison. A detailed analysis allowed us to determine the optimum operational regime for the nonreciprocal amplifier, where it was found that nonreciprocity could be used to protect the qubit against excessive dephasing by only allowing signal transmission from the cavity mode to the amplifier mode with near-negligible transmission in the reverse direction. The addition of the amplifier allowed for an increase in the measurement rate beyond a single-mode setup, with added amplifier noise also helping to overwhelm added noise from further down in the measurement chain. This more than compensated for any loss of efficiency that resulted from signal loss within the nonreciprocal amplifier due to the increased number of bosonic modes. For the opposite direction of nonreciprocal scattering, it was found that increasing amplifier gain also helped to overcome off-chip noise. However, using physically motivated parameters, it was found that eventually the excess parasitic dephasing caused by amplified noise in the cavity mode would become a significant part of the total qubit dephasing, reducing the achievable measurement efficiency.

While it is well understood how the measurement-induced dephasing and the measurement rate are affected by changes in the system parameters, the behaviour of the parasitic dephasing is not entirely understood. The analysis in this chapter demonstrated that the parasitic dephasing resulting from the presence of amplification is minimised when the loop phase and cooperativities are set such that this noise is directed away from the dispersively coupled cavity mode. How the choice of parameters affects the magnitude of the parasitic dephasing, however, is still unknown. Unlike the other rates, the parasitic dephasing cannot be written solely in terms of the various cooperativities, resulting in a more complicated analysis due to the dependence on the bare dissipation and coupling rates. The difficulty in understanding the effect of varying the numerous parameters is compounded by the intractable analytic expression for the dephasing. Performing the full analysis is of critical importance since optimum efficiency requires that the parasitic dephasing be significantly smaller in magnitude compared to the measurement dephasing, which, due to physical limitations, cannot always be made arbitrarily large through increases in the drive amplitude. Based on the fact that parasitic dephasing arises only when the noise is above vacuum, it may be possible to glean some information from the covariance matrix of the dispersively coupled mode's internal state.

4.4.1 The Dispersive Regime

This work was performed under the assumption that the Hamiltonian in Eq. (4.83) can be obtained by bringing a system consisting of some parametrically coupled modes coupled to a two-level artificial atom into the dispersive regime. Such a derivation would be important to demonstrate the validity of the model and would provide insight into the conditions that will have to be fulfilled for this approximation to be valid. One of the most important conditions that we need to fulfill is the critical photon number. If the occupation of the bosonic modes is not well below their critical photon numbers, then higher energy levels of the transmon become accessible. This is of particular interest for

this system since the gain of the amplifier will alter this limit[6], and so will impact which gain values are physically attainable for a given drive amplitude. Working in the rotated frame, and including the necessary detunings, our initial Hamiltonian could look like

$$\begin{aligned}\hat{H} = \Delta_a \hat{a}^\dagger \hat{a} + \Delta_b \hat{b}^\dagger \hat{b} + \Delta_c \hat{c}^\dagger \hat{c} + \frac{\Delta_q}{2}\hat{\sigma}_z + \frac{\lambda}{2}\left(e^{i\theta}\hat{a}^{\dagger 2} + e^{-i\theta}\hat{a}^2\right) + g_q\left(\hat{c}^\dagger \hat{\sigma}_- + \hat{c}\hat{\sigma}_+\right) \\ + g_{ab}\left(\hat{a}^\dagger \hat{b} + \hat{a}\hat{b}^\dagger\right) + g_{bc}\left(\hat{b}^\dagger \hat{c} + \hat{b}\hat{c}^\dagger\right) + g_{ac}\left(e^{i\phi}\hat{a}^\dagger \hat{c} + e^{-i\phi}\hat{a}\hat{c}^\dagger\right).\end{aligned} \tag{4.131}$$

The goal here is to obtain a dispersive Hamiltonian like in Eq. (4.83), however, the addition of squeezing and multiple bosonic modes complicates the use of the usual method, described in Section 4.1.3 for a Jaynes-Cummings Hamiltonian. The introduction of squeezing also means that the total number of quanta is no longer conserved, however, a linearised unitary transformation which solves this been proposed for a single mode system with squeezing [220], providing insight into how to approach the inclusion of single-mode squeezing when transforming the nonreciprocal amplifier to the dispersive regime.

The dispersive limit for a system consisting of multiple bosonic modes, on the other hand, has not been investigated in the literature. For the passive three-mode loop, the total quanta is still a conserved quantity, and so the Hamiltonian can be brought to a multimode Jaynes-Cummings form by means of a rotation of the bosonic modes. Including the squeezing complicates things, since the form of the Hamiltonian is now a multimode Rabi Hamiltonian when written in the normal mode basis. While it is possible to bring the Rabi Hamiltonian, along with other models not within the RWA regime, to the dispersive regime [221–223], such methods have not, as of yet, been applied to our multimode Hamiltonian.

4.4.2 Extending the Moment Method

The moment method, as formulated in this section, can be applied to a system comprised of a single qubit coupled to a multimode system. A quantum computer requires that the states of multiple qubits be read out efficiently and simultaneously [153], and such multiplexed qubit readout has long since been realised using the circuit QED architecture [224, 225]. Extending the moment method to multiple qubits is straightforward, but requires some modification to our initial assumptions. We recall that, for a single qubit system, T1-processes were necessarily excluded when applying the method to the pointer states because the distinguishability of the pointer states was destroyed through qubit state transitions, however, this was not a concern when calculating the dephasing. When extending the method to multiplexed qubit readout, this is no longer the case, and all processes which stimulate qubit state transitions must be excluded, even for dephasing calculations. To demonstrate exactly why, we consider a two-qubit system. The state can be written as a matrix in the tensor product basis as

$$\hat{\rho} = \begin{pmatrix} \hat{\rho}_{ee} & \hat{\rho}_{eg} \\ \hat{\rho}_{ge} & \hat{\rho}_{gg} \end{pmatrix} = \begin{pmatrix} \begin{pmatrix} \rho_{ee,ee} & \rho_{ee,eg} \\ \rho_{ee,ge} & \rho_{ee,gg} \end{pmatrix} & \begin{pmatrix} \rho_{eg,ee} & \rho_{eg,eg} \\ \rho_{eg,ge} & \rho_{eg,gg} \end{pmatrix} \\ \begin{pmatrix} \rho_{ge,ee} & \rho_{ge,eg} \\ \rho_{ge,ge} & \rho_{ge,gg} \end{pmatrix} & \begin{pmatrix} \rho_{gg,ee} & \rho_{gg,eg} \\ \rho_{gg,ge} & \rho_{gg,gg} \end{pmatrix} \end{pmatrix}. \tag{4.132}$$

Focusing on one of the qubits in this multi-qubit system, the presence of T1-processes results in transitions between the excited and ground states of that qubit, $\hat{\rho}_{ee}$ and $\hat{\rho}_{gg}$. Consequently, these state components contain information about the coherence of the other qubit through the matrix elements $\rho_{ee,eg}$ and $\rho_{gg,eg}$. For the Gaussian moment method to be used, these elements cannot couple to each other, and so all processes which result in qubit transitions must be excluded. As a result, the measurement must preserve the probability of the pointer states, and hence have the Pauli spin-z operators as QND-observables. The only non-trivial operators which do this are the individual Pauli spin-z operators, as well as combinations of these operators, such as ZZ-couplings. This same logic can be applied to any number of qubits, as well as combinations of finite-level systems with more than two energy levels, all of which have relevance in cases where excitation to higher energy levels of the transmon is non-negligible [226].

Extending the method to include nonlinear mode dynamics is also of interest, though the resulting dynamics is considerably more complicated. Although the expressions in Eq. (4.62) relating the dephasing and frequency shift to the norm of the Wigner functions still hold, the non-linear equations of motion will no longer preserve the Gaussianity of the Wigner functions. The higher order central moments then become independent quantities, and the closed set of differential equations in Eq. (4.74) becomes an infinite set which must be truncated to be solvable. If, however, the nonlinearity is sufficiently weak so that the system may be approximated with sufficient accuracy by a linearised model, then the original method as presented here will still be usable.

[6] As an example, for the dispersive measurement in Ref. [209] it was found that the single-mode squeezing altered the critical photon number by $n_{\text{crit}} = (\Delta^2/4g^2)(1+\lambda^2/\Delta^2)^2$, resulting in a dispersive coupling of the form $\chi = (g^2/\Delta)(1+\lambda^2/\Delta^2)^{-1}$ [220], where λ is the amplitude of the squeezing as in Eq. (4.131), and all other parameters are identical to those used in Section 4.1.3.2.

5 Conclusion

Nonreciprocal quantum amplifiers were originally conceived to perform two signal processing tasks: the amplification of weak signals and the directional routing of amplified signals to prevent backaction on sensitive quantum systems. Their realisation was desirable because they could replace bulky and noisy classical devices with better noise characteristics determined by the standard quantum limit. The integration of both functions in one device also reduced the need for multiple components in certain parts of the measurement chain. Since they are at their core quantum devices, they are also suited to integration with quantum circuits. While all of these properties are desirable, their main purpose is to replace classical devices with quantum ones when performing the usual signal processing applications. In this dissertation, we investigated further uses for these nonreciprocal quantum amplifiers, specifically two possible configurations called the delta and bowtie amplifiers. The results demonstrate that nonreciprocal quantum amplifiers have utility beyond just signal processing, and that their inherently quantum nature allows for novel applications specific to the quantum realm.

In Chapter 3, the use of nonreciprocal amplifiers to generate high fidelity entangled states was first investigated, prompted by the possibility that they could distribute states to modes within a quantum network. While it was not apparent at the outset if entanglement would be possible between modes which scatter nonreciprocally, it was found that not only is this not an impediment, but that nonreciprocity can be used to improve the purity, and hence, the fidelity of flying states. This is accomplished by using the directional signal routing capabilities to redirect unwanted thermal noise away from the output of hot modes by swapping it with input noise from a cold mode acting as a reservoir. This allowed for a hot mode to generate high-fidelity propagating entangled states with another cold mode in the amplifier, while the thermal noise ended up in the output of the cold reservoir. This behaviour was observed for both the delta and bowtie amplifiers, demonstrating that it is not specific to one configuration and can be extended to other nonreciprocal amplifiers.

It was also observed that the three-mode configurations are unable to handle multiple sources of thermal noise, and so high fidelity entanglement of multiple hot modes necessitates the use of multiple amplifiers and an entanglement swapping protocol, or amplifier configurations with a larger number of modes. In addition, it was noted that there exist further nonclassical correlations in quantum systems which do not necessarily involve entanglement, termed quantum discord. Whether the routing ability of these nonreciprocal amplifiers is of any benefit for the generation of these other quantum correlations remains an open question.

Chapter 4 introduced the problem of qubit measurement in circuit QED, where the use of a quantum amplifier as the preamplifier in a measurement chain is necessary to improve the efficiency of the readout. Even if this preamplifier is a nonreciprocal quantum amplifier, loss has already occurred as the measurement signal is transferred from the measurement resonator. The proposed solution was to integrate the nonreciprocal amplifier with the qubit, where it could perform the dual function of measurement resonator and amplifier.

To accurately characterise the efficiency, both the measurement rate and the rate of the qubit dephasing due to measurement must be calculated. In order to calculate the latter quantity, an existing method using the Wigner phase-space representation was extended to accommodate measurement systems with an arbitrary number of modes, allowing for the calculation of the dephasing from an easily constructed system of ordinary differential equations. The expanded method allowed for the exact calculation of the steady-state dephasing of the qubit due to the nonreciprocal amplifier, in this case, the bowtie configuration, during a measurement. Here, it was found that when the amplifier is operated at its optimal point, the directional signal propagation protects the qubit from excess dephasing due to the amplification. It was also found that while the upper limit of the measurement efficiency is initially limited in comparison to simpler measurement schemes, the ability to amplify the measurement signal at the source more than compensates for this, rendering the signal more robust against added noise from further up the measurement chain.

With the general moment method developed, the analysis of a myriad number of measurement setups becomes a comparatively simple affair. Although this work demonstrated the usefulness of a single measurement configuration, that of an integrated one-port nonreciprocal amplifier directly coupled to a qubit measurement. Use of the moment method allows for the analysis of the time-dependent and steady-state efficiencies of other measurement apparatuses, such as

multi-port nonreciprocal amplifiers, or other measurement schemes beyond the traditional dispersive measurement. Additionally, the moment method also opens up the possibility of reevaluating the efficiencies of previous experiments involving on-chip amplifiers and other signal processing components, which, although not directly coupled to the qubit, still form a larger collective quantum system due to their coupling to the readout resonator. Since quantum computers would require that simultaneous readout of multiple qubits be performed through a single amplifier, the method should also be further generalised to accommodate such multiplexed readout schemes.

A Phase Space Formulation of Quantum Mechanics

A basic understanding of the Wigner phase-space representation of quantum mechanical states and operators is essential for the work done in this dissertation. The treatment of phase-space representations in optics books is often focused on very specific applications and so is lacking in details which provide the connection between quantum mechanics in Hilbert space and phase space. The goal of this section is to provide a summary of how these two are connected, starting with a short historical summary, followed by some definitions for phase-space quasi-probability distributions and their related expectation values. Finally, we move on to the Wigner representation and show how dynamics can be performed here using the noncommutative Moyal product.

A.1 A Brief History

The formulation of quantum mechanics in terms of phase-space quasi-probability distributions is nearly as old as the original wave function and matrix formulations of quantum theory, both of which date to 1925 [227, 228]. The first mapping from phase space to Hilbert space was introduced in 1927 by Hermann Weyl [229], who provided a correspondence rule to transform phase-space functions to symmetrised functions of quantum mechanical operators. The inverse map, from operator space to phase space, was introduced in 1932 by Eugene Wigner [230]; this mapping defines the celebrated *Wigner function*. Another fundamental contribution to this field comes from Groenewold in his 1946 doctoral dissertation [34]. It was demonstrated in this work that it is not possible to define a general linear map from all possible phase-space functions to Hermitian quantum mechanical operators such that all classical Poisson bracket relations are also preserved by the corresponding operator commutation relations, now known as Groenewold's theorem. The same dissertation also introduces a phase-space *star product*, which is the phase-space equivalent to the noncommutative operator product. This star product was an attempt to define a consistent phase-space bracket, and allows for the quantum operator calculus to be mapped exactly to phase space. Importantly, the resulting phase-space functions are not equivalent to the classically expected ones, and often involve correction terms involving $\hbar$. A relation using the Fourier transform, equivalent to the star product, had in fact been demonstrated years earlier by von Neumann, but the result was not fully appreciated at the time [231]. This star product is sometimes called the *Weyl-Groenewald product*, or more commonly the *Moyal product*, largely in honour of Moyal's contributions in the field.

The goal of this early approach to quantum mechanics in phase space was to establish a connection between smooth functions in real space and operators in Hilbert space which obeyed the canonical commutation relations, $[\hat{q}, \hat{p}] = i\hbar$. The phase-space treatment also provided a connection between quantum theory and classical statistical physics, a topic expounded upon by Moyal [35]. For systems which do not obey these relations, such as finite-dimensional systems, systems with rotational symmetry, et cetera, there are other phase-space formulations. The construction of these alternative formulations depends on which properties one wishes to preserve when defining the phase-space mapping. In the brief history provided here, the main motivation was to systematically establish the transition from classical to quantum systems, a process known as *quantisation*. The phase-space approach is specifically referred to as *deformation quantisation*, since the traditional phase-space structures must be modified, or *deformed* with the aforementioned correction terms involving $\hbar$, in the classical to quantum transition.

The phase-space treatment has proven to be popular in quantum optics, as well as other fields where the semiclassical treatment of systems is practical, and even more recently in quantum information. In these cases, it is the representation of quantum states in a classical-like phase space which is of interest. In addition to the aforementioned Wigner representation, two other phase-space mappings are commonly used in quantum optics: the Husimi Q representation developed in 1940 by Kôdi Husimi [232], and the Glauber–Sudarshan P representation, developed independently in 1963 by Roy Glauber [233] and George Sudarshan [234]. These two representations, along with the original from Wigner, belong to the same class of phase-space representations and correspond to different *ordering* prescriptions between phase-space symbols and quantum mechanical operators.

A.2 Quasi-Probability Distributions

At the beginning of the previous section, we referred to phase-space distributions corresponding to quantum states as *quasi-probability distributions* (QPDs) because, while they allow for the calculation of statistical quantities of the quantum state, they do not obey all the properties of true probability distributions [235]. Despite this, they permit a unique perspective in the study of quantum mechanics and provide a link between it and classical physics. In order to discuss exactly how these quantum QPDs fail to be true probability distributions, we start by listing the Kolmogorov axioms for a probability distribution:

1. A probability distribution is a real-valued and non-negative function.
2. The probability for the entire sample space is one.
3. For a set of disjoint events, the probability of the union of these events is equal to the sum of the probabilities of the individual events.

As previously stated, unlike in classical physics, phase-space distributions in quantum mechanics are QPDs because they do not obey all of these axioms [236]. The first axiom is broken in general by our phase-space functions since they can take on negative values [230], although, importantly, the size of an individual negative region is constrained to never be larger than $\hbar$. Since exact locations in phase space are obscured by the uncertainty principle, this size restriction guarantees that the area of uncertainty around a point in phase space includes some area with positive probability density. The meaning of these regions of negative probability is still a matter of debate; despite this, the integral of the QPD for a density operator $\hat{\rho}$ over the entire phase space is still equal to one since the density operator must have unit trace, and so the second axiom is obeyed. Lastly, no events in phase space are truly disjoint since this would again violate the uncertainty principle, meaning that points in phase space which are close to each other on the order of $\hbar$ are generally correlated, so the third axiom is also violated; in practical calculations this occurs as a result of the replacement of usual scalar multiplication by the nonlocal Moyal star product. The uncertainty relation between position and momentum variables also means that it is not physically meaningful to consider points of definite position and momentum in phase space, which must again be replaced by area elements on the order of $\hbar$ or larger. As a final note, although some phase-space distributions will always obey the first axiom, such as states with Gaussian phase-space representations, they will still violate the third axiom and are therefore still considered QPDs.

Despite this, QPDs still allow for the calculation of expectation values of operators through the computation of integrals over phase space, or by taking derivatives of their associated characteristic function. It is also still possible to obtain physically meaningful marginal distributions by integrating over some subset of the entire phase space. The first step is to define a characteristic function for a density operator which consists of N bosonic modes:

$$w_s(\boldsymbol{\xi}) := \mathrm{Tr}\Big[\hat{\rho} e^{i\boldsymbol{\xi}\cdot\hat{\boldsymbol{r}}}\Big] e^{s|\boldsymbol{\xi}|^2/4}. \tag{A.1}$$

where $\hat{\boldsymbol{r}}$ is a vector of $2N$ operators in the quadrature basis, and $\boldsymbol{\xi}$ is a vector of associated variables in the Fourier space of the same length. The free parameter s denotes the *ordering* of the expectation values encoded in the moments of the characteristic function, with respect to the basis of creation and annihilation operators for the system modes. Three particular values are of interest: $s = -1$ corresponds to antinormal ordered expectation values, $s = 0$ to symmetric ordering, and $s = 1$ to normal ordering [237]. Of course, expectation values for any ordering can be extracted from any characteristic function since the ordering of the mode operators can always be shuffled using the canonical commutation relations. We can define the QPD associated with this characteristic function as usual, by applying the Fourier transform:

$$W_s(\boldsymbol{r}) := \frac{1}{(2\pi)^{2N}} \int_{\mathbb{R}^{2N}} w_s(\boldsymbol{\xi}) e^{-i\boldsymbol{\xi}\cdot\boldsymbol{r}}\, d^{2N}\boldsymbol{\xi}. \tag{A.2}$$

The above expression returns one of the three most commonly used phase-space representations depending on the choice of the ordering parameter: $s = -1$ corresponds to the Husimi Q representation, $s = 0$ to the Wigner representation, and $s = 1$ to the Glauber–Sudarshan P representation [237]. As stated previously, this QPD must be normalised since the trace of $\hat{\rho}$ is one:

$$\int_{\mathbb{R}^{2N}} W_s(\boldsymbol{r})\, d^{2N}\boldsymbol{r} = 1, \tag{A.3}$$

which may be demonstrated by using Eq. (A.2):

$$\begin{aligned}\int_{\mathbb{R}^{2N}} W_s(\boldsymbol{r})\, d^{2N}\boldsymbol{r} &= \frac{1}{(2\pi)^{2N}} \int_{\mathbb{R}^{2N}} \int_{\mathbb{R}^{2N}} w_s(\boldsymbol{\xi}) e^{-i\boldsymbol{\xi}\cdot\boldsymbol{r}}\, d^{2N}\boldsymbol{r}\, d^{2N}\boldsymbol{\xi} \\ &= \int_{\mathbb{R}^{2N}} w_s(\boldsymbol{\xi})\delta(\boldsymbol{\xi})\, d^{2N}\boldsymbol{\xi} \;\text{ where } \delta(\boldsymbol{\xi}) := \delta(\xi_1)\delta(\xi_2)\ldots\delta(\xi_{2N}) \\ &= w_s(0) = \mathrm{Tr}[\hat{\rho}] = 1. \end{aligned} \tag{A.4}$$

Partial traces can be obtained by integrating over pairs of noncommuting quadratures in phase space. Specific details concerning these three distributions, and their relation to specifically ordered expectation values, can be found in several sources [45, 46]. The symmetrically ordered Wigner functions have the specific property that the marginal distributions correspond to expectation values of the density operator, a property which is shared by no other QPD [236]. The marginal probability distribution over the quadrature r corresponds to the expectation value of the observable $\hat{r}$, and is obtained by integrating over all other quadratures, labelled $\boldsymbol{r}_{\mathrm{int}}$, in the phase space,

$$\langle r|\hat{\rho}|r\rangle = \int_{\mathbb{R}^{2N-1}} W(\boldsymbol{r})\, d^{2N-1}\boldsymbol{r}_{\mathrm{int}}. \tag{A.5}$$

Since Wigner QPDs are the only quantum phase-space functions which produce the correct marginals, we will therefore focus solely on this representation. As previously mentioned, the Wigner representation corresponds to symmetrically ordered expectation values, the details of which we will now consider. From this point onward, we will use the following notation for the characteristic function and QPD of the Wigner representation, $w_0(\boldsymbol{\xi}) \equiv w(\boldsymbol{\xi})$ and $W_0(\boldsymbol{r}) \equiv W(\boldsymbol{r})$. We begin by writing again the symmetrically ordered characteristic function, this time for only a single mode for clarity:

$$w(\xi_q, \xi_p) := \mathrm{Tr}\Big[\hat{\rho} e^{i(\xi_q\hat{q} + \xi_p\hat{p})}\Big]. \tag{A.6}$$

Raw moments can be extracted from the characteristic function by differentiation:

$$\langle(\hat{q}^m\hat{p}^n)_S\rangle = (-i)^{m+n} \frac{\partial^{m+n}}{\partial\xi_q^m \partial\xi_p^n} w(\xi_q, \xi_p)\Big|_{\xi_q,\xi_p=0}. \tag{A.7}$$

The expression $(\hat{q}^m\hat{p}^n)_S$ denotes the symmetrically ordered combination of these operators, which are given by [238]:

$$(\hat{q}^m\hat{p}^n)_S := \frac{1}{2^m}\sum_{k=0}^{m} \binom{m}{k} \hat{q}^k\hat{p}^n\hat{q}^{m-k} \equiv \frac{1}{2^n}\sum_{k=0}^{n} \binom{n}{k} \hat{p}^k\hat{q}^m\hat{p}^{n-k}. \tag{A.8}$$

We can apply the inverse Fourier transform and instead represent this expectation value as an integral over the entire phase space,

$$\langle(\hat{q}^m\hat{p}^n)_S\rangle = \int_{\mathbb{R}^2} W(q,p)\, q^m p^n\, dq\, dp. \tag{A.9}$$

In the case of Gaussian states, Isserlis' theorem can be used to further decompose higher-order moments into products of first- and second-order moments. The above formulae will be important when defining equations of motion for the means and covariances of Gaussian states, since dynamical equations for the state map to partial differential equations (PDEs) in phase space and the associated Fourier space. In order to construct these PDEs systematically, we will now introduce some additional machinery to describe how one maps not just a density operator but any operator to phase space, and how products of operators are mapped to phase space.

A.3 The Wigner Representation

The Wigner function can be seen as a map from Hilbert space to phase space, so to complete this description, we need the inverse map from phase space to Hilbert space, or in other words, a quantisation procedure. As mentioned earlier, this was first provided by Hermann Weyl, and is known as Weyl quantisation. It is possible to characterise this map entirely from the following correspondence [48]:

$$\big(u\hat{q} + v\hat{p}\big)^k \xleftrightarrow[\text{Wigner}]{\text{Weyl}} \big(uq + vp\big)^k. \tag{A.10}$$

The Weyl quantisation map that performs this is [229],

$$\mathcal{Q}[f(\boldsymbol{r})] := \frac{1}{(2\pi)^{2N}} \int_{\mathbb{R}^{2N}} f(\boldsymbol{r}) e^{-i\boldsymbol{\xi}\cdot(\hat{\boldsymbol{r}}-\boldsymbol{r})} d^{2N}\boldsymbol{\xi}\, d^{2N}\boldsymbol{r}, \tag{A.11}$$

and the map to phase space comes from Wigner [230],

$$\mathcal{W}\big[\hat{f}(\hat{\boldsymbol{r}})\big] := \frac{1}{(2\pi)^{2N}} \int_{\mathbb{R}^{2N}} \mathrm{Tr}\Big[\hat{f}(\hat{\boldsymbol{r}}) e^{i\boldsymbol{\xi}\cdot(\hat{\boldsymbol{r}}-\boldsymbol{r})}\Big]\, d^{2N}\boldsymbol{\xi}. \tag{A.12}$$

Here we have used an arbitrary operator $\hat{f}$, and have defined its Wigner representation as $f(\boldsymbol{r})$. These two maps are naturally the inverses of each other, $\mathcal{Q}^{-1}[\hat{f}] \equiv \mathcal{W}[\hat{f}]$, and together form the *Wigner-Weyl transform*. By substituting Eq. (A.12) into Eq. (A.11), we can retrieve the following relation

$$\mathcal{Q}[f(\boldsymbol{r})] \equiv \frac{1}{(2\pi)^{2N}} \int_{\mathbb{R}^{2N}} \mathrm{Tr}\Big[\hat{f}(\hat{\boldsymbol{r}}) e^{i\boldsymbol{\xi}\cdot\hat{\boldsymbol{r}}}\Big]\, e^{-i\boldsymbol{\xi}\cdot\hat{\boldsymbol{r}}} d^{2N}\boldsymbol{\xi}. \tag{A.13}$$

With the exception of expressions which take the same form as Eq. (A.10), in general, the form of $\hat{f}$ will not match the form of $f(\boldsymbol{r})$. In addition to this, when mapping the product of two operators to phase space the result will not generally be equal to the scalar multiplication of the individual distributions, $\mathcal{W}[\hat{f}\hat{g}] \neq \mathcal{W}[\hat{f}]\,\mathcal{W}[\hat{g}]$ for all possible $\hat{f}$ and $\hat{g}$. It is natural that scalar multiplication of distributions in phase space will not yield the correct distributions and is hence not equal to the operator product, and so we must define an additional noncommutative product which is the phase-space equivalent of the noncommutative operator product. The answer is the renowned *Moyal star product* [34, 35, 235]:

$$\mathcal{W}\big[\hat{f}\hat{g}\big] = \mathcal{W}\big[\hat{f}\big] \star \mathcal{W}\big[\hat{g}\big], \text{ or equivalently, } \mathcal{Q}[f]\mathcal{Q}[g] = \mathcal{Q}[f \star g]. \tag{A.14}$$

There are numerous formulations of this star product; the form most used in this dissertation is the differential operator form

$$f(\boldsymbol{r}) \star g(\boldsymbol{r}) := f(\boldsymbol{r})\, \exp\left[\frac{i\hbar}{2} \overleftarrow{\boldsymbol{\partial r}}^T \boldsymbol{\Omega}\, \overrightarrow{\boldsymbol{\partial r}}\right] g(\boldsymbol{r}) \tag{A.15}$$

where $f(\boldsymbol{r})$ and $g(\boldsymbol{r})$ are arbitrary phase-space functions, and $\boldsymbol{\Omega}$ is the symplectic form. The vector $\boldsymbol{\partial r}$ has elements $\partial/\partial \boldsymbol{r}_k$, and we take the transposition operation to only apply to the shape of the vector. The overhead arrows, $\overleftarrow{\partial}$ and $\overrightarrow{\partial}$, denote that these are directional derivatives which act to the left or right. From Eq. (A.15) we can see that the Moyal star product is associative and noncommutative. Using this form, we can also write the Moyal star product in terms of so-called Bopp shifts [239]:

$$f(\boldsymbol{r}) \star g(\boldsymbol{r}) \equiv f\left(\boldsymbol{r} + \frac{i\hbar}{2}\boldsymbol{\Omega}\overrightarrow{\boldsymbol{\partial r}}\right)\, g(\boldsymbol{r}) \equiv f(\boldsymbol{r})\, g\left(\boldsymbol{r} - \frac{i\hbar}{2}\boldsymbol{\Omega}\overleftarrow{\boldsymbol{\partial r}}\right). \tag{A.16}$$

The final common form for the Moyal star product casts it as a Fourier transform over the two functions [231, 235, 240]:

$$\begin{aligned} f(\boldsymbol{r}) \star g(\boldsymbol{r}) &\equiv \frac{1}{(\pi\hbar)^{2N}} \int_{\mathbb{R}^{2N}} \int_{\mathbb{R}^{2N}} f(\boldsymbol{r}_a)\, g(\boldsymbol{r}_b)\, \exp\left[\frac{2i}{\hbar}\,(\boldsymbol{r}_a - \boldsymbol{r})^T\, \boldsymbol{\Omega}\,(\boldsymbol{r}_b - \boldsymbol{r})\right]\, d^{2N}\boldsymbol{r}_a\, d^{2N}\boldsymbol{r}_b \\ &\equiv \frac{1}{(\pi\hbar)^{2N}} \int_{\mathbb{R}^{2N}} \int_{\mathbb{R}^{2N}} f(\boldsymbol{r} + \boldsymbol{r}_a)\, g(\boldsymbol{r} + \boldsymbol{r}_b)\, \exp\left[\frac{2i}{\hbar}\, \boldsymbol{r}_a^T\, \boldsymbol{\Omega}\, \boldsymbol{r}_b\right]\, d^{2N}\boldsymbol{r}_a\, d^{2N}\boldsymbol{r}_b. \end{aligned} \tag{A.17}$$

Every phase-space representation will have a unique form of the star product, which plays the role of the Hilbert space operator product. The Wigner phase-space star product has another singular feature that is not shared with any of the other phase-space distributions defined by Eq. (A.2): within an integral over the entire phase space, exactly one star product may be "cancelled," that is:

$$\mathrm{Tr}\big[\hat{f}\hat{g}\big] \equiv \int_{\mathbb{R}^{2N}} f(\boldsymbol{r}) \star g(\boldsymbol{r})\, d^{2N}\boldsymbol{r} = \int_{\mathbb{R}^{2N}} g(\boldsymbol{r}) \star f(\boldsymbol{r})\, d^{2N}\boldsymbol{r} = \int_{\mathbb{R}^{2N}} f(\boldsymbol{r})\, g(\boldsymbol{r})\, d^{2N}\boldsymbol{r}. \tag{A.18}$$

Using this result, the expectation value $\langle\hat{f}\rangle \equiv \mathrm{Tr}[\hat{\rho}\hat{f}]$ can be easily retrieved by solving the following integral,

$$\mathrm{Tr}\big[\hat{\rho}\hat{f}\big] = \int_{\mathbf{R}^{2N}} W(\boldsymbol{r})\, f(\boldsymbol{r})\, d^{2N}\boldsymbol{r}, \tag{A.19}$$

where we have used the definitions $f(\boldsymbol{r}) := \mathcal{W}[\hat{f}]$ and $W(\boldsymbol{r}) := \mathcal{W}[\hat{\rho}]$. Lastly, it is possible to obtain probabilities for specific measurement outcomes from the Wigner representation; as an example, integrating $W(q,p)$ along the line $uq + vp = z$ in phase space provides the probability that a measurement of $u\hat{q} + v\hat{p}$ on the state $\hat{\rho}$ has the result z. If we generalise this to the N mode system, expressing observable as $\boldsymbol{u}\cdot\hat{\boldsymbol{r}}$, then the probability of measuring z corresponds to the integral

$$P\big(\langle \boldsymbol{u}\cdot\hat{\boldsymbol{r}}\rangle = z\big) = \int_{\mathbb{R}^{2n}} W(\boldsymbol{r})\,\delta(\boldsymbol{u}\cdot\boldsymbol{r} - z)\,d^{2N}\boldsymbol{r}. \tag{A.20}$$

In fact, the Wigner representation can be uniquely determined as the phase-space representation satisfying Eqs. (A.18) and (A.20), with the additional property that for all Hermitian operators, the Wigner representation is a real valued function [241, 242]. Now that we have defined a noncommutative phase-space product, we can move on and define dynamics on the phase space. The time derivative commutes with the Wigner transformation, which allows us to write,

$$\mathcal{W}\left[\frac{d}{dt}\hat{f}\right] = \frac{d}{dt}\mathcal{W}[\hat{f}]. \tag{A.21}$$

The commutator, normalised by the factor $-i/\hbar$, maps to the so-called sine bracket, also termed the *Moyal bracket*:

$$-\frac{i}{\hbar}[\hat{f},\hat{g}] \longleftrightarrow \frac{1}{i\hbar}\Big(f(\boldsymbol{r})\star g(\boldsymbol{r}) - g(\boldsymbol{r})\star f(\boldsymbol{r})\Big) = \frac{2}{\hbar}f(\boldsymbol{r})\,\sin\left[\frac{\hbar}{2}\overleftarrow{\boldsymbol{\partial r}}^{T}\boldsymbol{\Omega}\,\overrightarrow{\boldsymbol{\partial r}}\right] g(\boldsymbol{r}) =: \{\{f,g\}\}. \tag{A.22}$$

The Moyal bracket obeys the same properties as the commutator, and by extension, the Poisson bracket. Importantly, it is anticommutative $\{\{f,g\}\} = -\{\{g,f\}\}$, linear in the first and second arguments, obeys the Leibniz rule, and the Jacobi identity. As with the star product, it is also possible to express this as a Fourier transform of the QPDs, however, we only give this form since it will be heavily used for calculations in this dissertation. With the definition of this bracket, the Heisenberg and von Neumann equations can now be mapped to phase-space PDEs:

$$\frac{d}{dt}\hat{A} = \frac{i}{\hbar}[\hat{H},\hat{A}] \longleftrightarrow \frac{d}{dt}A = \{\{A,H\}\} \quad \text{and} \quad \frac{d}{dt}\hat{\rho} = -\frac{i}{\hbar}[\hat{H},\hat{\rho}] \longleftrightarrow \frac{d}{dt}W = \{\{H,W\}\}. \tag{A.23}$$

We can see that the Heisenberg equation has mapped to an equation which is similar in form to the famous Hamilton's equation from classical physics, but where the Poisson bracket $\{f,g\}$ has been replaced by the Moyal bracket $\{\{f,g\}\}$; the same has also happened with von-Neumann equations, which shares a similar relation with Liouville's equation. In addition to this, the anticommutator, which will appear in dynamical equations containing dissipation, can also be expressed as a similar cosine bracket [240]:

$$[\hat{f},\hat{g}]_{+} \longleftrightarrow \Big(f(\boldsymbol{r})\star g(\boldsymbol{r}) + g(\boldsymbol{r})\star f(\boldsymbol{r})\Big) = \frac{2}{\hbar}f(\boldsymbol{r})\,\cos\left[\frac{\hbar}{2}\overleftarrow{\boldsymbol{\partial r}}^{T}\boldsymbol{\Omega}\,\overrightarrow{\boldsymbol{\partial r}}\right] g(\boldsymbol{r}) =: ((f,g)). \tag{A.24}$$

Now that the necessary expressions for solving quantum mechanical problems exactly in phase space have been provided, we will give a short review of how these expressions relate to the classical to quantum transition.

A.4 Star Products and the Classical Limit

Here we will review some aspects of phase-space star products and the link they provide between classical physics and quantum mechanics. In general, a star product is a differential function acting on two parameters, which is written as,

$$f\star g = fg + \sum_{n=1}^{\infty}(i\hbar)^n C_n(f,g) \tag{A.25}$$

where $\hbar$ is the deformation parameter [243]. Classical phase space expressions should be retrieved in the limit $\hbar\to 0$; it is termed the deformation parameter because it allows for the smooth deformation of classical phase-space structures to quantum ones. The functions $C_n(f,g)$ consist of n-th order derivatives of the phase-space functions f and g, and will in general cause this product to be noncommutative, $f\star g \neq g\star f$, except when one of them is a number, $1\star f = f\star 1 = f$. We also require that this product be associative, $(f\star g)\star h = f\star(g\star h)$, which places considerable constraints on the form that the $C_n(f,g)$ can take [43]. The restrictions placed on the star product functions are as follows [244]:

- The $\mathcal{O}[\hbar^0]$ order term is the usual multiplication, $f\star g = fg + \mathcal{O}[\hbar]$. This ensures that, in the classical limit $\hbar\to 0$, the star product reduces to the normal commutative multiplication.

- The first term in the series should have the property that $C_1(f,g) - C_1(g,f) = \{f,g\}$. This constraint ensures that the Poisson bracket is retrieved in the classical limit,

$$\lim_{\hbar\to 0} \frac{1}{i\hbar}\{\{f,g\}\} = \{f,g\}, \tag{A.26}$$

  providing a connection between classical and quantum dynamics. It is important to note that in this limit, the functions f and g will also have lost any dependence on $\hbar$, and will also be reduced to their equivalent classical phase-space distributions.

- Demanding that the star product be associative yields the following relation among the C_n terms:

$$\sum_{k+l=n} C_k(C_l(f,g),h) = \sum_{k+l=n} C_k(f,C_l(g,h)). \tag{A.27}$$

- The star product should be Hermitian, $\overline{f\star g} = \bar{g}\star\bar{f}$, which follows from the identical property from Hilbert space, $(\hat{f}\hat{g})^\dagger = \hat{g}^\dagger\hat{f}^\dagger$.

In addition, the linearity of the derivative is enough to ensure that the star product obeys the rest of the properties of multiplication. Many star products can be constructed which satisfy these criteria, each of which corresponds to its own mapping between phase space and Hilbert space. Therefore, it is also possible to define the Wigner-Weyl transform just from the definition of the Moyal product, Eq. (A.15). The star product can be defined for other phase-space formulations beyond the Wigner phase-space representation, including the popular Glauber–Sudarshan P and Husimi Q representations, where the different ordering prescriptions result in orderings of the differential operators. The star products for these representation are usually more easily expressed in the optical phase-space basis, that is the phase-space symbols corresponding to the ladder operators, $a := (q+ip)/\sqrt{2}$ and $a^* := (q-ip)/\sqrt{2}$, rather than the quadrature basis. The star-product is a necessary tool for the exact treatment of quantum mechanics in phase space, but despite this, it seems to receive little attention in the optics community when using phase-space methods, and it was this common oversight which motivated this review of its basic properties.

B Linking Master Equations and Differential Equations of Gaussian Moments

In this section, it will be shown how one can map equations of motion for operators acting on a Hilbert space to PDEs in phase space, along with the associated Fourier space. From there, these PDEs will be used to generate systems of ODEs for the moments of Gaussian Wigner functions. This can be used for the open system dynamics from Section 2.2. These results go beyond coherent and open system dynamics, and are critical for the moment method used for calculating the cavity backaction on a qubit from Section 4.2, where the dynamics does not preserve any properties of a density operator.

B.1 From Hilbert Space to Phase Space

The first step is to map cavity operator terms to expressions involving phase space symbols and their derivatives. A property of phase space distributions is that linear operators map to an associated phase space symbol, $\hat{r}_k \to r_k$; the partial derivative with respect to this phase space coordinate will be denoted $\partial r_k := \partial/\partial r_k$. The Fourier space coordinate associated with the phase space variable r_k will be denoted ξ_k, and similarly, the derivative with respect to this coordinate will be represented using the notation $\partial \xi_k := \partial/\partial \xi_k$. In order to work out the corresponding phase space expressions for operator products, the Moyal star-product from Appendix A.3 will be used, which may be written as:

$$f(\boldsymbol{r}) \star g(\boldsymbol{r}) = f(\boldsymbol{r}) \exp\left[\frac{i\hbar}{2}\overleftarrow{\boldsymbol{\partial r}}^T \boldsymbol{\Omega}\, \overrightarrow{\boldsymbol{\partial r}}\right] g(\boldsymbol{r}). \tag{B.1}$$

Any element in the operator expressions can be expressed as a combination of a commutator and anti-commutator, along with a "jump"-term for components of second order. As was also discussed in Appendix A.3, the phase-space equivalents of the commutator and anti-commutator are the sine and cosine brackets:

$$\begin{aligned} -\frac{i}{\hbar}[\hat{f},\hat{g}] &\longleftrightarrow \frac{1}{i\hbar}\Big(f(\boldsymbol{r}) \star g(\boldsymbol{r}) - g(\boldsymbol{r}) \star f(\boldsymbol{r})\Big) = \frac{2}{\hbar} f(\boldsymbol{r}) \sin\left[\frac{\hbar}{2}\overleftarrow{\boldsymbol{\partial r}}^T \boldsymbol{\Omega}\, \overrightarrow{\boldsymbol{\partial r}}\right] g(\boldsymbol{r}) =: \{\{f,g\}\} \\ [\hat{f},\hat{g}]_+ &\longleftrightarrow \Big(f(\boldsymbol{r}) \star g(\boldsymbol{r}) + g(\boldsymbol{r}) \star f(\boldsymbol{r})\Big) = \frac{2}{\hbar} f(\boldsymbol{r}) \cos\left[\frac{\hbar}{2}\overleftarrow{\boldsymbol{\partial r}}^T \boldsymbol{\Omega}\, \overrightarrow{\boldsymbol{\partial r}}\right] g(\boldsymbol{r}) =: ((f,g)). \end{aligned} \tag{B.2}$$

Expressions for important terms will be worked out and then combined to obtain PDEs of the Wigner function and the associated characteristic function. Natural units will also be used, and so we set $\hbar = 1$ from here. Lastly, in order to transform from phase space to Fourier space coordinates, the following Fourier transforms will be used:

$$\begin{aligned} &\mathcal{F}[r_j^n r_k^m W(\boldsymbol{r})] = (i\partial\xi_j)^n (i\partial\xi_k)^m w(\boldsymbol{\xi}) \qquad \mathcal{F}[\partial r_j^n \partial r_k^m W(\boldsymbol{r})] = (i\xi_j)^n (i\xi_k)^m w(\boldsymbol{\xi}) \\ &\mathcal{F}[r_j \partial r_k W(\boldsymbol{r})] = -(\delta_{jk} + \xi_k \partial\xi_j) w(\boldsymbol{\xi}). \end{aligned} \tag{B.3}$$

Einstein summation notation is used throughout this section, and so repeated indices imply summation over that index. The transpose is also denoted $\left(A^T\right)_{jk} \equiv A_{kj}$. Additionally, when the directional arrow is omitted, the differential operator is to be treated as if it is acting to the right, like the usual derivative.

First Order Terms

Since the commutator is related to a sine series of the differential operators, and the Hamiltonian is at most linear in the quadrature operators, this expansion may be terminated at the linear term in phase space. We start with the commutator:

$$-i[\hat{r}_j,\hat{\rho}] \xrightarrow{\text{Wigner}} 2r_j \sin\left[\frac{1}{2}\overleftarrow{\partial r_k}\, \Omega_{kl}\, \overrightarrow{\partial r_l}\right] W(\boldsymbol{r}) = \Omega_{jl}\partial r_l W(\boldsymbol{r}) \xrightarrow{\text{Fourier}} i\Omega_{jl}\xi_l w(\boldsymbol{\xi}). \tag{B.4}$$

Things are even simpler for the anti-commutator involving linear combinations of quadrature operators, where the result is just multiplication as the second-order differential terms vanish:

$$[\hat{r}_j, \hat{\rho}]_+ \xrightarrow{\text{Wigner}} 2r_j \cos\left[\frac{1}{2}\overleftarrow{\partial r_k}\Omega_{kl}\overrightarrow{\partial r_l}\right] W(\boldsymbol{r}) = 2r_j W(\boldsymbol{r}) \xrightarrow{\text{Fourier}} 2i\partial\xi_j w(\boldsymbol{\xi}). \tag{B.5}$$

Second Order Terms

The commutator term containing combinations of operators up to second order still results in simple expressions, since the differential terms of order greater than one in the sine series will vanish:

$$\begin{aligned}
-i[\hat{r}_j\hat{r}_k, \hat{\rho}] &\xrightarrow{\text{Wigner}} 2(r_j \star r_k)\sin\left[\frac{1}{2}\overleftarrow{\partial r_l}\Omega_{lm}\overrightarrow{\partial r_m}\right] W(\boldsymbol{r}) \\
&= \left(r_j r_k + \frac{i}{2}\Omega_{jk}\right)\left(\overleftarrow{\partial r_l}\Omega_{lm}\overrightarrow{\partial r_m}\right) W(\boldsymbol{r}) \\
&= \left(r_j\Omega_{kl} + r_k\Omega_{jl}\right)\partial r_l W(\boldsymbol{r}) \\
&\xrightarrow{\text{Fourier}} \xi_l\Big(-\Omega_{kl}\partial\xi_j - \Omega_{jl}\partial\xi_k\Big) w(\boldsymbol{\xi}) \\
&= \xi_l\Big(\Omega_{lk}\partial\xi_j + \Omega_{lj}\partial\xi_k\Big) w(\boldsymbol{\xi}).
\end{aligned} \tag{B.6}$$

The anti-commutator term is slightly more complicated, since a second-order differential term is now present:

$$\begin{aligned}
[\hat{r}_j\hat{r}_k, \hat{\rho}]_+ &\xrightarrow{\text{Wigner}} 2(r_j \star r_k)\cos\left[\frac{1}{2}\overleftarrow{\partial r_l}\Omega_{lm}\overrightarrow{\partial r_m}\right] W(\boldsymbol{r}) \\
&= \left(r_j r_k + \frac{i}{2}\Omega_{jk}\right)\left[2 - \frac{1}{4}\overleftarrow{\partial r_l}\overleftarrow{\partial r_{l'}}\Omega_{lm}\Omega_{l'm'}\overrightarrow{\partial r_m}\overrightarrow{\partial r_{m'}}\right] W(\boldsymbol{r}) \\
&= \left(2r_j r_k + i\Omega_{jk} + \frac{1}{2}\Omega_{lj}\Omega_{km}\partial r_l\partial r_m\right) W(\boldsymbol{r}) \\
&\xrightarrow{\text{Fourier}} \left(-\frac{1}{2}\Omega_{lj}\Omega_{km}\xi_l\xi_m + i\Omega_{jk} - 2\partial\xi_j\partial\xi_k\right) w(\boldsymbol{\xi}).
\end{aligned} \tag{B.7}$$

We must make sure to note that in the above sum, that although the $(\partial r_l(r_j))(\partial r_{l'}(r_k))$ and $(\partial r_l(r_k))(\partial r_{l'}(r_j))$ terms are distinct, both terms make identical contributions to the sum. We now consider the jump terms, which are expanded simply using the star product since there is no special bracket that may be used here:

$$\begin{aligned}
\hat{r}_j\hat{\rho}\hat{r}_k &\xrightarrow{\text{Wigner}} r_j \star W(\boldsymbol{r}) \star r_k = r_j \star \left(r_k - \frac{i}{2}\Omega_{km}\partial r_m\right) W(\boldsymbol{r}) \\
&= \left(r_j r_k + \frac{i}{2}\Omega_{jk} - \frac{i}{2}r_j\Omega_{kl}\partial r_l + \frac{i}{2}r_k\Omega_{jl}\partial r_l + \frac{1}{4}\Omega_{jl}\Omega_{km}\partial r_l\partial r_m\right) W(\boldsymbol{r}) \\
&\xrightarrow{\text{Fourier}} \left(\frac{1}{4}\Omega_{lj}\Omega_{km}\xi_l\xi_m - \frac{i}{2}\Omega_{jk} - \frac{i}{2}\xi_l\Omega_{lk}\partial\xi_j + \frac{i}{2}\xi_l\Omega_{lj}\partial\xi_k - \partial\xi_j\partial\xi_k\right) w(\boldsymbol{\xi}).
\end{aligned} \tag{B.8}$$

Dissipation Terms

Lastly, we consider the dissipation terms acting on the cavity, which can be written as follows:

$$\sum_k \gamma_k \mathcal{D}[z_k](\hat{\rho}) = \sum_{j,k} h_{jk}\left(\hat{r}_k\hat{\rho}\hat{r}_j - \frac{1}{2}[\hat{r}_j\hat{r}_k, \hat{\rho}]_+\right) \quad \text{where} \quad h_{jk} = h^*_{kj}. \tag{B.9}$$

The h_{jk} are elements of a positive definite Hermitian matrix, which has the dissipation rates γ_k as its eigenvalues. The individual terms in the sum can be worked out:

$$\begin{aligned}
\hat{r}_k\hat{\rho}\hat{r}_j - \frac{1}{2}[\hat{r}_j\hat{r}_k, \hat{\rho}]_+ &\xrightarrow{\text{Wigner}} \left(i\Omega_{kj} - \frac{i}{2}r_k\Omega_{jl}\partial r_l + \frac{i}{2}r_j\Omega_{kl}\partial r_l - \frac{1}{4}\left(\Omega_{lk}\Omega_{jm} + \Omega_{lj}\Omega_{km}\right)\partial r_l\partial r_m\right) W(\boldsymbol{r}) \\
&\xrightarrow{\text{Fourier}} \left(\frac{1}{2}\left(\Omega_{lk}\Omega_{jm} + \Omega_{lj}\Omega_{km}\right)\xi_l\xi_m - \frac{i}{2}\xi_l\Omega_{lj}\partial\xi_k + \frac{i}{2}\xi_l\Omega_{lk}\partial\xi_j\right) w(\boldsymbol{\xi}).
\end{aligned} \tag{B.10}$$

We could use the fact that $\Omega_{lk}\Omega_{jm} = \Omega_{mj}\Omega_{kl}$ and that the labels l, m are arbitrary, to make the above expression more compact, but this form is easier to work with later.

Thermal Bath Terms

The thermal noise terms combine several of the above results, however, they deserve special attention since they are usually expressed in the basis of ladder operators, rather than the quadrature basis. Here, for clarity, we focus on a single-mode system. The usual thermal dissipation can be expressed as follows in the quadrature basis:

$$\kappa(\bar{n}+1)\mathcal{D}[\hat{a}](\hat{\rho})+\kappa\bar{n}\mathcal{D}[\hat{a}^\dagger](\hat{\rho}) = \kappa\left(\bar{n}+\frac{1}{2}\right)\left(\mathcal{D}[\hat{q}](\hat{\rho})+\mathcal{D}[\hat{p}](\hat{\rho})\right)-\frac{i\kappa}{2}\left(\hat{q}\hat{\rho}\hat{p}-\frac{1}{2}[\hat{p}\hat{q},\hat{\rho}]_+\right)+\frac{i\kappa}{2}\left(\hat{p}\hat{\rho}\hat{q}-\frac{1}{2}[\hat{q}\hat{p},\hat{\rho}]_+\right). \tag{B.11}$$

We use the convention $(\hat{q},\hat{p}) = (\hat{r}_1,\hat{r}_2)$, so that associated phase space and Fourier space variables are (r_1, r_2) and (ξ_1, ξ_2), respectively. We can then write:

$$\begin{aligned}\kappa(\bar{n}+1)\mathcal{D}[\hat{a}](\hat{\rho}) + \kappa\bar{n}\mathcal{D}[\hat{a}^\dagger](\hat{\rho}) &\xrightarrow{\text{Wigner}} \frac{\kappa}{2}\left[(2+r_1\partial r_1+r_2\partial r_2)+\left(\bar{n}+\frac{1}{2}\right)\left(\partial r_1^2+\partial r_2^2\right)\right]W(\boldsymbol{r})\\ &\xrightarrow{\text{Fourier}} -\frac{\kappa}{2}\left[(\xi_1\partial\xi_1+\xi_2\partial\xi_2)+\left(n+\frac{1}{2}\right)\left(\xi_1^2+\xi_2^2\right)\right]w(\boldsymbol{\xi}).\end{aligned} \tag{B.12}$$

Collecting the Fourier space coordinates into a vector, this can be rewritten in the following compact form:

$$\kappa(\bar{n}+1)\mathcal{D}[\hat{a}](\hat{\rho}) + \kappa\bar{n}\mathcal{D}[\hat{a}^\dagger](\hat{\rho}) \to -\frac{\kappa}{2}\left[\left(\boldsymbol{\xi}^T\boldsymbol{\partial\xi}+\left(\bar{n}+\frac{1}{2}\right)\boldsymbol{\xi}^T\boldsymbol{\xi}\right)\right]w(\boldsymbol{\xi}). \tag{B.13}$$

This expression can then be generalised to the case of uncorrelated thermal noise acting on N cavity modes:

$$\left(\boldsymbol{\xi}^T\left(-\frac{1}{2}\boldsymbol{\kappa}\right)\boldsymbol{\partial\xi}-\frac{1}{2}\boldsymbol{\xi}^T\mathbf{D}\boldsymbol{\xi}\right)w(\xi) \quad \text{where} \quad \boldsymbol{\kappa}=\bigoplus_{k=1}^{N}\kappa_k\mathbf{I}_2 \quad \text{and} \quad \mathbf{D}=\bigoplus_{k=1}^{N}\kappa_k\left(\bar{n}_k+\frac{1}{2}\right)\mathbf{I}_2. \tag{B.14}$$

B.2 From Phase Space PDE to Moment ODEs

Combining the various terms from the previous section, it can be concluded that, provided the equation in Hilbert space is at most a quadratic polynomial of the quadrature operators, the associated PDEs will be at most linear second-order differential equations. Combining these terms, the phase-space PDE for the Wigner function can, in general, be written as

$$\frac{\partial}{\partial t}W(\boldsymbol{r}) = \left[\varpi-\boldsymbol{\partial r}^T\mathbf{f}-\boldsymbol{r}^T\mathbf{g}+\frac{1}{2}\boldsymbol{\partial r}^T\mathbf{C}\boldsymbol{\partial r}-\frac{1}{2}\boldsymbol{r}^T\mathbf{B}\boldsymbol{r}-\boldsymbol{\partial r}^T\mathbf{A}\boldsymbol{r}\right]W(\boldsymbol{r}), \tag{B.15}$$

which is a Fokker-Planck equation for the Wigner function $W(\boldsymbol{r})$. The constant coefficients are generally assumed to be complex-valued. It is easier to access the moments of $W(\boldsymbol{r})$ through its characteristic function $w(\boldsymbol{r})$, so in order to generate differential equations for the moments, we start by Fourier transforming this PDE to generate another Fokker-Planck equation in terms of the Fourier space coordinates:

$$\begin{aligned}\frac{\partial}{\partial t}w(\boldsymbol{\xi}) &= \left[\varpi-i\boldsymbol{\xi}^T\mathbf{f}-i\boldsymbol{\partial\xi}^T\mathbf{g}-\frac{1}{2}\boldsymbol{\xi}^T\mathbf{C}\boldsymbol{\xi}+\frac{1}{2}\boldsymbol{\partial\xi}^T\mathbf{B}\boldsymbol{\partial\xi}+\boldsymbol{\xi}^T\mathbf{A}\boldsymbol{\partial\xi}\right]w(\boldsymbol{\xi})\\ &= \left[\varpi-i\mathrm{f}_j\xi_j-i\mathrm{g}_j\partial\xi_j-\frac{1}{2}\mathrm{C}_{jk}\xi_j\xi_k+\frac{1}{2}\mathrm{B}_{jk}\partial\xi_j\partial\xi_k+\mathrm{A}_{jk}\xi_j\partial\xi_k\right]w(\boldsymbol{\xi}).\end{aligned} \tag{B.16}$$

Since the terms $\mathrm{B}_{jk}\partial\xi_j\partial\xi_k$ and $\mathrm{C}_{jk}\xi_j\xi_k$ will sum over identical terms twice, the matrices by construction are symmetric, and so $\mathrm{B}_{jk} = \mathrm{B}_{kj}$ and $\mathrm{C}_{jk} = \mathrm{C}_{kj}$. Assuming that the Wigner function is a Gaussian, and for the sake of the dephasing calculations, a potentially complex-valued non-normalised Gaussian, the associated characteristic function must therefore take the form:

$$w(\boldsymbol{\xi}) = \exp\left[-\frac{1}{2}\boldsymbol{\xi}^T\boldsymbol{\sigma\xi}-i\boldsymbol{\xi}^T\boldsymbol{\mu}-\upsilon\right] = \exp\left[-\frac{1}{2}\xi_j\sigma_{jk}\xi_k-i\xi_k\mu_k-\upsilon\right] \quad \text{where} \quad \sigma_{jk}=\sigma_{kj}. \tag{B.17}$$

Provided the Wigner function corresponds to a true quantum state, then the normalisation condition for the state $\mathrm{Tr}[\hat{\rho}] = 1$ implies that $w(0) = 1$, and therefore $\upsilon = 0$ always. Since the Wigner function will always be a Gaussian, the time-dependence can be assigned to the moments of the Gaussian. To work out the system of ODEs for these moments, we apply the PDE to $w(\boldsymbol{\xi})$ and pair up the coefficients of the ξ_j and $\xi_j\xi_k$ terms on the left and right-hand

side of the equation. Starting with the left-hand side, the time derivative of the characteristic function is:

$$\frac{\partial}{\partial t}w(\boldsymbol{\xi}) = \left[-\frac{1}{2}\xi_j\dot{\sigma}_{jk}\xi_k - i\xi_k\dot{\mu}_k - \dot{\upsilon}\right]w(\boldsymbol{\xi}). \tag{B.18}$$

Now, considering the right-hand side, we only need to work out the derivatives with respect to the Fourier space coordinates. The terms which have a single derivative become:

$$\begin{aligned}\partial\xi_j w(\boldsymbol{\xi}) &= \left[-\frac{1}{2}\delta_{jl}\xi_k\sigma_{lk} - \frac{1}{2}\delta_{jl}\xi_k\sigma_{kl} - i\delta_{ja}\mu_a\right]w(\boldsymbol{\xi}) \\ &= \left[-\frac{1}{2}\xi_a\left(\sigma_{ja}+\sigma_{aj}\right) - i\mu_j\right]w(\boldsymbol{\xi}).\end{aligned} \tag{B.19}$$

The second derivative terms are then:

$$\begin{aligned}\partial\xi_k\partial\xi_j w(\boldsymbol{\xi}) &= \partial\xi_k\left[-\frac{1}{2}\xi_b\sigma_{jb} - \frac{1}{2}\xi_a\sigma_{aj} - i\mu_j\right]w(\boldsymbol{\xi}) \\ &= \left(\left[-\frac{1}{2}\delta_{kb}\sigma_{jb} - \frac{1}{2}\delta_{ka}\sigma_{aj}\right] + \left[-\frac{1}{2}\xi_{b'}\sigma_{kb'} - \frac{1}{2}\xi_{a'}\sigma_{a'k} - i\mu_k\right]\left[-\frac{1}{2}\xi_b\sigma_{jb} - \frac{1}{2}\xi_a\sigma_{aj} - i\mu_j\right]\right)w(\boldsymbol{\xi}) \\ &= \Bigg(\frac{i}{2}\xi_a\mu_j\left[\sigma_{ka}+\sigma_{ak}\right] + \frac{i}{2}\xi_a\mu_k\left[\sigma_{ja}+\sigma_{aj}\right] - \mu_j\mu_k \\ &\quad + \frac{1}{4}\xi_a\xi_b\left[\sigma_{ka}+\sigma_{ak}\right]\left[\sigma_{jb}+\sigma_{bj}\right] - \frac{1}{2}\left(\sigma_{jk}+\sigma_{kj}\right)\Bigg)w(\boldsymbol{\xi})\end{aligned} \tag{B.20}$$

The differential equation $\dot{\sigma}_{ab}$ can be constructed from terms proportional to $\xi_a\xi_b$. Similarly, the differential equation $\dot{\mu}_a$ comes from terms proportional to ξ_a only, and the $\dot{\upsilon}$ differential equation is constructed from the terms with no dependence on the Fourier space coordinate. Putting everything together, the general form of the ODEs for the various moments are as follows:

$$\begin{aligned}\dot{\sigma}_{ab} &= \frac{1}{2}\mathrm{A}_{ak}\left(\sigma_{kb}+\sigma_{bk}\right) + \frac{1}{2}\mathrm{A}_{bk}\left(\sigma_{ka}+\sigma_{ak}\right) - \frac{\mathrm{B}_{jk}}{8}\Big[\left(\sigma_{ka}+\sigma_{ak}\right)\left(\sigma_{jb}+\sigma_{bj}\right) + \left(\sigma_{ja}+\sigma_{aj}\right)\left(\sigma_{kb}+\sigma_{bk}\right)\Big] + \mathrm{C}_{ab} \\ \dot{\mu}_a &= \mathrm{A}_{ak}\mu_k - \frac{\mathrm{B}_{jk}}{4}\left[\mu_j\left(\sigma_{ka}+\sigma_{ak}\right) + \mu_k\left(\sigma_{ja}+\sigma_{aj}\right)\right] + \mathrm{f}_a - \frac{\mathrm{g}_k}{2}\left(\sigma_{ka}+\sigma_{ak}\right) \\ \dot{\upsilon} &= -\varpi + \mathrm{g}_k\mu_k + \frac{\mathrm{B}_{jk}}{2}\left(\mu_j\mu_k + \frac{1}{2}\left(\sigma_{jk}+\sigma_{kj}\right)\right).\end{aligned} \tag{B.21}$$

We can convert these into the following vector and matrix equations:

$$\begin{aligned}\dot{\boldsymbol{\sigma}} &= \frac{1}{2}\mathbf{A}\left(\boldsymbol{\sigma}+\boldsymbol{\sigma}^T\right) + \frac{1}{2}\left(\boldsymbol{\sigma}+\boldsymbol{\sigma}^T\right)\mathbf{A}^T - \frac{1}{4}\left(\boldsymbol{\sigma}+\boldsymbol{\sigma}^T\right)\mathbf{B}\left(\boldsymbol{\sigma}+\boldsymbol{\sigma}^T\right) + \mathbf{C} \\ \dot{\boldsymbol{\mu}} &= \mathbf{A}\boldsymbol{\mu} - \frac{1}{2}\left(\boldsymbol{\sigma}+\boldsymbol{\sigma}^T\right)\mathbf{B}\boldsymbol{\mu} + \mathbf{f} - \frac{1}{2}\left(\boldsymbol{\sigma}+\boldsymbol{\sigma}^T\right)\mathbf{g} \\ \dot{\upsilon} &= -\varpi + \boldsymbol{\mu}^T\mathbf{g} + \frac{1}{2}\boldsymbol{\mu}^T\mathbf{B}\boldsymbol{\mu} + \frac{1}{4}\mathrm{Tr}\left[\mathbf{B}\left(\boldsymbol{\sigma}+\boldsymbol{\sigma}^T\right)\right].\end{aligned} \tag{B.22}$$

The covariance matrix, as defined in Eq. (2.9), is always symmetric, even when the expectation values are complex. Using this fact, we can simplify the above expressions to arrive at the following result:

$$\begin{aligned}\dot{\boldsymbol{\sigma}} &= \mathbf{A}\boldsymbol{\sigma} + \boldsymbol{\sigma}\mathbf{A}^T - \boldsymbol{\sigma}\mathbf{B}\boldsymbol{\sigma} + \mathbf{C} \\ \dot{\boldsymbol{\mu}} &= (\mathbf{A} - \boldsymbol{\sigma}\mathbf{B})\boldsymbol{\mu} + \mathbf{f} - \boldsymbol{\sigma}\mathbf{g} \\ \dot{\upsilon} &= -\varpi + \boldsymbol{\mu}^T\mathbf{g} + \frac{1}{2}\boldsymbol{\mu}^T\mathbf{B}\boldsymbol{\mu} + \frac{1}{2}\mathrm{Tr}\left[\mathbf{B}\boldsymbol{\sigma}\right].\end{aligned} \tag{B.23}$$

B.3 From Lindblad Master Equation to Moment ODEs

Now that the machinery to convert dynamical equations for Gaussian operators from Hilbert space to phase space has been established, we will apply it to the Lindbladian for a Gaussian state. We start with a Lindblad master equation for N cavity modes of the form

$$\frac{d}{dt}\hat{\rho} = \mathcal{L}_r(\hat{\rho}) \quad \text{where} \quad \mathcal{L}_r(\hat{\rho}) = -i[\hat{H}_r, \hat{\rho}] + \sum_{j,k=1}^{2N} \Gamma_{jk}\left(\hat{r}_j\hat{\rho}\hat{r}_k - \frac{1}{2}[\hat{r}_k\hat{r}_j, \hat{\rho}]_+\right). \tag{B.24}$$

The Hamiltonian is written as

$$\hat{H}_r = \frac{1}{2}\hat{\boldsymbol{r}}^T\boldsymbol{H}_r^{(2)}\hat{\boldsymbol{r}} + \hat{\boldsymbol{r}}^T\boldsymbol{h}_r^{(1)} = \frac{1}{2}\hat{r}_k\big(H_r^{(2)}\big)_{kl}\hat{r}_l + \big(h_r^{(1)}\big)_k\hat{r}_k \tag{B.25}$$

where $\boldsymbol{H}_r^{(2)}$ is a real-symmetric matrix, and $\boldsymbol{h}_r^{(1)}$ is a real-valued vector. We then proceed to work out the terms for the first and second order components in the Fourier coordinate space:

$$-i[\hat{r}_k\big(h_r^{(1)}\big)_k, \hat{\rho}] \to i\big(h_r^{(1)}\big)_k\Omega_{kj}\xi_j w_\rho(\boldsymbol{\xi}) = -i\boldsymbol{\xi}^T\boldsymbol{\Omega}\boldsymbol{h}_r^{(1)}w_\rho(\boldsymbol{\xi}) \tag{B.26}$$

and

$$\begin{aligned}
-\frac{i}{2}[\hat{r}_j\big(H_r^{(2)}\big)_{jk}\hat{r}_k, \hat{\rho}] \to \frac{\xi_l}{2}\big(H_r^{(2)}\big)_{jk}\Big(\Omega_{lk}\partial\xi_j + \Omega_{lj}\partial\xi_k\Big)w_\rho(\boldsymbol{\xi}) \\
= \frac{\xi_l}{2}\Big(\Omega_{lk}\big(H_r^{(2)}\big)_{kj}\partial\xi_j + \Omega_{lj}\big(H_r^{(2)}\big)_{jk}\partial\xi_k\Big)w_\rho(\boldsymbol{\xi}) \\
= \boldsymbol{\xi}^T(\boldsymbol{\Omega}\boldsymbol{H}_r^{(2)})\boldsymbol{\partial\xi}\, w_\rho(\boldsymbol{\xi}).
\end{aligned} \tag{B.27}$$

Finally, we work out the dissipation terms:

$$\begin{aligned}
\sum_{j,k=1}^{N}\Gamma_{jk}\left(\hat{r}_k\hat{\rho}\hat{r}_j - \frac{1}{2}[\hat{r}_j\hat{r}_k, \hat{\rho}]_+\right) \to \sum_{j,k=1}^{N}\Gamma_{jk}\left(\frac{1}{4}\xi_l\left(\Omega_{lk}\Omega_{jm} + \Omega_{lj}\Omega_{km}\right)\xi_m - \frac{i}{2}\xi_l\Omega_{lj}\partial\xi_k + \frac{i}{2}\xi_l\Omega_{lk}\partial\xi_j\right)w_\rho(\boldsymbol{\xi}) \\
= \sum_{j,k=1}^{N}\left(\frac{1}{4}\xi_m\Omega_{mj}\Gamma_{jk}\Omega_{kl}\xi_l + \frac{1}{4}\xi_m\Omega_{mk}\Gamma^*_{kj}\Omega_{jl}\xi_l \right. \\
\left. - \frac{i}{2}\xi_l\Omega_{lj}\Gamma_{jk}\partial\xi_k + \frac{i}{2}\xi_l\Omega_{lk}\Gamma^*_{kj}\partial\xi_j\right)w_\rho(\boldsymbol{\xi}) \\
= \left(\frac{1}{4}\boldsymbol{\xi}^T\boldsymbol{\Omega}\left(\boldsymbol{\Gamma} + \boldsymbol{\Gamma}^*\right)\boldsymbol{\Omega}\boldsymbol{\xi} - \frac{i}{2}\boldsymbol{\xi}^T\boldsymbol{\Omega}\left(\boldsymbol{\Gamma} - \boldsymbol{\Gamma}^*\right)\boldsymbol{\partial\xi}\right)w_\rho(\boldsymbol{\xi}).
\end{aligned} \tag{B.28}$$

The term $\boldsymbol{\Gamma}^*$ denotes element-by-element conjugation, and so is not the conjugate transpose. Assuming that the matrix $\boldsymbol{\Gamma}$ is Hermitian, we can replace this with the transpose $\boldsymbol{\Gamma}^* = \boldsymbol{\Gamma}^T$. The terms can then be replaced by the real and imaginary components of the matrix $\boldsymbol{\Gamma}$ using $\mathrm{Re}[\boldsymbol{\Gamma}] = (\boldsymbol{\Gamma} + \boldsymbol{\Gamma}^T)/2$ and $\mathrm{Im}[\boldsymbol{\Gamma}] = (\boldsymbol{\Gamma} - \boldsymbol{\Gamma}^T)/2i$. Combining the coherent and dissipative terms will result in the following expression:

$$\frac{\partial}{\partial t}w_\rho(\boldsymbol{\xi}) = \left[-i\boldsymbol{\xi}^T\left(\boldsymbol{\Omega}\boldsymbol{h}_r^{(1)}\right) + \frac{1}{2}\boldsymbol{\xi}^T\left(\boldsymbol{\Omega}\mathrm{Re}[\boldsymbol{\Gamma}]\boldsymbol{\Omega}\right)\boldsymbol{\xi} + \boldsymbol{\xi}^T\left(\boldsymbol{\Omega}\boldsymbol{H}_r^{(2)} + \boldsymbol{\Omega}\mathrm{Im}[\boldsymbol{\Gamma}]\right)\boldsymbol{\partial\xi}\right]w_\rho(\boldsymbol{\xi}). \tag{B.29}$$

With the PDE defined, we can plug the arrays into the expressions from the previous section to write a system of ODEs for the moments

$$\dot{\boldsymbol{\sigma}} = \mathbf{A}\boldsymbol{\sigma} + \boldsymbol{\sigma}\mathbf{A}^T + \mathbf{C} \qquad \dot{\boldsymbol{\mu}} = \mathbf{A}\boldsymbol{\mu} + \mathbf{f} \tag{B.30}$$

where the arrays are

$$\mathbf{A} = \boldsymbol{\Omega}\left(\boldsymbol{H}_r^{(2)} + \mathrm{Im}[\boldsymbol{\Gamma}]\right) \qquad \mathbf{C} = \boldsymbol{\Omega}\mathrm{Re}[\boldsymbol{\Gamma}]\boldsymbol{\Omega} \qquad \mathbf{f} = \boldsymbol{\Omega}\boldsymbol{h}_r^{(1)}. \tag{B.31}$$

B.4 Calculating Mode Backaction with Moment ODEs

The moments can also be used to calculate the backaction of a cavity on coupled qubits. Here we consider a qubit-cavity mode system that is coherently coupled, where the master equation is

$$\frac{d}{dt}\hat{\rho} = \mathcal{L}_r(\hat{\rho}) - i[\hat{H}_{qr}\hat{\sigma}_z, \hat{\rho}]. \tag{B.32}$$

$\mathcal{L}_r$ is the cavity Lindbladian defined in Eq. (B.24) in the previous section, and the qubit-cavity mode Hamiltonian is $\hat{H}_{qr}\hat{\sigma}_z$, where the cavity component is a Gaussian transformation:

$$\hat{H}_{qr} = \frac{1}{2}\hat{\boldsymbol{r}}^T\boldsymbol{H}_{qr}^{(2)}\hat{\boldsymbol{r}} + \hat{\boldsymbol{r}}^T\boldsymbol{h}_{qr}^{(1)} + h_{qr}^{(0)} = \frac{1}{2}\hat{r}_k\big(H_{qr}^{(2)}\big)_{kl}\hat{r}_l + \big(h_{qr}^{(1)}\big)_k\hat{r}_k + h_{qr}^{(0)}, \tag{B.33}$$

where $\boldsymbol{H}_{qr}^{(2)}$ is a real-symmetric matrix, $\boldsymbol{h}_{qr}^{(1)}$ is a real-valued vector, and $h_{qr}^{(0)}$ is a real constant. Calculating the backaction of the cavity on the qubit involves solving the dynamics of the norm of the $\hat{\rho}_{eg}$ sub-component of the total qubit-cavity state $\hat{\rho}$, which is not a true quantum state, using the equation

$$\frac{d}{dt}\hat{\rho}_{eg} = \mathcal{L}_r(\hat{\rho}_{eg}) - i[\hat{H}_{qr}, \hat{\rho}_{eg}]_+. \tag{B.34}$$

where the commutator is replaced with an anti-commutator due to the $\hat{\sigma}_z$ coupling; this is taken from Eq. (4.63). The solution to the $\mathcal{L}_r$ component of the dynamics is identical to the previous section. We therefore only have to solve for the terms which arise due to the qubit-cavity mode interaction Hamiltonian. The constant term usually arises when the Hamiltonian is not a symmetrically ordered function of the creation and annihilation operators, and contributes the term:

$$-i[h_{qr}^{(0)}, \hat{\rho}_{eg}]_+ \to -2ih_{qr}^{(0)}w_{eg}(\boldsymbol{\xi}). \tag{B.35}$$

Next, the first and second order terms in the quadrature operators are:

$$-i[\hat{r}_k\big(h_{qr}^{(1)}\big)_k, \hat{\rho}_{eg}]_+ \to 2\big(h_{qr}^{(1)}\big)_k\partial\xi_k w_{eg}(\boldsymbol{\xi}) = 2\boldsymbol{\partial\xi}^T\boldsymbol{h}_{qr}^{(1)}w_{eg}(\boldsymbol{\xi}), \tag{B.36}$$

along with,

$$\begin{aligned}
-\frac{i}{2}[\hat{r}_j\big(H_{qr}^{(2)}\big)_{jk}\hat{r}_k, \hat{\rho}_{eg}]_+ \to& -i\left(\frac{1}{4}\Omega_{jl}\big(H_{qr}^{(2)}\big)_{jk}\Omega_{km}\xi_l\xi_m + \frac{i}{2}\Omega_{jk}\big(H_{qr}^{(2)}\big)_{jk} - \big(H_{qr}^{(2)}\big)_{jk}\partial\xi_j\partial\xi_k\right)w_{eg}(\boldsymbol{\xi}) \\
=& \, i\left(\frac{1}{4}\xi_l\Omega_{lj}\big(H_{qr}^{(2)}\big)_{jk}\Omega_{km}\xi_m + \partial\xi_j\big(H_{qr}^{(2)}\big)_{jk}\partial\xi_k\right)w_{eg}(\boldsymbol{\xi}) \\
=& \, i\left(\frac{1}{4}\boldsymbol{\xi}^T\boldsymbol{\Omega}\boldsymbol{H}_{qr}^{(2)}\boldsymbol{\Omega}\boldsymbol{\xi} + \boldsymbol{\partial\xi}^T\boldsymbol{H}_{qr}^{(2)}\boldsymbol{\partial\xi}\right)w_{eg}(\boldsymbol{\xi}).
\end{aligned} \tag{B.37}$$

Since the dynamics is linear, these terms can be combined with the PDE in Eq. (B.29) to yield

$$\begin{aligned}
\frac{\partial}{\partial t}w_{eg}(\boldsymbol{\xi}) = \Bigg[& -2ih_{qr}^{(0)} - i\boldsymbol{\xi}^T\left(\boldsymbol{\Omega}\boldsymbol{h}_r^{(1)}\right) + 2\boldsymbol{\partial\xi}^T\boldsymbol{h}_{qr}^{(1)} + \frac{1}{2}\boldsymbol{\xi}^T\boldsymbol{\Omega}\left(\frac{i}{2}\boldsymbol{H}_{qr}^{(2)} + \mathrm{Re}[\boldsymbol{\Gamma}]\right)\boldsymbol{\Omega}\boldsymbol{\xi} \\
& + \boldsymbol{\xi}^T\left(\boldsymbol{\Omega}\boldsymbol{H}_r^{(2)} + \boldsymbol{\Omega}\mathrm{Im}[\boldsymbol{\Gamma}]\right)\boldsymbol{\partial\xi} + i\boldsymbol{\partial\xi}^T\boldsymbol{H}_{qr}^{(2)}\boldsymbol{\partial\xi}\Bigg]w_{eg}(\boldsymbol{\xi}).
\end{aligned} \tag{B.38}$$

Combining this expression with the results from Appendix B.2 linking PDEs of the form Eq. (B.16) to the moment ODEs in Eq. (B.23), the expressions used to calculate the cavity backaction detailed in Section 4.2.2.2 of the main text can be obtained.

C Gaussian States and Transformations

C.1 The Symplectic Group

As stated in Section 2.1.5, all covariance matrices can be diagonalised by symplectic transformations, which correspond to certain unitary transformations acting on the Hilbert space. For a system of N bosonic modes, the full set of unitary transformations corresponds to the real symplectic group, $Sp(2N, \mathbb{R})$, which has dimension $N(2N+1)$ and can be defined as a subset of the group of $2N \times 2N$ invertible matrices, $M_{2N\times 2N}$,

$$Sp(2N, \mathbb{R}) = \{\boldsymbol{S} \in M_{2N\times 2N}(\mathbb{R}) : \boldsymbol{S}^T \boldsymbol{\Omega} \boldsymbol{S} = \boldsymbol{\Omega}\}, \tag{C.1}$$

where $\boldsymbol{\Omega}$ is the symplectic form. The associated Lie algebra may be denoted $sp(2N, \mathbb{R})$, and is defined as

$$sp(2N, \mathbb{R}) = \{\boldsymbol{X} \in M_{2N\times 2N}(\mathbb{R}) : \boldsymbol{\Omega} \boldsymbol{X} + \boldsymbol{X}^T \boldsymbol{\Omega} = 0\}. \tag{C.2}$$

These two sets are related in the usual way, through the exponential map, $\exp : sp \to Sp$. There is one caveat, the exponential map from the symplectic Lie algebra to the group fails to be surjective, and as a result there are elements of the symplectic group which cannot be represented by $e^{\boldsymbol{X}}$; this results from the fact that the symplectic group is connected but not compact. It is, however, possible to represent any element of the real symplectic group using the product of at most two exponentials of elements in the symplectic Lie algebra, or in other words, for all $\boldsymbol{S} \in Sp(2N, \mathbb{R})$ there exists two elements $\boldsymbol{X}_1, \boldsymbol{X}_2 \in sp(2N, \mathbb{R})$ such that $\boldsymbol{S} = e^{\boldsymbol{X}_1} e^{\boldsymbol{X}_2}$. As a result, at most only two unitary transformations, involving quadratic Hamiltonians, are required to represent any symplectic transformation acting on a Gaussian covariance matrix.

Williamson's Theorem tells us that any valid covariance matrix can be represented as a symplectic transformation on a Gaussian thermal state, representing the state of the system's normal modes. This decomposition provides a useful way to relate the possibly complicated physical processes encapsulated in the covariance matrix to some effective unitary transformation on the normal modes of the Gaussian state. Provided that the Hamiltonian is quadratic, and so can be written as $\hat{H} = \frac{1}{2}\hat{\boldsymbol{r}}^T \boldsymbol{H} \hat{\boldsymbol{r}}$, where $\boldsymbol{H}$ is a $2N \times 2N$ symmetric matrix, then the corresponding unitary operators acting on the Hilbert space are equivalent to symplectic transformations of the quadrature operators through the following relations:

$$\hat{U} = e^{i\hat{H}} = e^{i\hat{\boldsymbol{r}}^T \boldsymbol{H} \hat{\boldsymbol{r}}/2} \to \hat{U}^\dagger \hat{\boldsymbol{r}} \hat{U} = e^{-i\hat{\boldsymbol{r}}^T \boldsymbol{H} \hat{\boldsymbol{r}}/2} \hat{\boldsymbol{r}} e^{i\hat{\boldsymbol{r}}^T \boldsymbol{H} \hat{\boldsymbol{r}}/2} = e^{\boldsymbol{\Omega H}} \hat{\boldsymbol{r}}. \tag{C.3}$$

The final replacement with $e^{\boldsymbol{\Omega H}} \hat{\boldsymbol{r}}$ results from the use of the BCH identity, along with the fact that the canonical commutation relation in the quadrature basis can be expressed as $[\hat{r}_j, \hat{r}_k] = i\Omega_{jk}$. Using the fact that the symplectic form $\boldsymbol{\Omega}$ is anti-symmetric, it may be shown using the above definitions that $\boldsymbol{\Omega H}$ is an element of the symplectic Lie algebra, and $e^{\boldsymbol{\Omega H}}$ an element of the symplectic Lie group.

To understand these unitary processes, we would therefore like to characterise every element of the symplectic Lie algebra, which may be divided into two subsets: the $N(N+1)$ elements representing active processes in the system, single and two-mode squeezing, and the N^2 elements representing passive processes, phase shifters and beam splitters. Translations will also be included, which correspond to a displacement of the Gaussian state. Combining these gives us the group of symplectic-affine transformations. As a reminder, affine transformations are linear translations of the form $\hat{\boldsymbol{r}} \to \mathbf{A}\hat{\boldsymbol{r}} + \mathbf{d}$, comprising both a linear displacement by the vector $\mathbf{d}$, along with multiplication by an invertible matrix $\mathbf{A}$, which in this instance is a symplectic matrix. From the main body of the text, recall that a unitary transformation corresponds to a symplectic-affine transformation on the quadrature operators through,

$$\hat{\boldsymbol{r}} \to \hat{U}^\dagger \hat{\boldsymbol{r}} \hat{U} \equiv \mathbf{S}\hat{\boldsymbol{r}} + \mathbf{d}. \tag{C.4}$$

Considering a state $\hat{\rho}$ with a Gaussian Wigner function of the form,

$$W(\boldsymbol{r}) = \frac{1}{(2\pi)^N \sqrt{\det[\boldsymbol{\sigma}]}} \exp\left[-\frac{1}{2}(\boldsymbol{r}-\boldsymbol{\mu})^T \boldsymbol{\sigma}^{-1}(\boldsymbol{r}-\boldsymbol{\mu})\right], \tag{C.5}$$

applying the Gaussian unitary transformation to this state, $\hat{U}\hat{\rho}\hat{U}^\dagger$, results in the following transformation on the moments of the Gaussian state,

$$\boldsymbol{\mu} \to \mathbf{S}\boldsymbol{\mu} + \mathbf{d} \quad \text{and} \quad \boldsymbol{\sigma} \to \mathbf{S}\boldsymbol{\sigma}\mathbf{S}^T. \tag{C.6}$$

This set of operations is also termed the canonical transformations, since they may be represented as transformations on the canonical coordinate system of the Wigner phase space. From this equivalent viewpoint, the unitary transformation transforms not the moments of the Gaussian, but the coordinate system,

$$W(\boldsymbol{r}) \to W(\mathbf{S}^{-1}(\boldsymbol{r}-\mathbf{d})). \tag{C.7}$$

In this appendix, we will provide the unitary transformations $\hat{U}$, along with the corresponding matrix transformations, where all provided expressions will be written in the quadrature basis. Physically relevant Gaussian Wigner functions and their moments will also be given. Important matrix decompositions for the elements of the symplectic group are also provided. Finally, for full details on the use of the symplectic group in quantum mechanics, consult the papers from R Simon in Refs. [33, 245, 246].

C.2 Bloch-Messiah and Polar Decompositions

The Bloch-Messiah and polar decompositions allow for arbitrary symplectic matrices, which represent Gaussian unitary transformations, to be broken down into a series of potentially simpler symplectic matrices. Since it can be difficult to understand what processes are represented in a symplectic transformation, these decompositions can be used to break the transformation up into *passive* and *active* processes [246].

Passive processes are interactions where photon number is conserved, which correspond to combinations of single mode processes of the form $\hat{a}_k^\dagger \hat{a}_k$, or two mode processes of the form $e^{i\theta}\hat{a}_k^\dagger \hat{a}_l + e^{-i\theta}\hat{a}_k \hat{a}_l^\dagger$ when expressed in the basis of the ladder operators. Since they conserve total quanta, a symplectic transformation consisting entirely of passive processes leaves the trace of the covariance matrix unchanged, $\mathrm{Tr}[\mathbf{S}\boldsymbol{\sigma}\mathbf{S}^T] = \mathrm{Tr}[\boldsymbol{\sigma}]$ [247]. This implies that $\mathbf{S}^T = \mathbf{S}^{-1}$, meaning that passive processes correspond to orthogonal matrices.

Active processes, on the other hand, do not preserve the trace of the covariance matrix, and correspond to combinations of single and two-mode squeezing processes: $e^{i\theta}\hat{a}_k^{\dagger 2} + e^{-i\theta}\hat{a}_k^2$ and $e^{i\theta}\hat{a}_k^\dagger \hat{a}_l^\dagger + e^{-i\theta}\hat{a}_k \hat{a}_l$. The symplectic matrices corresponding to active processes cannot be orthogonal, but are instead symmetric matrices. With this information, we can now provide a physical interpretation to the following matrix decompositions.

Bloch-Messiah Decomposition

Also called the Euler decomposition, this is simply the singular value decomposition (SVD) applied to a symplectic matrix [143]. The content of the decomposition is that a symplectic matrix can be written in the form

$$\mathbf{S} = \mathbf{O}_a \mathbf{S}_\mathrm{r} \mathbf{O}_b \quad \text{where} \quad \mathbf{S}_\mathrm{r} = \bigoplus_{k=1}^{N} \begin{pmatrix} e^{\mathrm{r}_k} & 0 \\ 0 & e^{-\mathrm{r}_k} \end{pmatrix}. \tag{C.8}$$

The matrices $\mathbf{O}_a$ and $\mathbf{O}_b$ are orthogonal matrices, and so purely consist of passive processes, such as single-mode phase shifters and two-mode beam splitters. The matrix $\mathbf{S}_\mathrm{r}$ is a real positive-definite matrix, and corresponds to a series of single-mode squeezing interactions acting in parallel on the modes, with some amount of squeezing r_k. The physical interpretation of this decomposition is that the action of any Gaussian unitary transformation is equivalent to a passive multi-mode interaction, followed by individual squeezing interactions applied to each mode, followed by another passive multi-mode interaction [144, 248, 249].

Polar Decomposition

A symplectic matrix can be written in polar form, either using the left polar decomposition or the right polar decomposition [142, 143], written as

$$\mathbf{S} = \mathbf{R}_\mathrm{L}\mathbf{U}_\mathrm{L} \quad \text{and} \quad \mathbf{S} = \mathbf{U}_\mathrm{R}\mathbf{R}_\mathrm{R}, \tag{C.9}$$

respectively. Here, $\mathbf{U}_\mathrm{L}, \mathbf{U}_\mathrm{R} \in Sp(2N,\mathbb{R}) \cap O(2N,\mathbb{R})$ are real symplectic orthogonal matrices, whereas the terms $\mathbf{R}_\mathrm{L}, \mathbf{R}_\mathrm{R} \in Sp(2N,\mathbb{R}) \cap \mathrm{Sym}^+(2N)$ are real symplectic symmetric positive definite matrices. In general, the matrices

$\mathbf{R}_{\mathrm{L}}$ and $\mathbf{R}_{\mathrm{R}}$ are not identical, while the matrices $\mathbf{U}_{\mathrm{L}}$ and $\mathbf{U}_{\mathrm{R}}$ must be similar matrices. It is possible to calculate the elements in both decompositions using different powers of the symplectic matrix $\mathbf{S}$:

$$\begin{aligned} \text{Left polar decomposition:} \quad & \mathbf{R}_{\mathrm{L}} = \left(\mathbf{S}\mathbf{S}^{T}\right)^{1/2} \quad \text{and} \quad \mathbf{U}_{\mathrm{L}} = \left(\mathbf{S}\mathbf{S}^{T}\right)^{-1/2}\mathbf{S} \\ \text{Right polar decomposition:} \quad & \mathbf{R}_{\mathrm{R}} = \left(\mathbf{S}^{T}\mathbf{S}\right)^{1/2} \quad \text{and} \quad \mathbf{U}_{\mathrm{R}} = \mathbf{S}\left(\mathbf{S}^{T}\mathbf{S}\right)^{-1/2}. \end{aligned} \tag{C.10}$$

The interpretation of this is similar to the Bloch-Messiah decomposition: the matrices $\mathbf{U}_{\mathrm{L}}$ and $\mathbf{U}_{\mathrm{R}}$ correspond to a passive multi-mode interaction, whereas the matrices $\mathbf{R}_{\mathrm{L}}$ and $\mathbf{R}_{\mathrm{R}}$ are comprised of only active multi-mode interactions, and therefore represent some combination of squeezing interactions. The polar decomposition then says that any Gaussian unitary transformation is equivalent to a passive multi-mode interaction followed by multi-mode squeezing interactions for the left decomposition, and the opposite in the case of the right decomposition, and that the active interactions involved in both will not necessarily be identical.

Comparing The Decompositions

These two decompositions are closely related, and it is possible to use the form of one to determine the other. Starting with the Bloch-Messiah decomposition, we can write $\mathbf{S} = (\mathbf{O}_a\mathbf{S}_{\mathrm{r}}\mathbf{O}_a^T)(\mathbf{O}_a\mathbf{O}_b)$ or $\mathbf{S} = (\mathbf{O}_a\mathbf{O}_b)(\mathbf{O}_b^T\mathbf{S}_{\mathrm{r}}\mathbf{O}_b)$ since $\mathbf{O}_a$ and $\mathbf{O}_b$ are orthogonal. The elements of the left and right polar decomposition can then be read off:

$$\begin{aligned} \text{Left polar decomposition:} \quad & \mathbf{U}_{\mathrm{L}} = \mathbf{O}_a\mathbf{O}_b \quad \text{and} \quad \mathbf{R}_{\mathrm{L}} = \mathbf{O}_a\mathbf{S}_{\mathrm{r}}\mathbf{O}_a^T \\ \text{Right polar decomposition:} \quad & \mathbf{U}_{\mathrm{R}} = \mathbf{O}_a\mathbf{O}_b \quad \text{and} \quad \mathbf{R}_{\mathrm{R}} = \mathbf{O}_b^T\mathbf{S}_{\mathrm{r}}\mathbf{O}_b. \end{aligned} \tag{C.11}$$

The forms of $\mathbf{R}_{\mathrm{L}}$ and $\mathbf{R}_{\mathrm{R}}$ follows from the fact that they are both real symmetric matrices, and so may be diagonalised by orthogonal matrices; diagonalisation by $\mathbf{O}_a$ or $\mathbf{O}_b$ is guaranteed to be unique, up to choice of an orthonormal basis. In addition, since these matrices are positive definite, their eigenvalues must be positive definite, a property which is fulfilled by the diagonal matrix $\mathbf{S}_{\mathrm{r}}$. Writing symplectic matrices in this form also tells us that any combination of squeezing process may be represented by a passive transformation, followed by single-mode squeezing with fixed phase, followed by the inverse of the first passive transformation. We can also see from the above that the passive matrices from the left and right polar decompositions are similar matrices, $\mathbf{U}_{\mathrm{R}} \sim \mathbf{U}_{\mathrm{L}}$.

C.3 Transformations on Gaussian States

Displacement Operator

The displacement operator in quantum optics acts as a shift operator on the first moments of the Wigner function, or equivalently, as a shift of the field operators. The usual convention is to define the displacement operator acting on a single mode as,

$$\hat{D}(\alpha) := \exp\left[\alpha\hat{a}^{\dagger} - \alpha^{*}\hat{a}\right] = \exp\left[-i\left(\hat{p}\bar{q} - \hat{q}\bar{p}\right)\right] \quad \text{where} \quad \alpha = \frac{1}{\sqrt{2}}(\bar{q} + i\bar{p}), \tag{C.12}$$

which will therefore transform the ladder operators as $\hat{D}^{\dagger}(\alpha)\hat{a}\hat{D}(\alpha) = \hat{a} + \alpha$. The inverse of this operator is by definition a transformation by $-\alpha$, $\hat{D}^{\dagger}(\alpha) = \hat{D}(-\alpha)$. In this work, displacement of the cavity mode often occurs due to drive terms in the Hamiltonian, which we express as $\epsilon\hat{a}^{\dagger} + \epsilon^{*}\hat{a}$. Since a different convention is used in the definition of this drive term, we define the corresponding displacement operator for a drive as follows:

$$\hat{U}_D := \exp\left[-i\left(\epsilon\hat{a}^{\dagger} + \epsilon^{*}\hat{a}\right)\right] = \exp\left[-i\sqrt{2}\left(\mathrm{Re}[\epsilon]\hat{q} + \mathrm{Im}[\epsilon]\hat{p}\right)\right]. \tag{C.13}$$

This is the only transformation which is not symplectic, and is purely a translation. The coordinate transformation in this instance is given by

$$\hat{\boldsymbol{r}} \to \hat{U}_D^{\dagger}\hat{\boldsymbol{r}}\hat{U}_D = \hat{\boldsymbol{r}} + \mathbf{d} \quad \text{where} \quad \mathbf{d} = \sqrt{2}\begin{pmatrix} \mathrm{Im}[\epsilon] \\ -\mathrm{Re}[\epsilon] \end{pmatrix}, \tag{C.14}$$

where $\hat{\boldsymbol{r}} = (\hat{q}, \hat{p})$. For completeness, displacement by $\hat{D}(\alpha)$ results in the following phase space transformation:

$$\hat{\boldsymbol{r}} \to \hat{D}^{\dagger}(\alpha)\hat{\boldsymbol{r}}\hat{D}(\alpha) = \hat{\boldsymbol{r}} + \mathbf{d} \quad \text{where} \quad \mathbf{d} = \begin{pmatrix} \bar{q} \\ \bar{p} \end{pmatrix}. \tag{C.15}$$

This is the only Gaussian transformation which displaces the Gaussian state; all others that will be considered are symplectic transformations which can alter the first moments but cannot generate any displacement if none is present.

Phase Shifters and Rotations
When working with harmonic modes, terms of the form $\theta\hat{a}^\dagger\hat{a}$ in the system Hamiltonian correspond to the frequency of the mode with respect to the choice of frame. The corresponding unitary operation, appropriately symmetrised, is given by:

$$\hat{U}_R := \exp\left[-i\frac{\theta}{2}\left(\hat{a}^\dagger\hat{a} + \hat{a}\hat{a}^\dagger\right)\right] = \exp\left[-i\frac{\theta}{2}\left(\hat{q}^2 + \hat{p}^2\right)\right]. \tag{C.16}$$

This unitary transforms the ladder operators as $\hat{U}_R^\dagger\hat{a}\hat{U}_R = e^{-i\theta}\hat{a}$, and so this operation is termed a phase shifter. Working in the quadrature basis, $\hat{\boldsymbol{r}} = (\hat{q}, \hat{p})$, the Hamiltonian may be expressed as a simple matrix diagonal in the quadrature basis:

$$\boldsymbol{H}_R = \theta\begin{pmatrix}1 & 0\\ 0 & 1\end{pmatrix}. \tag{C.17}$$

The unitary transformation can therefore be written as

$$\hat{\boldsymbol{r}} \to \hat{U}_R^\dagger\hat{\boldsymbol{r}}\hat{U}_R = \exp\left[\boldsymbol{\Omega}\boldsymbol{H}_R\right]\hat{\boldsymbol{r}} = \boldsymbol{R}(\theta)\hat{\boldsymbol{r}} \quad \text{where} \quad \boldsymbol{\Omega}\boldsymbol{H}_R = \theta\begin{pmatrix}0 & 1\\ -1 & 0\end{pmatrix}. \tag{C.18}$$

Calculating the matrix exponential, the symplectic transformation corresponds to an orthogonal rotation matrix, $\boldsymbol{R}^T(\theta) = \boldsymbol{R}(-\theta)$, acting on the quadrature basis:

$$\boldsymbol{R}(\theta) = \begin{pmatrix}\cos(\theta) & \sin(\theta)\\ -\sin(\theta) & \cos(\theta)\end{pmatrix}. \tag{C.19}$$

Applying this transformation to the Wigner distribution results in a rotation of the Wigner function in phase space about the origin. For an N-mode system, there are N phase shifter operations, one for each mode.

Beam Splitters and Two-Mode Rotations
The other set of passive transformations that may be applied to Gaussian systems are beam splitters, which give rise to the following unitary transformation acting on a two-mode system Hilbert space:

$$\hat{U}_B := \exp\left[-i\theta\left(e^{i\phi}\hat{a}_1^\dagger\hat{a}_2 + e^{-i\phi}\hat{a}_1\hat{a}_2^\dagger\right)\right] = \exp\left[-i\theta\Big(\cos(\phi)(\hat{q}_1\hat{q}_2 + \hat{p}_1\hat{p}_2) + \sin(\phi)(\hat{p}_1\hat{q}_2 - \hat{q}_1\hat{p}_2)\Big)\right]. \tag{C.20}$$

This unitary transformation will not only shift the phases of the different ladder operators but will also rotate the field operators between the two modes. The above unitary operator may be written as an operator acting on the basis of quadrature operators $\hat{\boldsymbol{r}} = (\hat{q}_1, \hat{p}_1, \hat{q}_2, \hat{p}_2)$ as follows:

$$\boldsymbol{H}_B = \theta\begin{pmatrix}\mathbf{0} & \cos(\phi)\mathbf{I} - \sin(\phi)\mathbf{J}\\ \cos(\phi)\mathbf{I} + \sin(\phi)\mathbf{J} & \mathbf{0}\end{pmatrix}. \tag{C.21}$$

This beam splitter unitary transformation will then transform the quadrature vector as,

$$\hat{\boldsymbol{r}} \to \hat{U}_B^\dagger\hat{\boldsymbol{r}}\hat{U}_B = \exp\left[\boldsymbol{\Omega}\boldsymbol{H}_B\right]\hat{\boldsymbol{r}} = \boldsymbol{B}(\theta,\phi)\hat{\boldsymbol{r}} \quad \text{where} \quad \boldsymbol{\Omega}\boldsymbol{H}_B = \theta\begin{pmatrix}\mathbf{0} & \cos(\phi)\mathbf{J} + \sin(\phi)\mathbf{I}\\ \cos(\phi)\mathbf{J} - \sin(\phi)\mathbf{I} & \mathbf{0}\end{pmatrix}. \tag{C.22}$$

The symplectic transformation in the Wigner phase space takes the form of the following two-mode rotation matrix:

$$\boldsymbol{B}(\theta,\phi) = \begin{pmatrix}\cos(\theta)\mathbf{I} & \sin(\theta)\left(\cos(\phi)\mathbf{J} + \sin(\phi)\mathbf{I}\right)\\ \sin(\theta)\left(\cos(\phi)\mathbf{J} - \sin(\phi)\mathbf{I}\right) & \cos(\theta)\mathbf{I}\end{pmatrix}. \tag{C.23}$$

This matrix is necessarily orthogonal, $\boldsymbol{B}^T(\theta,\phi) = \boldsymbol{B}^{-1}(\theta,\phi)$. The set of phase shifters and beam splitters acting on N-modes corresponds to the unitary group $U(N)$, which forms a subgroup of $Sp(2n,\mathbb{R})$; since the dimension of $U(N)$ is N^2, removing the phase shifters means that the number of distinct beam splitter operations for an N-mode system is $N(N-1)$.

Single-Mode Squeezing
As with the displacement operator, the single-mode squeezing operator is usually defined using the following convention in the quantum optics literature:

$$\hat{S}_1(r,\varphi) := \exp\left[-\frac{r}{2}\left(e^{i\varphi}\hat{a}^{\dagger 2} - e^{-i\varphi}\hat{a}^2\right)\right] = \exp\left[-i\frac{r}{2}\left(\sin(\varphi)(\hat{q}^2 - \hat{p}^2) - \cos(\varphi)(\hat{q}\hat{p} + \hat{p}\hat{q})\right)\right]. \tag{C.24}$$

The squeezing operator acts to squeeze or anti-squeeze the quadrature fields, with the axis of the squeezing given by the choice of phase φ. For example, when $\varphi = 0$, the position quadrature is squeezed, $\hat{S}_1^\dagger(r,0)\hat{q}\hat{S}_1(r,0) = e^{-r}\hat{q}$, and the momentum quadrature is anti-squeezed, $\hat{S}_1^\dagger(r,0)\hat{p}\hat{S}_1(r,0) = e^{r}\hat{p}$. However, given the expressions for single-mode squeezing that are used in the Hamiltonians within this work, the following unitary operator is more convenient in certain circumstances:

$$\hat{U}_{S1} := \exp\left[-i\frac{r}{2}\left(e^{i\phi}\hat{a}^{\dagger 2} + e^{-i\phi}\hat{a}^2\right)\right] = \exp\left[-i\frac{r}{2}\left(\cos(\phi)(\hat{q}^2 - \hat{p}^2) + \sin(\phi)(\hat{q}\hat{p} + \hat{p}\hat{q})\right)\right]. \tag{C.25}$$

We can convert between these two conventions through a change of the squeezing phase, $\phi \to \varphi - \pi/2$. The symmetric Hamiltonian matrix is written in the quadrature basis, $\hat{\boldsymbol{r}} = (q, p)$, as:

$$\boldsymbol{H}_{S1} = r\begin{pmatrix}\cos(\phi) & \sin(\phi)\\ \sin(\phi) & -\cos(\phi)\end{pmatrix} \tag{C.26}$$

The transformation of the quadrature operators proceeds as follows,

$$\hat{\boldsymbol{r}} \to \hat{U}_{S1}^\dagger \hat{\boldsymbol{r}} \hat{U}_{S1} = \exp\left[\boldsymbol{\Omega}\boldsymbol{H}_{S1}\right]\hat{\boldsymbol{r}} = \boldsymbol{S}_1(r,\phi)\hat{\boldsymbol{r}} \quad \text{where} \quad \boldsymbol{\Omega}\boldsymbol{H}_{S1} = r\begin{pmatrix}\sin(\phi) & -\cos(\phi)\\ -\cos(\phi) & -\sin(\phi)\end{pmatrix}, \tag{C.27}$$

where the symplectic transformation, $\boldsymbol{S}_1(r,\phi)$, is a real and positive-definite matrix:

$$\boldsymbol{S}_1(r,\phi) := \begin{pmatrix}\cosh(r) + \sin(\phi)\sinh(r) & -\cos(\phi)\sinh(r)\\ -\cos(\phi)\sinh(r) & \cosh(r) - \sin(\phi)\sinh(r)\end{pmatrix}. \tag{C.28}$$

All possible single-mode squeezing operations on a single mode can be constructed using a linear combination of two orthogonal elements of the symplectic Lie algebra; for an N-mode system, the subset of single-mode squeezing operations therefore has size $2N$.

Two-Mode Squeezing

The final active process to be considered is the two-mode squeezer, which is conventionally defined as follows:

$$\hat{S}_2(r,\varphi) := \exp\left[-r\left(e^{i\varphi}\hat{a}_1^\dagger\hat{a}_2^\dagger - e^{-i\varphi}\hat{a}_1\hat{a}_2\right)\right], \tag{C.29}$$

However, we again choose to use a different phase, $\phi \to \varphi - \pi/2$, in our definition:

$$\hat{U}_{S2} := \exp\left[-ir\left(e^{i\phi}\hat{a}_1^\dagger\hat{a}_2^\dagger + e^{-i\phi}\hat{a}_1\hat{a}_2\right)\right] = \exp\left[-ir\Big(\cos(\phi)(\hat{q}_1\hat{q}_2 - \hat{p}_1\hat{p}_2) + \sin(\phi)(\hat{p}_a\hat{q}_2 + \hat{q}_1\hat{p}_2)\Big)\right]. \tag{C.30}$$

The associated matrix of coefficients in the two-mode squeezer Hamiltonian is,

$$\boldsymbol{H}_{S2} = r\begin{pmatrix}\mathbf{0} & \cos(\phi)\mathbf{Z} + \sin(\phi)\mathbf{X}\\ \cos(\phi)\mathbf{Z} + \sin(\phi)\mathbf{X} & \mathbf{0}\end{pmatrix}, \tag{C.31}$$

so the quadrature operators transform as

$$\begin{aligned}&\hat{\boldsymbol{r}} \to \hat{U}_{S2}^\dagger \hat{\boldsymbol{r}} \hat{U}_{S2} = \exp\left[\boldsymbol{\Omega}\boldsymbol{H}_{S2}\right]\hat{\boldsymbol{r}} = \boldsymbol{S}_2(r,\phi)\hat{\boldsymbol{r}}\\ &\text{where} \quad \boldsymbol{\Omega}\boldsymbol{H}_{S2} = r\begin{pmatrix}\mathbf{0} & -\cos(\phi)\mathbf{X} + \sin(\phi)\mathbf{Z}\\ -\cos(\phi)\mathbf{X} + \sin(\phi)\mathbf{Z} & \mathbf{0}\end{pmatrix}.\end{aligned} \tag{C.32}$$

The symplectic transformation is therefore given by the following positive-definite symmetric matrix:

$$\boldsymbol{S}_2(r,\phi) := \begin{pmatrix}\cosh(r)\mathbf{I} & \sinh(r)\left(-\cos(\phi)\mathbf{X} + \sin(\phi)\mathbf{Z}\right)\\ \sinh(r)\left(-\cos(\phi)\mathbf{X} + \sin(\phi)\mathbf{Z}\right) & \cosh(r)\mathbf{I}\end{pmatrix}. \tag{C.33}$$

The total size of the subset of $sp(2N,\mathbb{R})$ representing active processes is $N(N+1)$, and after removing the single-mode squeezing processes, the number of distinct two-mode squeezing operations for an N mode system is therefore $N(N-1)$.

C.4 Standard Gaussian States

Vacuum and Displaced States

Perhaps the most important Gaussian state is the vacuum state of the harmonic oscillator Hamiltonian, $|0\rangle$, from which many other states can be generated through symplectic-affine transformations. The Wigner function for the vacuum state is just a simple Gaussian distribution centred at the origin of the phase space, with an associated characteristic function given by:

$$W_0(q,p) = \frac{1}{\pi}\exp\left[-\frac{1}{2}(q^2+p^2)\right] \xrightarrow{\text{Fourier}} w_0(\xi_q,\xi_p) = \exp\left[-\frac{1}{4}\left(\xi_q^2+\xi_p^2\right)\right]. \tag{C.34}$$

Also of interest are the states generated by applying the displacement operator to the vacuum state, resulting in so-called displaced states, also termed the canonical coherent states. Using the quantum optics convention for the displacement operator from Eq. (C.12), the displaced state is generated from the vacuum state via $|\alpha\rangle = \hat{D}(\alpha)\,|0\rangle$. Using $\alpha = (\bar{q}+i\bar{p})/\sqrt{2}$, the Wigner function and associated characteristic function are:

$$W_\alpha(q,p) = \frac{1}{\pi}\exp\left[-(q-\bar{q})^2-(p-\bar{p})^2\right] \xrightarrow{\text{Fourier}} w_\alpha(\xi_q,\xi_p) = \exp\left[-\frac{1}{4}\left(\xi_q^2+\xi_p^2\right) - i\bar{q}\xi_q - i\bar{p}\xi_p\right]. \tag{C.35}$$

Defining the quadrature basis vector as $\boldsymbol{r} = (q,p)$, the statistical moments for the displaced state may be written as

$$\boldsymbol{\sigma}_\alpha = \frac{1}{2}\begin{pmatrix}1 & 0\\ 0 & 1\end{pmatrix} \qquad \boldsymbol{\mu}_\alpha = \begin{pmatrix}\bar{q}\\ \bar{p}\end{pmatrix}. \tag{C.36}$$

The moments for the vacuum state can be retrieved by setting $\alpha = 0$.

Squeezed States

Squeezed states are perhaps the most important states for this work, since the presence of anti-squeezing is an indication of gain from the amplifier. The sharing of squeezed correlations between two or more modes is also a necessary component for the generation of entanglement between Gaussian states. A single-mode squeezed-vacuum (SMSV) state can be realised by applying the squeezing operator to the vacuum state, $|\text{SMSV}\rangle = \hat{S}_1(r,\varphi)\,|0\rangle$, where the squeezing operator used here is given in Eq. (C.24). The Wigner function and characteristic function are given by:

$$\begin{aligned} W_{S1}(q,p) \;&= \frac{1}{\pi}\exp\left[-e^{-2r}\left(q\cos\frac{\varphi}{2}+p\sin\frac{\varphi}{2}\right)^2 - e^{2r}\left(q\sin\frac{\varphi}{2}-p\cos\frac{\varphi}{2}\right)^2\right] \\ \xrightarrow{\text{Fourier}}\; w_{S1}(\xi_q,\xi_p) \;&= \exp\Bigg[-\frac{1}{4}\Big(\xi_q^2\left(\cosh(2r)+\cos(\varphi)\sinh(2r)\right)+\xi_p^2\left(\cosh(2r)-\cos(\varphi)\sinh(2r)\right) \\ &\qquad -2\xi_q\xi_p\sin(\varphi)\sinh(2r)\Big)\Bigg]. \end{aligned} \tag{C.37}$$

Reading off the moments from w_{S1}, the statistical moments for the SMSV state are therefore:

$$\boldsymbol{\sigma}_{S1} = \frac{1}{2}\begin{pmatrix}\cosh(2r)+\cos(\varphi)\sinh(2r) & -\sin(\varphi)\sinh(2r)\\ -\sin(\varphi)\sinh(2r) & \cosh(2r)-\cos(\varphi)\sinh(2r)\end{pmatrix} \qquad \boldsymbol{\mu}_{S1} = \begin{pmatrix}0\\0\end{pmatrix}. \tag{C.38}$$

Rather than going through the effort of computing the Wigner function and then performing the Fourier transform to obtain these moments, we can use the previously defined symplectic transformation for single-mode squeezing from Eq. (C.28) and transform the moments of the vacuum state directly using Eq. (C.6). Since the covariance matrix for the vacuum state is proportional to the identity matrix, the above covariance matrix for an SMSV is therefore more easily obtained using,

$$\boldsymbol{\sigma}_{S1} = \boldsymbol{S}_1(r,\varphi-\pi/2)\boldsymbol{\sigma}_0\boldsymbol{S}_1^T(r,\varphi-\pi/2), \tag{C.39}$$

with the means unchanged since the vacuum state has no displacement, $\boldsymbol{\mu}_{S1} = \boldsymbol{\mu}_0$.

The transformation matrices make it easier to generate any state we wish. As an example, we will look at the difference between a displaced squeezed state, $\hat{D}(\alpha)\hat{S}_1(r,\varphi)\,|0\rangle$, and a squeezed coherent state, $\hat{S}_1(r,\varphi)\hat{D}(\gamma)\,|0\rangle$, which in general are distinct since the two operations do not commute. Applying the single-mode squeezing and displacement transformations to the moments of the vacuum state results in the following set of moments:

$$\begin{aligned} &\hat{D}(\alpha)\hat{S}_1(r,\varphi)\,|0\rangle \;:\; \boldsymbol{\sigma} = \boldsymbol{S}_1\boldsymbol{\sigma}_0\boldsymbol{S}_1 \quad\text{and}\quad \boldsymbol{\mu} = \boldsymbol{S}_1\boldsymbol{\mu}_0 + \mathbf{d}_\alpha = \mathbf{d}_\alpha \\ &\hat{S}_1(r,\varphi)\hat{D}(\gamma)\,|0\rangle \;:\; \boldsymbol{\sigma} = \boldsymbol{S}_1\boldsymbol{\sigma}_0\boldsymbol{S}_1 \quad\text{and}\quad \boldsymbol{\mu} = \boldsymbol{S}_1(\boldsymbol{\mu}_0+\mathbf{d}_\gamma) = \boldsymbol{S}_1\mathbf{d}_\gamma. \end{aligned} \tag{C.40}$$

The second moments are the same no matter the order in which the operators are applied, since the displacement only affects the first moments of the state. For the displaced-squeezed state the final displacement in the same as the coherent state $|\alpha\rangle$, whereas for a squeezed-coherent state the squeezing alters the displacement of the final state, which is squeezed or anti-squeezed along an axis determined by the phase of $\hat{S}_1$. In order for the final displacement to be the same, we can set $\boldsymbol{S}_1\mathbf{d}_\gamma = \mathbf{d}_\alpha$, and after some matrix multiplication, retrieve $\gamma = \alpha\cosh(r) + \alpha^* e^{i\varphi}\sinh(r)$; this is equivalent to solving $\hat{D}(\alpha)\hat{S}_1(r,\varphi) = \hat{S}_1(r,\varphi)\hat{D}(\gamma)$.

The final squeezed state that we will consider is the two-mode squeezed-vacuum (TMSV) state, $|\text{TMSV}\rangle = \hat{S}_2(r,\varphi)\,|0\rangle$. Here we can ignore the Wigner function and work directly with the covariance and means of the two-mode vacuum state; since additional modes correspond to a direct sum, the covariance matrix of the vacuum is just the 4×4 identity matrix, while the means are all zero. The means for the TMSV will be unchanged, $\boldsymbol{\mu}_{S2} = \boldsymbol{\mu}_0$, while the covariance matrix is,

$$\boldsymbol{\sigma}_{S2} = \frac{1}{2}\begin{pmatrix} \cosh(2r)\,\mathbf{I} & -\sinh(2r)\,(\cos(\varphi)\mathbf{Z} + \sin(\varphi)\mathbf{X}) \\ -\sinh(2r)\,(\cos(\varphi)\mathbf{Z} + \sin(\varphi)\mathbf{X}) & \cosh(2r)\,\mathbf{I} \end{pmatrix}, \tag{C.41}$$

which is obtained by calculating $\boldsymbol{\sigma}_{S2} = \boldsymbol{S}_2(r,\varphi-\pi/2)\boldsymbol{\sigma}_0\boldsymbol{S}_2^T(r,\varphi-\pi/2)$.

Thermal States

There is one Gaussian state which cannot be obtained by applying canonical transformations to the vacuum state, and that is the thermal state. In order to work out the covariances, we start with the density operator for an uncorrelated cavity in a thermal state, written as follows:

$$\hat{\rho}_\beta = \left(1 - e^{-\beta\omega}\right)\sum_{n=0}^{\infty} e^{-\beta\Omega k}\,|n\rangle\langle n| = \sum_n \frac{(\bar{n})^n}{(\bar{n}+1)^{n+1}}\,|n\rangle\langle n|\,. \tag{C.42}$$

We can relate the thermodynamic β to average thermal occupation $\bar{n}$, assuming thermal equilibrium, through the relation $\bar{n} = 1/(e^{\beta\omega}-1)$, or equivalently $\beta\omega = \ln[(\bar{n}+1)/\bar{n}]$. The Wigner function for this can be obtained using the series expansion of the thermal state in the number eigenstate basis, along with the following expression for the Wigner function of the number eigenstates, $|n\rangle$:

$$W_n(q,p) = \frac{(-1)^n}{\pi} L_n\left[2(x^2+p^2)\right]\exp\left[-(x^2+p^2)\right]. \tag{C.43}$$

The Wigner function for the thermal state is then a weighted sum over these Wigner functions,

$$W_\beta(q,p) = \sum_n \frac{(\bar{n})^n}{(\bar{n}+1)^{n+1}} W_n(q,p), \tag{C.44}$$

which may be evaluated using the generating function for the Laguerre polynomials,

$$\sum_n s^n L_n[z] = (1-s)^{-1}\exp[-sz/(1-s)]. \tag{C.45}$$

The Wigner function for the thermal state, along with the characteristic function, is then,

$$W_\beta(q,p) = \frac{1}{\pi(2\bar{n}+1)}\exp\left[-\frac{1}{2\bar{n}+1}(q^2+p^2)\right] \xrightarrow{\text{Fourier}} w_\beta(\xi_q,\xi_p) = \exp\left[-\frac{1}{2}\left(\bar{n}+\frac{1}{2}\right)\left(\xi_x^2+\xi_p^2\right)\right], \tag{C.46}$$

where the thermal occupation plus vacuum in the above is equal to $2\bar{n}+1 = \coth(\beta\omega/2)$. The statistical moments for a thermal state are then easily read off from the characteristic function,

$$\boldsymbol{\sigma}_\beta = \frac{1}{2}\begin{pmatrix} 2\bar{n}+1 & 0 \\ 0 & 2\bar{n}+1 \end{pmatrix} \qquad \boldsymbol{\mu}_\beta = \begin{pmatrix} 0 \\ 0 \end{pmatrix}. \tag{C.47}$$

A larger temperature increases $\bar{n}$, leading to an increase in the variance of the state in Wigner phase space. In the absence of any photon occupation, equivalent to the low-temperature limit, it can be seen that the thermal state is equal to a vacuum state.

D Further Details on The Entangling Properties of the Delta Amplifier

D.1 Comparison of the Scattering Properties of the Delta Amplifier and the Open Two-Mode Squeezer

The delta amplifier can be optimised to allow swapping of thermal noise from mode a_1 to mode a_3 by setting the TMS cooperativities to be identical, $\mathcal{C}_{12}, \mathcal{C}_{23} = \mathcal{C}$, and the BS cooperativity to $\mathcal{C}_{13} = 1$. We additionally set the loop phase to $\phi = +\pi/2$ so that modes a_1 and a_2 are entangled. Substituting these values into Eq. (3.81), the steady-state scattering matrix on resonance written in the quadrature basis matrix will then have the following form:

$$\mathbf{S}_{\Delta} = \begin{pmatrix} \mathbf{0} & \frac{2\sqrt{\mathcal{C}}}{1-\mathcal{C}}\mathbf{X} & -\frac{1+\mathcal{C}}{1-\mathcal{C}}\mathbf{J} \\ \mathbf{0} & -\frac{1+\mathcal{C}}{1-\mathcal{C}}\mathbf{I} & -\frac{2\sqrt{\mathcal{C}}}{1-\mathcal{C}}\mathbf{Z} \\ -\mathbf{J} & \mathbf{0} & \mathbf{0} \end{pmatrix}. \tag{D.1}$$

Replacing the cooperativity with the squeezing parameter, $r = \operatorname{artanh}[2\sqrt{\mathcal{C}}/(1+\mathcal{C})]$, we can rewrite the above scattering matrix as follows:

$$\mathbf{S}_{\Delta} \equiv \begin{pmatrix} \mathbf{0} & \sinh(r)\mathbf{X} & -\cosh(r)\mathbf{J} \\ \mathbf{0} & -\cosh(r)\mathbf{I} & -\sinh(r)\mathbf{Z} \\ -\mathbf{J} & \mathbf{0} & \mathbf{0} \end{pmatrix}. \tag{D.2}$$

This makes clear the behaviour of the system at this point of nonreciprocity. Modes a_1 and a_2 are independent of the input noise on mode a_1, which only appears in mode a_3, showing how the noise is rerouted there. Meanwhile, modes a_2 and a_3 share some squeezed correlations. We can also calculate the steady-state scattering matrix for an open system with a TMS Hamiltonian given by $\hat{H}_{\mathrm{TMS}} = ig_{12}(\hat{a}_1^{\dagger}\hat{a}_2^{\dagger} - \hat{a}_1\hat{a}_2)$ using Eq. (3.56):

$$\mathbf{S}_{\mathrm{TMS}} = \begin{pmatrix} -\frac{1+\mathcal{C}}{1-\mathcal{C}}\mathbf{I} & -\frac{2\sqrt{\mathcal{C}}}{1-\mathcal{C}}\mathbf{Z} \\ -\frac{2\sqrt{\mathcal{C}}}{1-\mathcal{C}}\mathbf{Z} & -\frac{1+\mathcal{C}}{1-\mathcal{C}}\mathbf{I} \end{pmatrix}. \tag{D.3}$$

Note that selecting the TMS phase to be zero is not appropriate here, this comes from the polar decomposition in Eq. (3.85). Defining the squeezing in terms of the cooperativity in the same way as with the delta amplifier, we arrive at the following scattering matrix:

$$\mathbf{S}_{\mathrm{TMS}} \equiv \begin{pmatrix} -\cosh(r)\mathbf{I} & -\sinh(r)\mathbf{Z} \\ -\sinh(r)\mathbf{Z} & -\cosh(r)\mathbf{I} \end{pmatrix}. \tag{D.4}$$

While the covariance matrix of the TMS and modes a_1 and a_2 from the delta amplifier will be identical, the scattering behaviour is markedly different. This is expected given the circuit decomposition for the delta amplifier; since the squeezing is swapped from mode a_3 to mode a_1 by a beam splitter, the quadratures are rotated during this swap in a manner that cannot be replicated in a TMS alone.

D.2 A Reciprocal Three-Mode Loop Cannot Route Thermal Fluctuations And Generate Entanglement

In order to reroute thermal noise away from the output of one mode in the delta and bowtie amplifiers, it is required that the input noise not be reflected into the output field. Additionally, if this mode is to be entangled with another mode in the amplifier, the scattering between the pair of modes must be made nonreciprocal to prevent this thermal noise from appearing in the output field of the other mode in the entangled pair.

It is simple to demonstrate that it is not possible to do both in a three-mode system where the scattering between the pair of modes is reciprocal. We consider an example three-mode system, where the goal is to entangle modes a_1 and a_2, and route thermal noise coming from the input of mode a_1 away from the entangled state. If the scattering between modes a_1 and a_2 is reciprocal, this scattering matrix must take the form:

$$\mathbf{S} = \begin{pmatrix} \mathbf{0} & \mathbf{0} & \mathbf{S}_{13} \\ \mathbf{0} & \mathbf{S}_{22} & \mathbf{S}_{23} \\ \mathbf{S}_{31} & \mathbf{S}_{32} & \mathbf{S}_{33} \end{pmatrix}. \tag{D.5}$$

Writing the initial covariance matrix in block-form as $\boldsymbol{\sigma}_{\text{in}} = \text{diag}(\boldsymbol{\sigma}_{1,\text{in}}, \boldsymbol{\sigma}_{2,\text{in}}, \boldsymbol{\sigma}_{3,\text{in}})$, the covariance matrix for the output of modes a_1 and a_2 is then

$$\boldsymbol{\sigma}_{12,\text{out}} = \begin{pmatrix} \mathbf{S}_{13}\boldsymbol{\sigma}_{3,\text{in}}\mathbf{S}_{13}^T & \mathbf{S}_{13}\boldsymbol{\sigma}_{3,\text{in}}\mathbf{S}_{23}^T \\ \mathbf{S}_{23}\boldsymbol{\sigma}_{3,\text{in}}\mathbf{S}_{13}^T & \mathbf{S}_{22}\boldsymbol{\sigma}_{2,\text{in}}\mathbf{S}_{22}^T + \mathbf{S}_{23}\boldsymbol{\sigma}_{3,\text{in}}\mathbf{S}_{23}^T \end{pmatrix} \tag{D.6}$$

which is independent of $\boldsymbol{\sigma}_{1,\text{in}}$, as desired. Assuming that Eq. (D.5) is a valid scattering matrix, it must be symplectic and hence satisfy the condition $\mathbf{S}\boldsymbol{\Omega}_3\mathbf{S}^T = \boldsymbol{\Omega}_3$ where $\boldsymbol{\Omega}_3 = \text{diag}(\boldsymbol{\Omega}_1, \boldsymbol{\Omega}_1, \boldsymbol{\Omega}_1)$ is the symplectic form. Using this condition for the scattering matrix, it is possible to come up with conditions for the block elements of Eq. (D.5):

$$\begin{pmatrix} \mathbf{S}_{13}\boldsymbol{\Omega}_1\mathbf{S}_{13}^T & \mathbf{S}_{13}\boldsymbol{\Omega}_1\mathbf{S}_{23}^T & \mathbf{S}_{13}\boldsymbol{\Omega}_1\mathbf{S}_{33}^T \\ \mathbf{S}_{23}\boldsymbol{\Omega}_1\mathbf{S}_{13}^T & \mathbf{S}_{22}\boldsymbol{\Omega}_1\mathbf{S}_{22}^T + \mathbf{S}_{23}\boldsymbol{\Omega}_1\mathbf{S}_{23}^T & \mathbf{S}_{22}\boldsymbol{\Omega}_1\mathbf{S}_{32}^T + \mathbf{S}_{23}\boldsymbol{\Omega}_1\mathbf{S}_{33}^T \\ \mathbf{S}_{33}\boldsymbol{\Omega}_1\mathbf{S}_{13}^T & \mathbf{S}_{32}\boldsymbol{\Omega}_1\mathbf{S}_{22}^T + \mathbf{S}_{33}\boldsymbol{\Omega}_1\mathbf{S}_{23}^T & \mathbf{S}_{31}\boldsymbol{\Omega}_1\mathbf{S}_{31}^T + \mathbf{S}_{32}\boldsymbol{\Omega}_1\mathbf{S}_{32}^T + \mathbf{S}_{33}\boldsymbol{\Omega}_1\mathbf{S}_{33}^T \end{pmatrix} = \begin{pmatrix} \boldsymbol{\Omega}_1 & \mathbf{0} & \mathbf{0} \\ \mathbf{0} & \boldsymbol{\Omega}_1 & \mathbf{0} \\ \mathbf{0} & \mathbf{0} & \boldsymbol{\Omega}_1 \end{pmatrix}. \tag{D.7}$$

First, it may be determined from the above expression that $\mathbf{S}_{13}\boldsymbol{\Omega}_1\mathbf{S}_{13}^T = \boldsymbol{\Omega}_1$, which indicates that $\mathbf{S}_{13} \in Sp(2,\mathbb{R})$. We also have to satisfy $\mathbf{S}_{13}\boldsymbol{\Omega}_1\mathbf{S}_{23}^T = \mathbf{0}$ in order for $\mathbf{S}\boldsymbol{\Omega}_3\mathbf{S}^T = \boldsymbol{\Omega}_3$ to hold; since $\mathbf{S}_{13}\boldsymbol{\Omega}_1 \in Sp(2,\mathbb{R})$ must be invertible it follows that $\mathbf{S}_{23}^T = (\mathbf{S}_{13}\boldsymbol{\Omega}_1)^{-1}\mathbf{0}$ and so $\mathbf{S}_{23} = \mathbf{0}$. As a consequence, the off-diagonal blocks in Eq. (D.6) vanish, indicating that the output of modes a_1 and a_2 are never entangled. It is therefore not possible to realise thermal noise rerouting and entanglement in a reciprocal three-mode loop.

D.3 Steady-State Scattering as a Coherent Process

In Chapter 3, it was shown that, in the steady state, the scattering of the propagating modes off the internal modes of a Gaussian system could be modelled as a coherent process. In particular, the steady-state scattering matrix for the delta and bowtie amplifiers at points of perfect nonreciprocity can be decomposed into circuits comprised of the individual elements found within their respective Hamiltonians, with the original coherent coupling strengths replaced with couplings in terms of the cooperativities. In this section, we will show why this is the case for the delta amplifier. For the delta amplifier system, the scattering matrix may be related to a pseudo-coherent process when $\phi = \pm\pi/2$ as follows:

$$-\mathbf{S}_\Delta^{(\pm\pi/2)}\hat{\boldsymbol{r}} = (\hat{U}_\Delta^\pm)^\dagger \hat{\boldsymbol{r}} \hat{U}_\Delta^\pm \quad \text{where} \quad \hat{U}_\Delta^\pm = \exp\left[-i\frac{1}{\text{C}}\text{arcosh}\left(\frac{1+\text{C}^2}{1-\text{C}^2}\right)\tilde{H}_\Delta^\pm\right],\ \text{C} = \sqrt{\mathcal{C}_{12} - \mathcal{C}_{13} + \mathcal{C}_{23}}. \tag{D.8}$$

The Hamiltonian for the pseudo-coherent process is

$$\tilde{H}_\Delta^\pm = \sqrt{\mathcal{C}_{12}}\left(\hat{a}_1^\dagger\hat{a}_2^\dagger + \hat{a}_1\hat{a}_2\right) + \sqrt{\mathcal{C}_{13}}\left(\hat{a}_1^\dagger\hat{a}_3 + \hat{a}_1\hat{a}_3^\dagger\right) \pm \sqrt{\mathcal{C}_{23}}\left(i\hat{a}_2^\dagger\hat{a}_3^\dagger - i\hat{a}_2\hat{a}_3\right), \tag{D.9}$$

which is remarkably similar to the true Hamiltonian for the delta amplifier at these values of the loop phase:

$$\hat{H}_\Delta^{(\pm\pi/2)} = g_{12}\left(\hat{a}_1^\dagger\hat{a}_2^\dagger + \hat{a}_1\hat{a}_2\right) + g_{13}\left(\hat{a}_1^\dagger\hat{a}_3 + \hat{a}_1\hat{a}_3^\dagger\right) \pm g_{23}\left(i\hat{a}_2^\dagger\hat{a}_3^\dagger - i\hat{a}_2\hat{a}_3\right). \tag{D.10}$$

Working in the quadrature basis, we can write both Hamiltonians as

$$\hat{H}_{\Delta}^{(\pm\pi/2)} = \frac{1}{2}\hat{\boldsymbol{r}}^{T}\boldsymbol{H}_{\Delta}^{\pm}\hat{\boldsymbol{r}}\,,\ \text{and}\ \ \tilde{H}_{\Delta} = \frac{1}{2}\hat{\boldsymbol{r}}^{T}\tilde{\boldsymbol{H}}_{\Delta}^{\pm}\hat{\boldsymbol{r}}\ \longrightarrow \tilde{\boldsymbol{H}}_{\Delta}^{\pm} = 2\boldsymbol{\kappa}^{-1/2}\boldsymbol{H}_{\Delta}^{\pm}\boldsymbol{\kappa}^{-1/2}. \tag{D.11}$$

Using the definition $\mathcal{C}_{jk} = 4g_{jk}^{2}/\kappa_j\kappa_k$, the elements of $\tilde{\boldsymbol{H}}_{\Delta}^{\pm}$ are then just square roots of the cooperativities. At this point, using this definition, we can establish the connection in Eq. (D.8) by rewriting the scattering matrix in terms of $\tilde{\boldsymbol{H}}_{\Delta}^{\pm}$:

$$\begin{aligned}
-\mathbf{S}_{\Delta}^{(\pm\pi/2)} &= -\mathbf{I}_6 - \boldsymbol{\kappa}^{1/2}\left(\mathbf{A}_{\Delta}^{(\pm\pi/2)}\right)^{-1}\boldsymbol{\kappa}^{1/2}\ \ \text{where}\ \ \mathbf{A}_{\Delta}^{(\pm\pi/2)} = -\frac{1}{2}\boldsymbol{\kappa} + \boldsymbol{\Omega}\boldsymbol{H}_{\Delta}^{\pm} \\
&= -\mathbf{I}_6 + 2\left(\mathbf{I}_6 - 2\boldsymbol{\kappa}^{-1/2}\boldsymbol{\Omega}\boldsymbol{H}_{\Delta}^{\pm}\boldsymbol{\kappa}^{-1/2}\right)^{-1} \\
&= -\mathbf{I}_6 + 2\left(\mathbf{I}_6 - \boldsymbol{\Omega}\tilde{\boldsymbol{H}}_{\Delta}^{\pm}\right)^{-1}\ \text{since}\ [\boldsymbol{\kappa},\boldsymbol{\Omega}] = 0 \\
&= \exp\left[\frac{1}{\mathrm{C}}\mathrm{arcosh}\left(\frac{1+\mathrm{C}^2}{1-\mathrm{C}^2}\right)\boldsymbol{\Omega}\tilde{\boldsymbol{H}}_{\Delta}^{\pm}\right].
\end{aligned} \tag{D.12}$$

The ability to write the scattering matrix so simply in terms of the matrix exponential comes down to the spectrum of the matrix $\boldsymbol{\Omega}\tilde{\boldsymbol{H}}_{\Delta}^{\pm}$. Since the system is stable, it is guaranteed from the Routh-Hurwitz criterion that the cooperativities satisfy $0 < \mathcal{C}_{12} - \mathcal{C}_{13} + \mathcal{C}_{23} < 1$. The eigenvalues of $\boldsymbol{\Omega}\tilde{\boldsymbol{H}}_{\Delta}^{\pm}$ are coincidentally,

$$\nu = \left(\pm 0, \pm\sqrt{\mathcal{C}_{12} - \mathcal{C}_{13} + \mathcal{C}_{23}}, \pm\sqrt{\mathcal{C}_{12} - \mathcal{C}_{13} + \mathcal{C}_{23}}\right) = (0, \pm\mathrm{C}, \pm\mathrm{C})\,, \tag{D.13}$$

and are therefore entirely real and in the range $0 < |\nu| < 1$. The last line in Eq. (D.12) is obtained by performing a diagonalisation, $\boldsymbol{\Omega}\tilde{\boldsymbol{H}}_{\Delta}^{\pm} = \boldsymbol{Q}\boldsymbol{D}\boldsymbol{Q}^{-1}$, after which the following equation must then be solved to convert the matrix inverse into a matrix exponential:

$$\boldsymbol{Q}\left(2\left(\mathbf{I}_6 - \boldsymbol{D}\right)^{-1} - \mathbf{I}_6\right)\boldsymbol{Q}^{-1} = \boldsymbol{Q}e^{a\boldsymbol{D}}\boldsymbol{Q}^{-1} \rightarrow \frac{2}{1+\nu} - 1 = e^{a\nu}\,, a \in \mathbb{R}. \tag{D.14}$$

This is trivially satisfied for $\nu = 0$, and so only yields two unique equations to solve for the two degenerate eigenvalues:

$$\frac{2}{1 \mp \mathrm{C}} - 1 = e^{\pm a\mathrm{C}},\ a \in \mathbb{R} \rightarrow a = \frac{1}{\mathrm{C}}\ln\left(\frac{1+\mathrm{C}}{1-\mathrm{C}}\right) = \frac{1}{\mathrm{C}}\mathrm{arcosh}\left(\frac{1+\mathrm{C}^2}{1-\mathrm{C}^2}\right),\ |\mathrm{C}| < 1. \tag{D.15}$$

In this way, the last line of Eq. (D.12), and hence the simple connection between the scattering matrix and a coherent process with a similar form, is established with little effort. This simple relation only holds for the loop phase $\phi = \pm\pi/2$ due to the fact that the eigenvalues of $\tilde{\boldsymbol{H}}_{\Delta}^{\pm}$ are zero, or else are real-valued and have identical magnitude, allowing for the expression in Eq. (D.14) to have a single solution. So although the relation is useful, it is highly specific to this particular system and these particular parameters, and does not generalise to other values of the loop phase. The expression for the scattering matrix in terms of the matrix exponential,

$$-\mathbf{S}_{\Delta}^{(\pm\pi/2)} = \exp\left[\frac{1}{\mathrm{C}}\mathrm{arcosh}\left(\frac{1+\mathrm{C}^2}{1-\mathrm{C}^2}\right)\boldsymbol{\Omega}\tilde{\boldsymbol{H}}_{\Delta}^{\pm}\right] \tag{D.16}$$

is also what allows for the simple circuit representations obtained for the delta amplifier at the points of perfect nonreciprocity. This follows from the fact that the interactions in $\tilde{H}_{\Delta}^{\pm}$ form a closed subset of the full $sp(6,\mathbb{R})$ Lie algebra, equivalent to $sp(2,\mathbb{R})$:

$$\begin{aligned}
[\hat{a}_1^{\dagger}\hat{a}_2^{\dagger} + \hat{a}_1\hat{a}_2, \hat{a}_1^{\dagger}\hat{a}_3 + \hat{a}_1\hat{a}_3^{\dagger}] &= i\left(i\hat{a}_2^{\dagger}\hat{a}_3^{\dagger} - i\hat{a}_2\hat{a}_3\right) \\
[\hat{a}_1^{\dagger}\hat{a}_3 + \hat{a}_1\hat{a}_3^{\dagger}, i\hat{a}_2^{\dagger}\hat{a}_3^{\dagger} - i\hat{a}_2\hat{a}_3] &= i\left(\hat{a}_1^{\dagger}\hat{a}_2^{\dagger} + \hat{a}_1\hat{a}_2\right) \\
[i\hat{a}_2^{\dagger}\hat{a}_3^{\dagger} - i\hat{a}_2\hat{a}_3, \hat{a}_1^{\dagger}\hat{a}_2^{\dagger} + \hat{a}_1\hat{a}_2] &= -i\left(\hat{a}_1^{\dagger}\hat{a}_3 + \hat{a}_1\hat{a}_3^{\dagger}\right).
\end{aligned} \tag{D.17}$$

The interactions in $\boldsymbol{\Omega}\tilde{\boldsymbol{H}}_{\Delta}^{\pm}$ therefore form the same sub-algebra, and so $-\mathbf{S}_{\Delta}^{(\pm\pi/2)}$ belongs to an $Sp(2,\mathbb{R})$ sub-group of $Sp(6,\mathbb{R})$, where the latter group represents the full set of scattering matrices acting on three-mode bosonic systems. For the circuit decomposition, it is important that any element of $Sp(2,\mathbb{R})$ can be written as a product of operator exponentials

$$-\mathbf{S}_{\Delta}^{(\pm\pi/2)} = e^{X_1}e^{X_2}e^{X_3}, \tag{D.18}$$

where X_1,X_2, and X_3 span the entire Lie algebra $sp(2,\mathbb{R})$. This means that $-\mathbf{S}_\Delta^{(\pm\pi/2)}$ can be written as a product of symplectic matrices, where the X_k can be related to the three coherent processes in $\tilde{H}_\Delta^\pm$ as follows:

$$\{X_1, X_2, X_3\} \longleftrightarrow \{u_{12}(\hat{a}_1^\dagger \hat{a}_2^\dagger + \hat{a}_1\hat{a}_2), u_{13}(\hat{a}_1^\dagger \hat{a}_3 + \hat{a}_1\hat{a}_3^\dagger), u_{23}(i\hat{a}_2^\dagger \hat{a}_3^\dagger - i\hat{a}_2\hat{a}_3)\}. \tag{D.19}$$

The assignment is arbitrary, meaning that an X_k can correspond to any of the unitary processes generated by the operators on the right. The different orderings of the coherent processes which may be chosen will only change the coefficients u_{jk}, with some orderings resulting in simpler functional forms for the u_{jk} compared to others. These coefficients are not necessarily simpler at points of perfect nonreciprocity, however, it was found that out of all the possible orderings, only one ordering would provide simple forms for the u_{jk} coefficients, and consequently a simple representation of the scattering matrix. The simplest orderings happened to correspond to particular polar decompositions of the symplectic matrix, and are listed in the table below:

NR Scattering	Decomposition	Coop. Condition	Phase (ϕ)	Stability Criteria
$a_1 \to a_2$	$\mathbf{R}_-^{(2,3)}\mathbf{U}^{(1,3)}$	$\mathcal{C}_{12} = \mathcal{C}_{13}\mathcal{C}_{23}$	$-\pi/2$	$0 \le \mathcal{C}_{13}$ & $0 \le \mathcal{C}_{23} < 1$
$a_1 \leftarrow a_2$	$\mathbf{U}^{(1,3)}\mathbf{R}_+^{(2,3)}$	$\mathcal{C}_{12} = \mathcal{C}_{13}\mathcal{C}_{23}$	$+\pi/2$	$0 \le \mathcal{C}_{13}$ & $0 \le \mathcal{C}_{23} < 1$
$a_2 \to a_3$	$\mathbf{U}^{(1,3)}\mathbf{R}^{(1,2)}$	$\mathcal{C}_{23} = \mathcal{C}_{12}\mathcal{C}_{13}$	$-\pi/2$	$0 \le \mathcal{C}_{13}$ & $0 \le \mathcal{C}_{12} < 1$
$a_2 \leftarrow a_3$	$\mathbf{R}^{(1,2)}\mathbf{U}^{(1,3)}$	$\mathcal{C}_{23} = \mathcal{C}_{12}\mathcal{C}_{13}$	$+\pi/2$	$0 \le \mathcal{C}_{13}$ & $0 \le \mathcal{C}_{12} < 1$
$a_1 \to a_3$	$\mathbf{R}_-^{(2,3)}\mathbf{R}^{(1,2)}$	$\mathcal{C}_{13} = \mathcal{C}_{12}\mathcal{C}_{23}$	$-\pi/2$	$0 \le \mathcal{C}_{12} < 1$ & $0 \le \mathcal{C}_{23} < 1$
$a_1 \leftarrow a_3$	$\mathbf{R}^{(1,2)}\mathbf{R}_+^{(2,3)}$	$\mathcal{C}_{13} = \mathcal{C}_{12}\mathcal{C}_{23}$	$+\pi/2$	$0 \le \mathcal{C}_{12} < 1$ & $0 \le \mathcal{C}_{23} < 1$

. (D.20)

The expressions of the symplectic matrices in the decomposition were provided in Eq. (3.83), and are listed below for completeness:

$$\begin{aligned}
\mathbf{R}^{(1,2)} &\longleftrightarrow \hat{U}^{(1,2)} := \exp\left[-2i\,\mathrm{artanh}\left(\sqrt{\mathcal{C}_{12}}\right)\left(\hat{a}_1^\dagger\hat{a}_2^\dagger + \hat{a}_1\hat{a}_2\right)\right] \\
\mathbf{U}^{(1,3)} &\longleftrightarrow \hat{U}^{(1,3)} := \exp\left[-2i\,\arctan\left(\sqrt{\mathcal{C}_{13}}\right)\left(\hat{a}_1^\dagger\hat{a}_3 + \hat{a}_1\hat{a}_3^\dagger\right)\right] \\
\mathbf{R}_{\mathrm{sgn}(\phi)}^{(2,3)} &\longleftrightarrow \hat{U}^{(2,3)} := \exp\left[-2i\,\mathrm{sgn}(\phi)\,\mathrm{artanh}\left(\sqrt{\mathcal{C}_{23}}\right)\left(i\hat{a}_2^\dagger\hat{a}_3^\dagger - i\hat{a}_2\hat{a}_3\right)\right].
\end{aligned} \tag{D.21}$$

E Further Details on Gaussian-State Preserving Qubit-Cavity Interactions

E.1 Preserving Gaussian Cavity Operators

It has been stated many times in the text that only Lindblad master equations which preserve the Gaussian nature of the Wigner distribution of the harmonic modes can be handled using the moment method. The case of a single qubit coupled to an arbitrary number of cavity modes is considered in Section 4.2.1.2, where the general form of the Lindblad master equation is discussed. The restrictions listed are necessary to use the moment method for calculating the cavity backaction on the qubit. The restrictions on the cavity terms are discussed in Section 2.2; here, it will be shown how the restrictions on the qubit operator terms are determined.

In order to establish the limitations on the coherent terms, we can write a general Hamiltonian in the $\hat{\sigma}_z$ basis as follows

$$\vec{H}\cdot\vec{\sigma} = \begin{pmatrix} \hat{H}_0+\hat{H}_z & \hat{H}_x - i\hat{H}_y \\ \hat{H}_x + i\hat{H}_y & \hat{H}_0 - \hat{H}_z \end{pmatrix} \equiv \begin{pmatrix} \hat{H}_0+\hat{H}_z & \hat{H}_+ \\ \hat{H}_- & \hat{H}_0 - \hat{H}_z \end{pmatrix} \quad \text{where} \quad \hat{H}_k^\dagger = \hat{H}_k,\ k=0,x,y,z. \tag{E.1}$$

We have defined a vector of Hamiltonians which act on the cavity Hilbert space, $\vec{H} = (\hat{H}_0, \hat{H}_x, \hat{H}_y, \hat{H}_z)$, and a vector of Pauli operators, $\vec{\sigma} = (\hat{\sigma}_0, \hat{\sigma}_x, \hat{\sigma}_y, \hat{\sigma}_z)$, where the Pauli operators have the usual definitions:

$$\hat{\sigma}_0 = \begin{pmatrix} 1 & 0 \\ 0 & 1 \end{pmatrix} \qquad \hat{\sigma}_x = \begin{pmatrix} 0 & 1 \\ 1 & 0 \end{pmatrix} \qquad \hat{\sigma}_y = \begin{pmatrix} 0 & -i \\ i & 0 \end{pmatrix} \qquad \hat{\sigma}_z = \begin{pmatrix} 1 & 0 \\ 0 & -1 \end{pmatrix}. \tag{E.2}$$

Only Hamiltonians which conserve the qubit state probabilities will preserve the Gaussian nature of the cavity operator, which can be shown by calculating the commutator of $\vec{H}\cdot\vec{\sigma}$ and $\hat{\rho}$. In order to calculate this, the state $\hat{\rho}$ will be decomposed as in Eq. (4.45):

$$\hat{\rho} = \begin{pmatrix} \hat{\rho}_{ee} & \hat{\rho}_{eg} \\ \hat{\rho}_{ge} & \hat{\rho}_{gg} \end{pmatrix} \quad \text{where} \quad \hat{\rho}_{ee}^\dagger = \hat{\rho}_{ee},\ \hat{\rho}_{gg}^\dagger = \hat{\rho}_{gg},\ \hat{\rho}_{eg}^\dagger = \hat{\rho}_{ge}. \tag{E.3}$$

The commutator can then be written as

$$[\vec{H}\cdot\vec{\sigma}, \hat{\rho}] = \begin{pmatrix} [\hat{H}_0+\hat{H}_z, \hat{\rho}_{ee}] + \hat{H}_-\hat{\rho}_{ge} - \hat{\rho}_{eg}\hat{H}_+ & [\hat{H}_0, \hat{\rho}_{eg}] + [\hat{H}_z, \hat{\rho}_{eg}]_+ + \hat{H}_-\hat{\rho}_{gg} - \hat{\rho}_{ee}\hat{H}_- \\ [\hat{H}_0, \hat{\rho}_{ge}] - [\hat{H}_z, \hat{\rho}_{ge}]_+ + \hat{H}_+\hat{\rho}_{ee} - \hat{\rho}_{gg}\hat{H}_+ & [\hat{H}_0 - \hat{H}_z, \hat{\rho}_{gg}] + \hat{H}_+\hat{\rho}_{eg} - \hat{\rho}_{ge}\hat{H}_- \end{pmatrix}. \tag{E.4}$$

In order for the dynamics to preserve the Gaussian nature of the cavity operator, the dynamics of $\hat{\rho}_{jk}$ can only depend on $\hat{\rho}_{jk}$, where $j,k = e,g$, and no other terms from the Gaussian cavity operator. This is required since the sum of two non-identical Gaussians is not a Gaussian. The only form for the coherent dynamics is therefore $\vec{H}\cdot\vec{\sigma} = \hat{H}_0\hat{\sigma}_0 + \hat{H}_z\hat{\sigma}_z$, where the off-diagonal elements of $\vec{H}\cdot\vec{\sigma}$ must be zero. Therefore, cavity-qubit Hamiltonians that do not preserve the populations of the qubit states cannot be modelled using the moment method, which includes the Hamiltonian for the Rabi model, $\hat{\sigma}_x\hat{q}$, as well as the Jaynes-Cummings model, $\hat{\sigma}_+\hat{a} + \hat{\sigma}_-\hat{a}^\dagger$.

Things are more difficult for dissipation terms, however, the general form is still solvable. We can follow a similar procedure and proceed to write a general non-Hermitian jump operator expanded in the qubit basis:

$$\vec{z}_k\cdot\vec{\sigma} = \begin{pmatrix} \hat{z}_{k,0}+\hat{z}_{k,z} & \hat{z}_{k,x} - i\hat{z}_{k,y} \\ \hat{z}_{k,x} + i\hat{z}_{k,y} & \hat{z}_{k,0} - \hat{z}_{k,z} \end{pmatrix} \equiv \begin{pmatrix} \hat{z}_{k,e} & \hat{z}_{k,+} \\ \hat{z}_{k,e} & \hat{z}_{k,g} \end{pmatrix}. \tag{E.5}$$

The elements of $\vec{z}$ act on the cavity Hilbert space only, and can only consist of linear combinations of cavity quadrature operators for the Gaussian assumption to hold. Assuming that the cavity-qubit system undergoes Lindblad-type

evolution, the dissipation terms can, in general, be written as follows,

$$\mathcal{J}\big[(\vec{z}_1\cdot\vec{\sigma}),(\vec{z}_2\cdot\vec{\sigma})\big](\hat{\rho}) = (\vec{z}_1\cdot\vec{\sigma})\hat{\rho}(\vec{z}_2\cdot\vec{\sigma})^\dagger - \frac{1}{2}[(\vec{z}_2\cdot\vec{\sigma})^\dagger(\vec{z}_1\cdot\vec{\sigma}),\hat{\rho}]_+ \tag{E.6}$$

where there are two possibly distinct jump operators present. This can be expanded similarly to the coherent terms, and terms which do not preserve the Gaussian state can be eliminated by again demanding that the dynamics of $\hat{\rho}_{jk}$ can only depend on $\hat{\rho}_{jk}$. The conditions for the diagonal elements $\hat{\rho}_{ee}$ and $\hat{\rho}_{gg}$ are different from those for the off-diagonal elements $\hat{\rho}_{eg}$ and $\hat{\rho}_{ge}$, and so will be listed separately. To summarise, the Gaussianity of the cavity components $\hat{\rho}_{eg}$ and $\hat{\rho}_{ge}$ is preserved in the following cases:

- For $k=1,2$, if $\hat{\mathrm{z}}_{k,+}=0$ and $\hat{\mathrm{z}}_{k,-}=0$, then any values for $\hat{\mathrm{z}}_{k,e}$ and $\hat{\mathrm{z}}_{k,g}$ will preserve Gaussianity. The corresponding dissipation term is of the form:

$$\mathcal{J}\big[(\hat{\mathrm{z}}_{1,0}\hat{\sigma}_0+\hat{\mathrm{z}}_{1,z}\hat{\sigma}_z),(\hat{\mathrm{z}}_{2,0}\hat{\sigma}_0+\hat{\mathrm{z}}_{2,z}\hat{\sigma}_z)\big](\hat{\rho}). \tag{E.7}$$

- For $k=1,2$, if $\hat{\mathrm{z}}_{k,+}=0$ and $\hat{\mathrm{z}}_{k,-}\neq 0$, or, $\hat{\mathrm{z}}_{k,+}\neq 0$ and $\hat{\mathrm{z}}_{k,-}=0$, then we must have $\hat{\mathrm{z}}_{k,e}=0$ and $\hat{\mathrm{z}}_{k,g}=0$ for Gaussianity to be preserved. The corresponding dissipation terms are:

$$\mathcal{J}\big[(\hat{\mathrm{z}}_{1,+}\hat{\sigma}_+),(\hat{\mathrm{z}}_{2,+}\hat{\sigma}_+)\big](\hat{\rho}) \quad \text{or} \quad \mathcal{J}\big[(\hat{\mathrm{z}}_{1,-}\hat{\sigma}_-),(\hat{\mathrm{z}}_{2,-}\hat{\sigma}_-)\big](\hat{\rho}). \tag{E.8}$$

- If $\hat{\mathrm{z}}_{k,+}\neq 0$ and $\hat{\mathrm{z}}_{k,-}\neq 0$, then preserving Gaussianity is not possible.

As a result, the jump operators can only contain the qubit operators $\hat{\sigma}_z$, $\hat{\sigma}_+$, or $\hat{\sigma}_-$ jump operators in order for the moment method to be used to calculate the state of $\hat{\rho}_{eg}$ and $\hat{\rho}_{ge}$; this corresponds to the Lindbladians in Eq. (4.50) and (4.51). Next, the conditions for the components $\hat{\rho}_{ee}$ and $\hat{\rho}_{gg}$ can be summarised as:

- For $k=1,2$, if $\hat{\mathrm{z}}_{k,+}=0$ and $\hat{\mathrm{z}}_{k,-}=0$, then any values for $\hat{\mathrm{z}}_{k,e}$ and $\hat{\mathrm{z}}_{k,g}$ will preserve Gaussianity. The corresponding dissipation term is of the form:

$$\mathcal{J}\big[(\hat{\mathrm{z}}_{1,0}\hat{\sigma}_0+\hat{\mathrm{z}}_{1,z}\hat{\sigma}_z),(\hat{\mathrm{z}}_{2,0}\hat{\sigma}_0+\hat{\mathrm{z}}_{2,z}\hat{\sigma}_z)\big](\hat{\rho}). \tag{E.9}$$

- If $\hat{\mathrm{z}}_{k,+}\neq 0$ or $\hat{\mathrm{z}}_{k,-}\neq 0$, then preserving Gaussianity is not possible.

Ignoring the identity $\hat{\sigma}_0$, the only qubit operator allowed in a jump term is therefore $\hat{\sigma}_z$. The operators $\hat{\sigma}_-$ and $\hat{\sigma}_+$, which correspond to qubit T1-processes, therefore render the diagonal components non-Gaussian. Applying this condition will yield the Lindbladians from Eq. (4.49).

E.2 Dressed Dephasing of the Qubit

When performing the transformation to the dispersive regime, the effects of the transformation on the dissipation terms present in the full cavity-qubit Lindblad master equation are usually ignored. The effect of the transformation on dissipation is, in fact, not trivial, and the result is dissipation terms which couple the cavity system to the qubit [157, 196, 197]. The most interesting of these are the dressed dephasing terms, which take the form $\gamma_\Delta(\mathcal{D}[\hat{a}^\dagger\hat{\sigma}_-]+\mathcal{D}[\hat{a}\hat{\sigma}_+])$; here extra dephasing on the qubit state arises from qubit state transitions driven by photons in the cavity system [157]. As was shown above, these terms only preserve the Gaussian nature of the off-diagonal components of the cavity state, and so can be included in dephasing calculations for single-qubit systems.

In this section, we will demonstrate how terms from the dissipators coupling the cavity and qubit would appear in our equations of motion for the density matrix elements. Using expressions from Appendix B, these terms can then be included in future dephasing calculations. We first consider the dissipators $\mathcal{D}[\hat{\mathrm{z}}\hat{\sigma}_-]$ and $\mathcal{D}[\hat{\mathrm{z}}\hat{\sigma}_+]$, where $\hat{\mathrm{z}}$ is an arbitrary linear combination of cavity quadrature operators:

$$\begin{aligned}
\mathcal{D}[\hat{\mathrm{z}}\hat{\sigma}_-](\hat{\rho}) &= \hat{\sigma}_-\hat{\mathrm{z}}\hat{\rho}\hat{\sigma}_+\hat{\mathrm{z}}^\dagger - \frac{1}{2}[\hat{\sigma}_+\hat{\sigma}_-\hat{\mathrm{z}}^\dagger\hat{\mathrm{z}},\hat{\rho}]_+ = \frac{1}{2}\begin{pmatrix} -[\hat{\mathrm{z}}^\dagger\hat{\mathrm{z}},\hat{\rho}_{ee}]_+ & -\hat{\mathrm{z}}^\dagger\hat{\mathrm{z}}\hat{\rho}_{eg} \\ -\hat{\rho}_{ge}\hat{\mathrm{z}}^\dagger\hat{\mathrm{z}} & 2\hat{\mathrm{z}}\hat{\rho}_{ee}\hat{\mathrm{z}}^\dagger \end{pmatrix} \\
\mathcal{D}[\hat{\mathrm{z}}\hat{\sigma}_+](\hat{\rho}) &= \hat{\mathrm{z}}\hat{\sigma}_+\hat{\rho}\hat{\sigma}_-\hat{\mathrm{z}}^\dagger - \frac{1}{2}[\hat{\sigma}_-\hat{\sigma}_+\hat{\mathrm{z}}^\dagger\hat{\mathrm{z}},\hat{\rho}]_+ = \frac{1}{2}\begin{pmatrix} 2\hat{\mathrm{z}}\hat{\rho}_{gg}\hat{\mathrm{z}}^\dagger & -\hat{\rho}_{eg}\hat{z}^\dagger\hat{\mathrm{z}} \\ -\hat{\mathrm{z}}^\dagger\hat{\mathrm{z}}\hat{\rho}_{ge} & -[\hat{\mathrm{z}}^\dagger\hat{\mathrm{z}},\hat{\rho}_{gg}]_+ \end{pmatrix}.
\end{aligned} \tag{E.10}$$

Using the above, the expression for the dressed dephasing term is:

$$\begin{aligned}\big(\mathcal{D}[\hat{a}^\dagger\hat{\sigma}_-]+\mathcal{D}[\hat{a}\hat{\sigma}_+]\big)(\hat{\rho}) &= \frac{1}{2}\begin{pmatrix} 2\hat{a}\hat{\rho}_{gg}\hat{a}^\dagger - [\hat{a}\hat{a}^\dagger,\hat{\rho}_{ee}]_+ & -(\hat{a}\hat{a}^\dagger\hat{\rho}_{eg}+\hat{\rho}_{eg}\hat{a}^\dagger\hat{a}) \\ -(\hat{\rho}_{ge}\hat{a}\hat{a}^\dagger+\hat{a}^\dagger\hat{a}\hat{\rho}_{ge}) & 2\hat{a}^\dagger\hat{\rho}_{ee}\hat{a}-[\hat{a}^\dagger\hat{a},\hat{\rho}_{gg}]_+\end{pmatrix} \\ &= \frac{1}{2}\begin{pmatrix} 2\hat{a}\hat{\rho}_{gg}\hat{a}^\dagger - [\hat{a}\hat{a}^\dagger,\hat{\rho}_{ee}]_+ & -[\hat{a}^\dagger\hat{a}+1/2,\hat{\rho}_{eg}]_+ \\ -[\hat{a}^\dagger\hat{a}+1/2,\hat{\rho}_{ge}]_+ & 2\hat{a}^\dagger\hat{\rho}_{ee}\hat{a}-[\hat{a}^\dagger\hat{a},\hat{\rho}_{gg}]_+\end{pmatrix}. \end{aligned} \tag{E.11}$$

The dressed dephasing therefore gives rise to an anti-commutator term in the dynamics of the off-diagonal elements, and so behaves as dissipation on the cavity without the usual jump term. Transforming the full dispersive regime Lindblad master equation also results in dissipation terms coupling cavity operators to the $\hat{\sigma}_z$ operator [197]. Unlike dressed dephasing, the physical effect of these terms is usually ignored, however, expressions are provided for completeness:

$$\begin{aligned}\mathcal{D}[\hat{z}\hat{\sigma}_z](\hat{\rho}) &= \hat{z}\hat{\sigma}_z\hat{\rho}\hat{\sigma}_z\hat{z}^\dagger - \frac{1}{2}[\hat{z}^\dagger\hat{z},\hat{\rho}]_+ = \begin{pmatrix} \mathcal{D}[\hat{z}](\hat{\rho}_{ee}) & -2\hat{z}\hat{\rho}_{eg}\hat{z}^\dagger+\mathcal{D}[\hat{z}](\hat{\rho}_{eg}) \\ -2\hat{z}\hat{\rho}_{ge}\hat{z}^\dagger+\mathcal{D}[\hat{z}](\hat{\rho}_{ge}) & \mathcal{D}[\hat{z}](\hat{\rho}_{gg})\end{pmatrix} \\ \mathcal{D}\Big[\hat{z}_e\,|e\rangle\langle e| + \hat{z}_g\,|g\rangle\langle g|\Big](\hat{\rho}) &= \begin{pmatrix} \mathcal{D}[\hat{z}_e](\hat{\rho}_{ee}) & \hat{z}_e\hat{\rho}_{eg}\hat{z}_g^\dagger - \frac{1}{2}\hat{z}_e^\dagger\hat{z}_e\hat{\rho}_{eg} - \frac{1}{2}\hat{\rho}_{eg}\hat{z}_g^\dagger\hat{z}_g \\ \hat{z}_g\hat{\rho}_{ge}\hat{z}_e^\dagger - \frac{1}{2}\hat{z}_g^\dagger\hat{z}_g\hat{\rho}_{ge} - \frac{1}{2}\hat{\rho}_{ge}\hat{z}_e^\dagger\hat{z}_e & \mathcal{D}[\hat{z}_g](\hat{\rho}_{gg})\end{pmatrix}. \end{aligned} \tag{E.12}$$

F Explicit Solutions for the Qubit Dephasing and Measurement Rate

F.1 The Matrix Riccati Equation

For the physical systems which are of interest to us, the cavity backaction on the qubit rapidly approaches a constant value during the measurement process. Therefore, calculation of the steady state of the matrix equations from Eq. (4.74) is of importance. While analytic solutions are possible in certain instances, obtaining them can take some effort since the differential equation for $\boldsymbol{\sigma}$ is nonlinear:

$$\frac{d}{dt}\boldsymbol{\sigma} = \mathbf{A}\boldsymbol{\sigma} + \boldsymbol{\sigma}\mathbf{A}^T - \boldsymbol{\sigma}\mathbf{B}\boldsymbol{\sigma} + \mathbf{C}. \tag{F.1}$$

This differential equation is a type of differential equation called a *Riccati matrix differential equation* (RMDE), while the equation for the steady state solution belongs to a well-studied class of matrix equations called *continuous algebraic Riccati equations* (CARE). It is possible to solve the CARE by first linearising the RMDE. The solution for the CARE can be extracted by solving for the space of stable solutions of the linearised differential equations [250, 251]. This is not a straightforward process, and so it deserves a review. We will start with the generic form of the RMDE for a matrix $\boldsymbol{X}$:

$$\frac{d}{dt}\boldsymbol{X} = \boldsymbol{A}\boldsymbol{X} + \boldsymbol{X}\boldsymbol{D} + \boldsymbol{X}\boldsymbol{B}\boldsymbol{X} + \boldsymbol{C}. \tag{F.2}$$

The RMDE, and by extension the CARE, are closely related to the following system of linear matrix differential equations:

$$\frac{d}{dt}\begin{pmatrix}\boldsymbol{U}\\ \boldsymbol{V}\end{pmatrix} = \mathbf{H}\begin{pmatrix}\boldsymbol{U}\\ \boldsymbol{V}\end{pmatrix} \quad \text{where} \quad \mathbf{H} = \begin{pmatrix}\boldsymbol{D} & \boldsymbol{B}\\ -\boldsymbol{C} & -\boldsymbol{A}\end{pmatrix}. \tag{F.3}$$

The proposed relation is that provided that $\boldsymbol{U}, \boldsymbol{V}$ are solutions to the above system of equations, where $\boldsymbol{U}$ is an invertible matrix, then $\boldsymbol{X} = \boldsymbol{V}\boldsymbol{U}^{-1}$ is a solution to the RMDE. If $\boldsymbol{X}$ is a steady-state solution then $\dot{\boldsymbol{X}} = 0$, and using the above relations we can determine that $\dot{\boldsymbol{V}} = \boldsymbol{X}\dot{\boldsymbol{U}}$. Substituting in the expressions from Eq. (F.3) and multiplying by $\boldsymbol{U}^{-1}$ from the right, we can retrieve the CARE:

$$\begin{aligned} 0 &= (\boldsymbol{X}\dot{\boldsymbol{U}} - \dot{\boldsymbol{V}})\boldsymbol{U}^{-1} = (\boldsymbol{X}(\boldsymbol{D}\boldsymbol{U} + \boldsymbol{B}\boldsymbol{V}) + (\boldsymbol{C}\boldsymbol{U} + \boldsymbol{A}\boldsymbol{V}))\,\boldsymbol{U}^{-1} = \boldsymbol{X}\boldsymbol{D} + \boldsymbol{X}\boldsymbol{B}\boldsymbol{V}\boldsymbol{U}^{-1} + \boldsymbol{C} + \boldsymbol{A}\boldsymbol{V}\boldsymbol{U}^{-1} \\ &= \boldsymbol{A}\boldsymbol{X} + \boldsymbol{X}\boldsymbol{D} + \boldsymbol{X}\boldsymbol{B}\boldsymbol{X} + \boldsymbol{C} \quad \text{using} \quad \boldsymbol{V}\boldsymbol{U}^{-1} = \boldsymbol{X}. \end{aligned} \tag{F.4}$$

The stable steady-state solution to $\boldsymbol{X}$, and therefore the solution to the CARE, can be obtained by solving for $\boldsymbol{U}$ and $\boldsymbol{V}$. Additionally, in order for $\boldsymbol{V}\boldsymbol{U}^{-1}$ to be a solution to the CARE, it is required that $(\boldsymbol{U}\ \boldsymbol{V})^T \in \mathcal{V}$ be $\mathbf{H}$-invariant, that is multiplying any element of the space $\mathcal{V}$ by $\mathbf{H}$ returns another element of that space, $\mathbf{H}\mathcal{V} \in \mathcal{V}$. In order for $\mathcal{V}$ to be $\mathbf{H}$-invariant, there must exist a matrix $\mathbf{L}$ such that $\mathbf{H}(\boldsymbol{U}\ \boldsymbol{V})^T = (\boldsymbol{U}\ \boldsymbol{V})^T\mathbf{L}$. For this to be true, then $\mathbf{L}$ must satisfy the relations $\boldsymbol{L} = \boldsymbol{U}^{-1}(\boldsymbol{D}\boldsymbol{U} + \boldsymbol{B}\boldsymbol{V})$ and $\boldsymbol{V}\boldsymbol{L} = -(\boldsymbol{C}\boldsymbol{U} + \boldsymbol{A}\boldsymbol{V})$. Substituting the expression for $\boldsymbol{L}$ into the expression for $\boldsymbol{V}\boldsymbol{L}$, the CARE is again retrieved:

$$\begin{aligned} \boldsymbol{V}\boldsymbol{L} &= \boldsymbol{V}\boldsymbol{U}^{-1}(\boldsymbol{D}\boldsymbol{U} + \boldsymbol{B}\boldsymbol{V}) = -(\boldsymbol{C}\boldsymbol{U} + \boldsymbol{A}\boldsymbol{V}) \\ \rightarrow 0 &= \left(\boldsymbol{V}\boldsymbol{U}^{-1}\boldsymbol{D}\boldsymbol{U} + \boldsymbol{V}\boldsymbol{U}^{-1}\boldsymbol{B}\boldsymbol{V} + \boldsymbol{C}\boldsymbol{U} + \boldsymbol{A}\boldsymbol{V}\right)\boldsymbol{U}^{-1} \\ \rightarrow 0 &= \boldsymbol{A}\boldsymbol{X} + \boldsymbol{X}\boldsymbol{D} + \boldsymbol{X}\boldsymbol{B}\boldsymbol{X} + \boldsymbol{C} \quad \text{using} \quad \boldsymbol{V}\boldsymbol{U}^{-1} = \boldsymbol{X}. \end{aligned} \tag{F.5}$$

This confirms that solutions for the CARE can be found in $\mathbf{H}$-invariant subspaces. Since we are interested in stable solutions for $\boldsymbol{X}$, we are interested in solutions $(\boldsymbol{U}\ \boldsymbol{V})^T$ that lie in the stable subspace of the differential system Eq. (F.3). In order to find the stable subspace, we must find the eigenvalues of $\mathbf{H}$ with negative real part and their corresponding eigenvectors, which span the stable subspace. By definition, the span of a single eigenvector is an

invariant subspace, so the stable subspace must be $\mathbf{H}$-invariant. The $N \times 2N$ matrix $(\boldsymbol{U}\ \boldsymbol{V})^T$ is therefore a solution if the columns of the matrix span the entire stable subspace, and if $\boldsymbol{U}$ is non-singular. Additionally, the N eigenvalues of $\mathbf{L}$ correspond to the eigenvalues of $\mathbf{H}$ with negative real part. The existence of a solution for the CARE is therefore dependent on the spectrum of the $2N \times 2N$ matrix $\mathbf{H}$.

We can now apply this to Eq. (F.1), and therefore obtain solutions for the covariance matrix using $\boldsymbol{\sigma} = \boldsymbol{V}\boldsymbol{U}^{-1}$. The linearised system of differential equations takes the following form:

$$\frac{d}{dt}\begin{pmatrix}\boldsymbol{U}\\ \boldsymbol{V}\end{pmatrix} = \begin{pmatrix}\mathbf{A}^T & -\mathbf{B}\\ -\mathbf{C} & -\mathbf{A}\end{pmatrix}\begin{pmatrix}\boldsymbol{U}\\ \boldsymbol{V}\end{pmatrix}. \tag{F.6}$$

As stated above, provided that the stable solution does exist, then the eigenvalues of $\mathbf{L} = \mathbf{A}^T - \mathbf{B}\boldsymbol{\sigma}$ must have a negative real part. The same must then be true of the transpose of $\mathbf{L}$, $\mathbf{L}^T = \mathbf{A} - \boldsymbol{\sigma}\mathbf{B}$. This has interesting consequences for the differential equation for $\boldsymbol{\mu}$:

$$\frac{d}{dt}\boldsymbol{\mu} = (\mathbf{A} - \boldsymbol{\sigma}\mathbf{B})\boldsymbol{\mu} + \mathbf{f} - \boldsymbol{\sigma}\mathbf{g} \equiv \mathbf{L}^T\boldsymbol{\mu} + \mathbf{f} - \boldsymbol{\sigma}\mathbf{g}. \tag{F.7}$$

Since the eigenvalues of $\mathbf{L}^T$ all must have negative real part if the CARE has a solution, the existence of a stable solution for $\boldsymbol{\sigma}$ guarantees that a stable solution exists for the differential equation for $\boldsymbol{\mu}$.

As a final point, the availability of analytic solutions for $\boldsymbol{\sigma}$ is dependent on the spectrum of $\mathbf{H}$, which may become too difficult to handle for sufficiently complicated systems. The solutions for some sample dispersively coupled systems which admit analytic solutions will be provided in the remaining sections of this appendix to demonstrate the invariant subspace method in practice.

F.2 Single Cavity-Mode System

F.2.1 Cavity Induced Dephasing

The system under consideration is a single cavity dispersively coupled to a qubit, with a drive applied to enable readout, and a single-mode squeezing interaction to realise amplification. A detailed solution to the steady-state dephasing of this system is provided to demonstrate the moment method from Section 4.2 in action. The Hamiltonian under consideration is

$$\hat{H} = \chi\hat{a}^\dagger\hat{a}\hat{\sigma}_z + \frac{\lambda}{2}\left(e^{i\theta}\hat{a}^{\dagger 2} + e^{-i\theta}\hat{a}^2\right) + \sqrt{\kappa}\,|\alpha|\left(e^{i\varphi}\hat{a}^\dagger + e^{-i\varphi}\hat{a}\right), \tag{F.8}$$

and the Lindblad master equation for the cavity-qubit system is

$$\frac{d}{dt}\hat{\rho} = -i[\hat{H},\hat{\rho}] + \frac{\Gamma_\varphi}{2}\mathcal{D}[\hat{\sigma}_z](\hat{\rho}) + \kappa(\bar{n}+1)\mathcal{D}[\hat{a}](\hat{\rho}) + \kappa\bar{n}\mathcal{D}[\hat{a}^\dagger](\hat{\rho}). \tag{F.9}$$

In order to solve the time dynamics of the dephasing, it is required that we solve the matrix differential equations for the moments,

$$\frac{d}{dt}\boldsymbol{\sigma} = \mathbf{A}\boldsymbol{\sigma} + \boldsymbol{\sigma}\mathbf{A}^T - \boldsymbol{\sigma}\mathbf{B}\boldsymbol{\sigma} + \mathbf{C} \qquad \frac{d}{dt}\boldsymbol{\mu} = (\mathbf{A} - \boldsymbol{\sigma}\mathbf{B})\,\boldsymbol{\mu} + \mathbf{f} \tag{F.10}$$

where the arrays are given by

$$\begin{aligned}
\mathbf{A} &= \begin{pmatrix}-\kappa/2 + \lambda\sin(\theta) & -\lambda\cos(\theta)\\ -\lambda\cos(\theta) & -\kappa/2 - \lambda\sin(\theta)\end{pmatrix} & \mathbf{B} &= \begin{pmatrix}2i\chi & 0\\ 0 & 2i\chi\end{pmatrix}\\
\mathbf{C} &= \frac{1}{2}\begin{pmatrix}i\chi + \kappa(2\bar{n}+1) & 0\\ 0 & i\chi + \kappa(2\bar{n}+1)\end{pmatrix} & \mathbf{f} &= \sqrt{2\kappa}\,|\alpha|\begin{pmatrix}\sin(\varphi)\\ -\cos(\varphi)\end{pmatrix}.
\end{aligned} \tag{F.11}$$

The moment arrays can also be written as

$$\boldsymbol{\sigma} = \begin{pmatrix}\sigma_{qq} & \sigma_{qp}\\ \sigma_{qp} & \sigma_{pp}\end{pmatrix} \qquad \boldsymbol{\mu} = \begin{pmatrix}\mu_q\\ \mu_p\end{pmatrix}. \tag{F.12}$$

Instead of solving the expressions for arbitrary amplifier phase θ, we solve them for a specific phase $\theta = \pi/2$, where the expressions for the variances are

$$\begin{aligned}
\frac{d}{dt}\tilde{\sigma}_{qq} &= 2\left(-\frac{\kappa}{2}+\lambda\right)\tilde{\sigma}_{qq} - 2i\chi\left(\tilde{\sigma}_{qq}^2+\tilde{\sigma}_{qp}^2\right) + \frac{i\chi}{2} + \frac{\kappa}{2}(2\bar{n}+1) \\
\frac{d}{dt}\tilde{\sigma}_{pp} &= 2\left(-\frac{\kappa}{2}-\lambda\right)\tilde{\sigma}_{pp} - 2i\chi\left(\tilde{\sigma}_{pp}^2+\tilde{\sigma}_{xp}^2\right) + \frac{i\chi}{2} + \frac{\kappa}{2}(2\bar{n}+1) \\
\frac{d}{dt}\tilde{\sigma}_{qp} &= -\kappa\tilde{\sigma}_{qp} - 2i\chi\tilde{\sigma}_{qp}\left(\tilde{\sigma}_{qq}+\tilde{\sigma}_{pp}\right).
\end{aligned} \tag{F.13}$$

The covariance for an arbitrary amplifier phase can then be retrieved by combining the above expressions:

$$\boldsymbol{\sigma} = \frac{1}{2}\begin{pmatrix} (1+\sin(\theta))\tilde{\sigma}_{qq} + (1-\sin(\theta))\tilde{\sigma}_{pp} + 2\cos(\theta)\tilde{\sigma}_{qp} & -\cos(\theta)(\tilde{\sigma}_{qq}-\tilde{\sigma}_{pp}) + 2\sin(\theta)\tilde{\sigma}_{qp} \\ -\cos(\theta)(\tilde{\sigma}_{qq}-\tilde{\sigma}_{pp}) + 2\sin(\theta)\tilde{\sigma}_{qp} & (1-\sin(\theta))\tilde{\sigma}_{qq} + (1+\sin(\theta))\tilde{\sigma}_{pp} - 2\cos(\theta)\tilde{\sigma}_{qp} \end{pmatrix}. \tag{F.14}$$

We note that the trace of the matrix is independent of the choice of the phase of the squeezing, $\sigma_{qq}+\sigma_{pp} = \tilde{\sigma}_{qq}+\tilde{\sigma}_{pp}$, and so the parasitic dephasing must also be independent of the choice of amplifier phase. Next, we find the steady-state solutions to Eq. (F.13). Since the steady-state solution for the cross-covariance is $\tilde{\sigma}_{qp} = 0$, the other covariances are then just roots of a quadratic polynomial:

$$\begin{aligned}
\tilde{\sigma}_{qq} &= \frac{i}{2\chi}\left[\left(\frac{\kappa}{2}-\lambda\right) - \sqrt{\left(\frac{\kappa}{2}-\lambda\right)^2 - \chi^2 + i\chi\kappa(2n+1)}\right] \\
\tilde{\sigma}_{pp} &= \frac{i}{2\chi}\left[\left(\frac{\kappa}{2}+\lambda\right) - \sqrt{\left(\frac{\kappa}{2}+\lambda\right)^2 - \chi^2 + i\chi\kappa(2n+1)}\right].
\end{aligned} \tag{F.15}$$

We will now demonstrate that the solution method from Section F.1 will yield the same results. This will allow for the steady-state covariances to be more easily solved as the number of cavity modes increases. Recall that the invariant subspace method requires us to solve the following linear matrix differential equation:

$$\frac{d}{dt}\begin{pmatrix}\boldsymbol{U}\\ \boldsymbol{V}\end{pmatrix} = \mathbf{H}\begin{pmatrix}\boldsymbol{U}\\ \boldsymbol{V}\end{pmatrix} \quad \text{where} \quad \mathbf{H} = \begin{pmatrix}\mathbf{A}^T & -\mathbf{B}\\ -\mathbf{C} & -\mathbf{A}\end{pmatrix}. \tag{F.16}$$

The solution for the covariance matrix is then $\boldsymbol{\sigma} = \boldsymbol{V}\boldsymbol{U}^{-1}$, which lies in the stable subspace of $\mathbf{H}$. For simplicity, we will solve for the stable eigenspace of $\mathbf{H}$ when the phase of the amplifier is $\theta = \pi/2$. The characteristic polynomial of $\mathbf{H}$ is independent of this choice of phase and is

$$0 = \left[s^2 + \left(\chi^2 - i\kappa\chi(2\bar{n}+1) - (\kappa/2-\lambda)^2\right)\right]\left[s^2 + \left(\chi^2 - i\kappa\chi(2\bar{n}+1) - (\kappa/2+\lambda)^2\right)\right], \tag{F.17}$$

and so the four eigenvalues are

$$\pm\sqrt{\mathfrak{r}(\pm\lambda)} \quad \text{where} \quad \mathfrak{r}(\pm\lambda) = (\kappa/2 \mp \lambda)^2 - \chi^2 + i\kappa\chi(2\bar{n}+1). \tag{F.18}$$

The stable subspace is spanned by the eigenvectors associated with the stable eigenvalues $-\sqrt{\mathfrak{r}(\pm\lambda)}$, which may be written as follows:

$$v(+\lambda) = \begin{pmatrix}\frac{\kappa/2-\lambda+\sqrt{\mathfrak{r}(+\lambda)}}{\kappa(\bar{n}+1/2)+i\chi/2} & 0 & 1 & 0\end{pmatrix}^T \qquad v(-\lambda) = \begin{pmatrix}0 & \frac{\kappa/2+\lambda+\sqrt{\mathfrak{r}(-\lambda)}}{\kappa(\bar{n}+1/2)+i\chi/2} & 0 & 1\end{pmatrix}^T. \tag{F.19}$$

The matrix solution, therefore, has the form $(U\ V)^T = (v(+\lambda)\ v(-\lambda))$, and so we have the following steady state solution to the above system of differential equations:

$$\boldsymbol{U} = \frac{1}{\kappa(\bar{n}+1/2)+i\chi/2}\begin{pmatrix}\kappa/2-\lambda+\sqrt{\mathfrak{r}(+\lambda)} & 0\\ 0 & \kappa/2+\lambda+\sqrt{\mathfrak{r}(-\lambda)}\end{pmatrix} \qquad \boldsymbol{V} = \begin{pmatrix}1 & 0\\ 0 & 1\end{pmatrix}. \tag{F.20}$$

It should be noted that any set of vectors which spans the stable subspace of $\mathbf{H}$ constitutes a valid solution, so any normalisation factor will come out in the wash when calculating $\boldsymbol{V}\boldsymbol{U}^{-1}$. The above solutions for $\boldsymbol{U}$ and $\boldsymbol{V}$ are

therefore not unique. We can now solve the covariance matrix:

$$\begin{pmatrix} \tilde{\sigma}_{qq} & \tilde{\sigma}_{qp} \\ \tilde{\sigma}_{qp} & \tilde{\sigma}_{pp} \end{pmatrix} = \begin{pmatrix} \frac{\kappa(\bar{n}+1/2)+i\chi/2}{\kappa/2-\lambda+\sqrt{\mathfrak{r}(+\lambda)}} & 0 \\ 0 & \frac{\kappa(\bar{n}+1/2)+i\chi/2}{\kappa/2+\lambda+\sqrt{\mathfrak{r}(-\lambda)}} \end{pmatrix} = \frac{i}{2\chi} \begin{pmatrix} \kappa/2-\lambda-\sqrt{\mathfrak{r}(+\lambda)} & 0 \\ 0 & \kappa/2+\lambda-\sqrt{\mathfrak{r}(-\lambda)} \end{pmatrix}. \tag{F.21}$$

When substituting the expressions for $\mathfrak{r}(\pm\lambda)$, we can confirm that this is the same solution that we obtained by solving the differential equations directly. The means are now easily calculated by solving the linear matrix equation, after which expressions for the steady-state dephasing can be constructed. We know that the contributions to the cavity-induced dephasing can be calculated from the moments using the following expressions:

$$\Gamma_{\mathrm{d,p}} = \frac{1}{2}\mathrm{Re}\left[\mathrm{Tr}[\mathbf{B}\boldsymbol{\sigma}]\right] = \chi\mathrm{Re}\left[i\left(\sigma_{qq}+\sigma_{pp}\right)\right] \qquad \Gamma_{\mathrm{d,m}} = \frac{1}{2}\mathrm{Re}\left[\boldsymbol{\mu}^T\mathbf{B}\boldsymbol{\mu}\right] = \chi\mathrm{Re}\left[i\left(\mu_q^2+\mu_p^2\right)\right]. \tag{F.22}$$

Looking at the individual components, the parasitic dephasing is equal to

$$\begin{aligned} \Gamma_{\mathrm{d,p}} &= -\frac{\kappa}{2} + \frac{1}{2}\mathrm{Re}\Big[\sqrt{\mathfrak{r}(+\lambda)}+\sqrt{\mathfrak{r}(-\lambda)}\Big] \quad \text{where} \quad \mathfrak{r}(\pm\lambda) = (\kappa/2\mp\lambda)^2 - \chi^2 + i\chi\kappa(2\bar{n}+1) \\ &= -\frac{\kappa}{2} + \frac{1}{2\sqrt{2}}\sqrt{\left(\frac{\kappa}{2}-\lambda\right)^2 - \chi^2 + \sqrt{\left[\left(\frac{\kappa}{2}-\lambda\right)^2-\chi^2\right]^2 + \chi^2\kappa^2(2\bar{n}+1)^2}} \\ &\quad + \frac{1}{2\sqrt{2}}\sqrt{\left(\frac{\kappa}{2}+\lambda\right)^2 - \chi^2 + \sqrt{\left[\left(\frac{\kappa}{2}+\lambda\right)-\chi^2\right]^2 + \chi^2\kappa^2(2\bar{n}+1)^2}}. \end{aligned} \tag{F.23}$$

Given the above expressions, in the case where the squeezing and thermal noise vanish, $\lambda = 0$ and $\bar{n} = 0$, the parasitic dephasing goes to zero. Next, the measurement-induced dephasing is equal to

$$\begin{aligned} \Gamma_{\mathrm{d,m}} &= \kappa\left|\alpha\right|^2 \mathrm{Re}\left[i\chi\left(\frac{1}{\mathfrak{r}(+\lambda)}(1+\sin(2\varphi-\theta)) + \frac{1}{\mathfrak{r}(-\lambda)}(1-\sin(2\varphi-\theta))\right)\right] \\ &= \left|\alpha\right|^2\chi^2\kappa^2\left(2\bar{n}+1\right)\left[\frac{1-\sin(\theta-2\varphi)}{((\kappa/2-\lambda)^2-\chi^2)^2+\chi^2\kappa^2(2\bar{n}+1)^2} + \frac{1+\sin(\theta-2\varphi)}{((\kappa/2+\lambda)^2-\chi^2)^2+\chi^2\kappa^2(2\bar{n}+1)^2}\right]. \end{aligned} \tag{F.24}$$

The expressions for the dephasing in the presence of squeezing but with no thermal noise [209], and in the presence of thermal noise but with no squeezing [210], can both be obtained from the above expressions. In particular, we can write a series expression for $\Gamma_{\mathrm{d,p}}$ about small values of the thermal occupation $\bar{n}$ in the absence of squeezing to obtain the widely cited expression:

$$\Gamma_{\mathrm{d,p}} = \frac{4\kappa\chi^2}{\kappa^2+4\chi^2}\bar{n} + \mathcal{O}\left[\bar{n}^2\right]. \tag{F.25}$$

F.2.2 Measurement Rate

In this section, we will calculate the measurement rate. Using the Hamiltonian from Eq. (F.8), the Heisenberg-Langevin equations can be written in the quadrature basis as

$$\frac{d}{dt}\begin{pmatrix}\hat{q}\\ \hat{p}\end{pmatrix} = \begin{pmatrix} -\kappa/2+\lambda\sin(\theta) & \chi\langle\hat{\sigma}_z\rangle - \lambda\cos(\theta) \\ -\chi\langle\hat{\sigma}_z\rangle - \lambda\cos(\theta) & -\kappa/2-\lambda\sin(\theta)\end{pmatrix}\begin{pmatrix}\hat{q}\\ \hat{p}\end{pmatrix} + \sqrt{2\kappa}\left|\alpha\right|\begin{pmatrix}\sin(\varphi)\\ -\cos(\varphi)\end{pmatrix} - \sqrt{\kappa}\begin{pmatrix}\hat{q}_{\mathrm{in}}\\ \hat{p}_{\mathrm{in}}\end{pmatrix}. \tag{F.26}$$

We make the assumption that the input noise is Gaussian white noise, with the thermal fluctuations characterised by the number of thermal quanta in the thermal bath state, $\bar{n}$. In addition, we assume that the system is stable, and hence the eigenvalues of the dynamical matrix, $-\kappa/2 \pm \sqrt{\chi^2+\lambda^2}$, are negative. From here, we move to frequency space. Using the input-output relations, we can write the output fields as

$$\begin{pmatrix}\hat{q}_{\mathrm{out}}[\omega]\\ \hat{p}_{\mathrm{out}}[\omega]\end{pmatrix} = \mathbf{S}[\omega]\begin{pmatrix}\hat{q}_{\mathrm{in}}[\omega] - \sqrt{2}\left|\alpha\right|\sin(\varphi)\\ \hat{p}_{\mathrm{in}}[\omega] + \sqrt{2}\left|\alpha\right|\cos(\varphi)\end{pmatrix} \tag{F.27}$$

where the scattering matrix is

$$\mathbf{S}[\omega] = \frac{1}{(\kappa/2+i\omega)^2-\lambda^2+\chi^2} \times \begin{pmatrix} -\left((\kappa^2/4+\kappa\lambda\sin(\theta)+(\omega^2+\lambda^2-\chi^2)\right) & \kappa\left(-\chi\langle\hat{\sigma}_z\rangle+\lambda\cos(\theta)\right) \\ \kappa\left(\chi\langle\hat{\sigma}_z\rangle+\lambda\cos(\theta)\right) & -\left(\kappa^2/4-\kappa\lambda\sin(\theta)+(\omega^2+\lambda^2-\chi^2)\right) \end{pmatrix}. \tag{F.28}$$

The expressions for the expectation values of the output quadratures on resonance, $\omega = 0$, are:

$$\begin{aligned} \langle\hat{q}_{\text{out}}[0]\rangle &= \frac{\sqrt{2}\,|\alpha|}{\kappa^2/4-\lambda^2+\chi^2}\Big(\left(\kappa^2/4+\kappa\lambda\sin(\theta)+\lambda^2-\chi^2\right)\sin(\varphi)+\kappa\left(-\chi\langle\hat{\sigma}_z\rangle+\lambda\cos(\theta)\right)\cos(\varphi)\Big) \\ \langle\hat{p}_{\text{out}}[0]\rangle &= \frac{-\sqrt{2}\,|\alpha|}{\kappa^2/4-\lambda^2+\chi^2}\Big(\left(\kappa^2/4-\kappa\lambda\sin(\theta)+\lambda^2-\chi^2\right)\cos(\varphi)+\kappa\left(\chi\langle\hat{\sigma}_z\rangle+\lambda\cos(\theta)\right)\sin(\varphi)\Big). \end{aligned} \tag{F.29}$$

We can now work out the output noise-power matrix on resonance, assuming thermal noise from the input fields. For practical purposes, this is calculated in the same manner as the output covariance matrix:

$$\bar{S}[0] = \frac{(n+1/2)}{(\kappa^2/4-\lambda^2+\chi^2)^2}\begin{pmatrix} \kappa^2\left(-\chi\langle\hat{\sigma}_z\rangle+\lambda\cos(\theta)\right)^2 & -2\kappa\lambda\big[(\kappa^2/4+\lambda^2-\chi^2)\cos(\theta) \\ +\left(\kappa^2/4+\lambda^2-\chi^2+\kappa\lambda\sin(\theta)\right)^2 & +\kappa\chi\langle\hat{\sigma}_z\rangle\sin(\theta)\big] \\ -2\kappa\lambda\big[(\kappa^2/4+\lambda^2-\chi^2)\cos(\theta) & \kappa^2\left(\chi\langle\hat{\sigma}_z\rangle+\lambda\cos(\theta)\right)^2 \\ +\kappa\chi\langle\hat{\sigma}_z\rangle\sin(\theta)\big] & +\left(\kappa^2/4+\lambda^2-\chi^2-\kappa\lambda\sin(\theta)\right)^2 \end{pmatrix}. \tag{F.30}$$

We can now calculate the measurement rate using the following measurement operator:

$$\hat{M} = \cos(\vartheta)\hat{q}_{\text{out}} + \sin(\vartheta)\hat{p}_{\text{out}}. \tag{F.31}$$

The ground and excited-state conditioned expressions can then be combined to get the necessary expectation values for the measurement quadrature. We begin with the expectation values:

$$\langle\hat{q}_{\text{out}}[0]\rangle_e - \langle\hat{q}_{\text{out}}[0]\rangle_g = \frac{-2\sqrt{2}\,|\alpha|\,\chi\kappa}{\kappa^2/4-\lambda^2+\chi^2}\cos(\varphi) \qquad \langle\hat{p}_{\text{out}}[0]\rangle_e - \langle\hat{p}_{\text{out}}[0]\rangle_g = \frac{-2\sqrt{2}\,|\alpha|\,\chi\kappa}{\kappa^2/4-\lambda^2+\chi^2}\sin(\varphi) \tag{F.32}$$

The signal part of the measurement rate is then:

$$\langle\hat{M}[0]\rangle_e - \langle\hat{M}[0]\rangle_g = \frac{-2\sqrt{2}\,|\alpha|\,\chi\kappa}{\kappa^2/4-\lambda^2+\chi^2}\cos(\vartheta-\varphi) \tag{F.33}$$

In order to maximise the difference in the displacement, it is required that $\vartheta = \varphi$, and so the phase of the measurement quadrature should be identical to the phase of the drive. Moving on, the output noise-power of the measurement quadrature can be written in terms of the matrix elements of $\bar{S}[0]$ as:

$$\bar{S}_{MM,e/g}[0] = \cos^2(\vartheta)\bar{S}_{qq,e/g}[0] + 2\cos(\vartheta)\sin(\vartheta)\bar{S}_{qp,e/g}[0] + \sin^2(\vartheta)\bar{S}_{pp,e/g}[0] \quad \text{where} \quad \bar{S}[0] \equiv \begin{pmatrix} \bar{S}_{qq}[0] & \bar{S}_{qp}[0] \\ \bar{S}_{qp}[0] & \bar{S}_{pp}[0] \end{pmatrix}. \tag{F.34}$$

The different components of the output noise power are as follows:

$$\begin{aligned} \bar{S}_{qq,e}[0] + \bar{S}_{qq,g}[0] &= \frac{2(n+1/2)}{(\kappa^2/4-\lambda^2+\chi^2)^2}\left[\kappa^2\left(\chi^2+\lambda^2\cos^2(\theta)\right)+\left(\kappa^2/4+\lambda^2-\chi^2+\kappa\lambda\sin(\theta)\right)^2\right] \\ \bar{S}_{pp,e}[0] + \bar{S}_{pp,g}[0] &= \frac{2(n+1/2)}{(\kappa^2/4-\lambda^2+\chi^2)^2}\left[\kappa^2\left(\chi^2+\lambda^2\cos^2(\theta)\right)+\left(\kappa^2/4+|\lambda|^2-\chi^2-\kappa\lambda\sin(\theta)\right)^2\right] \\ \bar{S}_{qp,e}[0] + \bar{S}_{qp,g}[0] &= \frac{-4\kappa(n+1/2)}{(\kappa^2/4-\lambda^2+\chi^2)^2}\left(\kappa^2/4+\lambda^2-\chi^2\right)\lambda\cos(\theta). \end{aligned} \tag{F.35}$$

Combining these expressions and using the fact that the measurement phase $\vartheta = \varphi$ is optimal, we arrive at the following expression for the averaged output noise power of the measurement quadrature:

$$\bar{S}_{MM,e}[0] + \bar{S}_{MM,g}[0] = \frac{2n+1}{(\kappa^2/4 - \lambda^2 + \chi^2)^2}\Big[\kappa^2\chi^2 + \frac{1}{2}\left((\kappa/2-\lambda)^2 - \chi^2\right)^2(1-\sin(\theta-2\varphi)) + \frac{1}{2}\left((\kappa/2+\lambda)^2 - \chi^2\right)^2(1+\sin(\theta-2\varphi))\Big]. \tag{F.36}$$

If there are zero quanta of added off-chip noise, then the measurement rate is:

$$\Gamma_{\text{meas}} = \frac{2|\alpha|^2\chi^2\kappa^2}{(2n+1)}\left(\frac{1}{2}\left[\left((\kappa/2-\lambda)^2 - \chi^2\right)^2 + \kappa^2\chi^2\right](1-\sin(\theta-2\varphi)) + \frac{1}{2}\left[\left((\kappa/2+\lambda)^2 - \chi^2\right)^2 + \kappa^2\chi^2\right](1+\sin(\theta-2\varphi))\right)^{-1}. \tag{F.37}$$

With expressions for the measurement rate and dephasing, we can now calculate the maximum efficiency of the dispersive measurement. This is achieved when there is no squeezing or thermal noise, in which case the cavity-induced dephasing and measurement rate are identical:

$$\Gamma_{\text{meas}}\,,\,\Gamma_{\text{d}} = \frac{2|\alpha|^2\chi^2\kappa^2}{(\kappa^2/4+\chi^2)^2} = \frac{8|\alpha|^2\mathcal{X}^2}{(1+\mathcal{X}^2)^2}. \tag{F.38}$$

There is only drive-induced dephasing here, with no parasitic dephasing present. Since these quantities are the same, the measurement efficiency is therefore $\eta = \Gamma_{\text{meas}}/\Gamma_{\text{d}} = 1$. By appropriately balancing the strength of the dispersive coupling and the damping rate for the cavity mode, these rates can be maximised so that the measurement is performed as quickly as possible; the optimum values are then $\chi = \kappa/2$. Defining a dimensionless parameter, analogous to the cooperativity, $\mathcal{X} := 2\chi/\kappa$, the measurement rate is then maximised when $\mathcal{X} = 1$.

F.3 Two Passively Coupled Cavity-Modes

F.3.1 Cavity Induced Dephasing

Here we work out the expressions for a two-mode system where one mode is dispersively coupled to the qubit while a measurement drive is applied to the other qubit. The two modes are coupled via a beam splitter interaction and are subject to thermal noise from their baths. All other qubit terms in the Hamiltonian, along with their innate dissipation and dephasing, are omitted in this calculation. The Hamiltonian for this system is,

$$\hat{H} = \chi\hat{a}_2^\dagger\hat{a}_2\hat{\sigma}_z + g_{12}\left(e^{i\phi}\hat{a}_1^\dagger\hat{a}_2 + e^{-i\phi}\hat{a}_1\hat{a}_2^\dagger\right) + \sqrt{\kappa_1}\,|\alpha|\left(e^{i\varphi}\hat{a}_1^\dagger + e^{-i\phi}\hat{a}_1\right), \tag{F.39}$$

and the Lindblad master equation has the form

$$\frac{d}{dt}\hat{\rho} = -i[\hat{H},\hat{\rho}] + \sum_{k=1,2}\kappa_k\left((\bar{n}_k+1)\mathcal{D}[\hat{a}_k](\hat{\rho}) + \bar{n}_k\mathcal{D}[\hat{a}_k^\dagger](\hat{\rho})\right). \tag{F.40}$$

The phase of the beam splitter does not affect this calculation, so we set it to $\phi = 0$. To extract the steady state of the cavity-induced dephasing, we must solve the following matrix equations:

$$0 = \mathbf{A}\boldsymbol{\sigma} + \boldsymbol{\sigma}\mathbf{A}^T - \boldsymbol{\sigma}\mathbf{B}\boldsymbol{\sigma} + \mathbf{C} \qquad 0 = (\mathbf{A} - \boldsymbol{\sigma}\mathbf{B})\,\boldsymbol{\mu} + \mathbf{f}. \tag{F.41}$$

The matrices are written in the quadrature basis $\hat{\boldsymbol{r}} = (\hat{q}_1, \hat{p}_1, \hat{q}_2, \hat{p}_2)$ in block form as follows:

$$\mathbf{A} = \begin{pmatrix} -(\kappa_1/2)\mathbf{I} & g\mathbf{J} \\ g_{12}\mathbf{J} & -(\kappa_2/2)\mathbf{I}\end{pmatrix} \qquad \mathbf{B} = \begin{pmatrix}\mathbf{0} & \mathbf{0}\\ \mathbf{0} & 2i\chi\mathbf{I}\end{pmatrix} \qquad \mathbf{C} = \frac{1}{2}\begin{pmatrix}\kappa_1(2\bar{n}_1+1)\mathbf{I} & \mathbf{0}\\ \mathbf{0} & (i\chi + \kappa_2(2\bar{n}_2+1))\mathbf{I}\end{pmatrix}. \tag{F.42}$$

Additionally, the vector in the equation for the means is:

$$\mathbf{f} = \sqrt{2\kappa_1}\,|\alpha|\begin{pmatrix}\sin(\varphi) & -\cos(\varphi) & 0 & 0\end{pmatrix}^T. \tag{F.43}$$

The steady state of the covariance matrix and means will have the following forms

$$\boldsymbol{\sigma} = \begin{pmatrix} \sigma_{q_1q_1} & 0 & 0 & \sigma_{q_1p_2} \\ 0 & \sigma_{p_1p_1} & \sigma_{p_1q_2} & 0 \\ 0 & \sigma_{p_1q_2} & \sigma_{q_2q_2} & 0 \\ \sigma_{q_1p_2} & 0 & 0 & \sigma_{p_2p_2} \end{pmatrix} \qquad \boldsymbol{\mu} = \begin{pmatrix} \mu_{q_1} & \mu_{p_1} & \mu_{q_2} & \mu_{p_2} \end{pmatrix}^T, \tag{F.44}$$

and so the parasitic and measurement dephasing can be extracted using the following expressions:

$$\Gamma_{\mathrm{d,p}} = \frac{1}{2}\mathrm{Re}\left[\mathrm{Tr}[\mathbf{B}\boldsymbol{\sigma}]\right] = \chi \mathrm{Re}\left[i\left(\sigma_{q_2q_2} + \sigma_{p_2p_2}\right)\right] \qquad \Gamma_{\mathrm{d,m}} = \frac{1}{2}\mathrm{Re}\left[\boldsymbol{\mu}^T\mathbf{B}\boldsymbol{\mu}\right] = \chi \mathrm{Re}\left[i\left(\mu_{q_2}^2 + \mu_{p_2}^2\right)\right]. \tag{F.45}$$

Following the method from Section F.1 to solve the matrix equation for $\boldsymbol{\sigma}$, we start by constructing the matrix,

$$\mathbf{H} = \begin{pmatrix} \mathbf{A}^T & -\mathbf{B} \\ -\mathbf{C} & -\mathbf{A} \end{pmatrix} \tag{F.46}$$

The columns and rows are then reordered to yield the matrix $\tilde{\mathbf{H}}$, which is constructed so that it may be written in block form as follows:

$$\tilde{\mathbf{H}} = \begin{pmatrix} \mathbf{H}_+ & \mathbf{0}_4 \\ \mathbf{0}_4 & \mathbf{H}_- \end{pmatrix} \quad \text{where} \quad \mathbf{H}_\pm = \begin{pmatrix} \kappa_1/2 & \pm g_{12} & 0 & 0 \\ \mp g_{12} & \kappa_2/2 & 0 & 2i\chi \\ \kappa_1(\bar{n}_1 + 1/2) & 0 & -\kappa_1/2 & \pm g_{12} \\ 0 & \kappa_2(\bar{n}_2 + 1/2) + i\chi/2 & \mp g_{12} & -\kappa_2/2 \end{pmatrix} \tag{F.47}$$

The characteristic polynomial for $\mathbf{H}_+$ and $\mathbf{H}_-$ are identical, so the characteristic polynomial for $\mathbf{H}$ can be written as

$$0 = \left[s^4 + v_1 s^2 + v_0\right]\left[s^4 + v_1 s^2 + v_0\right] \tag{F.48}$$

with the coefficients defined as follows:

$$\begin{aligned} v_1 &= \chi^2 - i\chi\kappa_2(2\bar{n}_2 + 1) + 2g_{12}^2 - \left(\left(\frac{\kappa_1}{2}\right)^2 + \left(\frac{\kappa_2}{2}\right)^2\right) \\ v_0 &= -\chi^2\left(\frac{\kappa_1}{2}\right)^2 + i\chi\kappa_1\left[g_{12}^2(2\bar{n}_1 + 1) + \frac{\kappa_1}{2}\frac{\kappa_2}{2}(2\bar{n}_2 + 1)\right] + \left(g_{12}^2 + \frac{\kappa_1}{2}\frac{\kappa_2}{2}\right)^2. \end{aligned} \tag{F.49}$$

This polynomial is solvable and has the following 4 distinct eigenvalues,

$$\pm\sqrt{\mathfrak{r}_1}, \pm\sqrt{\mathfrak{r}_2} \quad \text{each with multiplicity of 2.} \tag{F.50}$$

The parameters $\mathfrak{r}_1$ and $\mathfrak{r}_2$ are the two roots for the quadratic polynomial:

$$0 = s^2 + v_1 s + v_0 \quad \text{and so} \quad \mathfrak{r}_1 = \frac{1}{2}\left(-v_1 + \sqrt{v_1^2 - 4v_0}\right), \mathfrak{r}_2 = \frac{1}{2}\left(-v_1 - \sqrt{v_1^2 - 4v_0}\right). \tag{F.51}$$

The four eigenvectors for the two degenerate eigenvalues, $-\sqrt{\mathfrak{r}_1}$ and $-\sqrt{\mathfrak{r}_2}$, can then be used to construct the stable subspace for the matrix $\mathbf{H}$. After some matrix multiplication, we get the following expressions for the covariances of mode a_2:

$$\sigma_{q_2q_2}, \sigma_{p_2p_2} = \frac{i}{2\chi}\left(\frac{\kappa_1}{2} + \frac{\kappa_2}{2} - \sqrt{\mathfrak{r}_1} - \sqrt{\mathfrak{r}_2}\right). \tag{F.52}$$

Combining everything, the parasitic dephasing should be:

$$\Gamma_{\mathrm{d,p}} = -\frac{1}{2}(\kappa_1 + \kappa_2) + \mathrm{Re}\left[\sqrt{\mathfrak{r}_1} + \sqrt{\mathfrak{r}_2}\right]. \tag{F.53}$$

Using the solution for the covariance matrix and the means, the measurement-induced dephasing can be readily calculated:

$$\Gamma_{\mathrm{d,m}} = \frac{2\left|\alpha\right|^2\chi^2\kappa_1^2 g_{12}^2 z_{\mathrm{th}}}{\left[(g_{12}^2 + \kappa_1\kappa_2/4))^2 - \chi^2(\kappa_1/2)^2\right]^2 + \chi^2\kappa_1^2 z_{\mathrm{th}}^2} \quad \text{where} \quad z_{\mathrm{th}} = g_{12}^2(2\bar{n}_1 + 1) + (\kappa_1\kappa_2/4)(2\bar{n}_2 + 1). \tag{F.54}$$

F.3.2 Measurement Rate

Once again, we will now calculate the measurement rate for this system. Since the drive is applied to mode a_1, it is the output fields of this mode that will be used to collect the measurement. The measurement quadrature is then defined as

$$\hat{M} = \cos(\vartheta)\hat{q}_{1,\text{out}} + \sin(\vartheta)\hat{p}_{1,\text{out}}. \tag{F.55}$$

Due to the added drive, the input noise operators of mode a_1 have the following forms:

$$\tilde{q}_{1,\text{in}}[\omega] = \hat{q}_{1,\text{in}}[\omega] - \sqrt{2}\,|\alpha|\sin(\varphi) \qquad \tilde{p}_{1,\text{in}}[\omega] = \hat{p}_{1,\text{in}}[\omega] + \sqrt{2}\,|\alpha|\cos(\varphi). \tag{F.56}$$

The bare input noise is Gaussian white noise, and so has an expectation value of zero; the non-zero value of the expectation value for the above input fields is then due to the presence of the drive. The signal component is then

$$\langle \hat{M}[0]\rangle_e - \langle \hat{M}[0]\rangle_g = \frac{-2\sqrt{2}\,|\alpha|\,\chi\kappa_1 g_{12}^2}{\left(g_{12}^2 + \kappa_1\kappa_2/4\right)^2 + \chi^2(\kappa_1/2)^2}\cos(\vartheta - \varphi). \tag{F.57}$$

Once again, the signal is maximised when the phase $\hat{M}$ matches the phase of the drive $\vartheta = \varphi$. The qubit state-dependent noise-power spectra of the measurement quadrature can be calculated using the values for the quadratures as follows

$$\bar{S}_{MM,e/g}[0] = \cos^2(\vartheta)\bar{S}_{q_1q_1,e/g}[0] + 2\cos(\vartheta)\sin(\vartheta)\bar{S}_{q_1p_1,e/g}[0] + \sin^2(\vartheta)\bar{S}_{p_1p_1,e/g}[0]. \tag{F.58}$$

The averaged noise-power spectrum is then

$$\begin{aligned}&\bar{S}_{MM,e}[0] + \bar{S}_{MM,g}[0]\\ &= \frac{1}{2\left(\left(g_{12}^2 + \kappa_1\kappa_2/4\right)^2 + \chi^2(\kappa_1/2)^2\right)}\left((2\bar{n}_1+1)\left[\left(g_{12}^2 - \kappa_1\kappa_2/4\right)^2 + \chi^2(\kappa_1/2)^2\right] + (2\bar{n}_2+1)g_{12}^2\kappa_1\kappa_2\right)\end{aligned} \tag{F.59}$$

In the absence of added noise, these two expressions can be combined to yield the following expression for the measurement rate:

$$\Gamma_{\text{meas}} = \frac{2\,|\alpha|^2\,\chi^2\kappa_1^2 g_{12}^4}{(g_{12}^2 + \kappa_1\kappa_2/4)^2 + \chi^2(\kappa_1/2)^2}\left((2\bar{n}_1+1)\left[\left(g_{12}^2 - \kappa_1\kappa_2/4\right)^2 + \chi^2(\kappa_1/2)^2\right] + (2\bar{n}_2+1)g_{12}^2\kappa_1\kappa_2\right)^{-1}. \tag{F.60}$$

With this defined, we can determine the maximum efficiency of a measurement. This will occur when there is no thermal noise from either of the baths, resulting in no parasitic dephasing. In this instance, the dephasing and measurement rate are easily expressed:

$$\Gamma_{\text{d}} = \frac{2\,|\alpha|^2\,\chi^2\kappa_1^2 g_{12}^2\left(g_{12}^2 + \kappa_1\kappa_2/4\right)}{\left((g_{12}^2 + \kappa_1\kappa_2/4)^2 + \chi^2\kappa_1^2/4\right)^2} \qquad \Gamma_{\text{meas}} = \frac{2\,|\alpha|^2\,\chi^2\kappa_1^2 g_{12}^4}{\left((g_{12}^2 + \kappa_1\kappa_2/4)^2 + \chi^2\kappa_1^2/4\right)^2}. \tag{F.61}$$

The measurement efficiency is then:

$$\eta = \frac{\Gamma_{\text{meas}}}{\Gamma_{\text{d}}} = \frac{g_{12}^2}{g_{12}^2 + \kappa_1\kappa_2/4} \equiv \frac{\mathcal{C}_{12}}{\mathcal{C}_{12}+1}. \tag{F.62}$$

The measurement is never perfectly efficient due to the fact that mode a_1 is not directly coupled to the qubit; however, by increasing the cooperativity of the beam splitter interaction, $\mathcal{C}_{12} = 4g_{12}^2/\kappa_1\kappa_2$, the efficiency can approach one. This corresponds to an increase in the rate of the beam splitter compared to the decay rates, so the efficiency increases as the rate of information exchange between modes a_1 and a_2 becomes larger than the rate at which qubit state information is lost to the baths. It is also important to balance the dispersive coupling and beam splitter cooperativity to maximise the magnitude of the measurement rate. This is achieved when the dispersive shift is $\chi = (\kappa_2/2)(\mathcal{C}_{12}+1)$, or equivalently if the cooperativity is set to $\mathcal{C}_{12} = \sqrt{(2\chi/\kappa_2)^2 + 1}$. We could again define a dimensionless parameter balancing the dispersive coupling with the damping rate of the dispersively coupled mode, $\mathcal{X} := 2\chi/\kappa_2$. Using this parameter, the optimum value is then $\mathcal{X} = \mathcal{C}_{12} + 1$, or if we are varying the cooperativity, $\mathcal{C}_{12} = \sqrt{\mathcal{X}^2 + 1}$.

F.4 Three-Mode Nonreciprocal Amplifier

F.4.1 Cavity Induced Dephasing

This section contains a detailed calculation for the added qubit dephasing from the integrated non-reciprocal amplifier presented in Section 4.3. The Hamiltonian is defined as in Eq. (4.83):

$$\begin{aligned}\hat{H} = g_{12}\left(\hat{a}_1^\dagger\hat{a}_2 + \hat{a}_1\hat{a}_1^\dagger\right) + g_{23}\left(\hat{a}_2^\dagger\hat{a}_3 + \hat{a}_2\hat{a}_3^\dagger\right) + g_{13}\left(e^{i\phi}\hat{a}_1^\dagger\hat{a}_3 + e^{-i\phi}\hat{a}_1\hat{a}_3^\dagger\right) \\ + \frac{\lambda}{2}\left(e^{i\theta}\hat{a}_1^{\dagger 2} + e^{-i\theta}\hat{a}_1^2\right) + \sqrt{\kappa_2}\,|\alpha|\left(e^{i\varphi}\hat{a}_2^\dagger + e^{-i\varphi}\hat{a}_2\right) + \chi\hat{a}_3^\dagger\hat{a}_3\hat{\sigma}_z,\end{aligned} \tag{F.63}$$

where we have redefined the modes from Section 4.3 according to, $\hat{a} \to \hat{a}_1$, $\hat{b} \to \hat{a}_2$, and $\hat{c} \to \hat{a}_3$ for notational convenience. The Lindblad master equation for the cavity-qubit system is given in Eq. (4.84):

$$\frac{d}{dt}\hat{\rho} = -i[\hat{H},\hat{\rho}] + \frac{\Gamma_\varphi}{2}\mathcal{D}[\hat{\sigma}_z](\hat{\rho}) + \sum_{k=1,2,3}\kappa_k\left((\bar{n}_k+1)\mathcal{D}[\hat{a}_k](\hat{\rho}) + \bar{n}_k\mathcal{D}[\hat{a}_k^\dagger](\hat{\rho})\right). \tag{F.64}$$

Since the expressions used in this work require that we work in the quadrature basis, we will first rewrite the Lindblad master equation in the following form:

$$\begin{aligned}&\frac{d}{dt}\hat{\rho} = -i[\hat{H},\hat{\rho}] + \frac{\Gamma_\varphi}{2}\mathcal{D}[\hat{\sigma}_z](\hat{\rho}) + \sum_{j,k=1}^{6}\Gamma_{jk}\left(\hat{r}_j\hat{\rho}\hat{r}_k - \frac{1}{2}[\hat{r}_k\hat{r}_j,\hat{\rho}]_+\right) \\ &\text{where}\;\; \hat{H} = \frac{1}{2}\hat{\boldsymbol{r}}^T\left(\boldsymbol{H}_r^{(2)} + \hat{\sigma}_z\boldsymbol{H}_{qr}^{(2)}\right)\hat{\boldsymbol{r}} + \hat{\boldsymbol{r}}^T\boldsymbol{h}_r^{(1)} + \left(h_{qr}^{(0)} + \frac{\tilde{\omega}_q}{2}\right)\hat{\sigma}_z.\end{aligned} \tag{F.65}$$

The vector of quadrature operators is defined as $\hat{\boldsymbol{r}} = (\hat{q}_1,\hat{p}_1,\hat{q}_2,\hat{p}_2,\hat{q}_3,\hat{p}_3)$, and so the symmetric form is the block diagonal matrix $\boldsymbol{\Omega} = \mathrm{diag}(\boldsymbol{\Omega}_1,\boldsymbol{\Omega}_1,\boldsymbol{\Omega}_1)$. The arrays of coefficients which appear in the cavity component of the Hamiltonian can be expressed as follows,

$$\boldsymbol{H}_r^{(2)} = \begin{pmatrix}\lambda(\cos(\theta)\mathbf{Z} + \sin(\theta)\mathbf{X}) & g_{12}\mathbf{I} & g_{13}(\cos(\phi)\mathbf{I} - \sin(\phi)\mathbf{J}) \\ g_{12}\mathbf{I} & \mathbf{0} & g_{23}\mathbf{I} \\ g_{13}(\cos(\phi)\mathbf{I} + \sin(\phi)\mathbf{J}) & g_{23}\mathbf{I} & \mathbf{0}\end{pmatrix} \qquad \boldsymbol{H}_{qr}^{(2)} = \begin{pmatrix}\mathbf{0} & \mathbf{0} & \mathbf{0} \\ \mathbf{0} & \mathbf{0} & \mathbf{0} \\ \mathbf{0} & \mathbf{0} & \chi\mathbf{I}\end{pmatrix} \tag{F.66}$$

along with the linear contribution from the drive term on the buffer mode

$$\boldsymbol{h}_r^{(1)} = \sqrt{2\kappa_2}\,|\alpha|\begin{pmatrix}0 & 0 & \cos(\varphi) & \sin(\varphi) & 0 & 0\end{pmatrix}^T. \tag{F.67}$$

The term $h_{qr}^{(0)} = -\chi/2$ is present because the dispersive coupling $\chi\hat{a}_3^\dagger\hat{a}_3\hat{\sigma}_z$ term does not correspond to a symmetrically ordered function of the quadrature operators. Lastly, the decay terms Γ_{jk} are elements of the Hermitian matrix $\boldsymbol{\Gamma}$:

$$\boldsymbol{\Gamma} = \begin{pmatrix}\kappa_1(\bar{n}_1+1/2)\mathbf{I} + i(\kappa_1/2)\mathbf{J} & \mathbf{0} & \mathbf{0} \\ \mathbf{0} & \kappa_2(\bar{n}_2+1/2)\mathbf{I} + i(\kappa_2/2)\mathbf{J} & \mathbf{0} \\ \mathbf{0} & \mathbf{0} & \kappa_3(\bar{n}_3+1/2)\mathbf{I} + i(\kappa_3/2)\mathbf{J}\end{pmatrix}. \tag{F.68}$$

We can now start defining the arrays that will be used for the moment method calculation, beginning with the dynamical matrix arising from the coherent and dissipative cavity processes:

$$\mathbf{A} = \boldsymbol{\Omega}(\boldsymbol{H}_r^{(2)} + \mathrm{Im}[\boldsymbol{\Gamma}]) = \begin{pmatrix}-(\kappa_1/2)\mathbf{I} + \lambda(-\cos(\theta)\mathbf{X} + \sin(\theta)\mathbf{Z}) & g_{12}\mathbf{J} & g_{13}(\cos(\phi)\mathbf{J} + \sin(\phi)\mathbf{I}) \\ g_{12}\mathbf{J} & -(\kappa_2/2)\mathbf{I} & g_{23}\mathbf{J} \\ g_{13}(\cos(\phi)\mathbf{J} - \sin(\phi)\mathbf{I}) & g_{23}\mathbf{J} & -(\kappa_3/2)\mathbf{I}\end{pmatrix}, \tag{F.69}$$

followed by the other two matrices necessary for the calculation of $\boldsymbol{\sigma}$:

$$\mathbf{B} = 2i\boldsymbol{H}_{qr}^{(2)} = \begin{pmatrix} \mathbf{0} & \mathbf{0} & \mathbf{0} \\ \mathbf{0} & \mathbf{0} & \mathbf{0} \\ \mathbf{0} & \mathbf{0} & 2i\chi\mathbf{I} \end{pmatrix}$$
$$\mathbf{C} = -\boldsymbol{\Omega}\left(\frac{i}{2}\boldsymbol{H}_{qr}^{(2)} + \mathrm{Re}[\boldsymbol{\Gamma}]\right)\boldsymbol{\Omega} = \frac{1}{2}\begin{pmatrix} \kappa_1(2\bar{n}_1+1)\mathbf{I} & \mathbf{0} & \mathbf{0} \\ \mathbf{0} & \kappa_2(2\bar{n}_2+1)\mathbf{I} & \mathbf{0} \\ \mathbf{0} & \mathbf{0} & (i\chi+\kappa_3(2\bar{n}_3+1))\mathbf{I} \end{pmatrix}. \tag{F.70}$$

Lastly, the drive term in the Hamiltonian will give rise to the following vector

$$\mathbf{f} = \boldsymbol{\Omega}\boldsymbol{h}_r^{(1)} = \sqrt{2\kappa_2}\,|\alpha|\begin{pmatrix} 0 & 0 & \sin(\varphi) & -\cos(\varphi) & 0 & 0 \end{pmatrix}^T. \tag{F.71}$$

We can now proceed to solve the matrix equations required to calculate the dephasing:

$$0 = \mathbf{A}\boldsymbol{\sigma} + \boldsymbol{\sigma}\mathbf{A}^T - \boldsymbol{\sigma}\mathbf{B}\boldsymbol{\sigma} + \mathbf{C} \qquad 0 = (\mathbf{A} - \boldsymbol{\sigma}\mathbf{B})\,\boldsymbol{\mu} + \mathbf{f}. \tag{F.72}$$

A Note on the Phases

In order for this system to have analytic solutions, the loop phase must be set to $\phi = \pm\pi/2$, which corresponds to the two different directions of circulation. The system is also much easier to solve when the phase of the amplifier is set to $\theta = \pm\pi/2$. Without loss of generality, we select $\theta = \pi/2$. The off-diagonal components of the dynamical matrix $\mathbf{A}$, which arise due to the squeezing, can be rotated away through a rotation by the angle $(\theta - \pi/2)/2$:

$$\mathbf{R}^T(\theta)\mathbf{A}(\theta)\mathbf{R}(\theta) = \mathbf{A}(\pi/2) \quad \text{where} \quad \mathbf{R}(\theta) = \frac{1}{\sqrt{2}}\Big(\big(\cos(\theta/2)+\sin(\theta/2)\big)\mathbf{I} + \big(\cos(\theta/2)-\sin(\theta/2)\big)\mathbf{J}\Big) \otimes \mathbf{I}_3. \tag{F.73}$$

Due to the form of $\mathbf{R}(\theta)$, it commutes with the two other dynamical matrices in the CARE:

$$\mathbf{R}^T(\theta)\mathbf{B}\mathbf{R}(\theta) = \mathbf{B} \qquad \mathbf{R}^T(\theta)\mathbf{C}\mathbf{R}(\theta) = \mathbf{C}. \tag{F.74}$$

The variances, means, and drive will all experience a rotation, but solutions for arbitrary values of the amplifier phase θ are easily obtained by appropriately combining the results for the $\theta = +\pi/2$ case. We will denote the variance for $\boldsymbol{\sigma}(\pi/2) \equiv \tilde{\boldsymbol{\sigma}}$. When calculating the dephasing, the variances for arbitrary phase are then retrieved using results for the phase $\pi/2$ as follows: $\boldsymbol{\sigma} = \mathbf{R}(\theta)\tilde{\boldsymbol{\sigma}}\mathbf{R}^T(\theta)$. The differential equation for $\boldsymbol{\sigma}$ can now be transformed to the rotated frame:

$$\frac{d}{dt}\boldsymbol{\sigma} = \mathbf{A}(\theta)\boldsymbol{\sigma} + \boldsymbol{\sigma}\mathbf{A}^T(\theta) - \boldsymbol{\sigma}\mathbf{B}\boldsymbol{\sigma} + \mathbf{C} \quad \rightarrow \quad \frac{d}{dt}\tilde{\boldsymbol{\sigma}} = \mathbf{A}(\pi/2)\tilde{\boldsymbol{\sigma}} + \tilde{\boldsymbol{\sigma}}\mathbf{A}^T(\pi/2) - \tilde{\boldsymbol{\sigma}}\mathbf{B}\tilde{\boldsymbol{\sigma}} + \mathbf{C}. \tag{F.75}$$

As will be shown, analytic solutions are possible for the steady state of $\tilde{\boldsymbol{\sigma}}$. When calculating the dephasing, the parasitic component will necessarily be independent of the value of the amplifier phase due to the cyclic nature of the trace and the fact that the rotation matrix is orthogonal:

$$\begin{aligned} \Gamma_{\mathrm{d,p}} &= \frac{1}{2}\mathrm{Re}\big[\mathrm{Tr}\,[\mathbf{B}\boldsymbol{\sigma}]\,\big] = \frac{1}{2}\mathrm{Re}\big[\mathrm{Tr}\,[\mathbf{R}^T(\theta)\mathbf{B}\mathbf{R}(\theta)\mathbf{R}^T(\theta)\boldsymbol{\sigma}\mathbf{R}(\theta)]\,\big] = \frac{1}{2}\mathrm{Re}\big[\mathrm{Tr}\,[\mathbf{B}\tilde{\boldsymbol{\sigma}}]\,\big] \\ \text{and hence} \quad \Gamma_{\mathrm{d,p}} &= \mathrm{Re}\big[i\chi\big(\sigma_{q_3q_3} + \sigma_{p_3p_3}\big)\big] = \mathrm{Re}\big[i\chi\big(\tilde{\sigma}_{q_3q_3} + \tilde{\sigma}_{p_3p_3}\big)\big]. \end{aligned} \tag{F.76}$$

If we similarly define $\tilde{\boldsymbol{\mu}} = \mathbf{R}(\theta)\boldsymbol{\mu}$, then we can rotate the equation of motion for the means as follows:

$$\frac{d}{dt}\boldsymbol{\mu} = (\mathbf{A}(\theta) - \boldsymbol{\sigma}\mathbf{B})\,\boldsymbol{\mu} + \mathbf{f} \quad \rightarrow \quad \frac{d}{dt}\tilde{\boldsymbol{\mu}} = (\mathbf{A}(\pi/2) - \tilde{\boldsymbol{\sigma}}\mathbf{B})\,\tilde{\boldsymbol{\mu}} + \mathbf{R}(\theta)\mathbf{f}. \tag{F.77}$$

The steady state of $\boldsymbol{\mu}$ can also be expressed as follows:

$$\boldsymbol{\mu} = -\,(\mathbf{A} - \boldsymbol{\sigma}\mathbf{B})^{-1}\,\mathbf{f} = -\mathbf{R}(\theta)\,(\mathbf{A}(\pi/2) - \tilde{\boldsymbol{\sigma}}\mathbf{B})^{-1}\,\mathbf{R}^T(\theta)\mathbf{f} \tag{F.78}$$

In this case, the rotation not only simplifies the calculation of $\tilde{\boldsymbol{\sigma}}$, the inverse matrix required to solve for the means, $(\mathbf{A}(\pi/2) - \tilde{\boldsymbol{\sigma}}\mathbf{B})^{-1} =: \mathbf{M}$, now takes on a simpler form as well. Due to the rotation, this matrix has the following

structure:

$$\mathbf{M} = \begin{pmatrix} M_{q_1q_1} & 0 & 0 & M_{q_1p_2} & M_{q_1q_3} & 0 \\ 0 & M_{p_1p_1} & M_{p_1q_2} & 0 & 0 & M_{p_1p_3} \\ 0 & M_{p_1q_2} & M_{q_2q_2} & 0 & 0 & M_{q_2p_3} \\ M_{q_1p_2} & 0 & 0 & M_{p_2p_2} & M_{p_2q_3} & 0 \\ M_{q_1q_3} & 0 & 0 & M_{p_2q_3} & M_{q_3q_3} & 0 \\ 0 & M_{p_1p_3} & M_{q_2p_3} & 0 & 0 & M_{p_3p_3} \end{pmatrix}. \tag{F.79}$$

With this we can obtain an explicit expression for $\boldsymbol{\mu} = -\mathbf{R}(\theta)\mathbf{M}\mathbf{R}^T(\theta)\mathbf{f}$:

$$\begin{pmatrix} \mu_{q_3} \\ \mu_{p_3} \end{pmatrix} = \sqrt{\frac{\kappa_2}{2}}\,|\alpha| \begin{pmatrix} (\cos(\varphi)+\sin(\theta-\varphi))M_{p_2q_3} + (\sin(\theta-\varphi)-\cos(\varphi))M_{q_2p_3} \\ (-\cos(\theta-\varphi)+\sin(\varphi))M_{p_2q_3} + (-\cos(\theta-\varphi)-\sin(\varphi))M_{q_2p_3} \end{pmatrix}. \tag{F.80}$$

The means can then be used to write an expression for the measurement-induced dephasing,

$$\begin{aligned} \Gamma_{\mathrm{d,m}} &= \frac{1}{2}\mathrm{Re}\big[\boldsymbol{\mu}^T\mathbf{B}\boldsymbol{\mu}\big] \\ &= \mathrm{Re}\big[i\chi\big(\mu_{q_3}^2+\mu_{p_3}^2\big)\big] \\ &= -\,|\alpha|^2\,\chi\kappa_2\left((1+\sin(\theta-2\varphi))\mathrm{Im}\big[M_{p_2q_3}^2\big] + (1-\sin(\theta-2\varphi))\mathrm{Im}\big[M_{q_2p_3}^2\big]\right). \end{aligned} \tag{F.81}$$

This way, when calculating the drive-induced component of the dephasing, we can focus entirely on calculating these two components of $\mathbf{M}$ rather than the entire matrix.

The Detailed Calculation

We begin the actual calculation by setting the phase of the amplifier to $\theta = \pi/2$ and the phase of the loop to $\phi = \pm\pi/2$, which will simply control the sign on g_{13} through the function $\mathrm{sgn}(\phi)$. We will use the stable subspace method from Section F.1 to solve the equation for $\tilde{\boldsymbol{\sigma}}$, and so must determine the eigenvalues and eigenvectors of the following matrix:

$$\mathbf{H} = \begin{pmatrix} \mathbf{A}^T(\pi/2) & -\mathbf{B} \\ -\mathbf{C} & -\mathbf{A}(\pi/2) \end{pmatrix}. \tag{F.82}$$

For these choices of the phases, we can permute the rows and columns of this matrix, $\tilde{\mathbf{H}} = \mathbf{P}\mathbf{H}\mathbf{P}^T$, into two 6×6 blocks:

$$\tilde{\mathbf{H}} = \begin{pmatrix} \mathbf{H}_+ & \mathbf{0}_6 \\ \mathbf{0}_6 & \mathbf{H}_- \end{pmatrix} \text{ where}$$

$$\mathbf{H}_\pm = \begin{pmatrix} -\kappa_1/2 \mp \lambda & \mp g_{12} & -\mathrm{sgn}(\phi)g_{13} & 0 & 0 & 0 \\ \pm g_{12} & -\kappa_2/2 & \pm g_{23} & 0 & 0 & 0 \\ \mathrm{sgn}(\phi)g_{13} & \mp g_{23} & -\kappa_3/2 & 0 & 0 & -2i\chi \\ -\kappa_1(\bar{n}_1+1/2) & 0 & 0 & \kappa_1/2 \mp \lambda & \mp g_{12} & -\mathrm{sgn}(\phi)g_{13} \\ 0 & -\kappa_2(\bar{n}_2+1/2) & 0 & \pm g_{12} & \kappa_2/2 & \pm g_{23} \\ 0 & 0 & -\kappa_3(\bar{n}_3+1/2)-i\chi/2 & \mathrm{sgn}(\phi)g_{13} & \mp g_{23} & \kappa_3/2 \end{pmatrix} \tag{F.83}$$

The characteristic polynomial for the $\mathbf{H}$ matrix is then the product of the characteristic polynomials for $\mathbf{H}_+$ and $\mathbf{H}_-$:

$$0 = \Big[s^6 + v_2(+\lambda)s^4 + v_1(+\lambda)s^2 + v_0(+\lambda,\mathrm{sgn}(\phi))\Big]\Big[s^6 + v_2(-\lambda)s^4 + v_1(-\lambda)s^2 + v_0(-\lambda,\mathrm{sgn}(\phi))\Big]. \tag{F.84}$$

The polynomials are solvable, and we write the 12 eigenvalues of $\mathbf{H}$ in the following form:

$$\pm\sqrt{\mathfrak{r}_k(+\lambda)}\,,\ \pm\sqrt{\mathfrak{r}_k(-\lambda)} \quad \text{where} \quad k = 1,2,3 \tag{F.85}$$

where the roots $\mathfrak{r}_k(\pm\lambda)$ are the solutions to the cubic polynomial

$$0 = s^3 + v_2(\pm\lambda)s^2 + v_1(\pm\lambda)s + v_0(\pm\lambda). \tag{F.86}$$

The polynomial coefficients may be written as:

$$
\begin{aligned}
v_2(\pm\lambda) &= \chi^2 - i\chi\kappa_3(2\bar{n}_3+1) + 2\left(g_{12}^2+g_{13}^2+g_{23}^2\right) - \left[\left(\frac{\kappa_1}{2}\mp\lambda\right)^2+\left(\frac{\kappa_2}{2}\right)^2+\left(\frac{\kappa_3}{2}\right)^2\right] \\
v_1(\pm\lambda) &= \chi^2\left[2g_{12}^2-\left(\left(\frac{\kappa_1}{2}\mp\lambda\right)^2+\left(\frac{\kappa_2}{2}\right)^2\right)\right] \\
&\quad + i\chi\left[\kappa_1(2\bar{n}_1+1)g_{13}^2+\kappa_2(2\bar{n}_2+1)g_{23}^2+\kappa_3(2\bar{n}_3+1)\left(-2g_{12}^2+\left[\left(\frac{\kappa_1}{2}\mp\lambda\right)^2+\left(\frac{\kappa_2}{2}\right)^2\right]\right)\right] \\
&\quad + \left(g_{12}^2+g_{23}^2+g_{13}^2\right)^2+\left[\left(\frac{\kappa_1}{2}\mp\lambda\right)^2\left(\frac{\kappa_2}{2}\right)^2+\left(\frac{\kappa_2}{2}\right)^2\left(\frac{\kappa_3}{2}\right)^2+\left(\frac{\kappa_1}{2}\mp\lambda\right)^2\left(\frac{\kappa_3}{2}\right)^2\right] \\
&\quad + 2g_{12}^2\left[\left(\frac{\kappa_1}{2}\mp\lambda\right)\left(\frac{\kappa_2}{2}\right)-\left(\frac{\kappa_2}{2}\right)^2\right]+2g_{23}^2\left[\left(\frac{\kappa_2}{2}\right)\left(\frac{\kappa_3}{2}\right)-\left(\frac{\kappa_1}{2}\mp\lambda\right)^2\right]+2g_{13}^2\left[\left(\frac{\kappa_1}{2}\mp\lambda\right)\left(\frac{\kappa_3}{2}\right)-\left(\frac{\kappa_2}{2}\right)^2\right] \\
v_0(\pm\lambda) &= \chi^2\left[g_{12}^2+\left(\frac{\kappa_1}{2}\mp\lambda\right)\left(\frac{\kappa_2}{2}\right)\right]^2-\left[g_{12}^2\frac{\kappa_3}{2}+g_{23}^2\left(\frac{\kappa_1}{2}\mp\lambda\right)+g_{13}^2\frac{\kappa_2}{2}+\left(\frac{\kappa_1}{2}\mp\lambda\right)\frac{\kappa_2}{2}\frac{\kappa_3}{2}\right]^2 \\
&\quad - i\chi\Bigg[\kappa_1(2\bar{n}_1+1)\left(g_{12}g_{23}+\operatorname{sgn}(\phi)g_{13}\frac{\kappa_2}{2}\right)^2+\kappa_2(2\bar{n}_2+1)\left(\operatorname{sgn}(\phi)g_{12}g_{13}-g_{23}\left(\frac{\kappa_1}{2}\mp\lambda\right)\right)^2 \\
&\qquad + \kappa_3(2\bar{n}_3+1)\left(g_{12}^2+\left(\frac{\kappa_1}{2}\mp\lambda\right)\left(\frac{\kappa_2}{2}\right)\right)^2\Bigg].
\end{aligned}
\tag{F.87}
$$

We note that only one of the coefficients, $v_0(\pm\lambda, \operatorname{sgn}(\phi))$, is dependent on the circulation direction. While the roots of the characteristic polynomial can technically be expressed in terms of radicals, the above coefficients result in complicated expressions, and so explicit expressions for the roots are omitted. The solutions for the eigenvectors are also too complicated to be included. However, with much effort, we can write down the expressions for the only two relevant variances in terms of the roots as follows:

$$
\begin{aligned}
\tilde{\sigma}_{q_3q_3} &= \frac{i}{2\chi}\left(\left(\frac{\kappa_1}{2}-\lambda\right)+\frac{\kappa_2}{2}+\frac{\kappa_3}{2}-\left(\sqrt{\mathfrak{r}_1(+\lambda)}+\sqrt{\mathfrak{r}_2(+\lambda)}+\sqrt{\mathfrak{r}_3(+\lambda)}\right)\right) \\
\tilde{\sigma}_{p_3p_3} &= \frac{i}{2\chi}\left(\left(\frac{\kappa_1}{2}+\lambda\right)+\frac{\kappa_2}{2}+\frac{\kappa_3}{2}-\left(\sqrt{\mathfrak{r}_1(-\lambda)}+\sqrt{\mathfrak{r}_2(-\lambda)}+\sqrt{\mathfrak{r}_3(-\lambda)}\right)\right).
\end{aligned}
\tag{F.88}
$$

In general, solving $\boldsymbol{\sigma}$ would require us to determine the expressions for all 21 unique covariances; however, when solving $\tilde{\boldsymbol{\sigma}}$, only 12 of the covariances are non-zero thanks to the choice of amplifier and loop phases. Moving on to $\boldsymbol{\mu}$, since the measurement-induced dephasing is only dependent on the values of μ_{q_3} and μ_{p_3}, we will only calculate these two means. To accomplish this, we solve for the two relevant elements of $\mathbf{M}$:

$$
\begin{aligned}
M_{p_2q_3} &= -\left(2\operatorname{sgn}(\phi)g_{12}g_{13}-g_{23}[\kappa_1-2\lambda]\right) \\
&\quad\times\Big[g_{13}^2\kappa_2+g_{23}^2[\kappa_1-2\lambda]+g_{12}^2\kappa_3+\frac{1}{4}[\kappa_1-2\lambda]\kappa_2\kappa_3+i\chi\left(4g_{12}^2+[\kappa_1-2\lambda]\kappa_2\right)\tilde{\sigma}_{q_3q_3} \\
&\qquad - 2i\chi\left(2g_{12}g_{23}+\operatorname{sgn}(\phi)g_{13}\kappa_2\right)\tilde{\sigma}_{q_1q_3}+2i\chi\left(-2\operatorname{sgn}(\phi)g_{12}g_{13}+g_{23}[\kappa_1-2\lambda]\right)\tilde{\sigma}_{p_2q_3}\Big]^{-1} \\
M_{q_2p_3} &= \left(2\operatorname{sgn}(\phi)g_{12}g_{13}-g_{23}[\kappa_1+2\lambda]\right) \\
&\quad\times\Big[g_{13}^2\kappa_2+g_{23}^2[\kappa_1+2\lambda]+g_{12}^2\kappa_3+\frac{1}{4}[\kappa_1+2\lambda]\kappa_2\kappa_3+i\chi\left(4g_{12}^2+[\kappa_1+2\lambda]\kappa_2\right)\tilde{\sigma}_{p_3p_3} \\
&\qquad - 2i\chi\left(2g_{12}g_{23}+\operatorname{sgn}(\phi)g_{13}\kappa_2\right)\tilde{\sigma}_{p_1p_3}-2i\chi\left(-2\operatorname{sgn}(\phi)g_{12}g_{13}+g_{23}[\kappa_1+2\lambda]\right)\tilde{\sigma}_{q_2p_3}\Big]^{-1}.
\end{aligned}
\tag{F.89}
$$

The other covariances which appear in these expressions are difficult to simplify, but with a bit of work, the denominators can be simplified to yield

$$
M_{q_3p_2} = -\frac{\operatorname{sgn}(\phi)g_{12}g_{13}-g_{23}[\kappa_1/2-\lambda]}{\sqrt{\mathfrak{r}_1(+\lambda)\,\mathfrak{r}_2(+\lambda)\,\mathfrak{r}_3(+\lambda)}} \qquad M_{q_2p_3} = \frac{\operatorname{sgn}(\phi)g_{12}g_{13}-g_{23}[\kappa_1/2+\lambda]}{\sqrt{\mathfrak{r}_1(-\lambda)\,\mathfrak{r}_2(-\lambda)\,\mathfrak{r}_3(-\lambda)}}.
\tag{F.90}
$$

These expressions can then be used to obtain a compact expression for the sum of the squared means which appear in the measurement induced dephasing, $\boldsymbol{\mu}^T\mathbf{B}\boldsymbol{\mu} = i\chi(\mu_{q_3}^2 + \mu_{p_3}^2)$:

$$\begin{aligned}\mu_{q_3}^2 + \mu_{p_3}^2 \;= |\alpha|^2\,\kappa_2\Bigg(&\frac{(\mathrm{sgn}(\phi)g_{12}g_{13} - g_{23}[\kappa_1/2-\lambda])^2}{\mathfrak{r}_1(+\lambda)\,\mathfrak{r}_2(+\lambda)\,\mathfrak{r}_3(+\lambda)}(1+\sin(\theta-2\varphi))\\ &+\frac{(\mathrm{sgn}(\phi)g_{12}g_{13} - g_{23}[\kappa_1/2+\lambda])^2}{\mathfrak{r}_1(-\lambda)\,\mathfrak{r}_2(-\lambda)\,\mathfrak{r}_3(-\lambda)}(1-\sin(\theta-2\varphi))\Bigg).\end{aligned} \tag{F.91}$$

Since these are roots of a cubic polynomial, the product in the denominator can be replaced by a coefficient from the characteristic polynomial for $\mathbf{H}_\pm$. As a reminder, the roots of a cubic polynomial satisfy

$$(s-\mathfrak{r}_1)(s-\mathfrak{r}_2)(s-\mathfrak{r}_3) = s^3 - (\mathfrak{r}_1+\mathfrak{r}_2+\mathfrak{r}_3)s^2 + (\mathfrak{r}_1\mathfrak{r}_2+\mathfrak{r}_2\mathfrak{r}_3+\mathfrak{r}_1\mathfrak{r}_3)s - \mathfrak{r}_1\mathfrak{r}_2\mathfrak{r}_3 \equiv s^3 + v_2 s^2 + v_1 s + v_0. \tag{F.92}$$

We can, therefore, replace the product of the roots with the coefficient $\mathfrak{r}_1(\pm\lambda)\,\mathfrak{r}_2(\pm\lambda)\,\mathfrak{r}_3(\pm\lambda) = -b_0(\pm\lambda, \mathrm{sgn}(\phi))$. It is worth noting that $-b_0(\pm\lambda,\mathrm{sgn}(\phi)) = \det[\mathbf{H}_\pm]$ and so $\mathfrak{r}_1(\pm\lambda)\,\mathfrak{r}_2(\pm\lambda)\,\mathfrak{r}_3(\pm\lambda) = \det[\mathbf{H}_\pm]$. With this, the worst of the calculation is complete, and we first proceed to the expression for the parasitic dephasing:

$$\Gamma_{\mathrm{d,p}} = -\frac{1}{2}(\kappa_1+\kappa_2+\kappa_3) + \frac{1}{2}\mathrm{Re}\Big[\sqrt{\mathfrak{r}_1(+\lambda)} + \sqrt{\mathfrak{r}_2(+\lambda)} + \sqrt{\mathfrak{r}_3(+\lambda)} + \sqrt{\mathfrak{r}_1(-\lambda)} + \sqrt{\mathfrak{r}_2(-\lambda)} + \sqrt{\mathfrak{r}_3(-\lambda)}\Big]. \tag{F.93}$$

For the measurement-induced dephasing, we start by writing the denominator in a more useful form to highlight the presence of the dispersive coupling χ:

$$\mathfrak{r}_1(\pm\lambda)\,\mathfrak{r}_2(\pm\lambda)\,\mathfrak{r}_3(\pm\lambda) = -v_0(\pm\lambda,\mathrm{sgn}(\phi)) = -\chi^2 c_2(\pm\lambda) + i\chi c_1(\pm\lambda,\mathrm{sgn}(\phi)) + c_0(\pm\lambda). \tag{F.94}$$

Using this, we can write the measurement-induced dephasing as follows:

$$\begin{aligned}\Gamma_{\mathrm{d,m}} = |\alpha|^2\,\chi^2\kappa_2\Bigg(&\frac{c_1(+\lambda,\mathrm{sgn}(\phi))\big(\mathrm{sgn}(\phi)g_{12}g_{13} - g_{23}[\kappa_1/2-\lambda]\big)^2}{\big[c_0(+\lambda)-\chi^2c_2(+\lambda)\big]^2 + \big[\chi c_1(+\lambda,\mathrm{sgn}(\phi))\big]^2}\big(1+\sin(\theta-2\varphi)\big)\\ &+\frac{c_1(-\lambda,\mathrm{sgn}(\phi))\big(\mathrm{sgn}(\phi)g_{12}g_{13} - g_{23}[\kappa_1/2+\lambda]\big)^2}{\big[c_0(-\lambda)-\chi^2c_2(-\lambda)\big]^2 + \big[\chi c_1(-\lambda,\mathrm{sgn}(\phi))\big]^2}\big(1-\sin(\theta-2\varphi)\big)\Bigg)\\ \text{where}\quad &c_0(\pm\lambda) = \big[g_{12}^2\kappa_3/2 + g_{23}^2(\kappa_1/2\mp\lambda) + g_{13}^2\kappa_2/2 + (\kappa_1/2\mp\lambda)(\kappa_2/2)(\kappa_3/2)\big]^2\\ &c_1(\pm\lambda,\mathrm{sgn}(\phi)) = \Big[\kappa_1(2\bar{n}_1+1)\,(g_{12}g_{23}+\mathrm{sgn}(\phi)g_{13}\kappa_2/2)^2\\ &\qquad\qquad + \kappa_2(2\bar{n}_2+1)\,(\mathrm{sgn}(\phi)g_{12}g_{13} - g_{23}(\kappa_1/2\mp\lambda))^2\\ &\qquad\qquad + \kappa_3(2\bar{n}_3+1)\,\big(g_{12}^2 + (\kappa_1/2\mp\lambda)(\kappa_2/2)\big)^2\Big]\\ &c_2(\pm\lambda) = \big(g_{12}^2 + (\kappa_1/2\mp\lambda)(\kappa_2/2)\big)^2.\end{aligned} \tag{F.95}$$

F.4.2 Measurement Rate

Assuming no detuning, the measurement rate can be defined as follows in terms of the qubit-state conditioned values of the output signal and output power noise at the resonance frequency:

$$\Gamma_{\mathrm{meas}} = \frac{|\langle\hat{M}[0]\rangle_e - \langle\hat{M}[0]\rangle_g|^2/4}{\bar{S}_{MM,e}[0] + \bar{S}_{MM,g}[0] + 2\bar{n}_{\mathrm{add}}}. \tag{F.96}$$

Since the measurement is performed through the buffer mode, a_2, the measurement quadrature is defined purely in terms of the buffer mode output quadratures:

$$\hat{M} = \cos(\vartheta)\hat{q}_{2,\mathrm{out}} + \sin(\vartheta)\hat{p}_{2,\mathrm{out}}. \tag{F.97}$$

Due to the added drive term, the input noise operators of the buffer mode have the following forms:

$$\tilde{q}_{2,\mathrm{in}}[\omega] = \hat{q}_{2,\mathrm{in}}[\omega] - \sqrt{2}\,|\alpha|\sin(\varphi) \qquad \tilde{p}_{2,\mathrm{in}}[\omega] = \hat{p}_{2,\mathrm{in}}[\omega] + \sqrt{2}\,|\alpha|\cos(\varphi). \tag{F.98}$$

We are again only concerned with the behaviour at the optimal values of the loop-phase, $\phi = \pm\pi/2$. The following expressions are then understood to only apply for these values of the loop phase, and the function of $\mathrm{sgn}(\phi)$ is used

when there is a sign difference depending on the circulation direction. Therefore, this function only accepts the values $\phi = \pm\pi/2$. We can now work out the following expression for the signal:

$$\langle\hat{M}[0]\rangle_e - \langle\hat{M}[0]\rangle_g = \frac{-2\sqrt{2}\,|\alpha|\,\chi\kappa_2}{\det[\mathbf{A}]}\Big(\left[g_{12}^2 g_{13}^2 - g_{23}^2\left((\kappa_1/2)^2 - \lambda^2\right)\right]\cos(\vartheta-\varphi) \\ + 2\,\mathrm{sgn}(\phi)\lambda\, g_{12}g_{23}g_{13}\sin(\theta-(\vartheta+\varphi))\Big) \tag{F.99}$$

where $\det[\mathbf{A}]$ is the determinant of the dynamical matrix of the system with the qubit state dependent dephasing included on the dispersively coupled mode a_3, and so is equivalent to Eq. (F.69) with an additional term:

$$\mathbf{A} = \begin{pmatrix} -(\kappa_1/2)\mathbf{I} + \lambda(-\cos(\theta)\mathbf{X} + \sin(\theta)\mathbf{Z}) & g_{12}\mathbf{J} & g_{13}(\cos(\phi)\mathbf{J} + \sin(\phi)\mathbf{I}) \\ g_{12}\mathbf{J} & -(\kappa_2/2)\mathbf{I} & g_{23}\mathbf{J} \\ g_{13}(\cos(\phi)\mathbf{J} - \sin(\phi)\mathbf{I}) & g_{23}\mathbf{J} & -(\kappa_3/2)\mathbf{I} + \sigma_z\chi\mathbf{J} \end{pmatrix}, \tag{F.100}$$

where $\sigma_z = \pm 1$. The determinant is identical for both the excited and ground qubit state conditioned scattering matrices, and is also independent of the circulation direction, as well as the value of the amplifier phase θ. The determinant of the dynamical matrix may be written as:

$$\det[\mathbf{A}] = \left(g_{12}^2\frac{\kappa_3}{2} + g_{23}^2\left(\frac{\kappa_1}{2}+\lambda\right) + g_{13}^2\frac{\kappa_2}{2} + \left(\frac{\kappa_1}{2}+\lambda\right)\frac{\kappa_2}{2}\frac{\kappa_3}{2}\right)\left(g_{12}^2\frac{\kappa_3}{2} + g_{23}^2\left(\frac{\kappa_1}{2}-\lambda\right) + g_{13}^2\frac{\kappa_2}{2} + \left(\frac{\kappa_1}{2}-\lambda\right)\frac{\kappa_2}{2}\frac{\kappa_3}{2}\right) \\ + \chi^2\left(g_{12}^2 + \left(\frac{\kappa_1}{2}+\lambda\right)\frac{\kappa_2}{2}\right)\left(g_{12}^2 + \left(\frac{\kappa_1}{2}-\lambda\right)\frac{\kappa_2}{2}\right). \tag{F.101}$$

It can be determined that when the loop phase is set $\phi = \pm\pi/2$, the optimum value of the phase for the measurement quadrature is the same phase as the measurement drive, $\vartheta = \varphi$. With this, we arrive at the following expression for the measurement signal:

$$\begin{aligned} &\langle\hat{M}[0]\rangle_e - \langle\hat{M}[0]\rangle_g \\ &= \frac{-2\sqrt{2}\,|\alpha|\,\chi\kappa_2}{\det[\mathbf{A}]}\Big(\left[g_{12}^2 g_{13}^2 - g_{23}^2\left((\kappa_1/2)^2 - \lambda^2\right)\right] + 2\,\mathrm{sgn}(\phi)\lambda\, g_{12}g_{23}g_{13}\sin(\theta-2\varphi)\Big) \\ &= \frac{-2\sqrt{2}\,|\alpha|\,\chi\kappa_2}{\det[\mathbf{A}]}\Bigg[\frac{1}{2}\left(\mathrm{sgn}(\phi)g_{12}g_{13} - g_{23}\left(\frac{\kappa_1}{2}-\lambda\right)\right)\left(\mathrm{sgn}(\phi)g_{12}g_{13} + g_{23}\left(\frac{\kappa_1}{2}+\lambda\right)\right)(1+\sin(\theta-2\varphi)) \\ &\qquad + \frac{1}{2}\left(\mathrm{sgn}(\phi)g_{12}g_{13} + g_{23}\left(\frac{\kappa_1}{2}-\lambda\right)\right)\left(\mathrm{sgn}(\phi)g_{12}g_{13} - g_{23}\left(\frac{\kappa_1}{2}+\lambda\right)\right)(1-\sin(\theta-2\varphi))\Bigg]. \end{aligned} \tag{F.102}$$

For the output noise-power spectra, we use the following expression to combine the results

$$\bar{S}_{MM,e/g}[0] = \cos^2(\vartheta)\bar{S}_{q_2q_2,e/g}[0] + 2\cos(\vartheta)\sin(\vartheta)\bar{S}_{q_2p_2,e/g}[0] + \sin^2(\vartheta)\bar{S}_{p_2p_2,e/g}[0], \tag{F.103}$$

The combination of the ground and excited state conditioned output power spectra may be expressed as follows:

$$\bar{S}_{MM,e}[0] + \bar{S}_{MM,g}[0] = \frac{1}{2\det[\mathbf{A}]^2}\Big(\bar{S}(+\lambda,\mathrm{sgn}(\phi))\,(1+\sin(\theta-2\varphi)) + \bar{S}(-\lambda,\mathrm{sgn}(\phi))\,(1-\sin(\theta-2\varphi))\Big). \tag{F.104}$$

The functions $\bar{S}(\pm\lambda,\mathrm{sgn}(\phi))$ in the above are defined as,

$$\bar{S}(\pm\lambda,\mathrm{sgn}(\phi)) = (2\bar{n}_1+1)\bar{S}_1(\pm\lambda,\mathrm{sgn}(\phi)) + (2\bar{n}_2+1)\bar{S}_2(\pm\lambda,\mathrm{sgn}(\phi)) + (2\bar{n}_3+1)\bar{S}_3(\pm\lambda,\mathrm{sgn}(\phi)), \tag{F.105}$$

where the coefficients for the individual bath contributions to the noise are:

$$\begin{aligned}
\bar{S}_1(\pm\lambda, \mathrm{sgn}(\phi)) = \kappa_1\kappa_2\Bigg(&\chi^2\big(g_{12}g_{23} + \mathrm{sgn}(\phi)g_{13}\kappa_2/2\big)^2\big(\mathrm{sgn}(\phi)g_{12}g_{13} + g_{23}(\kappa_1/2 \pm \lambda)\big)^2 \\
&+ \Big[\big(\mathrm{sgn}(\phi)g_{13}g_{23} - g_{12}\kappa_3/2\big)\Big(g_{12}^2\kappa_3/2 + g_{23}^2(\kappa_1/2 \mp \lambda) + g_{13}^2\kappa_2/2 + (\kappa_1/2 \mp \lambda)(\kappa_2\kappa_3/4)\Big) \\
&\quad - \chi^2 g_{12}\big(g_{12}^2 + (\kappa_1/2 \mp \lambda)(\kappa_2/2)\big)\Big]^2\Bigg) \\
\bar{S}_2(\pm\lambda, \mathrm{sgn}(\phi)) = \Bigg(&\kappa_2^2\chi^2\big(\mathrm{sgn}(\phi)g_{12}g_{13} + g_{23}(\kappa_1/2 \pm \lambda)\big)^2\big(\mathrm{sgn}(\phi)g_{12}g_{13} - g_{23}(\kappa_1/2 \mp \lambda)\big)^2 \\
&+ \Big[\Big(g_{12}^2\kappa_3/2 + g_{23}^2(\kappa_1/2 \mp \lambda) + g_{13}^2\kappa_2/2 + (\kappa_1/2 \mp \lambda)(\kappa_2\kappa_3/4)\Big) \\
&\quad \times \Big(g_{12}^2\kappa_3/2 + g_{23}^2(\kappa_1/2 \pm \lambda) - g_{13}^2\kappa_2/2 - (\kappa_1/2 \pm \lambda)(\kappa_2\kappa_3/4)\Big) \\
&\quad + \chi^2\big(g_{12}^2 + (\kappa_1/2 \mp \lambda)(\kappa_2/2)\big)\big(g_{12}^2 - (\kappa_1/2 \pm \lambda)(\kappa_2/2)\big)\Big]^2\Bigg) \\
\bar{S}_3(\pm\lambda, \mathrm{sgn}(\phi)) = \Bigg(&\Big(g_{12}^2\kappa_3/2 + g_{23}^2(\kappa_1/2 \mp \lambda) + g_{13}^2\kappa_2/2 + (\kappa_1/2 \mp \lambda)(\kappa_2\kappa_3/4)\Big)^2 + \chi^2\big(g_{12}^2 + (\kappa_1/2 \mp \lambda)(\kappa_2/2)\big)^2\Bigg) \\
&\times \Big(\kappa_2\kappa_3\big(\mathrm{sgn}(\phi)g_{12}g_{13} + g_{23}(\kappa_1/2 \pm \lambda)\big)^2\Big). \qquad \text{(F.106)}
\end{aligned}$$

Bibliography

[1] J. P. Dowling and G. J. Milburn, "Quantum technology: the second quantum revolution", Philosophical Transactions of the Royal Society of London. Series A: Mathematical, Physical and Engineering Sciences **361**, edited by A. G. J. MacFarlane, 1655 (2003).

[2] M. Planck, "Ueber das Gesetz der Energieverteilung im Normalspectrum", Annalen der Physik **309**, 553 (1901).

[3] C. L. Degen, F. Reinhard, and P. Cappellaro, "Quantum sensing", Reviews of Modern Physics **89**, 10.1103/revmodphys.89.035002 (2017).

[4] V. Giovannetti, S. Lloyd, and L. Maccone, "Advances in quantum metrology", Nature Photonics **5**, 222 (2011).

[5] G. Wendin, "Quantum information processing with superconducting circuits: a review", Reports on Progress in Physics **80**, 106001 (2017).

[6] N. P. de Leon, K. M. Itoh, D. Kim, K. K. Mehta, T. E. Northup, H. Paik, B. S. Palmer, N. Samarth, S. Sangtawesin, and D. W. Steuerman, "Materials challenges and opportunities for quantum computing hardware", Science **372**, 10.1126/science.abb2823 (2021).

[7] N. Gisin and R. Thew, "Quantum communication", Nature Photonics **1**, 165 (2007).

[8] N. Gisin, G. Ribordy, W. Tittel, and H. Zbinden, "Quantum cryptography", Reviews of Modern Physics **74**, 145 (2002).

[9] C. H. Bennett and D. P. DiVincenzo, "Quantum information and computation", Nature **404**, 247 (2000).

[10] A. A. Clerk, M. H. Devoret, S. M. Girvin, F. Marquardt, and R. J. Schoelkopf, "Introduction to quantum noise, measurement, and amplification", Reviews of Modern Physics **82**, 1155 (2010).

[11] C. M. Caves, "Quantum limits on noise in linear amplifiers", Physical Review D **26**, 1817 (1982).

[12] H. A. Haus and J. A. Mullen, "Quantum Noise in Linear Amplifiers", Physical Review **128**, 2407 (1962).

[13] H. Zimmer, "Parametric Amplificiation of Microwaves in Superconducting Josephson Tunnel Junctions", Applied Physics Letters **10**, 193 (1967).

[14] J. Aumentado, "Superconducting Parametric Amplifiers: The State of the Art in Josephson Parametric Amplifiers", IEEE Microwave Magazine **21**, 45 (2020).

[15] A. Metelmann and A. A. Clerk, "Nonreciprocal Photon Transmission and Amplification via Reservoir Engineering", Physical Review X **5**, 10.1103/physrevx.5.021025 (2015).

[16] L. Ranzani and J. Aumentado, "Graph-based analysis of nonreciprocity in coupled-mode systems", New Journal of Physics **17**, 023024 (2015).

[17] B. Abdo, K. Sliwa, S. Shankar, M. Hatridge, L. Frunzio, R. Schoelkopf, and M. Devoret, "Josephson Directional Amplifier for Quantum Measurement of Superconducting Circuits", Physical Review Letters **112**, 10.1103/physrevlett.112.167701 (2014).

[18] K. M. Sliwa, M. Hatridge, A. Narla, S. Shankar, L. Frunzio, R. J. Schoelkopf, and M. H. Devoret, "Reconfigurable Josephson Circulator/Directional Amplifier", Physical Review X **5**, 10.1103/physrevx.5.041020 (2015).

[19] F. Lecocq, L. Ranzani, G. A. Peterson, K. Cicak, R. W. Simmonds, J. D. Teufel, and J. Aumentado, "Nonreciprocal Microwave Signal Processing with a Field-Programmable Josephson Amplifier", Physical Review Applied **7**, 10.1103/physrevapplied.7.024028 (2017).

[20] F. Lecocq, L. Ranzani, G. Peterson, K. Cicak, A. Metelmann, S. Kotler, R. Simmonds, J. Teufel, and J. Aumentado, "Microwave Measurement beyond the Quantum Limit with a Nonreciprocal Amplifier", Physical Review Applied **13**, 10.1103/physrevapplied.13.044005 (2020).

[21] Z. Shen, Y.-L. Zhang, Y. Chen, F.-W. Sun, X.-B. Zou, G.-C. Guo, C.-L. Zou, and C.-H. Dong, "Reconfigurable optomechanical circulator and directional amplifier", Nature Communications **9**, 10.1038/s41467-018-04187-8 (2018).

[22] D. Malz, L. D. Tóth, N. R. Bernier, A. K. Feofanov, T. J. Kippenberg, and A. Nunnenkamp, "Quantum-Limited Directional Amplifiers with Optomechanics", Physical Review Letters **120**, 10.1103/physrevlett.120.023601 (2018).

[23] L. Ranzani, S. Kotler, A. J. Sirois, M. P. DeFeo, M. Castellanos-Beltran, K. Cicak, L. R. Vale, and J. Aumentado, "Wideband Isolation by Frequency Conversion in a Josephson-Junction Transmission Line", Physical Review Applied **8**, 10.1103/physrevapplied.8.054035 (2017).

[24] L. Ranzani and J. Aumentado, "Circulators at the Quantum Limit: Recent Realizations of Quantum-Limited Superconducting Circulators and Related Approaches", IEEE Microwave Magazine **20**, 112 (2019).

[25] C. Müller, S. Guan, N. Vogt, J. H. Cole, and T. M. Stace, "Passive On-Chip Superconducting Circulator Using a Ring of Tunnel Junctions", Physical Review Letters **120**, 10.1103/physrevlett.120.213602 (2018).

[26] B. Abdo, N. T. Bronn, O. Jinka, S. Olivadese, A. D. Córcoles, V. P. Adiga, M. Brink, R. E. Lake, X. Wu, D. P. Pappas, and J. M. Chow, "Active protection of a superconducting qubit with an interferometric Josephson isolator", Nature Communications **10**, 10.1038/s41467-019-11101-3 (2019).

[27] K. Fang, J. Luo, A. Metelmann, M. H. Matheny, F. Marquardt, A. A. Clerk, and O. Painter, "Generalized non-reciprocity in an optomechanical circuit via synthetic magnetism and reservoir engineering", Nature Physics **13**, 465 (2017).

[28] G. A. Peterson, F. Lecocq, K. Cicak, R. W. Simmonds, J. Aumentado, and J. D. Teufel, "Demonstration of Efficient Nonreciprocity in a Microwave Optomechanical Circuit", Physical Review X **7**, 10.1103/physrevx.7.031001 (2017).

[29] N. R. Bernier, L. D. Tóth, A. Koottandavida, M. A. Ioannou, D. Malz, A. Nunnenkamp, A. K. Feofanov, and T. J. Kippenberg, "Nonreciprocal reconfigurable microwave optomechanical circuit", Nature Communications **8**, 10.1038/s41467-017-00447-1 (2017).

[30] F. Lecocq, L. Ranzani, G. A. Peterson, K. Cicak, X. Y. Jin, R. W. Simmonds, J. D. Teufel, and J. Aumentado, "Efficient Qubit Measurement with a Nonreciprocal Microwave Amplifier", Physical Review Letters **126**, 10.1103/physrevlett.126.020502 (2021).

[31] L. Orr, S. A. Khan, N. Buchholz, S. Kotler, and A. Metelmann, "High-Purity Entanglement of Hot Propagating Modes Using Nonreciprocity", PRX Quantum **4**, 10.1103/prxquantum.4.020344 (2023).

[32] C. Fabre and N. Treps, "Modes and states in quantum optics", Reviews of Modern Physics **92**, 10.1103/revmodphys.92.035005 (2020).

[33] R. Simon, N. Mukunda, and B. Dutta, "Quantum-noise matrix for multimode systems: U(n) invariance, squeezing, and normal forms", Physical Review A **49**, 1567 (1994).

[34] H. Groenewold, "On the principles of elementary quantum mechanics", Physica **12**, 405 (1946).

[35] J. E. Moyal, "Quantum mechanics as a statistical theory", Mathematical Proceedings of the Cambridge Philosophical Society **45**, 99 (1949).

[36] B. L. Schumaker, "Quantum mechanical pure states with gaussian wave functions", Physics Reports **135**, 317 (1986).

[37] B. C. Hall, *Lie Groups, Lie Algebras, and Representations: An Elementary Introduction* (Springer International Publishing, 2015).

[38] J. Williamson, "On the Algebraic Problem Concerning the Normal Forms of Linear Dynamical Systems", American Journal of Mathematics **58**, 141 (1936).

[39] J. L. Pereira, L. Banchi, and S. Pirandola, "Symplectic decomposition from submatrix determinants", Proceedings of the Royal Society A: Mathematical, Physical and Engineering Sciences **477**, 10.1098/rspa.2021.0513 (2021).

[40] F. Caruso, J. Eisert, V. Giovannetti, and A. S. Holevo, "Multi-mode bosonic Gaussian channels", New Journal of Physics **10**, 083030 (2008).

[41] G. Lindblad, "On the generators of quantum dynamical semigroups", Communications in Mathematical Physics **48**, 119 (1976).

[42] V. Gorini, A. Kossakowski, and E. C. G. Sudarshan, "Completely positive dynamical semigroups of N-level systems", Journal of Mathematical Physics **17**, 821 (1976).

[43] H.-P. Breuer and F. Petruccione, *The Theory of Open Quantum Systems* (Oxford University Press, Jan. 2007).

[44] D. Grimmer, E. Brown, A. Kempf, R. B. Mann, and E. Martín-Martínez, "A classification of open Gaussian dynamics", Journal of Physics A: Mathematical and Theoretical **51**, 245301 (2018).

[45] H. J. Carmichael, *Statistical Methods in Quantum Optics 1* (Springer Berlin Heidelberg, 1999).

[46] C. Gardiner and P. Zoller, *Quantum Noise: A Handbook of Markovian and Non-Markovian Quantum Stochastic Methods with Applications to Quantum Optics*, 3rd ed., Springer Series in Synergetics (Springer, Aug. 2004).

[47] A. B. Klimov and S. M. Chumakov, *A Group-Theoretical Approach to Quantum Optics: Models of Atom-Field Interactions* (Wiley, Jan. 2009).

[48] B. C. Hall, *Quantum Theory for Mathematicians* (Springer New York, 2013).

[49] N. Van Kampen, *Stochastic Processes in Physics and Chemistry*, North-Holland Personal Library (North Holland, 2011).

[50] C. W. Gardiner and M. J. Collett, "Input and output in damped quantum systems: Quantum stochastic differential equations and the master equation", Physical Review A **31**, 3761 (1985).

[51] G. A. Peterson, *Parametric coupling between microwaves and motion in quantum circuits: Fundamental limits and applications*, Doctoral Dissertation (University of Colorado at Boulder, 2020).

[52] A. Metelmann, "Parametric couplings in engineered quantum systems", SciPost Physics Lecture Notes, 10.21468/scipostphyslectnotes.66 (2023).

[53] M. H. Devoret and J. M. Martinis, "Implementing Qubits with Superconducting Integrated Circuits", in *Experimental Aspects of Quantum Computing* (Springer US, 2005), pp. 163–203.

[54] B. Josephson, "Possible new effects in superconductive tunnelling", Physics Letters **1**, 251 (1962).

[55] P. W. Anderson and J. M. Rowell, "Probable Observation of the Josephson Superconducting Tunneling Effect", Physical Review Letters **10**, 230 (1963).

[56] A. Barone and G. Paternò, *Physics and Applications of the Josephson Effect* (Wiley, July 1982).

[57] T.-C. Chien, O. Lanes, C. Liu, X. Cao, P. Lu, S. Motz, G. Liu, D. Pekker, and M. Hatridge, "Multiparametric amplification and qubit measurement with a Kerr-free Josephson ring modulator", Physical Review A **101**, 10.1103/physreva.101.042336 (2020).

[58] R. C. Jaklevic, J. Lambe, A. H. Silver, and J. E. Mercereau, "Quantum Interference Effects in Josephson Tunneling", Physical Review Letters **12**, 159 (1964).

[59] J. M. Martinis and J. Clarke, "Signal and noise theory for a dc SQUID amplifier", Journal of Low Temperature Physics **61**, 227 (1985).

[60] T. Yamamoto, K. Inomata, M. Watanabe, K. Matsuba, T. Miyazaki, W. D. Oliver, Y. Nakamura, and J. S. Tsai, "Flux-driven Josephson parametric amplifier", Applied Physics Letters **93**, 10.1063/1.2964182 (2008).

[61] J. Clarke, "A superconducting galvanometer employing Josephson tunnelling", Philosophical Magazine **13**, 115 (1966).

[62] G. J. Ribeill, D. Hover, Y.-F. Chen, S. Zhu, and R. McDermott, "Superconducting low-inductance undulatory galvanometer microwave amplifier: Theory", Journal of Applied Physics **110**, 10.1063/1.3660217 (2011).

[63] D. Hover, Y.-F. Chen, G. J. Ribeill, S. Zhu, S. Sendelbach, and R. McDermott, "Superconducting low-inductance undulatory galvanometer microwave amplifier", Applied Physics Letters **100**, 10.1063/1.3682309 (2012).

[64] D. Hover, S. Zhu, T. Thorbeck, G. J. Ribeill, D. Sank, J. Kelly, R. Barends, J. M. Martinis, and R. McDermott, "High fidelity qubit readout with the superconducting low-inductance undulatory galvanometer microwave amplifier", Applied Physics Letters **104**, 10.1063/1.4871088 (2014).

[65] N. E. Frattini, U. Vool, S. Shankar, A. Narla, K. M. Sliwa, and M. H. Devoret, "3-wave mixing Josephson dipole element", Applied Physics Letters **110**, 10.1063/1.4984142 (2017).

[66] N. E. Frattini, V. V. Sivak, A. Lingenfelter, S. Shankar, and M. H. Devoret, "Optimizing the Nonlinearity and Dissipation of a SNAIL Parametric Amplifier for Dynamic Range", Physical Review Applied **10**, 10.1103/physrevapplied.10.054020 (2018).

[67] C. Zhou, P. Lu, M. Praquin, T.-C. Chien, R. Kaufman, X. Cao, M. Xia, R. S. K. Mong, W. Pfaff, D. Pekker, and M. Hatridge, "Realizing all-to-all couplings among detachable quantum modules using a microwave quantum state router", npj Quantum Information **9**, 10.1038/s41534-023-00723-7 (2023).

[68] N. Bergeal, R. Vijay, V. E. Manucharyan, I. Siddiqi, R. J. Schoelkopf, S. M. Girvin, and M. H. Devoret, "Analog information processing at the quantum limit with a Josephson ring modulator", Nature Physics **6**, 296 (2010).

[69] N. Bergeal, F. Schackert, M. Metcalfe, R. Vijay, V. E. Manucharyan, L. Frunzio, D. E. Prober, R. J. Schoelkopf, S. M. Girvin, and M. H. Devoret, "Phase-preserving amplification near the quantum limit with a Josephson ring modulator", Nature **465**, 64 (2010).

[70] B. Abdo, F. Schackert, M. Hatridge, C. Rigetti, and M. Devoret, "Josephson amplifier for qubit readout", Applied Physics Letters **99**, 10.1063/1.3653473 (2011).

[71] B. Abdo, A. Kamal, and M. Devoret, "Nondegenerate three-wave mixing with the Josephson ring modulator", Physical Review B **87**, 10.1103/physrevb.87.014508 (2013).

[72] B. Abdo, K. Sliwa, L. Frunzio, and M. Devoret, "Directional Amplification with a Josephson Circuit", Physical Review X **3**, 10.1103/physrevx.3.031001 (2013).

[73] A. Roy and M. Devoret, "Quantum-limited parametric amplification with Josephson circuits in the regime of pump depletion", Physical Review B **98**, 10.1103/physrevb.98.045405 (2018).

[74] V. Sivak, N. Frattini, V. Joshi, A. Lingenfelter, S. Shankar, and M. Devoret, "Kerr-Free Three-Wave Mixing in Superconducting Quantum Circuits", Physical Review Applied **11**, 10.1103/physrevapplied.11.054060 (2019).

[75] H. A. Lorentz, "The theorem of Poynting concerning the energy in the electromagnetic field and two general propositions concerning the propagation of light", Amsterdammer Akademie der Wetenschappen **4**, 176 (1896).

[76] Rayleigh, "On the Magnetic Rotation of Light and the Second Law of Thermo-Dynamics", Nature **64**, 577 (1901).

[77] R. J. Potton, "Reciprocity in optics", Reports on Progress in Physics **67**, 717 (2004).

[78] D. Jalas, A. Petrov, M. Eich, W. Freude, S. Fan, Z. Yu, R. Baets, M. Popović, A. Melloni, J. D. Joannopoulos, M. Vanwolleghem, C. R. Doerr, and H. Renner, "What is — and what is not — an optical isolator", Nature Photonics **7**, 579 (2013).

[79] C. Caloz, A. Alù, S. Tretyakov, D. Sounas, K. Achouri, and Z.-L. Deck-Léger, "Electromagnetic Nonreciprocity", Physical Review Applied **10**, 10.1103/physrevapplied.10.047001 (2018).

[80] S. Ramo, J. R. Whinnery, and T. Van Duzer, *Fields and waves in communication electronics* (John Wiley & Sons, 1994).

[81] M. L. Kales, "Modes in Wave Guides Containing Ferrites", Journal of Applied Physics **24**, 604 (1953).

[82] A. Kamal and A. Metelmann, "Minimal Models for Nonreciprocal Amplification Using Biharmonic Drives", Physical Review Applied **7**, 10.1103/physrevapplied.7.034031 (2017).

[83] A. Metelmann and A. A. Clerk, "Nonreciprocal quantum interactions and devices via autonomous feedforward", Physical Review A **95**, 10.1103/physreva.95.013837 (2017).

[84] H. J. Carmichael, "Quantum trajectory theory for cascaded open systems", Physical Review Letters **70**, 2273 (1993).

[85] C. W. Gardiner, "Driving a quantum system with the output field from another driven quantum system", Physical Review Letters **70**, 2269 (1993).

[86] L. Ranzani and J. Aumentado, "A geometric description of nonreciprocity in coupled two-mode systems", New Journal of Physics **16**, 103027 (2014).

[87] S. J. van Enk, J. I. Cirac, and P. Zoller, "Photonic Channels for Quantum Communication", Science **279**, 205 (1998).

[88] J. I. Cirac, P. Zoller, H. J. Kimble, and H. Mabuchi, "Quantum State Transfer and Entanglement Distribution among Distant Nodes in a Quantum Network", Physical Review Letters **78**, 3221 (1997).

[89] A. Acín, J. I. Cirac, and M. Lewenstein, "Entanglement percolation in quantum networks", Nature Physics **3**, 256 (2007).

[90] H. J. Kimble, "The quantum internet", Nature **453**, 1023 (2008).

[91] N. Roch, M. E. Schwartz, F. Motzoi, C. Macklin, R. Vijay, A. W. Eddins, A. N. Korotkov, K. B. Whaley, M. Sarovar, and I. Siddiqi, "Observation of Measurement-Induced Entanglement and Quantum Trajectories of Remote Superconducting Qubits", Physical Review Letters **112**, 10.1103/physrevlett.112.170501 (2014).

[92] C. Simon, "Towards a global quantum network", Nature Photonics **11**, 678 (2017).

[93] S. Wehner, D. Elkouss, and R. Hanson, "Quantum internet: A vision for the road ahead", Science **362**, 10.1126/science.aam9288 (2018).

[94] A. Ferraro, S. Olivares, and M. G. Paris, "Gaussian states in continuous variable quantum information", arXiv preprint quant-ph/0503237 (2005).

[95] S. L. Braunstein and P. van Loock, "Quantum information with continuous variables", Reviews of Modern Physics **77**, 513 (2005).

[96] P. Kok, W. J. Munro, K. Nemoto, T. C. Ralph, J. P. Dowling, and G. J. Milburn, "Linear optical quantum computing with photonic qubits", Reviews of Modern Physics **79**, 135 (2007).

[97] X. Wang, T. Hiroshima, A. Tomita, and M. Hayashi, "Quantum information with Gaussian states", Physics Reports **448**, 1 (2007).

[98] C. Weedbrook, S. Pirandola, R. García-Patrón, N. J. Cerf, T. C. Ralph, J. H. Shapiro, and S. Lloyd, "Gaussian quantum information", Reviews of Modern Physics **84**, 621 (2012).

[99] G. Adesso, S. Ragy, and A. R. Lee, "Continuous Variable Quantum Information: Gaussian States and Beyond", Open Systems & Information Dynamics **21**, 1440001 (2014).

[100] S. L. Braunstein, "Error Correction for Continuous Quantum Variables", Physical Review Letters **80**, 4084 (1998).

[101] S. L. Braunstein, "Quantum error correction for communication with linear optics", Nature **394**, 47 (1998).

[102] J. Eisert, S. Scheel, and M. B. Plenio, "Distilling Gaussian States with Gaussian Operations is Impossible", Physical Review Letters **89**, 10.1103/physrevlett.89.137903 (2002).

[103] L.-M. Duan, G. Giedke, J. I. Cirac, and P. Zoller, "Entanglement Purification of Gaussian Continuous Variable Quantum States", Physical Review Letters **84**, 4002 (2000).

[104] J. Fiurášek, "Gaussian Transformations and Distillation of Entangled Gaussian States", Physical Review Letters **89**, 10.1103/physrevlett.89.137904 (2002).

[105] G. Giedke, L.-M. Duan, I. Cirac, and P. Zoller, "Distillability criterion for all bipartite Gaussian states", Quantum Information and Computation **1**, 79 (2001).

[106] G. Giedke and J. Ignacio Cirac, "Characterization of Gaussian operations and distillation of Gaussian states", Physical Review A **66**, 10.1103/physreva.66.032316 (2002).

[107] D. E. Browne, J. Eisert, S. Scheel, and M. B. Plenio, "Driving non-Gaussian to Gaussian states with linear optics", Physical Review A **67**, 10.1103/physreva.67.062320 (2003).

[108] H. Takahashi, J. S. Neergaard-Nielsen, M. Takeuchi, M. Takeoka, K. Hayasaka, A. Furusawa, and M. Sasaki, "Entanglement distillation from Gaussian input states", Nature Photonics **4**, 178 (2010).

[109] G. Y. Xiang, T. C. Ralph, A. P. Lund, N. Walk, and G. J. Pryde, "Heralded noiseless linear amplification and distillation of entanglement", Nature Photonics **4**, 316 (2010).

[110] M. F. Gely, M. Kounalakis, C. Dickel, J. Dalle, R. Vatré, B. Baker, M. D. Jenkins, and G. A. Steele, "Observation and stabilization of photonic Fock states in a hot radio-frequency resonator", Science **363**, 1072 (2019).

[111] J. Li and S. Gröblacher, "Stationary quantum entanglement between a massive mechanical membrane and a low frequency LC circuit", New Journal of Physics **22**, 063041 (2020).

[112] G. Steele, M. Gely, I. Rodrigues, D. Bothner, M. Kounalakis, C. Dickel, J. Dalle, R. Vatré, B. Baker, and M. Jenkins, "Photonics at radio frequency: Quantum sensing of radio-frequency photons and vibrations", in Optical and Quantum Sensing and Precision Metrology, Vol. 11700 (Mar. 2021), 117001B.

[113] D. Vitali, S. Gigan, A. Ferreira, H. R. Böhm, P. Tombesi, A. Guerreiro, V. Vedral, A. Zeilinger, and M. Aspelmeyer, "Optomechanical Entanglement between a Movable Mirror and a Cavity Field", Physical Review Letters **98**, 10.1103/physrevlett.98.030405 (2007).

[114] C. Genes, A. Mari, P. Tombesi, and D. Vitali, "Robust entanglement of a micromechanical resonator with output optical fields", Physical Review A **78**, 10.1103/physreva.78.032316 (2008).

[115] Y.-D. Wang and A. A. Clerk, "Reservoir-Engineered Entanglement in Optomechanical Systems", Physical Review Letters **110**, 10.1103/physrevlett.110.253601 (2013).

[116] Y.-D. Wang, S. Chesi, and A. A. Clerk, "Bipartite and tripartite output entanglement in three-mode optomechanical systems", Physical Review A **91**, 10.1103/physreva.91.013807 (2015).

[117] A. Bienfait, K. J. Satzinger, Y. P. Zhong, H.-S. Chang, M.-H. Chou, C. R. Conner, É. Dumur, J. Grebel, G. A. Peairs, R. G. Povey, and A. N. Cleland, "Phonon-mediated quantum state transfer and remote qubit entanglement", Science **364**, 368 (2019).

[118] S. Barzanjeh, E. S. Redchenko, M. Peruzzo, M. Wulf, D. P. Lewis, G. Arnold, and J. M. Fink, "Stationary entangled radiation from micromechanical motion", Nature **570**, 480 (2019).

[119] J. Chen, M. Rossi, D. Mason, and A. Schliesser, "Entanglement of propagating optical modes via a mechanical interface", Nature Communications **11**, 10.1038/s41467-020-14768-1 (2020).

[120] M. B. Plenio and S. Virmani, "An introduction to entanglement measures", arXiv preprint quant-ph/0504163 (2005).

[121] C. H. Bennett, H. J. Bernstein, S. Popescu, and B. Schumacher, "Concentrating partial entanglement by local operations", Physical Review A **53**, 2046 (1996).

[122] R. Horodecki, P. Horodecki, M. Horodecki, and K. Horodecki, "Quantum entanglement", Reviews of Modern Physics **81**, 865 (2009).

[123] G. Vidal and R. F. Werner, "Computable measure of entanglement", Physical Review A **65**, 10.1103/physreva.65.032314 (2002).

[124] M. B. Plenio, "Logarithmic Negativity: A Full Entanglement Monotone That is not Convex", Physical Review Letters **95**, 10.1103/physrevlett.95.090503 (2005).

[125] C. H. Bennett, D. P. DiVincenzo, J. A. Smolin, and W. K. Wootters, "Mixed-state entanglement and quantum error correction", Physical Review A **54**, 3824 (1996).

[126] C. H. Bennett, G. Brassard, S. Popescu, B. Schumacher, J. A. Smolin, and W. K. Wootters, "Purification of Noisy Entanglement and Faithful Teleportation via Noisy Channels", Physical Review Letters **76**, 722 (1996).

[127] M. Horodecki, P. Horodecki, and R. Horodecki, "Mixed-State Entanglement and Distillation: Is there a "Bound" Entanglement in Nature?", Physical Review Letters **80**, 5239 (1998).

[128] R. F. Werner and M. M. Wolf, "Bound Entangled Gaussian States", Physical Review Letters **86**, 3658 (2001).

[129] A. Peres, "Separability Criterion for Density Matrices", Physical Review Letters **77**, 1413 (1996).

[130] M. Horodecki, P. Horodecki, and R. Horodecki, "Separability of mixed states: necessary and sufficient conditions", Physics Letters A **223**, 1 (1996).

[131] P. Horodecki, "Separability criterion and inseparable mixed states with positive partial transposition", Physics Letters A **232**, 333 (1997).

[132] R. Simon, "Peres-Horodecki Separability Criterion for Continuous Variable Systems", Physical Review Letters **84**, 2726 (2000).

[133] A. Serafini, G. Adesso, and F. Illuminati, "Unitarily localizable entanglement of Gaussian states", Physical Review A **71**, 10.1103/physreva.71.032349 (2005).

[134] F. G. S. L. Brandão, "Quantifying entanglement with witness operators", Physical Review A **72**, 10.1103/physreva.72.022310 (2005).

[135] P. Hyllus and J. Eisert, "Optimal entanglement witnesses for continuous-variable systems", New Journal of Physics **8**, 51 (2006).

[136] L. Lami, B. Regula, X. Wang, R. Nichols, A. Winter, and G. Adesso, "Gaussian quantum resource theories", Physical Review A **98**, 10.1103/physreva.98.022335 (2018).

[137] G. Giedke, B. Kraus, M. Lewenstein, and J. I. Cirac, "Entanglement Criteria for All Bipartite Gaussian States", Physical Review Letters **87**, 10.1103/physrevlett.87.167904 (2001).

[138] L.-M. Duan, G. Giedke, J. I. Cirac, and P. Zoller, "Inseparability Criterion for Continuous Variable Systems", Physical Review Letters **84**, 2722 (2000).

[139] G. Adesso, A. Serafini, and F. Illuminati, "Determination of Continuous Variable Entanglement by Purity Measurements", Physical Review Letters **92**, 10.1103/physrevlett.92.087901 (2004).

[140] E. J. Routh, *A treatise on the stability of a given state of motion, particularly steady motion: being the essay to which the Adams prize was adjudged in 1877, in the University of Cambridge* (Macmillan and Company, 1877).

[141] A. Hurwitz, "Ueber die Bedingungen, unter welchen eine Gleichung nur Wurzeln mit negativen reellen Theilen besitzt", Mathematische Annalen **46**, 273 (1895).

[142] M. A. de Gosson, *Symplectic Methods in Harmonic Analysis and in Mathematical Physics* (Springer Basel, 2011).

[143] M. Houde, W. McCutcheon, and N. Quesada, "Matrix decompositions in quantum optics: Takagi/Autonne, Bloch–Messiah/Euler, Iwasawa, and Williamson", Canadian Journal of Physics **102**, 497 (2024).

[144] S. L. Braunstein, "Squeezing as an irreducible resource", Physical Review A **71**, 10.1103/physreva.71.055801 (2005).

[145] J. Hoelscher-Obermaier and P. van Loock, "Optimal Gaussian entanglement swapping", Physical Review A **83**, 10.1103/physreva.83.012319 (2011).

[146] P. van Loock, "Quantum Communication with Continuous Variables", Fortschritte der Physik **50**, 1177 (2002).

[147] G. Liu, A. Lingenfelter, V. Joshi, N. Frattini, V. Sivak, S. Shankar, and M. Devoret, "Fully directional quantum-limited phase-preserving amplifier", Physical Review Applied **21**, 10.1103/physrevapplied.21.014021 (2024).

[148] B. Dakić, Y. O. Lipp, X. Ma, M. Ringbauer, S. Kropatschek, S. Barz, T. Paterek, V. Vedral, A. Zeilinger, C. Brukner, and P. Walther, "Quantum discord as resource for remote state preparation", Nature Physics **8**, 666 (2012).

[149] V. Madhok and A. Datta, "Quantum discord as a resource in quantum communication", International Journal of Modern Physics B **27**, 1345041 (2012).

[150] S. Pirandola, "Quantum discord as a resource for quantum cryptography", Scientific Reports **4**, 10.1038/srep06956 (2014).

[151] P. Giorda and M. G. A. Paris, "Gaussian Quantum Discord", Physical Review Letters **105**, 10.1103/physrevlett.105.020503 (2010).

[152] G. Adesso and A. Datta, "Quantum versus Classical Correlations in Gaussian States", Physical Review Letters **105**, 10.1103/physrevlett.105.030501 (2010).

[153] D. P. DiVincenzo, "The Physical Implementation of Quantum Computation", Fortschritte der Physik **48**, 771 (2000).

[154] M. H. Devoret and R. J. Schoelkopf, "Superconducting Circuits for Quantum Information: An Outlook", Science **339**, 1169 (2013).

[155] R. Barends, J. Kelly, A. Megrant, A. Veitia, D. Sank, E. Jeffrey, T. C. White, J. Mutus, A. G. Fowler, B. Campbell, Y. Chen, Z. Chen, B. Chiaro, A. Dunsworth, C. Neill, P. O'Malley, P. Roushan, A. Vainsencher, J. Wenner, A. N. Korotkov, A. N. Cleland, and J. M. Martinis, "Superconducting quantum circuits at the surface code threshold for fault tolerance", Nature **508**, 500 (2014).

[156] M. Kjaergaard, M. E. Schwartz, J. Braumüller, P. Krantz, J. I.-J. Wang, S. Gustavsson, and W. D. Oliver, "Superconducting Qubits: Current State of Play", Annual Review of Condensed Matter Physics **11**, 369 (2020).

[157] A. Blais, A. L. Grimsmo, S. M. Girvin, and A. Wallraff, "Circuit quantum electrodynamics", Reviews of Modern Physics **93**, 10.1103/revmodphys.93.025005 (2021).

[158] E. I. Rosenthal, C. M. F. Schneider, M. Malnou, Z. Zhao, F. Leditzky, B. J. Chapman, W. Wustmann, X. Ma, D. A. Palken, M. F. Zanner, L. R. Vale, G. C. Hilton, J. Gao, G. Smith, G. Kirchmair, and K. W. Lehnert, "Efficient and Low-Backaction Quantum Measurement Using a Chip-Scale Detector", Physical Review Letters **126**, 10.1103/physrevlett.126.090503 (2021).

[159] W. H. Zurek, "Pointer basis of quantum apparatus: Into what mixture does the wave packet collapse?", Physical Review D **24**, 1516 (1981).

[160] V. B. Braginsky, Y. I. Vorontsov, and K. S. Thorne, "Quantum Nondemolition Measurements", Science **209**, 547 (1980).

[161] A. Peres, ed., *Quantum Theory: Concepts and Methods* (Springer Netherlands, 2002).

[162] A. N. Korotkov, "Continuous quantum measurement of a double dot", Physical Review B **60**, 5737 (1999).

[163] A. Blais, J. Gambetta, A. Wallraff, D. I. Schuster, S. M. Girvin, M. H. Devoret, and R. J. Schoelkopf, "Quantum-information processing with circuit quantum electrodynamics", Physical Review A **75**, 10.1103/physreva.75.032329 (2007).

[164] A. Blais, R.-S. Huang, A. Wallraff, S. M. Girvin, and R. J. Schoelkopf, "Cavity quantum electrodynamics for superconducting electrical circuits: An architecture for quantum computation", Physical Review A **69**, 10.1103/physreva.69.062320 (2004).

[165] M. H. Devoret, "Quantum fluctuations in electrical circuits", Les Houches, Session LXIII **7**, 133 (1995).

[166] P. Dirac, *The Principles of Quantum Mechanics*, International series of monographs on physics (Clarendon Press, 1967).

[167] P. Carruthers and M. M. Nieto, "Phase and Angle Variables in Quantum Mechanics", Reviews of Modern Physics **40**, 411 (1968).

[168] H. A. Kastrup, "Quantization of the canonically conjugate pair angle and orbital angular momentum", Physical Review A **73**, 10.1103/physreva.73.052104 (2006).

[169] B. D. Josephson, "The discovery of tunnelling supercurrents", Reviews of Modern Physics **46**, 251 (1974).

[170] E. B. Sonin, "Quantum rotator and Josephson junction: Compact vs. extended phase and dissipative quantum phase transition", Low Temperature Physics **48**, 400 (2022).

[171] P. Dirac, *Lectures on Quantum Mechanics*, Dover Books on Physics (Dover Publications, Mineola, NY, Mar. 2001).

[172] P. A. M. Dirac, "Generalized Hamiltonian Dynamics", Canadian Journal of Mathematics **2**, 129 (1950).

[173] J. L. Anderson and P. G. Bergmann, "Constraints in Covariant Field Theories", Physical Review **83**, 1018 (1951).

[174] M. Henneaux and C. Teitelboim, *Quantization of Gauge Systems* (Princeton University Press, June 2020).

[175] A. Parra-Rodriguez and I. L. Egusquiza, "Geometrical description and Faddeev-Jackiw quantization of electrical networks", Quantum **8**, 1466 (2024).

[176] A. Osborne, T. Larson, S. G. Jones, R. W. Simmonds, A. Gyenis, and A. Lucas, "Symplectic Geometry and Circuit Quantization", PRX Quantum **5**, 10.1103/prxquantum.5.020309 (2024).

[177] M. Rymarz and D. P. DiVincenzo, "Consistent Quantization of Nearly Singular Superconducting Circuits", Physical Review X **13**, 10.1103/physrevx.13.021017 (2023).

[178] I. L. Egusquiza and A. Parra-Rodriguez, *On "Consistent Quantization of Nearly Singular Superconducting Circuits"*, 2024.

[179] A. Wallraff, D. I. Schuster, A. Blais, L. Frunzio, R. S. Huang, J. Majer, S. Kumar, S. M. Girvin, and R. J. Schoelkopf, "Strong coupling of a single photon to a superconducting qubit using circuit quantum electrodynamics", Nature **431**, 162 (2004).

[180] H. Paik, D. I. Schuster, L. S. Bishop, G. Kirchmair, G. Catelani, A. P. Sears, B. R. Johnson, M. J. Reagor, L. Frunzio, L. I. Glazman, S. M. Girvin, M. H. Devoret, and R. J. Schoelkopf, "Observation of High Coherence in Josephson Junction Qubits Measured in a Three-Dimensional Circuit QED Architecture", Physical Review Letters **107**, 10.1103/physrevlett.107.240501 (2011).

[181] Y. Makhlin, G. Schön, and A. Shnirman, "Quantum-state engineering with Josephson-junction devices", Reviews of Modern Physics **73**, 357 (2001).

[182] M. H. Devoret, A. Wallraff, and J. M. Martinis, *Superconducting Qubits: A Short Review*, 2004.

[183] J. Clarke and F. K. Wilhelm, "Superconducting quantum bits", Nature **453**, 1031 (2008).

[184] P. Krantz, M. Kjaergaard, F. Yan, T. P. Orlando, S. Gustavsson, and W. D. Oliver, "A quantum engineer's guide to superconducting qubits", Applied Physics Reviews **6**, 10.1063/1.5089550 (2019).

[185] J. Koch, T. M. Yu, J. Gambetta, A. A. Houck, D. I. Schuster, J. Majer, A. Blais, M. H. Devoret, S. M. Girvin, and R. J. Schoelkopf, "Charge-insensitive qubit design derived from the Cooper pair box", Physical Review A **76**, 10.1103/physreva.76.042319 (2007).

[186] V. Bouchiat, D. Vion, P. Joyez, D. Esteve, and M. H. Devoret, "Quantum Coherence with a Single Cooper Pair", Physica Scripta **T76**, 165 (1998).

[187] A. Shnirman, G. Schön, and Z. Hermon, "Quantum Manipulations of Small Josephson Junctions", Physical Review Letters **79**, 2371 (1997).

[188] Y. Nakamura, Y. A. Pashkin, and J. S. Tsai, "Coherent control of macroscopic quantum states in a single-Cooper-pair box", Nature **398**, 786 (1999).

[189] J. A. Schreier, A. A. Houck, J. Koch, D. I. Schuster, B. R. Johnson, J. M. Chow, J. M. Gambetta, J. Majer, L. Frunzio, M. H. Devoret, S. M. Girvin, and R. J. Schoelkopf, "Suppressing charge noise decoherence in superconducting charge qubits", Physical Review B **77**, 10.1103/physrevb.77.180502 (2008).

[190] F. Yoshihara, K. Harrabi, A. O. Niskanen, Y. Nakamura, and J. S. Tsai, "Decoherence of Flux Qubits due to $1/f$ Flux Noise", Physical Review Letters **97**, 10.1103/physrevlett.97.167001 (2006).

[191] R. C. Bialczak, R. McDermott, M. Ansmann, M. Hofheinz, N. Katz, E. Lucero, M. Neeley, A. D. O'Connell, H. Wang, A. N. Cleland, and J. M. Martinis, "$1/f$ Flux Noise in Josephson Phase Qubits", Physical Review Letters **99**, 10.1103/physrevlett.99.187006 (2007).

[192] B. Douçot and L. B. Ioffe, "Physical implementation of protected qubits", Reports on Progress in Physics **75**, 072001 (2012).

[193] A. Gyenis, A. Di Paolo, J. Koch, A. Blais, A. A. Houck, and D. I. Schuster, "Moving beyond the Transmon: Noise-Protected Superconducting Quantum Circuits", PRX Quantum **2**, 10.1103/prxquantum.2.030101 (2021).

[194] D. Sank, Z. Chen, M. Khezri, J. Kelly, R. Barends, B. Campbell, Y. Chen, B. Chiaro, A. Dunsworth, A. Fowler, E. Jeffrey, E. Lucero, A. Megrant, J. Mutus, M. Neeley, C. Neill, P. J. J. O'Malley, C. Quintana, P. Roushan, A. Vainsencher, T. White, J. Wenner, A. N. Korotkov, and J. M. Martinis, "Measurement-Induced State Transitions in a Superconducting Qubit: Beyond the Rotating Wave Approximation", Physical Review Letters **117**, 10.1103/physrevlett.117.190503 (2016).

[195] M. Khezri, A. Opremcak, Z. Chen, K. C. Miao, M. McEwen, A. Bengtsson, T. White, O. Naaman, D. Sank, A. N. Korotkov, Y. Chen, and V. Smelyanskiy, "Measurement-induced state transitions in a superconducting qubit: Within the rotating-wave approximation", Physical Review Applied **20**, 10.1103/physrevapplied.20.054008 (2023).

[196] M. Boissonneault, J. M. Gambetta, and A. Blais, "Nonlinear dispersive regime of cavity QED: The dressed dephasing model", Physical Review A **77**, 10.1103/physreva.77.060305 (2008).

[197] M. Boissonneault, J. M. Gambetta, and A. Blais, "Dispersive regime of circuit QED: Photon-dependent qubit dephasing and relaxation rates", Physical Review A **79**, 10.1103/physreva.79.013819 (2009).

[198] G. Zhu, D. G. Ferguson, V. E. Manucharyan, and J. Koch, "Circuit QED with fluxonium qubits: Theory of the dispersive regime", Physical Review B **87**, 10.1103/physrevb.87.024510 (2013).

[199] A. A. Houck, J. A. Schreier, B. R. Johnson, J. M. Chow, J. Koch, J. M. Gambetta, D. I. Schuster, L. Frunzio, M. H. Devoret, S. M. Girvin, and R. J. Schoelkopf, "Controlling the Spontaneous Emission of a Superconducting Transmon Qubit", Physical Review Letters **101**, 10.1103/physrevlett.101.080502 (2008).

[200] D. I. Schuster, A. Wallraff, A. Blais, L. Frunzio, R.-S. Huang, J. Majer, S. M. Girvin, and R. J. Schoelkopf, "ac Stark Shift and Dephasing of a Superconducting Qubit Strongly Coupled to a Cavity Field", Physical Review Letters **94**, 10.1103/physrevlett.94.123602 (2005).

[201] P. Bertet, I. Chiorescu, G. Burkard, K. Semba, C. J. P. M. Harmans, D. P. DiVincenzo, and J. E. Mooij, "Dephasing of a Superconducting Qubit Induced by Photon Noise", Physical Review Letters **95**, 10.1103/physrevlett.95.257002 (2005).

[202] J. Gambetta, A. Blais, D. I. Schuster, A. Wallraff, L. Frunzio, J. Majer, M. H. Devoret, S. M. Girvin, and R. J. Schoelkopf, "Qubit-photon interactions in a cavity: Measurement-induced dephasing and number splitting", Physical Review A **74**, 10.1103/physreva.74.042318 (2006).

[203] A. P. Sears, A. Petrenko, G. Catelani, L. Sun, H. Paik, G. Kirchmair, L. Frunzio, L. I. Glazman, S. M. Girvin, and R. J. Schoelkopf, "Photon shot noise dephasing in the strong-dispersive limit of circuit QED", Physical Review B **86**, 10.1103/physrevb.86.180504 (2012).

[204] C. A. Ryan, B. R. Johnson, J. M. Gambetta, J. M. Chow, M. P. da Silva, O. E. Dial, and T. A. Ohki, "Tomography via correlation of noisy measurement records", Physical Review A **91**, 10.1103/physreva.91.022118 (2015).

[205] C. C. Bultink, B. Tarasinski, N. Haandbæk, S. Poletto, N. Haider, D. J. Michalak, A. Bruno, and L. DiCarlo, "General method for extracting the quantum efficiency of dispersive qubit readout in circuit QED", Applied Physics Letters **112**, 10.1063/1.5015954 (2018).

[206] J. Gambetta, A. Blais, M. Boissonneault, A. A. Houck, D. I. Schuster, and S. M. Girvin, "Quantum trajectory approach to circuit QED: Quantum jumps and the Zeno effect", Physical Review A **77**, 10.1103/physreva.77.012112 (2008).

[207] P.-M. Billangeon, J. S. Tsai, and Y. Nakamura, "Circuit-QED-based scalable architectures for quantum information processing with superconducting qubits", Physical Review B **91**, 10.1103/physrevb.91.094517 (2015).

[208] T. Walter, P. Kurpiers, S. Gasparinetti, P. Magnard, A. Potočnik, Y. Salathé, M. Pechal, M. Mondal, M. Oppliger, C. Eichler, and A. Wallraff, "Rapid High-Fidelity Single-Shot Dispersive Readout of Superconducting Qubits", Physical Review Applied **7**, 10.1103/physrevapplied.7.054020 (2017).

[209] A. Eddins, J. M. Kreikebaum, D. M. Toyli, E. M. Levenson-Falk, A. Dove, W. P. Livingston, B. A. Levitan, L. C. G. Govia, A. A. Clerk, and I. Siddiqi, "High-Efficiency Measurement of an Artificial Atom Embedded in a Parametric Amplifier", Physical Review X **9**, 10.1103/physrevx.9.011004 (2019).

[210] A. A. Clerk and D. W. Utami, "Using a qubit to measure photon-number statistics of a driven thermal oscillator", Physical Review A **75**, 10.1103/physreva.75.042302 (2007).

[211] I. Serban, E. Solano, and F. K. Wilhelm, "Phase-space theory for dispersive detectors of superconducting qubits", Physical Review B **76**, 10.1103/physrevb.76.104510 (2007).

[212] I. Serban, E. Solano, and F. K. Wilhelm, "Crossover from weak- to strong-coupling regime in dispersive circuit QED", Europhysics Letters (EPL) **80**, 40011 (2007).

[213] I. Serban, B. L. T. Plourde, and F. K. Wilhelm, "Quantum nondemolition-like fast measurement scheme for a superconducting qubit", Physical Review B **78**, 10.1103/physrevb.78.054507 (2008).

[214] N. Didier, A. Kamal, W. D. Oliver, A. Blais, and A. A. Clerk, "Heisenberg-Limited Qubit Read-Out with Two-Mode Squeezed Light", Physical Review Letters **115**, 10.1103/physrevlett.115.093604 (2015).

[215] N. Didier, J. Bourassa, and A. Blais, "Fast Quantum Nondemolition Readout by Parametric Modulation of Longitudinal Qubit-Oscillator Interaction", Physical Review Letters **115**, 10.1103/physrevlett.115.203601 (2015).

[216] S. Richer and D. DiVincenzo, "Circuit design implementing longitudinal coupling: A scalable scheme for superconducting qubits", Physical Review B **93**, 10.1103/physrevb.93.134501 (2016).

[217] A. Eddins, S. Schreppler, D. M. Toyli, L. S. Martin, S. Hacohen-Gourgy, L. C. G. Govia, H. Ribeiro, A. A. Clerk, and I. Siddiqi, "Stroboscopic Qubit Measurement with Squeezed Illumination", Physical Review Letters **120**, 10.1103/physrevlett.120.040505 (2018).

[218] J. Gambetta, W. A. Braff, A. Wallraff, S. M. Girvin, and R. J. Schoelkopf, "Protocols for optimal readout of qubits using a continuous quantum nondemolition measurement", Physical Review A **76**, 10.1103/physreva.76.012325 (2007).

[219] A. W. Eddins, *Superconducting Circuits for Quantum Metrology with Nonclassical Light*, Doctoral Dissertation (University of California, Berkeley, 2017).

[220] B. Levitan, *Dispersive qubit measurement using an on-chip parametric amplifier*, M.Sc. Thesis (McGill University, 2015).

[221] G. Zhu, S. Schmidt, and J. Koch, "Dispersive regime of the Jaynes–Cummings and Rabi lattice", New Journal of Physics **15**, 115002 (2013).

[222] C. Müller, "Dissipative Rabi model in the dispersive regime", Physical Review Research **2**, 10.1103/physrevresearch.2.033046 (2020).

[223] D. Zueco, G. M. Reuther, S. Kohler, and P. Hänggi, "Qubit-oscillator dynamics in the dispersive regime: Analytical theory beyond the rotating-wave approximation", Physical Review A **80**, 10.1103/physreva.80.033846 (2009).

[224] S. Filipp, P. Maurer, P. J. Leek, M. Baur, R. Bianchetti, J. M. Fink, M. Göppl, L. Steffen, J. M. Gambetta, A. Blais, and A. Wallraff, "Two-Qubit State Tomography Using a Joint Dispersive Readout", Physical Review Letters **102**, 10.1103/physrevlett.102.200402 (2009).

[225] J. Heinsoo, C. K. Andersen, A. Remm, S. Krinner, T. Walter, Y. Salathé, S. Gasparinetti, J.-C. Besse, A. Potočnik, A. Wallraff, and C. Eichler, "Rapid High-fidelity Multiplexed Readout of Superconducting Qubits", Physical Review Applied **10**, 10.1103/physrevapplied.10.034040 (2018).

[226] M. Boissonneault, A. C. Doherty, F. R. Ong, P. Bertet, D. Vion, D. Esteve, and A. Blais, "Back-action of a driven nonlinear resonator on a superconducting qubit", Physical Review A **85**, 10.1103/physreva.85.022305 (2012).

[227] E. Schrödinger, "An Undulatory Theory of the Mechanics of Atoms and Molecules", Physical Review **28**, 1049 (1926).

[228] B. L. van der Waerden, ed., *Sources of Quantum Mechanics*, Dover Books on Physics (Dover Publications, Mineola, NY, Feb. 2007).

[229] H. Weyl, "Quantenmechanik und Gruppentheorie", Zeitschrift für Physik **46**, 1 (1927).

[230] E. Wigner, "On the Quantum Correction For Thermodynamic Equilibrium", Physical Review **40**, 749 (1932).

[231] J. v. Neumann, "Die Eindeutigkeit der Schrödingerschen Operatoren", Mathematische Annalen **104**, 570 (1931).

[232] K. Husimi, "Some formal properties of the density matrix", Proceedings of the Physico-Mathematical Society of Japan. 3rd Series **22**, 264 (1940).

[233] R. J. Glauber, "Coherent and Incoherent States of the Radiation Field", Physical Review **131**, 2766 (1963).

[234] E. C. G. Sudarshan, "Equivalence of Semiclassical and Quantum Mechanical Descriptions of Statistical Light Beams", Physical Review Letters **10**, 277 (1963).

[235] M. Hillery, R. O'Connell, M. Scully, and E. Wigner, "Distribution functions in physics: Fundamentals", Physics Reports **106**, 121 (1984).

[236] T. L. Curtright, D. B. Fairlie, and C. K. Zachos, *A Concise Treatise on Quantum Mechanics in Phase Space* (World Scientific, June 2013).

[237] K. E. Cahill and R. J. Glauber, "Density Operators and Quasiprobability Distributions", Physical Review **177**, 1882 (1969).

[238] N. H. McCoy, "On the Function in Quantum Mechanics Which Corresponds to a Given Function in Classical Mechanics", Proceedings of the National Academy of Sciences **18**, 674 (1932).

[239] F. Bopp, *Werner Heisenberg und die Physik unserer Zeit* (Vieweg+Teubner Verlag, 1961).

[240] G. A. Baker, "Formulation of Quantum Mechanics Based on the Quasi-Probability Distribution Induced on Phase Space", Physical Review **109**, 2198 (1958).

[241] J. Bertrand and P. Bertrand, "A tomographic approach to Wigner's function", Foundations of Physics **17**, 397 (1987).

[242] C. Ferrie, "Quasi-probability representations of quantum theory with applications to quantum information science", Reports on Progress in Physics **74**, 116001 (2011).

[243] A. C. Hirshfeld and P. Henselder, "Deformation quantization in the teaching of quantum mechanics", American Journal of Physics **70**, 537 (2002).

[244] M. Gerstenhaber, "On the Deformation of Rings and Algebras", The Annals of Mathematics **79**, 59 (1964).

[245] R. Simon, E. C. G. Sudarshan, and N. Mukunda, "Gaussian pure states in quantum mechanics and the symplectic group", Physical Review A **37**, 3028 (1988).

[246] Arvind, B. Dutta, N. Mukunda, and R. Simon, "The real symplectic groups in quantum mechanics and optics", Pramana **45**, 471 (1995).

[247] B. Demoen, P. Vanheuverzwijn, and A. Verbeure, "Completely positive maps on the CCR-algebra", Letters in Mathematical Physics **2**, 161 (1977).

[248] G. Cariolaro and G. Pierobon, "Reexamination of Bloch-Messiah reduction", Physical Review A **93**, `10.1103/physreva.93.062115` (2016).

[249] G. Cariolaro and G. Pierobon, "Bloch-Messiah reduction of Gaussian unitaries by Takagi factorization", Physical Review A **94**, `10.1103/physreva.94.062109` (2016).

[250] S. Bittanti, A. J. Laub, and J. C. Willems, eds., *The Riccati Equation* (Springer Berlin Heidelberg, 1991).

[251] P. Lancaster and L. Rodman, *Algebraic Riccati Equations* (Oxford University Press, Sept. 1995).